Living Rev. Relativity, **16**, (2013), 6
http://www.livingreviews.org/lrr-2013-6
doi:10.12942/lrr-2013-6

LIVING REVIEWS in relativity

Cosmology and Fundamental Physics with the Euclid Satellite

Luca Amendola*, Stephen Appleby, David Bacon, Tessa Baker, Marco Baldi, Nicola Bartolo, Alain Blanchard, Camille Bonvin, Stefano Borgani, Enzo Branchini, Clare Burrage, Stefano Camera*, Carmelita Carbone, Luciano Casarini, Mark Cropper, Claudia de Rham, Cinzia Di Porto*, Anne Ealet, Pedro G. Ferreira*, Fabio Finelli, Juan García-Bellido*, Tommaso Giannantonio, Luigi Guzzo, Alan Heavens, Lavinia Heisenberg, Catherine Heymans, Henk Hoekstra, Lukas Hollenstein, Rory Holmes, Ole Horst, Knud Jahnke, Thomas D. Kitching*, Tomi Koivisto, Martin Kunz*, Giuseppe La Vacca, Marisa March, Elisabetta Majerotto, Katarina Markovic, David Marsh, Federico Marulli, Richard Massey, Yannick Mellier, David F. Mota, Nelson J. Nunes, Will Percival, Valeria Pettorino*, Cristiano Porciani*, Claudia Quercellini, Justin Read, Massimiliano Rinaldi, Domenico Sapone, Roberto Scaramella, Constantinos Skordis, Fergus Simpson, Andy Taylor, Shaun Thomas, Roberto Trotta*, Licia Verde*, Filippo Vernizzi, Adrian Vollmer, Yun Wang*, Jochen Weller, Tom Zlosnik
(The Euclid Theory Working Group)[1]

* Corresponding authors.
[1] Please contact euclidtheoryreview@gmail.com for questions and comments.

Accepted: 13 June 2013
Published: 2 September 2013

Abstract

Euclid is a European Space Agency medium-class mission selected for launch in 2019 within the Cosmic Vision 2015 – 2025 program. The main goal of Euclid is to understand the origin of the accelerated expansion of the universe. Euclid will explore the expansion history of the universe and the evolution of cosmic structures by measuring shapes and red-shifts of galaxies as well as the distribution of clusters of galaxies over a large fraction of the sky.

Although the main driver for Euclid is the nature of dark energy, Euclid science covers a vast range of topics, from cosmology to galaxy evolution to planetary research. In this review we focus on cosmology and fundamental physics, with a strong emphasis on science beyond the current standard models. We discuss five broad topics: dark energy and modified gravity, dark matter, initial conditions, basic assumptions and questions of methodology in the data analysis.

This review has been planned and carried out within Euclid's Theory Working Group and is meant to provide a guide to the scientific themes that will underlie the activity of the group during the preparation of the Euclid mission.

Keywords: dark energy, cosmology, galaxy evolution

Imprint / Terms of Use

Living Reviews in Relativity is a peer reviewed open access journal published by the Max Planck Institute for Gravitational Physics, Am Mühlenberg 1, 14476 Potsdam, Germany. ISSN 1433-8351.

Because a *Living Reviews* article can evolve over time, we recommend to cite the article as follows:

Luca Amendola et al. (The Euclid Theory Working Group),
"Cosmology and Fundamental Physics with the Euclid Satellite",
Living Rev. Relativity, **16**, (2013), 6. URL (accessed <date>):
http://www.livingreviews.org/lrr-2013-6

The date given as <date> then uniquely identifies the version of the article you are referring to.

Article Revisions

Living Reviews supports two ways of keeping its articles up-to-date:

Fast-track revision. A fast-track revision provides the author with the opportunity to add short notices of current research results, trends and developments, or important publications to the article. A fast-track revision is refereed by the responsible subject editor. If an article has undergone a fast-track revision, a summary of changes will be listed here.

Major update. A major update will include substantial changes and additions and is subject to full external refereeing. It is published with a new publication number.

For detailed documentation of an article's evolution, please refer to the history document of the article's online version at http://www.livingreviews.org/lrr-2013-6.

Credits

Euclid Theory Working Group Editorial Board (2012):

Valeria Pettorino (editor in chief)
Tessa Baker
Stefano Camera
Elisabetta Majerotto
Marisa March
Cinzia Di Porto
Martin Kunz (Euclid Theory Working Group Coordinator)
Luca Amendola (Euclid Theory Working Group Coordinator)

Corresponding authors (2012):

Luca Amendola
Stefano Camera
Cinzia Di Porto
Pedro G. Ferreira
Juan García-Bellido
Thomas D. Kitching
Martin Kunz
Valeria Pettorino
Cristiano Porciani
Roberto Trotta
Licia Verde
Yun Wang

DISCLAIMER: This is not an official Euclid document and its content reflects solely the views of the contributing authors.

Contents

List of acronyms . . . 11
List of symbols . . . 13

Introduction **15**

Part 1: Dark Energy **17**

1.1 Introduction **17**

1.2 Background evolution **18**
1.2.1 Parametrization of the background evolution . . . 19

1.3 Perturbations **20**
1.3.1 Cosmological perturbation theory . . . 21
1.3.2 Modified growth parameters . . . 23
1.3.2.1 Two new degrees of freedom . . . 24
1.3.2.2 Parameterizations and non-parametric approaches . . . 25
1.3.2.3 Trigger relations . . . 26

1.4 Models of dark energy and modified gravity **26**
1.4.1 Quintessence . . . 27
1.4.2 K-essence . . . 29
1.4.3 A definition of modified gravity . . . 30
1.4.4 Coupled dark-energy models . . . 31
1.4.4.1 Dark energy and baryons . . . 33
1.4.4.2 Dark energy and dark matter . . . 33
1.4.4.3 Dark energy and neutrinos . . . 34
1.4.4.4 Scalar-tensor theories . . . 34
1.4.5 Phantom crossing . . . 35
1.4.5.1 Parameterizing the pressure perturbation . . . 36
1.4.5.2 Regularizing the divergences . . . 37
1.4.5.3 A word on perturbations when $w = -1$ . . . 38
1.4.6 *f(R)* gravity . . . 39
1.4.7 Massive gravity and higher-dimensional models . . . 43
1.4.7.1 Self-acceleration . . . 43
1.4.7.2 Observations . . . 47
1.4.7.3 Screening mechanisms . . . 47
1.4.7.4 Density dependent couplings . . . 48
1.4.8 Einstein Aether and its generalizations . . . 49
1.4.9 The Tensor-Vector-Scalar theory of gravity . . . 50

1.5 Generic properties of dark energy and modified gravity models **53**
1.5.1 To which precision should we measure w? . . . 53
1.5.1.1 Lessons from inflation . . . 53
1.5.1.2 Higgs-Dilaton Inflation: a connection between the early and late universe acceleration . . . 56
1.5.1.3 When should we stop: Bayesian model comparison . . . 56
1.5.2 The effective anisotropic stress as evidence for modified gravity . . . 59

1.5.2.1 Modified gravity models with a single degree of freedom 59
1.5.2.2 Balancing multiple degrees of freedom 60
1.5.3 Parameterized frameworks for theories of modified gravity 61

1.6 Nonlinear aspects **63**
1.6.1 N-body simulations of dark energy and modified gravity 63
1.6.1.1 Quintessence and early dark-energy models 63
1.6.1.2 Interacting dark-energy models 65
1.6.1.3 Growing neutrinos 67
1.6.1.4 Modified gravity 67
1.6.2 The spherical collapse model 68
1.6.2.1 Clustering dark energy 69
1.6.2.2 Coupled dark energy 71
1.6.2.3 Early dark energy 73

1.7 Observational properties of dark energy and modified gravity **74**
1.7.1 General remarks 74
1.7.2 Observing modified gravity with weak lensing 75
1.7.2.1 Magnification matrix 76
1.7.2.2 Observable quantities 77
1.7.3 Observing modified gravity with redshift surveys 80
1.7.4 Cosmological bulk flows 83

1.8 Forecasts for Euclid **85**
1.8.1 A review of forecasts for parametrized modified gravity with Euclid 85
1.8.2 Euclid surveys 88
1.8.3 Forecasts for the growth rate from the redshift survey 89
1.8.4 Weak lensing non-parametric measurement of expansion and growth rate . . . 100
1.8.5 Testing the nonlinear corrections for weak lensing forecasts 103
1.8.6 Forecasts for the dark-energy sound speed 105
1.8.7 Weak lensing constraints on $f(R)$ gravity 110
1.8.8 Forecast constraints on coupled quintessence cosmologies 113
1.8.9 Extra-Euclidean data and priors 115
1.8.9.1 The Planck prior 118

1.9 Summary and outlook **120**

Part 2: Dark Matter and Neutrinos **122**

2.1 Introduction **122**

2.2 Dark matter halo properties **124**
2.2.1 The halo mass function as a function of redshift 124
2.2.1.1 Weak and strong lensing measurements of the halo mass function . . . 125
2.2.1.2 The advantage of going to high redshift 126
2.2.2 The dark matter density profile 126

2.3 Euclid dark matter studies: wide-field X-ray complementarity **129**

2.4 Dark matter mapping **130**
2.4.1 Charting the universe in 3D . . . 130

2.5 Scattering cross sections **131**
2.5.1 Dark matter–dark matter interactions . . . 131
2.5.2 Dark matter–baryonic interactions . . . 131
2.5.3 Dark matter–dark energy interactions . . . 132

2.6 Cross-section constraints from galaxy clusters **132**
2.6.1 Bulleticity . . . 133

2.7 Constraints on warm dark matter **133**
2.7.1 Warm dark matter particle candidates . . . 133
2.7.2 Dark matter free-streaming . . . 135
2.7.3 Current constraints on the WDM particle from large-scale structure . . . 135

2.8 Neutrino properties **136**
2.8.1 Evidence of relic neutrinos . . . 137
2.8.2 Neutrino mass . . . 138
2.8.3 Hierarchy and the nature of neutrinos . . . 138
2.8.4 Number of neutrino species . . . 139
2.8.5 Model dependence . . . 140
2.8.6 Σ forecasted error bars and degeneracies . . . 140
2.8.6.1 Hierarchy dependence . . . 140
2.8.6.2 Growth and incoherent peculiar velocity dependence . . . 140
2.8.7 $N_{\rm eff}$ forecasted errors and degeneracies . . . 141
2.8.8 Nonlinear effects of massive cosmological neutrinos on bias and RSD . . . 142

2.9 Coupling between dark energy and neutrinos **143**

2.10 Unified Dark Matter **150**
2.10.1 Theoretical background . . . 151
2.10.2 Euclid observables . . . 151

2.11 Dark energy and dark matter **152**

2.12 Ultra-light scalar fields **154**
2.12.1 Requirements . . . 158

2.13 Dark-matter surrogates in theories of modified gravity **158**
2.13.1 Extra fields in modified gravity . . . 158
2.13.2 Vector dark matter in Einstein-Aether models . . . 159
2.13.3 Scalar and tensors in TeVeS . . . 161
2.13.4 Tensor dark matter in models of bigravity . . . 161

2.14 Outlook **161**

Part 3: Initial Conditions **163**

3.1 Introduction **163**

3.2 Constraining inflation **164**
3.2.1 Primordial perturbations from inflation . . . 164
3.2.2 Forecast constraints on the power spectrum . . . 165

3.3 Probing the early universe with non-Gaussianities **169**
3.3.1 Local non-Gaussianity . . . 169
3.3.2 Shapes: what do they tell us? . . . 171
3.3.3 Beyond shapes: scale dependence and the squeezed limit . . . 172
3.3.4 Beyond inflation . . . 173

3.4 Primordial Non-Gaussianity and Large-Scale Structure **174**
3.4.1 Constraining primordial non-Gaussianity and gravity from 3-point statistics . . . 174
3.4.2 Non-Gaussian halo bias . . . 175
3.4.3 Number counts of nonlinear structures . . . 177
3.4.4 Forecasts for Euclid . . . 177
3.4.5 Complementarity . . . 179

3.5 Isocurvature modes **180**
3.5.1 The origin of isocurvature perturbations . . . 180
3.5.2 Constraining isocurvature perturbations . . . 182

3.6 Summary and outlook **183**

Part 4: Testing the Basic Cosmological Hypotheses **184**

4.1 Introduction **184**

4.2 Transparency and Etherington Relation **184**
4.2.1 Violation of photon conservation . . . 184
4.2.2 Axion-like particles . . . 185
4.2.3 Mini-charged particles . . . 186

4.3 Beyond homogeneity and isotropy **187**
4.3.1 Anisotropic models . . . 187
4.3.1.1 Late-time anisotropy . . . 189
4.3.2 Late-time inhomogeneity . . . 190
4.3.3 Inhomogeneous models: Large voids . . . 191
4.3.4 Inhomogeneous models: Backreaction . . . 195

4.4 Reconstructing the global curvature at different redshifts **198**

4.5 Speculative avenues: non-standard models of primordial fluctuations **200**
4.5.1 Probing the quantum origin of primordial fluctuations . . . 200
4.5.2 Early-time anisotropy . . . 203
4.5.2.1 Vector field models . . . 204
4.5.2.2 Modulated perturbations . . . 204
4.5.3 Current and future constraints from CMB and LSS on an anisotropic power spectrum . . . 205

Part 5: Statistical Methods for Performance Forecasts **207**

5.1 Introduction **207**

5.2 Predicting the science return of a future experiment **207**
5.2.1 The Gaussian linear model 207
5.2.2 Fisher-matrix error forecast 210
5.2.3 Figure of merits 212
5.2.4 The Bayesian approach 213

5.3 Survey design and optimization **215**

5.4 Future activities and open challenges **216**

Acknowledgments **218**

References **219**

List of Tables

1 Strength of evidence disfavoring the three benchmark models against a cosmological constant model, using an indicative accuracy on $w = -1$ from present data, $\sigma \sim 0.1$. 58
2 Required accuracy for future surveys in order to disfavor the three benchmark models against $w = -1$ for two different strengths of evidence. 58
3 Expected galaxy number densities in units of $(h/\mathrm{Mpc})^3$ for Euclid survey. 89
4 1σ marginalized errors for the bias and the growth rates in each redshift bin. . . . 93
5 Numerical values for 1σ constraints on parameters in Figure 16 and figures of merit. Here we have fixed Ω_k to its fiducial value, $\Omega_k = 0$. 97
6 Numerical values for 1σ constraints on parameters γ and w (assumed constant), relative to the red ellipses in Figures 17, 18 and figures of merit. Here we have marginalized over Ω_k. 97
7 Numerical values for marginalized 1σ constraints on cosmological parameters using constant γ and w. 97
8 1σ marginalized errors for parameters γ and w expressed through γ and η parameterizations. 98
9 Numerical values for 1σ constraints on parameters in right panel of Figure 16 and figures of merit. 98
10 Numerical values for 1σ constraints on parameters in Figure 19 and figures of merit. 98
11 1σ marginalized errors for the parameters w_0 and w_1, obtained with three different methods (reference case, see Figure 20). 100
12 Values used in our computation. The values of the fiducial model (WMAP7, on the left) and the survey parameters (on the right). 102
13 1-σ errors for the set $\Theta \equiv \{\beta^2, \alpha, \Omega_c, h, \Omega_b, n_s\, \sigma_8, \log(A)\}$ of cosmological parameters, combining CMB $+P(k)$ and CMB + $P(k)$ + WL. 115
14 1-σ errors for β^2, for CMB, $P(k)$, WL and CMB + $P(k)$ + WL. 115
15 R, l_a, $\Omega_b h^2$ and n_s estimated from Planck simulated data. 119
16 Covariance matrix for $(R, l_a, \Omega_b h^2, n_s)$ from Planck. 119
17 Fisher matrix for (w_0, w_a, Ω_{DE}, Ω_k, ω_m, ω_b, n_S) derived from the covariance matrix for $(R, l_a, \Omega_b h^2, n_s)$ from Planck. 119
18 $\sigma(M_\nu)$ and $\sigma(N_{\mathrm{eff}})$ marginalized errors from LSS+CMB 142
19 Instrument specifics for the Planck satellite with 30 months of integration. 166
20 Cosmological parameters 168

21 Specifications of the surveys used in the Euclid forecasts given in Table 22. 178
22 Forecast 1σ errors for the nonlinearity parameter $f_{\rm NL}$ based on two-point statistics (power spectra) of the Euclid redshift and weak-lensing surveys. 179
23 Forecast 1σ errors for a scale-dependent local model of primordial non-Gaussianity. 179
24 Bianchi models containing FRW limit and their structure constants. 189

List of acronyms

AGN	Active Galactic Nucleus
ALP	Axio-Like Particle
BAO	Baryonic Acoustic Oscillations
BBKS	Bardeen–Bond–Kaiser–Szalay
BOSS	Baryon Oscillation Spectroscopic Survey
BPol	B-Polarization Satellite
BigBOSS	Baryon Oscillation Spectroskopic Survey
CAMB	Code for Anisotropies in the Microwave Background
CDE	Coupled Dark Energy
CDM	Cold Dark Matter
CDMS	Cryogenic Dark Matter Search
CL	Confidence Level
CMB	Cosmic Microwave Background
COMBO-17	Classifying Objects by Medium-Band Observations
COSMOS	Cosmological Evolution Survey
CPL	Chevallier–Polarski–Linder
CQ	Coupled Quintessence
CRESST	Cryogenic Rare Event Search with Superconducting Thermometers
DE	Dark Energy
DES	Dark Energy Survey
DETF	Dark Energy Task Force
DGP	Dvali–Gabadadze–Porrati
DM	Dark Matter
EBI	Eddington–Born–Infeld
EDE	Early Dark Energy
EROS	Expérience pour la Recherche d'Objets Sombres
eROSITA	Extended ROentgen Survey with an Imaging Telescope Array
FCDM	Fuzzy Cold Dark Matter
FFT	Fast Fourier Transform
FLRW	Friedmann–Lemaître–Robertson–Walker
FoM	Figure of Merit
FoG	Fingers of God
GEA	Generalized Einstein-Aether
GR	General Relativity
HETDEX	Hobby-Eberly Telescope Dark Energy Experiment
ICM	Intracluster Medium
IH	Inverted Hierarchy
IR	Infrared
ISW	Integrated Sachs–Wolfe

KL	Kullback–Leibler divergence
LCDM	Lambda Cold Dark Matter
LHC	Large Hadron Collider
LRG	Luminous Red Galaxy
LSB	Low Surface Brightness
LSS	Large Scale Structure
LSST	Large Synoptic Survey Telescope
LTB	Lemaître–Tolman–Bondi
MACHO	MAssive Compact Halo Object
MCMC	Markov Chain Monte Carlo
MCP	Mini-Charged Particles
MF	Mass Function
MG	Modified Gravity
MOND	MOdified Newtonian Dynamics
MaVaNs	Mass Varying Neutrinos
NFW	Navarro–Frenk–White
NH	Normal Hierarchy
PCA	Principal Component Analysis
PDF	Probability Distribution Function
PGB	Pseudo-Goldstein Boson
PKDGRAV	Parallel K-D tree GRAVity code
PPF	Parameterized Post-Friedmann
PPN	Parameterized Post-Newtonian
PPOD	Predictive Posterior Odds Distribution
PSF	Point Spread Function
QCD	Quantum ChromoDynamics
RDS	Redshift Space Distortions
RG	Renormalization Group
SD	Savage–Dickey
SDSS	Sloan Digital Sky Survey
SIDM	Self Interacting Dark Matter
SN	Supernova
TeVeS	Tensor Vector Scalar
UDM	Unified Dark Matter
UV	Ultra Violett
WDM	Warm Dark Matter
WFXT	Wide-Field X-Ray Telescope
WIMP	Weakly Interacting Massive Particle
WKB	Wentzel–Kramers–Brillouin
WL	Weak Lensing
WLS	Weak Lensing Survey
WMAP	Wilkinson Microwave Anisotropy Probe
XMM-Newton	X-ray Multi-Mirror Mission
vDVZ	van Dam–Veltman–Zakharov

List of symbols

c_a	Adiabatic sound speed	p. 36
$D_A(z)$	Angular diameter distance	p. 81
$\eth$	Angular spin raising operator	p. 76
Π^i_j	Anisotropic stress perturbation tensor	p. 21
σ	Uncertainty	
Bo	Bayes factor	p. 213
b	Bias (ratio of galaxy to total matter perturbations)	p. 82
$B_\Phi(k_1, k_2, k_3)$	Bispectrum of the Bardeen's potential	p. 202
$g(X)$	Born–Infeld kinetic term	p. 151
$\mathbf{b}$	Bulleticity	p. 133
ζ	Comoving curvature perturbation	p. 164
$r(z)$	Comoving distance	
$\mathcal{H}$	Conformal Hubble parameter, $\mathcal{H} = aH$	p. 18
η, τ	Conformal time	p. 18
κ	Convergence	p. 76
t	Cosmic time	p. 33
Λ	Cosmological constant	
$\mathbf{\Theta}$	Cosmological parameters	p. 207
r_c	Cross over scale	p. 44
$\Box$	d'Alembertian, $\Box = \nabla^2$	
F	Derivative of $f(R)$	p. 39
θ	Divergence of velocity field	p. 22
μ	Direction cosine	p. 166
π	Effective anisotropic stress	p. 38
$\eta(a, k)$	Effective anisotropic stress parameterization	p. 24
ρ	Energy density	
$T_{\mu\nu}$	Energy momentum tensor	p. 21
w	Equation of state	p. 19
$F_{\alpha\beta}$	Fisher information matrix	p. 211
σ_8	Fluctuation amplitude at 8 km/s/Mpc	
u^μ	Four-velocity	p. 21
Ω_m	Fractional matter density	
$f_{\rm sky}$	Fraction of sky observed	p. 101
Δ_M	Gauge invariant comoving density contrast	p. 23
$\tau(z)$	Generic opacity parameter	p. 185
ϖ	Gravitational slip parameter	p. 25
$G(a)$	Growth function/Growth factor	p. 26

γ	Growth index/Shear	p. 26/p. 76
f_g	Growth rate	p. 23
$b_{\rm eff}$	Halo effective linear bias factor	p. 143
h	Hubble constant in units of 100 km/s/Mpc	
$H(z)$	Hubble parameter	
ξ_i	Killing field	p. 188
δ_{ij}	Kronecker delta	
$f(R)$	Lagrangian in modified gravity	p. 39
$P_l(\mu)$	Legendre polynomials	p. 83
$\mathcal{L}(\mathbf{\Theta})$	Likelihood function	p. 207
$\beta(z)$	Linear redshift-space distortion parameter	p. 82
$D_L(z)$	Luminosity distance	p. 184
$Q(a,k)$	Mass screening effect	p. 24
δ_m	Matter density perturbation	
$g_{\mu\nu}$	Metric tensor	p. 21
μ	Modified gravity function: $\mu = Q/\eta$	p. 25
C_ℓ	Multipole power spectrum	p. 166
G	Newton's gravitational constant	
N	Number of e-folds, $N = \ln a$	p. 165
$P(k)$	Matter power spectrum	
p	Pressure	
δp	Pressure perturbation	
$\chi(z)$	Radial, dimensionless comoving distance	p. 81
z	Redshift	
R	Ricci scalar	
ϕ	Scalar field	p. 32
A	Scalar potential	p. 21
Ψ, Φ	Scalar potentials	p. 21
n_s	Scalar spectral index	p. 164
a	Scale factor	
f_a	Scale of Peccei–Quinn symmetry breaking	p. 155
ℓ	Spherical harmonic multipoles	
c_s	Sound speed	p. 106
Σ	Total neutrino mass/Inverse covariance matrix/PPN parameter	p. 136/p. 210/p. 25
H_T^{ij}	Trace-free distortion	p. 21
$T(k)$	Transfer function	p. 174
B_i	Vector shift	p. 21
$\mathbf{k}$	Wavenumber	

Introduction

Euclid[1] [551, 760, 239] is an ESA medium-class mission selected for the second launch slot (expected for 2019) of the Cosmic Vision 2015 – 2025 program. The main goal of Euclid is to understand the physical origin of the accelerated expansion of the universe. Euclid is a satellite equipped with a 1.2 m telescope and three imaging and spectroscopic instruments working in the visible and near-infrared wavelength domains. These instruments will explore the expansion history of the universe and the evolution of cosmic structures by measuring shapes and redshifts of galaxies over a large fraction of the sky. The satellite will be launched by a Soyuz ST-2.1B rocket and transferred to the L2 Lagrange point for a six-year mission that will cover at least 15 000 square degrees of sky. Euclid plans to image a billion galaxies and measure nearly 100 million galaxy redshifts.

These impressive numbers will allow Euclid to realize a detailed reconstruction of the clustering of galaxies out to a redshift 2 and the pattern of light distortion from weak lensing to redshift 3. The two main probes, redshift clustering and weak lensing, are complemented by a number of additional cosmological probes: cross correlation between the cosmic microwave background and the large scale structure; luminosity distance through supernovae Ia; abundance and properties of galaxy clusters and strong lensing. To extract the maximum of information also in the nonlinear regime of perturbations, these probes will require accurate high-resolution numerical simulations. Besides cosmology, Euclid will provide an exceptional dataset for galaxy evolution, galaxy structure, and planetary searches. All Euclid data will be publicly released after a relatively short proprietary period and will constitute for many years the ultimate survey database for astrophysics.

A huge enterprise like Euclid requires highly considered planning in terms not only of technology but also for the scientific exploitation of future data. Many ideas and models that today seem to be abstract exercises for theorists will in fact finally become testable with the Euclid surveys. The main science driver of Euclid is clearly the nature of dark energy, the enigmatic substance that is driving the accelerated expansion of the universe. As we discuss in detail in Part 1, under the label "dark energy" we include a wide variety of hypotheses, from extradimensional physics to higher-order gravity, from new fields and new forces to large violations of homogeneity and isotropy. The simplest explanation, Einstein's famous cosmological constant, is still currently acceptable from the observational point of view, but is not the only one, nor necessarily the most satisfying, as we will argue. Therefore, it is important to identify the main observables that will help distinguish the cosmological constant from the alternatives and to forecast Euclid's performance in testing the various models.

Since clustering and weak lensing also depend on the properties of dark matter, Euclid is a dark matter probe as well. In Part 2 we focus on the models of dark matter that can be tested with Euclid data, from massive neutrinos to ultra-light scalar fields. We show that Euclid can measure the neutrino mass to a very high precision, making it one of the most sensitive neutrino experiments of its time, and it can help identify new light fields in the cosmic fluid.

The evolution of perturbations depends not only on the fields and forces active during the cosmic eras, but also on the initial conditions. By reconstructing the initial conditions we open a window on the inflationary physics that created the perturbations, and allow ourselves the chance of determining whether a single inflaton drove the expansion or a mixture of fields. In Part 3 we review the choices of initial conditions and their impact on Euclid science. In particular we discuss deviations from simple scale invariance, mixed isocurvature-adiabatic initial conditions, non-Gaussianity, and the combined forecasts of Euclid and CMB experiments.

Practically all of cosmology is built on the Copernican Principle, a very fruitful idea postulating a homogeneous and isotropic background. Although this assumption has been confirmed time and again since the beginning of modern cosmology, Euclid's capabilities can push the test to new levels. In Part 4 we challenge some of the basic cosmological assumptions and predict how

[1] Continuously updated information on Euclid is available on http://www.euclid-ec.org.

well Euclid can constrain them. We explore the basic relation between luminosity and angular diameter distance that holds in any metric theory of gravity if the universe is transparent to light, and the existence of large violations of homogeneity and isotropy, either due to local voids or to the cumulative stochastic effects of perturbations, or to intrinsically anisotropic vector fields or spacetime geometry.

Finally, in Part 5 we review some of the statistical methods that are used to forecast the performance of probes like Euclid, and we discuss some possible future developments.

This review has been planned and carried out within Euclid's Theory Working Group and is meant to provide a guide to the scientific themes that will underlie the activity of the group during the preparation of the mission. At the same time, this review will help us and the community at large to identify the areas that deserve closer attention, to improve the development of Euclid science and to offer new scientific challenges and opportunities.

Part 1: Dark Energy

1.1 Introduction

With the discovery of cosmic acceleration at the end of the 1990s, and its possible explanation in terms of a cosmological constant, cosmology has returned to its roots in Einstein's famous 1917 paper that simultaneously inaugurated modern cosmology and the history of the constant Λ. Perhaps cosmology is approaching a robust and all-encompassing standard model, like its cousin, the very successful standard model of particle physics. In this scenario, the cosmological standard model could essentially close the search for a broad picture of cosmic evolution, leaving to future generations only the task of filling in a number of important, but not crucial, details.

The cosmological constant is still in remarkably good agreement with almost all cosmological data more than ten years after the observational discovery of the accelerated expansion rate of the universe. However, our knowledge of the universe's evolution is so incomplete that it would be premature to claim that we are close to understanding the ingredients of the cosmological standard model. If we ask ourselves what we know for certain about the expansion rate at redshifts larger than unity, or the growth rate of matter fluctuations, or about the properties of gravity on large scales and at early times, or about the influence of extra dimensions (or their absence) on our four dimensional world, the answer would be surprisingly disappointing.

Our present knowledge can be succinctly summarized as follows: we live in a universe that is consistent with the presence of a cosmological constant in the field equations of general relativity, and as of 2012, the value of this constant corresponds to a fractional energy density today of $\Omega_\Lambda \approx 0.73$. However, far from being disheartening, this current lack of knowledge points to an exciting future. A decade of research on dark energy has taught many cosmologists that this ignorance can be overcome by the same tools that revealed it, together with many more that have been developed in recent years.

Why then is the cosmological constant not the end of the story as far as cosmic acceleration is concerned? There are at least three reasons. The first is that we have no simple way to explain its small but non-zero value. In fact, its value is unexpectedly small with respect to any physically meaningful scale, except the *current* horizon scale. The second reason is that this value is not only small, but also surprisingly close to another unrelated quantity, the *present* matter-energy density. That this happens just by coincidence is hard to accept, as the matter density is diluted rapidly with the expansion of space. Why is it that we happen to live at the precise, fleeting epoch when the energy densities of matter and the cosmological constant are of comparable magnitude? Finally, observations of coherent acoustic oscillations in the cosmic microwave background (CMB) have turned the notion of accelerated expansion in the very early universe (inflation) into an integral part of the cosmological standard model. Yet the simple truth that we exist as observers demonstrates that this early accelerated expansion was of a finite duration, and hence cannot be ascribable to a true, constant Λ; this sheds doubt on the nature of the current accelerated expansion. The very fact that we know so little about the past dynamics of the universe forces us to enlarge the theoretical parameter space and to consider phenomenology that a simple cosmological constant cannot accommodate.

These motivations have led many scientists to challenge one of the most basic tenets of physics: Einstein's law of gravity. Einstein's theory of general relativity (GR) is a supremely successful theory on scales ranging from the size of our solar system down to micrometers, the shortest distances at which GR has been probed in the laboratory so far. Although specific predictions about such diverse phenomena as the gravitational redshift of light, energy loss from binary pulsars, the rate of precession of the perihelia of bound orbits, and light deflection by the sun are not unique to GR, it must be regarded as highly significant that GR is consistent with each of these tests and

more. We can securely state that GR has been tested to high accuracy *at these distance scales*.

The success of GR on larger scales is less clear. On astrophysical and cosmological scales, tests of GR are complicated by the existence of invisible components like dark matter and by the effects of spacetime geometry. We do not know whether the physics underlying the apparent cosmological constant originates from modifications to GR (i.e., an extended theory of gravity), or from a new fluid or field in our universe that we have not yet detected directly. The latter phenomena are generally referred to as 'dark energy' models.

If we only consider observations of the expansion rate of the universe we cannot discriminate between a theory of modified gravity and a dark-energy model. However, it is likely that these two alternatives will cause perturbations around the 'background' universe to behave differently. Only by improving our knowledge of the growth of structure in the universe can we hope to progress towards breaking the degeneracy between dark energy and modified gravity. Part 1 of this review is dedicated to this effort. We begin with a review of the background and linear perturbation equations in a general setting, defining quantities that will be employed throughout. We then explore the nonlinear effects of dark energy, making use of analytical tools such as the spherical collapse model, perturbation theory and numerical N-body simulations. We discuss a number of competing models proposed in literature and demonstrate what the Euclid survey will be able to tell us about them.

1.2 Background evolution

Most of the calculations in this review are performed in the Friedmann–Lemaître–Robertson–Walker (FLRW) metric

$$\mathrm{d}s^2 = -\mathrm{d}t^2 + a(t)^2\left(\frac{\mathrm{d}r^2}{1-kr^2} + r^2\,\mathrm{d}\theta^2 + r^2\sin^2\theta\,\mathrm{d}\phi^2\right), \tag{1.2.1}$$

where $a(t)$ is the scale factor and k the spatial curvature. The usual symbols for the Hubble function $H = \dot{a}/a$ and the density fractions Ω_x, where x stands for the component, are employed. We characterize the components with the subscript M or m for matter, γ or r for radiation, b for baryons, K for curvature and Λ for the cosmological constant. Whenever necessary for clarity, we append a subscript 0 to denote the present epoch, e.g., $\Omega_{M,0}$. Sometimes the conformal time $\eta = \int \mathrm{d}t/a$ and the conformal Hubble function $\mathcal{H} = aH = \mathrm{d}a/(a\mathrm{d}\eta)$ are employed. Unless otherwise stated, we denote with a dot derivatives w.r.t. cosmic time t (and sometimes we employ the dot for derivatives w.r.t. conformal time η) while we use a prime for derivatives with respect to $\ln a$.

The energy density due to a cosmological constant with $p = -\rho$ is obviously constant over time. This can easily be seen from the covariant conservation equation $T^{\nu}_{\mu;\nu} = 0$ for the homogeneous and isotropic FLRW metric,

$$\dot{\rho} + 3H(\rho + p) = 0\,. \tag{1.2.2}$$

However, since we also observe radiation with $p = \rho/3$ and non-relativistic matter for which $p \approx 0$, it is natural to assume that the dark energy is not necessarily limited to a constant energy density, but that it could be dynamical instead.

One of the simplest models that explicitly realizes such a dynamical dark energy scenario is described by a minimally-coupled canonical scalar field evolving in a given potential. For this reason, the very concept of dynamical dark energy is often associated with this scenario, and in this context it is called 'quintessence' [954, 754]. In the following, the scalar field will be indicated with ϕ. Although in this simplest framework the dark energy does not interact with other species and influences spacetime only through its energy density and pressure, this is not the only possibility

and we will encounter more general models later on. The homogeneous energy density and pressure of the scalar field ϕ are defined as

$$\rho_\phi = \frac{\dot{\phi}^2}{2} + V(\phi)\,, \quad p_\phi = \frac{\dot{\phi}^2}{2} - V(\phi)\,, \quad w_\phi = \frac{p_\phi}{\rho_\phi}\,, \tag{1.2.3}$$

and w_ϕ is called the equation-of-state parameter. Minimally-coupled dark-energy models can allow for attractor solutions [252, 573, 867]: if an attractor exists, depending on the potential $V(\phi)$ in which dark energy rolls, the trajectory of the scalar field in the present regime converges to the path given by the attractor, though starting from a wide set of different initial conditions for ϕ and for its first derivative $\dot{\phi}$. Inverse power law and exponential potentials are typical examples of potential that can lead to attractor solutions. As constraints on w_ϕ become tighter [e.g., 526], the allowed range of initial conditions to follow into the attractor solution shrinks, so that minimally-coupled quintessence is actually constrained to have very flat potentials. The flatter the potential, the more minimally-coupled quintessence mimics a cosmological constant, the more it suffers from the same fine-tuning and coincidence problems that affect a ΛCDM scenario [646].

However, when GR is modified or when an interaction with other species is active, dark energy may very well have a non-negligible contribution at early times. Therefore, it is important, already at the background level, to understand the best way to characterize the main features of the evolution of quintessence and dark energy in general, pointing out which parameterizations are more suitable and which ranges of parameters are of interest to disentangle quintessence or modified gravity from a cosmological constant scenario.

In the following we briefly discuss how to describe the cosmic expansion rate in terms of a small number of parameters. This will set the stage for the more detailed cases discussed in the subsequent sections. Even within specific physical models it is often convenient to reduce the information to a few phenomenological parameters.

Two important points are left for later: from Eq. (1.2.3) we can easily see that $w_\phi \geq -1$ as long as $\rho_\phi > 0$, i.e., uncoupled canonical scalar field dark energy never crosses $w_\phi = -1$. However, this is not necessarily the case for non-canonical scalar fields or for cases where GR is modified. We postpone to Section 1.4.5 the discussion of how to parametrize this 'phantom crossing' to avoid singularities, as it also requires the study of perturbations.

The second deferred part on the background expansion concerns a basic statistical question: what is a sensible precision target for a measurement of dark energy, e.g., of its equation of state? In other words, how close to $w_\phi = -1$ should we go before we can be satisfied and declare that dark energy is the cosmological constant? We will address this question in Section 1.5.

1.2.1 Parametrization of the background evolution

If one wants to parametrize the equation of state of dark energy, two general approaches are possible. The first is to start from a set of dark-energy models given by the theory and to find parameters describing their w_ϕ as accurately as possible. Only later can one try and include as many theoretical models as possible in a single parametrization. In the context of scalar-field dark-energy models (to be discussed in Section 1.4.1), [266] parametrize the case of slow-rolling fields, [796] study thawing quintessence, [446] and [232] include non-minimally coupled fields, [817] quintom quintessence, [325] parametrize hilltop quintessence, [231] extend the quintessence parametrization to a class of k-essence models, [459] study a common parametrization for quintessence and phantom fields. Another convenient way to parametrize the presence of a non-negligible homogeneous dark energy component at early times (usually labeled as EDE) was presented in [956]. We recall it here because we will refer to this example in Section 1.6.1.1. In this case the equation of state is parametrized as:

$$w_X(z) = \frac{w_0}{1 + b\ln(1+z)}, \tag{1.2.4}$$

where b is a constant related to the amount of dark energy at early times, i.e.,

$$b = -\frac{3\bar{w}_0}{\ln\frac{1-\Omega_{\mathrm{X},e}}{\Omega_{\mathrm{X},e}} + \ln\frac{1-\Omega_{m,0}}{\Omega_{m,0}}} \,. \tag{1.2.5}$$

Here the subscripts '0' and 'e' refer to quantities calculated today or early times, respectively. With regard to the latter parametrization, we note that concrete theoretical and realistic models involving a non-negligible energy component at early times are often accompanied by further important modifications (as in the case of interacting dark energy), not always included in a parametrization of the sole equation of state such as (1.2.4) (for further details see Section 1.6 on nonlinear aspects of dark energy and modified gravity).

The second approach is to start from a simple expression of w without assuming any specific dark-energy model (but still checking afterwards whether known theoretical dark-energy models can be represented). This is what has been done by [470, 623, 953] (linear and logarithmic parametrization in z), [229], [584] (linear and power law parametrization in a), [322], [97] (rapidly varying equation of state).

The most common parametrization, widely employed in this review, is the linear equation of state [229, 584]

$$w_X(a) = w_0 + w_a(1-a)\,, \tag{1.2.6}$$

where the subscript X refers to the generic dark-energy constituent. While this parametrization is useful as a toy model in comparing the forecasts for different dark-energy projects, it should not be taken as all-encompassing. In general a dark-energy model can introduce further significant terms in the effective $w_X(z)$ that cannot be mapped onto the simple form of Eq. (1.2.6).

An alternative to model-independent constraints is measuring the dark-energy density $\rho_X(z)$ (or the expansion history $H(z)$) as a free function of cosmic time [942, 881, 274]. Measuring $\rho_X(z)$ has advantages over measuring the dark-energy equation of state $w_X(z)$ as a free function; $\rho_X(z)$ is more closely related to observables, hence is more tightly constrained for the same number of redshift bins used [942, 941]. Note that $\rho_X(z)$ is related to $w_X(z)$ as follows [942]:

$$\frac{\rho_X(z)}{\rho_X(0)} = \exp\left\{\int_0^z \mathrm{d}z' \, \frac{3[1+w_X(z')]}{1+z'}\right\} \,. \tag{1.2.7}$$

Hence, parametrizing dark energy with $w_X(z)$ implicitly assumes that $\rho_X(z)$ does not change sign in cosmic time. This precludes whole classes of dark-energy models in which $\rho_X(z)$ becomes negative in the future ("Big Crunch" models, see [943] for an example) [944].

Note that the measurement of $\rho_X(z)$ is straightforward once $H(z)$ is measured from baryon acoustic oscillations, and Ω_m is constrained tightly by the combined data from galaxy clustering, weak lensing, and cosmic microwave background data – although strictly speaking this requires a choice of perturbation evolution for the dark energy as well, and in addition one that is not degenerate with the evolution of dark matter perturbations; see [534].

Another useful possibility is to adopt the principal component approach [468], which avoids any assumption about the form of w and assumes it to be constant or linear in redshift bins, then derives which combination of parameters is best constrained by each experiment.

For a cross-check of the results using more complicated parameterizations, one can use simple polynomial parameterizations of w and $\rho_{\mathrm{DE}}(z)/\rho_{\mathrm{DE}}(0)$ [939].

1.3 Perturbations

This section is devoted to a discussion of linear perturbation theory in dark-energy models. Since we will discuss a number of non-standard models in later sections, we present here the main

equations in a general form that can be adapted to various contexts. This section will identify which perturbation functions the Euclid survey [551] will try to measure and how they can help us to characterize the nature of dark energy and the properties of gravity.

1.3.1 Cosmological perturbation theory

Here we provide the perturbation equations in a dark-energy dominated universe for a general fluid, focusing on scalar perturbations.

For simplicity, we consider a flat universe containing only (cold dark) matter and dark energy, so that the Hubble parameter is given by

$$H^2 = \left(\frac{1}{a}\frac{\mathrm{d}a}{\mathrm{d}t}\right)^2 = H_0^2\left[\Omega_{m_0}a^{-3} + (1-\Omega_{m_0})\exp\left(-3\int_1^a \frac{1+w(a')}{a'}\,\mathrm{d}a\right)\right]. \tag{1.3.1}$$

We will consider linear perturbations on a spatially-flat background model, defined by the line of element

$$\mathrm{d}s^2 = a^2\left[-(1+2A)\,\mathrm{d}\eta^2 + 2B_i\,\mathrm{d}\eta\,\mathrm{d}x^i + ((1+2H_L)\,\delta_{ij} + 2H_{Tij})\,\mathrm{d}x_i\,\mathrm{d}x^j\right], \tag{1.3.2}$$

where A is the scalar potential; B_i a vector shift; H_L is the scalar perturbation to the spatial curvature; H_T^{ij} is the trace-free distortion to the spatial metric; $\mathrm{d}\eta = \mathrm{d}t/a$ is the conformal time.

We will assume that the universe is filled with perfect fluids only, so that the energy momentum tensor takes the simple form

$$T^{\mu\nu} = (\rho + p)\,u^\mu u^\nu + p\,g^{\mu\nu} + \Pi^{\mu\nu}, \tag{1.3.3}$$

where ρ and p are the density and the pressure of the fluid respectively, u^μ is the four-velocity and $\Pi^{\mu\nu}$ is the anisotropic-stress perturbation tensor that represents the traceless component of the T^i_j.

The components of the perturbed energy momentum tensor can be written as:

$$T^0_0 = -(\bar\rho + \delta\rho) \tag{1.3.4}$$
$$T^0_j = (\bar\rho + \bar p)\,(v_j - B_j) \tag{1.3.5}$$
$$T^i_0 = (\bar\rho + \bar p)\,v^i \tag{1.3.6}$$
$$T^i_j = (\bar p + \delta p)\,\delta^i_j + \bar p\,\Pi^i_j. \tag{1.3.7}$$

Here $\bar\rho$ and $\bar p$ are the energy density and pressure of the homogeneous and isotropic background universe, $\delta\rho$ is the density perturbation, δp is the pressure perturbation, v^i is the velocity vector. Here we want to investigate only the scalar modes of the perturbation equations. So far the treatment of the matter and metric is fully general and applies to any form of matter and metric. We now choose the Newtonian gauge (also known as the longitudinal gauge), characterized by zero non-diagonal metric terms (the shift vector $B_i = 0$ and $H_T^{ij} = 0$) and by two scalar potentials Ψ and Φ; the metric Eq. (1.3.2) then becomes

$$\mathrm{d}s^2 = a^2\left[-(1+2\Psi)\,\mathrm{d}\eta^2 + (1-2\Phi)\,\mathrm{d}x_i\,\mathrm{d}x^i\right]. \tag{1.3.8}$$

The advantage of using the Newtonian gauge is that the metric tensor $g_{\mu\nu}$ is diagonal and this simplifies the calculations. This choice not only simplifies the calculations but is also the most intuitive one as the observers are attached to the points in the unperturbed frame; as a consequence, they will detect a velocity field of particles falling into the clumps of matter and will measure their gravitational potential, represented directly by Ψ; Φ corresponds to the perturbation to the spatial

curvature. Moreover, as we will see later, the Newtonian gauge is the best choice for observational tests (i.e., for perturbations smaller than the horizon).

In the conformal Newtonian gauge, and in Fourier space, the first-order perturbed Einstein equations give [see 599, for more details]:

$$k^2\Phi + 3\frac{\dot{a}}{a}\left(\dot{\Phi} + \frac{\dot{a}}{a}\Psi\right) = -4\pi G a^2 \sum_\alpha \bar{\rho}_\alpha \delta_\alpha \,, \tag{1.3.9}$$

$$k^2\left(\dot{\Phi} + \frac{\dot{a}}{a}\Psi\right) = 4\pi G a^2 \sum_\alpha (\bar{\rho}_\alpha + \bar{p}_\alpha)\theta_\alpha \,, \tag{1.3.10}$$

$$\ddot{\Phi} + \frac{\dot{a}}{a}(\dot{\Psi} + 2\dot{\Phi}) + \left(2\frac{\ddot{a}}{a} - \frac{\dot{a}^2}{a^2}\right)\Psi + \frac{k^2}{3}(\Phi - \Psi) = 4\pi G a^2 \sum_\alpha \delta p_\alpha \,, \tag{1.3.11}$$

$$k^2(\Phi - \Psi) = 12\pi G a^2 \sum_\alpha (\bar{\rho}_\alpha + \bar{p}_\alpha)\,\pi_\alpha \,, \tag{1.3.12}$$

where a dot denotes $d/d\eta$, $\delta_\alpha = \delta\rho_\alpha/\bar{\rho}_\alpha$, the index α indicates a sum over all matter components in the universe and π is related to Π^i_j through:

$$(\bar{\rho} + \bar{p})\,\pi = -\left(\hat{k}_i\hat{k}_j - \frac{1}{3}\delta_{ij}\right)\Pi^i_j. \tag{1.3.13}$$

The energy-momentum tensor components in the Newtonian gauge become:

$$T^0_0 = -(\bar{\rho} + \delta\rho) \tag{1.3.14}$$

$$ik_i T^i_0 = -ik_i T^0_i = (\bar{\rho} + \bar{p})\,\theta \tag{1.3.15}$$

$$T^i_j = (\bar{p} + \delta p)\,\delta^i_j + \bar{p}\Pi^i_j \tag{1.3.16}$$

where we have defined the variable $\theta = ik_j v^j$ that represents the divergence of the velocity field.

Perturbation equations for a single fluid are obtained taking the covariant derivative of the perturbed energy momentum tensor, i.e., $T^\mu_{\nu;\mu} = 0$. We have

$$\dot{\delta} = -(1+w)\left(\theta - 3\dot{\Phi}\right) - 3\frac{\dot{a}}{a}\left(\frac{\delta p}{\bar{\rho}} - w\delta\right) \qquad \text{for} \quad \nu = 0 \tag{1.3.17}$$

$$\dot{\theta} = -\frac{\dot{a}}{a}(1 - 3w)\,\theta - \frac{\dot{w}}{1+w}\theta + k^2\frac{\delta p/\bar{\rho}}{1+w} + k^2\Psi - k^2\pi \qquad \text{for} \quad \nu = i. \tag{1.3.18}$$

The equations above are valid for any fluid. The evolution of the perturbations depends on the characteristics of the fluids considered, i.e., we need to specify the equation of state parameter w, the pressure perturbation δp and the anisotropic stress π. For instance, if we want to study how matter perturbations evolve, we simply substitute $w = \delta p = \pi = 0$ (matter is pressureless) in the above equations. However, Eqs. (1.3.17) – (1.3.18) depend on the gravitational potentials Ψ and Φ, which in turn depend on the evolution of the perturbations of the other fluids. For instance, if we assume that the universe is filled by dark matter and dark energy then we need to specify δp and π for the dark energy.

The problem here is not only to parameterize the pressure perturbation and the anisotropic stress for the dark energy (there is not a unique way to do it, see below, especially Section 1.4.5 for what to do when w crosses -1) but rather that we need to run the perturbation equations for each model we assume, making predictions and compare the results with observations. Clearly, this approach takes too much time. In the following Section 1.3.2 we show a general approach to understanding the observed late-time accelerated expansion of the universe through the evolution of the matter density contrast.

In the following, whenever there is no risk of confusion, we remove the overbars from the background quantities.

1.3.2 Modified growth parameters

Even if the expansion history, $H(z)$, of the FLRW background has been measured (at least up to redshifts ~ 1 by supernova data), it is not yet possible yet to identify the physics causing the recent acceleration of the expansion of the universe. Information on the growth of structure at different scales and different redshifts is needed to discriminate between models of dark energy (DE) and modified gravity (MG). A definition of what we mean by DE and MG will be postponed to Section 1.4.

An alternative to testing predictions of specific theories is to parameterize the possible departures from a fiducial model. Two conceptually-different approaches are widely discussed in the literature:

- *Model parameters* capture the degrees of freedom of DE/MG and modify the evolution equations of the energy-momentum content of the fiducial model. They can be associated with physical meanings and have uniquely-predicted behavior in specific theories of DE and MG.
- *Trigger relations* are derived directly from observations and only hold in the fiducial model. They are constructed to break down if the fiducial model does not describe the growth of structure correctly.

As the current observations favor concordance cosmology, the fiducial model is typically taken to be spatially flat FLRW in GR with cold dark matter and a cosmological constant, hereafter referred to as ΛCDM.

For a large-scale structure and weak lensing survey the crucial quantities are the matter-density contrast and the gravitational potentials and we therefore focus on scalar perturbations in the Newtonian gauge with the metric (1.3.8).

We describe the matter perturbations using the gauge-invariant comoving density contrast $\Delta_M \equiv \delta_M + 3aH\theta_M/k^2$ where δ_M and θ_M are the matter density contrast and the divergence of the fluid velocity for matter, respectively. The discussion can be generalized to include multiple fluids.

In ΛCDM, after radiation-matter equality there is no anisotropic stress present and the Einstein constraint equations at "sub-Hubble scales" $k \gg aH$ become

$$-k^2\Phi = 4\pi G a^2 \rho_M \Delta_M\,, \qquad \Phi = \Psi\,. \tag{1.3.19}$$

These can be used to reduce the energy-momentum conservation of matter simply to the second-order growth equation

$$\Delta_M'' + [2 + (\ln H)']\,\Delta_M' = \frac{3}{2}\Omega_M(a)\Delta_M\,. \tag{1.3.20}$$

Primes denote derivatives with respect to $\ln a$ and we define the time-dependent fractional matter density as $\Omega_M(a) \equiv 8\pi G\rho_M(a)/(3H^2)$. Notice that the evolution of Δ_M is driven by $\Omega_M(a)$ and is scale-independent throughout (valid on sub- and super-Hubble scales after radiation-matter equality). We define the growth factor $G(a)$ as $\Delta = \Delta_0 G(a)$. This is very well approximated by the expression

$$G(a) \approx \exp\left\{\int_1^a \frac{\mathrm{d}a'}{a'}\,[\Omega_M(a')^\gamma]\right\} \tag{1.3.21}$$

and

$$f_g \equiv \frac{\mathrm{d}\log G}{\mathrm{d}\log a} \approx \Omega_M(a)^\gamma \tag{1.3.22}$$

defines the growth rate and the growth index γ that is found to be $\gamma_\Lambda \simeq 0.545$ for the ΛCDM solution [see 937, 585, 466, 363].

Clearly, if the actual theory of structure growth is not the ΛCDM scenario, the constraints (1.3.19) will be modified, the growth equation (1.3.20) will be different, and finally the growth factor (1.3.21) is changed, i.e., the growth index is different from γ_Λ and may become time and scale dependent. Therefore, the inconsistency of these three points of view can be used to test the ΛCDM paradigm.

1.3.2.1 Two new degrees of freedom

Any generic modification of the dynamics of scalar perturbations with respect to the simple scenario of a smooth dark-energy component that only alters the background evolution of ΛCDM can be represented by introducing two new degrees of freedom in the Einstein constraint equations. We do this by replacing (1.3.19) with

$$-k^2\Phi = 4\pi G Q(a,k) a^2 \rho_M \Delta_M\,, \qquad \Phi = \eta(a,k)\Psi\,. \tag{1.3.23}$$

Non-trivial behavior of the two functions Q and η can be due to a clustering dark-energy component or some modification to GR. In MG models the function $Q(a,k)$ represents a mass screening effect due to local modifications of gravity and effectively modifies Newton's constant. In dynamical DE models Q represents the additional clustering due to the perturbations in the DE. On the other hand, the function $\eta(a,k)$ parameterizes the effective anisotropic stress introduced by MG or DE, which is absent in ΛCDM.

Given an MG or DE theory, the scale- and time-dependence of the functions Q and η can be derived and predictions projected into the (Q,η) plane. This is also true for interacting dark sector models, although in this case the identification of the total matter density contrast (DM plus baryonic matter) and the galaxy bias become somewhat contrived [see, e.g., 848, for an overview of predictions for different MG/DE models].

Using the above-defined modified constraint equations (1.3.23), the conservation equations of matter perturbations can be expressed in the following form (see [737])

$$\begin{aligned}
\Delta'_M &= -\frac{1/\eta - 1 + (\ln Q)'}{x_Q^2 + \frac{9}{2}\Omega_M}\,\frac{9}{2}\Omega_M\Delta_M - \frac{x_Q^2 - 3(\ln H)'/Q}{x_Q^2 + \frac{9}{2}\Omega_M}\,\frac{\theta_M}{aH} \\
\theta'_M &= -\theta_M - \frac{3}{2}aH\Omega_M\frac{Q}{\eta}\Delta_M,
\end{aligned} \tag{1.3.24}$$

where we define $x_Q \equiv k/(aH\sqrt{Q})$. Remember $\Omega_M = \Omega_M(a)$ as defined above. Notice that it is Q/η that modifies the source term of the θ_M equation and therefore also the growth of Δ_M. Together with the modified Einstein constraints (1.3.23) these evolution equations form a closed system for $(\Delta_M, \theta_M, \Phi, \Psi)$ which can be solved for given (Q,η).

The influence of the Hubble scale is modified by Q, such that now the size of x_Q determines the behavior of Δ_M; on "sub-Hubble" scales, $x_Q \gg 1$, we find

$$\Delta''_M + [2 + (\ln H)']\,\Delta'_M = \frac{3}{2}\Omega_M(a)\frac{Q}{\eta}\Delta_M \tag{1.3.25}$$

and $\theta_M = -aH\Delta'_M$. The growth equation is only modified by the factor Q/η on the RHS with respect to ΛCDM (1.3.20). On "super-Hubble" scales, $x_Q \ll 1$, we have

$$\begin{aligned}
\Delta'_M &= -\left[1/\eta - 1 + (\ln Q)'\right]\Delta_M + \frac{2}{3\Omega_M}\frac{(\ln H)'}{aH}\frac{1}{Q}\theta_M, \\
\theta'_M &= -\theta_M - \frac{3}{2}\Omega_M\, aH\frac{Q}{\eta}\Delta_M\,.
\end{aligned} \tag{1.3.26}$$

Q and η now create an additional drag term in the Δ_M equation, except if $\eta > 1$ when the drag term could flip sign. [737] also showed that the metric potentials evolve independently and scale-invariantly on super-Hubble scales as long as $x_Q \to 0$ for $k \to 0$. This is needed for the comoving curvature perturbation, ζ, to be constant on super-Hubble scales.

Many different names and combinations of the above defined functions (Q, η) have been used in the literature, some of which are more closely related to actual observables and are less correlated than others in certain situations [see, e.g., 41, 667, 848, 737, 278, 277, 363].

For instance, as observed above, the combination Q/η modifies the source term in the growth equation. Moreover, peculiar velocities are following gradients of the Newtonian potential, Ψ, and therefore the comparison of peculiar velocities with the density field is also sensitive to Q/η. So we define

$$\mu \equiv Q\,/\,\eta \qquad \Rightarrow \qquad -k^2\Psi = 4\pi G a^2 \mu(a,k)\rho_M \Delta_M\,. \tag{1.3.27}$$

Weak lensing and the integrated Sachs–Wolfe (ISW) effect, on the other hand, are measuring $(\Phi + \Psi)/2$, which is related to the density field via

$$\Sigma \equiv \frac{1}{2}Q(1+1/\eta) = \frac{1}{2}\mu(\eta+1) \qquad \Rightarrow \qquad -k^2(\Phi+\Psi) = 8\pi G a^2 \Sigma(a,k)\rho_M\Delta_M\,. \tag{1.3.28}$$

A summary of different other variables used was given by [278]. For instance, the gravitational slip parameter introduced by [194] and widely used is related through $\varpi \equiv 1/\eta - 1$. Recently [277] used $\{\mathcal{G} \equiv \Sigma,\ \mu \equiv Q,\ \mathcal{V} \equiv \mu\}$, while [115] defined $R \equiv 1/\eta$. All these variables reflect the same two degrees of freedom additional to the linear growth of structure in ΛCDM.

Any combination of two variables out of $\{Q, \eta, \mu, \Sigma, \ldots\}$ is a valid alternative to (Q, η). It turns out that the pair (μ, Σ) is particularly well suited when CMB, WL and LSS data are combined as it is less correlated than others [see 980, 277, 68].

1.3.2.2 Parameterizations and non-parametric approaches

So far we have defined two free functions that can encode any departure of the growth of linear perturbations from ΛCDM. However, these free functions are not measurable, but have to be inferred via their impact on the observables. Therefore, one needs to specify a parameterization of, e.g., (Q, η) such that departures from ΛCDM can be quantified. Alternatively, one can use non-parametric approaches to infer the time and scale-dependence of the modified growth functions from the observations.

Ideally, such a parameterization should be able to capture all relevant physics with the least number of parameters. Useful parameterizations can be motivated by predictions for specific theories of MG/DE [see 848] and/or by pure simplicity and measurability [see 41]. For instance, [980] and [278] use scale-independent parameterizations that model one or two smooth transitions of the modified growth parameters as a function of redshift. [115] also adds a scale dependence to the parameterization, while keeping the time-dependence a simple power law:

$$\begin{aligned} Q(a,k) &\equiv 1 + \left[Q_0 e^{-k/k_c} + Q_\infty(1-e^{-k/k_c}) - 1\right] a^s\,, \\ \eta(a,k)^{-1} &\equiv 1 + \left[R_0 e^{-k/k_c} + R_\infty(1-e^{-k/k_c}) - 1\right] a^s\,, \end{aligned} \tag{1.3.29}$$

with constant Q_0, Q_∞, R_0, R_∞, s and k_c. Generally, the problem with any kind of parameterization is that it is difficult – if not impossible – for it to be flexible enough to describe all possible modifications.

Daniel et al. [278, 277] investigate the modified growth parameters binned in z and k. The functions are taken constant in each bin. This approach is simple and only mildly dependent on the size and number of the bins. However, the bins can be correlated and therefore the data might

not be used in the most efficient way with fixed bins. Slightly more sophisticated than simple binning is a principal component analysis (PCA) of the binned (or pixelized) modified growth functions. In PCA uncorrelated linear combinations of the original pixels are constructed. In the limit of a large number of pixels the model dependence disappears. At the moment however, computational cost limits the number of pixels to only a few. Zhao et al. [982, 980] employ a PCA in the (μ, η) plane and find that the observables are more strongly sensitive to the scale-variation of the modified growth parameters rather than the time-dependence and their average values. This suggests that simple, monotonically or mildly-varying parameterizations as well as only time-dependent parameterizations are poorly suited to detect departures from ΛCDM.

1.3.2.3 Trigger relations

A useful and widely popular trigger relation is the value of the growth index γ in ΛCDM. It turns out that the value of γ can also be fitted also for simple DE models and sub-Hubble evolution in some MG models [see, e.g., 585, 466, 587, 586, 692, 363]. For example, for a non-clustering perfect fluid DE model with equation of state $w(z)$ the growth factor $G(a)$ given in (1.3.21) with the fitting formula

$$\gamma = 0.55 + 0.05\,[1 + w(z=1)] \tag{1.3.30}$$

is accurate to the 10^{-3} level compared with the actual solution of the growth equation (1.3.20). Generally, for a given solution of the growth equation the growth index can simply be computed using

$$\gamma(a,k) = \frac{\ln(\Delta_M') - \ln\Delta_M}{\ln\Omega_M(a)}\,. \tag{1.3.31}$$

The other way round, the modified gravity function μ can be computed for a given γ [737]

$$\mu = \frac{2}{3}\Omega_M^{\gamma-1}(a)\,[\Omega_M^{\gamma}(a) + 2 + (\ln H)' - 3\gamma + \gamma'\ln\gamma]\,. \tag{1.3.32}$$

The fact that the value of γ is quite stable in most DE models but strongly differs in MG scenarios means that a large deviation from γ_Λ signifies the breakdown of GR, a substantial DE clustering or a breakdown of another fundamental hypothesis like near-homogeneity. Furthermore, using the growth factor to describe the evolution of linear structure is a very simple and computationally cheap way to carry out forecasts and compare theory with data. However, several drawbacks of this approach can be identified:

- As only one additional parameter is introduced, a second parameter, such as η, is needed to close the system and be general enough to capture all possible modifications.
- The growth factor is a solution of the growth equation on sub-Hubble scales and, therefore, is not general enough to be consistent on all scales.
- The framework is designed to describe the evolution of the matter density contrast and is not easily extended to describe all other energy-momentum components and integrated into a CMB-Boltzmann code.

1.4 Models of dark energy and modified gravity

In this section we review a number of popular models of dynamical DE and MG. This section is more technical than the rest and it is meant to provide a quick but self-contained review of the current research in the theoretical foundations of DE models. The selection of models is of course somewhat arbitrary but we tried to cover the most well-studied cases and those that introduce new and interesting observable phenomena.

1.4.1 Quintessence

In this review we refer to scalar field models with canonical kinetic energy in Einstein's gravity as "quintessence models". Scalar fields are obvious candidates for dark energy, as they are for the inflaton, for many reasons: they are the simplest fields since they lack internal degrees of freedom, do not introduce preferred directions, are typically weakly clustered (as discussed later on), and can easily drive an accelerated expansion. If the kinetic energy has a canonical form, the only degree of freedom is then provided by the field potential (and of course by the initial conditions). The typical requirement is that the potentials are flat enough to lead to the slow-roll inflation today with an energy scale $\rho_{\rm DE} \simeq 10^{-123} m_{\rm pl}^4$ and a mass scale $m_\phi \lesssim 10^{-33}$ eV.

Quintessence models are the protoypical DE models [195] and as such are the most studied ones. Since they have been explored in many reviews of DE, we limit ourselves here to a few remarks.[2]

The quintessence model is described by the action

$$S = \int \mathrm{d}^4x\sqrt{-g}\left[\frac{1}{2\kappa^2}R + \mathcal{L}_\phi\right] + S_M\,, \qquad \mathcal{L}_\phi = -\frac{1}{2}g^{\mu\nu}\partial_\mu\phi\partial_\nu\phi - V(\phi)\,, \tag{1.4.1}$$

where $\kappa^2 = 8\pi G$ and R is the Ricci scalar and S_M is the matter action. The fluid satisfies the continuity equation

$$\dot\rho_M + 3H(\rho_M + p_M) = 0\,. \tag{1.4.2}$$

The energy-momentum tensor of quintessence is

$$T^{(\phi)}_{\mu\nu} = -\frac{2}{\sqrt{-g}}\frac{\delta(\sqrt{-g}\mathcal{L}_\phi)}{\delta g^{\mu\nu}} \tag{1.4.3}$$

$$= \partial_\mu\phi\partial_\nu\phi - g_{\mu\nu}\left[\frac{1}{2}g^{\alpha\beta}\partial_\alpha\phi\partial_\beta\phi + V(\phi)\right]\,. \tag{1.4.4}$$

As we have already seen, in a FLRW background, the energy density ρ_ϕ and the pressure p_ϕ of the field are

$$\rho_\phi = -T^{0(\phi)}_0 = \frac{1}{2}\dot\phi^2 + V(\phi)\,, \quad p_\phi = \frac{1}{3}T^{i(\phi)}_i = \frac{1}{2}\dot\phi^2 - V(\phi)\,, \tag{1.4.5}$$

which give the equation of state

$$w_\phi \equiv \frac{p_\phi}{\rho_\phi} = \frac{\dot\phi^2 - 2V(\phi)}{\dot\phi^2 + 2V(\phi)}\,. \tag{1.4.6}$$

In the flat universe, Einstein's equations give the following equations of motion:

$$H^2 = \frac{\kappa^2}{3}\left[\frac{1}{2}\dot\phi^2 + V(\phi) + \rho_M\right]\,, \tag{1.4.7}$$

$$\dot H = -\frac{\kappa^2}{2}\left(\dot\phi^2 + \rho_M + p_M\right)\,, \tag{1.4.8}$$

where $\kappa^2 = 8\pi G$. The variation of the action (1.4.1) with respect to ϕ gives

$$\ddot\phi + 3H\dot\phi + V_{,\phi} = 0\,, \tag{1.4.9}$$

[2] This subsection is based on [49].

where $V_{,\phi} \equiv \mathrm{d}V/\mathrm{d}\phi$.

During radiation or matter dominated epochs, the energy density ρ_M of the fluid dominates over that of quintessence, i.e., $\rho_M \gg \rho_\phi$. If the potential is steep so that the condition $\dot{\phi}^2/2 \gg V(\phi)$ is always satisfied, the field equation of state is given by $w_\phi \simeq 1$ from Eq. (1.4.6). In this case the energy density of the field evolves as $\rho_\phi \propto a^{-6}$, which decreases much faster than the background fluid density.

The condition $w_\phi < -1/3$ is required to realize the late-time cosmic acceleration, which translates into the condition $\dot{\phi}^2 < V(\phi)$. Hence the scalar potential needs to be shallow enough for the field to evolve slowly along the potential. This situation is similar to that in inflationary cosmology and it is convenient to introduce the following slow-roll parameters [104]

$$\epsilon_s \equiv \frac{1}{2\kappa^2}\left(\frac{V_{,\phi}}{V}\right)^2, \qquad \eta_s \equiv \frac{V_{,\phi\phi}}{\kappa^2 V}. \tag{1.4.10}$$

If the conditions $\epsilon_s \ll 1$ and $|\eta_s| \ll 1$ are satisfied, the evolution of the field is sufficiently slow so that $\dot{\phi}^2 \ll V(\phi)$ and $|\ddot{\phi}| \ll |3H\dot{\phi}|$ in Eqs. (1.4.7) and (1.4.9).

From Eq. (1.4.9) the deviation of w_ϕ from -1 is given by

$$1 + w_\phi = \frac{V_{,\phi}^2}{9H^2(\xi_s+1)^2\rho_\phi}, \tag{1.4.11}$$

where $\xi_s \equiv \ddot{\phi}/(3H\dot{\phi})$. This shows that w_ϕ is always larger than -1 for a positive potential and energy density. In the slow-roll limit, $|\xi_s| \ll 1$ and $\dot{\phi}^2/2 \ll V(\phi)$, we obtain $1 + w_\phi \simeq 2\epsilon_s/3$ by neglecting the matter fluid in Eq. (1.4.7), i.e., $3H^2 \simeq \kappa^2 V(\phi)$. The deviation of w_ϕ from -1 is characterized by the slow-roll parameter ϵ_s. It is also possible to consider Eq. (1.4.11) as a prescription for the evolution of the potential given $w_\phi(z)$ and to reconstruct a potential that gives a desired evolution of the equation of state (subject to $w \in [-1, 1]$). This was used, for example, in [102].

However, in order to study the evolution of the perturbations of a quintessence field it is not even necessary to compute the field evolution explicitly. Rewriting the perturbation equations of the field in terms of the perturbations of the density contrast δ_ϕ and the velocity θ_ϕ in the conformal Newtonian gauge, one finds [see, e.g., 536, Appendix A] that they correspond precisely to those of a fluid, (1.3.17) and (1.3.18), with $\pi = 0$ and $\delta p = c_s^2\delta\rho + 3aH(c_s^2 - c_a^2)(1+w)\rho\theta/k^2$ with $c_s^2 = 1$. The adiabatic sound speed, c_a, is defined in Eq. (1.4.31). The large value of the sound speed c_s^2, equal to the speed of light, means that quintessence models do not cluster significantly inside the horizon [see 785, 786, and Section 1.8.6 for a detailed analytical discussion of quintessence clustering and its detectability with future probes, for arbitrary c_s^2].

Many quintessence potentials have been proposed in the literature. A simple crude classification divides them into two classes, (i) "freezing" models and (ii) "thawing" models [196]. In class (i) the field was rolling along the potential in the past, but the movement gradually slows down after the system enters the phase of cosmic acceleration. The representative potentials that belong to this class are

(i) Freezing models

- $V(\phi) = M^{4+n}\phi^{-n} \quad (n > 0)$,
- $V(\phi) = M^{4+n}\phi^{-n}\exp(\alpha\phi^2/m_{\rm pl}^2)$.

The former potential does not possess a minimum and hence the field rolls down the potential toward infinity. This appears, for example, in the fermion condensate model as a dynamical supersymmetry breaking [138]. The latter potential has a minimum at which the field is eventually

trapped (corresponding to $w_\phi = -1$). This potential can be constructed in the framework of supergravity [170].

In thawing models (ii) the field (with mass m_ϕ) has been frozen by Hubble friction (i.e., the term $H\dot{\phi}$ in Eq. (1.4.9)) until recently and then it begins to evolve once H drops below m_ϕ. The equation of state of DE is $w_\phi \simeq -1$ at early times, which is followed by the growth of w_ϕ. The representative potentials that belong to this class are

(ii) Thawing models

- $V(\phi) = V_0 + M^{4-n}\phi^n \quad (n > 0)\,,$
- $V(\phi) = M^4 \cos^2(\phi/f)\,.$

The former potential is similar to that of chaotic inflation ($n = 2, 4$) used in the early universe (with $V_0 = 0$) [577], while the mass scale M is very different. The model with $n = 1$ was proposed by [487] in connection with the possibility to allow for negative values of $V(\phi)$. The universe will collapse in the future if the system enters the region with $V(\phi) < 0$. The latter potential appears as a potential for the Pseudo-Nambu–Goldstone Boson (PNGB). This was introduced by [370] in response to the first tentative suggestions that the universe may be dominated by the cosmological constant. In this model the field is nearly frozen at the potential maximum during the period in which the field mass m_ϕ is smaller than H, but it begins to roll down around the present ($m_\phi \simeq H_0$).

Potentials can also be classified in several other ways, e.g., on the basis of the existence of special solutions. For instance, tracker solutions have approximately constant w_ϕ and Ω_ϕ along special attractors. A wide range of initial conditions converge to a common, cosmic evolutionary tracker. Early DE models contain instead solutions in which DE was not negligible even during the last scattering. While in the specific Euclid forecasts section (1.8) we will not explicitly consider these models, it is worthwhile to note that the combination of observations of the CMB and of large scale structure (such as Euclid) can dramatically constrain these models drastically improving the inverse area figure of merit compared to current constraints, as discussed in [467].

1.4.2 K-essence

In a quintessence model it is the potential energy of a scalar field that leads to the late-time acceleration of the expansion of the universe; the alternative, in which the kinetic energy of the scalar field which dominates, is known as k-essence. Models of k-essence are characterized by an action for the scalar field of the following form

$$S = \int \mathrm{d}^4x\, \sqrt{-g}p(\phi, X)\,, \tag{1.4.12}$$

where $X = (1/2)g^{\mu\nu}\nabla_\mu\phi\nabla_\nu\phi$. The energy density of the scalar field is given by

$$\rho_\phi = 2X\frac{\mathrm{d}p}{\mathrm{d}X} - p\,, \tag{1.4.13}$$

and the pressure is simply $p_\phi = p(\phi, X)$. Treating the k-essence scalar as a perfect fluid, this means that k-essence has the equation of state

$$w_\phi = \frac{p_\phi}{\rho_\phi} = -\frac{p}{p - 2Xp_{,X}}\,, \tag{1.4.14}$$

where the subscript $_{,X}$ indicates a derivative with respect to X. Clearly, with a suitably chosen p the scalar can have an appropriate equation of state to allow it to act as dark energy.

The dynamics of the k-essence field are given by a continuity equation

$$\dot{\rho}_\phi = -3H(\rho_\phi + p_\phi)\,, \tag{1.4.15}$$

or equivalently by the scalar equation of motion

$$G^{\mu\nu}\nabla_\mu\nabla_\nu\phi + 2X\frac{\partial^2 p}{\partial X\partial\phi} - \frac{\partial p}{\partial\phi} = 0\,, \tag{1.4.16}$$

where

$$G^{\mu\nu} = \frac{\partial p}{\partial X}g^{\mu\nu} + \frac{\partial^2 p}{\partial X^2}\nabla^\mu\phi\nabla^\nu\phi\,. \tag{1.4.17}$$

For this second order equation of motion to be hyperbolic, and hence physically meaningful, we must impose

$$1 + 2X\frac{p_{,XX}}{p_{,X}} > 0\,. \tag{1.4.18}$$

K-essence was first proposed by [61, 62], where it was also shown that tracking solutions to this equation of motion, which are attractors in the space of solutions, exist during the radiation and matter-dominated eras for k-essence in a similar manner to quintessence.

The speed of sound for k-essence fluctuation is

$$c_s^2 = \frac{p_{,X}}{p_{,X} + 2Xp_{,XX}}\,. \tag{1.4.19}$$

So that whenever the kinetic terms for the scalar field are not linear in X, the speed of sound of fluctuations differs from unity. It might appear concerning that superluminal fluctuations are allowed in k-essence models, however it was shown in [71] that this does not lead to any causal paradoxes.

1.4.3 A definition of modified gravity

In this review we often make reference to DE and MG models. Although in an increasing number of publications a similar dichotomy is employed, there is currently no consensus on where to draw the line between the two classes. Here we will introduce an operational definition for the purpose of this document.

Roughly speaking, what most people have in mind when talking about standard dark energy are models of minimally-coupled scalar fields with standard kinetic energy in 4-dimensional Einstein gravity, the only functional degree of freedom being the scalar potential. Often, this class of model is referred to simply as "quintessence". However, when we depart from this picture a simple classification is not easy to draw. One problem is that, as we have seen in the previous sections, both at background and at the perturbation level, different models can have the same observational signatures [537]. This problem is not due to the use of perturbation theory: any modification to Einstein's equations can be interpreted as standard Einstein gravity with a modified "matter" source, containing an arbitrary mixture of scalars, vectors and tensors [457, 535].

The simplest example can be discussed by looking at Eqs. (1.3.23). One can modify gravity and obtain a modified Poisson equation, and therefore $Q \neq 1$, or one can introduce a clustering dark energy (for example a k-essence model with small sound speed) that also induces the same $Q \neq 1$ (see Eq. 1.3.23). This extends to the anisotropic stress η: there is in general a one-to-one relation at first order between a fluid with arbitrary equation of state, sound speed, and anisotropic stress and a modification of the Einstein–Hilbert Lagrangian.

Therefore, we could simply abandon any attempt to distinguish between DE and MG, and just analyse different models, comparing their properties and phenomenology. However, there

is a possible classification that helps us set targets for the observations, which is often useful in concisely communicating the results of complex arguments. In this review, we will use the following notation:

- *Standard dark energy:* These are models in which dark energy lives in standard Einstein gravity *and* does not cluster appreciably on sub-horizon scales. As already noted, the prime example of a standard dark-energy model is a minimally-coupled scalar field with standard kinetic energy, for which the sound speed equals the speed of light.
- *Clustering dark energy:* In clustering dark-energy models, there is an additional contribution to the Poisson equation due to the dark-energy perturbation, which induces $Q \neq 1$. However, in this class we require $\eta = 1$, i.e., no extra effective anisotropic stress is induced by the extra dark component. A typical example is a k-essence model with a low sound speed, $c_s^2 \ll 1$.
- *Explicit modified gravity models:* These are models where from the start the Einstein equations are modified, for example scalar-tensor and $f(R)$ type theories, Dvali–Gabadadze–Porrati (DGP) as well as interacting dark energy, in which effectively a fifth force is introduced in addition to gravity. Generically they change the clustering and/or induce a non-zero anisotropic stress. Since our definitions are based on the phenomenological parameters, we also add dark-energy models that live in Einstein's gravity but that have non-vanishing anisotropic stress into this class since they cannot be distinguished by cosmological observations.

Notice that both clustering dark energy and explicit modified gravity models lead to deviations from what is often called 'general relativity' (or, like here, standard dark energy) in the literature when constraining extra perturbation parameters like the growth index γ. For this reason we generically call both of these classes MG models. In other words, in this review we use the simple and by now extremely popular (although admittedly somewhat misleading) expression "modified gravity" to denote models in which gravity is modified and/or dark energy clusters or interacts with other fields. Whenever we feel useful, we will remind the reader of the actual meaning of the expression "modified gravity" in this review.

Therefore, on sub-horizon scales and at first order in perturbation theory our definition of MG is straightforward: models with $Q = \eta = 1$ (see Eq. 1.3.23) are standard DE, otherwise they are MG models. In this sense the definition above is rather convenient: we can use it to quantify, for instance, how well Euclid will distinguish between standard dynamical dark energy and modified gravity by forecasting the errors on Q, η or on related quantities like the growth index γ.

On the other hand, it is clear that this definition is only a practical way to group different models and should not be taken as a fundamental one. We do not try to set a precise threshold on, for instance, how much dark energy should cluster before we call it modified gravity: the boundary between the classes is therefore left undetermined but we think this will not harm the understanding of this document.

1.4.4 Coupled dark-energy models

A first class of models in which dark energy shows dynamics, in connection with the presence of a fifth force different from gravity, is the case of 'interacting dark energy': we consider the possibility that dark energy, seen as a dynamical scalar field, may interact with other components in the universe. This class of models effectively enters in the "explicit modified gravity models" in the classification above, because the gravitational attraction between dark matter particles is modified by the presence of a fifth force. However, we note that the anisotropic stress for DE is still zero in the Einstein frame, while it is, in general, non-zero in the Jordan frame. In some cases (when a universal coupling is present) such an interaction can be explicitly recast in a non-minimal coupling

to gravity, after a redefinition of the metric and matter fields (Weyl scaling). We would like to identify whether interactions (couplings) of dark energy with matter fields, neutrinos or gravity itself can affect the universe in an observable way.

In this subsection we give a general description of the following main interacting scenarios:

1. couplings between dark energy and baryons;
2. couplings between dark energy and dark matter (coupled quintessence);
3. couplings between dark energy and neutrinos (growing neutrinos, MaVaNs);
4. universal couplings with all species (scalar-tensor theories and $f(R)$).

In all these cosmologies the coupling introduces a fifth force, in addition to standard gravitational attraction. The presence of a new force, mediated by the DE scalar field (sometimes called the 'cosmon' [954], seen as the mediator of a cosmological interaction) has several implications and can significantly modify the process of structure formation. We will discuss cases (2) and (3) in Section 2.

In these scenarios the presence of the additional interaction couples the evolution of components that in the standard Λ-FLRW would evolve independently. The stress-energy tensor $T^{\mu}{}_{\nu}$ of each species is, in general, not conserved – only the total stress-energy tensor is. Usually, at the level of the Lagrangian, the coupling is introduced by allowing the mass m of matter fields to depend on a scalar field ϕ via a function $m(\phi)$ whose choice specifies the interaction. This wide class of cosmological models can be described by the following action:

$$\mathcal{S} = \int \mathrm{d}^4x\sqrt{-g}\left[-\frac{1}{2}\partial^{\mu}\phi\partial_{\mu}\phi - U(\phi) - m(\phi)\bar{\psi}\psi + \mathcal{L}_{\rm kin}[\psi]\right], \tag{1.4.20}$$

where $U(\phi)$ is the potential in which the scalar field ϕ rolls, ψ describes matter fields, and g is defined in the usual way as the determinant of the metric tensor, whose background expression is $g_{\mu\nu} = \mathrm{diag}[-a^2, a^2, a^2, a^2]$.

For a general treatment of background and perturbation equations we refer to [514, 33, 35, 724]. Here the coupling of the dark-energy scalar field to a generic matter component (denoted by index α) is treated as an external source $Q_{(\alpha)\mu}$ in the Bianchi identities:

$$\nabla_{\nu}T^{\nu}_{(\alpha)\mu} = Q_{(\alpha)\mu}\,, \tag{1.4.21}$$

with the constraint

$$\sum_{\alpha} Q_{(\alpha)\mu} = 0\,. \tag{1.4.22}$$

The zero component of (1.4.21) gives the background conservation equations:

$$\frac{\mathrm{d}\rho_{\phi}}{\mathrm{d}\eta} = -3\mathcal{H}(1+w_{\phi})\rho_{\phi} + \beta(\phi)\frac{\mathrm{d}\phi}{\mathrm{d}\eta}(1-3w_{\alpha})\rho_{\alpha}\,, \tag{1.4.23}$$

$$\frac{\mathrm{d}\rho_{\alpha}}{\mathrm{d}\eta} = -3\mathcal{H}(1+w_{\alpha})\rho_{\alpha} - \beta(\phi)\frac{\mathrm{d}\phi}{\mathrm{d}\eta}(1-3w_{\alpha})\rho_{\alpha}\,, \tag{1.4.24}$$

for a scalar field ϕ coupled to one single fluid α with a function $\beta(\phi)$, which in general may not be constant. The choice of the mass function $m(\phi)$ corresponds to a choice of $\beta(\phi)$ and equivalently to a choice of the source $Q_{(\alpha)\mu}$ and specifies the strength of the coupling according to the following relations:

$$Q_{(\phi)\mu} = \frac{\partial \ln m(\phi)}{\partial\phi}T_{\alpha}\,\partial_{\mu}\phi\,,\; m_{\alpha} = \bar{m}_{\alpha}\; e^{-\beta(\phi)\phi}\,, \tag{1.4.25}$$

where $\bar{m}_\alpha$ is the constant Jordan-frame bare mass. The evolution of dark energy is related to the trace T_α and, as a consequence, to density and pressure of the species α. We note that a description of the coupling via an action such as (1.4.20) is originally motivated by the wish to modify GR with an extension such as scalar-tensor theories. In general, one of more couplings can be active [176].

As for perturbation equations, it is possible to include the coupling in a modified Euler equation:

$$\frac{\mathrm{d}\mathbf{v}_\alpha}{\mathrm{d}\eta} + \left(\mathcal{H} - \beta(\phi)\frac{\mathrm{d}\phi}{\mathrm{d}\eta}\right)\mathbf{v}_\alpha - \nabla\left[\Phi_\alpha + \beta\phi\right] = 0\,. \tag{1.4.26}$$

The Euler equation in cosmic time ($\mathrm{d}t = a\,\mathrm{d}\tau$) can also be rewritten in the form of an acceleration equation for particles at position $\mathbf{r}$:

$$\dot{\mathbf{v}}_\alpha = -\tilde{H}\mathbf{v}_\alpha - \nabla\frac{\tilde{G}_\alpha m_\alpha}{r}\,. \tag{1.4.27}$$

The latter expression explicitly contains all the main ingredients that affect dark-energy interactions:

1. a fifth force $\nabla\left[\Phi_\alpha + \beta\phi\right]$ with an effective $\tilde{G}_\alpha = G_N[1 + 2\beta^2(\phi)]$;
2. a velocity dependent term $\tilde{H}\mathbf{v}_\alpha \equiv H\left(1 - \beta(\phi)\frac{\dot{\phi}}{H}\right)\mathbf{v}_\alpha$
3. a time-dependent mass for each particle α, evolving according to (1.4.25).

The relative significance of these key ingredients can lead to a variety of potentially observable effects, especially on structure formation. We will recall some of them in the following subsections as well as, in more detail, for two specific couplings in the dark matter section (2.11, 2.9) of this report.

1.4.4.1 Dark energy and baryons

A coupling between dark energy and baryons is active when the baryon mass is a function of the dark-energy scalar field: $m_b = m_b(\phi)$. Such a coupling is constrained to be very small: main bounds come from tests of the equivalence principle and solar system constraints [130]. More in general, depending on the coupling, bounds on the variation of fundamental constants over cosmological time-scales may have to be considered ([631, 303, 304, 639] and references therein). It is presumably very difficult to have significant cosmological effects due to a coupling to baryons only. However, uncoupled baryons can still play a role in the presence of a coupling to dark matter (see Section 1.6 on nonlinear aspects).

1.4.4.2 Dark energy and dark matter

An interaction between dark energy and dark matter (CDM) is active when CDM mass is a function of the dark-energy scalar field: $m_c = m_c(\phi)$. In this case the coupling is not affected by tests on the equivalence principle and solar-system constraints and can therefore be stronger than the one with baryons. One may argue that dark-matter particles are themselves coupled to baryons, which leads, through quantum corrections, to direct coupling between dark energy and baryons. The strength of such couplings can still be small and was discussed in [304] for the case of neutrino–dark-energy couplings. Also, quantum corrections are often recalled to spoil the flatness of a quintessence potential. However, it may be misleading to calculate quantum corrections up to a cutoff scale, as contributions above the cutoff can possibly compensate terms below the cutoff, as discussed in [958].

Typical values of β presently allowed by observations (within current CMB data) are within the range $0 < \beta < 0.06$ (at 95% CL for a constant coupling and an exponential potential) [114, 47, 35, 44], or possibly more [539, 531] if neutrinos are taken into account or for more realistic time-dependent choices of the coupling. This framework is generally referred to as 'coupled quintessence' (CQ). Various choices of couplings have been investigated in literature, including constant and varying $\beta(\phi)$ [33, 619, 35, 518, 414, 747, 748, 724, 377].

The presence of a coupling (and therefore, of a fifth force acting among dark-matter particles) modifies the background expansion and linear perturbations [34, 33, 35], therefore affecting CMB and cross-correlation of CMB and LSS [44, 35, 47, 45, 114, 539, 531, 970, 612, 42].

Furthermore, structure formation itself is modified [604, 618, 518, 611, 870, 3, 666, 129, 962, 79, 76, 77, 80, 565, 562, 75, 980, 640].

An alternative approach, also investigated in the literature [619, 916, 915, 613, 387, 388, 193, 794, 192], where the authors consider as a starting point Eq. (1.4.21): the coupling is then introduced by choosing directly a covariant stress-energy tensor on the RHS of the equation, treating dark energy as a fluid and in the absence of a starting action. The advantage of this approach is that a good parameterization allows us to investigate several models of dark energy at the same time. Problems connected to instabilities of some parameterizations or to the definition of a physically-motivated speed of sound for the density fluctuations can be found in [916]. It is also possible to both take a covariant form for the coupling and a quintessence dark-energy scalar field, starting again directly from Eq. (1.4.21). This has been done, e.g., in [145], [144]. At the background level only, [235], [237], [302] and [695] have also considered which background constraints can be obtained when starting from a fixed present ratio of dark energy and dark matter. The disadvantage of this approach is that it is not clear how to perturb a coupling that has been defined as a background quantity.

A Yukawa-like interaction was investigated [357, 279], pointing out that coupled dark energy behaves as a fluid with an effective equation of state $w \lesssim -1$, though staying well defined and without the presence of ghosts [279].

For an illustration of observable effects related to dark-energy–dark-matter interaction see also Section (2.11) of this report.

1.4.4.3 Dark energy and neutrinos

A coupling between dark energy and neutrinos can be even stronger than the one with dark matter and as compared to gravitational strength. Typical values of β are order $50-100$ or even more, such that even the small fraction of cosmic energy density in neutrinos can have a substantial influence on the time evolution of the quintessence field. In this scenario neutrino masses change in time, depending on the value of the dark-energy scalar field ϕ. Such a coupling has been investigated within MaVaNs [356, 714, 135, 12, 952, 280, 874, 856, 139, 178, 177] and more recently within growing neutrino cosmologies [36, 957, 668, 963, 962, 727, 179, 78]. In this latter case, DE properties are related to the neutrino mass and to a cosmological event, i.e., neutrinos becoming non-relativistic. This leads to the formation of stable neutrino lumps [668, 963, 78] at very large scales only ($\sim$ 100 Mpc and beyond) as well as to signatures in the CMB spectra [727]. For an illustration of observable effects related to this case see Section (2.9) of this report.

1.4.4.4 Scalar-tensor theories

Scalar-tensor theories [954, 471, 472, 276, 216, 217, 955, 912, 722, 354, 146, 764, 721, 797, 646, 725, 726, 205, 54] extend GR by introducing a non-minimal coupling between a scalar field (acting also as dark energy) and the metric tensor (gravity); they are also sometimes referred to as 'extended quintessence'. We include scalar-tensor theories among 'interacting cosmologies' because, via a Weyl transformation, they are equivalent to a GR framework (minimal coupling to gravity) in which

the dark-energy scalar field ϕ is coupled (universally) to all species [954, 608, 936, 351, 724, 219]. In other words, these theories correspond to the case where, in action (1.4.20), the mass of all species (baryons, dark matter, ...) is a function $m = m(\phi)$ with the same coupling for every species α. Indeed, a description of the coupling via an action such as (1.4.20) is originally motivated by extensions of GR such as scalar-tensor theories. Typically the strength of the scalar-mediated interaction is required to be orders of magnitude weaker than gravity ([553], [725] and references therein for recent constraints). It is possible to tune this coupling to be as small as is required – for example by choosing a suitably flat potential $V(\phi)$ for the scalar field. However, this leads back to naturalness and fine-tuning problems.

In Sections 1.4.6 and 1.4.7 we will discuss in more detail a number of ways in which new scalar degrees of freedom can naturally couple to standard model fields, while still being in agreement with observations. We mention here only that the presence of chameleon mechanisms [171, 672, 670, 172, 464, 173, 282] can, for example, modify the coupling depending on the environment. In this way, a small (screened) coupling in high-density regions, in agreement with observations, is still compatible with a bigger coupling ($\beta \sim 1$) active in low density regions. In other words, a dynamical mechanism ensures that the effects of the coupling are screened in laboratory and solar system tests of gravity.

Typical effects of scalar-tensor theories on CMB and structure formation include:

- enhanced ISW [725, 391, 980];
- violation of the equivalence principle: extended objects such as galaxies do not all fall at the same rate [45, 464].

However, it is important to remark that screening mechanisms are meant to protect the scalar field in high-density regions (and therefore allow for bigger couplings in low density environments) but they do not address problems related to self-acceleration of the DE scalar field, which still usually require some fine-tuning to match present observations on w. $f(R)$ theories, which can be mapped into a subclass of scalar-tensor theories, will be discussed in more detail in Section 1.4.6.

1.4.5 Phantom crossing

In this section we pay attention to the evolution of the perturbations of a general dark-energy fluid with an evolving equation of state parameter w. Current limits on the equation of state parameter $w = p/\rho$ of the dark energy indicate that $p \approx -\rho$, and so do not exclude $p < -\rho$, a region of parameter space often called *phantom energy*. Even though the region for which $w < -1$ may be unphysical at the quantum level, it is still important to probe it, not least to test for coupled dark energy and alternative theories of gravity or higher dimensional models that can give rise to an effective or apparent phantom energy.

Although there is no problem in considering $w < -1$ for the background evolution, there are apparent divergences appearing in the perturbations when a model tries to cross the limit $w = -1$. This is a potential headache for experiments like Euclid that directly probe the perturbations through measurements of the galaxy clustering and weak lensing. To analyze the Euclid data, we need to be able to consider models that cross the phantom divide $w = -1$ at the level of first-order perturbations (since the only dark-energy model that has no perturbations at all is the cosmological constant).

However, at the level of cosmological first-order perturbation theory, there is no fundamental limitation that prevents an effective fluid from crossing the phantom divide.

As $w \to -1$ the terms in Eqs. (1.3.17) and (1.3.18) containing $1/(1+w)$ will generally diverge. This can be avoided by replacing θ with a new variable V defined via $V = \rho\,(1+w)\,\theta$. This corresponds to rewriting the 0-i component of the energy momentum tensor as $ik_jT_0^j = V$, which

avoids problems if $T_0^j \neq 0$ when $\bar{p} = -\bar{\rho}$. Replacing the time derivatives by a derivative with respect to the logarithm of the scale factor $\ln a$ (denoted by a prime), we obtain [599, 450, 536]:

$$\delta' = 3(1+w)\Phi' - \frac{V}{Ha} - 3\left(\frac{\delta p}{\bar{\rho}} - w\delta\right) \tag{1.4.28}$$

$$V' = -(1-3w)V + \frac{k^2}{Ha}\frac{\delta p}{\bar{\rho}} + (1+w)\frac{k^2}{Ha}(\Psi - \pi)\ . \tag{1.4.29}$$

In order to solve Eqs. (1.4.28) and (1.4.29) we still need to specify the expressions for δp and π, quantities that characterize the physical, intrinsic nature of the dark-energy fluid at first order in perturbation theory. While in general the anisotropic stress plays an important role as it gives a measure of how the gravitational potentials Φ and Ψ differ, we will set it in this section to zero, $\pi = 0$. Therefore, we will focus on the form of the pressure perturbation. There are two important special cases: barotropic fluids, which have no internal degrees of freedom and for which the pressure perturbation is fixed by the evolution of the average pressure, and non-adiabatic fluids like, e.g., scalar fields for which internal degrees of freedom can change the pressure perturbation.

1.4.5.1 Parameterizing the pressure perturbation

Barotropic fluids. We define a fluid to be barotropic if the pressure p depends strictly only on the energy density ρ: $p = p(\rho)$. These fluids have only adiabatic perturbations, so that they are often called adiabatic. We can write their pressure as

$$p(\rho) = p(\bar{\rho} + \delta\rho) = p(\bar{\rho}) + \left.\frac{\mathrm{d}p}{\mathrm{d}\rho}\right|_{\bar{\rho}} \delta\rho + O\left[(\delta\rho)^2\right]. \tag{1.4.30}$$

Here $p(\bar{\rho}) = \bar{p}$ is the pressure of the isotropic and homogeneous part of the fluid. The second term in the expansion (1.4.30) can be re-written as

$$\left.\frac{\mathrm{d}p}{\mathrm{d}\rho}\right|_{\bar{\rho}} = \frac{\dot{\bar{p}}}{\dot{\bar{\rho}}} = w - \frac{\dot{w}}{3aH(1+w)} \equiv c_a^2, \tag{1.4.31}$$

where we used the equation of state and the conservation equation for the dark-energy density in the background. We notice that the adiabatic sound speed c_a^2 will necessarily diverge for any fluid where w crosses -1.

However, for a perfect barotropic fluid the adiabatic sound speed c_a^2 turns out to be the physical propagation speed of perturbations. Therefore, it should never be larger than the speed of light – otherwise our theory becomes acausal – and it should never be negative ($c_a^2 < 0$) – otherwise classical, and possible quantum, instabilities appear. Even worse, the pressure perturbation

$$\delta p = c_a^2 \delta\rho = \left(w - \frac{\dot{w}}{3aH(1+w)}\right)\delta\rho \tag{1.4.32}$$

will necessarily diverge if w crosses -1 and $\delta\rho \neq 0$. Even if we find a way to stabilize the pressure perturbation, for instance an equation of state parameter that crosses the -1 limit with zero slope ($\dot{w}$), there will always be the problem of a negative speed of sound that prevents these models from being viable dark-energy candidates.

Non-adiabatic fluids. To construct a model that can cross the phantom divide, we therefore need to violate the constraint that p is a unique function of ρ. At the level of first-order perturbation theory, this amounts to changing the prescription for δp, which now becomes an arbitrary function of k and t. One way out of this problem is to choose an appropriate gauge where the equations

are simple; one choice is, for instance, the rest frame of the fluid where the pressure perturbation reads (in this frame)

$$\hat{\delta p} = \hat{c}_s^2 \hat{\delta\rho}, \tag{1.4.33}$$

where now the $\hat{c}_s^2$ is the speed with which fluctuations in the fluid propagate, i.e., the sound speed. We can write Eq. (1.4.33), with an appropriate gauge transformation, in a form suitable for the Newtonian frame, i.e., for Eqs. (1.4.28) and (1.4.29). We find that the pressure perturbation is given by [347, 112, 214]

$$\delta p = \hat{c}_s^2 \delta\rho + 3aH\,(a)\left(\hat{c}_s^2 - c_a^2\right)\bar{\rho}\frac{V}{k^2}. \tag{1.4.34}$$

The problem here is the presence of c_a^2, which goes to infinity at the crossing and it is impossible that this term stays finite except if $V \to 0$ fast enough or $\dot{w} = 0$, but this is not, in general, the case.

This divergence appears because for $w = -1$ the energy momentum tensor Eq. (1.3.3) reads: $T^{\mu\nu} = pg^{\mu\nu}$. Normally the four-velocity u^μ is the time-like eigenvector of the energy-momentum tensor, but now all vectors are eigenvectors. So the problem of fixing a unique rest-frame is no longer well posed. Then, even though the pressure perturbation looks fine for *the observer in the rest-frame*, because it does not diverge, the badly-defined gauge transformation to the Newtonian frame does, as it also contains c_a^2.

1.4.5.2 Regularizing the divergences

We have seen that neither barotropic fluids nor canonical scalar fields, for which the pressure perturbation is of the type (1.4.34), can cross the phantom divide. However, there is a simple model [called the quintom model 360, 451] consisting of two fluids of the same type as in the previous Section 1.4.5.1 but with a constant w on either side of $w = -1$. The combination of the two fluids then effectively crosses the phantom divide if we start with $w_{\rm tot} > -1$, as the energy density in the fluid with $w < -1$ will grow faster, so that this fluid will eventually dominate and we will end up with $w_{\rm tot} < -1$.

The perturbations in this scenario were analyzed in detail in [536], where it was shown that in addition to the rest-frame contribution, one also has relative and non-adiabatic perturbations. All these contributions apparently diverge at the crossing, but their sum stays finite. When parameterizing the perturbations in the Newtonian gauge as

$$\delta p(k,t) = \gamma(k,t)\,\delta\rho(k,t) \tag{1.4.35}$$

the quantity γ will, in general, have a complicated time and scale dependence. The conclusion of the analysis is that indeed single canonical scalar fields with pressure perturbations of the type (1.4.34) in the Newtonian frame cannot cross $w = -1$, but that this is not the most general case. More general models have *a priori* no problem crossing the phantom divide, at least not with the classical stability of the perturbations.

Kunz and Sapone [536] found that a good approximation to the quintom model behavior can be found by regularizing the adiabatic sound speed in the gauge transformation with

$$c_a^2 = w - \frac{\dot{w}(1+w)}{3Ha[(1+w)^2 + \lambda]} \tag{1.4.36}$$

where λ is a tunable parameter which determines how close to $w = -1$ the regularization kicks in. A value of $\lambda \approx 1/1000$ should work reasonably well. However, the final results are not too sensitive on the detailed regularization prescription.

This result appears also related to the behavior found for coupled dark-energy models (originally introduced to solve the coincidence problem) where dark matter and dark energy interact not only

through gravity [33]. The effective dark energy in these models can also cross the phantom divide without divergences [462, 279, 534].

The idea is to insert (by hand) a term in the continuity equations of the two fluids

$$\dot{\rho}_M + 3H\rho_M = \lambda \tag{1.4.37}$$

$$\dot{\rho}_x + 3H\left(1 + w_x\right)\rho_x = -\lambda, \tag{1.4.38}$$

where the subscripts m, x refer to dark matter and dark energy, respectively. In this approximation, the adiabatic sound speed c_a^2 reads

$$c_{a,x}^2 = \frac{\dot{p}_x}{\dot{\rho}_x} = w_x - \frac{\dot{w}_x}{3aH\left(1 + w_x\right) + \lambda/\rho_x}, \tag{1.4.39}$$

which stays finite at crossing as long as $\lambda \neq 0$.

However in this class of models there are other instabilities arising at the perturbation level regardless of the coupling used, [cf. 916].

1.4.5.3 A word on perturbations when $w = -1$

Although a cosmological constant has $w = -1$ and no perturbations, the converse is not automatically true: $w = -1$ does not necessarily imply that there are no perturbations. It is only when we set from the beginning (in the calculation):

$$p = -\rho \tag{1.4.40}$$

$$\delta p = -\delta\rho \tag{1.4.41}$$

$$\pi = 0\,, \tag{1.4.42}$$

i.e., $T^{\mu\nu} \propto g^{\mu\nu}$, that we have as a solution $\delta = V = 0$.

For instance, if we set $w = -1$ and $\delta p = \gamma\delta\rho$ (where γ can be a generic function) in Eqs. (1.4.28) and (1.4.29) we have $\delta \neq 0$ and $V \neq 0$. However, the solutions are decaying modes due to the $-\frac{1}{a}\left(1 - 3w\right)V$ term so they are not important at late times; but it is interesting to notice that they are in general not zero.

As another example, if we have a non-zero anisotropic stress π then the Eqs. (1.4.28) – (1.4.29) will have a source term that will influence the growth of δ and V in the same way as Ψ does (just because they appear in the same way). The $(1 + w)$ term in front of π should not worry us as we can always define the anisotropic stress through

$$\rho\left(1 + w\right)\pi = -\left(\hat{k}_i\hat{k}_j - \frac{1}{3}\delta_{ij}\right)\Pi^i_{\ j}\,, \tag{1.4.43}$$

where $\Pi^i_{\ j} \neq 0$ when $i \neq j$ is the *real* traceless part of the energy momentum tensor, probably the quantity we need to look at: as in the case of $V = (1 + w)\theta$, there is no need for $\Pi \propto (1 + w)\pi$ to vanish when $w = -1$.

It is also interesting to notice that when $w = -1$ the perturbation equations tell us that dark-energy perturbations are not influenced through Ψ and Φ' (see Eq. (1.4.28) and (1.4.29)). Since Φ and Ψ are the quantities directly entering the metric, they must remain finite, and even much smaller than 1 for perturbation theory to hold. Since, in the absence of direct couplings, the dark energy only feels the other constituents through the terms $(1 + w)\Psi$ and $(1 + w)\Phi'$, it decouples completely in the limit $w = -1$ and just evolves on its own. But its perturbations still enter the Poisson equation and so the dark matter perturbation will feel the effects of the dark-energy perturbations.

Although this situation may seem contrived, it might be that the acceleration of the universe is just an observed effect as a consequence of a modified theory of gravity. As was shown in [537], any modified gravity theory can be described as an effective fluid both at background and at perturbation level; in such a situation it is imperative to describe its perturbations properly as this effective fluid may manifest unexpected behavior.

1.4.6 *f(R)* gravity

In parallel to models with extra degrees of freedom in the matter sector, such as interacting quintessence (and k-essence, not treated here), another promising approach to the late-time acceleration enigma is to modify the left-hand side of the Einstein equations and invoke new degrees of freedom, belonging this time to the gravitational sector itself. One of the simplest and most popular extensions of GR and a known example of modified gravity models is the $f(R)$ gravity in which the 4-dimensional action is given by some generic function $f(R)$ of the Ricci scalar R (for an introduction see, e.g., [49]):

$$S = \frac{1}{2\kappa^2}\int \mathrm{d}^4x\sqrt{-g}f(R) + S_m(g_{\mu\nu}, \Psi_m)\,, \tag{1.4.44}$$

where as usual $\kappa^2 = 8\pi G$, and S_m is a matter action with matter fields Ψ_m. Here G is a *bare* gravitational constant: we will see that the observed value will in general be different. As mentioned in the previously, it is possible to show that $f(R)$ theories can be mapped into a subset of scalar-tensor theories and, therefore, to a class of interacting scalar field dark-energy models universally coupled to all species. When seen in the Einstein frame [954, 608, 936, 351, 724, 219], action (1.4.44) can, therefore, be related to the action (1.4.20) shown previously. Here we describe $f(R)$ in the Jordan frame: the matter fields in S_m obey standard conservation equations and, therefore, the metric $g_{\mu\nu}$ corresponds to the physical frame (which here is the Jordan frame).

There are two approaches to deriving field equations from the action (1.4.44).

- **(I) The metric formalism**

  The first approach is the *metric formalism* in which the connections $\Gamma^{\alpha}_{\beta\gamma}$ are the usual connections defined in terms of the metric $g_{\mu\nu}$. The field equations can be obtained by varying the action (1.4.44) with respect to $g_{\mu\nu}$:

  $$F(R)R_{\mu\nu}(g) - \frac{1}{2}f(R)g_{\mu\nu} - \nabla_\mu\nabla_\nu F(R) + g_{\mu\nu}\Box F(R) = \kappa^2 T_{\mu\nu}\,, \tag{1.4.45}$$

  where $F(R) \equiv \partial f/\partial R$ (we also use the notation $f_{,R} \equiv \partial f/\partial R$, $f_{,RR} \equiv \partial^2 f/\partial R^2$), and $T_{\mu\nu}$ is the matter energy-momentum tensor. The trace of Eq. (1.4.45) is given by

  $$3\,\Box F(R) + F(R)R - 2f(R) = \kappa^2 T\,, \tag{1.4.46}$$

  where $T = g^{\mu\nu}T_{\mu\nu} = -\rho + 3P$. Here ρ and P are the energy density and the pressure of the matter, respectively.

- **(II) The Palatini formalism**

  The second approach is the *Palatini formalism*, where $\Gamma^{\alpha}_{\beta\gamma}$ and $g_{\mu\nu}$ are treated as independent variables. Varying the action (1.4.44) with respect to $g_{\mu\nu}$ gives

  $$F(R)R_{\mu\nu}(\Gamma) - \frac{1}{2}f(R)g_{\mu\nu} = \kappa^2 T_{\mu\nu}\,, \tag{1.4.47}$$

where $R_{\mu\nu}(\Gamma)$ is the Ricci tensor corresponding to the connections $\Gamma^{\alpha}_{\beta\gamma}$. In general this is different from the Ricci tensor $R_{\mu\nu}(g)$ corresponding to the metric connections. Taking the trace of Eq. (1.4.47), we obtain

$$F(R)R - 2f(R) = \kappa^2 T\,, \tag{1.4.48}$$

where $R(T) = g^{\mu\nu}R_{\mu\nu}(\Gamma)$ is directly related to T. Taking the variation of the action (1.4.44) with respect to the connection, and using Eq. (1.4.47), we find

$$R_{\mu\nu}(g) - \frac{1}{2}g_{\mu\nu}R(g) = \frac{\kappa^2 T_{\mu\nu}}{F} - \frac{FR(T) - f}{2F}g_{\mu\nu} + \frac{1}{F}(\nabla_\mu\nabla_\nu F - g_{\mu\nu}\Box F) - \frac{3}{2F^2}\left[\partial_\mu F\partial_\nu F - \frac{1}{2}g_{\mu\nu}(\nabla F)^2\right]. \tag{1.4.49}$$

In GR we have $f(R) = R - 2\Lambda$ and $F(R) = 1$, so that the term $\Box F(R)$ in Eq. (1.4.46) vanishes. In this case both the metric and the Palatini formalisms give the relation $R = -\kappa^2 T = \kappa^2(\rho - 3P)$, which means that the Ricci scalar R is directly determined by the matter (the trace T).

In modified gravity models where $F(R)$ is a function of R, the term $\Box F(R)$ does not vanish in Eq. (1.4.46). This means that, in the metric formalism, there is a propagating scalar degree of freedom, $\psi \equiv F(R)$. The trace equation (1.4.46) governs the dynamics of the scalar field ψ – dubbed "scalaron" [862]. In the Palatini formalism the kinetic term $\Box F(R)$ is not present in Eq. (1.4.48), which means that the scalar-field degree of freedom does not propagate freely [32, 563, 567, 566].

The de Sitter point corresponds to a vacuum solution at which the Ricci scalar is constant. Since $\Box F(R) = 0$ at this point, we get

$$F(R)R - 2f(R) = 0\,, \tag{1.4.50}$$

which holds for both the metric and the Palatini formalisms. Since the model $f(R) = \alpha R^2$ satisfies this condition, it possesses an exact de Sitter solution [862].

It is important to realize that the dynamics of $f(R)$ dark-energy models is different depending on the two formalisms. Here we confine ourselves to the metric case only.

Already in the early 1980s it was known that the model $f(R) = R + \alpha R^2$ can be responsible for inflation in the early universe [862]. This comes from the fact that the presence of the quadratic term αR^2 gives rise to an asymptotically exact de Sitter solution. Inflation ends when the term αR^2 becomes smaller than the linear term R. Since the term αR^2 is negligibly small relative to R at the present epoch, this model is not suitable to realizing the present cosmic acceleration.

Since a late-time acceleration requires modification for small R, models of the type $f(R) = R - \alpha/R^n$ ($\alpha > 0, n > 0$) were proposed as a candidate for dark energy [204, 212, 687]. While the late-time cosmic acceleration is possible in these models, it has become clear that they do not satisfy local gravity constraints because of the instability associated with negative values of $f_{,RR}$ [230, 319, 852, 697, 355]. Moreover a standard matter epoch is not present because of a large coupling between the Ricci scalar and the non-relativistic matter [43].

Then, we can ask what are the conditions for the viability of $f(R)$ dark-energy models in the metric formalism. In the following we first present such conditions and then explain step by step why they are required.

- (i) $f_{,R} > 0$ for $R \geq R_0$ (> 0), where R_0 is the Ricci scalar at the present epoch. Strictly speaking, if the final attractor is a de Sitter point with the Ricci scalar R_1 (> 0), then the condition $f_{,R} > 0$ needs to hold for $R \geq R_1$.

  This is required to avoid a negative effective gravitational constant.

- (ii) $f_{,RR} > 0$ for $R \geq R_0$.

  This is required for consistency with local gravity tests [319, 697, 355, 683], for the presence of the matter-dominated epoch [43, 39], and for the stability of cosmological perturbations [213, 849, 110, 358].

- (iii) $f(R) \to R - 2\Lambda$ for $R \gg R_0$.

  This is required for consistency with local gravity tests [48, 456, 864, 53, 904] and for the presence of the matter-dominated epoch [39].

- (iv) $0 < \frac{Rf_{,RR}}{f_{,R}}(r = -2) < 1$ at $r = -\frac{Rf_{,R}}{f} = -2$.

  This is required for the stability of the late-time de Sitter point [678, 39].

For example, the model $f(R) = R - \alpha/R^n$ ($\alpha > 0$, $n > 0$) does not satisfy the condition (ii).

Below we list some viable $f(R)$ models that satisfy the above conditions.

$$\text{(A) } f(R) = R - \mu R_c (R/R_c)^p \qquad \text{with} \quad 0 < p < 1, \quad \mu, R_c > 0\,, \tag{1.4.51}$$

$$\text{(B) } f(R) = R - \mu R_c \frac{(R/R_c)^{2n}}{(R/R_c)^{2n} + 1} \qquad \text{with} \quad n, \mu, R_c > 0\,, \tag{1.4.52}$$

$$\text{(C) } f(R) = R - \mu R_c \left[1 - \left(1 + R^2/R_c^2\right)^{-n}\right] \qquad \text{with} \quad n, \mu, R_c > 0\,, \tag{1.4.53}$$

$$\text{(D) } f(R) = R - \mu R_c \tanh\left(R/R_c\right) \qquad \text{with} \quad \mu, R_c > 0\,. \tag{1.4.54}$$

The models (A), (B), (C), and (D) have been proposed in [39], [456], [864], and [904], respectively. A model similar to (D) has been also proposed in [53], while a generalized model encompassing (B) and (C) has been studied in [660]. In model (A), the power p needs to be close to 0 to satisfy the condition (iii). In models (B) and (C) the function $f(R)$ asymptotically behaves as $f(R) \to R - \mu R_c[1 - (R^2/R_c^2)^{-n}]$ for $R \gg R_c$ and hence the condition (iii) can be satisfied even for $n = \mathcal{O}(1)$. In model (D) the function $f(R)$ rapidly approaches $f(R) \to R - \mu R_c$ in the region $R \gg R_c$. These models satisfy $f(R = 0) = 0$, so the cosmological constant vanishes in the flat spacetime.

Let us consider the cosmological dynamics of $f(R)$ gravity in the metric formalism. It is possible to carry out a general analysis without specifying the form of $f(R)$. In the flat FLRW spacetime the Ricci scalar is given by

$$R = 6(2H^2 + \dot{H})\,, \tag{1.4.55}$$

where H is the Hubble parameter. As a matter action S_m we take into account non-relativistic matter and radiation, which satisfy the usual conservation equations $\dot{\rho}_m + 3H\rho_m = 0$ and $\dot{\rho}_r + 4H\rho_r = 0$ respectively. From Eqs. (1.4.45) and (1.4.46) we obtain the following equations

$$3FH^2 = \kappa^2 (\rho_m + \rho_r) + (FR - f)/2 - 3H\dot{F}\,, \tag{1.4.56}$$

$$-2F\dot{H} = \kappa^2 [\rho_m + (4/3)\rho_r] + \ddot{F} - H\dot{F}\,. \tag{1.4.57}$$

We introduce the dimensionless variables:

$$x_1 \equiv -\frac{\dot{F}}{HF}\,, \quad x_2 \equiv -\frac{f}{6FH^2}\,, \quad x_3 \equiv \frac{R}{6H^2}\,, \quad x_4 \equiv \frac{\kappa^2 \rho_r}{3FH^2}\,, \tag{1.4.58}$$

together with the following quantities

$$\Omega_m \equiv \frac{\kappa^2 \rho_m}{3FH^2} = 1 - x_1 - x_2 - x_3 - x_4\,, \qquad \Omega_r \equiv x_4\,, \qquad \Omega_{\rm DE} \equiv x_1 + x_2 + x_3\,. \tag{1.4.59}$$

It is straightforward to derive the following differential equations [39]:

$$x_1' = -1 - x_3 - 3x_2 + x_1^2 - x_1 x_3 + x_4\,, \tag{1.4.60}$$
$$x_2' = \frac{x_1 x_3}{m} - x_2(2x_3 - 4 - x_1)\,, \tag{1.4.61}$$
$$x_3' = -\frac{x_1 x_3}{m} - 2x_3(x_3 - 2)\,, \tag{1.4.62}$$
$$x_4' = -2x_3 x_4 + x_1 x_4\,, \tag{1.4.63}$$

where the prime denotes $\mathrm{d}/\mathrm{d}\ln a$ and

$$m \equiv \frac{\mathrm{d}\ln F}{\mathrm{d}\ln R} = \frac{R f_{,RR}}{f_{,R}}\,, \tag{1.4.64}$$
$$r \equiv -\frac{\mathrm{d}\ln f}{\mathrm{d}\ln R} = -\frac{R f_{,R}}{f} = \frac{x_3}{x_2}\,. \tag{1.4.65}$$

From Eq. (1.4.65) one can express R as a function of x_3/x_2. Since m is a function of R, it follows that m is a function of r, i.e., $m = m(r)$. The ΛCDM model, $f(R) = R - 2\Lambda$, corresponds to $m = 0$. Hence the quantity m characterizes the deviation from the ΛCDM model. Note also that the model, $f(R) = \alpha R^{1+m} - 2\Lambda$, gives a constant value of m. The analysis using Eqs. (1.4.60)–(1.4.63) is sufficiently general in the sense that the form of $f(R)$ does not need to be specified.

The effective equation of state of the system (i.e., $p_{\rm tot}/\rho_{\rm tot}$) is

$$w_{\rm eff} = -\frac{1}{3}(2x_3 - 1)\,. \tag{1.4.66}$$

The dynamics of the full system can be investigated by analyzing the stability properties of the critical phase-space points as in, e.g., [39]. The general conclusions is that only models with a characteristic function $m(r)$ positive and close to ΛCDM, i.e., $m \geq 0$, are cosmologically viable. That is, only for these models one finds a sequence of a long decelerated matter epoch followed by a stable accelerated attractor.

The perturbation equations have been derived in, e.g., [473, 907]. Neglecting the contribution of radiation one has

$$\begin{aligned}
&\delta_m'' + \left(x_3 - \frac{1}{2}x_1\right)\delta_m' - \frac{3}{2}(1 - x_1 - x_2 - x_3)\delta_m \\
&\quad = \frac{1}{2}\left[\left\{\frac{k^2}{x_5^2} - 6 + 3x_1^2 - 3x_1' - 3x_1(x_3 - 1)\right\}\delta\tilde{F}\right. \\
&\qquad \left. + 3(-2x_1 + x_3 - 1)\delta\tilde{F}' + 3\delta\tilde{F}''\right]\,,
\end{aligned} \tag{1.4.67}$$

$$\begin{aligned}
&\delta\tilde{F}'' + (1 - 2x_1 + x_3)\delta\tilde{F}' \\
&\quad + \left[\frac{k^2}{x_5^2} - 2x_3 + \frac{2x_3}{m} - x_1(x_3 + 1) - x_1' + x_1^2\right]\delta\tilde{F} \\
&\qquad = (1 - x_1 - x_2 - x_3)\delta_m - x_1\delta_m'\,,
\end{aligned} \tag{1.4.68}$$

where $\delta\tilde{F} \equiv \delta F/F$, and the new variable $x_5 \equiv aH$ satisfies

$$x_5' = (x_3 - 1)\, x_5\,. \tag{1.4.69}$$

The perturbation δF can be written as $\delta F = f_{,RR}\delta R$ and, therefore, $\delta\tilde{F} = m\delta R/R$. These equations can be integrated numerically to derive the behavior of δ_m at all scales. However, at

sub-Hubble scales they can be simplified and the following expression for the two MG functions Q, η of Eq. (1.3.23) can be obtained:

$$Q = 1 - \frac{k^2}{3(a^2M^2 + k^2)}$$
$$\eta = 1 - \frac{2k^2}{3a^2M^2 + 4k^2} \tag{1.4.70}$$

where

$$M^2 = \frac{1}{3f_{,RR}}. \tag{1.4.71}$$

Note that in the ΛCDM limit $f_{,RR} \to 0$ and $Q, \eta \to 1$.

These relations can be straightforwardly generalized. In [287] the perturbation equations for the $f(R)$ Lagrangian have been extended to include coupled scalar fields and their kinetic energy $X \equiv -\phi_{,\mu}\phi^{\mu}/2$, resulting in a $f(R, \phi, X)$-theory. In the slightly simplified case in which $f(R, \phi, X) = f_1(R, \phi) + f_2(\phi, X)$, with arbitrary functions $f_1, 2$, one obtains

$$Q = -\frac{1}{F}\frac{(1 + 2r_1)(f_{,X} + 2r_2) + 2F^2_{,\phi}/F}{(1 + 3r_1)(f_{,X} + 2r_2) + 3F^2_{,\phi}/F},$$
$$\eta = \frac{(1 + 2r_1)(f_{,X} + 2r_2) + 2F^2_{,\phi}/F}{(1 + 4r_1)(f_{,X} + 2r_2) + 4F^2_{,\phi}/F}, \tag{1.4.72}$$

where the notation $f_{,X}$ or $F_{,\phi}$ denote differentiation wrt X or ϕ, respectively, and where $r_1 \equiv \frac{k^2}{a^2}\frac{m}{R}$ and $r_2 \equiv \frac{a^2}{k^2}M^2_{\phi}$, $M_{\phi} = -f_{,\phi\phi}/2$ being the scalar field effective mass. In the same paper [287] an extra term proportional to $X\Box\phi$ in the Lagrangian is also taken into account.

Euclid forecasts for the $f(R)$ models will be presented in Section 1.8.7.

1.4.7 Massive gravity and higher-dimensional models

Instead of introducing new scalar degrees of freedom such as in $f(R)$ theories, another philosophy in modifying gravity is to modify the graviton itself. In this case the new degrees of freedom belong to the gravitational sector itself; examples include massive gravity and higher-dimensional frameworks, such as the Dvali–Gabadadze–Porrati (DGP) model [326] and its extensions. The new degrees of freedom can be responsible for a late-time speed-up of the universe, as is summarized below for a choice of selected models. We note here that while such self-accelerating solutions are interesting in their own right, they do not tackle the old cosmological constant problem: why the observed cosmological constant is so much smaller than expected in the first place. Instead of answering this question directly, an alternative approach is the idea of degravitation [see 327, 328, 58, 330], where the cosmological constant could be as large as expected from standard field theory, but would simply gravitate very little (see the paragraph in Section 1.4.7.1 below).

1.4.7.1 Self-acceleration

DGP. The DGP model is one of the important infrared (IR) modified theories of gravity. From a four-dimensional point of view this corresponds effectively to a theory in which the graviton acquires a soft mass m. In this braneworld model our visible universe is confined to a brane of four dimensions embedded into a five-dimensional bulk. At small distances, the four-dimensional gravity is recovered due to an intrinsic Einstein–Hilbert term sourced by the brane curvature causing a gravitational force law that scales as r^{-2}. At large scales the gravitational force law asymptotes to an r^{-3} behavior. The cross over scale $r_c = m^{-1}$ is given by the ratio of the Planck masses in four

(M_4) and five (M_5) dimensions. One can study perturbations around flat spacetime and compute the gravitational exchange amplitude between two conserved sources, which does not reduce to the GR result even in the limit m$\to$ 0. However, the successful implementation of the Vainshtein mechanism for decoupling the additional modes from gravitational dynamics at sub-cosmological scales makes these theories still very attractive [913]. Hereby, the Vainshtein effect is realized through the nonlinear interactions of the helicity-0 mode π, as will be explained in further detail below. Thus, this vDVZ discontinuity does not appear close to an astrophysical source where the π field becomes nonlinear and these nonlinear effects of π restore predictions to those of GR. This is most easily understood in the limit where $M_4, M_5 \to \infty$ and $m \to 0$ while keeping the strong coupling scale $\Lambda = (M_4 m^2)^{1/3}$ fixed. This allows us to treat the usual helicity-2 mode of gravity linearly while treating the helicity-0 mode π nonlinearly. The resulting effective action is then

$$\mathcal{L}_\pi = 3\pi\Box\pi - \frac{1}{\Lambda^3}(\partial\pi)^2\Box\pi\,, \tag{1.4.73}$$

where interactions already become important at the scale $\Lambda \ll M_{\rm Pl}$ [593].

Furthermore, in this model, one can recover an interesting range of cosmologies, in particular a modified Friedmann equation with a self-accelerating solution. The Einstein equations thus obtained reduce to the following modified Friedmann equation in a homogeneous and isotropic metric [298]

$$H^2 \pm mH = \frac{8\pi G}{3}\rho\,, \tag{1.4.74}$$

such that at higher energies one recovers the usual four-dimensional behavior, $H^2 \sim \rho$, while at later time corrections from the extra dimensions kick in. As is clear in this Friedmann equation, this braneworld scenario holds two branches of cosmological solutions with distinct properties. The self-accelerating branch (minus sign) allows for a de Sitter behavior $H = \text{const} = m$ even in the absence of any cosmological constant $\rho_\Lambda = 0$ and as such it has attracted a lot of attention. Unfortunately, this branch suffers from a ghost-like instability. The normal branch (the plus sign) instead slows the expansion rate but is stable. In this case a cosmological constant is still required for late-time acceleration, but it provides significant intuition for the study of degravitation.

The Galileon. Even though the DGP model is interesting for several reasons like giving the Vainshtein effect a chance to work, the self-acceleration solution unfortunately introduces extra ghost states as outlined above. However, it has been generalized to a "Galileon" model, which can be considered as an effective field theory for the helicity-0 field π. Galileon models are invariant under shifts of the field π and shifts of the gradients of π (known as the Galileon symmetry), meaning that a Galileon model is invariant under the transformation

$$\pi \to \pi + c + v_\mu x^\mu\,, \tag{1.4.75}$$

for arbitrary constant c and v_μ. In induced gravity braneworld models, this symmetry is naturally inherited from the five-dimensional Poincaré invariance [295]. The Galileon theory relies strongly on this symmetry to constrain the possible structure of the effective π Lagrangian, and insisting that the effective field theory for π bears no ghost-like instabilities further restricts the possibilities [686]. It can be shown that there exist only five derivative interactions, which preserve the Galilean symmetry without introducing ghosts. These interactions are symbolically of the form $\mathcal{L}_\pi^{(1)} = \pi$ and $\mathcal{L}_\pi^{(n)} = (\partial\pi)^2(\partial\partial\pi)^{n-2}$, for $n = 2, \ldots 5$. A general Galileon Lagrangian can be constructed as a linear combination of these Lagrangian operators. The effective action for the DGP scalar (1.4.73) can be seen to be a combination of $\mathcal{L}_\pi^{(2)}$ and $\mathcal{L}_\pi^{(3)}$. Such interactions have been shown to naturally arise from Lovelock invariants in the bulk of generalized braneworld models [295]. However, the

Galileon does not necessarily require a higher-dimensional origin and can be consistently treated as a four-dimensional effective field theory.

As shown in [686], such theories can allow for self-accelerating de Sitter solutions without any ghosts, unlike in the DGP model. In the presence of compact sources, these solutions can support spherically-symmetric, Vainshtein-like nonlinear perturbations that are also stable against small fluctuations. However, this is constrained to the subset of the third-order Galileon, which contains only $\mathcal{L}_\pi^{(1)}$, $\mathcal{L}_\pi^{(2)}$ and $\mathcal{L}_\pi^{(3)}$ [669].

The Galileon terms described above form a subset of the "generalized Galileons". A generalized Galileon model allows nonlinear derivative interactions of the scalar field π in the Lagrangian while insisting that the equations of motion remain at most second order in derivatives, thus removing any ghost-like instabilities. However, unlike the pure Galileon models, generalized Galileons do not impose the symmetry of Eq. (1.4.75). These theories were first written down by Horndeski [445] and later rediscoved by Deffayet et al. [300]. They are a linear combination of Lagrangians constructed by multiplying the Galileon Lagrangians $\mathcal{L}_\pi^{(n)}$ by an arbitrary scalar function of the scalar π and its first derivatives. Just like the Galileon, generalized Galileons can give rise to cosmological acceleration and to Vainshtein screening. However, as they lack the Galileon symmetry these theories are not protected from quantum corrections. Many other theories can also be found within the spectrum of generalized Galileon models, including k-essence.

Degravitation. The idea behind degravitation is to modify gravity in the IR, such that the vacuum energy could have a weaker effect on the geometry, and therefore reconcile a natural value for the vacuum energy as expected from particle physics with the observed late-time acceleration. Such modifications of gravity typically arise in models of massive gravity [327, 328, 58, 330], i.e., where gravity is mediated by a massive spin-2 field. The extra-dimensional DGP scenario presented previously, represents a specific model of soft mass gravity, where gravity weakens down at large distance, with a force law going as $1/r$. Nevertheless, this weakening is too weak to achieve degravitation and tackle the cosmological constant problem. However, an obvious way out is to extend the DGP model to higher dimensions, thereby diluting gravity more efficiently at large distances. This is achieved in models of cascading gravity, as is presented below. An alternative to cascading gravity is to work directly with theories of constant mass gravity (hard mass graviton).

Cascading gravity. Cascading gravity is an explicit realization of the idea of degravitation, where gravity behaves as a high-pass filter, allowing sources with characteristic wavelength (in space and in time) shorter than a characteristic scale r_c to behave as expected from GR, but weakening the effect of sources with longer wavelengths. This could explain why a large cosmological constant does not backreact as much as anticipated from standard GR. Since the DGP model does not modify gravity enough in the IR, "cascading gravity" relies on the presence of at least two infinite extra dimensions, while our world is confined on a four-dimensional brane [293]. Similarly as in DGP, four-dimensional gravity is recovered at short distances thanks to an induced Einstein–Hilbert term on the brane with associated Planck scale M_4. The brane we live in is then embedded in a five-dimensional brane, which bears a five-dimensional Planck scale M_5, itself embedded in six dimensions (with Planck scale M_6). From a four-dimensional perspective, the relevant scales are the 5d and 6d masses $m_4 = M_5^3/M_4^2$ and $m_5 = M_6^4/M_5^3$, which characterize the transition from the 4d to 5d and 5d to 6d behavior respectively.

Such theories embedded in more-than-one extra dimensions involve at least one additional scalar field that typically enters as a ghost. This ghost is independent of the ghost present in the self-accelerating branch of DGP but is completely generic to any codimension-two and higher framework with brane localized kinetic terms. However, there are two ways to cure the ghost, both of which are natural when considering a realistic higher codimensional scenario, namely smoothing

out the brane, or including a brane tension [293, 290, 294].

When properly taking into account the issue associated with the ghost, such models give rise to a theory of massive gravity (soft mass graviton) composed of one helicity-2 mode, helicity-1 modes that decouple and 2 helicity-0 modes. In order for this theory to be consistent with standard GR in four dimensions, both helicity-0 modes should decouple from the theory. As in DGP, this decoupling does not happen in a trivial way, and relies on a phenomenon of strong coupling. Close enough to any source, both scalar modes are strongly coupled and therefore freeze.

The resulting theory appears as a theory of a massless spin-2 field in four-dimensions, in other words as GR. If $r \ll m_5$ and for $m_6 \leq m_5$, the respective Vainshtein scale or strong coupling scale, i.e., the distance from the source M within which each mode is strongly coupled is $r_i^3 = M/m_i^2 M_4^2$, where $i = 5, 6$. Around a source M, one recovers four-dimensional gravity for $r \ll r_5$, five-dimensional gravity for $r_5 \ll r \ll r_6$ and finally six-dimensional gravity at larger distances $r \gg r_6$.

Massive gravity. While laboratory experiments, solar systems tests and cosmological observations have all been in complete agreement with GR for almost a century now, these bounds do not eliminate the possibility for the graviton to bear a small hard mass $m \lesssim 6.10^{-32}$ eV [400]. The question of whether or not gravity could be mediated by a hard-mass graviton is not only a purely fundamental but an abstract one. Since the degravitation mechanism is also expected to be present if the graviton bears a hard mass, such models can play an important role for late-time cosmology, and more precisely when the age of the universe becomes on the order of the graviton Compton wavelength.

Recent progress has shown that theories of hard massive gravity can be free of any ghost-like pathologies in the decoupling limit where $M_{\rm Pl} \to \infty$ and $m \to 0$ keeping the scale $\Lambda_3^3 = M_{\rm Pl} m^2$ fixed [291, 292]. The absence of pathologies in the decoupling limit does not guarantee the stability of massive gravity on cosmological backgrounds, but provides at least a good framework to understand the implications of a small graviton mass. Unlike a massless spin-2 field, which only bears two polarizations, a massive one bears five of them, namely two helicity-2 modes, two helicity-1 modes which decouple, and one helicity-0 mode (denoted as π). As in the braneworld models presented previously, this helicity-0 mode behaves as a scalar field with specific derivative interactions of the form

$$\mathcal{L}_\pi = h^{\mu\nu} \left(X^{(1)}_{\mu\nu} + \frac{1}{\Lambda_3^3} X^{(2)}_{\mu\nu} + \frac{1}{\Lambda_3^6} X^{(3)}_{\mu\nu} \right) . \tag{1.4.76}$$

Here, $h_{\mu\nu}$ denotes the canonically-normalized (rescaled by $M_{\rm pl}$) tensor field perturbation (helicity-2 mode), while $X^{(1)}_{\mu\nu}, X^{(2)}_{\mu\nu}$, and $X^{(3)}_{\mu\nu}$ are respectively, linear, quadratic and cubic in the helicity-0 mode π. Importantly, they are all transverse (for instance, $X^{(1)}_{\mu\nu} \propto \eta_{\mu\nu}\Box\pi - \partial_\mu\partial_\nu\pi$). Not only do these interactions automatically satisfy the Bianchi identity, as they should to preserve diffeomorphism invariance, but they are also at most second order in time derivatives. Hence, the interactions (1.4.76) are linear in the helicity-2 mode, and are free of any ghost-like pathologies. Therefore, such interactions are very similar in spirit to the Galileon ones, and bear the same internal symmetry (1.4.75), and present very similar physical properties. When $X^{(3)}_{\mu\nu}$ is absent, one can indeed recover an Einstein frame picture for which the interactions are of the form

$$\begin{aligned} \mathcal{L} = {} & \frac{M_{\rm Pl}^2}{2}\sqrt{-g}R + \frac{3}{2}\pi\Box\pi + \frac{3\beta}{2\Lambda_3^3}(\partial\pi)^2\Box\pi + \frac{\beta^2}{2\Lambda_3^6}(\partial\pi)^2\left((\partial_\alpha\partial_\beta\pi)^2 - (\Box\pi)^2\right) \\ & + \mathcal{L}_{\rm mat}[\psi, \tilde{g}_{\mu\nu}] , \end{aligned} \tag{1.4.77}$$

where β is an arbitrary constant and matter fields ψ do not couple to the metric $g_{\mu\nu}$ but to $\tilde{g}_{\mu\nu} = g_{\mu\nu} + \pi\eta_{\mu\nu} + \frac{\beta}{\Lambda_3^3}\partial_\mu\pi\partial_\nu\pi$. Here again, the recovery of GR in the UV is possible via a strong coupling phenomena, where the interactions for π are already important at the scale $\Lambda_3 \ll M_{\rm Pl}$,

well before the interactions for the usual helicity-2 mode. This strong coupling, as well as the peculiar coupling to matter sources, have distinguishable features in cosmology as is explained below [11, 478].

1.4.7.2 Observations

All models of modified gravity presented in this section have in common the presence of at least one additional helicity-0 degree of freedom that is not an arbitrary scalar, but descends from a full-fledged spin-two field. As such it has no potential and enters the Lagrangian via very specific derivative terms fixed by symmetries. However, tests of gravity severely constrain the presence of additional scalar degrees of freedom. As is well known, in theories of massive gravity the helicity-0 mode can evade fifth-force constraints in the vicinity of matter if the helicity-0 mode interactions are important enough to freeze out the field fluctuations [913]. This Vainshtein mechanism is similar in spirit but different in practice to the chameleon and symmetron mechanisms presented in detail in the next Sections 1.4.7.3 and 1.4.7.4. One key difference relies on the presence of derivative interactions rather than a specific potential. So, rather than becoming massive in dense regions, in the Vainshtein mechanism the helicity-0 mode becomes weakly coupled to matter (and light, i.e., sources in general) at high energy. This screening of scalar mode can yet have distinct signatures in cosmology and in particular for structure formation.

1.4.7.3 Screening mechanisms

While quintessence introduces a new degree of freedom to explain the late-time acceleration of the universe, the idea behind modified gravity is instead to tackle the core of the cosmological constant problem and its tuning issues as well as screening any fifth forces that would come from the introduction of extra degrees of freedom. As mentioned in Section 1.4.4.1, the strength with which these new degrees of freedom can couple to the fields of the standard model is very tightly constrained by searches for fifth forces and violations of the weak equivalence principle. Typically the strength of the scalar mediated interaction is required to be orders of magnitude weaker than gravity. It is possible to tune this coupling to be as small as is required, leading however to additional naturalness problems. Here we discuss in more detail a number of ways in which new scalar degrees of freedom can naturally couple to standard model fields, whilst still being in agreement with observations, because a dynamical mechanism ensures that their effects are screened in laboratory and solar system tests of gravity. This is done by making some property of the field dependent on the background environment under consideration. These models typically fall into two classes; either the field becomes massive in a dense environment so that the scalar force is suppressed because the Compton wavelength of the interaction is small, or the coupling to matter becomes weaker in dense environments to ensure that the effects of the scalar are suppressed. Both types of behavior require the presence of nonlinearities.

Density dependent masses: The chameleon. The chameleon [499] is the archetypal model of a scalar field with a mass that depends on its environment, becoming heavy in dense environments and light in diffuse ones. The ingredients for construction of a chameleon model are a conformal coupling between the scalar field and the matter fields of the standard model, and a potential for the scalar field, which includes relevant self-interaction terms.

In the presence of non-relativistic matter these two pieces conspire to give rise to an effective potential for the scalar field

$$V_{\rm eff}(\phi) = V(\phi) + \rho A(\phi), \tag{1.4.78}$$

where $V(\phi)$ is the bare potential, ρ the local energy density and $A(\phi)$ the conformal coupling function. For suitable choices of $A(\phi)$ and $V(\phi)$ the effective potential has a minimum and the

position of the minimum depends on ρ. Self-interaction terms in $V(\phi)$ ensure that the mass of the field in this minimum also depends on ρ so that the field becomes more massive in denser environments.

The environmental dependence of the mass of the field allows the chameleon to avoid the constraints of fifth-force experiments through what is known as the thin-shell effect. If a dense object is embedded in a diffuse background the chameleon is massive inside the object. There, its Compton wavelength is small. If the Compton wavelength is smaller than the size of the object, then the scalar mediated force felt by an observer at infinity is sourced, not by the entire object, but instead only by a thin shell of matter (of depth the Compton wavelength) at the surface. This leads to a natural suppression of the force without the need to fine tune the coupling constant.

1.4.7.4 Density dependent couplings

The Vainshtein Mechanism. In models such as DGP and the Galileon, the effects of the scalar field are screened by the Vainshtein mechanism [913, 299]. This occurs when nonlinear, higher-derivative operators are present in the Lagrangian for a scalar field, arranged in such a way that the equations of motion for the field are still second order, such as the interactions presented in Eq. (1.4.73).

In the presence of a massive source the nonlinear terms force the suppression of the scalar force in the vicinity of a massive object. The radius within which the scalar force is suppressed is known as the Vainshtein radius. As an example in the DGP model the Vainshtein radius around a massive object of mass M is

$$r_\star \sim \left(\frac{M}{4\pi M_{\rm Pl}}\right)^{1/3} \frac{1}{\Lambda}\,, \tag{1.4.79}$$

where Λ is the strong coupling scale introduced in section 1.4.7.1. For the Sun, if $m \sim 10^{-33}$ eV, or in other words, $\Lambda^{-1} = 1000$ km, then the Vainshtein radius is $r_\star \sim 10^2$ pc.

Inside the Vainshtein radius, when the nonlinear, higher-derivative terms become important they cause the kinetic terms for scalar fluctuations to become large. This can be interpreted as a relative weakening of the coupling between the scalar field and matter. In this way the strength of the interaction is suppressed in the vicinity of massive objects.

The Symmetron. The symmetron model [436] is in many ways similar to the chameleon model discussed above. It requires a conformal coupling between the scalar field and the standard model and a potential of a certain form. In the presence of non-relativistic matter this leads to an effective potential for the scalar field

$$V_{\rm eff}(\phi) = -\frac{1}{2}\left(\frac{\rho}{M^2} - \mu^2\right)\phi^2 + \frac{1}{4}\lambda\phi^4\,, \tag{1.4.80}$$

where M, μ and λ are parameters of the model, and ρ is the local energy density.

In sufficiently dense environments, $\rho > \mu^2 M^2$, the field sits in a minimum at the origin. As the local density drops the symmetry of the field is spontaneously broken and the field falls into one of the two new minima with a non-zero vacuum expectation value. In high-density symmetry-restoring environments, the scalar field vacuum expectation value should be near zero and fluctuations of the field should not couple to matter. Thus, the symmetron force in the exterior of a massive object is suppressed because the field does not couple to the core of the object.

The Olive–Pospelov model. The Olive–Pospelov model [696] again uses a scalar conformally coupled to matter. In this construction both the coupling function and the scalar field potential are chosen to have quadratic minima. If the background field takes the value that minimizes the

coupling function, then fluctuations of the scalar field decouple from matter. In non-relativistic environments the scalar field feels an effective potential, which is a combinations of these two functions. In high-density environments the field is very close to the value that minimizes the form of the coupling function. In low-density environments the field relaxes to the minimum of the bare potential. Thus, the interactions of the scalar field are suppressed in dense environments.

1.4.8 Einstein Aether and its generalizations

In 1983 it was suggested by Milgrom [659] that the emerging evidence for the presence of dark matter in galaxies could follow from a modification either to how 'baryonic' matter responded to the Newtonian gravitational field it created or to how the gravitational field was related to the baryonic matter density. Collectively these ideas are referred to as MOdified Newtonian Dynamics (MOND). By way of illustration, MOND may be considered as a modification to the non-relativistic Poisson equation:

$$\nabla \cdot \left(\mu \left(\frac{|\nabla \Psi|}{a_0} \right) \nabla \Psi \right) = 4\pi G \rho \,, \tag{1.4.81}$$

where Ψ is the gravitational potential, a_0 is a number with dimensions Length^{-1} and ρ is the baryonic matter density. The number a_0 is determined by looking at the dynamics of visible matter in galaxies [783]. The function $\mu(x)$ would simply be equal to unity in Newtonian gravity. In MOND, the functional form is only fixed at its limits: $\mu \to 1$ as $x \to \infty$ and $\mu \to x$ as $x \to 0$.

We are naturally interested in a relativistic version of such a proposal. The building block is the perturbed spacetime metric already introduced in Eq. 1.3.8

$$ds^2 = -(1+2\Psi)\,\mathrm{d}t^2 + (1-2\Phi)a^2(t)(\mathrm{d}R^2 + R^2\,\mathrm{d}\Omega^2). \tag{1.4.82}$$

A simple approach is to introduce a dynamical clock field, which we will call A^μ. If it has solutions aligned with the time-like coordinate t^μ then it will be sensitive to Ψ. The dynamical nature of the field implies that it should have an action that will contain gradients of the field and thus potentially scalars formed from gradients of Ψ, as we seek. A family of covariant actions for the clock field is as follows [988]:

$$I[g^{ab}, A^a, \lambda] = \frac{1}{16\pi G} \int \mathrm{d}^4x \sqrt{-g} \left[\frac{1}{\ell^2} F(K) + \lambda \left(A^a A_a + 1 \right) \right],$$

where

$$K = \ell^2 K^{\mu\nu\gamma\delta} \nabla_\mu A_\nu \nabla_\gamma A_\delta \tag{1.4.83}$$

with

$$K^{\mu\nu\gamma\delta} = c_1 g^{\mu\gamma} g^{\nu\delta} + c_2 g^{\mu\nu} g^{\gamma\delta} + c_3 g^{\mu\delta} g^{\nu\delta} \,. \tag{1.4.84}$$

The quantity ℓ is a number with dimensions of length, the c_A are dimensionless constants, the Lagrange multiplier field λ enforces the unit-timelike constraint on A^a, and F is a function. These models have been termed Generalized Einstein-Aether (GEA) theories, emphasizing the coexistence of general covariance and a 'preferred' state of rest in the model, i.e., keeping time with A^μ.

Indeed, when the geometry is of the form (1.4.82), anisotropic stresses are negligible and A^μ is aligned with the flow of time t^μ, then one can find appropriate values of the c_A and ℓ such that K is dominated by a term equal to $|\nabla\Psi|^2/a_0^2$. This influence then leads to a modification to the time-time component of Einstein's equations: instead of reducing to Poisson's equation, one recovers an equation of the form (1.4.81). Therefore the models are successful covariant realizations of MOND.

Interestingly, in the FLRW limit $\Phi, \Psi \to 0$, the time-time component of Einstein's equations in the GEA model becomes a modified Friedmann equation:

$$\beta\left(\frac{H^2}{a_0^2}\right) H^2 = \frac{8\pi G\rho}{3}\,, \tag{1.4.85}$$

where the function β is related to F and its derivatives with respect to K. The dynamics in galaxies prefer a value a_0 on the order the Hubble parameter today H_0 [783] and so one typically gets a modification to the background expansion with a characteristic scale H_0, i.e., the scale associated with modified gravity models that produce dark-energy effects. Ultimately the GEA model is a phenomenological one and as such there currently lack deeper reasons to favor any particular form of F. However, one may gain insight into the possible solutions of (1.4.85) by looking at simple forms for F. In [991] the monomial case $F \propto K^{n_{ae}}$ was considered where the kinetic index n_{ae} was allowed to vary. Solutions with accelerated expansion were found that could mimic dark energy.

Returning to the original motivation behind the theory, the next step is to look at the theory on cosmological scales and see whether the GEA models are realistic alternatives to dark matter. As emphasized, the additional structure in spacetime is dynamical and so possesses independent degrees of freedom. As the model is assumed to be uncoupled to other matter, the gravitational field equations would regard the influence of these degrees of freedom as a type of dark matter (possibly coupled non-minimally to gravity, and not necessarily 'cold').

The possibility that the model may then be a viable alternative to the dark sector in background cosmology and linear cosmological perturbations has been explored in depth in [989, 564] and [991]. As an alternative to dark matter, it was found that the GEA models could replicate some but not all of the following features of cold dark matter: influence on background dynamics of the universe; negligible sound speed of perturbations; growth rate of dark matter 'overdensity'; absence of anisotropic stress and contribution to the cosmological Poisson equation; effective minimal coupling to the gravitational field. When compared to the data from large scale structure and the CMB, the model fared significantly less well than the Concordance Model and so is excluded. If one relaxes the requirement that the vector field be responsible for the effects of cosmological dark matter, one can look at the model as one responsible only for the effects of dark energy. It was found [991] that the current most stringent constraints on the model's success as dark energy were from constraints on the size of large scale CMB anisotropy. Specifically, possible variation in $w(z)$ of the 'dark energy' along with new degrees of freedom sourcing anisotropic stress in the perturbations was found to lead to new, non-standard time variation of the potentials Φ and Ψ. These time variations source large scale anisotropies via the integrated Sachs–Wolfe effect, and the parameter space of the model is constrained in avoiding the effect becoming too pronounced.

In spite of this, given the status of current experimental bounds it is conceivable that a more successful alternative to the dark sector may share some of these points of departure from the Concordance Model and yet fare significantly better at the level of the background and linear perturbations.

1.4.9 The Tensor-Vector-Scalar theory of gravity

Another proposal for a theory of modified gravity arising from Milgrom's observation is the Tensor-Vector-Scalar theory of gravity, or TeVeS. TeVeS theory is *bimetric* with two frames: the "geometric frame" for the gravitational fields, and the "physical frame", for the matter fields. The three gravitational fields are the metric $\tilde{g}_{ab}$ (with connection $\tilde{\nabla}_a$) that we refer to as the geometric metric, the vector field A_a and the scalar field ϕ. The action for all matter fields, uses a single physical metric g_{ab} (with connection ∇_a). The two metrics are related via an algebraic, disformal relation [116] as

$$g_{ab} = e^{-2\phi}\tilde{g}_{ab} - 2\sinh(2\phi)A_a A_b\,. \tag{1.4.86}$$

Just like in the Generalized Einstein-Aether theories, the vector field is further enforced to be unit-timelike with respect to the geometric metric, i.e.,

$$\tilde{g}^{ab}A_aA_b = A^aA_a = -1. \tag{1.4.87}$$

The theory is based on an action S, which is split as $S = S_{\tilde{g}} + S_A + S_\phi + S_m$ where

$$S_{\tilde{g}} = \frac{1}{16\pi G}\int \mathrm{d}^4x\,\sqrt{-\tilde{g}}\,\tilde{R}\,, \tag{1.4.88}$$

where $\tilde{g}$ and $\tilde{R}$ are the determinant and scalar curvature of $\tilde{g}_{\mu\nu}$ respectively and G is the bare gravitational constant,

$$S_A = -\frac{1}{32\pi G}\int \mathrm{d}^4x\,\sqrt{-\tilde{g}}\,\left[KF^{ab}F_{ab} - 2\lambda(A_aA^a+1)\right], \tag{1.4.89}$$

where $F_{ab} = \nabla_aA_b - \nabla_bA_a$ leads to a Maxwellian kinetic term and λ is a Lagrange multiplier ensuring the unit-timelike constraint on A_a and K is a dimensionless constant (note that indices on F_{ab} are raised using the geometric metric, i.e., $F^a{}_b = \tilde{g}^{ac}F_{cb}$) and

$$S_\phi = -\frac{1}{16\pi G}\int \mathrm{d}^4x\sqrt{-\tilde{g}}\left[\mu\,\hat{g}^{ab}\tilde{\nabla}_a\phi\tilde{\nabla}_b\phi + V(\mu)\right], \tag{1.4.90}$$

where μ is a non-dynamical dimensionless scalar field, $\hat{g}^{ab} = \tilde{g}^{ab} - A^aA^b$ and $V(\mu)$ is an arbitrary function that typically depends on a scale ℓ_B. The matter is coupled only to the physical metric g_{ab} and defines the matter stress-energy tensor T_{ab} through $\delta S_m = -\frac{1}{2}\int \mathrm{d}^4x\sqrt{-g}\,T_{ab}\,\delta g^{ab}$. The TeVeS action can be written entirely in the physical frame [987, 840] or in a diagonal frame [840] where the scalar and vector fields decouple.

In a Friedmann universe, the cosmological evolution is governed by the Friedmann equation

$$3\tilde{H}^2 = 8\pi G e^{-2\phi}\left(\rho_\phi + \rho\right), \tag{1.4.91}$$

where $\tilde{H}$ is the Hubble rate in terms of the geometric scale factor, ρ is the physical matter density that obeys the energy conservation equation with respect to the physical metric and where the scalar field energy density is

$$\rho_\phi = \frac{e^{2\phi}}{16\pi G}\left(\mu\frac{\mathrm{d}V}{\mathrm{d}\mu} + V\right) \tag{1.4.92}$$

Exact analytical and numerical solutions with the Bekenstein free function have been found in [841] and in [318]. It turns out that energy density tracks the matter fluid energy density. The ratio of the energy density of the scalar field to that of ordinary matter is approximately constant, so that the scalar field exactly tracks the matter dynamics. In realistic situations, the radiation era tracker is almost never realized, as has been noted by Dodelson and Liguori, but rather ρ_ϕ is subdominant and slowly-rolling and $\phi \propto a^{4/5}$. [157] studied more general free functions which have the Bekenstein function as a special case and found a whole range of behavior, from tracking and accelerated expansion to finite time singularities. [309] have studied cases where the cosmological TeVeS equations lead to inflationary/accelerated expansion solutions.

Although no further studies of accelerated expansion in TeVeS have been performed, it is very plausible that certain choices of function will inevitably lead to acceleration. It is easy to see that the scalar field action has the same form as a k-essence/k-inflation [61] action which has been considered as a candidate theory for acceleration. It is unknown in general whether this has similar features as the uncoupled k-essence, although Zhao's study indicates that this a promising research direction [984].

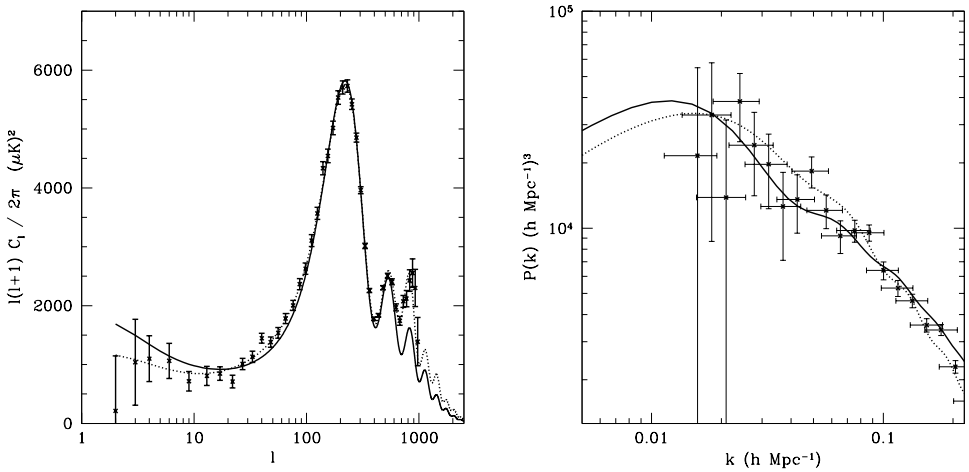

Figure 1: *Left:* the cosmic microwave background angular power spectrum $l(l+1)C_l/(2\pi)$ for TeVeS (solid) and ΛCDM (dotted) with WMAP 5-year data [689]. *Right:* the matter power spectrum $P(k)$ for TeVeS (solid) and ΛCDM (dotted) plotted with SDSS data.

In TeVeS, cold dark matter is absent. Therefore, in order to get acceptable values for the physical Hubble constant today (i.e., around $H_0 \sim 70$ km/s/Mpc), we have to supplement the absence of CDM with something else. Possibilities include the scalar field itself, massive neutrinos [841, 364] and a cosmological constant. At the same time, one has to get the right angular diameter distance to recombination [364]. These two requirements can place severe constraints on the allowed free functions.

Until TeVeS was proposed and studied in detail, MOND-type theories were assumed to be fatally flawed: their lack of a dark matter component would necessarily prevent the formation of large-scale structure compatible with current observational data. In the case of an Einstein universe, it is well known that, since baryons are coupled to photons before recombination they do not have enough time to grow into structures on their own. In particular, on scales smaller than the diffusion damping scale perturbations in such a universe are exponentially damped due to the Silk-damping effect. CDM solves all of these problems because it does not couple to photons and therefore can start creating potential wells early on, into which the baryons fall.

TeVeS contains two additional fields, which change the structure of the equations significantly. The first study of TeVeS predictions for large-scale structure observations was conducted in [841]. They found that TeVeS can indeed form large-scale structure compatible with observations depending on the choice of TeVeS parameters in the free function. In fact the form of the matter power spectrum $P(k)$ in TeVeS looks quite similar to that in ΛCDM. Thus TeVeS can produce matter power spectra that cannot be distinguished from ΛCDM by current observations. One would have to turn to other observables to distinguish the two models. The power spectra for TeVeS and ΛCDM are plotted on the right panel of Figure 1. [318] provided an analytical explanation of the growth of structure seen numerically by [841] and found that the growth in TeVeS is due to the vector field perturbation.

It is premature to claim (as in [843, 855]) that only a theory with CDM can fit CMB observations; a prime example to the contrary is the EBI theory [83]. Nevertheless, in the case of TeVeS [841] numerically solved the linear Boltzmann equation in the case of TeVeS and calculated the CMB angular power spectrum for TeVeS. By using initial conditions close to adiabatic the spectrum thus found provides very poor fit as compared to the ΛCDM model (see the left panel

of Figure 1). The CMB seems to put TeVeS into trouble, at least for the Bekenstein free function. The result of [318] has a further direct consequence. The difference $\Phi - \Psi$, sometimes named the gravitational slip (see Section 1.3.2), has additional contributions coming from the perturbed vector field α. Since the vector field is required to grow in order to drive structure formation, it will inevitably lead to a growing $\Phi - \Psi$. If the difference $\Phi - \Psi$ can be measured observationally, it can provide a substantial test of TeVeS that can distinguish TeVeS from ΛCDM.

1.5 Generic properties of dark energy and modified gravity models

This section explores some generic issues that are not connected to particular models (although we use some specific models as examples). First, we ask ourselves to which precision we should measure w in order to make a significant progress in understanding dark energy. Second, we discuss the role of the anisotropic stress in distinguishing between dark energy and modified gravity models. Finally, we present some general consistency relations among the perturbation variables that all models of modified gravity should fulfill.

1.5.1 To which precision should we measure w?

Two crucial questions that are often asked in the context of dark-energy surveys:

- Since w is so close to -1, do we not already know that the dark energy is a cosmological constant?
- To which precision should we measure w? Or equivalently, why is the Euclid target precision of about 0.01 on w_0 and 0.1 on w_a interesting?

In this section we will attempt to answer these questions at least partially, in two different ways. We will start by examining whether we can draw useful lessons from inflation, and then we will look at what we can learn from arguments based on Bayesian model comparison.

In the first part we will see that for single field slow-roll inflation models we effectively measure $w \sim -1$ with percent-level accuracy (see Figure 2); however, the deviation from a scale invariant spectrum means that we nonetheless observe a dynamical evolution and, thus, a deviation from an exact and constant equation of state of $w = -1$. Therefore, we know that inflation was not due to a cosmological constant; we also know that we can see no deviation from a de Sitter expansion for a precision smaller than the one Euclid will reach.

In the second part we will consider the Bayesian evidence in favor of a true cosmological constant if we keep finding $w = -1$; we will see that for priors on w_0 and w_a of order unity, a precision like the one for Euclid is necessary to favor a true cosmological constant decisively. We will also discuss how this conclusion changes depending on the choice of priors.

1.5.1.1 Lessons from inflation

In all probability the observed late-time acceleration of the universe is not the first period of accelerated expansion that occurred during its evolution: the current standard model of cosmology incorporates a much earlier phase with $\ddot{a} > 0$, called inflation. Such a period provides a natural explanation for several late-time observations:

- Why is the universe very close to being spatially flat?
- Why do we observe homogeneity and isotropy on scales that were naively never in causal contact?

- What created the initial fluctuations?

In addition, inflation provides a mechanism to get rid of unwanted relics from phase transitions in the early universe, like monopoles, that arise in certain scenarios (e.g., grand-unified theories).

While there is no conclusive proof that an inflationary phase took place in the early universe, it is surprisingly difficult to create the observed fluctuation spectrum in alternative scenarios that are strictly causal and only act on sub-horizon scales [854, 803].

If, however, inflation took place, then it seems natural to ask the question whether its observed properties appear similar to the current knowledge about the dark energy, and if yes, whether we can use inflation to learn something about the dark energy. The first lesson to draw from inflation is that it was not due to a pure cosmological constant. This is immediately clear since we exist: inflation ended. We can go even further: if Planck confirms the observations of a deviation from a scale invariant initial spectrum ($n_s \neq 1$) of WMAP [526] then this excludes an exactly exponential expansion during the observable epoch and, thus, also a temporary, effective cosmological constant.

If there had been any observers during the observationally accessible period of inflation, what would they have been seeing? Following the analysis in [475], we notice that

$$1 + w = -\frac{2}{3}\frac{\dot{H}}{H^2} = \frac{2}{3}\varepsilon_H \,, \tag{1.5.1}$$

where $\epsilon_H \equiv 2M_{\rm Pl}^2(H'/H)^2$ and here the prime denotes a derivative with respect to the inflaton field. Since, therefore, the tensor-to-scalar ratio is linked to the equation of state parameter through $r \sim 24(1+w)$ we can immediately conclude that no deviation of from $w = -1$ during inflation has been observed so far, just as no such deviation has been observed for the contemporary dark energy. At least in this respect inflation and the dark energy look similar. However, we also know that

$$\frac{d\ln(1+w)}{dN} = 2(\eta_H - \varepsilon_H) \tag{1.5.2}$$

where $\eta_H \equiv 2M_{\rm Pl}^2 H''/H$ is related to the scalar spectral index by $2\eta_H = (n_s - 1) + 4\varepsilon_H$. Thus, if $n_s \neq 1$ we have that either $\eta_H \neq 0$ or $\varepsilon_H \neq 0$, and consequently either $w \neq -1$ or w is not constant.

As already said earlier, we conclude that inflation is not due to a cosmological constant. However, an observer back then would nonetheless have found $w \approx -1$. Thus, observation of $w \approx -1$ (at least down to an error of about 0.02, see Figure 2) does not provide a very strong reason to believe that we are dealing with a cosmological constant.

We can rewrite Eq. (1.5.2) as

$$(1+w) = -\frac{1}{6}(n_s - 1) + \frac{\eta_H}{3} \approx 0.007 + \frac{\eta_H}{3} \,. \tag{1.5.3}$$

Naively it would appear rather fine-tuned if η_H precisely canceled the observed contribution from $n_s - 1$. Following this line of reasoning, if ε_H and η_H are of about the same size, then we would expect $1 + w$ to be about 0.005 to 0.015, well within current experimental bounds and roughly at the limit of what Euclid will be able to observe.

However, this last argument is highly speculative, and at least for inflation we know that there are classes of models where the cancellation is indeed natural, which is why one cannot give a lower limit for the amplitude of primordial gravitational waves. On the other hand, the observed period of inflation is probably in the middle of a long slow-roll phase during which w tends to be close to -1 (cf. Figure 3), while near the end of inflation the deviations become large. Additionally, inflation happened at an energy scale somewhere between 1 MeV and the Planck scale, while the energy scale of the late-time accelerated expansion is of the order of 10^{-3} eV. At least in this respect the two are very different.

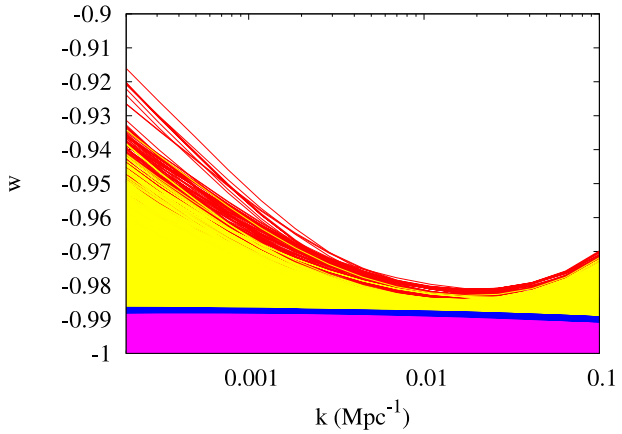

Figure 2: The evolution of w as a function of the comoving scale k, using only the 5-year WMAP CMB data. Red and yellow are the 95% and 68% confidence regions for the LV formalism. Blue and purple are the same for the flow-equation formalism. From the outside inward, the colored regions are red, yellow, blue, and purple. Image reproduced by permission from [475]; copyright by APS.

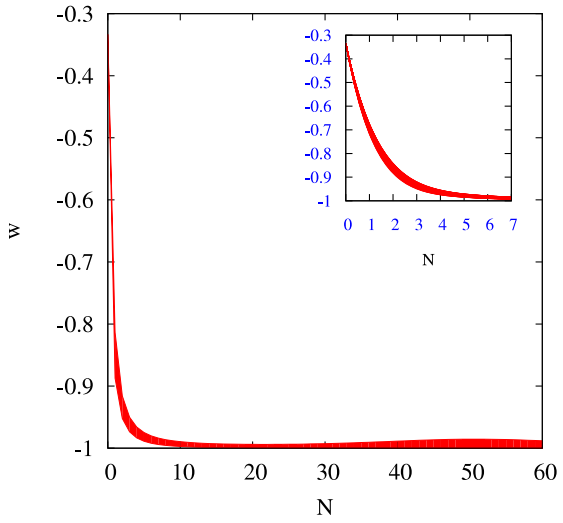

Figure 3: The complete evolution of $w(N)$, from the flow-equation results accepted by the CMB likelihood. Inflation is made to end at $N = 0$ where $w(N = 0) = -1/3$ corresponding to $\epsilon_H(N = 0) = 1$. For our choice of priors on the slow-roll parameters at $N = 0$, we find that w decreases rapidly towards -1 (see inset) and stays close to it during the period when the observable scales leave the horizon ($N \approx 40-60$). Image reproduced by permission from [475]; copyright by APS.

1.5.1.2 Higgs-Dilaton Inflation: a connection between the early and late universe acceleration

Despite previous arguments, it is natural to ask for a connection between the two known acceleration periods. In fact, in the last few years there has been a renewal of model building in inflationary cosmology by considering the fundamental Higgs as the inflaton field [133]. Such an elegant and economical model can give rise to the observed amplitude of CMB anisotropies when we include a large non-minimal coupling of the Higgs to the scalar curvature. In the context of quantum field theory, the running of the Higgs mass from the electroweak scale to the Planck scale is affected by this non-minimal coupling in such a way that the beta function of the Higgs' self-coupling vanishes at an intermediate scale ($\mu \sim 10^{15}$ GeV), if the mass of the Higgs is precisely 126 GeV, as measured at the LHC. This partial fixed point (other beta functions do not vanish) suggests an enhancement of symmetry at that scale, and the presence of a Nambu–Goldstone boson (the dilaton field) associated with the breaking of scale invariance [820]. In a subsequent paper [383], the Higgs-Dilaton scenario was explored in full detail. The model predicts a bound on the scalar spectral index, $n_s < 0.97$, with negligible associated running, $-0.0006 < d\ln n_s/d\ln k < 0.00015$, and a scalar to tensor ratio, $0.0009 < r < 0.0033$, which, although out of reach of the Planck satellite mission, is within the capabilities of future CMB satellite projects like PRISM [52]. Moreover, the model predicts that, after inflation, the dilaton plays the role of a thawing quintessence field, whose slow motion determines a concrete relation between the early universe fluctuations and the equation of state of dark energy, $3(1+w) = 1 - n_s > 0.03$, which could be within reach of Euclid satellite mission [383]. Furthermore, within the HDI model, there is also a relation between the running of the scalar tilt and the variation of $w(a)$, $d\ln n_s/d\ln k = 3w_a$, a prediction that can easily be ruled out with future surveys.

These relationships between early and late universe acceleration parameters constitute a fundamental physics connection within a very concrete and economical model, where the Higgs plays the role of the inflaton and the dilaton is a thawing quintessence field, whose dynamics has almost no freedom and satisfies all of the present constraints [383].

1.5.1.3 When should we stop: Bayesian model comparison

In the previous section we saw that inflation provides an argument why an observation of $w \approx -1$ need not support a cosmological constant strongly. Let us now investigate this argument more precisely with Bayesian model comparison. One model, M_0, posits that the accelerated expansion is due to a cosmological constant. The other models assume that the dark energy is dynamical, in a way that is well parametrized either by an arbitrary constant w (model M_1) or by a linear fit $w(a) = w_0 + (1-a)w_a$ (model M_2). Under the assumption that no deviation from $w = -1$ will be detected in the future, at which point should we stop trying to measure w ever more accurately? The relevant target here is to quantify at what point we will be able to rule out an entire class of theoretical dark-energy models (when compared to ΛCDM) at a certain threshold for the strength of evidence.

Here we are using the constant and linear parametrization of w because on the one hand we can consider the constant w to be an effective quantity, averaged over redshift with the appropriate weighting factor for the observable, see [838], and on the other hand because the precision targets for observations are conventionally phrased in terms of the figure of merit (FoM) given by $1/\sqrt{|\mathrm{Cov}(w_0, w_a)|}$. We will, therefore, find a direct link between the model probability and the FoM. It would be an interesting exercise to repeat the calculations with a more general model, using e.g. PCA, although we would expect to reach a similar conclusion.

Bayesian model comparison aims to compute the relative model probability

$$\frac{P(M_0|d)}{P(M_1|d)} = \frac{P(d|M_0)}{P(d|M_1)}\frac{P(M_0)}{P(M_1)} \tag{1.5.4}$$

where we used Bayes formula and where $B_{01} \equiv P(d|M_0)/P(d|M_1)$ is called the Bayes factor. The Bayes factor is the amount by which our relative belief in the two models is modified by the data, with $\ln B_{01} > (< 0)$ indicating a preference for model 0 (model 1). Since the model M_0 is nested in M_1 at the point $w = -1$ and in model M_2 at $(w_0 = -1, w_a = 0)$, we can use the Savage–Dickey (SD) density ratio [e.g. 894]. Based on SD, the Bayes factor between the two models is just the ratio of posterior to prior at $w = -1$ or at $(w_0 = -1, w_a = 0)$, marginalized over all other parameters.

Let us start by following [900] and consider the Bayes factor B_{01} between a cosmological constant model $w = -1$ and a free but constant effective w. If we assume that the data are compatible with $w_{\rm eff} = -1$ with an uncertainty σ, then the Bayes factor in favor of a cosmological constant is given by

$$B = \sqrt{\frac{2}{\pi}} \frac{\Delta_+ + \Delta_-}{\sigma} \left[\mathrm{erfc}\left(-\frac{\Delta_+}{\sqrt{2}\sigma} \right) - \mathrm{erfc}\left(\frac{\Delta_-}{\sqrt{2}\sigma} \right) \right]^{-1}, \tag{1.5.5}$$

where for the evolving dark-energy model we have adopted a flat prior in the region $-1 - \Delta_- \leq w_{\rm eff} \leq -1 + \Delta_+$ and we have made use of the Savage–Dickey density ratio formula [see 894]. The prior, of total width $\Delta = \Delta_+ + \Delta_-$, is best interpreted as a factor describing the predictivity of the dark-energy model under consideration. For instance, in a model where dark energy is a fluid with a negative pressure but satisfying the strong energy condition we have that $\Delta_+ = 2/3, \Delta_- = 0$. On the other hand, phantom models will be described by $\Delta_+ = 0, \Delta_- > 0$, with the latter being possibly rather large. A model with a large Δ will be more generic and less predictive, and therefore is disfavored by the Occam's razor of Bayesian model selection, see Eq. (1.5.5). According to the Jeffreys' scale for the strength of evidence, we have a moderate (strong) preference for the cosmological constant model for $2.5 < \ln B_{01} < 5.0$ ($\ln B_{01} > 5.0$), corresponding to posterior odds of 12:1 to 150:1 (above 150:1).

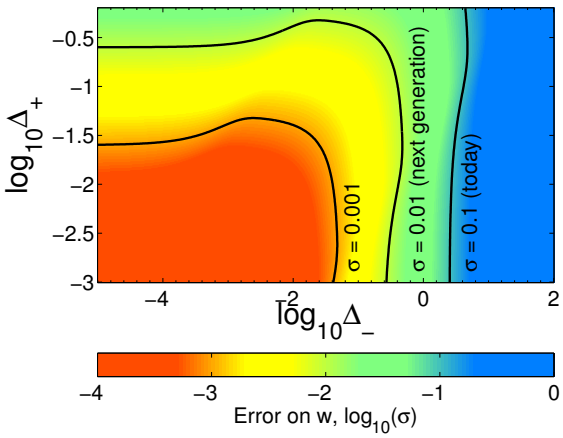

Figure 4: Required accuracy on $w_{\rm eff} = -1$ to obtain strong evidence against a model where $-1 - \Delta_- \leq w_{\rm eff} \leq -1 + \Delta_+$ as compared to a cosmological constant model, $w = -1$. For a given σ, models to the right and above the contour are disfavored with odds of more than 20:1.

We plot in Figure 4 contours of constant observational accuracy σ in the model predictivity space (Δ_-, Δ_+) for $\ln B = 3.0$ from Eq. (1.5.5), corresponding to odds of 20 to 1 in favor of a cosmological constant (slightly above the "moderate" threshold. The figure can be interpreted as giving the space of extended models that can be significantly disfavored with respect to $w = -1$ at a given accuracy. The results for the 3 benchmark models mentioned above (fluid-like, phantom or small departures from $w = -1$) are summarized in Table 1. Instead, we can ask the question which precision needs to reached to support ΛCDM at a given level. This is shown in Table 2 for odds 20:1 and 150:1. We see that to rule out a fluid-like model, which also covers the parameter

Table 1: Strength of evidence disfavoring the three benchmark models against a cosmological constant model, using an indicative accuracy on $w = -1$ from present data, $\sigma \sim 0.1$.

Model	(Δ_+, Δ_-)	$\ln B$ today ($\sigma = 0.1$)
Phantom	$(0, 10)$	4.4 (strongly disfavored)
Fluid-like	$(2/3, 0)$	1.7 (slightly disfavored)
Small departures	$(0.01, 0.01)$	0.0 (inconclusive)

space expected for canonical scalar field dark energy, we need to reach a precision comparable to the one that the Euclid satellite is expected to attain.

Table 2: Required accuracy for future surveys in order to disfavor the three benchmark models against $w = -1$ for two different strengths of evidence.

Model	(Δ_+, Δ_-)	Required σ for odds	
		$> 20:1$	$> 150:1$
Phantom	$(0, 10)$	0.4	$5 \cdot 10^{-2}$
Fluid-like	$(2/3, 0)$	$3 \cdot 10^{-2}$	$3 \cdot 10^{-3}$
Small departures	$(0.01, 0.01)$	$4 \cdot 10^{-4}$	$5 \cdot 10^{-5}$

By considering the model M_2 we can also provide a direct link with the target DETF FoM: Let us choose (fairly arbitrarily) a flat probability distribution for the prior, of width Δw_0 and Δw_a in the dark-energy parameters, so that the value of the prior is $1/(\Delta w_0 \Delta w_a)$ everywhere. Let us assume that the likelihood is Gaussian in w_0 and w_a and centered on ΛCDM (i.e., the data fully supports Λ as the dark energy).

As above, we need to distinguish different cases depending on the width of the prior. If you accept the argument of the previous section that we expect only a small deviation from $w = -1$, and set a prior width of order 0.01 on both w_0 and w_a, then the posterior is dominated by the prior, and the ratio will be of order 1 if the future data is compatible with $w = -1$. Since the precision of the experiment is comparable to the expected deviation, both ΛCDM and evolving dark energy are equally probable (as argued above and shown for model M_1 in Table 1), and we have to wait for a detection of $w \neq -1$ or a significant further increase in precision (cf. the last row in Table 2).

However, one often considers a much wider range for w, for example the fluid-like model with $w_0 \in [-1/3, -1]$ and $w_a \in [-1, 1]$ with equal probability (and neglecting some subtleties near $w = -1$). If the likelihood is much narrower than the prior range, then the value of the normalized posterior at $w = -1$ will be $2/(2\pi\sqrt{|\mathrm{Cov}(w_0, w_a)|} = \mathrm{FoM}/\pi$ (since we excluded $w < -1$, else it would half this value). The Bayes factor is then given by

$$B_{01} = \frac{\Delta w_0 \Delta w_a \mathrm{FoM}}{\pi} . \tag{1.5.6}$$

For the prior given above, we end up with $B_{01} \approx 4\mathrm{FoM}/(3\pi) \approx 0.4\mathrm{FoM}$. In order to reach a "decisive" Bayes factor, usually characterized as $\ln B > 5$ or $B > 150$, we thus need a figure of merit exceeding 375. Demanding that Euclid achieve a FoM > 500 places us, therefore, on the safe side and allows to reach the same conclusions (the ability to favor ΛCDM decisively *if* the data is in full agreement with $w = -1$) under small variations of the prior as well.

A similar analysis could be easily carried out to compare the cosmological constant model against departures from Einstein gravity, thus giving some useful insight into the potential of future surveys in terms of Bayesian model selection.

To summarize, we used inflation as a dark-energy prototype to show that the current experimental bounds of $w \approx -1.0 \pm 0.1$ are not yet sufficient to significantly favor a cosmological constant

over other models. In addition, even when expecting a deviation of $w = -1$ of order unity, our current knowledge of w does not allow us to favor Λ strongly in a Bayesian context. Here we showed that we need to reach a percent level accuracy both to have any chance of observing a deviation of w from -1 if the dark energy is similar to inflation, and because it is at this point that a cosmological constant starts to be favored decisively for prior widths of order 1. In either scenario, we do not expect to be able to improve much our knowledge with a lower precision measurement of w. The dark energy can of course be quite different from the inflaton and may lead to larger deviations from $w = -1$. This indeed would be the preferred situation for Euclid, as then we will be able to investigate much more easily the physical origin of the accelerate expansion. We can, however, have departures from ΛCDM even if w is very close to -1 today. In fact most present models of modified gravity and dynamical dark energy have a value of w_0 which is asymptotically close to -1 (in the sense that large departures from this value is already excluded). In this sense, for example, early dark-energy parameterizations (Ω_e) test the amount of dark energy in the past, which can still be non negligible (ex. [723]). Similarly, a fifth force can lead to a background similar to LCDM but different effects on perturbations and structure formation [79].

1.5.2 The effective anisotropic stress as evidence for modified gravity

As discussed in Section 1.4, all dark energy and modified gravity models can be described with the same effective metric degrees of freedom. This makes it impossible in principle to distinguish clearly between the two possibilities with cosmological observations alone. But while the cleanest tests would come from laboratory experiments, this may well be impossible to achieve. We would expect that model comparison analyses would still favor the correct model as it should provide the most elegant and economical description of the data. However, we may not know the correct model a priori, and it would be more useful if we could identify generic differences between the different classes of explanations, based on the phenomenological description that can be used directly to analyze the data.

Looking at the effective energy momentum tensor of the dark-energy sector, we can either try to find a hint in the form of the pressure perturbation δp or in the effective anisotropic stress π. Whilst all scalar field dark energy affects δp (and for multiple fields with different sound speeds in potentially quite complex ways), they generically have $\pi = 0$. The opposite is also true, modified gravity models have generically $\pi \neq 0$ [537]. Radiation and neutrinos will contribute to anisotropic stress on cosmological scales, but their contribution is safely negligible in the late-time universe. In the following sections we will first look at models with single extra degrees of freedom, for which we will find that $\pi \neq 0$ is a firm prediction. We will then consider the $f(R, G)$ case as an example for multiple degrees of freedom [782].

1.5.2.1 Modified gravity models with a single degree of freedom

In the prototypical scalar-tensor theory, where the scalar φ is coupled to R through $F(\varphi)R$, we find that $\pi \propto (F'/F)\delta\varphi$. This is very similar to the $f(R)$ case for which $\pi \propto (F'/F)\delta R$ (where now $F = df/dR$). In both cases the generic model with vanishing anisotropic stress is given by $F' = 0$, which corresponds to a constant coupling (for scalar-tensor) or $f(R) \propto R + \Lambda$. In both cases we find the GR limit. The other possibility, $\delta\varphi = 0$ or $\delta R = 0$, imposes a very specific evolution on the perturbations that in general does not agree with observations.

Another possible way to build a theory that deviates from GR is to use a function of the second-order Lovelock function, the Gauss–Bonnet term $G \equiv R^2 - 4R_{\mu\nu}R^{\mu\nu} + R_{\alpha\beta\mu\nu}R^{\alpha\beta\mu\nu}$. The Gauss–Bonnet term by itself is a topological invariant in 4 spacetime dimensions and does not contribute to the equation of motion. It is useful here since it avoids an Ostrogradski-type instability [967].

In $R + f(G)$ models, the situation is slightly more complicated than for the scalar-tensor case, as

$$\pi \sim \Phi - \Psi = 4H\dot{\xi}\Psi - 4\ddot{\xi}\Phi + 4\left(H^2 + \dot{H}\right)\delta\xi \tag{1.5.7}$$

where the dot denotes derivative with respect to ordinary time and $\xi = df/dG$ (see, e.g., [782]). An obvious choice to force $\pi = 0$ is to take ξ constant, which leads to $R + G + \Lambda$ in the action, and thus again to GR in four spacetime dimensions. There is no obvious way to exploit the extra ξ terms in Eq. (1.5.7), with the exception of curvature dominated evolution and on small scales (which is not very relevant for realistic cosmologies).

Finally, in DGP one has, with the notation of [41],

$$\Phi - \Psi = \frac{2Hr_c - 1}{1 + Hr_c(3Hr_c - 2)}\Phi\,. \tag{1.5.8}$$

This expression vanishes for $Hr_c = 1/2$ (which is never reached in the usual scenario in which $Hr_c \to 1$ from above) and for $Hr_c \to \infty$ (for large Hr_c the expression in front of Φ in (1.5.8) vanishes like $1/(Hr_c)$). In the DGP scenario the absolute value of the anisotropic stress grows over time and approaches the limiting value of $\Phi - \Psi = \Phi/2$. The only way to avoid this limit is to set the crossover scale to be unobservably large, $r_c \propto M_4^2/M_5^3 \to \infty$. In this situation the five-dimensional part of the action is suppressed and we end up with the usual 4D GR action.

In all of these examples only the GR limit has consistently no effective anisotropic stress in situations compatible with observational results (matter dominated evolution with a transition towards a state with $w \ll -1/3$).

1.5.2.2 Balancing multiple degrees of freedom

In models with multiple degrees of freedom it is at least in principle possible to balance the contributions in order to achieve a net vanishing π. [782] explicitly study the case of $f(R, G)$ gravity (please refer to this paper for details). The general equation,

$$\Phi - \Psi = \frac{1}{F}\left[\delta F + 4H\dot{\xi}\Psi - 4\ddot{\xi}\Phi + 4\left(H^2 + \dot{H}\right)\delta\xi\right], \tag{1.5.9}$$

is rather complicated, and generically depends, e.g., on scale of the perturbations (except for ξ constant, which in turn requires F constant for $\pi = 0$ and corresponds again to the GR limit). Looking only at small scales, $k \gg aH$, one finds

$$f_{RR} + 16(H^2 + \dot{H})(H^2 + 2\dot{H})f_{GG} + 4(2H^2 + 3\dot{H})f_{RG} = 0\,. \tag{1.5.10}$$

It is in principle possible to find simultaneous solutions of this equation and the modified Friedmann (0-0 Einstein) equation, for a given $H(t)$. As an example, the model $f(R, G) = R + G^n R^m$ with

$$n = \frac{1}{90}\left(11 \pm \sqrt{41}\right), \quad m = \frac{1}{180}\left(61 \pm 11\sqrt{41}\right) \tag{1.5.11}$$

allows for matter dominated evolution, $H = 2/(3t)$, and has no anisotropic stress. It is however not clear at all how to connect this model to different epochs and especially how to move towards a future accelerated epoch with $\pi = 0$ as the above exponents are fine-tuned to produce no anisotropic stress specifically only during matter domination. Additionally, during the transition to a de Sitter fixed point one encounters generically severe instabilities.

In summary, none of the standard examples with a single extra degree of freedom discussed above allows for a viable model with $\pi = 0$. While finely balanced solutions can be constructed for models with several degrees of freedom, one would need to link the motion in model space to

the evolution of the universe, in order to preserve $\pi = 0$. This requires even more fine tuning, and in some cases is not possible at all, most notably for evolution to a de Sitter state. The effective anisotropic stress appears therefore to be a very good quantity to look at when searching for generic conclusions on the nature of the accelerated expansion from cosmological observations.

1.5.3 Parameterized frameworks for theories of modified gravity

As explained in earlier sections of this report, modified-gravity models cannot be distinguished from dark-energy models by using solely the FLRW background equations. But by comparing the background expansion rate of the universe with observables that depend on linear perturbations of an FRW spacetime we can hope to distinguish between these two categories of explanations. An efficient way to do this is via a parameterized, model-independent framework that describes cosmological perturbation theory in modified gravity. We present here one such framework, the parameterized post-Friedmann formalism [73][3] that implements possible extensions to the linearized gravitational field equations.

The parameterized post-Friedmann approach (PPF) is inspired by the parameterized post-Newtonian (PPN) formalism [961, 960], which uses a set of parameters to summarize leading-order deviations from the metric of GR. PPN was developed in the 1970s for the purpose of testing of alternative gravity theories in the solar system or binary systems, and is valid in weak-field, low-velocity scenarios. PPN itself cannot be applied to cosmology, because we do not know the exact form of the linearized metric for our Hubble volume. Furthermore, PPN can only test for constant deviations from GR, whereas the cosmological data we collect contain inherent redshift dependence.

For these reasons the PPF framework is a parameterization of the gravitational field equations (instead of the metric) in terms of a set of functions of redshift. A theory of modified gravity can be analytically mapped onto these PPF functions, which in turn can be constrained by data.

We begin by writing the perturbed Einstein field equations for spin-0 (scalar) perturbations in the form:

$$\delta G_{\mu\nu} \;=\; 8\pi G\,\delta T_{\mu\nu} + \delta U_{\mu\nu}^{\rm metric} + \delta U_{\mu\nu}^{\rm d.o.f} + \text{ gauge invariance fixing terms}\,, \tag{1.5.12}$$

where $\delta T_{\mu\nu}$ is the usual perturbed stress-energy tensor of all cosmologically-relevant fluids. The tensor $\delta U_{\mu\nu}^{\rm metric}$ holds new terms that may appear in a modified theory, containing perturbations of the metric (in GR such perturbations are entirely accounted for by $\delta G_{\mu\nu}$). $\delta U_{\mu\nu}^{\rm d.o.f.}$ holds perturbations of any new degrees of freedom that are introduced by modifications to gravity. A simple example of the latter is a new scalar field, such as introduced by scalar-tensor or Galileon theories. However, new degrees of freedom could also come from spin-0 perturbations of new tensor or vector fields, Stückelberg fields, effective fluids and actions based on curvature invariants (such as $f\,(R)$ gravity).

In principle there could also be new terms containing matter perturbations on the RHS of Eq. (1.5.12). However, for theories that maintain the weak equivalence principle – i.e., those with a Jordan frame where matter is uncoupled to any new fields – these matter terms can be eliminated in favor of additional contributions to $\delta U_{\mu\nu}^{\rm metric}$ and $\delta U_{\mu\nu}^{\rm d.o.f.}$.

The tensor $\delta U_{\mu\nu}^{\rm metric}$ is then expanded in terms of two gauge-invariant perturbation variables $\hat{\Phi}$ and $\hat{\Gamma}$. $\hat{\Phi}$ is one of the standard gauge-invariant Bardeen potentials, while $\hat{\Gamma}$ is the following combination of the Bardeen potentials: $\hat{\Gamma} = 1/k(\dot{\hat{\Phi}} + \mathcal{H}\hat{\Psi})$. We use $\hat{\Gamma}$ instead of the usual Bardeen potential $\hat{\Psi}$ because $\hat{\Gamma}$ has the same derivative order as $\hat{\Phi}$ (whereas $\hat{\Psi}$ does not). We then deduce that the only possible structure of $\delta U_{\mu\nu}^{\rm metric}$ that maintains the gauge-invariance of the field

[3] Not to be confused with a different formalism of the same name by other authors [457].

equations is a linear combination of $\hat{\Phi}$, $\hat{\Gamma}$ and their derivatives, multiplied by functions of the cosmological background (see Eqs. (1.5.13) – (1.5.17) below).

$\delta U^{\rm d.o.f.}_{\mu\nu}$ is similarly expanded in a set of gauge-invariant potentials $\{\hat{\chi}_i\}$ that contain the new degrees of freedom. [73] presented an algorithm for constructing the relevant gauge-invariant quantities in any theory.

For concreteness we will consider here a theory that contains only one new degree of freedom and is second-order in its equations of motion (a generic but not watertight requirement for stability, see [967]). Then the four components of Eq. (1.5.12) are:

$$-a^2\delta G^0_0 = 8\pi a^2 G\,\rho_M\delta_M + A_0k^2\hat{\Phi} + F_0k^2\hat{\Gamma} + \alpha_0k^2\hat{\chi} + \alpha_1k\dot{\hat{\chi}} + k^3M_\Delta(\dot{\nu}+2\epsilon) \tag{1.5.13}$$

$$-a^2\delta G^0_i = \nabla_i\left[8\pi a^2 G\,\rho_M(1+\omega_M)\theta_M + B_0k\hat{\Phi} + I_0k\hat{\Gamma} + \beta_0k\hat{\chi} + \beta_1\dot{\hat{\chi}} + k^2M_\Theta(\dot{\nu}+2\epsilon)\right] \tag{1.5.14}$$

$$a^2\delta G^i_i = 3\,8\pi a^2 G\,\rho_M\Pi_M + C_0k^2\hat{\Phi} + C_1k\dot{\hat{\Phi}} + J_0k^2\hat{\Gamma} + J_1k\dot{\hat{\Gamma}} + \gamma_0k^2\hat{\chi} + \gamma_1k\dot{\hat{\chi}} + \gamma_2\ddot{\hat{\chi}} \tag{1.5.15}$$

$$+ k^3M_P(\dot{\nu}+2\epsilon) \tag{1.5.16}$$

$$a^2\delta\hat{G}^i_j = 8\pi a^2 G\,\rho_M(1+\omega_M)\Sigma_M + D_0\hat{\Phi} + \frac{D_1}{k}\dot{\hat{\Phi}} + K_0\hat{\Gamma} + \frac{K_1}{k}\dot{\hat{\Gamma}} + \epsilon_0\hat{\chi} + \frac{\epsilon_1}{k}\dot{\hat{\chi}} + \frac{\epsilon_2}{k^2}\ddot{\hat{\chi}} \tag{1.5.17}$$

where $\delta\hat{G}^i_j = \delta G^i_j - \frac{\delta^i_j}{3}\delta G^k_k$. Each of the lettered coefficients in Eqs. (1.5.13) – (1.5.17) is a function of cosmological background quantities, i.e., functions of time or redshift; this dependence has been suppressed above for clarity. Potentially the coefficients could also depend on scale, but this dependence is not arbitrary [832]). These PPF coefficients are the analogy of the PPN parameters; they are the objects that a particular theory of gravity 'maps onto', and the quantities to be constrained by data. Numerous examples of the PPF coefficients corresponding to well-known theories are given in [73].

The final terms in Eqs. (1.5.13) – (1.5.16) are present to ensure the gauge invariance of the modified field equations, as is required for any theory governed by a covariant action. The quantities M_Δ, M_Θ and M_P are all pre-determined functions of the background. ϵ and ν are off-diagonal metric perturbations, so these terms vanish in the conformal Newtonian gauge. The gauge-fixing terms should be regarded as a piece of mathematical book-keeping; there is no constrainable freedom associated with them.

One can then calculate observable quantities – such as the weak lensing kernel or the growth rate of structure $f(z)$ – using the parameterized field equations (1.5.13) – (1.5.17). Similarly, they can be implemented in an Einstein–Boltzmann solver code such as CAMB [559] to utilize constraints from the CMB. If we take the divergence of the gravitational field equations (i.e., the unperturbed equivalent of Eq. (1.5.12)), the left-hand side vanishes due to the Bianchi identity, while the stress-energy tensor of matter obeys its standard conservation equations (since we are working in the Jordan frame). Hence the U-tensor must be separately conserved, and this provides the necessary evolution equation for the variable $\hat{\chi}$:

$$\delta\left(\nabla^\mu\left[U^{\rm metric}_{\mu\nu} + U^{\rm d.o.f.}_{\mu\nu}\right]\right) = 0. \tag{1.5.18}$$

Eq. (1.5.18) has two components. If one wishes to treat theories with more than two new degrees of freedom, further information is needed to supplement the PPF framework.

The full form of the parameterized equations (1.5.13) – (1.5.17) can be simplified in the 'quasistatic regime', that is, significantly sub-horizon scales on which the time derivatives of perturbations can be neglected in comparison to their spatial derivatives [457]. Quasistatic lengthscales are the relevant stage for weak lensing surveys and galaxy redshift surveys such as those of Euclid. A

common parameterization used on these scales has the form:

$$2\nabla^2\Phi = 8\pi a^2 G\,\mu(a,k)\,\bar{\rho}_M\Delta_M, \tag{1.5.19}$$

$$\frac{\Phi}{\Psi} = \gamma(a,k), \tag{1.5.20}$$

where $\{\mu,\gamma\}$ are two functions of time and scale to be constrained. This parameterization has been widely employed [131, 277, 587, 115, 737, 980, 320, 441, 442]. It has the advantages of simplicity and somewhat greater physical transparency: $\mu(a,k)$ can be regarded as describing evolution of the effective gravitational constant, while $\gamma(a,k)$ can, to a certain extent, be thought of as acting like a source of anisotropic stress (see Section 1.5.2).

Let us make a comment about the number of coefficient functions employed in the PPF formalism. One may justifiably question whether the number of unknown functions in Eqs. (1.5.13) – (1.5.17) could ever be constrained. In reality, the PPF coefficients are not all independent. The form shown above represents a fully agnostic description of the extended field equations. However, as one begins to impose restrictions in theory space (even the simple requirement that the modified field equations must originate from a covariant action), constraint relations between the PPF coefficients begin to emerge. These constraints remove freedom from the parameterization.

Even so, degeneracies will exist between the PPF coefficients. It is likely that a subset of them can be well-constrained, while another subset have relatively little impact on current observables and so cannot be tested. In this case it is justifiable to drop the untestable terms. Note that this realization, in itself, would be an interesting statement – that there are parts of the gravitational field equations that are essentially unknowable.

Finally, we note that there is also a completely different, complementary approach to parameterizing modifications to gravity. Instead of parameterizing the linearized field equations, one could choose to parameterize the perturbed gravitational action. This approach has been used recently to apply the standard techniques of effective field theory to modified gravity; see [107, 142, 411] and references therein.

1.6 Nonlinear aspects

In this section we discuss how the nonlinear evolution of cosmic structures in the context of different non-standard cosmological models can be studied by means of numerical simulations based on N-body algorithms and of analytical approaches based on the spherical collapse model.

1.6.1 *N*-body simulations of dark energy and modified gravity

Here we discuss the numerical methods presently available for this type of analyses, and we review the main results obtained so far for different classes of alternative cosmologies. These can be grouped into models where structure formation is affected only through a modified expansion history (such as quintessence and early dark-energy models, Section 1.4.1) and models where particles experience modified gravitational forces, either for individual particle species (interacting dark-energy models and growing neutrino models, Section 1.4.4.4) or for all types of particles in the universe (modified gravity models).

1.6.1.1 Quintessence and early dark-energy models

In general, in the context of flat FLRW cosmologies, any dynamical evolution of the dark-energy density ($\rho_{\rm DE} \neq$ const. $= \rho_\Lambda$) determines a modification of the cosmic expansion history with respect to the standard ΛCDM cosmology. In other words, if the dark energy is a dynamical quantity, i.e.,

if its equation of state parameter $w \neq -1$ exactly, for any given set of cosmological parameters (H_0, $\Omega_{\rm CDM}$, $\Omega_{\rm b}$, $\Omega_{\rm DE}$, $\Omega_{\rm rad}$), the redshift evolution of the Hubble function $H(z)$ will differ from the standard ΛCDM case $H_\Lambda(z)$.

Quintessence models of dark energy [954, 754] based on a classical scalar field ϕ subject to a self-interaction potential $V(\phi)$ have an energy density $\rho_\phi \equiv \dot\phi^2/2 + V(\phi)$ that evolves in time according to the dynamical evolution of the scalar field, which is governed by the homogeneous Klein–Gordon equation:

$$\ddot\phi + 3H\dot\phi + \frac{{\rm d}V}{{\rm d}\phi} = 0\,. \tag{1.6.1}$$

Here the dot denotes derivation w.r.t. ordinary time t.

For a canonical scalar field, the equation of state parameter $w_\phi \equiv \rho_\phi/p_\phi$, where $p_\phi \equiv \dot\phi^2/2 - V(\phi)$, will in general be larger than -1, and the density of dark energy ρ_ϕ will consequently be larger than ρ_Λ at any redshift $z > 0$. Furthermore, for some simple choices of the potential function such as those discussed in Section 1.4.1 (e.g., an exponential potential $V \propto \exp(-\alpha\phi/M_{\rm Pl})$ or an inverse-power potential $V \propto (\phi/M_{\rm Pl})^{-\alpha}$), scaling solutions for the evolution of the system can be analytically derived. In particular, for an exponential potential, a scaling solution exists where the dark energy scales as the dominant cosmic component, with a fractional energy density

$$\Omega_\phi \equiv \frac{8\pi G\rho_\phi}{3H^2} = \frac{n}{\alpha^2}\,, \tag{1.6.2}$$

with $n = 3$ for matter domination and $n = 4$ for radiation domination. This corresponds to a relative fraction of dark energy at high redshifts, which is in general not negligible, whereas during matter and radiation domination $\Omega_\Lambda \sim 0$ and, therefore, represents a phenomenon of an early emergence of dark energy as compared to ΛCDM where dark energy is for all purposes negligible until $z \sim 1$.

Early dark energy (EDE) is, therefore, a common prediction of scalar field models of dark energy, and observational constraints put firm bounds on the allowed range of Ω_ϕ at early times, and consequently on the potential slope α.

As we have seen in Section 1.2.1, a completely phenomenological parametrization of EDE, independent from any specific model of dynamical dark energy has been proposed by [956] as a function of the present dark-energy density $\Omega_{\rm DE}$, its value at early times $\Omega_{\rm EDE}$, and the present value of the equation of state parameter w_0. From Eq. 1.2.4, the full expansion history of the corresponding EDE model can be derived.

A modification of the expansion history indirectly influences also the growth of density perturbations and ultimately the formation of cosmic structures. While this effect can be investigated analytically for the linear regime, N-body simulations are required to extend the analysis to the nonlinear stages of structure formation. For standard Quintessence and EDE models, the only modification that is necessary to implement into standard N-body algorithms is the computation of the correct Hubble function $H(z)$ for the specific model under investigation, since this is the only way in which these non standard cosmological models can alter structure formation processes.

This has been done by the independent studies of [406] and [367], where a modified expansion history consistent with EDE models described by the parametrization of Eq. 1.2.4 has been implemented in the widely used N-body code GADGET-2 [857] and the properties of nonlinear structures forming in these EDE cosmologies have been analyzed. Both studies have shown that the standard formalism for the computation of the halo mass function still holds for EDE models at $z = 0$. In other words, both the standard fitting formulae for the number density of collapsed objects as a function of mass, and their key parameter $\delta_c = 1.686$ representing the linear overdensity at collapse for a spherical density perturbation, remain unchanged also for EDE cosmologies.

The work of [406], however, investigated also the internal properties of collapsed halos in EDE models, finding a slight increase of halo concentrations due to the earlier onset of structure forma-

tion and most importantly a significant increment of the line-of-sight velocity dispersion of massive halos. The latter effect could mimic a higher σ_8 normalization for cluster mass estimates based on galaxy velocity dispersion measurements and, therefore, represents a potentially detectable signature of EDE models.

1.6.1.2 Interacting dark-energy models

Another interesting class of non standard dark-energy models, as introduced in Section 1.4.4, is given by coupled dark energy where a direct interaction is present between a Quintessence scalar field ϕ and other cosmic components, in the form of a source term in the background continuity equations:

$$\frac{\mathrm{d}\rho_\phi}{\mathrm{d}\eta} = -3\mathcal{H}(1+w_\phi)\rho_\phi + \beta(\phi)\frac{\mathrm{d}\phi}{\mathrm{d}\eta}(1-3w_\alpha)\rho_\alpha\,, \tag{1.6.3}$$

$$\frac{\mathrm{d}\rho_\alpha}{\mathrm{d}\eta} = -3\mathcal{H}(1+w_\alpha)\rho_\alpha - \beta(\phi)\frac{\mathrm{d}\phi}{\mathrm{d}\eta}(1-3w_\alpha)\rho_\alpha\,, \tag{1.6.4}$$

where α represents a single cosmic fluid coupled to ϕ.

While such direct interaction with baryonic particles ($\alpha = b$) is tightly constrained by observational bounds, and while it is suppressed for relativistic particles ($\alpha = r$) by symmetry reasons ($1 - 3w_r = 0$), a selective interaction with cold dark matter (CDM hereafter) or with massive neutrinos is still observationally viable (see Section 1.4.4).

Since the details of interacting dark-energy models have been discussed in Section 1.4.4, here we simply recall the main features of these models that have a direct relevance for nonlinear structure formation studies. For the case of interacting dark energy, in fact, the situation is much more complicated than for the simple EDE scenario discussed above. The mass of a coupled particle changes in time due to the energy exchange with the dark-energy scalar field ϕ according to the equation:

$$m(\phi) = m_0 e^{-\int \beta(\phi')\,\mathrm{d}\phi'} \tag{1.6.5}$$

where m_0 is the mass at $z = 0$. Furthermore, the Newtonian acceleration of a coupled particle (subscript c) gets modified as:

$$\dot{\vec{v}}_c = -\tilde{H}\vec{v}_c - \vec{\nabla}\tilde{\Phi}_c - \vec{\nabla}\Phi_{nc}\,. \tag{1.6.6}$$

where $\tilde{H}$ contains a new velocity-dependent acceleration:

$$\tilde{H}\vec{v}_c = H\left(1 - \beta_\phi\frac{\dot{\phi}}{H}\right)\vec{v}_c\,, \tag{1.6.7}$$

and where a fifth-force acts only between coupled particles as

$$\tilde{\Phi}_c = (1+2\beta^2)\Phi_c\,, \tag{1.6.8}$$

while Φ_{nc} represents the gravitational potential due to all massive particles with no coupling to the dark energy that exert a standard gravitational pull.

As a consequence of these new terms in the Newtonian acceleration equation the growth of density perturbations will be affected, in interacting dark-energy models, not only by the different Hubble expansion due to the dynamical nature of dark energy, but also by a direct modification of the effective gravitational interactions at subhorizon scales. Therefore, linear perturbations of coupled species will grow with a higher rate in these cosmologies In particular, for the case of a coupling to CDM, a different amplitude of the matter power spectrum will be reached at $z = 0$ with respect to ΛCDM if a normalization in accordance with CMB measurements at high redshifts is assumed.

Clearly, the new acceleration equation (1.6.6) will have an influence also on the formation and evolution of nonlinear structures, and a consistent implementation of all the above mentioned effects into an N-body algorithm is required in order to investigate this regime.

For the case of a coupling to CDM (a coupling with neutrinos will be discussed in the next section) this has been done, e.g., by [604, 870] with 1D or 3D grid-based field solvers, and more recently by means of a suitable modification by [79] of the TreePM hydrodynamic N-body code GADGET-2 [857].

Nonlinear evolution within coupled quintessence cosmologies has been addressed using various methods of investigation, such as spherical collapse [611, 962, 618, 518, 870, 3, 129] and alternative semi-analytic methods [787, 45]. N-body and hydro-simulations have also been done [604, 79, 76, 77, 80, 565, 562, 75, 980]. We list here briefly the main observable features typical of this class of models:

- The suppression of power at small scales in the power spectrum of interacting dark-energy models as compared to ΛCDM;
- The development of a gravitational bias in the amplitude of density perturbations of uncoupled baryons and coupled CDM particles defined as $P_b(k)/P_c(k) < 1$, which determines a significant decrease of the baryonic content of massive halos at low redshifts in accordance with a large number of observations [79, 75];
- The increase of the number density of high-mass objects at any redshift as compared to ΛCDM [see 77];
- An enhanced ISW effect [33, 35, 612]; such effects may be partially reduced when taking into account nonlinearities, as described in [727];
- A less steep inner core halo profiles (depending on the interplay between fifth force and velocity-dependent terms) [79, 76, 565, 562, 75];
- A lower concentration of the halos [79, 76, 562];
- Voids are emptier when a coupling is active [80].

Subsequent studies based on Adaptive Mesh Refinement schemes for the solution of the local scalar field equation [561] have broadly confirmed these results.

The analysis has been extended to the case of non-constant coupling functions $\beta(\phi)$ by [76], and has shown how in the presence of a time evolution of the coupling some of the above mentioned results no longer hold:

- Small scale power can be both suppressed and enhanced when a growing coupling function is considered, depending on the magnitude of the coupling time derivative $\mathrm{d}\beta(\phi)/\mathrm{d}\phi$
- The inner overdensity of CDM halos, and consequently the halo concentrations, can both decrease (as always happens for the case of constant couplings) or increase, again depending on the rate of change of the coupling strength;

All these effects represent characteristic features of interacting dark-energy models and could provide a direct way to observationally test these scenarios. Higher resolution studies would be required in order to quantify the impact of a DE-CDM interaction on the statistical properties of halo substructures and on the redshift evolution of the internal properties of CDM halos.

As discussed in Section 1.6.1, when a variable coupling $\beta(\phi)$ is active the relative balance of the fifth-force and other dynamical effects depends on the specific time evolution of the coupling

strength. Under such conditions, certain cases may also lead to the opposite effect of larger halo inner overdensities and higher concentrations, as in the case of a steeply growing coupling function [see 76]. Alternatively, the coupling can be introduced by choosing directly a covariant stress-energy tensor, treating dark energy as a fluid in the absence of a starting action [619, 916, 193, 794, 915, 613, 387, 192, 388].

1.6.1.3 Growing neutrinos

In case of a coupling between the dark-energy scalar field ϕ and the relic fraction of massive neutrinos, all the above basic equations (1.6.5) – (1.6.8) still hold. However, such models are found to be cosmologically viable only for large negative values of the coupling β [as shown by 36], that according to Eq. 1.6.5 determines a neutrino mass that grows in time (from which these models have been dubbed "growing neutrinos"). An exponential growth of the neutrino mass implies that cosmological bounds on the neutrino mass are no longer applicable and that neutrinos remain relativistic much longer than in the standard scenario, which keeps them effectively uncoupled until recent epochs, according to Eqs. (1.6.3 and 1.6.4). However, as soon as neutrinos become non-relativistic at redshift $z_{\rm nr}$ due to the exponential growth of their mass, the pressure terms $1 - 3w_\nu$ in Eqs. (1.6.3 and 1.6.4) no longer vanish and the coupling with the DE scalar field ϕ becomes active.

Therefore, while before $z_{\rm nr}$ the model behaves as a standard ΛCDM scenario, after $z_{\rm nr}$ the non-relativistic massive neutrinos obey the modified Newtonian equation (1.6.6) and a fast growth of neutrino density perturbation takes place due to the strong fifth force described by Eq. (1.6.8).

The growth of neutrino overdensities in the context of growing neutrinos models has been studied in the linear regime by [668], predicting the formation of very large neutrino lumps at the scale of superclusters and above (10 – 100 Mpc/h) at redshift $z \approx 1$.

The analysis has been extended to the nonlinear regime in [963] by following the spherical collapse of a neutrino lump in the context of growing neutrino cosmologies. This study has witnessed the onset of virialization processes in the nonlinear evolution of the neutrino halo at $z \approx 1.3$, and provided a first estimate of the associated gravitational potential at virialization being of the order of $\Phi_\nu \approx 10^{-6}$ for a neutrino lump with radius $R \approx 15$ Mpc.

An estimate of the potential impact of such very large nonlinear structures onto the CMB angular power spectrum through the Integrated Sachs–Wolfe effect has been attempted by [727]. This study has shown that the linear approximation fails in predicting the global impact of the model on CMB anisotropies at low multipoles, and that the effects under consideration are very sensitive to the details of the transition between the linear and nonlinear regimes and of the virialization processes of nonlinear neutrino lumps, and that also significantly depend on possible backreaction effects of the evolved neutrino density field onto the local scalar filed evolution.

A full nonlinear treatment by means of specifically designed N-body simulations is, therefore, required in order to follow in further detail the evolution of a cosmological sample of neutrino lumps beyond virialization, and to assess the impact of growing neutrinos models onto potentially observable quantities as the low-multipoles CMB power spectrum or the statistical properties of CDM large scale structures.

1.6.1.4 Modified gravity

Modified gravity models, presented in Section 1.4, represent a different perspective to account for the nature of the dark components of the universe. Although most of the viable modifications of GR are constructed in order to provide an identical cosmic expansion history to the standard ΛCDM model, their effects on the growth of density perturbations could lead to observationally testable predictions capable of distinguishing modified gravity models from standard GR plus a cosmological constant.

Since a modification of the theory of gravity would affect all test masses in the universe, i.e., including the standard baryonic matter, an asymptotic recovery of GR for solar system environments, where deviations from GR are tightly constrained, is required for all viable modified gravity models. Such mechanism, often referred to as the "Chameleon effect", represents the main difference between modified gravity models and the interacting dark-energy scenarios discussed above, by determining a local dependence of the modified gravitational laws in the Newtonian limit.

While the linear growth of density perturbations in the context of modified gravity theories can be studied [see, e.g., 456, 674, 32, 54] by parametrizing the scale dependence of the modified Poisson and Euler equations in Fourier space (see the discussion in Section 1.3), the nonlinear evolution of the "Chameleon effect" makes the implementation of these theories into nonlinear N-body algorithms much more challenging. For this reason, very little work has been done so far in this direction. A few attempts to solve the modified gravity interactions in the nonlinear regime by means of mesh-based iterative relaxation schemes have been carried out by [700, 701, 800, 500, 981, 281, 964] and showed an enhancement of the power spectrum amplitude at intermediate and small scales. These studies also showed that this nonlinear enhancement of small scale power cannot be accurately reproduced by applying the linear perturbed equations of each specific modified gravity theory to the standard nonlinear fitting formulae [as, e.g., 844].

Higher resolution simulations and new numerical approaches will be necessary in order to extend these first results to smaller scales and to accurately evaluate the deviations of specific models of modified gravity from the standard GR predictions to a potentially detectable precision level.

1.6.2 The spherical collapse model

A popular analytical approach to study nonlinear clustering of dark matter without recurring to N-body simulations is the spherical collapse model, first studied by [413]. In this approach, one studies the collapse of a spherical overdensity and determines its critical overdensity for collapse as a function of redshift. Combining this information with the extended Press–Schechter theory ([743, 147]; see [976] for a review) one can provide a statistical model for the formation of structures which allows to predict the abundance of virialized objects as a function of their mass. Although it fails to match the details of N-body simulations, this simple model works surprisingly well and can give useful insigths into the physics of structure formation. Improved models accounting for the complexity of the collapse exist in the literature and offer a better fit to numerical simulations. For instance, [823] showed that a significant improvement can be obtained by considering an ellipsoidal collapse model. Furthermore, recent theoretical developments and new improvements in the excursion set theory have been undertaken by [609] and other authors (see e.g., [821]).

The spherical collapse model has been generalized to include a cosmological constant by [718, 948]. [540] have used it to study the observational consequences of a cosmological constant on the growth of perturbations. The case of standard quintessence, with speed of sound $c_s = 1$, have been studied by [937]. In this case, scalar fluctuations propagate at the speed of light and sound waves maintain quintessence homogeneous on scales smaller than the horizon scale. In the spherical collapse pressure gradients maintain the same energy density of quintessence between the inner and outer part of the spherical overdensity, so that the evolution of the overdensity radius is described by

$$\frac{\ddot{R}}{R} = -\frac{4\pi G}{3}(\rho_m + \bar{\rho}_Q + 3\bar{p}_Q)\,, \tag{1.6.9}$$

where ρ_m denotes the energy density of dark matter while $\bar{\rho}_Q$ and $\bar{p}_Q$ denote the homogeneous energy density and pressure of the quintessence field. Note that, although this equation looks like one of the Friedmann equations, the dynamics of R is not the same as for a FLRW universe. Indeed, ρ_m evolves following the scale factor R, while the quintessence follows the external scale factor a, according to the continuity equation $\dot{\bar{\rho}}_Q + 3(\dot{a}/a)(\bar{\rho}_Q + \bar{p}_Q) = 0$.

In the following we will discuss the spherical collapse model in the contest of other dark energy and modified gravity models.

1.6.2.1 Clustering dark energy

In its standard version, quintessence is described by a minimally-coupled canonical field, with speed of sound $c_s = 1$. As mentioned above, in this case clustering can only take place on scales larger than the horizon, where sound waves have no time to propagate. However, observations on such large scales are strongly limited by cosmic variance and this effect is difficult to observe. A minimally-coupled scalar field with fluctuations characterized by a practically zero speed of sound can cluster on all observable scales. There are several theoretical motivations to consider this case. In the limit of zero sound speed one recovers the Ghost Condensate theory proposed by [56] in the context of modification of gravity, which is invariant under shift symmetry of the field $\phi \to \phi +$ constant. Thus, there is no fine tuning in assuming that the speed of sound is very small: quintessence models with vanishing speed of sound should be thought of as deformations of this particular limit where shift symmetry is recovered. Moreover, it has been shown that minimally-coupled quintessence with an equation of state $w < -1$ can be free from ghosts and gradient instabilities only if the speed of sound is very tiny, $|c_s| \lesssim 10^{-15}$. Stability can be guaranteed by the presence of higher derivative operators, although their effect is absent on cosmologically relevant scales [260, 228, 259].

The fact that the speed of sound of quintessence may vanish opens up new observational consequences. Indeed, the absence of quintessence pressure gradients allows instabilities to develop on all scales, also on scales where dark matter perturbations become nonlinear. Thus, we expect quintessence to modify the growth history of dark matter not only through its different background evolution but also by actively participating to the structure formation mechanism, in the linear and nonlinear regime, and by contributing to the total mass of virialized halos.

Following [258], in the limit of zero sound speed pressure gradients are negligible and, as long as the fluid approximation is valid, quintessence follows geodesics remaining comoving with the dark matter (see also [574] for a more recent model with identical phenomenology). In particular, one can study the effect of quintessence with vanishing sound speed on the structure formation in the nonlinear regime, in the context of the spherical collapse model. The zero speed of sound limit represents the natural counterpart of the opposite case $c_s = 1$. Indeed, in both cases there are no characteristic length scales associated with the quintessence clustering and the spherical collapse remains independent of the size of the object (see [95, 671, 692] for a study of the spherical collapse when c_s of quintessence is small but finite).

Due to the absence of pressure gradients quintessence follows dark matter in the collapse and the evolution of the overdensity radius is described by

$$\frac{\ddot{R}}{R} = -\frac{4\pi G}{3}(\rho_m + \rho_Q + \bar{p}_Q)\,, \tag{1.6.10}$$

where the energy density of quintessence ρ_Q has now a different value inside and outside the overdensity, while the pressure remains unperturbed. In this case the quintessence inside the overdensity evolves following the internal scale factor R, $\dot{\rho}_Q + 3(\dot{R}/R)(\rho_Q + \bar{p}_Q) = 0$ and the comoving regions behave as closed FLRW universes. R satisfies the Friedmann equation and the spherical collapse can be solved exactly [258].

Quintessence with zero speed of sound modifies dark matter clustering with respect to the smooth quintessence case through the linear growth function and the linear threshold for collapse. Indeed, for $w > -1$ ($w < -1$), it enhances (diminishes) the clustering of dark matter, the effect being proportional to $1 + w$. The modifications to the critical threshold of collapse are small and the effects on the dark matter mass function are dominated by the modification on the linear

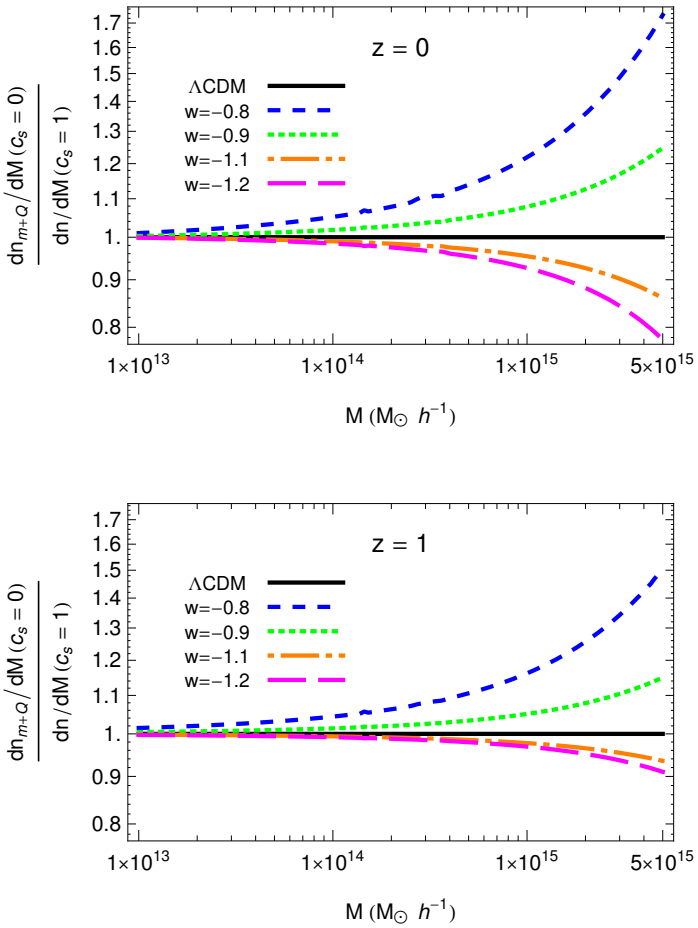

Figure 5: Ratio of the total mass functions, which include the quintessence contribution, for $c_s = 0$ and $c_s = 1$ at $z = 0$ (above) and $z = 1$ (below). Image reproduced by permission from [258]; copyright by IOP and SISSA.

dark matter growth function. Besides these conventional effects there is a more important and qualitatively new phenomenon: quintessence mass adds to the one of dark matter, contributing to the halo mass by a fraction of order $\sim (1+w)\Omega_Q/\Omega_m$. Importantly, it is possible to show that the mass associated with quintessence stays constant inside the virialized object, independently of the details of virialization. Moreover ,the ratio between the virialization and the turn-around radii is approximately the same as the one for ΛCDM computed by [540]. In Figure 5 we plot the ratio of the mass function including the quintessence mass contribution, for the $c_s = 0$ case to the smooth $c_s = 1$ case. The sum of the two effects is rather large: for values of w still compatible with the present data and for large masses the difference between the predictions of the $c_s = 0$ and the $c_s = 1$ cases is of order one.

1.6.2.2 Coupled dark energy

We now consider spherical collapse within coupled dark-energy cosmologies. The presence of an interaction that couples the cosmon dynamics to another species introduces a new force acting between particles (CDM or neutrinos in the examples mentioned in Section 1.4.4) and mediated by dark-energy fluctuations. Whenever such a coupling is active, spherical collapse, whose concept is intrinsically based on gravitational attraction via the Friedmann equations, has to be suitably modified in order to account for other external forces. As shown in [962] the inclusion of the fifth force within the spherical collapse picture deserves particular caution. Here we summarize the main results on this topic and we refer to [962] for a detailed illustration of spherical collapse in presence of a fifth force.

If CDM is coupled to a quintessence scalar field as described in Sections 1.4.4 and 2.11 of the present document, the full nonlinear evolution equations within the Newtonian limit read:

$$\dot{\delta}_m = -\mathbf{v}_m \nabla\delta_m - (1+\delta_m)\,\nabla\cdot\mathbf{v}_m \tag{1.6.11}$$

$$\dot{\mathbf{v}}_m = -(2\bar{H} - \beta\,\dot{\bar{\phi}})\,\mathbf{v}_m - (\mathbf{v}_m\nabla)\mathbf{v}_m - a^{-2}\,\nabla(\Phi - \beta\,\delta\phi) \tag{1.6.12}$$

$$\Delta\delta\phi = -\beta\,a^2\,\delta\rho_m \tag{1.6.13}$$

$$\Delta\Phi = -\frac{a^2}{2}\sum_\alpha \delta\rho_\alpha \tag{1.6.14}$$

These equations can be derived from the non-relativistic Navier–Stokes equations and from the Bianchi identities written in presence of an external source of the type:

$$\nabla_\gamma T^\gamma_\mu = Q_\mu = -\beta T^\gamma_\gamma \partial_\mu\phi\,, \tag{1.6.15}$$

where T^γ_μ is the stress energy tensor of the dark matter fluid and we are using comoving spatial coordinates $\mathbf{x}$ and cosmic time t. Note that $\mathbf{v}_m$ is the comoving velocity, related to the peculiar velocities by $\mathbf{v}_m = \mathbf{v}_{pec}/a$. They are valid for arbitrary quintessence potentials as long as the scalar field is sufficiently light, i.e., $m^2_\phi\delta\phi = V''(\phi)\delta\phi \ll \Delta\delta\phi$ for the scales under consideration. For a more detailed discussion see [962]. Combining the above equations yields to the following expression for the evolution of the matter perturbation δ_m:

$$\ddot{\delta}_m = -(2\bar{H} - \beta\,\dot{\bar{\phi}})\,\dot{\delta}_m + \frac{4}{3}\frac{\dot{\delta}^2_m}{1+\delta_m} + \frac{1+\delta_m}{a^2}\,\Delta\Phi_{\rm eff}\,, \tag{1.6.16}$$

Linearization leads to:

$$\ddot{\delta}_{m,L} = -(2\bar{H} - \beta\,\dot{\bar{\phi}})\,\dot{\delta}_{m,L} + a^{-2}\,\Delta\Phi_{\rm eff}\,. \tag{1.6.17}$$

where the effective gravitational potential follows the modified Poisson equation:

$$\Delta\Phi_{\rm eff} = -\frac{a^2}{2}\bar{\rho}_m\delta_m\left(1+2\beta^2\right) . \tag{1.6.18}$$

Eqs. (1.6.16) and (1.6.17) are the two main equations which correctly describe the nonlinear and linear evolution for a coupled dark-energy model. They can be used, among other things, for estimating the extrapolated linear density contrast at collapse δ_c in the presence of a fifth force. It is possible to reformulate Eqs. (1.6.16) and (1.6.17) into an effective spherical collapse:

$$\frac{\ddot{R}}{R} = -\beta\,\dot{\phi}\left(H-\frac{\dot{R}}{R}\right) - \frac{1}{6}\sum_\alpha\left[\rho_\alpha(1+3w_\alpha)\right] - \frac{1}{3}\,\beta^2\,\delta\rho_m\,. \tag{1.6.19}$$

Eq. (1.6.19) [611, 962], describes the general evolution of the radius of a spherical overdense region within coupled quintessence. Comparing with the standard case (1.6.9) we notice the presence of two additional terms: a 'friction' term and the coupling term $\beta^2\,\delta\rho_m$, the latter being responsible for the additional attractive fifth force. Note that the 'friction' term is actually velocity dependent and its effects on collapse depend, more realistically, on the direction of the velocity, information which is not contained within a *spherical* collapse picture and can be treated within simulations [77, 565, 76, 562, 75]. We stress that it is crucial to include these additional terms in the equations, as derived from the nonlinear equations, in order to correctly account for the presence of a fifth force. The outlined procedure can easily be generalized to include uncoupled components, for example baryons. In this case, the corresponding evolution equation for δ_b, will be fed by $\Phi_{\rm eff} = \Phi$. This yields an evolution equation for the uncoupled scale factor R_{uc} that is equivalent to the standard Friedmann equation. In Figure 6 we show the linear density contrast at collapse $\delta_c(z_c)$ for three coupled quintessence models with $\alpha = 0.1$ and $\beta = 0.05,\ 0.1,\ 0.15$.

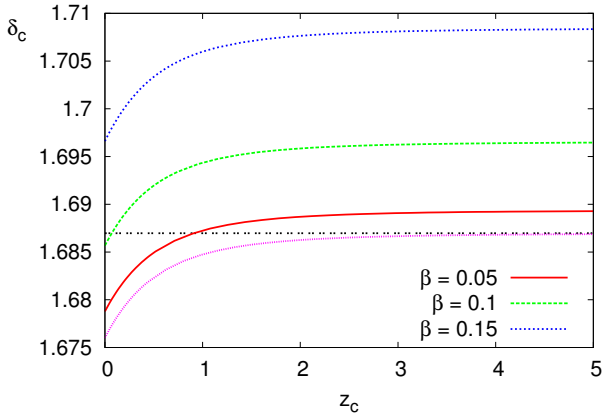

Figure 6: Extrapolated linear density contrast at collapse for coupled quintessence models with different coupling strength β. For all plots we use a constant $\alpha = 0.1$. We also depict δ_c for reference ΛCDM (dotted, pink) and EdS (double-dashed, black) models. Image reproduced by permission from [962]; copyright by APS.

An increase of β results in an increase of δ_c. As shown in [962], $\delta_c(\beta)$ is well described by a simple quadratic fitting formula,

$$\delta_c(\beta) = 1.686(1+a\beta^2)\,, a = 0.556\,, \tag{1.6.20}$$

valid for small $\beta \lesssim 0.4$ and $z_c \geq 5$. We recall that a nonlinear analysis beyond the spherical collapse method can be addressed by means of the time-renormalization-group method, extended to the case of couple quintessence in [787].

If a coupling between dark energy and neutrinos is present, as described in Sections 1.4.4 and 2.9, bound neutrino structures may form within these models [180]. It was shown in [668] that their formation will only start after neutrinos become non-relativistic. A nonlinear treatment of the evolution of neutrino densities is thus only required for very late times, and one may safely neglect neutrino pressure as compared to their density. The evolution equations (1.6.16) and (1.6.17) can then also be applied for the nonlinear and linear neutrino density contrast. The extrapolated linear density at collapse δ_c for growing neutrino quintessence reflects in all respects the characteristic features of this model and results in a δ_c which looks quite different from standard dark-energy cosmologies. We have plotted the dependence of δ_c on the collapse redshift z_c in Figure 7 for three values of the coupling. The oscillations seen are the result of the oscillations of the neutrino mass caused by the coupling to the scalar field: the latter has characteristic oscillations as it approaches the minimum of the effective potential in which it rolls, given by a combination of the self-interaction potential $U(\phi)$ and the coupling contribution $\beta(1-3w_\nu)\rho_\nu$. Furthermore, due to the strong coupling β, the average value of δ_c is found to be substantially higher than 1.686, corresponding to the Einstein de Sitter value, shown in black (double-dashed) in Figure 7. Such an effect can have a strong impact on structure formation and on CMB [727]. For the strongly coupled models, corresponding to a low present day neutrino mass $m_\nu(t_0)$, the critical density at collapse is only available for $z_c \lesssim 0.2$, 1 for $\beta = -560$, -112, respectively. This is again a reflection of the late transition to the non-relativistic regime. Nonlinear investigations of single lumps beyond the spherical collapse picture was performed in [963, 179], the latter showing the influence of the gravitational potentials induced by the neutrino inhomogeneities on the acoustic oscillations in the baryonic and dark-matter spectra.

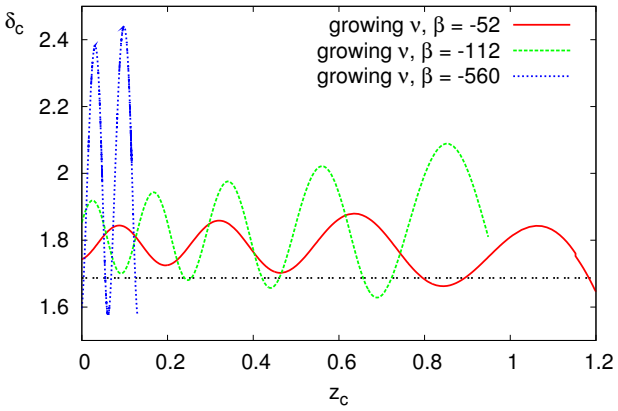

Figure 7: Extrapolated linear density contrast at collapse δ_c vs. collapse redshift z_c for growing neutrinos with $\beta = -52$ (solid, red), $\beta = -112$ (long-dashed, green) and $\beta = -560$ (short-dashed, blue). A reference EdS model (double-dashed. black) is also shown. Image reproduced by permission from [962]; copyright by APS.

1.6.2.3 Early dark energy

A convenient way to parametrize the presence of a nonnegligible homogeneous dark-energy component at early times was presented in [956] and has been illustrated in Section 1.2.1 of the present

review. If we specify the spherical collapse equations for this case, the nonlinear evolution of the density contrast follows the evolution equations (1.6.16) and (1.6.17) without the terms related to the coupling. As before, we assume relativistic components to remain homogeneous. In Figure 8 we show δ_c for two models of early dark energy, namely model I and II, corresponding to the choices $(\Omega_{m,0} = 0.332\,, \quad w_0 = -0.93\,, \quad \Omega_{\mathrm{DE},e} = 2 \cdot 10^{-4})$ and $(\Omega_{m,0} = 0.314\,, \quad w_0 = -0.99\,, \quad \Omega_{\mathrm{DE},e} = 8 \cdot 10^{-4})$ respectively. Results show $\delta_c(z_c = 5) \sim 1.685$ $(\sim 5 \cdot 10^{-2}\%)$ [368, 962].

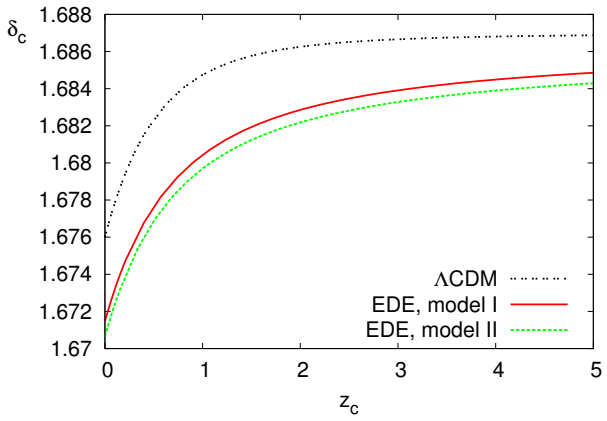

Figure 8: Extrapolated linear density contrast at collapse δ_c vs. collapse redshift z_c for EDE models I (solid, red) and II (long-dashed, green), as well as ΛCDM (double-dashed, black). Image reproduced by permission from [962]; copyright by APS.

1.7 Observational properties of dark energy and modified gravity

Both scalar field dark-energy models and modifications of gravity can in principle lead to any desired expansion history $H(z)$, or equivalently any evolution of the effective dark-energy equation of state parameter $w(z)$. For canonical scalar fields, this can be achieved by selecting the appropriate potential $V(\varphi)$ along the evolution of the scalar field $\varphi(t)$, as was done, e.g., in [102]. For modified gravity models, the same procedure can be followed for example for $f(R)$ type models [e.g. 736]. The evolution history on its own can thus not tell us very much about the physical nature of the mechanism behind the accelerated expansion (although of course a clear measurement showing that $w \neq -1$ would be a sensational discovery). A smoking gun for modifications of gravity can thus only appear at perturbation level.

In the next subsections we explore how dark energy or modified gravity effects can be detected through weak lensing and redshift surveys.

1.7.1 General remarks

Quite generally, cosmological observations fall into two categories: geometrical probes and structure formation probes. While the former provide a measurement of the Hubble function, the latter are a test of the gravitational theory in an almost Newtonian limit on subhorizon scales. Furthermore, possible effects on the geodesics of test particles need to be derived: naturally, photons follow null-geodesics while massive particles, which constitute the cosmic large-scale structure, move along geodesics for non-relativistic particles.

In some special cases, modified gravity models predict a strong deviation from the standard Friedmann equation as in, e.g., DGP, (1.4.74). While the Friedmann equation is not know explicitly in more general models of massive gravity (cascading gravity or hard mass gravity), similar modifications are expected to arise and provide characteristic features, [see, e.g., 11, 478]) that could distinguish these models from other scenarios of modified gravity or with additional dynamical degrees of freedom.

In general however the most interesting signatures of modified gravity models are to be found in the perturbation sector. For instance, in DGP, growth functions differ from those in dark-energy models by a few percent for identical Hubble functions, and for that reason, an observation of both the Hubble and the growth function gives a handle on constraining the gravitational theory, [592]. The growth function can be estimated both through weak lensing and through galaxy clustering and redshift distortions.

Concerning the interactions of light with the cosmic large-scale structure, one sees a modified coupling in general models and a difference between the metric potentials. These effects are present in the anisotropy pattern of the CMB, as shown in [792], where smaller fluctuations were found on large angular scales, which can possibly alleviate the tension between the CMB and the ΛCDM model on small multipoles where the CMB spectrum acquires smaller amplitudes due to the ISW-effect on the last-scattering surface, but provides a worse fit to supernova data. An interesting effect inexplicable in GR is the anticorrelation between the CMB temperature and the density of galaxies at high redshift due to a sign change in the integrated Sachs–Wolfe effect. Interestingly, this behavior is very common in modified gravity theories.

A very powerful probe of structure growth is of course weak lensing, but to evaluate the lensing effect it is important to understand the nonlinear structure formation dynamics as a good part of the total signal is generated by small structures. Only recently has it been possible to perform structure formation simulations in modified gravity models, although still without a mechanism in which GR is recovered on very small scales, necessary to be in accordance with local tests of gravity.

In contrast, the number density of collapsed objects relies only little on nonlinear physics and can be used to investigate modified gravity cosmologies. One needs to solve the dynamical equations for a spherically symmetric matter distribution. Modified gravity theories show the feature of lowering the collapse threshold for density fluctuations in the large-scale structure, leading to a higher comoving number density of galaxies and clusters of galaxies. This probe is degenerate with respect to dark-energy cosmologies, which generically give the same trends.

1.7.2 Observing modified gravity with weak lensing

The magnification matrix is a 2×2 matrix that relates the true shape of a galaxy to its image. It contains two distinct parts: the convergence, defined as the trace of the matrix, modifies the size of the image, whereas the shear, defined as the symmetric traceless part, distorts the shape of the image. At small scales the shear and the convergence are not independent. They satisfy a consistency relation, and they contain therefore the same information on matter density perturbations. More precisely, the shear and the convergence are both related to the sum of the two Bardeen potentials, $\Phi + \Psi$, integrated along the photon trajectory. At large scales however, this consistency relation does not hold anymore. Various relativistic effects contribute to the convergence, see [150]. Some of these effects are generated along the photon trajectory, whereas others are due to the perturbations of the galaxies redshift. These relativistic effects provide independent information on the two Bardeen potentials, breaking their degeneracy. The convergence is therefore a useful quantity that can increase the discriminatory power of weak lensing.

The convergence can be measured through its effect on the galaxy number density, see e.g. [175]. The standard method extracts the magnification from correlations of distant quasars with fore-

ground clusters, see [804, 657]. Recently, [977, 978] designed a new method that permits to accurately measure auto-correlations of the magnification, as a function of the galaxies redshift. This method potentially allows measurements of the relativistic effects in the convergence.

1.7.2.1 Magnification matrix

We are interested in computing the magnification matrix $\mathcal{D}_{ab}$ in a perturbed Friedmann universe. The magnification matrix relates the true shape of a galaxy to its image, and describes therefore the deformations encountered by a light bundle along its trajectory. $\mathcal{D}_{ab}$ can be computed by solving Sachs equation, see [775], that governs propagation of light in a generic geometry. The convergence κ and the shear $\gamma \equiv \gamma_1 + i\gamma_2$ are then defined respectively as the trace and the symmetric traceless part of $\mathcal{D}_{ab}$

$$\mathcal{D}_{ab} = \frac{\chi_S}{1+z_S}\begin{pmatrix} 1-\kappa-\gamma_1 & -\gamma_2 \\ -\gamma_2 & 1-\kappa+\gamma_1 \end{pmatrix}. \tag{1.7.1}$$

Here z_S is the redshift of the source and χ_S is a time coordinate related to conformal time η_S through $\chi_S = \eta_O - \eta_S$.

We consider a spatially flat ($K = 0$) Friedmann universe with scalar perturbations. We start from the usual longitudinal (or Newtonian) gauge where the metric is given by

$$g_{\mu\nu}\,\mathrm{d}x^\mu\,\mathrm{d}x^\nu = a^2\left[-(1+2\Psi)d\eta^2 + (1-2\Phi)\delta_{ij}\,\mathrm{d}x^i\,\mathrm{d}x^j\right]. \tag{1.7.2}$$

We compute $\mathcal{D}_{ab}$ at linear order in Φ and Ψ and then we extract the shear and the convergence. We find, see [150, 125]

$$\gamma = \frac{1}{2}\int_0^{\chi_S}\mathrm{d}\chi\frac{\chi_S-\chi}{\chi\chi_S}\,\eth^2(\Phi+\Psi), \tag{1.7.3}$$

$$\begin{aligned}\kappa = {}& \frac{1}{2}\int_0^{\chi_S}\mathrm{d}\chi\frac{\chi_S-\chi}{\chi\chi_S}\,\bar{\eth}\,\eth(\Phi+\Psi) + \Phi_S - \int_0^{\chi_S}\frac{\mathrm{d}\chi}{\chi_S}(\Phi+\Psi) \\ & + \left(\frac{1}{\mathcal{H}_S\chi_S}-1\right)\left(\Psi_S + \mathbf{n}\cdot\mathbf{v}_S - \int_0^{\chi_S}\mathrm{d}\chi(\dot{\Phi}+\dot{\Psi})\right),\end{aligned} \tag{1.7.4}$$

where $\mathbf{n}$ is the direction of observation and $\mathbf{v}_S$ is the peculiar velocity of the source. Here we are making use of the angular spin raising $\eth$ and lowering $\bar{\eth}$ operators (see e.g., [560] for a review of the properties of these operators) defined as

$$\eth\ {}_sX \equiv -\sin^s\theta(\partial_\theta + i\csc\theta\partial_\varphi)(\sin^{-s}\theta)\ {}_sX\,, \qquad \bar{\eth}\ {}_sX \equiv -\sin^{-s}\theta(\partial_\theta - i\csc\theta\partial_\varphi)(\sin^{s}\theta)\ {}_sX\,, \tag{1.7.5}$$

where ${}_sX$ is an arbitrary field of spin s and θ and φ are spherical coordinates.

Eq. (1.7.3) and the first term in Eq. (1.7.4) are the standard contributions of the shear and the convergence, but expressed here with the full-sky transverse operators

$$\frac{1}{\chi^2}\,\eth^2 = \frac{1}{\chi^2}\left(\partial_\theta^2 - \cot\theta\partial_\theta - \frac{1}{\sin^2\theta}\partial_\varphi\right) + \frac{2\mathrm{i}}{\chi^2\sin\theta}\Big(\partial_\theta\partial_\varphi - \cot\theta\partial_\theta\Big), \tag{1.7.6}$$

$$\frac{1}{\chi^2}\,\eth\,\bar{\eth} = \frac{1}{\chi^2}\left(\partial_\theta^2 + \cot\theta\partial_\theta + \frac{1}{\sin^2\theta}\partial_\varphi\right). \tag{1.7.7}$$

In the flat-sky approximation, where θ is very small, $\frac{1}{\chi^2}\,\eth\,\bar{\eth}$ reduces to the 2D Laplacian $\partial_x^2 + \partial_y^2$ and one recovers the standard expression for the convergence. Similarly, the real part of $\frac{1}{\chi^2}\,\eth^2$ that corresponds to γ_1 reduces to $\partial_y^2 - \partial_x^2$ and the imaginary part that corresponds to γ_2 becomes $\partial_x\partial_y$.

The other terms in Eq. (1.7.4) are relativistic corrections to the convergence, that are negligible at small scales but may become relevant at large scales. The terms in the first line are intrinsic corrections, generated respectively by the curvature perturbation at the source position and the Shapiro time-delay. The terms in the second line are due to the fact that we measure the convergence at a fixed redshift of the source z_S rather that at a fixed conformal time η_S. Since in a perturbed universe, the observable redshift is itself a perturbed quantity, this transformation generates additional contribution to the convergence. Those are respectively the Sachs–Wolfe contribution, the Doppler contribution and the integrated Sachs–Wolfe contribution. Note that we have neglected the contributions at the observer position since they only give rise to a monopole or dipole term. The dominant correction to the convergence is due to the Doppler term. Therefore in the following we are interested in comparing its amplitude with the amplitude of the standard contribution. To that end we define $\kappa_{\rm st}$ and $\kappa_{\rm vel}$ as

$$\kappa_{\rm st} = \int_0^{\chi_S} \mathrm{d}\chi \frac{\chi_S - \chi}{2\chi\chi_S} \eth\bar{\eth}(\Phi + \Psi)\,, \tag{1.7.8}$$

$$\kappa_{\rm vel} = \left(\frac{1}{\mathcal{H}_S\chi_S} - 1\right)\mathbf{n}\cdot\mathbf{v}_S\,. \tag{1.7.9}$$

1.7.2.2 Observable quantities

The convergence is not directly observable. However it can be measured through the modifications that it induces on the galaxy number density. Let us introduce the magnification

$$\mu = \frac{1}{\det\mathcal{D}} \simeq 1 + 2\kappa\,, \quad \text{when} \quad |\kappa|, |\gamma| \ll 1\,. \tag{1.7.10}$$

The magnification modifies the size of a source: $d\Omega_O = \mu d\Omega_S$, where $d\Omega_S$ is the true angular size of the source and $d\Omega_O$ is the solid angle measured by the observer, i.e. the size of the image. The magnification has therefore an impact on the observed galaxy number density. Let us call $\bar{n}(f)df$ the number of unlensed galaxies per unit solid angle, at a redshift z_S, and with a flux in the range $[f, f + df]$. The magnification μ modifies the flux measured by the observer, since it modifies the observed galaxy surface. It affects also the solid angle of observation and hence the number of galaxies per unit of solid angle. These two effects combine to give a galaxy number overdensity, see [175, 804]

$$\delta_g^\mu = \frac{n(f) - \bar{n}(f)}{\bar{n}(f)} \simeq 1 + 2\big(\alpha - 1\big)(\kappa_{\rm st} + \kappa_{\rm vel})\,. \tag{1.7.11}$$

Here $\alpha \equiv -N'(>f_c)f_c/N(f_c)$, where $N(>f_c)$ is the number of galaxies brighter than f_c and f_c is the flux limit adopted. Hence α is an observable quantity, see e.g. [977, 804]. Recent measurements of the galaxy number overdensity δ_g^μ are reported in [804, 657]. The challenge in those measurements is to eliminate intrinsic clustering of galaxies, which induces an overdensity δ_g^{cl} much larger than δ_g^μ. One possibility to separate these two effects is to correlate galaxy number overdensities at widely separated redshifts. One can then measure $\langle\delta_g^\mu(z_S)\delta_g^{cl}(z_{S'})\rangle$, where z_S is the redshift of the sources and $z_{S'} < z_S$ is the redshift of the lenses. Another possibility, proposed by [977, 978], is to use the unique dependence of δ_g^μ on galaxy flux (i.e., on α) to disentangle δ_g^μ from δ_g^{cl}. This method, combined with precise measurements of the galaxies redshift, allows to measure auto-correlations of δ_g^μ, i.e., $\langle\delta_g^\mu(z_S)\delta_g^\mu(z_{S'})\rangle$, either for $z_S \neq z_{S'}$ or for $z_S = z_{S'}$. The velocity contribution, $\kappa_{\rm vel}$, has only an effect on $\langle\delta_g^\mu(z_S)\delta_g^\mu(z_{S'})\rangle$. The correlations between $\delta_g^{cl}(z_{S'})$ and $\mathbf{v}_S$ are indeed completely negligible and hence the source peculiar velocity does not affect $\langle\delta_g^\mu(z_S)\delta_g^{cl}(z_{S'})\rangle$. In the following we study in detail the contribution of peculiar motion to $\langle\delta_g^\mu(z_S)\delta_g^\mu(z_S)\rangle$.

The two components of the convergence $\kappa_{\rm st}$ and $\kappa_{\rm vel}$ (and consequently the galaxy number overdensity) are functions of redshift z_S and direction of observation $\mathbf{n}$. We can therefore determine

the angular power spectrum

$$\langle \delta_g^\mu(z_S, \mathbf{n}) \delta_g^\mu(z_S, \mathbf{n}') \rangle = \sum_\ell \frac{2\ell+1}{4\pi} C_\ell(z_S) P_\ell(\mathbf{n}\cdot\mathbf{n}') \,. \tag{1.7.12}$$

The angular power spectrum $C_\ell(z_S)$ contains two contributions, generated respectively by $\langle \kappa_{\rm st}\kappa_{\rm st}\rangle$ and $\langle \kappa_{\rm vel}\kappa_{\rm vel}\rangle$. The cross-term $\langle \kappa_{\rm vel}\kappa_{\rm st}\rangle$ is negligible since $\kappa_{\rm st}$ contains only Fourier modes with a wave vector $\mathbf{k}_\perp$ perpendicular to the line of sight (see Eq. (1.7.8)), whereas $\kappa_{\rm vel}$ selects modes with wave vector along the line of sight (Eq. (1.7.9)).

So far the derivation has been completely generic. Eqs. (1.7.3) and (1.7.4) are valid in any theory of gravity whose metric can be written as in Eq. (1.7.2). To evaluate the angular power spectrum we now have to be more specific. In the following we assume GR, with no anisotropic stress such that $\Phi = \Psi$. We use the Fourier transform convention

$$\mathbf{v}(\mathbf{x}, \chi) = \frac{1}{(2\pi)^3} \int \mathrm{d}^3k\, \mathbf{v}(\mathbf{k}, \chi) e^{i\mathbf{k}\mathbf{x}} \,. \tag{1.7.13}$$

The continuity equation, see e.g., [317], allows us to express the peculiar velocity as

$$\mathbf{v}(\mathbf{k}, \chi) = -i \frac{\dot G(a)}{G(a)} \frac{\mathbf{k}}{k^2} \delta(\mathbf{k}, a) \,, \tag{1.7.14}$$

where $\delta(\mathbf{k}, a)$ is the density contrast, $G(a)$ is the growth function, and $\dot G(a)$ its derivative with respect to χ. With this we can express the angular power spectrum as

$$C_\ell^{\rm vel}(z_S) = \frac{16\pi\delta_H^2(\alpha_S-1)^2 \dot G(a_S)^2}{H_0^4 G^2(a=1)} \left(\frac{1}{\mathcal{H}_S\chi_S} - 1\right)^2 \int \mathrm{d}k\, k T^2(k) j_\ell'(k\chi_S)^2 \,. \tag{1.7.15}$$

Here δ_H is the density contrast at horizon and $T(k)$ is the transfer function defined through, see e.g., [317]

$$\Psi(\mathbf{k}, a) = \frac{9}{10} \Psi_p(\mathbf{k}) T(k) \frac{G(a)}{a} \,. \tag{1.7.16}$$

We assume a flat power spectrum, $n_s = 1$, for the primordial potential $\Psi_p(\mathbf{k})$. We want to compare this contribution with the standard contribution

$$C_\ell^{\rm st}(z_S) = \frac{36\pi\delta_H^2(\alpha_S-1)^2\Omega_m^2\ell^2(\ell+1)^2}{G^2(a=1)} \int \frac{\mathrm{d}k}{k} T^2(k) \left[\int_0^{\chi_S} \mathrm{d}\chi \frac{\chi_S - \chi}{\chi\chi_S} \frac{G(a)}{a} j_\ell(k\chi)\right]^2 \,. \tag{1.7.17}$$

We evaluate $C_\ell^{\rm vel}$ and $C_\ell^{\rm st}$ in a ΛCDM universe with $\Omega_m = 0.25$, $\Omega_\Lambda = 0.75$ and $\delta_H = 5.7\cdot 10^{-5}$. We approximate the transfer function with the BBKS formula, see [85]. In Figure 9, we plot $C_\ell^{\rm vel}$ and $C_\ell^{\rm st}$ for various source redshifts. The amplitude of $C_\ell^{\rm vel}$ and $C_\ell^{\rm st}$ depends on $(\alpha-1)^2$, which varies with the redshift of the source, the flux threshold adopted, and the sky coverage of the experiment. Since $(\alpha-1)^2$ influences $C_\ell^{\rm vel}$ and $C_\ell^{\rm st}$ in the same way we do not include it in our plot. Generally, at small redshifts, $(\alpha-1)$ is smaller than 1 and consequently the amplitude of both $C_\ell^{\rm vel}$ and $C_\ell^{\rm st}$ is slightly reduced, whereas at large redshifts $(\alpha-1)$ tends to be larger than 1 and to amplify $C_\ell^{\rm vel}$ and $C_\ell^{\rm st}$, see e.g., [978]. However, the general features of the curves and more importantly the ratio between $C_\ell^{\rm vel}$ and $C_\ell^{\rm st}$ are not affected by $(\alpha-1)$.

Figure 9 shows that $C_\ell^{\rm vel}$ peaks at rather small ℓ, between 30 and 120 depending on the redshift. This corresponds to rather large angle $\theta \sim 90-360$ arcmin. This behavior differs from the standard term (Figure 9) that peaks at large ℓ. Therefore, it is important to have large sky surveys to detect the velocity contribution. The relative importance of $C_\ell^{\rm vel}$ and $C_\ell^{\rm st}$ depends strongly on the redshift of the source. At small redshift, $z_S = 0.2$, the velocity contribution is about $4\cdot 10^{-5}$ and is hence

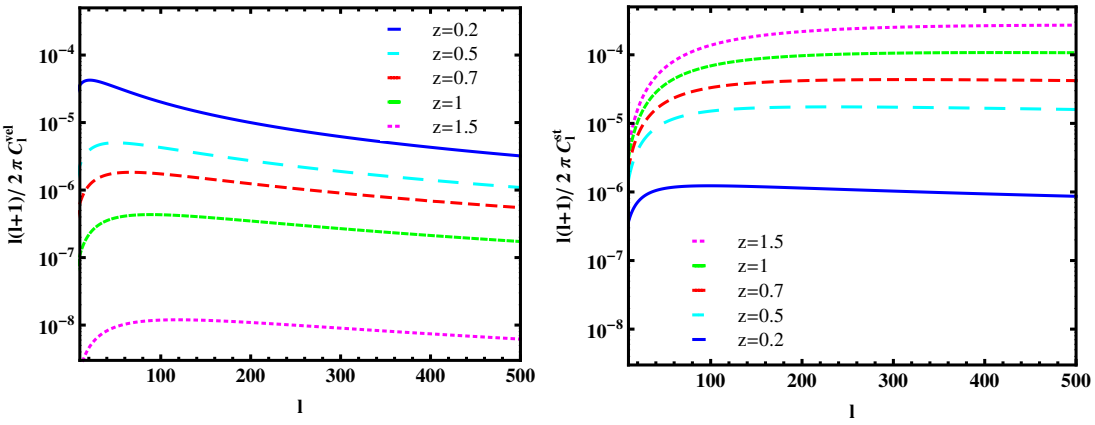

Figure 9: *Left:* The velocity contribution $C_\ell^{\rm vel}$ as a function of ℓ for various redshifts. *Right:* The standard contribution $C_\ell^{\rm st}$ as a function of ℓ for various redshifts.

larger than the standard contribution which reaches 10^{-6}. At redshift $z_S = 0.5$, $C_\ell^{\rm vel}$ is about 20% of $C_\ell^{\rm st}$, whereas at redshift $z_S = 1$, it is about 1 % of $C_\ell^{\rm st}$. Then at redshift $z_S = 1.5$ and above, $C_\ell^{\rm vel}$ becomes very small with respect to $C_\ell^{\rm st}$: $C_\ell^{\rm vel} \leq 10^{-4}\, C_\ell^{\rm st}$. The enhancement of $C_\ell^{\rm vel}$ at small redshift together with its fast decrease at large redshift are due to the prefactor $\left(\frac{1}{\mathcal{H}_S \chi_S} - 1\right)^2$ in Eq. (1.7.15). Thanks to this enhancement we see that if the magnification can be measured with an accuracy of 10%, then the velocity contribution is observable up to redshifts $z \leq 0.6$. If the accuracy reaches 1% then the velocity contribution becomes interesting up to redshifts of order 1.

The shear and the standard contribution in the convergence are not independent. One can easily show that their angular power spectra satisfy the consistency relation, see [449]

$$C_\ell^{\kappa\,{\rm st}} = \frac{\ell(\ell+1)}{(\ell+2)(\ell-1)} C_\ell^\gamma \,. \tag{1.7.18}$$

This relation is clearly modified by the velocity contribution. Using that the cross-correlation between the standard term and the velocity term is negligible, we can write a new consistency relation that relates the observed convergence $C_\ell^{\kappa\,{\rm tot}}$ to the shear

$$\frac{\ell(\ell+1)}{(\ell+2)(\ell-1)} C_\ell^\gamma = C_\ell^{\kappa\,{\rm tot}} - C_\ell^{\kappa\,{\rm vel}} \,. \tag{1.7.19}$$

Consequently, if one measures both the shear C_ℓ^γ and the magnification $C_\ell^{\kappa\,{\rm tot}}$ as functions of the redshift, Eq. (1.7.19) allows to extract the peculiar velocity contribution $C_\ell^{\kappa\,{\rm vel}}$. This provides a new way to measure peculiar velocities of galaxies.

Note that in practice, in weak lensing tomography, the angular power spectrum is computed in redshift bins and therefore the square bracket in Eq. (1.7.17) has to be integrated over the bin

$$\int_0^\infty {\rm d}\chi n_i(\chi) \int_0^\chi {\rm d}\chi' \frac{\chi - \chi'}{\chi\chi'} \frac{G(\chi')}{a(\chi')} j_\ell(k\chi') \,, \tag{1.7.20}$$

where n_i is the galaxy density for the i-th bin, convolved with a Gaussian around the mean redshift of the bin. The integral over χ' is then simplified using Limber approximation, i.e.,

$$\int_0^\chi {\rm d}\chi' F(\chi') J_\ell(k\chi') \simeq \frac{1}{k} F\left(\frac{\ell}{k}\right) \theta(k\chi - \ell) \,, \tag{1.7.21}$$

where J_ℓ is the Bessel function of order ℓ. The accuracy of Limber approximation increases with ℓ. Performing a change of coordinate such that $k = \ell/\chi$, Eq. (1.7.17) can be recast in the usual form used in weak lensing tomography, see e.g., Eq. (1.8.4).

1.7.3 Observing modified gravity with redshift surveys

Wide-deep galaxy redshift surveys have the power to yield information on both $H(z)$ and $f_g(z)$ through measurements of Baryon Acoustic Oscillations (BAO) and redshift-space distortions. In particular, if gravity is not modified and matter is not interacting other than gravitationally, then a detection of the expansion rate is directly linked to a unique prediction of the growth rate. Otherwise galaxy redshift surveys provide a unique and crucial way to make a combined analysis of $H(z)$ and $f_g(z)$ to test gravity. As a wide-deep survey, Euclid allows us to measure $H(z)$ directly from BAO, but also indirectly through the angular diameter distance $D_A(z)$ (and possibly distance ratios from weak lensing). Most importantly, Euclid survey enables us to measure the cosmic growth history using two independent methods: $f_g(z)$ from galaxy clustering, and $G(z)$ from weak lensing. In the following we discuss the estimation of $[H(z), D_A(z)$ and $f_g(z)]$ from galaxy clustering.

From the measure of BAO in the matter power spectrum or in the 2-point correlation function one can infer information on the expansion rate of the universe. In fact, the sound waves imprinted in the CMB can be also detected in the clustering of galaxies, thereby completing an important test of our theory of gravitational structure formation.

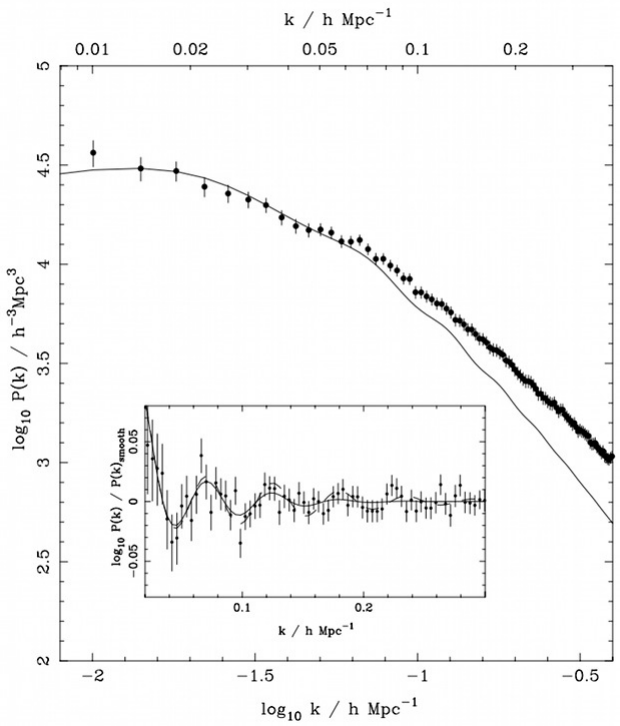

Figure 10: Matter power spectrum form measured from SDSS [720]

The BAO in the radial and tangential directions offer a way to measure the Hubble parameter and angular diameter distance, respectively. In the simplest FLRW universe the basis to define

distances is the dimensionless, radial, comoving distance:

$$\chi(z) \equiv \int_0^z \frac{dz'}{E(z')} \,. \tag{1.7.22}$$

The dimensionless version of the comoving distance (defined in the previous section by the same symbol χ) is:

$$E^2(z) = \Omega_m^{(0)}(1+z)^3 + (1-\Omega_m^{(0)}) \exp\left[\int_0^z \frac{3(1+w(\tilde{z}))}{1+\tilde{z}} \mathrm{d}\tilde{z}\right] . \tag{1.7.23}$$

The standard cosmological distances are related to $\chi(z)$ via

$$D_A(z) = \frac{c}{H_0(1+z)\sqrt{-\Omega_k}} \sin\left(\sqrt{-\Omega_k}\chi(z)\right) \tag{1.7.24}$$

where the luminosity distance, $D_L(z)$, is given by the distance duality:

$$D_L(z) = (1+z)^2 D_A(z). \tag{1.7.25}$$

The coupling between $D_A(z)$ and $D_L(z)$ persists in any metric theory of gravity as long as photon number is conserved (see Section 4.2 for cases in which the duality relation is violated). BAO yield both $D_A(z)$ and $H(z)$ making use of an almost completely linear physics (unlike for example SN Ia, demanding complex and poorly understood mechanisms of explosions). Furthermore, they provide the chance of constraining the growth rate through the change in the amplitude of the power spectrum.

The characteristic scale of the BAO is set by the sound horizon at decoupling. Consequently, one can attain the angular diameter distance and Hubble parameter separately. This scale along the line of sight ($s_{||}(z)$) measures $H(z)$ through $H(z) = c\Delta z/s_{||}(z)$, while the tangential mode measures the angular diameter distance $D_A(z) = s_\perp/\Delta\theta(1+z)$.

One can then use the power spectrum to derive predictions on the parameter constraining power of the survey (see e.g., [46, 418, 938, 945, 308]).

In order to explore the cosmological parameter constraints from a given redshift survey, one needs to specify the measurement uncertainties of the galaxy power spectrum. In general, the statistical error on the measurement of the galaxy power spectrum $P_\mathrm{g}(k)$ at a given wave-number bin is [359]

$$\left[\frac{\Delta P_\mathrm{g}}{P_\mathrm{g}}\right]^2 = \frac{2(2\pi)^2}{V_\mathrm{survey} k^2 \Delta k \Delta\mu}\left[1 + \frac{1}{n_\mathrm{g} P_\mathrm{g}}\right]^2 , \tag{1.7.26}$$

where n_g is the mean number density of galaxies, V_survey is the comoving survey volume of the galaxy survey, and μ is the cosine of the angle between $\mathbf{k}$ and the line-of-sight direction $\mu = \vec{k}\cdot\hat{r}/k$.

In general, the *observed* galaxy power spectrum is different from the *true* spectrum, and it can be reconstructed approximately assuming a reference cosmology (which we consider to be our fiducial cosmology) as (e.g., [815])

$$P_\mathrm{obs}(k_{\mathrm{ref}\perp}, k_{\mathrm{ref}\parallel}, z) = \frac{D_A(z)^2_\mathrm{ref} H(z)}{D_A(z)^2 H(z)_\mathrm{ref}} P_\mathrm{g}(k_{\mathrm{ref}\perp}, k_{\mathrm{ref}\parallel}, z) + P_\mathrm{shot} \,, \tag{1.7.27}$$

where

$$P_\mathrm{g}(k_{\mathrm{ref}\perp}, k_{\mathrm{ref}\parallel}, z) = b(z)^2 \left[1 + \beta(z)\frac{k^2_{\mathrm{ref}\parallel}}{k^2_{\mathrm{ref}\perp} + k^2_{\mathrm{ref}\parallel}}\right]^2 \times P_\mathrm{matter}(k, z) \,. \tag{1.7.28}$$

In Eq. (1.7.27), $H(z)$ and $D_A(z)$ are the Hubble parameter and the angular diameter distance, respectively, and the prefactor $(D_A(z)^2_\mathrm{ref} H(z))/(D_A(z)^2 H(z)_\mathrm{ref})$ encapsulates the geometrical distortions due to the Alcock–Paczynski effect [815, 81]. Their values in the reference cosmology are

distinguished by the subscript 'ref', while those in the true cosmology have no subscript. $k_\perp$ and $k_\parallel$ are the wave-numbers across and along the line of sight in the true cosmology, and they are related to the wave-numbers calculated assuming the reference cosmology by $k_{\mathrm{ref}\perp} = k_\perp D_A(z)/D_A(z)_{\mathrm{ref}}$ and $k_{\mathrm{ref}\parallel} = k_\parallel H(z)_{\mathrm{ref}}/H(z)$. P_{shot} is the unknown white shot noise that remains even after the conventional shot noise of inverse number density has been subtracted [815]. In Eq. (1.7.28), $b(z)$ is the *linear bias* factor between galaxy and matter density distributions, $f_g(z)$ is the linear growth rate,[4] and $\beta(z) = f_g(z)/b(z)$ is the linear redshift-space distortion parameter [485]. The linear matter power spectrum $P_{\mathrm{matter}}(k,z)$ in Eq. (1.7.27) takes the form

$$P_{\mathrm{matter}}(k,z) = \frac{8\pi^2 c^4 k_0 \Delta^2_{\mathcal{R}}(k_0)}{25 H_0^4 \Omega_m^2} T^2(k) \left[\frac{G(z)}{G(z=0)}\right]^2 \left(\frac{k}{k_0}\right)^{n_s} e^{-k^2\mu^2\sigma_r^2}, \tag{1.7.29}$$

where $G(z)$ is the usual *scale independent* linear growth-factor in the absence of massive neutrino free-streaming (see Eq. (25) in [337]), whose fiducial value in each redshift bin is computed through numerical integration of the differential equations governing the growth of linear perturbations in presence of dark energy [588] or employing the approximation of Eq. (1.3.22). $T(k)$ depends on matter and baryon densities[5] (neglecting dark energy at early times), and is computed in each redshift bin using a Boltzmann code like CAMB[6] [559] or CMBFAST.

In Eq. (1.7.29) a damping factor $e^{-k^2\mu^2\sigma_r^2}$ has been added, due to redshift uncertainties, where $\sigma_r = (\partial r/\partial z)\sigma_z$, $r(z)$ being the comoving distance [940, 815], and assumed that the power spectrum of primordial curvature perturbations, $P_{\mathcal{R}}(k)$, is

$$\Delta^2_{\mathcal{R}}(k) \equiv \frac{k^3 P_{\mathcal{R}}(k)}{2\pi^2} = \Delta^2_{\mathcal{R}}(k_0) \left(\frac{k}{k_0}\right)^{n_s}, \tag{1.7.30}$$

where $k_0 = 0.002/\mathrm{Mpc}$, $\Delta^2_{\mathcal{R}}(k_0)|_{\mathrm{fid}} = 2.45 \times 10^{-9}$ is the dimensionless amplitude of the primordial curvature perturbations evaluated at a pivot scale k_0, and n_s is the scalar spectral index [548].

In the limit where the survey volume is much larger than the scale of any features in $P_{\mathrm{obs}}(k)$, it has been shown that the redshift survey Fisher matrix for a given redshift bin can be approximated as [880]

$$F_{ij}^{\mathrm{LSS}} = \int_{-1}^{1} \int_{k_{\mathrm{min}}}^{k_{\mathrm{max}}} \frac{\partial \ln P_{\mathrm{obs}}(k,\mu)}{\partial p_i} \frac{\partial \ln P_{\mathrm{obs}}(k,\mu)}{\partial p_j} V_{\mathrm{eff}}(k,\mu) \frac{2\pi k^2 dk d\mu}{2(2\pi)^3}, \tag{1.7.31}$$

where the derivatives are evaluated at the parameter values p_i of the fiducial model, and V_{eff} is the effective volume of the survey:

$$V_{\mathrm{eff}}(k,\mu) = \left[\frac{n_{\mathrm{g}} P_{\mathrm{g}}(k,\mu)}{n_{\mathrm{g}} P_{\mathrm{g}}(k,\mu) + 1}\right]^2 V_{\mathrm{survey}}, \tag{1.7.32}$$

where the comoving number density $n_{\mathrm{g}}(z)$ is assumed to be spatially constant. Due to azimuthal symmetry around the line of sight, the three-dimensional galaxy redshift power spectrum $P_{\mathrm{obs}}(\vec{k})$ depends only on k and μ, i.e., is reduced to two dimensions by symmetry [815]. The total Fisher matrix can be obtained by summing over the redshift bins.

To minimize nonlinear effects, one should restrict wave-numbers to the quasi-linear regime, e.g., imposing that k_{max} is given by requiring that the variance of matter fluctuations in a sphere of radius R is, for instance, $\sigma^2(R) = 0.25$ for $R = \pi/(2k_{\mathrm{max}})$. Or one could model the nonlinear distortions as in [338]. On scales larger than ($\sim 100\,h^{-1}$ Mpc) where we focus our analysis,

[4] In presence of massive neutrinos f_g depends also on the scale k [501].

[5] If we assume that neutrinos have a non-vanishing mass, then the transfer function is also redshift-dependent.

[6] http://camb.info/

nonlinear effects can be represented in fact as a displacement field in Lagrangian space modeled by an elliptical Gaussian function. Therefore, following [338, 816], to model nonlinear effect we multiply $P(k)$ by the factor

$$\exp\left\{-k^2\left[\frac{(1-\mu^2)\Sigma_\perp^2}{2}+\frac{\mu^2\Sigma_\parallel^2}{2}\right]\right\}, \tag{1.7.33}$$

where $\Sigma_\perp$ and $\Sigma_\parallel$ represent the displacement across and along the line of sight, respectively. They are related to the growth factor G and to the growth rate f_g through $\Sigma_\perp = \Sigma_0 G$ and $\Sigma_\parallel = \Sigma_0 G(1+f_g)$. The value of Σ_0 is proportional to σ_8. For a reference cosmology where $\sigma_8 = 0.8$ [526], we have $\Sigma_0 = 11\,h^{-1}$ Mpc.

Finally, we note that when actual data are available, the usual way to measure $\beta = f_g/b$ is by fitting the measured galaxy redshift-space correlation function $\xi(\sigma,\pi)$ to a model [717]:

$$\xi(\sigma,\pi) = \int_{-\infty}^{\infty} \mathrm{d}v\, f(v)\,\tilde{\xi}(\sigma,\pi - v/H_0)\,, \tag{1.7.34}$$

where $f(v)$ describes the small-scale random motion (usually modeled by a Gaussian that depends on the galaxy pairwise peculiar velocity dispersion), and $\tilde{\xi}(\sigma,\pi)$ is the model accounting for coherent infall velocities:[7]

$$\tilde{\xi}(\sigma,\pi) = \xi_0(s)P_0(\mu) + \xi_2(s)P_2(\mu) + \xi_4(s)P_4(\mu). \tag{1.7.35}$$

$P_l(\mu)$ are Legendre polynomials; $\mu = \cos\theta$, where θ denotes the angle between $\mathbf{r}$ and π; $\xi_0(s)$, $\xi_2(s)$, and $\xi_4(s)$ depend on β and the real-space correlation function $\xi(r)$.

The bias between galaxy and matter distributions can be estimated from either galaxy clustering, or weak lensing. To determine bias, we can assume that the galaxy density perturbation δ_g is related to the matter density perturbation $\delta_m(\mathbf{x})$ as [371]:

$$\delta_g = b\delta_m(\mathbf{x}) + b_2\delta_m^2(\mathbf{x})/2. \tag{1.7.36}$$

Bias can be derived from galaxy clustering by measuring the galaxy bispectrum:

$$\begin{aligned}\langle\delta_{g\mathbf{k}_1}\delta_{g\mathbf{k}_2}\delta_{g\mathbf{k}_1}\rangle = (2\pi)^3\{&P(\mathbf{k}_1)P(\mathbf{k}_2)\left[J(\mathbf{k}_1,\mathbf{k}_2)/b + b_2/b^2\right]\\ &+\text{cyc.}\}\,\delta^D(\mathbf{k}_1+\mathbf{k}_2+\mathbf{k}_3),\end{aligned} \tag{1.7.37}$$

where J is a function that depends on the shape of the triangle formed by $(\mathbf{k}_1, \mathbf{k}_2, \mathbf{k}_3)$ in $\mathbf{k}$ space, but only depends very weakly on cosmology [648, 925].

In general, bias can be measured from weak lensing through the comparison of the shear-shear and shear-galaxy correlations functions. A combined constraint on bias and the growth factor $G(z)$ can be derived from weak lensing by comparing the cross-correlations of multiple redshift slices.

Of course, if bias is assumed to be linear ($b_2 = 0$) and scale independent, or is parametrized in some simple way, e.g., with a power law scale dependence, then it is possible to estimate it even from linear galaxy clustering alone, as we will see in Section 1.8.3.

1.7.4 Cosmological bulk flows

As we have seen, the additional redshift induced by the galaxy peculiar velocity field generates the redshift distortion in the power spectrum. In this section we discuss a related effect on the luminosity of the galaxies and on its use to measure the peculiar velocity in large volumes, the so-called bulk flow.

[7] See [420]. $\tilde{\xi}(\sigma,\pi)$ is the Fourier transform of $P_s(k) = (1+\beta\mu^2)^2 P_r(k)$ [485].

In the gravitational instability framework, inhomogeneities in the matter distribution induce gravitational accelerations $\mathbf{g}$, which result in galaxies having peculiar velocities $\mathbf{v}$ that add to the Hubble flow. In linear theory the peculiar velocity field is proportional to the peculiar acceleration

$$\mathbf{v}(\mathbf{r}) = \frac{2f_g}{3H_0\Omega_m}\mathbf{g}(\mathbf{r}) = \frac{H_0 f_g}{4\pi}\int \delta_m(\mathbf{r}')\frac{(\mathbf{r}'-\mathbf{r})}{|\mathbf{r}'-\mathbf{r}|^3}\,\mathrm{d}^3\mathbf{r}'\,, \tag{1.7.38}$$

and the bulk flow of a spherical region is solely determined by the gravitational pull of the dipole of the external mass distribution. For this reason, bulk flows are reliable indicators to deviations from homogeneity and isotropy on large scale, should they exist.

Constraints on the power spectrum and growth rate can be obtained by comparing the bulk flow estimated from the volume-averaged motion of the sphere of radius R:

$$\mathbf{B}_R \equiv \frac{\int \mathbf{v}(\mathbf{x})W(\mathbf{x}/R)\,\mathrm{d}^3\mathbf{x}}{\int W(\mathbf{x}/R)\,\mathrm{d}^3\mathbf{x}}\,, \tag{1.7.39}$$

with expected variance:

$$\sigma^2_{\mathbf{B},R} = \frac{H_0^2 f_g^2}{6\pi^2}\int P(k)\mathcal{W}(kR)^2(k)\,\mathrm{d}k\,, \tag{1.7.40}$$

where the window function $W(\mathbf{x}/R)$ and its Fourier transform $\mathcal{W}(kR)$ describe the spatial distribution of the dataset.

Over the years the bulk flows has been estimated from the measured peculiar velocities of a large variety of objects ranging from galaxies [397, 398, 301, 256, 271, 788] clusters of galaxies [549, 165, 461] and SN Ia [766]. Conflicting results triggered by the use of error-prone distance indicators have fueled a long lasting controversy on the amplitude and convergence of the bulk flow that is still on. For example, the recent claim of a bulk flow of 407 ± 81 km s^{-1} within $R = 50$ h^{-1} Mpc [947], inconsistent with expectation from the ΛCDM model, has been seriously challenged by the re-analysis of the same data by [694] who found a bulk flow amplitude consistent with ΛCDM expectations and from which they were able to set the strongest constraints on modified gravity models so far. On larger scales, [493] claimed the detection of a dipole anisotropy attributed to the kinetic SZ decrement in the WMAP temperature map at the position of X-ray galaxy clusters. When interpreted as a coherent motion, this signal would indicate a gigantic bulk flow of 1028 ± 265 km s^{-1} within $R = 528$ h^{-1} Mpc. This highly debated result has been seriously questioned by independent analyses of WMAP data [see, e.g., 699])

The large, homogeneous dataset expected from Euclid has the potential to settle these issues. The idea is to measure bulk flows in large redshift surveys, based on the apparent, dimming or brightening of galaxies due to their peculiar motion. The method, originally proposed by [875], has been recently extended by [693] who propose to estimate the bulk flow by minimizing systematic variations in galaxy luminosities with respect to a reference luminosity function measured from the whole survey. It turns out that, if applied to the photo-z catalog expected from Euclid, this method would be able to detect at 5σ significance a bulk flow like the one of [947] over ~ 50 independent spherical volumes at $z \geq 0.2$, provided that the systematic magnitude offset over the corresponding areas in the sky does not exceed the expected random magnitude errors of 0.02–0.04 mag. Additionally, photo-z or spectral-z could be used to validate or disproof with very large ($> 7\sigma$) significance the claimed bulk flow detection of [493] at $z = 0.5$.

Closely related to the bulk flow is the Local Group peculiar velocity inferred from the observed CMB dipole [483]

$$\mathbf{v}_{\rm CMB} = \mathbf{v}_{{\rm LG},R} - \frac{H_0 f_g}{3}\mathbf{x}_{c.m.} + \mathbf{B}_R\,, \tag{1.7.41}$$

where $\mathbf{v}_{{\rm LG},R}$ is the Local Group velocity resulting from the gravitational pull of all objects in the sample within the radius R, $\mathbf{x}_{\rm c.m.}$ is the position of the center of mass of the sample and $\mathbf{v}_{\rm CMB}$ is

the LG velocity inferred from the CMB dipole [121]. The convergence of $\mathbf{v}_{\mathrm{LG},R}$ with the radius and its alignment with the CMB dipole direction indicates a crossover to homogeneity [793] and allows to constrain the growth rate by comparing $\mathbf{v}_{\mathrm{CMB}}$ with $\mathbf{v}_{\mathrm{LG},R}$. The latter can be estimated from the dipole in the distribution of objects either using a number-weighting scheme if redshifts are available for all objects of the sample, or using a flux-weighting scheme. In this second case the fact that both gravitational acceleration and flux are inversely proportional to the distance allows to compute the dipole from photometric catalogs with no need to measure redshifts. The drawback is that the information on the convergence scale is lost.

As for the bulk flow case, despite the many measurements of cosmological dipoles using galaxies [972, 283, 654, 868, 801, 513] there is still no general consensus on the scale of convergence and even on the convergence itself. Even the recent analyses of measuring the acceleration of the Local Group from the 2MASS redshift catalogs provided conflicting results. [344] found that the galaxy dipole seems to converge beyond $R = 60\,h^{-1}$ Mpc, whereas [552] find no convergence within $R = 120\,h^{-1}$ Mpc.

Once again, Euclid will be in the position to solve this controversy by measuring the galaxy and cluster dipoles not only at the LG position and out to very large radii, but also in several independent ad truly all-sky spherical samples carved out from the the observed areas with $|b| > 20°$. In particular, coupling photometry with photo-z one expects to be able to estimate the convergence scale of the flux-weighted dipole over about 100 independent spheres of radius $200\,h^{-1}$ Mpc out to $z = 0.5$ and, beyond that, to compare number-weighted and flux-weighted dipoles over a larger number of similar volumes using spectroscopic redshifts.

1.8 Forecasts for Euclid

Here we describe forecasts for the constraints on modified gravity parameters which Euclid observations should be able to achieve. We begin with reviewing the relevant works in literature. Then, after we define our "Euclid model", i.e., the main specifics of the redshift and weak lensing survey, we illustrate a number of Euclid forecasts obtained through a Fisher matrix approach.

1.8.1 A review of forecasts for parametrized modified gravity with Euclid

Heavens et al. [429] have used Bayesian evidence to distinguish between models, using the Fisher matrices for the parameters of interest. This study calculates the ratio of evidences B for a 3D weak lensing analysis of the full Euclid survey, for a dark-energy model with varying equation of state, and modified gravity with additionally varying growth parameter γ. They find that Euclid can decisively distinguish between, e.g., DGP and dark energy, with $|\ln B| \simeq 50$. In addition, they find that it will be possible to distinguish any departure from GR which has a difference in γ greater than $\simeq 0.03$. A phenomenological extension of the DGP model [332, 11] has also been tested with Euclid. Specifically, [199] found that it will be possible to discriminate between this modification to gravity from ΛCDM at the 3σ level in a wide range of angular scale, approximately $1000 \lesssim \ell \lesssim 4000$.

Thomas et al. [886] construct Fisher matrix forecasts for the Euclid weak lensing survey, shown in Figure 11. The constraints obtained depend on the maximum wavenumber which we are confident in using; $\ell_{\mathrm{max}} = 500$ is relatively conservative as it probes the linear regime where we can hope to analytically track the growth of structure; $\ell_{\mathrm{max}} = 10000$ is more ambitious as it includes nonlinear power, using the [844] fitting function. This will not be strictly correct, as the fitting function was determined in a GR context. Note that γ is not very sensitive to ℓ_{max}, while Σ_0, defined in [41] as $\Sigma = 1 + \Sigma_0 a$ (and where Σ is defined in Eq. 1.3.28) is measured much more

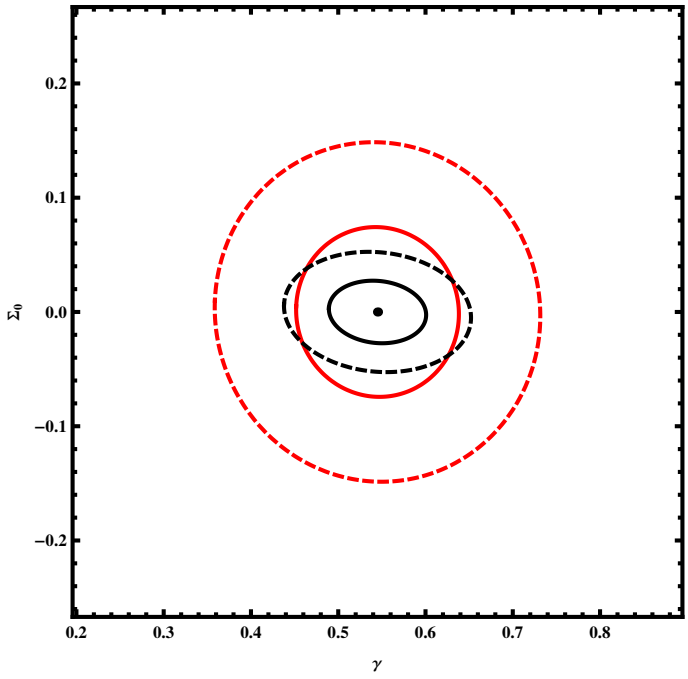

Figure 11: Marginalized $\gamma-\Sigma_0$ forecast for weak lensing only analysis with Euclid. Here Σ_0 is defined from $\Sigma = 1 + \Sigma_0 a$ and Σ, defined via Eq. 1.3.28, is related to the WL potential. Black contours correspond to $\ell_{\rm max} = 5000$, demonstrating an error of $0.089(1\sigma)$ on Σ_0, whereas the red contours correspond to $\ell_{\rm max} = 500$ giving an error of 0.034. In both cases, the inner and outer contours are 1σ and 2σ respectively. GR resides at [0.55, 0], while DGP resides at [0.68, 0].

accurately in the nonlinear regime.

Amendola et al. [41] find Euclid weak lensing constraints for a more general parameterization that includes evolution. In particular, $\Sigma(z)$ is investigated by dividing the Euclid weak lensing survey into three redshift bins with equal numbers of galaxies in each bin, and approximating that Σ is constant within that bin. Since Σ_1, i.e., the value of Σ in the $a = 1$ bin (present-day) is degenerate with the amplitude of matter fluctuations, it is set to unity. The study finds that a deviation from unit Σ (i.e., GR) of 3% can be detected in the second redshift bin, and a deviation of 10% is still detected in the furthest redshift bin.

Beynon et al. [132] make forecasts for modified gravity with Euclid weak lensing including [457] in interpolating between the linear spectrum predicted by modified gravity, and GR on small scales as required by Solar System tests. This requires parameters A (a measure of the abruptness of transitioning between these two regimes), α_1 (controlling the k-dependence of the transition) and α_2 (controlling the z-dependence of the transition).

The forecasts for modified gravity parameters are shown in Figure 12 for the Euclid lensing data. Even with this larger range of parameters to fit, Euclid provides a measurement of the growth factor γ to within 10%, and also allows some constraint on the α_1 parameter, probing the physics of nonlinear collapse in the modified gravity model.

Finally, Song et al. [848] have shown forecasts for measuring Σ and μ using both imaging and spectroscopic surveys. They combine 20,000 square-degree lensing data (corresponding to [550] rather than to the updated [551]) with the peculiar velocity dispersion measured from redshift space distortions in the spectroscopic survey, together with stringent background expansion measurements from the CMB and supernovae. They find that for simple models for the redshift

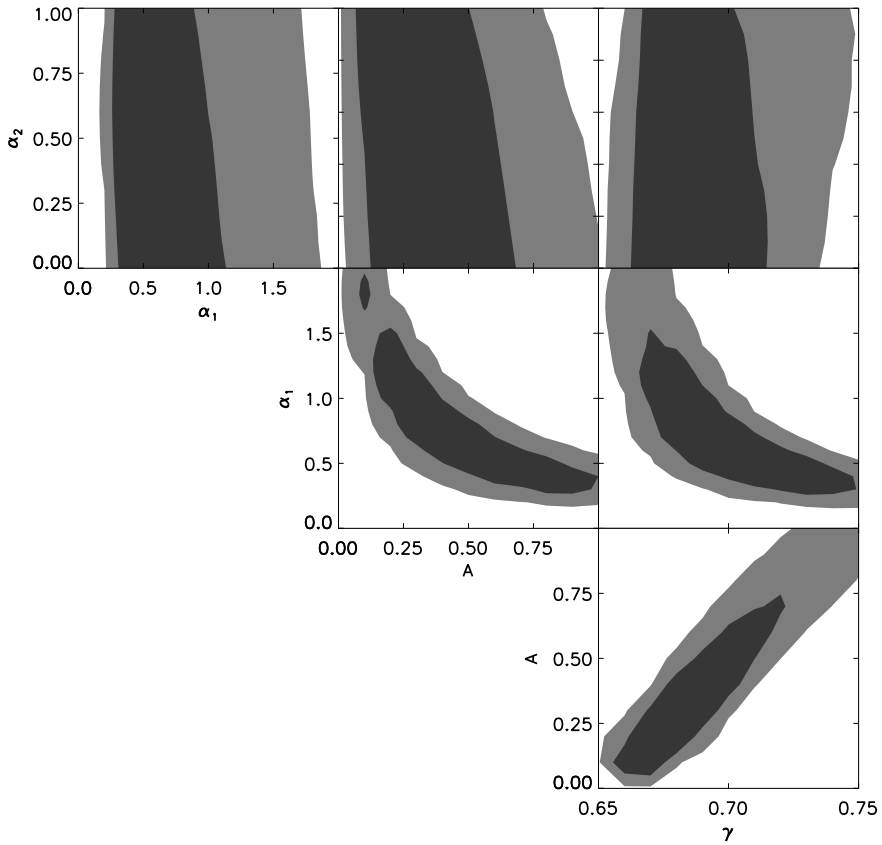

Figure 12: Constraints on γ, α_1, α_2 and A from Euclid, using a DGP fiducial model and 0.4 redshift bins between 0.3 and 1.5 for the central cosmological parameter values fitting WMAP+BAO+SNe.

evolution of Σ and μ, both quantities can be measured to 20% accuracy.

1.8.2 Euclid surveys

The Euclid mission will produce a catalog of up to 100 million galaxy redshifts and an imaging survey that should allow to estimate the galaxy ellipticity of up to 2 billion galaxy images. Here we discuss these surveys and fix their main properties into a "Euclid model", i.e., an approximation to the real Euclid survey that will be used as reference mission in the following.

Modeling the Redshift Survey.
The main goals of next generation redshift surveys will be to constrain the dark-energy parameters and to explore models alternative to standard Einstein gravity. For these purposes they will need to consider very large volumes that encompass $z \sim 1$, i.e., the epoch at which dark energy started dominating the energy budget, spanning a range of epochs large enough to provide a sufficient leverage to discriminate among competing models at different redshifts.

Here we consider a survey covering a large fraction of the extragalactic corresponding to ~ 15000 deg^2 capable to measure a large number of galaxy redshifts out to $z \sim 2$. A promising observational strategy is to target Hα emitters at near-infrared wavelengths (which implies $z > 0.5$) since they guarantee both relatively dense sampling (the space density of this population is expected to increase out to $z \sim 2$) and an efficient method to measure the redshift of the object. The limiting flux of the survey should be the tradeoff between the requirement of minimizing the shot noise, the contamination by other lines (chiefly among them the [O II] line), and that of maximizing the so-called efficiency ε, i.e., the fraction of successfully measured redshifts. To minimize shot noise one should obviously strive for a low flux. Indeed, [389] found that a limiting flux $f_{\mathrm{H}\alpha} \geq 1 \times 10^{-16}$ erg cm^{-2} s^{-1} would be able to balance shot noise and cosmic variance out to $z = 1.5$. However, simulated observations of mock Hα galaxy spectra have shown that ε ranges between 30% and 60% (depending on the redshift) for a limiting flux $f_{\mathrm{H}\alpha} \geq 3 \times 10^{-16}$ erg cm^{-2} s^{-1} [551]. Moreover, contamination from [O II] line drops from 12% to 1% when the limiting flux increases from 1×10^{-16} to 5×10^{-16} erg cm^{-2} s^{-1} [389].

Taking all this into account, in order to reach the top-level science requirement on the number density of Hα galaxies, the average effective Hα line flux limit from a 1-arcsec diameter source shall be lower than or equal to 3×10^{-16} erg cm^{-2} s^{-1}. However, a slitless spectroscopic survey has a success rate in measuring redshifts that is a function of the emission line flux. As such, the Euclid survey cannot be characterized by a single flux limit, as in conventional slit spectroscopy.

We use the number density of Hα galaxies at a given redshift, $n(z)$, estimated using the latest empirical data (see Figure 3.2 of [551]), where the values account for redshift – and flux – success rate, to which we refer as our reference efficiency ε_r.

However, in an attempt to bracket current uncertainties in modeling galaxy surveys, we consider two further scenarios, one where the efficiency is only the half of ε_r and one where it is increased by a factor of 40%. Then we define the following cases:

- *Reference case (ref.).* Galaxy number density $n(z)$ which include efficiency ε_r (column $n_2(z)$ in Table 3).
- *Pessimistic case (pess.).* Galaxy number density $n(z) \cdot 0.5$, i.e., efficiency is $\varepsilon_r \cdot 0.5$ (column $n_3(z)$ in Table 3).
- *Optimistic case (opt.).* Galaxy number density $n(z) \cdot 1.4$, i.e., efficiency is $\varepsilon_r \cdot 1.4$ (column $n_1(z)$ in Table 3).

The total number of observed galaxies ranges from $3 \cdot 10^7$ (pess.) to $9 \cdot 10^7$ (opt.). For all cases we assume that the error on the measured redshift is $\Delta z = 0.001(1 + z)$, independent of the

limiting flux of the survey.

Table 3: Expected galaxy number densities in units of $(h/\mathrm{Mpc})^3$ for Euclid survey. Let us notice that the galaxy number densities $n(z)$ depend on the fiducial cosmology adopted in the computation of the survey volume, needed for the conversion from the galaxy numbers dN/dz to $n(z)$.

z	$n_1(z)\ \times 10^{-3}$	$n_2(z)\ \times 10^{-3}$	$n_3(z)\ \times 10^{-3}$
0.65 – 0.75	1.75	1.25	0.63
0.75 – 0.85	2.68	1.92	0.96
0.85 – 0.95	2.56	1.83	0.91
0.95 – 1.05	2.35	1.68	0.84
1.05 – 1.15	2.12	1.51	0.76
1.15 – 1.25	1.88	1.35	0.67
1.25 – 1.35	1.68	1.20	0.60
1.35 – 1.45	1.40	1.00	0.50
1.45 – 1.55	1.12	0.80	0.40
1.55 – 1.65	0.81	0.58	0.29
1.65 – 1.75	0.53	0.38	0.19
1.75 – 1.85	0.49	0.35	0.18
1.85 – 1.95	0.29	0.21	0.10
1.95 – 2.05	0.16	0.11	0.06

Modeling the weak lensing survey. For the weak lensing survey, we assume again a sky coverage of 15,000 square degrees. For the number density we use the common parameterization

$$n(z) = z^2 \exp(-(z/z_0)^{3/2}) \,, \tag{1.8.1}$$

where $z_0 = z_{\mathrm{mean}}/1.412$ is the peak of $n(z)$ and z_{mean} the median and typically we assume $z_{\mathrm{mean}} = 0.9$ and a surface density of valid images of $n_g = 30$ per arcmin^2 [551]). We also assume that the photometric redshifts give an error of $\Delta z = 0.05(1+z)$. Other specifications will be presented in the relevant sections.

1.8.3 Forecasts for the growth rate from the redshift survey

In this section we forecast the constraints that future observations can put on the growth rate and on a scale-independent bias, employing the Fisher matrix method presented in Section 1.7.3. We use the representative Euclid survey presented in Section 1.8.2. We assess how well one can constrain the bias function from the analysis of the power spectrum itself and evaluate the impact that treating bias as a free parameter has on the estimates of the growth factor. We estimate how errors depend on the parametrization of the growth factor and on the number and type of degrees of freedom in the analysis. Finally, we explicitly explore the case of coupling between dark energy and dark matter and assess the ability of measuring the coupling constant. Our parametrization is defined as follows. More details can be found in [308].

Equation of state. In order to represent the evolution of the equation of state parameter w, we use the popular CPL parameterization [229, 584]

$$w(z) = w_0 + w_1 \frac{z}{1+z} \,. \tag{1.8.2}$$

As a special case we will also consider the case of a constant w. We refer to this as the w-parametrization.

Growth rate. Here we assume that the growth rate, f_g, is a function of time but not of scale. As usual, we use the simple prescription [716, 540, 738, 585, 937]

$$f_g = \Omega_m^\gamma \,, \tag{1.8.3}$$

where $\Omega_m(z)$ is the matter density in units of the critical density as a function of redshift. A value $\gamma \approx 0.545$ reproduces well the ΛCDM behavior while departures from this value characterize different models. Here we explore three different parameterizations of f_g:

- *f-parameterization.* This is in fact a non-parametric model in which the growth rate itself is modeled as a step-wise function $f_g(z) = f_i$, specified in different redshift bins. The errors are derived on f_i in each i-th redshift bin of the survey.

- *γ-parameterization.* As a second case we assume

$$f_g \equiv \Omega_m(z)^{\gamma(z)} \,. \tag{1.8.4}$$

  where the $\gamma(z)$ function is parametrized as

$$\gamma(z) = \gamma_0 + \gamma_1 \frac{z}{1+z} \,. \tag{1.8.5}$$

  As shown by [969, 372], this parameterization is more accurate than that of Eq. (1.8.3) for both ΛCDM and DGP models. Furthermore, this parameterization is especially effective to distinguish between a wCDM model (i.e., a dark-energy model with a constant equation of state) that has a negative γ_1 ($-0.020 \lesssim \gamma_1 \lesssim -0.016$) and a DGP model that instead, has a positive γ_1 ($0.035 < \gamma_1 < 0.042$). In addition, modified gravity models show a strongly evolving $\gamma(z)$ [378, 673, 372], in contrast with conventional dark-energy models. As a special case we also consider $\gamma =$ constant (only when w also is assumed constant), to compare our results with those of previous works.

- *η-parameterization.* To explore models in which perturbations grow faster than in the ΛCDM case, like in the case of a coupling between dark energy and dark matter [307], we consider a model in which γ is constant and the growth rate varies as

$$f_g \equiv \Omega_m(z)^\gamma (1+\eta) \,, \tag{1.8.6}$$

  where η quantifies the strength of the coupling. The example of the coupled quintessence model worked out by [307] illustrates this point. In that model, the numerical solution for the growth rate can be fitted by the formula (1.8.6), with $\eta = c\beta_c^2$, where β_c is the dark energy-dark matter coupling constant and best fit values $\gamma = 0.56$ and $c = 2.1$. In this simple case, observational constraints over η can be readily transformed into constraints over β_c.

Reference Cosmological Models. We assume as reference model a "pseudo" ΛCDM, where the growth rate values are obtained from Eq. (1.8.3) with $\gamma = 0.545$ and $\Omega_m(z)$ is given by the standard evolution. Then $\Omega_m(z)$ is completely specified by setting $\Omega_{m,0} = 0.271$, $\Omega_k = 0$, $w_0 = -0.95$, $w_1 = 0$. When the corresponding parameterizations are employed, we choose as fiducial values $\gamma_1 = 0$ and $\eta = 0$, We also assume a primordial slope $n_s = 0.966$ and a present normalization $\sigma_8 = 0.809$.

One of the goals of this work is to assess whether the analysis of the power spectrum in redshift-space can distinguish the fiducial model from alternative cosmologies, characterized by their own set of parameters (apart from $\Omega_{m,0}$ which is set equal to 0.27 for all of them). The alternative models that we consider in this work are:

- *DGP model.* We consider the flat space case studied in [602]. When we adopt this model then we set $\gamma_0 = 0.663$, $\gamma_1 = 0.041$ [372] or $\gamma = 0.68$ [587] and $w = -0.8$ when γ and w are assumed constant.

- *$f(R)$ model.* Here we consider different classes of $f(R)$ models: i) the one proposed in [456], depending on two parameters, n and λ, which we fix to $n = 0.5, 1, 2$ and $\lambda = 3$. For the model with $n = 2$ we assume $\gamma_0 = 0.43$, $\gamma_1 = -0.2$, values that apply quite generally in the limit of small scales (provided they are still linear, see [378]) or $\gamma = 0.4$ and $w = -0.99$. Unless differently specified, we will always refer to this specific model when we mention comparisons to a single $f(R)$ model. ii) The model proposed in [864] fixing $\lambda = 3$ and $n = 2$, which shows a very similar behavior to the previous one. iii) The one proposed in [904] fixing $\lambda = 1$.

- *Coupled dark-energy (CDE) model.* This is the coupled model proposed by [33, 955]. In this case we assume $\gamma_0 = 0.56$, $\eta = 0.056$ (this value comes from putting $\beta_c = 0.16$ as coupling, which is of the order of the maximal value allowed by CMB constraints) [44]. As already explained, this model cannot be reproduced by a constant γ. Forecasts on coupled quintessence based on [42, 33, 724] are discussed in more detail in Section 1.8.8.

For the fiducial values of the bias parameters in every bin, we assume $b(z) = \sqrt{1+z}$ (already used in [753]) since this function provides a good fit to Hα line galaxies with luminosity $L_{\mathrm{H}\alpha} = 10^{42}$ erg^{-1} s^{-1} h^{-2} modeled by [698] using the semi-analytic *GALFORM* models of [108]. For the sake of comparison, we will also consider the case of constant $b = 1$ corresponding to the rather unphysical case of a redshift-independent population of unbiased mass tracers.

The fiducial values for β are computed through

$$\beta^F(z) = \frac{\Omega_m^F(z)^{\gamma^F}}{b^F(z)} = \frac{f_g^F}{b^F}\,. \tag{1.8.7}$$

Now we express the growth function $G(z)$ and the redshift distortion parameter $\beta(z)$ in terms of the growth rate f_g (see Eqs. (1.8.8), (1.8.7)). When we compute the derivatives of the spectrum in the Fisher matrix $b(z)$ and $f_g(z)$ are considered as independent parameters in each redshift bin. In this way we can compute the errors on b (and f_g) self consistently by marginalizing over all other parameters.

Now we are ready to present the main result of the Fisher matrix analysis . We note that in all tables below we always quote errors at 68% probability level and draw in the plots the probability regions at 68% and/or 95% (denoted for shortness as 1 and 2σ values). Moreover, in all figures, all the parameters that are not shown have been marginalized over or fixed to a fiducial value when so indicated.

Results for the f-parameterization. The total number of parameters that enter in the Fisher matrix analysis is 45: 5 parameters that describe the background cosmology ($\Omega_{m,0}h^2, \Omega_{b,0}h^2$, h, n, Ω_k) plus 5 z-dependent parameters specified in 8 redshift bins evenly spaced in the range $z = [0.5, 2.1]$. They are $P_{\mathrm{s}}(z)$, $D(z)$, $H(z)$, $f_g(z)$, $b(z)$. However, since we are not interested in constraining $D(z)$ and $H(z)$, we always project them to the set of parameters they depend on (as explained in [815]) instead of marginalizing over, so extracting more information on the background parameters.

The fiducial growth function $G(z)$ in the $(i+1)$-th redshift bin is evaluated from a step-wise, constant growth rate $f_g(z)$ as

$$G(z) = \exp\left\{\int_0^z f_g(z)\frac{dz}{1+z}\right\} = \prod_i \left(\frac{1+z_i}{1+z_{i-1}}\right)^{f_i} \left(\frac{1+z}{1+z_i}\right)^{f_{i+1}}\,. \tag{1.8.8}$$

To obtain the errors on s_i and b_i we compute the elements of the Fisher matrix and marginalize over all other parameters. In this case one is able to obtain, self-consistently, the error on the bias and on the growth factor at different redshifts, as detailed in Table 4. In Figure 13 we show the contour plots at 68% and 95% of probability for all the pairs $s(z_i) - b(z_i)$ in several redshift bins (with $b = \sqrt{1+z}$), where z_i's are the central values of the bins. We do not show the ellipses for all the 14 bins to avoid overcrowding.

Table 4 illustrates one important result: through the analysis of the redshift-space galaxy power spectrum in a next-generation Euclid-like survey, it will be possible to measure galaxy biasing in $\Delta z = 0.1$ redshift bins with less than 1.6% error, provided that the bias function is independent of scale. We also tested a different choice for the fiducial form of the bias: $b(z) = 1$ finding that the precision in measuring the bias as well as the other parameters has a very little dependence on the $b(z)$ form. Given the robustness of the results on the choice of $b(z)$ in the following we only consider the $b(z) = \sqrt{1+z}$ case.

In Figure 14 we show the errors on the growth rate f_g as a function of redshift, overplotted to our fiducial ΛCDM (green solid curve). The three sets of error bars are plotted in correspondence of the 14 redshift bins and refer (from left to right) to the *Optimistic, Reference* and *Pessimistic* cases, respectively. The other curves show the expected growth rate in three alternative cosmological models: flat DGP (red, longdashed curve), CDE (purple, dot-dashed curve) and different $f(R)$ models (see description in the figure caption). This plot clearly illustrates the ability of next generation surveys to distinguish between alternative models, even in the less favorable choice of survey parameters.

The main results can be summarized as follows.

1. The ability of measuring the biasing function is not too sensitive to the characteristic of the survey ($b(z)$ can be constrained to within 1% in the *Optimistic* scenario and up to 1.6% in the *Pessimistic* one) provided that the bias function is independent of scale. Moreover, we checked that the precision in measuring the bias has a very little dependence on the $b(z)$ form.

2. The growth rate f_g can be estimated to within $1-2.5\%$ in each bin for the *Reference case* survey with no need of estimating the bias function $b(z)$ from some dedicated, independent analysis using higher order statistics [925] or full-PDF analysis [825].

3. The estimated errors on f_g depend weakly on the fiducial model of $b(z)$.

Next, we focus on the ability of determining γ_0 and γ_1, in the context of the γ-*parameterization* and γ, η in the η-*parameterization*. In both cases the Fisher matrix elements have been estimated by expressing the growth factor as

$$G(z) = \delta_0 \exp\left[(1+\eta)\int_0^z \Omega_m(z')^{\gamma(z)}\frac{dz'}{1+z'}\right], \tag{1.8.9}$$

where for the γ-*parameterization* we fix $\eta = 0$.

- γ-*parameterization*. We start by considering the case of constant γ and w in which we set $\gamma = \gamma^F = 0.545$ and $w = w^F = -0.95$. As we will discuss in the next Section, this simple case will allow us to cross-check our results with those in the literature. In Figure 16 we show the marginalized probability regions, at 1 and 2σ levels, for γ and w. The regions with different shades of green illustrate the *Reference case* for the survey whereas the blue long-dashed and the black short-dashed ellipses refer to the *Optimistic* and *Pessimistic* cases, respectively. Errors on γ and w are listed in Table 5 together with the corresponding figures of merit [FoM] defined to be the squared inverse of the Fisher matrix determinant and therefore equal

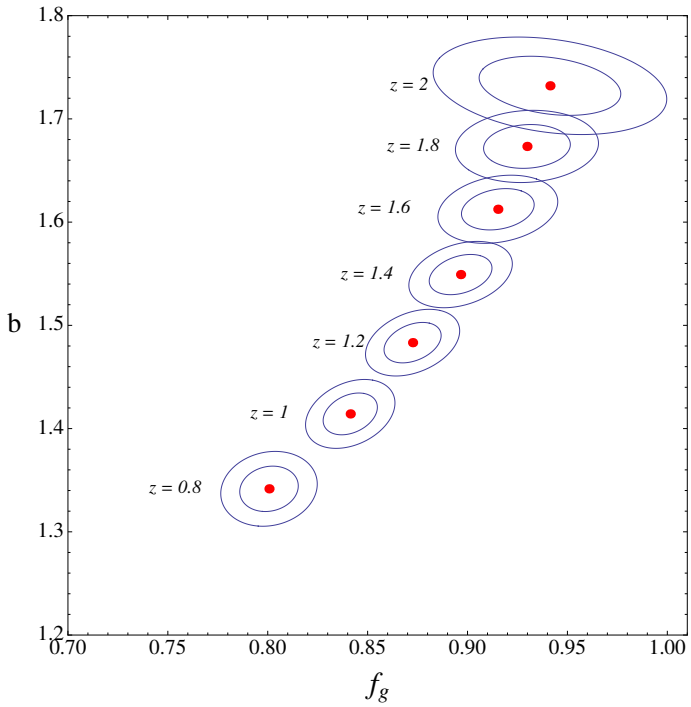

Figure 13: Contour plots at 68% and 98% of probability for the pairs $s(z_i) - b(z_i)$ in 7 redshift bins (with $b = \sqrt{1+z}$). The ellipses are centered on the fiducial values of the growth rate and bias parameters, computed in the central values of the bins, z_i.

Table 4: 1σ marginalized errors for the bias and the growth rates in each redshift bin.

z	σ_b			b^F	z	f_g^F	σ_{f_g}		
	ref.	opt.	pess.				ref.	opt.	pess.
0.7	0.016	0.015	0.019	1.30	0.7	0.76	0.011	0.010	0.012
0.8	0.014	0.014	0.017	1.34	0.8	0.80	0.010	0.009	0.011
0.9	0.014	0.013	0.017	1.38	0.9	0.82	0.009	0.009	0.011
1.0	0.013	0.012	0.016	1.41	1.0	0.84	0.009	0.008	0.011
1.1	0.013	0.012	0.016	1.45	1.1	0.86	0.009	0.008	0.011
1.2	0.013	0.012	0.016	1.48	1.2	0.87	0.009	0.009	0.011
1.3	0.013	0.012	0.016	1.52	1.3	0.88	0.010	0.009	0.012
1.4	0.013	0.012	0.016	1.55	1.4	0.89	0.010	0.009	0.013
1.5	0.013	0.012	0.016	1.58	1.5	0.91	0.011	0.010	0.014
1.6	0.013	0.012	0.016	1.61	1.6	0.91	0.012	0.011	0.016
1.7	0.014	0.013	0.017	1.64	1.7	0.92	0.014	0.012	0.018
1.8	0.014	0.013	0.018	1.67	1.8	0.93	0.014	0.013	0.019
1.9	0.016	0.014	0.021	1.70	1.9	0.93	0.017	0.015	0.025
2.0	0.019	0.016	0.028	1.73	2.0	0.94	0.023	0.019	0.037

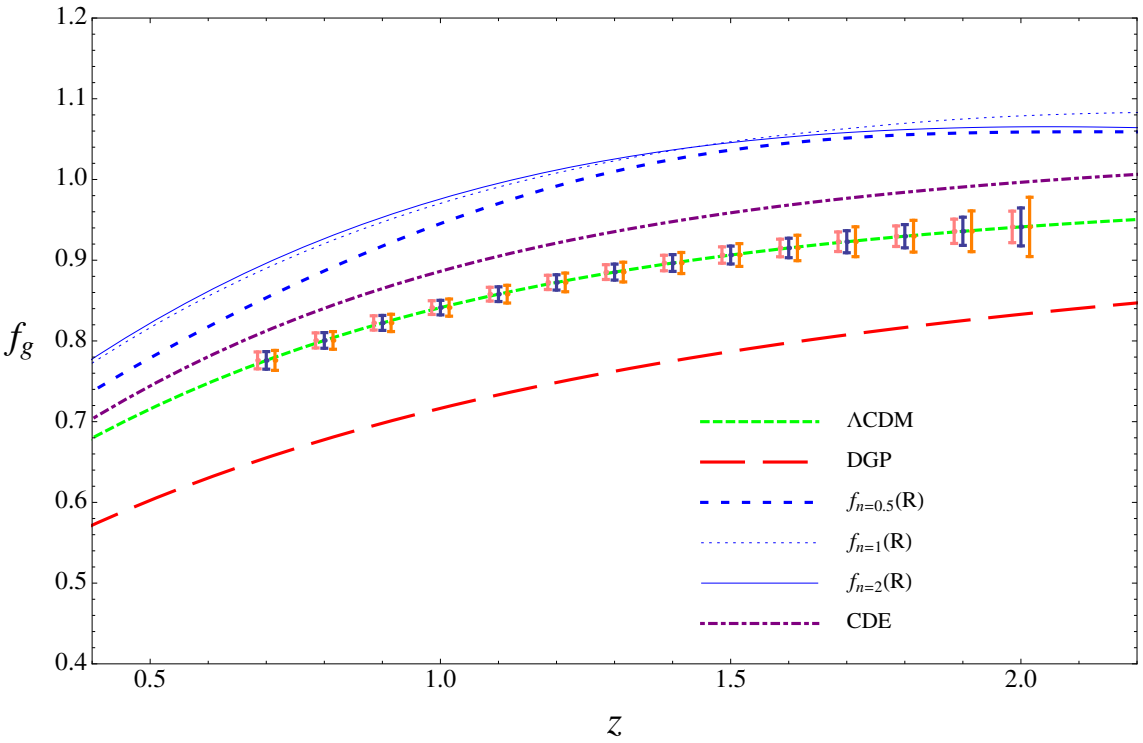

Figure 14: Expected constraints on the growth rates in each redshift bin. For each z the central error bars refer to the *Reference case* while those referring to the *Optimistic* and *Pessimistic* case have been shifted by -0.015 and $+0.015$ respectively. The growth rates for different models are also plotted: ΛCDM (green tight shortdashed curve), flat DGP (red longdashed curve) and a model with coupling between dark energy and dark matter (purple, dot-dashed curve). The blue curves (shortdashed, dotted and solid) represent the $f(R)$ model by [456] with $n = 0.5, 1, 2$ respectively. The plot shows that it will be possible to distinguish these models with next generation data.

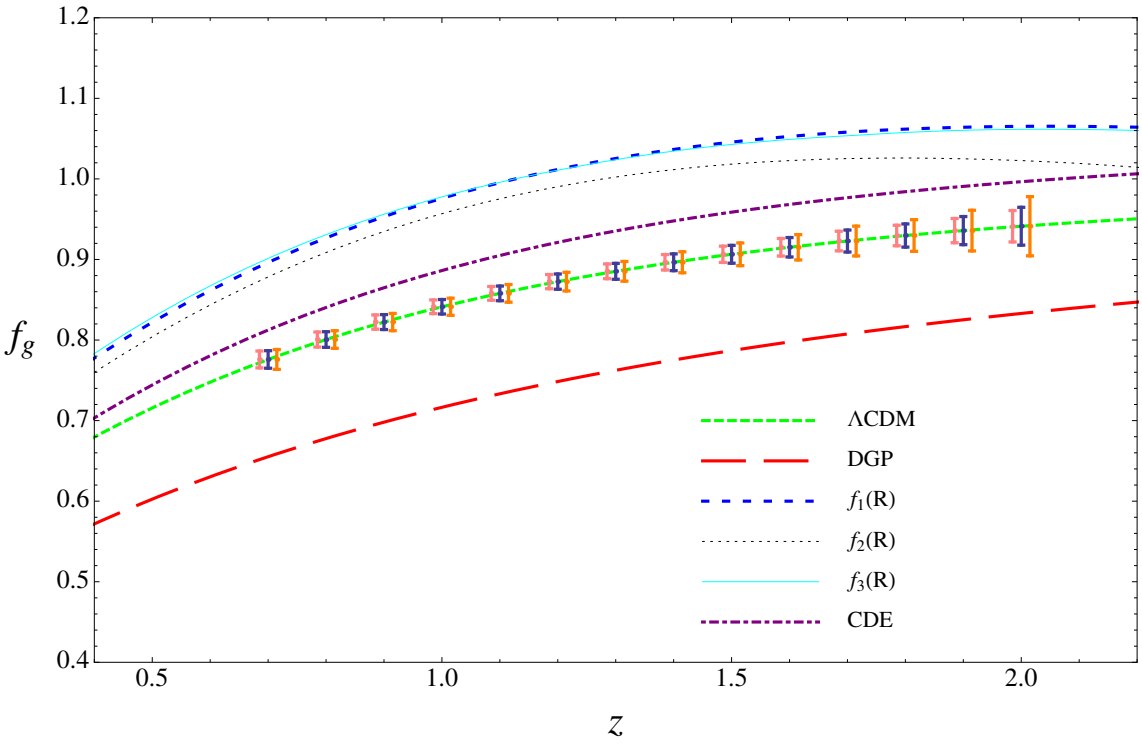

Figure 15: Expected constraints on the growth rates in each redshift bin. For each z the central error bars refer to the *Reference case* while those referring to the *Optimistic* and *Pessimistic* case have been shifted by -0.015 and $+0.015$ respectively. The growth rates for different models are also plotted: ΛCDM (green tight shortdashed curve), flat DGP (red longdashed curve) and a model with coupling between dark energy and dark matter (purple, dot-dashed curve). Here we plot again the $f(R)$ model by [456] with $n = 2$ (blue shortdashed curve) together with the model by [864] (cyan solid curve) and the one by [904] (black dotted curve). Also in this case it will be possible to distinguish these models with next generation data.

to the inverse of the product of the errors in the pivot point, see [21]. Contours are centered on the fiducial model. The blue triangle and the blue square represent the flat DGP and the $f(R)$ models' predictions, respectively. It is clear that, in the case of constant γ and w, the measurement of the growth rate in a Euclid-like survey will allow us to discriminate among these models. These results have been obtained by fixing the curvature to its fiducial value $\Omega_k = 0$. If instead, we consider curvature as a free parameter and marginalize over, the errors on γ and w increase significantly, as shown in Table 6, and yet the precision is good enough to distinguish the different models. For completeness, we also computed the fully marginalized errors over the other cosmological parameters for the reference survey, given in Table 7.

As a second step we considered the case in which γ and w evolve with redshift according to Eqs. (1.8.5) and (1.8.2) and then we marginalized over the parameters γ_1, w_1 and Ω_k. The marginalized probability contours are shown in Figure 17 in which we have shown the three survey setups in three different panels to avoid overcrowding. Dashed contours refer to the z-dependent parameterizations while red, continuous contours refer to the case of constant γ and w obtained after marginalizing over Ω_k. Allowing for time dependency increases the size of the confidence ellipses since the Fisher matrix analysis now accounts for the additional uncertainties in the extra-parameters γ_1 and w_1; marginalized error values are in columns $\sigma_{\gamma_{\rm marg,1}}$, $\sigma_{w_{\rm marg,1}}$ of Table 8. The uncertainty ellipses are now larger and show that DGP and fiducial models could be distinguished at $> 2\sigma$ level only if the redshift survey parameter will be more favorable than in the *Reference case*.

We have also projected the marginalized ellipses for the parameters γ_0 and γ_1 and calculated their marginalized errors and figures of merit, which are reported in Table 9. The corresponding uncertainties contours are shown in the right panel of Figure 16. Once again we overplot the expected values in the $f(R)$ and DGP scenarios to stress the fact that one is expected to be able to distinguish among competing models, irrespective on the survey's precise characteristics.

- *η-parameterization.*

  We have repeated the same analysis as for the *γ-parameterization* taking into account the possibility of coupling between DE and DM, i.e., we have modeled the growth factor according to Eq. (1.8.6) and the dark-energy equation of state as in Eq. (1.8.2) and marginalized over all parameters, including Ω_k. The marginalized errors are shown in columns $\sigma_{\gamma_{\rm marg,2}}$, $\sigma_{w_{\rm marg,2}}$ of Table 8 and the significance contours are shown in the three panels of Figure 18 which is analogous to Figure 17. Even if the ellipses are now larger we note that errors are still small enough to distinguish the fiducial model from the $f(R)$ and DGP scenarios at $> 1\sigma$ and $> 2\sigma$ level respectively.

  Marginalizing over all other parameters we can compute the uncertainties in the γ and η parameters, as listed in Table 10. The relative confidence ellipses are shown in the left panel of Figure 19. This plot shows that next generation Euclid-like surveys will be able to distinguish the reference model with no coupling (central, red dot) to the CDE model proposed by [44] (white square) only at the $1-1.5\sigma$ level.

Finally, in order to explore the dependence on the number of parameters and to compare our results to previous works, we also draw the confidence ellipses for w_0, w_1 with three different methods: i) fixing γ_0, γ_1 and Ω_k to their fiducial values and marginalizing over all the other parameters; ii) fixing only γ_0 and γ_1; iii) marginalizing over all parameters but w_0, w_1. As one can see in Figure 20 and Table 11 this progressive increase in the number of marginalized parameters reflects in a widening of the ellipses with a consequent decrease in the figures of merit. These results are in agreement with those of other authors (e.g., [945]).

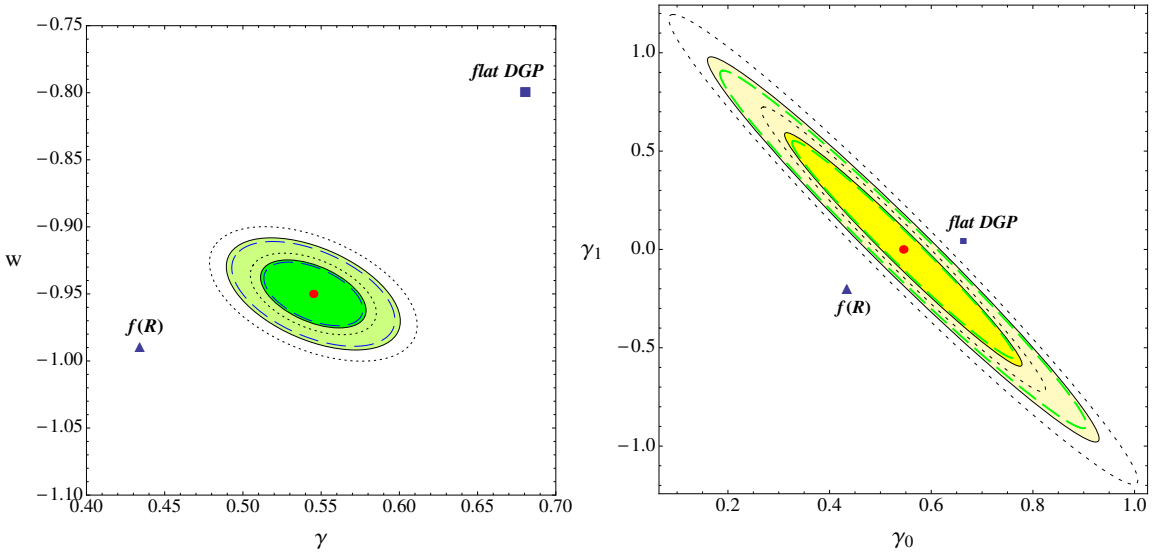

Figure 16: γ-parameterization. *Left panel:* 1 and 2σ marginalized probability regions for constant γ and w: the green (shaded) regions are relative to the *Reference case*, the blue long-dashed ellipses to the *Optimistic case*, while the black short-dashed ellipses are the probability regions for the *Pessimistic case*. The red dot marks the fiducial model; two alternative models are also indicated for comparison. *Right panel:* 1 and 2σ marginalized probability regions for the parameters γ_0 and γ_1, relative to the *Reference case* (shaded yellow regions), to the *Optimistic case* (green long-dashed ellipses), and to the *Pessimistic case* (black dotted ellipses). Red dots represent the fiducial model, blue squares mark the DGP while triangles stand for the $f(R)$ model. Then, in the case of γ-parameterization, one could distinguish these three models (at 95% probability).

Table 5: Numerical values for 1σ constraints on parameters in Figure 16 and figures of merit. Here we have fixed Ω_k to its fiducial value, $\Omega_k = 0$.

	case	σ_γ	σ_w	FoM
$b = \sqrt{1+z}$	ref.	0.02	0.017	3052
with	opt.	0.02	0.016	3509
Ω_k fixed	pess.	0.026	0.02	2106

Table 6: Numerical values for 1σ constraints on parameters γ and w (assumed constant), relative to the red ellipses in Figures 17, 18 and figures of merit. Here we have marginalized over Ω_k.

bias	case	σ_γ	FoM	
$b = \sqrt{1+z}$	ref.	0.03	0.04	1342
	opt.	0.03	0.03	1589
	pess.	0.04	0.05	864

Table 7: Numerical values for marginalized 1σ constraints on cosmological parameters using constant γ and w.

	case	σ_h	$\sigma_{\Omega_m h^2}$	$\sigma_{\Omega_b h^2}$	σ_{Ω_k}	σ_{n_s}	σ_{σ_8}
$b = \sqrt{1+z}$	ref.	0.007	0.002	0.0004	0.008	0.03	0.006

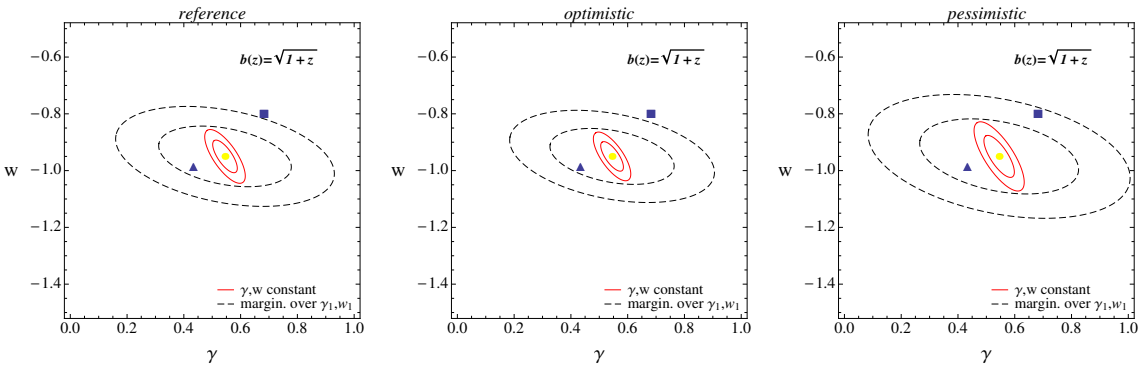

Figure 17: γ-parameterization. 1 and 2σ marginalized probability regions obtained assuming constant γ and w (red solid curves) or assuming the parameterizations (1.8.5) and (1.8.2) and marginalizing over γ_1 and w_1 (black dashed curves); marginalized error values are in columns $\sigma_{\gamma_{\rm marg,1}}$, $\sigma_{w_{\rm marg,1}}$ of Table 8. Yellow dots represent the fiducial model, the triangles a $f(R)$ model and the squares mark the flat DGP.

Table 8: 1σ marginalized errors for parameters γ and w expressed through γ and η parameterizations. Columns $\gamma_{0,\rm marg1}, w_{0,\rm marg1}$ refer to marginalization over γ_1, w_1 (Figure 17) while columns $\gamma_{0,\rm marg2}, w_{0,\rm marg2}$ refer to marginalization over η, w_1 (Figure 18).

bias	case	$\sigma_{\gamma_{\rm marg,1}}$	$\sigma_{w_{\rm marg,1}}$	FoM	$\sigma_{\gamma_{\rm marg,2}}$	$\sigma_{w_{\rm marg,2}}$	FoM
$b=\sqrt{1+z}$	ref.	0.15	0.07	97	0.07	0.07	216
	opt.	0.14	0.06	112	0.07	0.06	249
	pess.	0.18	0.09	66	0.09	0.09	147

Table 9: Numerical values for 1σ constraints on parameters in right panel of Figure 16 and figures of merit.

bias	case	σ_{γ_0}	σ_{γ_1}	FoM
$b=\sqrt{1+z}$	ref.	0.15	0.4	87
	opt.	0.14	0.36	102
	pess.	0.18	0.48	58

Table 10: Numerical values for 1σ constraints on parameters in Figure 19 and figures of merit.

bias	case	σ_γ	σ_η	FoM
$b=\sqrt{1+z}$	ref.	0.07	0.06	554
	opt.	0.07	0.06	650
	pess.	0.09	0.08	362

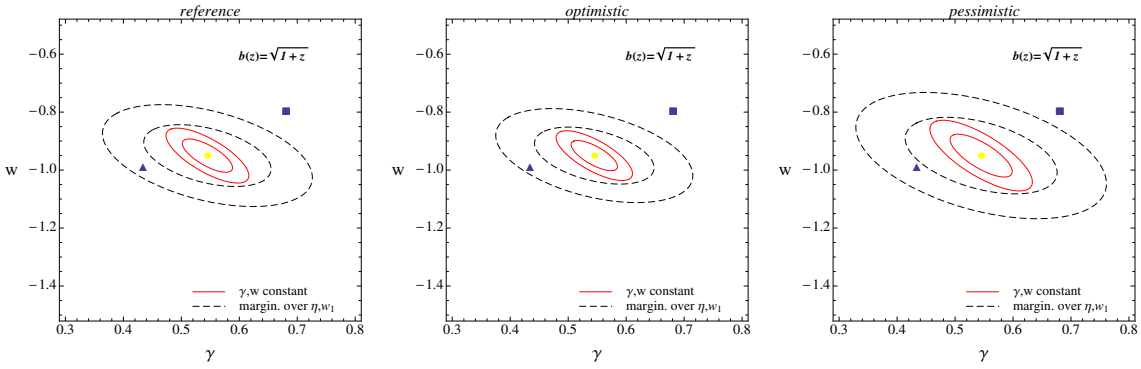

Figure 18: η-parameterization. 1 and 2σ marginalized probability regions obtained assuming constant γ and w (red solid curves) or assuming the parameterizations (1.8.6) and (1.8.2) and marginalizing over η and w_1 (black dashed curves); marginalized error values are in columns $\sigma_{\gamma_{\mathrm{marg},2}}$, $\sigma_{w_{\mathrm{marg},2}}$ of Table 9. Yellow dots represent the fiducial model, the triangles stand for a $f(R)$ model and the squares mark the flat DGP.

The results obtained in this section can be summarized as follows.

1. If both γ and w are assumed to be constant and setting $\Omega_k = 0$, then a redshift survey described by our *Reference case* will be able to constrain these parameters to within 4% and 2%, respectively.

2. Marginalizing over Ω_k degrades these constraints to 5.3% and 4% respectively.

3. If w and γ are considered redshift-dependent and parametrized according to Eqs. (1.8.5) and (1.8.2) then the errors on γ_0 and w_0 obtained after marginalizing over γ_1 and w_1 increase by a factor $\sim 7, 5$. However, with this precision we will be able to distinguish the fiducial model from the DGP and $f(R)$ scenarios with more than 2σ and 1σ significance, respectively.

4. The ability to discriminate these models with a significance above 2σ is confirmed by the confidence contours drawn in the γ_0-γ_1 plane, obtained after marginalizing over all other parameters.

5. If we allow for a coupling between dark matter and dark energy, and we marginalize over η rather than over γ_1, then the errors on w_0 are almost identical to those obtained in the case of the γ-*parameterization*, while the errors on γ_0 decrease significantly.

   However, our ability in separating the fiducial model from the CDE model is significantly hampered: the confidence contours plotted in the γ-η plane show that discrimination can only be performed wit $1-1.5\sigma$ significance. Yet, this is still a remarkable improvement over the present situation, as can be appreciated from Figure 19 where we compare the constraints expected by next generation data to the present ones. Moreover, the *Reference* survey will be able to constrain the parameter η to within 0.06. Reminding that we can write $\eta = 2.1\beta_c^2$ [307], this means that the coupling parameter β_c between dark energy and dark matter can be constrained to within 0.14, solely employing the growth rate information. This is comparable to existing constraints from the CMB but is complementary since obviously it is obtained at much smaller redshifts. A variable coupling could therefore be detected by comparing the redshift survey results with the CMB ones.

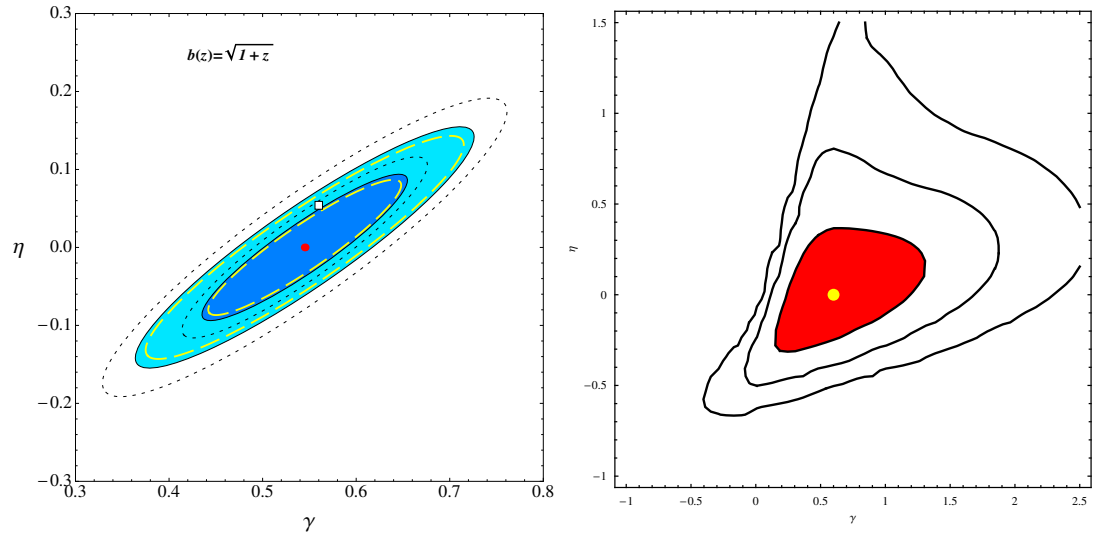

Figure 19: η-parameterization. *Left panel:* 1 and 2σ marginalized probability regions for the parameters γ and η in Eq. (1.8.6) relative to the reference case (shaded blue regions), to the optimistic case (yellow long-dashed ellipses) and to the pessimistic case (black short-dashed ellipses). The red dot marks the fiducial model while the square represents the coupling model. *Right panel:* present constraints on γ and η computed through a full likelihood method (here the red dot marks the likelihood peak) [307].

Table 11: 1σ marginalized errors for the parameters w_0 and w_1, obtained with three different methods (reference case, see Figure 20).

	σ_{w_0}	σ_{w_1}	FoM
γ_0, γ_1, Ω_k fixed	0.05	0.16	430
γ_0, γ_1 fixed	0.06	0.26	148
marginalization over all other parameters	0.07	0.3	87

It is worth pointing out that, whenever we have performed statistical tests similar to those already discussed by other authors in the context of a Euclid-like survey, we did find consistent results. Examples of this are the values of FoM and errors for w_0, w_1, similar to those in [945, 614] and the errors on constant γ and w [614]. However, let us notice that all these values strictly depend on the parametrizations adopted and on the numbers of parameters fixed or marginalized over (see, e.g., [753]).

1.8.4 Weak lensing non-parametric measurement of expansion and growth rate

In this section we apply power spectrum tomography [448] to the Euclid weak lensing survey without using any parameterization of the Hubble parameter $H(z)$ as well as the growth function $G(z)$. Instead, we add the fiducial values of those functions at the center of some redshift bins of our choice to the list of cosmological parameters. Using the Fisher matrix formalism, we can forecast the constraints that future surveys can put on $H(z)$ and $G(z)$. Although such a non-parametric approach is quite common for as concerns the equation-of-state ratio $w(z)$ in supernovae surveys [see, e.g., 22] and also in redshift surveys [815], it has not been investigated for weak lensing surveys.

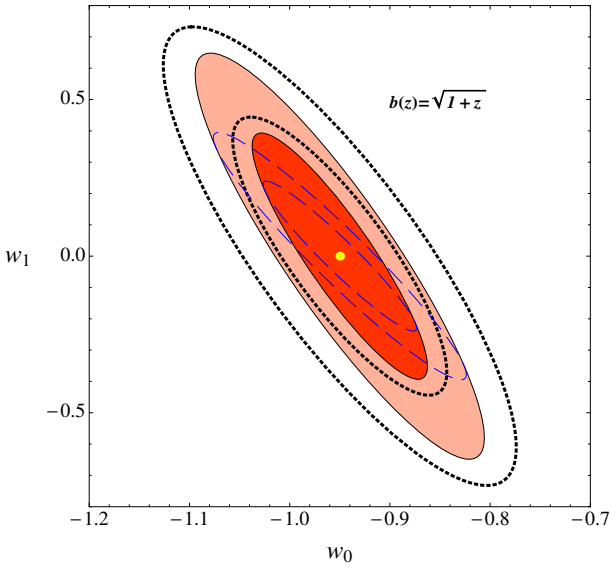

Figure 20: Errors on the equation of state. 1 and 2σ marginalized probability regions for the parameters w_0 and w_1, relative to the reference case and bias $b = \sqrt{(1+z)}$. The blue dashed ellipses are obtained fixing γ_0, γ_1 and $\Omega_k = 0$ to their fiducial values and marginalizing over all the other parameters; for the red shaded ellipses instead, we also marginalize over $\Omega_k = 0$ but we fix γ_0, γ_1. Finally, the black dotted ellipses are obtained marginalizing over all parameters but w_0 and w_1. The progressive increase in the number of parameters reflects in a widening of the ellipses with a consequent decrease in the figures of merit (see Table 11).

The Fisher matrix is given by [458]

$$F_{\alpha\beta} = f_{\rm sky} \sum_{\ell} \frac{(2\ell+1)\Delta\ell}{2} \frac{\partial P_{ij}(\ell)}{\partial p_\alpha} C^{-1}_{jk} \frac{\partial P_{km}(\ell)}{\partial p_\beta} C^{-1}_{mi}, \tag{1.8.10}$$

where $f_{\rm sky}$ is the observed fraction of the sky, C is the covariance matrix, $P(\ell)$ is the convergence power spectrum and $\mathbf{p}$ is the vector of the parameters defining our cosmological model. Repeated indices are being summed over from 1 to N, the number of redshift bins. The covariance matrix is defined as (no summation over j)

$$C_{jk} = P_{jk} + \delta_{jk}\gamma^2_{\rm int} n_j^{-1}, \tag{1.8.11}$$

where $\gamma_{\rm int}$ is the intrinsic galaxy shear and n_j is the fraction of galaxies per steradian belonging to the j-th redshift bin:

$$n_j = 3600 \left(\frac{180}{\pi}\right)^2 n_\theta \int_0^\infty n_j(z) {\rm d}z \tag{1.8.12}$$

where n_θ is the galaxy density per arc minute and $n_j(z)$ the galaxy density for the j-th bin, convolved with a gaussian around $\hat{z}_j$, the center of that bin, with a width of $\sigma_z(1+\hat{z}_j)$ in order to account for errors in the redshift measurement.

For the matter power spectrum we use the fitting formulae from [337] and for its nonlinear corrections the results from [844]. Note that this is where the growth function enters. The convergence power spectrum for the i-th and j-th bin can then be written as

$$P_{ij}(\ell) = \frac{9H_0^3}{4} \int_0^\infty \frac{W_i(z) W_j(z) E^3(z) \Omega_m^2(z)}{(1+z)^4} P_{\delta_m}\left(\frac{\ell}{\pi r(z)}\right) {\rm d}z. \tag{1.8.13}$$

Here we make use of the window function

$$W_i(z) = \int_z^\infty \frac{\mathrm{d}\tilde{z}}{H(\tilde{z})} \left[1 - \frac{r(z)}{r(\tilde{z})}\right] n_i[r(\tilde{z})] \tag{1.8.14}$$

(with $r(z)$ being the comoving distance) and the dimensionless Hubble parameter

$$E^2(z) = \Omega_m^{(0)}(1+z)^3 + (1-\Omega_m^{(0)}) \exp\left[\int_0^z \frac{3(1+w(\tilde{z}))}{1+\tilde{z}} \mathrm{d}\tilde{z}\right]. \tag{1.8.15}$$

For the equation-of-state ratio, finally, we use the usual CPL parameterization.

We determine N intervals in redshift space such that each interval contains the same amount of galaxies. For this we use the common parameterization

$$n(z) = z^2 \exp(-(z/z_0)^{3/2}), \tag{1.8.16}$$

where $z_0 = z_{\mathrm{mean}}/1.412$ is the peak of $n(z)$ and z_{mean} the median. Now we can define $\hat{z}_i$ as the center of the i-th redshift bin and add $h_i \equiv \log\left(H(\hat{z}_i)/H_0\right)$ as well as $g_i \equiv \log G(\hat{z}_i)$ to the list of cosmological parameters. The Hubble parameter and the growth function now become functions of the h_i and g_i respectively:

$$H(z; \Omega_m^{(0)}, w_0, w_1) \to H(z; h_1, \ldots, h_N) \tag{1.8.17}$$

$$G(z; \Omega_m^{(0)}, \gamma) \to G(z; g_1, \ldots, g_N) \tag{1.8.18}$$

This is being done by linearly interpolating the functions through their supporting points, e.g., $(\hat{z}_i, \exp(h_i))$ for $H(z)$. Any function that depends on either $H(z)$ or $G(z)$ hence becomes a function of the h_i and g_i as well.

Table 12: Values used in our computation. The values of the fiducial model (WMAP7, on the left) and the survey parameters (on the right).

ω_m	0.1341
ω_b	0.02258
τ	0.088
n_s	0.963
Ω_m	0.266
w_0	–1
w_1	0
γ	0.547
γ_{ppn}	0
σ_8	0.801

f_{sky}	0.375
z_{mean}	0.9
σ_z	0.05
n_θ	30
γ_{int}	0.22
ℓ_{max}	$5 \cdot 10^3$
$\Delta \log_{10} \ell$	0.02

The values for our fiducial model (taken from WMAP 7-year data [526]) and the survey parameters that we chose for our computation can be found in Table 12.

As for the sum in Eq. (1.8.10), we generally found that with a realistic upper limit of $\ell_{\mathrm{max}} = 5 \cdot 10^3$ and a step size of $\Delta \lg \ell = 0.2$ we get the best result in terms of a figure of merit (FoM), that we defined as

$$\mathrm{FoM} = \sum \sigma_i^{-2}. \tag{1.8.19}$$

Note that this is a fundamentally different FoM than the one defined by the Dark Energy Task Force. Our definition allows for a single large error without influencing the FoM significantly and should stay almost constant after dividing a bin arbitrarily in two bins, assuming the error scales roughly as the inverse of the root of the number of galaxies in a given bin.

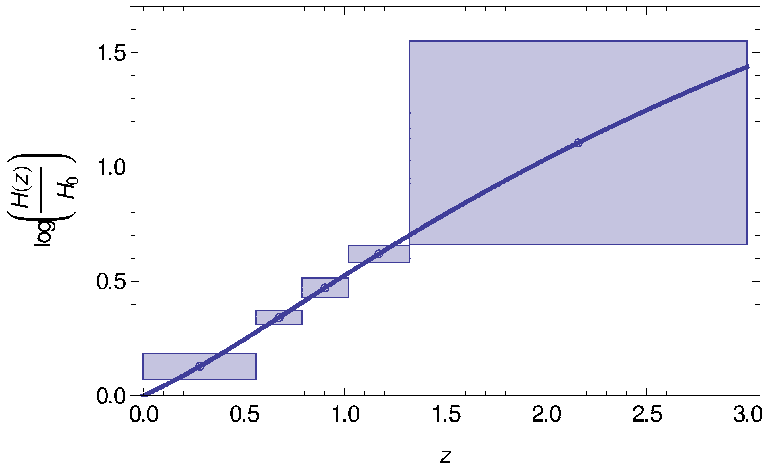

Figure 21: Error bars on the Hubble parameter $H(z)$ with five redshift bins. The exact height of the error bars respectively are $(0.23, 0.072, 0.089, 0.064, 0.76)$.

We first did the computation with just binning $H(z)$ and using the common fit for the growth function slope [937]

$$\frac{d\log G(z)}{d\log a} = \Omega_m(z)^\gamma, \tag{1.8.20}$$

yielding the result in Figure 21. Binning both $H(z)$ and $G(z)$ and marginalizing over the h_is yields the plot for $G(z)$ seen in Figure 22.

Notice that here we assumed no prior information. Of course one could improve the FoM by taking into account some external constraints due to other experiments.

1.8.5 Testing the nonlinear corrections for weak lensing forecasts

In order to fully exploit next generation weak lensing survey potentialities, accurate knowledge of nonlinear power spectra up to $\sim 1\%$ is needed [465, 469]. However, such precision goes beyond the claimed $\pm 3\%$ accuracy of the popular HALOFIT code [844].

[651] showed that, using HALOFIT for non-ΛCDM models, requires suitable corrections. In spite of that, HALOFIT has been often used to calculate the spectra of models with non-constant DE state parameter $w(z)$. This procedure was dictated by the lack of appropriate extensions of HALOFIT to non-ΛCDM cosmologies.

In this paragraph we quantify the effects of using the HALOFIT code instead of N-body outputs for nonlinear corrections for DE spectra, when the nature of DE is investigated through weak lensing surveys. Using a Fisher-matrix approach, we evaluate the discrepancies in error forecasts for w_0, w_a and Ω_m and compare the related confidence ellipses. See [215] for further details.

The weak lensing survey is as specified in Section 1.8.2. Tests are performed assuming three different fiducial cosmologies: ΛCDM model ($w_0 = -1$, $w_a = 0$) and two dynamical DE models, still consistent with the WMAP+BAO+SN combination [526] at 95% C.L. They will be dubbed M1 ($w_0 = -0.67$, $w_a = 2.28$) and M3 ($w_0 = -1.18$, $w_a = 0.89$). In this way we explore the dependence of our results on the assumed fiducial model. For the other parameters we adopt the fiducial cosmology of Secton 1.8.2.

The derivatives to calculate the Fisher matrix are evaluated by extracting the power spectra from the N-body simulations of models close to the fiducial ones, obtained by considering parameter increments $\pm 5\%$. For the ΛCDM case, two different initial seeds were also considered, to test the

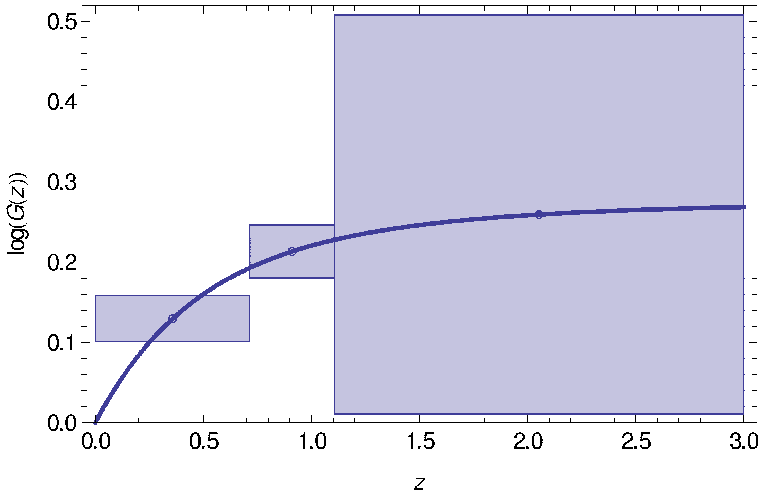

Figure 22: Error bars on the growth function $G(z)$ with three redshift bins while marginalizing over the h_is. The exact height of the error bars respectively are $(0.029, 0.033, 0.25)$.

dependence on initial conditions, finding that Fisher matrix results are almost insensitive to it. For the other fiducial models, only one seed is used.

N-body simulations are performed by using a modified version of PKDGRAV [859] able to handle any DE state equation $w(a)$, with $N^3 = 256^3$ particles in a box with side $L = 256\,h^{-1}$ Mpc. Transfer functions generated using the CAMB package are employed to create initial conditions, with a modified version of the PM software by [510], also able to handle suitable parameterizations of DE.

Matter power spectra are obtained by performing a FFT (Fast Fourier Transform) of the matter density fields, computed from the particles distribution through a Cloud-in-Cell algorithm, by using a regular grid with $N_g = 2048$. This allows us to obtain nonlinear spectra in a large k-interval. In particular, our resolution allows to work out spectra up to $k \simeq 10\,h$ Mpc^{-1}. However, for $k > 2-3\,h$ Mpc^{-1} neglecting baryon physics is no longer accurate [481, 774, 149, 976, 426]. For this reason, we consider WL spectra only up to $\ell_{\rm max} = 2000$.

Particular attention has to be paid to matter power spectra normalizations. In fact, we found that, normalizing all models to the same linear $\sigma_8(z = 0)$, the shear derivatives with respect to w_0, w_a or Ω_m were largely dominated by the normalization shift at $z = 0$, σ_8 and $\sigma_{8,nl}$ values being quite different and the shift itself depending on w_0, w_a and Ω_m. This would confuse the z dependence of the growth factor, through the observational z-range. This normalization problem was not previously met in analogous tests with the Fisher matrix, as HALOFIT does not directly depend on the DE state equation.

As a matter of fact, one should keep in mind that, observing the galaxy distribution with future surveys, one can effectively measure $\sigma_{8,nl}$, and not its linear counterpart. For these reasons, we choose to normalize matter power spectra to $\sigma_{8,nl}$, assuming to know it with high precision.

In Figures 23 we show the confidence ellipses, when the fiducial model is ΛCDM, in the cases of 3 or 5 bins and with $\ell_{\rm max} = 2000$. Since the discrepancy between different seeds are small, discrepancies between HALOFIT and simulations are truly indicating an underestimate of errors in the HALOFIT case.

As expected, the error on Ω_m estimate is not affected by the passage from simulations to HALOFIT, since we are dealing with ΛCDM models only. On the contrary, using HALOFIT leads to underestimates of the errors on w_0 and w_a, by a substantial $30-40\%$ (see [215] for further details).

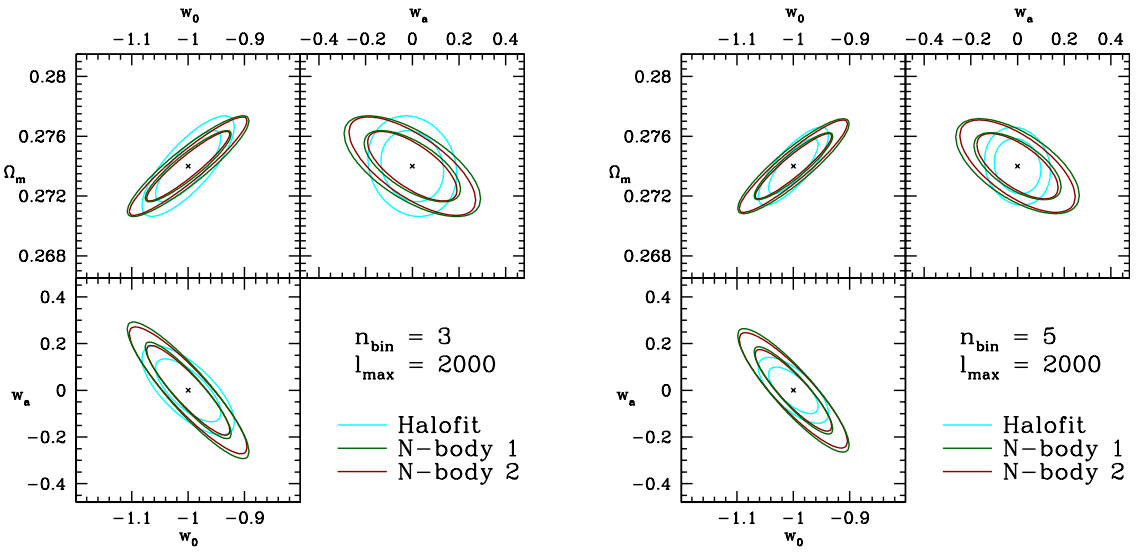

Figure 23: Likelihood contours, for 65% and 95% C.L., calculated including signals up to $\ell \simeq 2000$ for the ΛCDM fiducial. Here simulations and HALOFIT yield significantly different outputs.

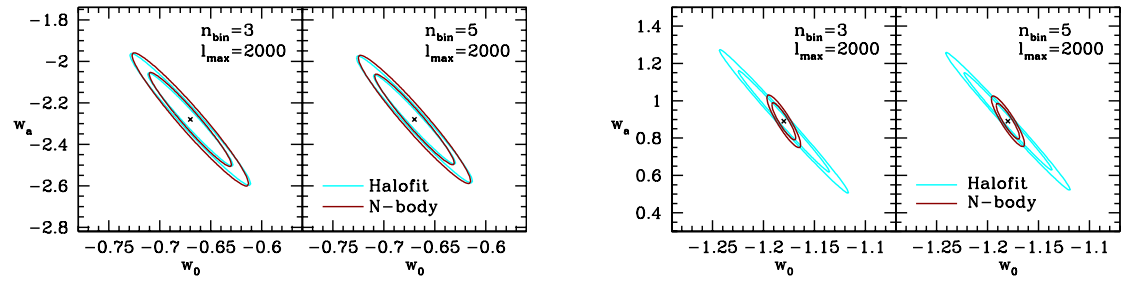

Figure 24: On the left (right) panel, 1- and 2-σ contours for the M1 (M3) model. The two fiducial models exhibit quite different behaviors.

This confirms that, when considering models different from ΛCDM, nonlinear correction obtained through HALOFIT may be misleading. This is true even when the fiducial model is ΛCDM itself and we just consider mild deviations of w from -1.

Figure 24 then show the results in the w_0-w_a plane, when the fiducial models are M1 or M3. It is evident that the two cases are quite different. In the M1 case, we see just quite a mild shift, even if they are $\mathcal{O}$ (10%) on error predictions. In the M3 case, errors estimated through HALOFIT exceed simulation errors by a substantial factor. Altogether, this is a case when estimates based on HALOFIT are not trustworthy.

The effect of baryon physics is another nonlinear correction to be considered. We note that the details of a study on the impact of baryon physics on the power spectrum and the parameter estimation can be found in [813]

1.8.6 Forecasts for the dark-energy sound speed

As we have seen in Section 1.3.1, when dark energy clusters, the standard sub-horizon Poisson equation that links matter fluctuations to the gravitational potential is modified and $Q \neq 1$. The deviation from unity will depend on the degree of DE clustering and therefore on the sound speed

c_s. In this subsection we try to forecast the constraints that Euclid can put on a constant c_s by measuring Q both via weak lensing and via redshift clustering. Here we assume standard Einstein gravity and zero anisotropic stress (and therefore we have $\Psi = \Phi$) and we allow c_s to assume different values in the range $0-1$.

Generically, while dealing with a non-zero sound speed, we have to worry about the sound horizon $k_{sh} = aH/c_s$, which characterizes the growth of the perturbations; then we have at least three regimes with different behavior of the perturbations:

1. perturbations larger than the causal horizon (where perturbations are not causally connected and their growth is suppressed),
2. perturbations smaller than the causal horizon but larger than the sound horizon, $k \ll aH/c_s$ (this is the only regime where perturbations are free to grow because the velocity dispersion, or equivalently the pressure perturbation, is smaller than the gravitational attraction),
3. perturbations smaller than the sound horizon, $k \gg aH/c_s$ (here perturbations stop growing because the pressure perturbation is larger than the gravitational attraction).

As we have set the anisotropic stress to zero, the perturbations are fully described by Q. The main problem is therefore to find an explicit expression that shows how Q depends on c_s. [785] have provided the following explicit approximate expression for $Q(k,a)$ which captures the behavior for both super- and sub-horizon scales:

$$Q(k,a) = 1 + \frac{1-\Omega_{M,0}}{\Omega_{M,0}} \frac{(1+w)a^{-3w}}{1-3w+\frac{2}{3}\nu(a)^2}. \tag{1.8.21}$$

Here $\nu(a)^2 = k^2 c_s^2 a/\left(\Omega_{M,0}H_0^2\right)$ which it is defined through $c_s k \equiv \nu aH$ so that ν counts how deep a mode is inside the sound horizon.

Eq. (1.8.21) depends substantially on the value of the sound speed or, to put it differently, on the scale considered. For scales larger than the sound horizon ($\nu \approx 0$), Eq. (1.8.21) scales as a^{-3w} and for $\Omega_{m,0} = 0.25$ and $w = -0.8$ we have that

$$Q - 1 \approx \frac{3}{17} a^{2.4} \simeq 0.18 a^{2.4}\,. \tag{1.8.22}$$

This is not a negligible deviation today, but it decreases rapidly as we move into the past, as the dark energy becomes less important.[8] As a scale enters the sound horizon, $Q-1$ grows with one power of the scale factor slower (since $\delta_{\rm DE}$ stops growing), suppressing the final deviation roughly by the ratio of horizon size to the scale of interest (as now $\nu^2 \gg 1$). In the observable range, $(k/H_0)^2 \approx 10^2 - 10^4$. Therefore, if $c_s \approx 1$, $Q \to 1$ and the dependence on c_s is lost. This shows that Q is sensitive to c_s only for small values, $c_s^2 \lesssim 10^{-2}$.

We can characterize the dependence of Q on the main perturbation parameter c_s^2 by looking at its derivative, a key quantity for Fisher matrix forecasts:

$$\frac{\partial \log Q}{\partial \log c_s^2} = -\frac{x}{(1+x)}\frac{Q-1}{Q}\,, \tag{1.8.23}$$

where $x = \frac{2}{3}\nu(a)^2/(1-3w) \simeq 0.2\nu(a)^2$ (with the last expression being for $w = -0.8$). For the values we are interested in here, this derivative has a peak at the present epoch at the sound horizon, i.e., for $c_s \approx H_0/k$, which in the observable range of k is $c_s \approx .01 - .001$, and declines rapidly for larger c_s. This means that the sensitivity of Q to the sound speed can be boosted by several orders of magnitude as the sound speed is decreased.

There are several observables that depend on Q:

[8] For this reason, early dark-energy models can have a much stronger impact.

- The growth of matter perturbations

  There are two ways to influence the growth factor: firstly at background level, with a different Hubble expansion. Secondly at perturbation level: if dark energy clusters then the gravitational potential changes because of the Poisson equation, and this will also affect the growth rate of dark matter. All these effects can be included in the growth index γ and we therefore expect that γ is a function of w and c_s^2 (or equivalently of w and Q).

  The growth index depends on dark-energy perturbations (through Q) as [785]

$$\gamma = \frac{3\left(1 - w - A\left(Q\right)\right)}{5 - 6w} \tag{1.8.24}$$

  where

$$A\left(Q\right) = \frac{Q - 1}{1 - \Omega_M\left(a\right)}. \tag{1.8.25}$$

  Clearly here, the key quantity is the derivative of the growth factor with respect to the sound speed:

$$\frac{\partial \log G}{\partial \ln c_s^2} \propto \int_{a_0}^{a_1} \frac{\partial \gamma}{\partial c_s^2} \mathrm{d}a \propto \int_{a_0}^{a_1} \frac{\partial Q}{\partial c_s^2} \mathrm{d}a \propto \int_{a_0}^{a_1} \left(Q - 1\right) \mathrm{d}a\,. \tag{1.8.26}$$

  From the above equation we also notice that the derivative of the growth factor does not depend on $Q - 1$ like the derivative Q, but on $Q - Q_0$ as it is an integral (being Q_0 the value of Q today). The growth factor is thus not directly probing the deviation of Q from unity, but rather how Q evolves over time, see [786] for more details.

- Redshift space distortions

  The distortion induced by redshift can be expressed in linear theory by the β factor, related to the bias factor and the growth rate via:

$$\beta(z, k) = \frac{\Omega_m\left(z\right)^{\gamma(k,z)}}{b(z)}\,. \tag{1.8.27}$$

  The derivative of the redshift distortion parameter with respect to the sound speed is:

$$\frac{\partial \log\left(1 + \beta\mu^2\right)}{\partial \log c_s^2} = -\frac{3}{5 - 6w} \frac{\beta\mu^2}{1 + \beta\mu^2} \frac{x}{1 + x} \left(Q - 1\right)\,. \tag{1.8.28}$$

  We see that the behavior versus c_s^2 is similar to the one for the Q derivative, so the same discussion applies. Once again, the effect is maximized for small c_s. The β derivative is comparable to that of G at $z = 0$ but becomes more important at low redshifts.

- Shape of the dark matter power spectrum

  Quantifying the impact of the sound speed on the matter power spectrum is quite hard as we need to run Boltzmann codes (such as CAMB, [559]) in order to get the full impact of dark-energy perturbations into the matter power spectrum. [786] proceeded in two ways: first using the CAMB output and then considering the analytic expression from [337] (which does not include dark energy perturbations, i.e., does not include c_s).

  They find that the impact of the derivative of the matter power spectrum with respect the sound speed on the final errors is only relevant if high values of c_s^2 are considered; by decreasing the sound speed, the results are less and less affected. The reason is that for low values of the sound speed other parameters, like the growth factor, start to be the dominant source of information on c_s^2.

Impact on weak lensing. Now it is possible to investigate the response of weak lensing (WL) to the dark-energy parameters. Proceeding with a Fisher matrix as in [41], the main difference here being that the parameter Q has an explicit form. Since Q depends on w and c_s^2, we can forecast the precision with which those parameters can be extracted. We can also try to trace where the constraints come from. For a vanishing anisotropic stress the WL potential becomes:

$$k^2 (\Phi + \Psi) = -2Q \frac{3H_0^2 \Omega_{M,0}}{2a} \Delta_M \tag{1.8.29}$$

which can be written, in linear perturbation theory as:

$$k^2 (\Phi + \Psi) = -3H (a)^2 a^3 Q (a,k) \Omega_M (a) G (a,k) \Delta_M (k) . \tag{1.8.30}$$

Hence, the lensing potential contains three conceptually different contributions from the dark-energy perturbations:

- The direct contribution of the perturbations to the gravitational potential through the factor Q.
- The impact of the dark-energy perturbations on the growth rate of the dark matter perturbations, affecting the time dependence of Δ_M, through $G(a,k)$.
- A change in the shape of the matter power spectrum $P(k)$, corresponding to the dark energy induced k dependence of Δ_M.

We use the representative Euclid survey presented in Section 1.8.2 and we extend our survey up to three different redshifts: $z_{\max} = 2, 3, 4$. We choose different values of c_s^2 and $w_0 = -0.8$ in order to maximize the impact on Q: values closer to -1 reduce the effect and therefore increase the errors on c_s.

In Figure 25 we report the $1-\sigma$ confidence region for w_0, c_s^2 for two different values of the sound speed and $z_{\max}$. For high value of the sound speed ($c_s^2 = 1$) we find $\sigma(w_0) = 0.0195$ and the relative error for the sound speed is $\sigma(c_s^2)/c_s^2 = 2615$. As expected, WL is totally insensitive to the clustering properties of quintessence dark-energy models when the sound speed is equal to 1. The presence of dark-energy perturbations leaves a w and c_s^2 dependent signature in the evolution of the gravitational potentials through $\Delta_{\rm DE}/\Delta_m$ and, as already mentioned, the increase of the c_s^2 enhances the suppression of dark-energy perturbations which brings $Q \to 1$.

Once we decrease the sound speed then dark-energy perturbations are free to grow at smaller scales. In Figure 25 the confidence region for w_0, c_s^2 for $c_s^2 = 10^{-6}$ is shown; we find $\sigma(w_0) = 0.0286$, $\sigma(c_s^2)/c_s^2 = 0.132$; in the last case the error on the measurement of the sound speed is reduced to the 70% of the total signal.

Impact on galaxy power spectrum. We now explore a second probe of clustering, the galaxy power spectrum. The procedure is the same outlined in Section 1.7.3. We use the representative Euclid survey presented in Section 1.8.2. Here too we also consider in addition possible extended surveys to $z_{\max} = 2.5$ and $z_{\max} = 4$.

In Figure 26 we report the confidence region for w_0, c_s^2 for two different values of the sound speed and $z_{\max}$. For high values of the sound speed ($c_s^2 = 1$) we find, for our benchmark survey: $\sigma(w_0) = 0.0133$, and $\sigma(c_s^2)/c_s^2 = 50.05$. Here again we find that galaxy power spectrum is not sensitive to the clustering properties of dark energy when the sound speed is of order unity. If we decrease the sound speed down to $c_s^2 = 10^{-6}$ then the errors are $\sigma(w_0) = 0.0125$, $\sigma(c_s^2)/c_s^2 = 0.118$.

In conclusion, as perhaps expected, we find that dark-energy perturbations have a very small effect on dark matter clustering unless the sound speed is extremely small, $c_s \leq 0.01$. Let us remind that in order to boost the observable effect, we always assumed $w = -0.8$; for values closer to -1

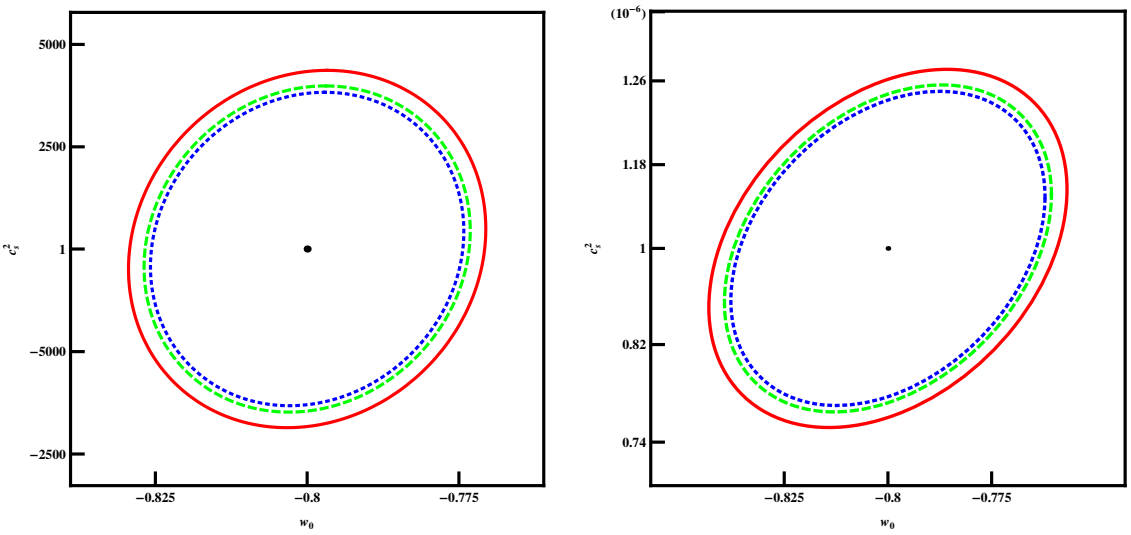

Figure 25: Confidence region at 68% for three different values of $z_{\max} = 2.5, 3.5, 4$, red solid, green long-dashed and blue dashed contour, respectively. The left panel shows the confidence region when the sound speed is $c_s^2 = 1$; the right panel with the sound speed $c_s^2 = 10^{-6}$. The equation of state parameter is for both cases $w_0 = -0.8$.

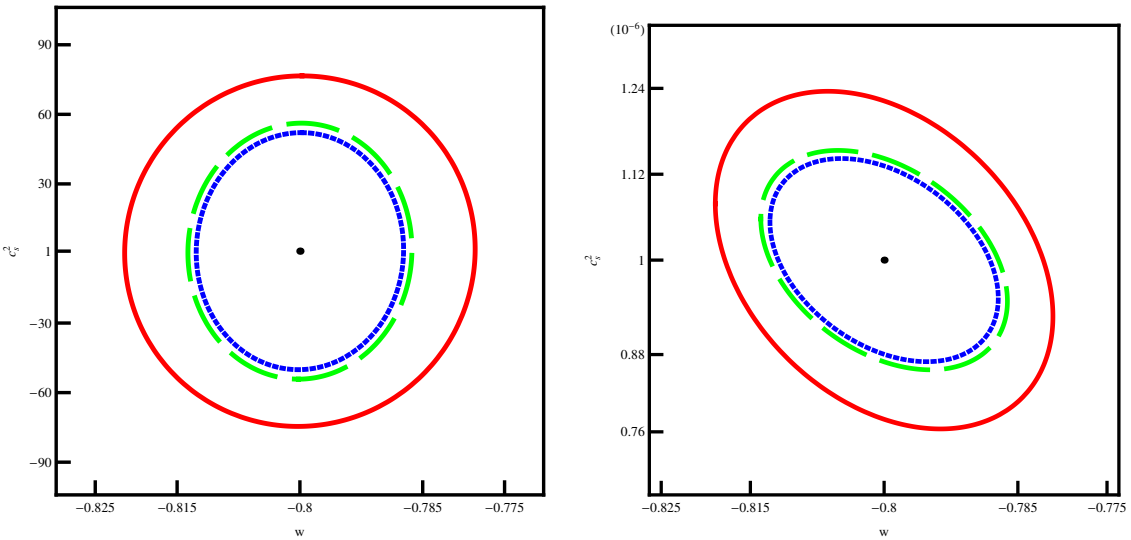

Figure 26: Confidence region at 68% for three different values of $z_{\max} = 2.5, 3.5, 4$, red solid, green long-dashed and blue dashed contour, respectively. The left panel shows the confidence region when the sound speed is $c_s^2 = 1$; the right panel with the sound speed $c_s^2 = 10^{-6}$. The equation of state parameter is for both cases $w_0 = -0.8$.

the sensitivity to c_s^2 is further reduced. As a test, [786] performed the calculation for $w = -0.9$ and $c_s^2 = 10^{-5}$ and found $\sigma_{c_s^2}/c_s^2 = 2.6$ and $\sigma_{c_s^2}/c_s^2 = 1.09$ for WL and galaxy power spectrum experiments, respectively.

Such small sound speeds are not in contrast with the fundamental expectation of dark energy being much smoother that dark matter: even with $c_s \approx 0.01$, dark-energy perturbations are more than one order of magnitude weaker than dark matter ones (at least for the class of models investigated here) and safely below nonlinearity at the present time at all scales. Models of "cold" dark energy are interesting because they can cross the phantom divide [536] and contribute to the cluster masses [258] (see also Section 1.6.2 of this review). Small c_s could be constructed for instance with scalar fields with non-standard kinetic energy terms.

1.8.7 Weak lensing constraints on *f(R)* gravity

In this section, we present the Euclid weak lensing forecasts of a specific, but very popular, class of models, the so-called $f(R)$ models of gravity. As we have already seen in Section 1.4.6 these models are described by the action

$$S_{\rm grav} = \int \sqrt{-g}\, \mathrm{d}^4x \left[\frac{f(R)}{16\pi G} - \mathcal{L}_{\rm m}\right], \tag{1.8.31}$$

where $f(R)$ is an arbitrary function of the Ricci scalar and $\mathcal{L}_{\rm m}$ is the Lagrange density of standard matter and radiation.

In principle one has complete freedom to specify the function $f(R)$, and so any expansion history can be reproduced. However, as discussed in Section 1.4.6, those that remain viable are the subset that very closely mimic the standard ΛCDM background expansion, as this restricted subclass of models can evade solar system constraints [230, 906, 410], have a standard matter era in which the scale factor evolves according to $a(t) \propto t^{2/3}$ [43] and can also be free of ghost and tachyon instabilities [682, 415].

To this subclass belongs the popular $f(R)$ model proposed by [456] (1.4.52). [200] demonstrated that Euclid will have the power of distinguishing between it and ΛCDM with a good accuracy. They performed a tomographic analysis using several values of the maximum allowed wavenumber of the Fisher matrices; specifically, a conservative value of 1000, an optimistic value of 5000 and a bin-dependent setting, which increases the maximum angular wavenumber for distant shells and reduces it for nearby shells. Moreover, they computed the Bayesian expected evidence for the model of Eq. (1.4.52) over the ΛCDM model as a function of the extra parameter n. This can be done because the ΛCDM model is formally nested in this $f(R)$ model, and the latter is equivalent to the former when $n = 0$. Their results are shown in Figure 27. For another Bayesian evidence analysis of $f(R)$ models and the added value of probing the growth of structure with galaxy surveys see also [850].

This subclass of $f(R)$ models can be parameterized solely in terms of the mass of the scalar field, which as we have seen in Eq. (1.4.71) is related to the $f(R)$ functional form via the relation

$$M^2(a) = \frac{1}{3f_{,RR}[R_{\rm back}(a)]} \tag{1.8.32}$$

where R subscripts denote differentiation with respect to R. The function $f_{,RR}$ can be approximated by its standard ΛCDM form,

$$\frac{R_{\rm back}}{H_0^2} \simeq \frac{3\Omega_{\rm m0}}{a^3} + 12\Omega_\Lambda\,, \tag{1.8.33}$$

valid for $z \lesssim 1000$. The mass $M(a)$ is typically a function of redshift which decays from a large value in the early universe to its present day value M_0.

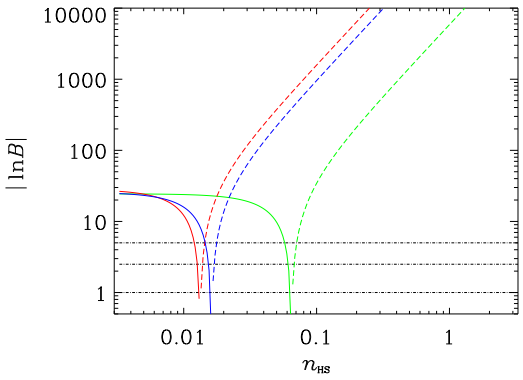

Figure 27: The Bayes factor $\ln B$ for the $f(R)$ model of Eq. (1.4.52) over standard ΛCDM as a function of the extra parameter n. The green, red and blue curves refer to the conservative, bin-dependent and optimistic $\ell_{\rm max}$, respectively. The horizontal lines denote the Jeffreys' scale levels of significance.

Whilst these models are practically indistinguishable from ΛCDM at the level of background expansion, there is a significant difference in the evolution of perturbations relative to the standard GR behavior.

The evolution of linear density perturbations in the context of $f(R)$ gravity is markedly different than in the standard ΛCDM scenario; $\delta_{\rm m} \equiv \delta\rho_{\rm m}/\rho_{\rm m}$ acquires a nontrivial scale dependence at late times. This is due to the presence of an additional scale $M(a)$ in the equations; as any given mode crosses the modified gravity 'horizon' $k = aM(a)$, said mode will feel an enhanced gravitational force due to the scalar field. This will have the effect of increasing the power of small scale modes.

Perturbations on sub-horizon scales in the Newtonian gauge evolve approximately according to

$$\Psi = \left(1 + \frac{2\bar{K}^2}{3 + 2\bar{K}^2}\right)\Phi, \tag{1.8.34}$$

$$k^2\Phi = -4\pi G\left(\frac{3 + 2\bar{K}^2}{3 + 3\bar{K}^2}\right)a^2\rho_{\rm m}\delta_{\rm m}, \tag{1.8.35}$$

$$\ddot{\delta}_{\rm m} + 2H\dot{\delta}_{\rm m} - 4\pi G\left(\frac{3 + 4\bar{K}^2}{3 + 3\bar{K}^2}\right)\rho_{\rm m}\delta_{\rm m} = 0\,, \tag{1.8.36}$$

where $\bar{K} = k/(aM(a))$. These equations represent a particular example of a general parameterization introduced in [636, 131, 983]. To solve them one should first parameterize the scalaron mass $M(a)$, choosing a form that broadly describes the behavior of viable $f(R)$ models. A suitable functional form, which takes into account the evolution of $M(a)$ in both the matter era and the late-time accelerating epoch, is given by [887]

$$M^2 = M_0^2\left(\frac{a^{-3} + 4a_*^{-3}}{1 + 4a_*^{-3}}\right)^{2\nu}, \tag{1.8.37}$$

where a_* is the scale factor at matter-Λ equality; $a_* = (\Omega_{\rm m0}/\Omega_\Lambda)^{1/3}$. There are two modified gravity parameters; M_0 is the mass of the scalaron at the present time and ν is the rate of increase of $M(a)$ to the past.

In Figure 28 the linear matter power spectrum is exhibited for this parameterization (dashed line), along with the standard ΛCDM power spectrum (solid line). The observed, redshift dependent tilt is due to the scalaron's influence on small scale modes, and represents a clear modified

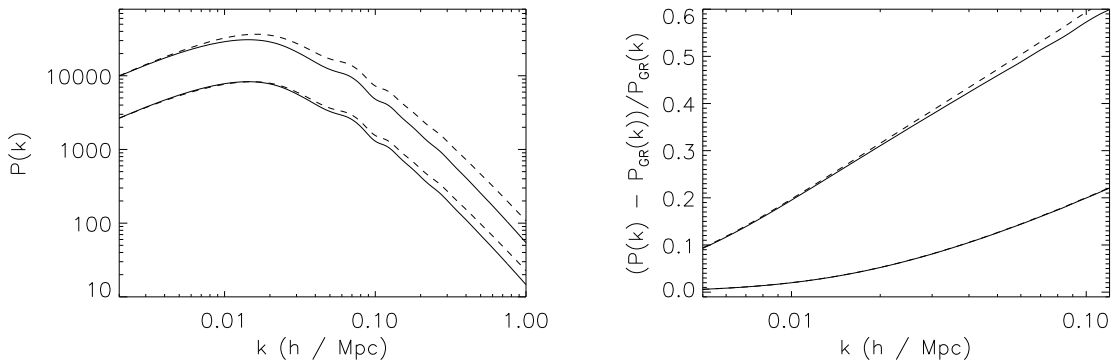

Figure 28: *Left panel:* Linear matter power spectra for ΛCDM (solid line; $M_0^{-1} = 0$, $\nu = 1.5$) and scalaron (dashed line; $M_0^{-1} = 375[10^{28}\ \mathrm{h}^{-1}\ \mathrm{eV}^{-1}]$, $\nu = 1.5$) cosmologies. The modification to gravity causes a sizeable scale dependent effect in the growth of perturbations. The redshift dependence of the scalaron can be seen by comparing the top and bottom pairs of power spectra evaluated at redshifts $z = 0.0$ and $z = 1.5$, respectively. *Right panel:* The environmental dependent chameleon mechanism can be seen in the mildly nonlinear regime. We exhibit the fractional difference $(P(k) - P_{\rm GR}(k))/P_{\rm GR}(k)$ between the $f(R)$ and GR power spectra for the model (1.8.37) with parameters $M_0^{-1} = 375[10^{28}\ \mathrm{h}^{-1}\ \mathrm{eV}^{-1}]$ and $\nu = 1.5$. The dashed lines represent linear power spectra ($P(k)$ and $P_{\rm GR}(k)$ calculated with no higher order effects) and the solid lines are the power spectra calculated to second order. We see that the nonlinearities decrease the modified gravity signal. This is a result of the chameleon mechanism. The top set of lines correspond to $z = 0$ and the bottom to $z = 0.9$; demonstrating that the modified gravity signal dramatically decreases for larger z. This is due to the scalaron mass being much larger at higher redshifts. Furthermore, nonlinear effects are less significant for increasing z.

gravity signal. Since weak lensing is sensitive to the underlying matter power spectrum, we expect Euclid to provide direct constraints on the mass of the scalar field.

By performing a Fisher analysis, using the standard Euclid specifications, [887] calculates the expected $f(R)$ parameter sensitivity of the weak lensing survey. By combining Euclid weak lensing and Planck Fisher matrices, both modified gravity parameters M_0 and ν are shown to be strongly constrained by the growth data in Figure 29. The expected 1σ bounds on M_0 and ν are quoted as $M_0 = 1.34 \pm 0.62 \times 10^{-30}$[h eV], $\nu = 1.5 \pm 0.18$ when using linear data $l < 400$ only and $M_0 = 1.34 \pm 0.25 \times 10^{-30}$[h eV], $\nu = 1.5 \pm 0.04$ when utilizing the full set of nonlinear modes $l < 10000$.

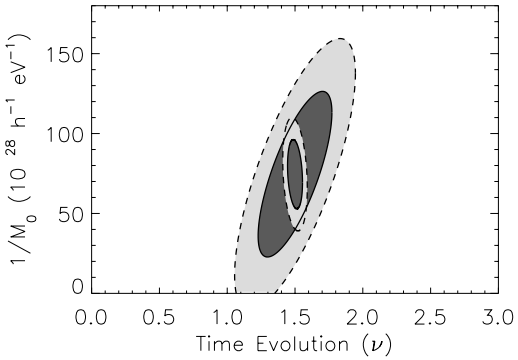

Figure 29: 68% (dark grey) and 95% (light grey) projected bounds on the modified gravity parameters M_0^{-1} and ν for the combined Euclid weak lensing and Planck CMB surveys. The smaller (larger) contours correspond to including modes $l = 400(10000)$ in the weak lensing analysis.

1.8.8 Forecast constraints on coupled quintessence cosmologies

In this section we present forecasts for coupled quintessence cosmologies [33, 955, 724], obtained when combining Euclid weak lensing, Euclid redshift survey (baryon acoustic oscillations, redshift distortions and full $P(k)$ shape) and CMB as obtained in Planck (see also the next section for CMB priors). Results reported here were obtained in [42] and we refer to it for details on the analysis and Planck specifications (for weak lensing and CMB constraints on coupled quintessence with a different coupling see also [637, 284]). In [42] the coupling is the one described in Section 1.4.4.4, as induced by a scalar-tensor model. The slope α of the Ratra–Peebles potential is included as an additional parameter and Euclid specifications refer to the Euclid Definition phase [551].

The combined Fisher confidence regions are plotted in Figure 30 and the results are in Table 13. The main result is that future surveys can constrain the coupling of dark energy to dark matter β^2 to less than $3 \cdot 10^{-4}$. Interestingly, some combinations of parameters (e.g., Ω_b vs α) seem to profit the most from the combination of the three probes.

We can also ask whether a better knowledge of the parameters $\{\alpha, \Omega_c, h, \Omega_b, n_s, \sigma_8, \log(A)\}$, obtained by independent future observations, can give us better constraints on the coupling β^2. In Table 14 we show the errors on β^2 when we have a better knowledge of only one other parameter, which is here fixed to the reference value. All remaining parameters are marginalized over.

It is remarkable to notice that the combination of CMB, power spectrum and weak lensing is already a powerful tool and a better knowledge of one parameter does not improve much the constraints on β^2. CMB alone, instead, improves by a factor 3 when Ω_c is known and by a factor 2 when h is known. The power spectrum is mostly influenced by Ω_c, which allows to improve

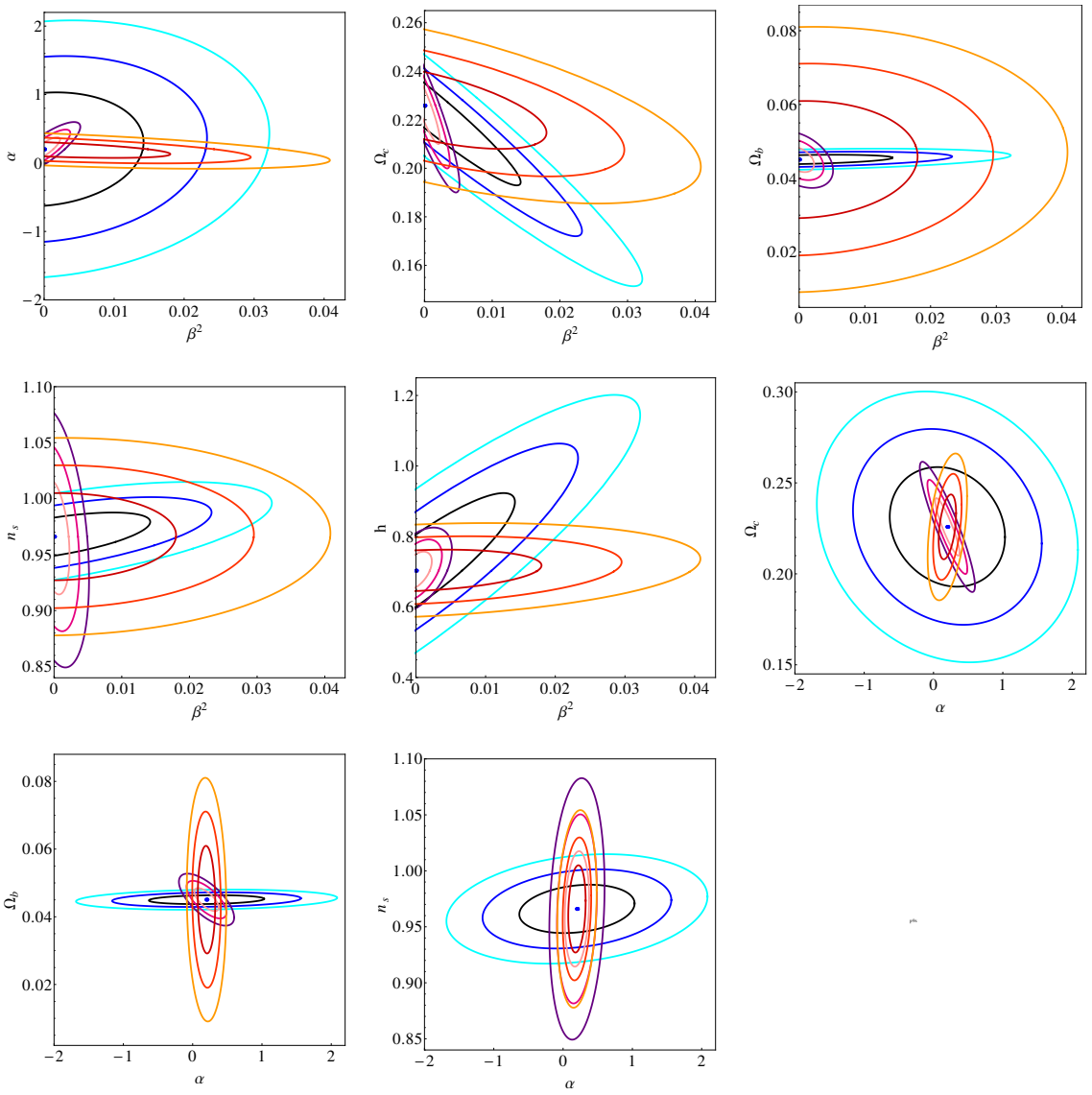

Figure 30: Comparison among predicted confidence contours for the cosmological parameter set $\Theta \equiv \{\beta^2, \alpha, \Omega_c, h, \Omega_b, n_s, \sigma_8, \log(A)\}$ using CMB (Planck, blue contours), $P(k)$ (pink-violet contours) and weak lensing (orange-red contours) with Euclid-like specifications. Image reproduced by permission from [42], copyright by APS.

Table 13: 1-σ errors for the set $\Theta \equiv \{\beta^2, \alpha, \Omega_c, h, \Omega_b, n_s\, \sigma_8, \log(A)\}$ of cosmological parameters, combining CMB + $P(k)$ (left column) and CMB + $P(k)$ + WL (right column).

Parameter	σ_i CMB + $P(k)$	σ_i CMB + $P(k)$ + WL
β^2	0.00051	0.00032
α	0.055	0.032
Ω_c	0.0037	0.0010
h	0.0080	0.0048
Ω_b	0.00047	0.00041
n_s	0.0057	0.0049
σ_8	0.0049	0.0036
$\log(A)$	0.0051	0.0027

constraints on the coupling by more than a factor 2. Weak lensing gains the most by a better knowledge of σ_8.

Table 14: 1-σ errors for β^2, for CMB, $P(k)$, WL and CMB + $P(k)$ + WL. For each line, only the parameter in the left column has been fixed to the reference value. The first line corresponds to the case in which we have marginalized over all parameters. Table reproduced by permission from [42], copyright by APS.

Fixed parameter	CMB	$P(k)$	WL	CMB + $P(k)$ + WL
(Marginalized on all params)	0.0094	0.0015	0.012	0.00032
α	0.0093	0.00085	0.0098	0.00030
Ω_c	0.0026	0.00066	0.0093	0.00032
h	0.0044	0.0013	0.011	0.00032
Ω_b	0.0087	0.0014	0.012	0.00030
n_s	0.0074	0.0014	0.012	0.00028
σ_8	0.0094	0.00084	0.0053	0.00030
$\log(A)$	0.0090	0.0015	0.012	0.00032

1.8.9 Extra-Euclidean data and priors

Other dark-energy projects will enable the cross-check of the dark-energy constraints from Euclid. These include Planck, BOSS, WiggleZ, HETDEX, DES, Panstarrs, LSST, BigBOSS and SKA.

Planck will provide exquisite constraints on cosmological parameters, but not tight constraints on dark energy by itself, as CMB data are not sensitive to the nature of dark energy (which has to be probed at $z < 2$, where dark energy becomes increasingly important in the cosmic expansion history and the growth history of cosmic large scale structure). Planck data in combination with Euclid data provide powerful constraints on dark energy and tests of gravity. In the next Section 1.8.9.1, we will discuss how to create a Gaussian approximation to the Planck parameter constraints that can be combined with Euclid forecasts in order to model the expected sensitivity until the actual Planck data is available towards the end of 2012.

The galaxy redshift surveys BOSS, WiggleZ, HETDEX, and BigBOSS are complementary to Euclid, since the overlap in redshift ranges of different galaxy redshift surveys, both space and ground-based, is critical for understanding systematic effects such as bias through the use of multiple tracers of cosmic large scale structure. Euclid will survey Hα emission line galaxies at $0.5 < z < 2.0$ over 20,000 square degrees. The use of multiple tracers of cosmic large scale structure can reduce systematic effects and ultimately increase the precision of dark-energy measurements

from galaxy redshift surveys [see, e.g., 811].

Currently on-going or recently completed surveys which cover a sufficiently large volume to measure BAO at several redshifts and thus have science goals common to Euclid, are the Sloan Digital Sky Survey III Baryon Oscillations Spectroscopic Survey (BOSS for short) and the WiggleZ survey.

BOSS[9] maps the redshifts of 1.5 million Luminous Red Galaxies (LRGs) out to $z \sim 0.7$ over 10,000 square degrees, measuring the BAO signal, the large-scale galaxy correlations and extracting information of the growth from redshift space distortions. A simultaneous survey of $2.2 < z < 3.5$ quasars measures the acoustic oscillations in the correlations of the Lyman-α forest. LRGs were chosen for their high bias, their approximately constant number density and, of course, the fact that they are bright. Their spectra and redshift can be measured with relatively short exposures in a 2.4 m ground-based telescope. The data-taking of BOSS will end in 2014.

The WiggleZ[10] survey is now completed, it measured redshifts for almost 240,000 galaxies over 1000 square degrees at $0.2 < z < 1$. The target are luminous blue star-forming galaxies with spectra dominated by patterns of strong atomic emission lines. This choice is motivated by the fact that these emission lines can be used to measure a galaxy redshift in relatively short exposures of a 4 m class ground-based telescope.

Red quiescent galaxies inhabit dense clusters environments, while blue star-forming galaxies trace better lower density regions such as sheets and filaments. It is believed that on large cosmological scales these details are unimportant and that galaxies are simply tracers of the underlying dark matter: different galaxy type will only have a different 'bias factor'. The fact that so far results from BOSS and WiggleZ agree well confirms this assumption.

Between now and the availability of Euclid data other wide-field spectroscopic galaxy redshift surveys will take place. Among them, eBOSS will extend BOSS operations focusing on 3100 square degrees using a variety of tracers. Emission line galaxies will be targeted in the redshift window $0.6 < z < 1$. This will extend to higher redshift and extend the sky coverage of the WiggleZ survey. Quasars in the redshift range $1 < z < 2.2$ will be used as tracers of the BAO feature instead of galaxies. The BAO LRG measurement will be extended to $z \sim 0.8$, and the quasar number density at $z > 2.2$ of BOSS will be tripled, thus improving the BAO Lyman-α forest measure.

HETDEX is expected to begin full science operation is 2014: it aims at surveying 1 million Lyman-α emitting galaxies at $1.9 < z < 3.5$ over 420 square degrees. The main science goal is to map the BAO feature over this redshift range.

Further in the future, we highlight here the proposed BigBOSS survey and SuMIRe survey with HyperSupremeCam on the Subaru telescope. The BigBOSS survey will target [OII] emission line galaxies at $0.6 < z < 1.5$ (and LRGs at $z < 0.6$) over 14,000 square degrees. The SuMIRe wide survey proposes to survey ~ 2000 square degrees in the redshift range $0.6 < z < 1.6$ targeting LRGs and [OII] emission-line galaxies. Both these surveys will likely reach full science operations roughly at the same time as the Euclid launch.

Wide field photometric surveys are also being carried out and planned. The on-going Dark Energy Survey (DES)[11] will cover 5000 square degrees out to $z \sim 1.3$ and is expected to complete observations in 2017; the Panoramic Survey Telescope & Rapid Response System (Pan-STARRS), on-going at the single-mirror stage, The PanSTARSS survey, which first phase is already on-going, will cover 30,000 square degrees with 5 photometry bands for redshifts up to $z \sim 1.5$. The second pause of the survey is expected to be competed by the time Euclid launches. More in the future the Large Synoptic Survey Telescope (LSST) will cover redshifts $0.3 < z < 3.6$ over 20,000 square degrees, but is expected to begin operations in 2021, after Euclid's planned launch date. The

[9] http://www.sdss3.org/surveys/boss.php

[10] http://wigglez.swin.edu.au/site/index.html

[11] http://www.darkenergysurvey.org

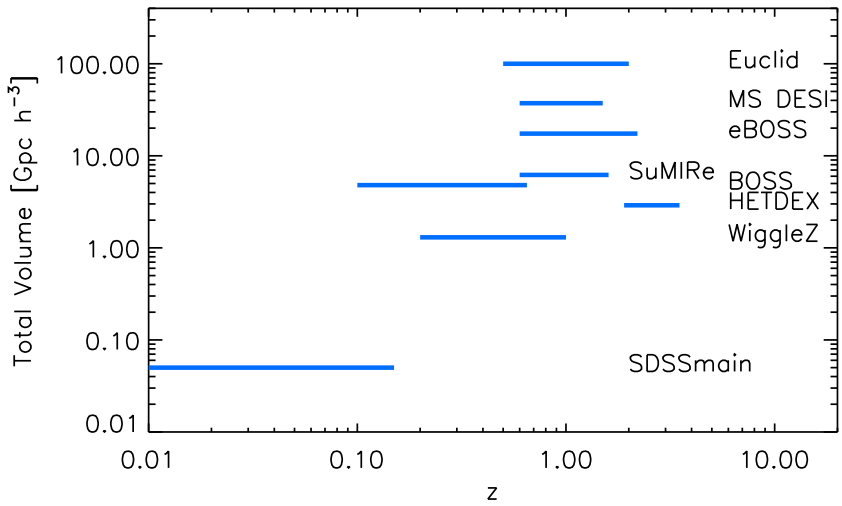

Figure 31: Redshift coverage and volume for the surveys mentioned in the text. Spectroscopic surveys only are shown. Recall that while future and forthcoming photometric surveys focus on weak gravitational lensing, spectroscopic surveys can extract the three dimensional galaxy clustering information and therefore measure radial and tangential BAO signal, the power spectrum shape and the growth of structure via redshift space distortions. The three-dimensional clustering information is crucial for BAO. For example to obtain the same figure of merit for dark-energy properties a photometric survey must cover a volume roughly ten times bigger than a spectroscopic one.

galaxy imaging surveys DES, Panstarrs, and LSST will complement Euclid imaging survey in both the choice of band passes, and the sky coverage.

SKA (which is expected to begin operations in 2020 and reach full operational capability in 2024) will survey neutral atomic hydrogen (HI) through the radio 21 cm line, over a very wide area of the sky. It is expected to detect HI emitting galaxies out to $z \sim 1.5$ making it nicely complementary to Euclid. Such galaxy redshift survey will of course offer the opportunity to measure the galaxy power spectrum (and therefore the BAO feature) out to $z \sim 1.5$. The well behaved point spread function of a synthesis array like the SKA should ensure superb image quality enabling cosmic shear to be accurately measured and tomographic weak lensing used to constrain cosmology and in particular dark energy. This weak lensing capability also makes SKA and Euclid very complementary. For more information see, e.g., [755, 140].

The Figure 31 puts Euclid into context. Euclid will survey Hα emission line galaxies at $0.5 < z < 2.0$ over 20,000 square degrees. Clearly, Euclid with both spectroscopic and photometric capabilities and wide field coverage surpasses all surveys that will be carried out by the time it launches. The large volume surveyed is crucial as the number of modes to sample for example the power spectrum and the BAO feature scales with the volume. The redshift coverage is also important especially at $z < 2$ where the dark-energy contribution to the density pod the universe is non-negligible (at $z > 2$ for most cosmologies the universe is effectively Einstein–de Sitter, therefore, high redshifts do not contribute much to constraints on dark energy). Having a single instrument, a uniform target selection and calibration is also crucial to perform precision tests of cosmology without having to build a 'ladder' from different surveys selecting different targets. On the other hand it is also easy to see the synergy between these ground-based surveys and Euclid: by mapping different targets (over the same sky area and ofter the same redshift range) one can

gain better control over issues such as bias factors. The use of multiple tracers of cosmic large scale structure can reduce systematic effects and ultimately increase the precision of dark-energy measurements from galaxy redshift surveys [see, e.g., 811].

Moreover, having both spectroscopic and imaging capabilities Euclid is uniquely poised to explore the clustering with both the three dimensional distribution of galaxies and weak gravitational lensing.

1.8.9.1 The Planck prior

Planck will provide highly accurate constraints on many cosmological parameters, which makes the construction of a Planck Fisher matrix somewhat non-trivial as it is very sensitive to the detailed assumptions. A relatively robust approach was used by [676] to construct a Gaussian approximation to the WMAP data by introducing two extra parameters,

$$R \equiv \sqrt{\Omega_m H_0^2}\, r(z_{\rm CMB})\,, \qquad l_a \equiv \pi r(z_{\rm CMB})/r_s(z_{\rm CMB})\,, \tag{1.8.38}$$

where $r(z)$ is the comoving distance from the observer to redshift z, and $r_s(z_{\rm CMB})$ is the comoving size of the sound-horizon at decoupling.

In this scheme, l_a describes the peak location through the angular diameter distance to decoupling and the size of the sound horizon at that time. If the geometry changes, either due to non-zero curvature or due to a different equation of state of dark energy, l_a changes in the same way as the peak structure. R encodes similar information, but in addition contains the matter density which is connected with the peak height. In a given class of models (for example, quintessence dark energy), these parameters are "observables" related to the shape of the observed CMB spectrum, and constraints on them remain the same independent of (the prescription for) the equation of state of the dark energy.

As a caveat we note that if some assumptions regarding the evolution of perturbations are changed, then the corresponding R and l_a constraints and covariance matrix will need to be recalculated under each such hypothesis, for instance, if massive neutrinos were to be included, or even if tensors were included in the analysis [255]. Further, R as defined in Eq. (1.8.38) can be badly constrained and is quite useless if the dark energy clusters as well, e.g., if it has a low sound speed, as in the model discussed in [534].

In order to derive a Planck fisher matrix, [676] simulated Planck data as described in [703] and derived constraints on our base parameter set $\{R, l_a, \Omega_b h^2, n_s\}$ with a MCMC based likelihood analysis. In addition to R and l_a they used the baryon density $\Omega_b h^2$, and optionally the spectral index of the scalar perturbations n_s, as these are strongly correlated with R and l_a, which means that we will lose information if we do not include these correlations. As shown in [676], the resulting Fisher matrix loses some information relative to the full likelihood when only considering Planck data, but it is very close to the full analysis as soon as extra data is used. Since this is the intended application here, it is perfectly sufficient for our purposes.

The following tables, from [676], give the covariance matrix for quintessence-like dark energy (high sound speed, no anisotropic stress) on the base parameters and the Fisher matrix derived from it. Please consult the appendix of that paper for the precise method used to compute R and l_a as the results are sensitive to small variations.

Table 15: R, l_a, $\Omega_b h^2$ and n_s estimated from Planck simulated data. Table reproduced by permission from [676], copyright by APS.

Parameter	mean	rms variance
	$\Omega_k \neq 0$	
R	1.7016	0.0055
l_a	302.108	0.098
$\Omega_b h^2$	0.02199	0.00017
n_s	0.9602	0.0038

Table 16: Covariance matrix for $(R, l_a, \Omega_b h^2, n_s)$ from Planck. Table reproduced by permission from [676], copyright by APS.

	R	l_a	$\Omega_b h^2$	n_s
		$\Omega_k \neq 0$		
R	0.303492E–04	0.297688E–03	–0.545532E–06	–0.175976E–04
l_a	0.297688E–03	0.951881E–02	–0.759752E–05	–0.183814E–03
$\Omega_b h^2$	–0.545532E–06	–0.759752E-05	0.279464E–07	0.238882E–06
n_s	–0.175976E–04	–0.183814E-03	0.238882E–06	0.147219E–04

Table 17: Fisher matrix for (w_0, w_a, $\Omega_{\rm DE}$, Ω_k, ω_m, ω_b, n_S) derived from the covariance matrix for $(R, l_a, \Omega_b h^2, n_s)$ from Planck. Table reproduced by permission from [676], copyright by APS.

	w_0	w_a	$\Omega_{\rm DE}$	Ω_k	ω_m	ω_b	n_S
w_0	.172276E+06	.490320E+05	.674392E+06	–.208974E+07	.325219E+07	–.790504E+07	–.549427E+05
w_a	.490320E+05	.139551E+05	.191940E+06	–.594767E+06	.925615E+06	–.224987E+07	–.156374E+05
$\Omega_{\rm DE}$	.674392E+06	.191940E+06	.263997E+07	–.818048E+07	.127310E+08	–.309450E+08	–.215078E+06
Ω_k	–.208974E+07	–.594767E+06	–.818048E+07	.253489E+08	–.394501E+08	.958892E+08	.666335E+06
ω_m	.325219E+07	.925615E+06	.127310E+08	–.394501E+08	.633564E+08	–.147973E+09	–.501247E+06
ω_b	–.790504E+07	–.224987E+07	–.309450E+08	.958892E+08	–.147973E+09	.405079E+09	.219009E+07
n_S	–.549427E+05	–.156374E+05	–.215078E+06	.666335E+06	–.501247E+06	.219009E+07	.242767E+06

1.9 Summary and outlook

This section introduced the main features of the most popular dark energy/modified gravity models. Here we summarize the performance of Euclid with respect to these models. Unless otherwise indicated, we always assume Euclid with no external priors and all errors fully marginalized over the standard cosmological parameters. Here RS denotes the redshift survey, WLS the weak lensing one.

1. Euclid (RS) should be able to measure the main standard cosmological parameters to percent or sub-percent level as detailed in Table 7 (all marginalized errors, including constant equation of state and constant growth rate, see Table 11 and Figure 20).

2. The two CPL parameters w_0, w_1 should be measured with errors 0.06 and 0.26, respectively (fixing the growth rate to fiducial), see Table 11 and Figure 20.

3. The equation of state w and the growth rate parameter γ, both assumed constant, should be simultaneously constrained to within 0.04 and 0.03, respectively.

4. The growth function should be constrained to within $0.01-0.02$ for each redshift bin from $z = 0.7$ to $z = 2$ (see Table 4).

5. A scale-independent bias function $b(z)$ should be constrained to within 0.02 for each redshift bin (see Table 4).

6. The growth rate parameters γ_0, γ_1 defined in Eq. 1.8.5 should be measured to within 0.08, 0.17, respectively.

7. Euclid will achieve an accuracy on measurements of the dark energy sound speed of $\sigma(c_s^2)/c_s^2 = 2615$ (WLS) and $\sigma(c_s^2)/c_s^2 = 50.05$ (RS), if $c_s^2 = 1$, or $\sigma(c_s^2)/c_s^2 = 0.132$ (WLS) and $\sigma(c_s^2)/c_s^2 = 0.118$ (RS), if $c_s^2 = 10^{-6}$.

8. The coupling β^2 between dark energy and dark matter can be constrained by Euclid (with Planck) to less than $3 \cdot 10^{-4}$ (see Figure 30 and Table 13).

9. Any departure from GR greater than $\simeq 0.03$ in the growth index γ will be distinguished by the WLS [429].

10. Euclid WLS can detect deviations between 3% and 10% from the GR value of the modified-gravity parameter Σ (Eq. 1.3.28), whilst with the RS there will be a 20% accuracy on both Σ and μ (Eq. 1.3.27).

11. With the WLS, Euclid should provide an upper limit to the present dimensionless scalaron inverse mass $\mu \equiv H_0/M_0$ of the $f(R)$ scalar (where the time dependent scalar field mass is defined in Eq. 1.8.37) as $\mu = 0.00 \pm 1.10 \times 10^{-3}$ for $l < 400$ and $\mu = 0.0 \pm 2.10 \times 10^{-4}$ for $l < 10000$

12. The WLS will be able to rule out the DGP model growth index with a Bayes factor $|\ln B| \simeq 50$ [429], and viable phenomenological extensions could be detected at the 3σ level for $1000 \lesssim \ell \lesssim 4000$ [199].

At the same time, there are several areas of research that we feel are important for the future of Euclid, both to improve the current analyses and to maximize its science return. Here we provide a preliminary, partial list.

1. The results of the redshift survey and weak lensing surveys should be combined in a statistically coherent way
2. The set of possible priors to be combined with Euclid data should be better defined
3. The forecasts for the parameters of the modified gravity and clustered dark-energy models should be extended to include more general cases
4. We should estimate the errors on a general reconstruction of the modified gravity functions Σ, μ or of the metric potentials Ψ, Φ as a function of both scale and time.

Part 2: Dark Matter and Neutrinos

2.1 Introduction

The identification of dark matter is one of the most important open problems in particle physics and cosmology. In standard cosmology, dark matter contributes 85% of all the matter in the universe, but we do not know what it is made of, as we have never observed dark matter particles in our laboratories. The foundations of the modern dark matter paradigm were laid in the 1970s and 1980s, after decades of slow accumulation of evidence. Back in the 1930s, it was noticed that the Coma cluster seemed to contain much more mass than what could be inferred from visible galaxies [992, 993], and a few years later, it became clear that the Andromeda galaxy M31 rotates anomalously fast at large radii, as if most of its mass resides in its outer regions. Several other pieces of evidence provided further support to the dark matter hypothesis, including the so called timing-argument. In the 1970s, rotation curves were extended to larger radii and to many other spiral galaxies, proving the presence of large amounts of mass on scales much larger than the size of galactic disks [712].

We are now in the position of determining the total abundance of dark matter relative to normal, baryonic matter, in the universe with exquisite accuracy; we have a much better understanding of how dark matter is distributed in structures ranging from dwarf galaxies to clusters of galaxies, thanks to gravitational lensing observations [see 644, for a review] and theoretically from high-resolution numerical simulations made possible by modern supercomputers (such as, for example, the Millennium or Marenostrum simulations).

Originally, Zwicky thought of dark matter as most likely baryonic – missing cold gas, or low mass stars. Rotation curve observation could be explained by dark matter in the form of MAssive Compact Halo Objects (MACHOs, e.g., a halo of black holes or brown dwarfs). However, the MACHO and EROS experiments have shown that dark matter cannot be in the mass range $0.6 \times 10^{-7}\, M_\odot < M < 15\, M_\odot$ if it comprises massive compact objects [23, 889]. Gas measurements are now extremely sensitive, ruling out dark matter as undetected gas ([134, 238, 765]; but see [728]). And the CMB and Big Bang Nucleosynthesis require the total mass in baryons in the universe to be significantly less that the total matter density [759, 246, 909].

This is one of the most spectacular results in cosmology obtained at the end of the 20th century: dark matter has to be non-baryonic. As a result, our expectation of the nature of dark matter shifted from an astrophysical explanation to particle physics, linking the smallest and largest scales that we can probe.

During the seventies the possibility of the neutrino to be the dark matter particle with a mass of tenth of eV was explored, but it was realized that such light particle would erase the primordial fluctuations on small scales, leading to a lack of structure formation on galactic scales and below. It was therefore postulated that the dark matter particle must be cold (low thermal energy, to allow structures on small scale to form), collisionless (or have a very low interaction cross section, because dark matter is observed to be pressureless) and stable over a long period of time: such a candidate is referred to as a weakly interacting massive particle (WIMP). This is the standard cold dark matter (CDM) picture [see 369, 719].

Particle physicists have proposed several possible dark matter candidates. Supersymmetry (SUSY) is an attractive extension of the Standard Model of particle physics. The lightest SUSY particle (the LSP) is stable, uncharged, and weakly interacting, providing a perfect WIMP candidate known as a neutralino. Specific realizations of SUSY each provide slightly different dark matter candidates [for a review see 482]. Another distinct dark matter candidate arising from extensions of the Standard Model is the axion, a hypothetical pseudo-Goldstone boson whose existence was postulated to solve the so called strong CP problem in quantum chromodynamics [715],

also arising generically in string theory [965, 871]. They are known to be very well motivated dark matter candidates [for a review of axions in cosmology see 826]. Other well-known candidates are sterile neutrinos, which interact only gravitationally with ordinary matter, apart from a small mixing with the familiar neutrinos of the Standard Model (which should make them ultimately unstable), and candidates arising from technicolor [see, e.g., 412]. A wide array of other possibilities have been discussed in the literature, and they are currently being searched for with a variety of experimental strategies [for a complete review of dark matter in particle physics see 51].

There remain some possible discrepancies in the standard cold dark matter model, such as the missing satellites problem, and the cusp-core controversy (see below for details and references) that have led some authors to question the CDM model and to propose alternative solutions. The physical mechanism by which one may reconcile the observations with the standard theory of structure formation is the suppression of the matter power spectrum at small scales. This can be achieved with dark matter particles with a strong self-scattering cross section, or with particles with a non-negligible velocity dispersion at the epoch of structure formation, also referred to as warm dark matter (WDM) particles.

Another possibility is that the extra gravitational degrees of freedom arising in modified theories of gravity play the role of dark matter. In particular this happens for the Einstein-Aether, TeVeS and bigravity models. These theories were developed following the idea that the presence of unknown dark components in the universe may be indicating us that it is not the matter component that is exotic but rather that gravity is not described by standard GR.

Finally, we note that only from astrophysical probes can any dark matter candidate found in either direct detection experiments or accelerators, such as the LHC, be confirmed. Any direct dark matter candidate discovery will give Euclid a clear goal to verify the existence of this particle on astrophysical scales. Within this context, Euclid can provide precious information on the nature of dark matter. In this part, we discuss the most relevant results that can be obtained with Euclid, and that can be summarized as follows:

- The discovery of an exponential suppression in the power spectrum at small scales, that would rule out CDM and favor WDM candidates, or, in absence of it, the determination of a lower limit on the mass of the WDM particle, $m_{\rm WDM}$, of 2 keV;

- the determination of an upper limit on the dark matter self-interaction cross section $\sigma/m \sim 10^{-27}$ cm^2 GeV^{-1} at 68% CL, which represents an improvement of three orders of magnitude compared to the best constraint available today, which arises from the analysis of the dynamics of the bullet cluster;

- the measurement of the slope of the dark matter distribution within galaxies and clusters of galaxies with unprecedented accuracy;

- the determination of the properties of the only known – though certainly subdominant – non-baryonic dark matter particle: the standard neutrino, for which Euclid can provide information on the absolute mass scale, its normal or inverted hierarchy, as well as its Dirac or Majorana nature;

- the test of unified dark matter (UDM, or quartessence) models, through the detection of characteristic oscillatory features predicted by these theories on the matter power spectrum, detectable through weak lensing or baryonic acoustic oscillations studies;

- a probe of the axiverse, i.e., of the legacy of string theory through the presence of ultra-light scalar fields that can affect the growth of structure, introducing features in the matter power spectrum and modifying the growth rate of structures.

Finally, Euclid will provide, through gravitational lensing measurement, a map of the dark matter distribution over the entire extragalactic sky, allowing us to study the effect of the dark matter environment on galaxy evolution and structure formation as a function of time. This map will pinpoint our place within the dark universe.

2.2 Dark matter halo properties

Dark matter was first proposed by [993] to explain the anomalously high velocity of galaxies in galaxy clusters. Since then, evidence for dark matter has been accumulating on all scales. The velocities of individual stars in dwarf galaxies suggest that these are the most dark matter dominated systems in the universe [e.g., 650, 509, 834, 635, 934]. Low surface brightness (LSB) and giant spiral galaxies rotate too fast to be supported by their stars and gas alone, indicating the presence of dark matter [286, 833, 153, 512]. Gravitationally lensed giant elliptical galaxies and galaxy clusters require dark matter to explain their observed image distributions [e.g., 761, 156, 935, 851, 244]. Finally, the temperature fluctuations in the cosmic microwave background (CMB) radiation indicate the need for dark matter in about the same amount as that required in galaxy clusters [e.g., 845, 968, 855].

While the case for particle dark matter is compelling, until we find direct evidence for such a particle, astrophysics remains a unique dark matter probe. Many varieties of dark matter candidates produce a noticeable change in the growth of structure in the universe [482, 865]. Warm dark matter (WDM) suppresses the growth of structure in the early universe producing a measurable effect on the small-scale matter power spectrum [143, 67, 87]. Self-interacting dark matter (SIDM) changes the expected density distribution *within* bound dark matter structures [273, 440]. In both cases, the key information about dark matter is contained on very small scales. In this section, we discuss previous work that has attempted to measure the small scale matter distribution in the universe, and discuss how Euclid will revolutionize the field. We divide efforts into three main areas: measuring the halo mass function on large scales, but at high redshift; measuring the halo mass function on small scales through lens *substructures*; measuring the dark matter density profile within galaxies and galaxy clusters.

2.2.1 The halo mass function as a function of redshift

Attempts have already been made to probe the small scale power in the universe through galaxy counts. Figure 32 shows the best measurement of the 'baryonic mass function' of galaxies to date [758]. This is the number of galaxies with a given total mass in baryons normalized to a volume of 1 Mpc. To achieve this measurement, [758] sewed together results from a wide range of surveys reaching a baryonic mass of just $\sim 10^6\, M_\odot$ – some of the smallest galaxies observed to date.

The baryonic mass function already turns up an interesting result. Over-plotted in blue on Figure 32 is the *dark matter* mass function expected assuming that dark matter is 'cold' – i.e., that it has no preferred scale. Notice that this has a different shape. On large scales, there should be bound dark matter structures with masses as large as $10^{14}\, M_\odot$, yet the number of observed galaxies drops off exponentially above a baryonic mass of $\sim 10^{12}\, M_\odot$. This discrepancy is well-understood. Such large dark matter haloes have been observed, but they no longer host a single galaxy; rather they are bound collections of galaxies – galaxy clusters [see e.g. 993]. However, there is also a discrepancy at low masses that is not so well understood. There should be far more bound dark matter haloes than observed small galaxies. This is the well-known 'missing satellite' problem [662, 511].

The missing satellite problem could be telling us that dark matter is not cold. The red line on Figure 32 shows the expected dark matter mass function for WDM with a (thermal relic) mass of $m_{\rm WDM} = 1$ keV. Notice that this gives an excellent match to the observed slope of the baryonic

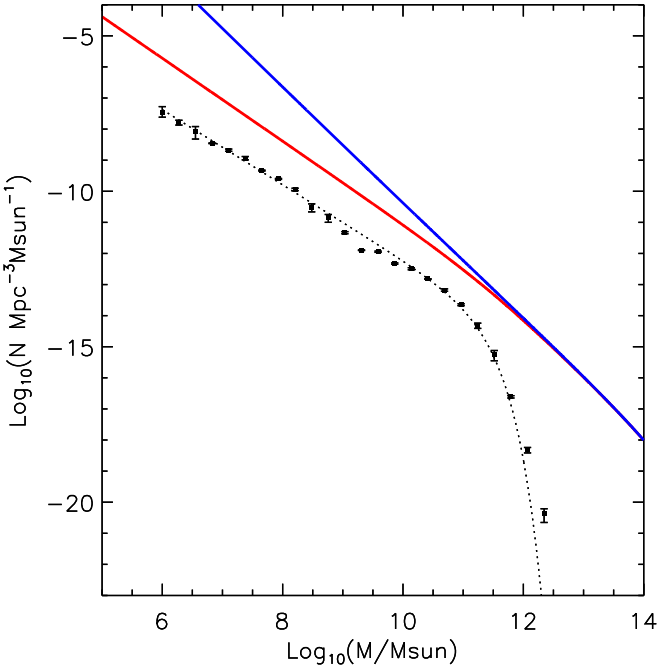

Figure 32: The baryonic mass function of galaxies (data points). The dotted line shows a Schechter function fit to the data. The blue line shows the predicted mass function of dark matter haloes, assuming that dark matter is cold. The red line shows the same assuming that dark matter is warm with a (thermal relic) mass of $m_{\rm WDM} = 1$ keV.

mass function on small scales. However, there may be a less exotic solution. It is likely that star formation becomes inefficient in galaxies on small scales. A combination of supernovae feedback, reionization and ram-pressure stripping is sufficient to fully explain the observed distribution assuming pure CDM [529, 756, 603]. Such 'baryon feedback' solutions to the missing satellite problem are also supported by recent measurements of the orbits of the Milky Way's dwarf galaxies [594].

2.2.1.1 Weak and strong lensing measurements of the halo mass function

To make further progress on WDM constraints from astrophysics, we must avoid the issue of baryonic physics by probing the halo mass function *directly*. The only tool for achieving this is gravitational lensing. In weak lensing this means stacking data for a very large number of galaxies to obtain an averaged mass function. In strong lensing, this means simply finding enough systems with 'good data.' Good data ideally means multiple sources with wide redshift separation [776]; combining independent data from dynamics with lensing may also prove a promising route [see e.g. 893].

Euclid will measure the halo mass function down to $\sim 10^{13}\,M_\odot$ using weak lensing. It will simultaneously find 1000s of strong lensing systems. However, in both cases, the lowest mass scale is limited by the lensing critical density. This limits us to probing down to a halo mass of $\sim 10^{11}\,M_\odot$ which gives poor constraints on the nature of dark matter. However, if such measurements can be made as a *function of redshift*, the constraints improve dramatically. We discuss this in the next Section.

2.2.1.2 The advantage of going to high redshift

Dark matter constraints from the halo mass function become much stronger if the halo mass function is measured as a function of redshift. This is because warm dark matter *delays* the growth of structure formation as well as suppressing small scale power. This is illustrated in Figure 33, which shows the fraction of mass in bound structures as a function of redshift, normalized to a halo of Milky Way's mass at redshift $z = 0$. Marked are different thermal relic WDM particle masses in keV (black solid lines). Notice that the differences between WDM models increase significantly towards higher redshift at a given mass scale. Thus we can obtain strong constraints on the nature of dark matter by moving to higher z's, rather than lower halo mass.

The utility of redshift information was illustrated recently by observations of the Lyman-α absorption spectra from Quasars [927, 812]. Quasars act as cosmic 'flashlights' shining light from the very distant universe. Some of this light is absorbed by intervening neutral gas leading to absorption features in the Quasar spectra. Such features contain rich information about the matter distribution in the universe at high redshift. Thus, the Lyman-α forest measurements have been able to place a lower bound of $m_{\rm WDM} > 4$ keV probing scales of ~ 1 Mpc. Key to the success of this measurement is that much of the neutral gas lies in-between galaxies in filaments. Thus, linear approximations for the growth of structures in WDM versus CDM remain acceptable, while assuming that the baryons are a good tracer of the underlying matter field is also a good approximation. However, improving on these early results means probing smaller scales where nonlinearities and baryon physics will creep in. For this reason, tighter bounds must come from techniques that either probe even higher redshifts, or even smaller scales. Lensing from Euclid is an excellent candidate since it will achieve both while measuring the halo mass function directly rather than through the visible baryons.

2.2.2 The dark matter density profile

An alternative approach to constraining dark matter models is to measure the distribution of dark matter *within* galaxies. Figure 34 shows the central log-slope of the density distribution for 9 galaxies/groups and 3 lensing clusters as a function of the enclosed lensing mass [777, 757, 776]. Over the visible region of galaxies, the dark matter distribution tends towards a single power law: $\rho \propto r^{\alpha}$. Marked in red is the prediction from structure-formation simulations of the standard cosmological model, that assume non-relativistic CDM, and that do not include any baryonic matter. Notice that above an enclosed lensing mass of $\sim 10^{12}\, M_{\odot}$, the agreement between theory and observations is very good. This lends support to the idea that dark matter is cold and not strongly self-interacting. However, this result is based on only a handful of galaxy clusters with excellent data. Furthermore, lower mass galaxies and groups can, in principle, give tighter constraints. In these mass ranges, however ($M_{\rm enc} < 10^{12}\, M_{\odot}$), the lensing mass is dominated by the visible stars. Determining the underlying dark matter distribution is then much more difficult. It is likely that the dark matter distribution is also altered from simple predictions by the dynamical interplay between the stars, gas and dark matter during galaxy formation [e.g., 296].

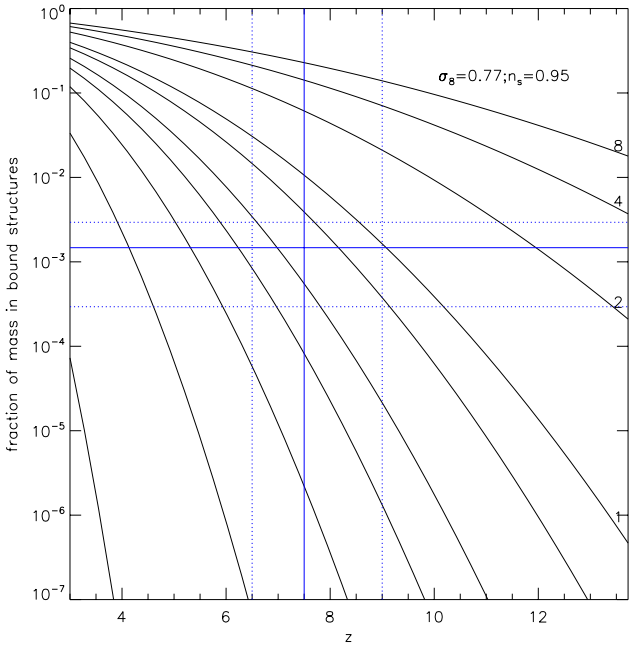

Figure 33: The fraction of mass in bound structures as a function of redshift, normalized to a halo of Milky Way's mass at redshift $z = 0$. Marked are different masses of thermal-relic WDM particles in keV (black solid lines). Notice that the differences between different WDM models increases towards higher redshift.

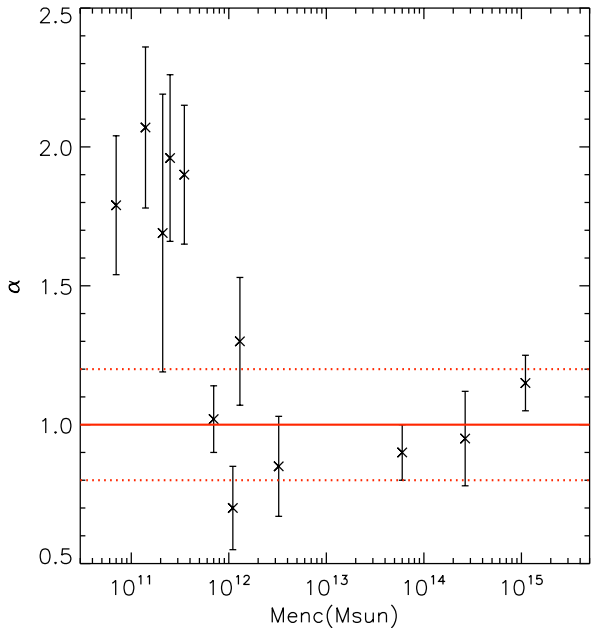

Figure 34: The central log-slope α of the density distribution $\rho \propto r^{\alpha}$ for 9 galaxies/groups and 3 lensing clusters as a function of the enclosed lensing mass. Marked in red is the prediction from structure formation simulations of the standard cosmological model, that assume non-relativistic CDM, and that do not include any baryonic matter.

2.3 Euclid dark matter studies: wide-field X-ray complementarity

The predominant extragalactic X-ray sources are AGNs and galaxy clusters. For dark matter studies the latter are the more interesting targets. X-rays from clusters are emitted as thermal bremsstrahlung by the hot intracluster medium (ICM) which contains most of the baryons in the cluster. The thermal pressure of the ICM supports it against gravitational collapse so that measuring the temperature through X-ray observations provides information about the mass of the cluster and its distribution. Hence, X-rays form a complementary probe of the dark matter in clusters to Euclid weak lensing measurements.

The ongoing X-ray missions XMM-Newton and Chandra have good enough angular resolution to measure the temperature and mass profiles in ~ 10 radial bins for clusters at reasonable redshifts, although this requires long exposures. Many planned X-ray missions aim to improve the spectral coverage, spectral resolution, and/or collection area of the present mission, but they are nonetheless mostly suited for targeted observations of individual objects. Two notable exceptions are eROSITA[12] [207, launch 2014] and the Wide Field X-ray Telescope[13] [WFXT 390, 931, 789, 773, 152, 790, proposed] which will both conduct full sky surveys and, in the case of WFXT, also smaller but deeper surveys of large fractions of the sky.

A sample of high-angular resolution X-ray cluster observations can be used to test the prediction from N-body simulations of structure formation that dark matter haloes are described by the NFW profile [684] with a concentration parameter c. This describes the steepness of the profile, which is related to the mass of the halo [685]. Weak or strong lensing measurements of the mass profile, such as those that will be provided from Euclid, can supplement the X-ray measurement and have different systematics. Euclid could provide wide field weak lensing data for such a purpose with very good point spread function (PSF) properties, but it is likely that the depth of the Euclid survey will make dedicated deep field observations a better choice for a lensing counterpart to the X-ray observations. However, if the WFXT mission becomes a reality, the sheer number of detected clusters with mass profiles would mean Euclid could play a much more important rôle.

X-ray observations of galaxy clusters can constrain cosmology by measuring the geometry of the universe through the baryon fraction $f_{\rm gas}$ [26] or by measuring the growth of structures by determining the high-mass tail of the mass function [622]. The latter method would make the most of the large number of clusters detected in full-sky surveys and there would be several benefits by combining an X-ray and a lensing survey. It is not immediately clear which type of survey would be able to better detect clusters at various redshifts and masses, and the combination of the two probes could improve understanding of the sample completeness. An X-ray survey alone cannot measure cluster masses with the required precision for cosmology. Instead, it requires a calibrated relation between the X-ray temperature and the cluster mass. Such a calibration, derived from a large sample of clusters, could be provided by Euclid. In any case, it is not clear yet whether the large size of a Euclid sample would be more beneficial than deeper observations of fewer clusters.

Finally, X-ray observations can also confirm the nature of possible 'bullet-like' merging clusters. In such systems the shock of the collision has displaced the ICM from the dark matter mass, which is identified through gravitational lensing. This offers the opportunity to study dark matter haloes with very few baryons and, e.g., search for signatures of decaying or annihilating dark matter.

[12] http://www.mpe.mpg.de/erosita/

[13] http://www.wfxt.eu/home/Overview.html

2.4 Dark matter mapping

Gravitational lensing offers a unique way to chart dark matter structures in the universe as it is sensitive to all forms of matter. Weak lensing has been used to map the dark matter in galaxy clusters [see for example 245] with high resolution reconstructions recovered for the most massive strong lensing clusters [see for example 164]. Several lensing studies have also mapped the projected surface mass density over degree scale-fields [386, 798, 532] to identify shear-selected groups and clusters. The minimum mass scale that can be identified is limited only by the intrinsic ellipticity noise in the lensing analysis and projection effects. Using a higher number density of galaxies in the shear measurement reduces this noise, and for this reason the Deep Field Euclid Survey will be truly unique for this area of research, permitting high resolution reconstructions of dark matter in the field [645, 432] and the study of lenses at higher redshift.

There are several non-parametric methods to reconstruct dark matter in 2D which can be broadly split into two categories: convergence techniques [486] and potential techniques [90]. In the former one measures the projected surface mass density (or convergence) κ directly by applying a convolution to the measured shear under the assumption that $\kappa \ll 1$. Potential techniques perform a χ^2 minimization and are better suited to the cluster regime and can also incorporate strong lensing information [163]. In the majority of methods, choices need to be made about smoothing scales to optimize signal-to-noise whilst preserving reconstruction resolution. Using a wavelet method circumvents this choice [860, 497] but makes the resulting significance of the reconstruction difficult to measure.

2.4.1 Charting the universe in 3D

The lensing distortion depends on the total projected surface mass density along the line of sight and a geometrical factor that increases with source distance. This redshift dependence can be used to recover the full 3D gravitational potential of the matter density as described in [455, 72] and applied to the COMBO-17 survey in [879] and the COSMOS survey in [645]. This work has been extended in [835] to reconstruct the full 3D mass density field and applied to the STAGES survey in [836].

All 3D mass reconstruction methods require the use of a prior based on the expected mean growth of matter density fluctuations. Without the inclusion of such a prior, [455] have shown that one is unable to reasonably constrain the radial matter distribution, even for densely sampled space-based quality lensing data. Therefore 3D maps cannot be directly used to infer cosmological parameters.

The driving motivation behind the development of 3D reconstruction techniques was to enable an unbiased 3D comparison of mass and light. Dark haloes for example would only be detected in this manner. However the detailed analysis of noise and the radial PSF in the 3D lensing reconstructions presented for the first time in [836] show how inherently noisy the process is. Given the limitations of the method to resolve only the most massive structures in 3D the future direction of the application of this method for the Euclid Wide survey should be to reconstruct large scale structures in the 3D density field. Using more heavily spatially smoothed data we can expect higher quality 3D resolution reconstructions as on degree scales the significance of modes in a 3D mass density reconstruction are increased [835]. Adding additional information from flexion may also improve mass reconstruction, although using flexion information alone is much less sensitive than shear [733].

2.5 Scattering cross sections

We now move towards discussing the particulate aspects of dark matter, starting with a discussion on the scattering cross-sections of dark matter. At present, many physical properties of the dark matter particle remain highly uncertain. Prospects for studying the scattering of dark matter with each of the three major constituents of the universe – itself, baryons, and dark energy – are outlined below.

2.5.1 Dark matter–dark matter interactions

Self-interacting dark matter (SIDM) was first postulated by [853], in an attempt to explain the apparent paucity of low-mass haloes within the Local Group. The key characteristic of this model is that CDM particles possess a large scattering cross-section, yet with negligible annihilation or dissipation. The process of elastic scattering erases small substructures and cuspy cores, whilst preserving the density profile of the haloes.

However, as highlighted by [399], cross-sections large enough to alleviate the structure formation issues would also allow significant heat transfer from particles within a large halo to the cooler sub-haloes. This effect is most prominent close to the centers of clusters. As the sub-halo evaporates, the galaxy residing within the halo would be disrupted. Limiting this rate of evaporation to exceed the Hubble time allows an upper bound to be placed on the scattering cross-section of approximately $\sigma_p/m_p \lesssim 0.3\ \mathrm{cm}^2\ \mathrm{g}^{-1}$ (neglecting any velocity dependence). Note the dependence on particle mass – a more massive CDM particle would be associated with a lower number density, thereby reducing the frequency of collisions.

[658] have performed ray-tracing through N-body simulations, and have discovered that the ability for galaxy clusters to generate giant arcs from strong lensing is compromized if the dark matter is subject to just a few collisions per particle. This constraint translates to an upper bound $\sigma_p/m_p \lesssim 0.1\ \mathrm{cm}^2\ \mathrm{g}^{-1}$. Furthermore, more recent analyses of SIDM models [629, 750] utilize data from the Bullet Cluster to provide another independent limit on the scattering cross section, though the upper bound remains unchanged. [643] have proposed that the tendency for baryonic and dark matter to become separated within dynamical systems, as seen in the Bullet Cluster, could be studied in greater detail if the analysis were to be extended over the full sky in Euclid. This concept is explored in further detail in the following section.

How do these cosmological constraints relate to the values anticipated by particle physics? WIMPs are expected to fall in the range of 10 GeV to a few TeV. The aforementioned values would then correspond to around $\sigma_p \lesssim 10^{-24}\ \mathrm{cm}^2$, at least twenty order of magnitudes greater than what one might expect to achieve from neutral current interactions. Therefore in a cosmological context WIMPs are essentially collisionless, as are axions, since they exhibit an even smaller cross section. Any cosmological detection of SIDM would thus point towards the more exotic candidates postulated by particle physicists, particularly those which are not point particles but instead comprise of extended objects such as Q-balls. A measurement of the scattering cross-section would also place an upper bound on the mass of the dark matter particle, since unitarity of the scattering matrix forbids extremely large cross sections [463], i.e.,

$$\sigma_{\mathrm{tot}} \leq 1.76 \times 10^{-17}\,\mathrm{cm}^2 \left(\frac{\mathrm{GeV}}{m_\chi}\right)^2 \left(\frac{10\,\mathrm{km\ s}^{-1}}{v_{\mathrm{rel}}}\right)^2 \tag{2.5.1}$$

2.5.2 Dark matter–baryonic interactions

Currently, a number of efforts are underway to directly detect WIMPs via the recoil of atomic nuclei. The underground experiments such as CDMS, CRESST, XENON, EDELWEISS and ZEPLIN have pushed observational limits for the spin-independent WIMP-nucleon cross-section

down to the $\sigma \lesssim 10^{-43}\mathrm{cm}^2$ régime.[14] A collection of the latest constraints can be found at http://dmtools.brown.edu.

Another opportunity to unearth the dark matter particle lies in accelerators such as the LHC. By 2018 it is possible these experiments will have yielded mass estimates for dark matter candidates, provided its mass is lighter than a few hundred GeV. However, the discovery of more detailed properties of the particle, which are essential to confirm the link to cosmological dark matter, would have to wait until the International Linear Collider is constructed.

2.5.3 Dark matter–dark energy interactions

Interactions in the dark sector have provided a popular topic for exploration, with a view to building models which alleviate the coincidence and fine-tuning issues associated with dark energy (see Section 1.4.4). The great uncertainty surrounding the physical nature of dark energy leaves plenty of scope for non-gravitational physics to play a rôle. These models are discussed at length in other sections of this review (1.4 and 2.11). Here, we only mention that [837] have explored the phenomenology associated with dark matter scattering elastically with dark energy. The growth rate of large-scale structures is artificially slowed, allowing a modest constraint of

$$\sigma_p/m_p \lesssim \frac{10}{1+w}\ \mathrm{cm}^2\ \mathrm{g}^{-1}\,. \tag{2.5.2}$$

It is clear that such dark sector interactions do not arise in the simplest models of dark matter and dark energy. However a rigorous refutation of GR will require not only a robust measure of the growth of cosmic structures, but confirmation that the anomalous dynamics are not simply due to physics within the dark sector.

2.6 Cross-section constraints from galaxy clusters

Clusters of galaxies present an interesting environment in which the dark matter density is high and where processes such as collisions present the possibility of distinguishing dark matter from baryonic matter as the two components interact differently. For instance, particulate dark matter and baryonic matter may be temporarily separated during collisions between galaxy clusters, such as 1E 0657-56 [244, 164] and MACS J0025.4-1222 [162]. These 'bullet clusters' have provided astrophysical constraints on the interaction cross-section of hypothesized dark matter particles [750], and may ultimately prove the most useful laboratory in which to test for any velocity dependence of the cross-section. Unfortunately, the contribution of individual systems is limited by uncertainties in the collision velocity, impact parameter and angle with respect to the plane of the sky. Current constraints are three orders of magnitude weaker than constraints from the shapes of haloes [361] and, since collisions between two massive progenitors are rare [818, 819], the total observable number of such systems may be inadequate to investigate a physically interesting regime of dark matter properties.

Current constraints from bullet clusters on the cross-section of particulate dark matter are ~ 18 orders of magnitude larger than that required to distinguish between plausible particle-physics dark matter candidates (for example from supersymmetric extensions to the standard model). In order to investigate a physically interesting régime of dark matter cross-section, and provide smaller error bars, many more individual bullet clusters are required. However collisions between two massive progenitors are rare and ultimately the total observable number of such systems may be inadequate.

[14] It is anyway worth noticing the controversial results of DAMA/LIBRA, and more recently of CoGeNT.

2.6.1 Bulleticity

In [643], a method for using every individual infalling substructure in every cluster has been proposed. For each piece of infalling substructure, a local vector from the dark matter peak (identified using weak lensing analysis) and the baryonic mass peak (from X-rays) – dubbed 'bulleticity' – can be defined

$$\mathbf{b} = b_r \hat{\boldsymbol{e}}_r + b_t \hat{\boldsymbol{e}}_t \,, \tag{2.6.1}$$

where the radial b_r and azimuthal b_t components are defined relative to unit vector towards the cluster center and tangentially and $b = |\mathbf{b}|$. An integrated bulleticity signal of zero would imply an equal cross sections for the dark matter and baryonic matter. By measuring the amplitude of the bulleticity one can empirically measure the ratio between the dark matter and baryonic cross sections.

In Figure 35 a result from full hydrodynamical simulations of dark and baryonic matter within clusters in shown. [643] have used these simulations to show that the measurement of a net bulleticity consistent with the cold dark matter used in the simulations is possible.

Finally, a Fisher matrix calculation has shown that, under the assumption that systematic effects can be controlled, Euclid could use such a technique to constrain the relative particulate cross-sections to 6×10^{-27} cm^2 GeV^{-1}.

The raw bulleticity measurement would constrain the relative cross-sections of the baryon-baryon interaction and the dark matter-dark matter interaction. However, since we know the baryonic cross-section relatively well, we can infer the dark matter-dark matter cross-section. The dark matter-dark matter interaction probed by Euclid using this technique will be complementary to the interactions constrained by direct detection and accelerator experiments where the primary constraints will be on the dark matter-baryon interaction.

2.7 Constraints on warm dark matter

N-body simulations of large-scale structures that assume a ΛCDM cosmology appear to over-predict the power on small scales when compared to observations [744]: 'the missing-satellite problem' [494, 511, 869, 188], the 'cusp-core problem' [568, 833, 974] and sizes of mini-voids [888]. These problems may be more or less solved by several different phenomena [e.g. 310], however one which could explain all of the above is warm dark matter (WDM) [143, 248, 159]. If the dark matter particle is very light, it can cause a suppression of the growth of structures on small scales via free-streaming of the dark matter particles whilst relativistic in the early universe.

2.7.1 Warm dark matter particle candidates

Numerous WDM particle models can be constructed, but there are two that occur most commonly in literature, because they are most plausible from particle physics theory as well as from cosmological observations:

- Sterile neutrinos may be constructed to extend the standard model of particle physics. The standard model active (left-handed) neutrinos can then receive the observed small masses through, e.g., a see-saw mechanism. This implies that right-handed sterile neutrinos must be rather heavy, but the lightest of them naturally has a mass in the keV region, which makes it a suitable WDM candidate. The simplest model of sterile neutrinos as WDM candidate assumes that these particles were produced at the same time as active neutrinos, but they never thermalized and were thus produced with a much reduced abundance due to their weak coupling [see 136, and references therein].

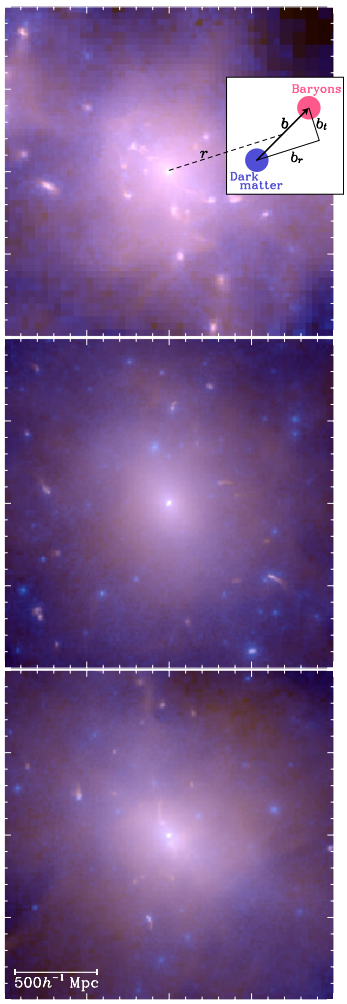

Figure 35: Full hydrodynamical simulations of massive clusters at redshift $z = 0.6$. Total projected mass is shown in blue, while X-ray emission from baryonic gas is in red. The preferential trailing of gas due to pressure from the ICM, and its consequent separation from the non interacting dark matter, is apparent in much of the infalling substructure.

- The gravitino appears as the supersymmetric partner of the graviton in supergravity models. If it has a mass in the keV range, it will be a suitable WDM candidate. It belongs to a more general class of *thermalized* WDM candidates. It is assumed that this class of particles achieved a full thermal equilibrium, but at an earlier stage, when the number of degrees of freedom was much higher and hence their relative temperature with respect to the CMB is much reduced. Note that in order for the gravitino to be a good dark matter particle in general, it must be very stable, which in most models corresponds to it being the LSP [e.g. 151, 221].

Other possible WDM candidates exist, for example a non-thermal neutralino [438] or a non-thermal gravitino [82] etc.

2.7.2 Dark matter free-streaming

The modification of the shape of the linear-theory power spectrum of CDM due to WDM can be calculated by multiplication by a transfer function [143]

$$T(k) \equiv \sqrt{\frac{P_{\rm WDM}(k)}{P_{\rm CDM}(k)}} = \left[1 + (\alpha k)^{2\mu}\right]^{-5/\mu}, \tag{2.7.1}$$

with suitable parameter $\mu = 1.12$ [929] and with the scale break parameter, α in the case of thermal relic DM

$$\alpha = 0.049 \left(\frac{m_{\rm WDM}}{\rm keV}\right)^{-1.11} \left(\frac{\Omega_{\rm WDM}}{0.25}\right)^{0.11} \left(\frac{h}{0.7}\right)^{1.22} h^{-1}\,{\rm Mpc}. \tag{2.7.2}$$

This is a fit to the solution of the full Boltzman equations.

There is a one-to-one relation between the mass of the thermalized WDM particle $m_{\rm WDM}$ (e.g., gravitino), and the mass of the simplest sterile neutrino $m_{\nu{\rm s}}$, such that the two models have an identical impact on cosmology [929]

$$m_{\nu{\rm s}} = 4.43 \left(\frac{m_{\rm WDM}}{\rm keV}\right)^{4/3} \left(\frac{\omega_{\rm WDM}}{0.1225}\right)^{-1/3} {\rm keV}, \tag{2.7.3}$$

where $\omega = \Omega h^2$. The difference comes from the fact that in the gravitino case the particle is fully thermalized, the number of effective degrees of freedom being determined by mass and energy density of dark matter, while in the simplest sterile neutrino case the number of degrees of freedom is fixed, while abundance is determined by mass and energy density of dark matter.

In order to extrapolate the matter power spectrum to later times one must take into account the nonlinear evolution of the matter density field. This is not straightforward in the WDM case [630] and most likely needs to be explored through further simulations [974].

2.7.3 Current constraints on the WDM particle from large-scale structure

Measurements in the particle-physics energy domain can only reach masses uninteresting in the WDM context, since direct detectors look mainly for a WIMP, whose mass should be in the GeV – TeV range. However, as described above, cosmological observations are able to place constraints on light dark matter particles. Observation of the flux power spectrum of the Lyman-α forest, which can indirectly measure the fluctuations in the dark matter density on scales between ~ 100 kpc and ~ 10 Mpc gives the limits of $m_{\rm WDM} > 4$ keV or equivalently $m_{\nu{\rm s}} > 28$ keV at 95% confidence level [927, 929, 812]. For the simplest sterile neutrino model, these lower limits are at odds with the upper limits derived from X-ray observations, which come from the lack of observed diffuse

X-ray background from sterile neutrino annihilation and set the limit $m_{\nu s} < 1.8$ keV at the 95% confidence limit [161]. However, these results do not rule the simplest sterile neutrino models out. There exist theoretical means of evading small-scale power constraints [see e.g. 160, and references therein]. The weak lensing power spectrum from Euclid will be able to constrain the dark matter particle mass to about $m_{\rm WDM} > 2$ keV [630].

2.8 Neutrino properties

The first significant evidence for a finite neutrino mass [373] indicated the incompleteness of the standard model of particle physics. Subsequent experiments have further strengthened this evidence and improved the determination of the neutrino mass splitting required to explain observations of neutrino oscillations.

As a summary of the last decade of neutrino experiments, two hierarchical neutrino mass splittings and three mixing angles have been measured. Furthermore, the standard model has three neutrinos: the motivation for considering deviations from the standard model in the form of extra sterile neutrinos has disappeared [655, 13]. Of course, deviations from the standard effective numbers of neutrino species could still indicate exotic physics which we will discuss below (Section 2.8.4).

New and future neutrino experiments aim to determine the remaining parameters of the neutrino mass matrix and the nature of the neutrino mass. Within three families of neutrinos, and given all neutrino oscillation data, there are three possible mass spectra: a) degenerate, with mass splitting smaller than the neutrino masses, and two non-degenerate cases, b) normal hierarchy (NH), with the larger mass splitting between the two more massive neutrinos and c) inverted hierarchy (IH), with the smaller spitting between the two higher mass neutrinos. Figure 36 [480] illustrates the currently allowed regions in the plane of total neutrino mass, Σ, vs. mass of the lightest neutrino, m. Note that a determination of $\Sigma < 0.1$ eV would indicate normal hierarchy and that there is an expected minimum mass $\Sigma > 0.054$ eV. The cosmological constraint is from [762].

Cosmological constraints on neutrino properties are highly complementary to particle physics experiments for several reasons:

- **Relic neutrinos** produced in the early universe are hardly detectable by weak interactions, making it impossible with foreseeable technology to detect them directly. But new cosmological probes such as Euclid offer the opportunity to detect (albeit indirectly) relic neutrinos, through the effect of their mass on the growth of cosmological perturbations.

- **Cosmology remains a key avenue to determine the absolute neutrino mass scale**. Particle physics experiments will be able to place lower limits on the *effective* neutrino mass, which depends on the hierarchy, with no rigorous limit achievable in the case of normal hierarchy [680]. Contrarily, neutrino free streaming suppresses the small-scale clustering of large-scale cosmological structures by an amount that depends on neutrino mass.

- **"What is the hierarchy (normal, inverted or degenerate)?"** Neutrino oscillation data are unable to resolve whether the mass spectrum consists in two light states with mass m and a heavy one with mass M – normal hierarchy – or two heavy states with mass M and a light one with mass m – inverted hierarchy – in a model-independent way. Cosmological observations, such as the data provided by Euclid, can determine the hierarchy, complementarily to data from particle physics experiments.

- **"Are neutrinos their own anti-particle?"** If the answer is yes, then neutrinos are Majorana fermions; if not, they are Dirac. If neutrinos and anti-neutrinos are identical,

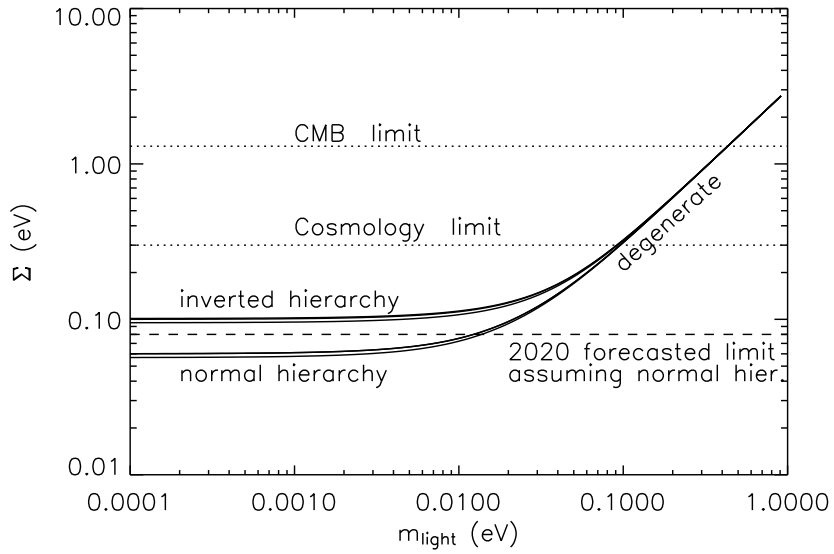

Figure 36: Constraints from neutrino oscillations and from cosmology in the m-Σ plane. Image reproduced by permission from [480]; copyright by IOP and SISSA.

there could have been a process in the early universe that affected the balance between particles and anti-particles, leading to the matter anti-matter asymmetry we need to exist [374]. This question can, in principle, be resolved if neutrino-less double-β decay is observed [see 680, and references therein]. However, if such experiments [ongoing and planned, e.g., 265] lead to a negative result, the implications for the nature of neutrinos depend on the hierarchy. As shown in [480], in this case cosmology can offer complementary information by helping determine the hierarchy.

2.8.1 Evidence of relic neutrinos

The hot big bang model predicts a background of relic neutrinos in the universe with an average number density of $\sim 100\, N_\nu$ cm^{-3}, where N_ν is the number of neutrino species. These neutrinos decouple from the CMB at redshift $z \sim 10^{10}$ when the temperature was $T \sim o(\mathrm{MeV})$, but remain relativistic down to much lower redshifts depending on their mass. A detection of such a neutrino background would be an important confirmation of our understanding of the physics of the early universe.

Massive neutrinos affect cosmological observations in different ways. Primary CMB data alone can constrain the total neutrino mass Σ, if it is above ~ 1 eV [526, finds $\Sigma < 1.3$ eV at 95% confidence] because these neutrinos become non-relativistic before recombination leaving an imprint in the CMB. Neutrinos with masses $\Sigma < 1$ eV become non-relativistic after recombination altering matter-radiation equality for fixed $\Omega_m h^2$; this effect is degenerate with other cosmological parameters from primary CMB data alone. After neutrinos become non-relativistic, their free streaming damps the small-scale power and modifies the shape of the matter power spectrum below the free-streaming length. The free-streaming length of each neutrino family depends on its mass.

Current cosmological observations do not detect any small-scale power suppression and break many of the degeneracies of the primary CMB, yielding constraints of $\Sigma < 0.3$ eV [762] if we assume the neutrino mass to be a constant. A detection of such an effect, however, would provide

a detection, although indirect, of the cosmic neutrino background. As shown in the next section, the fact that oscillations predict a minimum total mass $\Sigma \sim 0.054$ eV implies that Euclid has the statistical power to detect the cosmic neutrino background. We finally remark that the neutrino mass may also very well vary in time [957]; this might be tested by comparing (and not combining) measurements from CMB at decoupling with low-z measurements. An inconsistency would point out a direct measurement of a time varying neutrino mass [959].

2.8.2 Neutrino mass

Particle physics experiments are sensitive to neutrino flavours making a determination of the neutrino absolute-mass scales very model dependent. On the other hand, cosmology is not sensitive to neutrino flavour, but is sensitive to the total neutrino mass.

The small-scale power-suppression caused by neutrinos leaves imprints on CMB lensing: forecasts indicate that Planck should be able to constrain the sum of neutrino masses Σ, with a 1σ error of 0.13 eV [491, 557, 289].

Euclid's measurement of the galaxy power spectrum, combined with Planck (primary CMB only) priors should yield an error on Σ of 0.04 eV [for details see 211] which is in qualitative agreement with previous work [e.g. 779]), assuming a minimal value for Σ and constant neutrino mass. Euclid's weak lensing should also yield an error on Σ of 0.05 eV [507]. While these two determinations are not fully independent (the cosmic variance part of the error is in common given that the lensing survey and the galaxy survey cover the same volume of the universe) the size of the error-bars implies more than 1σ detection of even the minimum Σ allowed by oscillations. Moreover, the two independent techniques will offer cross-checks and robustness to systematics. The error on Σ depends on the fiducial model assumed, decreasing for fiducial models with larger Σ. Euclid will enable us not only to detect the effect of massive neutrinos on clustering but also to determine the absolute neutrino mass scale.

2.8.3 Hierarchy and the nature of neutrinos

Since cosmology is insensitive to flavour, one might expect that cosmology may not help in determining the neutrino mass hierarchy. However, for $\Sigma < 0.1$ eV, only normal hierarchy is allowed, thus a mass determination can help disentangle the hierarchy. There is however another effect: neutrinos of different masses become non-relativistic at slightly different epochs; the free streaming length is sightly different for the different species and thus the detailed shape of the small scale power suppression depends on the individual neutrino masses and not just on their sum. As discussed in [480], in cosmology one can safely neglect the impact of the solar mass splitting. Thus, two masses characterize the neutrino mass spectrum: the lightest m, and the heaviest M. The mass splitting can be parameterized by $\Delta = (M-m)/\Sigma$ for normal hierarchy and $\Delta = (m-M)/\Sigma$ for inverted hierarchy. The absolute value of Δ determines the mass splitting, whilst the sign of Δ gives the hierarchy. Cosmological data are very sensitive to $|\Delta|$; the direction of the splitting – i.e., the sign of Δ – introduces a sub-dominant correction to the main effect. Nonetheless, [480] show that weak gravitational lensing from Euclid data will be able to determine the hierarchy (i.e., the mass splitting and its sign) if far enough away from the degenerate hierarchy (i.e., if $\Sigma < 0.13$).

A detection of neutrino-less double-β decay from the next generation experiments would indicate that neutrinos are Majorana particles. A null result of such double-β decay experiments would lead to a definitive result pointing to the Dirac nature of the neutrino only for degenerate or inverted mass spectrum. This information can be obtained from large-scale structure cosmological data, improved data on the tritium beta decay, or the long-baseline neutrino oscillation experiments. If the small mixing in the neutrino mixing matrix is negligible, cosmology might be the most promising arena to help in this puzzle.

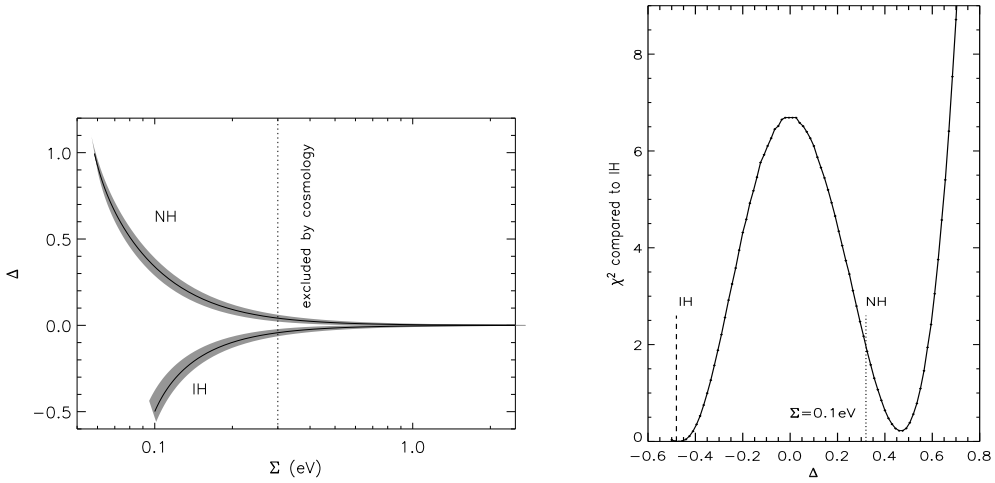

Figure 37: *Left:* region in the Δ-Σ parameter space allowed by oscillations data. *Right:* Weak lensing forecasts. The dashed and dotted vertical lines correspond to the central value for Δ given by oscillations data. In this case Euclid could discriminate NI from IH with a $\Delta\chi^2 = 2$. Image reproduced by permission from [480]; copyright by IOP and SISSA.

2.8.4 Number of neutrino species

Neutrinos decouple early in cosmic history and contribute to a relativistic energy density with an effective number of species $N_{\nu,\mathrm{eff}} = 3.046$. Cosmology is sensitive to the physical energy density in relativistic particles in the early universe, which in the standard cosmological model includes only photons and neutrinos: $\omega_{\mathrm{rel}} = \omega_\gamma + N_{\nu,\mathrm{eff}}\omega_\nu$, where ω_γ denotes the energy density in photons and is exquisitely constrained from the CMB, and ω_ν is the energy density in one neutrino. Deviations from the standard value for $N_{\nu,\mathrm{eff}}$ would signal non-standard neutrino features or additional relativistic species. $N_{\nu,\mathrm{eff}}$ impacts the big bang nucleosynthesis epoch through its effect on the expansion rate; measurements of primordial light element abundances can constrain $N_{\nu,\mathrm{eff}}$ and rely on physics at $T \sim$ MeV [158]. In several non-standard models – e.g., decay of dark matter particles, axions, quintessence – the energy density in relativistic species can change at some later time. The energy density of free-streaming relativistic particles alters the epoch of matter-radiation equality and leaves therefore a signature in the CMB and in the matter-transfer function. However, there is a degeneracy between $N_{\nu,\mathrm{eff}}$ and $\Omega_m h^2$ from CMB data alone (given by the combination of these two parameters that leave matter-radiation equality unchanged) and between $N_{\nu,\mathrm{eff}}$ and σ_8 and/or n_s. Large-scale structure surveys measuring the shape of the power spectrum at large scale can constrain independently the combination $\Omega_m h$ and n_s, thus breaking the CMB degeneracy. Furthermore, anisotropies in the neutrino background affect the CMB anisotropy angular power spectrum at a level of $\sim 20\%$ through the gravitational feedback of their free streaming damping and anisotropic stress contributions. Detection of this effect is now possible by combining CMB and large-scale structure observations. This yields an indication at more than 2σ level that there exists a neutrino background with characteristics compatible with what is expected under the cosmological standard model [901, 285].

The forecasted errors on $N_{\nu,\mathrm{eff}}$ for Euclid (with a Planck prior) are ± 0.1 at 1σ level [507], which is a factor ~ 5 better than current constraints from CMB and LSS and about a factor ~ 2 better than constraints from light element abundance and nucleosynthesis.

2.8.5 Model dependence

A recurring question is how much model dependent will the neutrino constraints be. It is important to recall that usually parameter-fitting is done within the context of a ΛCDM model and that the neutrino effects are seen indirectly in the clustering. Considering more general cosmological models, might degrade neutrino constraints, and vice versa, including neutrinos in the model might degrade dark-energy constraints. Here below we discuss the two cases of varying the total neutrino mass Σ and the number of relativistic species $N_{\rm eff}$, separately.

2.8.6 Σ forecasted error bars and degeneracies

In [211] it is shown that, for a general model which allows for a non-flat universe, and a redshift dependent dark-energy equation of state, the 1σ spectroscopic errors on the neutrino mass Σ are in the range $0.036-0.056$ eV, depending on the fiducial total neutrino mass Σ, for the combination Euclid+Planck.

On the other hand, looking at the effect that massive neutrinos have on the dark-energy parameter constraints, it is shown that the total CMB+LSS dark-energy FoM decreases only by $\sim 15\%-25\%$ with respect to the value obtained if neutrinos are supposed to be massless, when the forecasts are computed using the so-called "$P(k)$-method marginalized over growth-information" (see Methodology section), which therefore results to be quite robust in constraining the dark-energy equation of state.

For what concerns the parameter correlations, at the LSS level, the total neutrino mass Σ is correlated with all the cosmological parameters affecting the galaxy power spectrum shape and BAO positions. When Planck priors are added to the Euclid constraints, all degeneracies are either resolved or reduced, and the remaining dominant correlations among Σ and the other cosmological parameters are Σ-$\Omega_{\rm de}$, Σ-Ω_m, and Σ-w_a, with the Σ-$\Omega_{\rm de}$ degeneracy being the largest one.

2.8.6.1 Hierarchy dependence

In addition, the neutrino mass spectroscopic constraints depend also on the neutrino hierarchy. In fact, the 1σ errors on total neutrino mass for normal hierarchy are $\sim 17\%-20\%$ larger than for the inverted one. It appears that the matter power spectrum is less able to give information on the total neutrino mass when the normal hierarchy is assumed as fiducial neutrino mass spectrum. This is similar to what found in [480] for the constraints on the neutrino mass hierarchy itself, when a normal hierarchy is assumed as the fiducial one. On the other hand, when CMB information are included, the Σ-errors decrease by $\sim 35\%$ in favor of the normal hierarchy, at a given fiducial value $\Sigma|_{\rm fid}$. This difference arises from the changes in the free-streaming effect due to the assumed mass hierarchy, and is in agreement with the results of [556], which confirms that the expected errors on the neutrino masses depend not only on the sum of neutrino masses, but also on the order of the mass splitting between the neutrino mass states.

2.8.6.2 Growth and incoherent peculiar velocity dependence

Σ spectroscopic errors stay mostly unchanged whether growth-information are included or marginalised over, and decrease only by $10\%-20\%$ when adding $f_g\sigma_8$ measurements. This result is expected, if we consider that, unlike dark-energy parameters, Σ affects the shape of the power spectrum via a redshift-dependent transfer function $T(k,z)$, which is sampled on a very large range of scales including the $P(k)$ turnover scale, therefore this effect dominates over the information extracted from measurements of $f_g\sigma_8$. This quantity, in turn, generates new correlations with Σ via the σ_8-term, which actually is anti-correlated with M_ν [641]. On the other hand, if we suppose that early dark-energy is negligible, the dark-energy parameters $\Omega_{\rm de}$, w_0 and w_a do not enter the

transfer function, and consequently growth information have relatively more weight when added to constraints from $H(z)$ and $D_A(z)$ alone. Therefore, the value of the dark-energy FoM does increase when growth-information are included, even if it decreases by a factor $\sim 50\% - 60\%$ with respect to cosmologies where neutrinos are assumed to be massless, due to the correlation among Σ and the dark-energy parameters. As confirmation of this degeneracy, when growth-information are added and if the dark-energy parameters $\Omega_{\rm de}$, w_0, w_a are held fixed to their fiducial values, the errors $\sigma(\Sigma)$ decrease from 0.056 eV to 0.028 eV, for Euclid combined with Planck.

We expect that dark-energy parameter errors are somewhat sensitive also to the effect of incoherent peculiar velocities, the so-called "Fingers of God" (FoG). This can be understood in terms of correlation functions in the redshift-space; the stretching effect due to random peculiar velocities contrasts the flattening effect due to large-scale bulk velocities. Consequently, these two competing effects act along opposite directions on the dark-energy parameter constraints (see methodology Section 5).

On the other hand, the neutrino mass errors are found to be stable again at $\sigma(\Sigma) = 0.056$, also when FoG effects are taken into account by marginalising over $\sigma_v(z)$; in fact, they increase only by $10\% - 14\%$ with respect to the case where FoG are not taken into account.

Finally, in Table 18 we summarize the dependence of the Σ-errors on the model cosmology, for Euclid combined with Planck.[15] We conclude that, if Σ is > 0.1 eV, spectroscopy with Euclid will be able to determine the neutrino mass scale independently of the model cosmology assumed. If Σ is < 0.1 eV, the sum of neutrino masses, and in particular the minimum neutrino mass required by neutrino oscillations, can be measured in the context of a ΛCDM model.

2.8.7 $N_{\rm eff}$ forecasted errors and degeneracies

Regarding the $N_{\rm eff}$ spectroscopic errors, [211] finds $\sigma(N_{\rm eff}) \sim 0.56$ from Euclid, and $\sigma(N_{\rm eff}) \sim 0.086$, for Euclid+Planck. Concerning the effect of $N_{\rm eff}$ uncertainties on the dark-energy parameter errors, the CMB+LSS dark-energy FoM decreases only by $\sim 5\%$ with respect to the value obtained holding $N_{\rm eff}$ fixed at its fiducial value, meaning that also in this case the "$P(k)$-method marginalized over growth–information" is not too sensitive to assumptions about model cosmology when constraining the dark-energy equation of state.

About the degeneracies between $N_{\rm eff}$ and the other cosmological parameters, it is necessary to say that the number of relativistic species gives two opposite contributions to the observed power spectrum $P_{\rm obs}$ (see methodology Section 5), and the total sign of the correlation depends on the dominant one, for each single cosmological parameter. In fact, a larger $N_{\rm eff}$ value suppresses the transfer function $T(k)$ on scales $k \leq k_{\rm max}$. On the other hand, a larger $N_{\rm eff}$ value also increases the Alcock–Paczynski prefactor in $P_{\rm obs}$. For what concerns the dark-energy parameters $\Omega_{\rm de}$, w_0, w_a, and the dark-matter density Ω_m, the Alcock–Paczynski prefactor dominates, so that $N_{\rm eff}$ is positively correlated to $\Omega_{\rm de}$ and w_a, and anti-correlated to Ω_m and w_0. In contrast, for the other parameters, the $T(k)$ suppression produces the larger effect and $N_{\rm eff}$ results to be anti-correlated to Ω_b, and positively correlated to h and n_s. The degree of the correlation is very large in the n_s-$N_{\rm eff}$ case, being of the order ~ 0.8 with and without Planck priors. For the remaining cosmological parameters, all the correlations are reduced when CMB information are added, except for the covariance $N_{\rm eff}$-$\Omega_{\rm de}$, as happens also for the M_ν-correlations. To summarize, after the inclusion of Planck priors, the remaining dominant degeneracies among $N_{\rm eff}$ and the other cosmological parameters are $N_{\rm eff}$-n_s, $N_{\rm eff}$-$\Omega_{\rm de}$, and $N_{\rm eff}$-h, and the forecasted error is $\sigma(N_{\rm eff}) \sim 0.086$, from Euclid+Planck. Finally, if we fix to their fiducial values the dark-energy parameters $\Omega_{\rm de}$, w_0 and w_a, $\sigma(N_{\rm eff})$ decreases from 0.086 to 0.048, for the combination Euclid+Planck.

[15] In this case we have added the contribution from BOSS at redshifts $0.1 < z < z_{\rm min}$, where $z_{\rm min} = 0.5$ is the minimum redshift of the Euclid spectroscopic survey.

Table 18: $\sigma(M_\nu)$ and $\sigma(N_{\rm eff})$ marginalized errors from LSS+CMB

General cosmology						
fiducial $\rightarrow$	$\Sigma = 0.3\,{\rm eV}^a$	$\Sigma = 0.2\,{\rm eV}^a$	$\Sigma = 0.125\,{\rm eV}^b$	$\Sigma = 0.125\,{\rm eV}^c$	$\Sigma = 0.05\,{\rm eV}^b$	$N_{\rm eff} = 3.04^d$
EUCLID+Planck	0.0361	0.0458	0.0322	0.0466	0.0563	0.0862
ΛCDM cosmology						
EUCLID+Planck	0.0176	0.0198	0.0173	0.0218	0.0217	0.0224

[a] for degenerate spectrum: $m_1 \approx m_2 \approx m_3$; [b] for normal hierarchy: $m_3 \neq 0$, $m_1 \approx m_2 \approx 0$
[c] for inverted hierarchy: $m_1 \approx m_2$, $m_3 \approx 0$; [d] fiducial cosmology with massless neutrinos

2.8.8 Nonlinear effects of massive cosmological neutrinos on bias and RSD

In general, forecasted errors are obtained using techniques, like the Fisher-matrix approach, that are not particularly well suited to quantify systematic effects. These techniques forecast only statistical errors, which are meaningful as long as they dominate over systematic errors. Therefore, it is important to consider sources of systematics and their possible effects on the recovered parameters. Possible sources of systematic errors of major concern are the effect of nonlinearities and the effects of galaxy bias.

The description of nonlinearities in the matter power spectrum in the presence of massive neutrinos has been addressed in several different ways: [966, 779, 778, 780] have used perturbation theory, [555] the time-RG flow approach and [167, 166, 168, 928] different schemes of N-body simulations. Another nonlinear scheme that has been examined in the literature is the halo model. This has been applied to massive neutrino cosmologies in [1, 421, 422].

On the other hand, galaxy/halo bias is known to be almost scale-independent only on large, linear scales, but to become nonlinear and scale-dependent for small scales and/or for very massive haloes. From the above discussion and references, it is clear that the effect of massive neutrinos on the galaxy power spectrum in the nonlinear regime must be explored via N-body simulations to encompass all the relevant effects.

Here below we focus on the behavior of the DM-halo mass function (MF), the DM-halo bias, and the redshift-space distortions (RSD), in the presence of a cosmological background of massive neutrinos. To this aim, [168] and [641] have analysed a set of large N-body hydrodynamical simulations, developed with an extended version of the code GADGET-3 [928], which take into account the effect of massive free-streaming neutrinos on the evolution of cosmic structures.

The pressure produced by massive neutrino free-streaming contrasts the gravitational collapse which is the basis of cosmic structure formation, causing a significant suppression in the average number density of massive structures. This effect can be observed in the high mass tail of the halo MF in Figure 38, as compared with the analytic predictions of [824] (ST), where the variance in the density fluctuation field, $\sigma(M)$, has been computed via CAMB [559], using the same cosmological parameters of the simulations. In particular, here the MF of sub-structures is shown, identified using the SUBFIND package [858], while the normalization of the matter power spectrum is fixed by the dimensionless amplitude of the primordial curvature perturbations $\Delta^2_{\mathcal{R}}(k_0)|_{\rm fid} = 2.3 \times 10^{-9}$, evaluated at a pivot scale $k_0 = 0.002/{\rm Mpc}$ [548], which has been chosen to have the same value both in the ΛCDMν and in the ΛCDM cosmologies.

In Figures 38 and 39, two fiducial neutrino masses have been considered, $\Sigma = 0.3$ and $\Sigma = 0.6$ eV. From the comparison of the corresponding MFs, we confirm the theoretical predictions, i.e., that the higher the neutrino mass is, the larger the suppression in the comoving number density

of DM haloes becomes.

As is well known, massive neutrinos also strongly affect the spatial clustering of cosmic structures. A standard statistics generally used to quantify the degree of clustering of a population of sources is the two-point auto-correlation function. Although the free-streaming of massive neutrinos causes a suppression of the matter power spectrum on scales k larger than the neutrino free-streaming scale, the halo bias is significantly enhanced. This effect can be physically explained thinking that, due to neutrino structure suppression, the same halo bias would correspond, in a ΛCDM cosmology, to more massive haloes (than in a ΛCDMν cosmology), which as known are typically more clustered.

This effect is evident in Figure 39 which shows the two-point DM-halo correlation function measured with the Landy and Szalay [541] estimator, compared to the matter correlation function. In particular, the clustering difference between the ΛCDM and ΛCDMν cosmologies increases at higher redshifts, as it can be observed from Figures 40 and 41 and the windows at redshifts $z > 0$ of Figure 38. Note also the effect of nonlinearities on the bias, which clearly starts to become scale-dependent for separations $r < 20$ Mpc$/h$.

As it happens for the MF and clustering, also RSD are strongly affected by massive neutrinos. Figure 42 shows the real and redshift space correlation functions of DM haloes as a function of the neutrino mass. The effect of massive neutrinos is particularly evident when the correlation function is measured as a function of the two directions perpendicular and parallel to the line of sight. As a consequence, the value of the linear growth rate that can be derived by modelling galaxy clustering anisotropies can be greatly suppressed with respect to the value expected in a ΛCDM cosmology. Indeed, neglecting the cosmic relic massive neutrino background in data analysis might induce a bias in the inferred growth rate, from which a potentially fake signature of modified gravity might be inferred. Figure 43 demonstrates this point, showing the best-fit values of β and σ_{12}, as a function of Σ and redshift, where $\beta = \frac{f(\Omega_{\rm M})}{b_{\rm eff}}$, $b_{\rm eff}$ being the halo effective linear bias factor, $f(\Omega_{\rm M})$ the linear growth rate and σ_{12} the pairwise velocity dispersion.

2.9 Coupling between dark energy and neutrinos

As we have seen in Section 1.4.4, it is interesting to consider the possibility that dark energy, seen as a dynamical scalar field (quintessence), may interact with other components in the universe. In this section we focus on the possibility that a coupling may exist between dark energy and neutrinos.

The idea of such a coupling has been addressed and developed by several authors within MaVaNs theories first [356, 714, 135, 12, 952, 280, 874, 856, 139, 178, 177] and more recently within growing neutrino cosmologies [36, 957, 668, 963, 962, 727, 179]. It has been shown that neutrinos can play a crucial role in cosmology, setting naturally the desired scale for dark energy. Interestingly, a coupling between neutrinos and dark energy may help solving the 'why now' problem, explaining why dark energy dominates only in recent epochs. The coupling follows the description illustrated in Section 1.4.4 for a general interacting dark-energy cosmology, where now $m_\nu = m_\nu(\phi)$.

Typically, in growing neutrino cosmologies, the function $m_\nu(\phi)$ is such that the neutrino mass grows with time from low, nearly massless values (when neutrinos are non-relativistic) up to present masses in a range in agreement with current observations (see the previous section of this review for latest bounds on neutrino masses). The key feature of growing neutrino models is that the amount of dark energy today is triggered by a cosmological event, corresponding to the transition from relativistic to non-relativistic neutrinos at redshift $z_{\rm NR} \sim 5 \div 10$. As long as neutrinos are relativistic, the coupling plays no role on the dynamics of the scalar field, which follows attractor solutions of the type described in Section 1.4.4. From there on, the evolution of dark energy resembles that of a cosmological constant, plus small oscillations of the coupled dark energy-

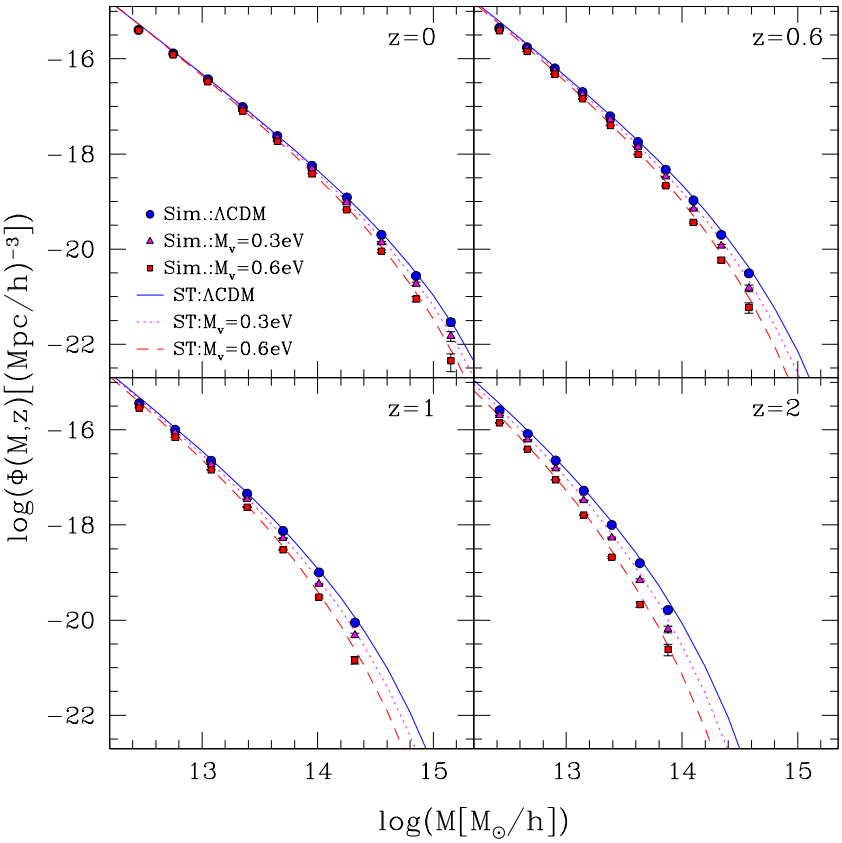

Figure 38: DM halo mass function (MF) as a function of Σ and redshift. MF of the SUBFIND haloes in the ΛCDM N-body simulation (blue circles) and in the two simulations with $\Sigma = 0.3$ eV (magenta triangles) and $\Sigma = 0.6$ eV (red squares). The blue, magenta and red lines show the halo MF predicted by [824], where the variance in the density fluctuation field, $\sigma(M)$, at the three cosmologies, $\Sigma = 0, 0.3, 0.6$ eV, has been computed with the software CAMB [559].

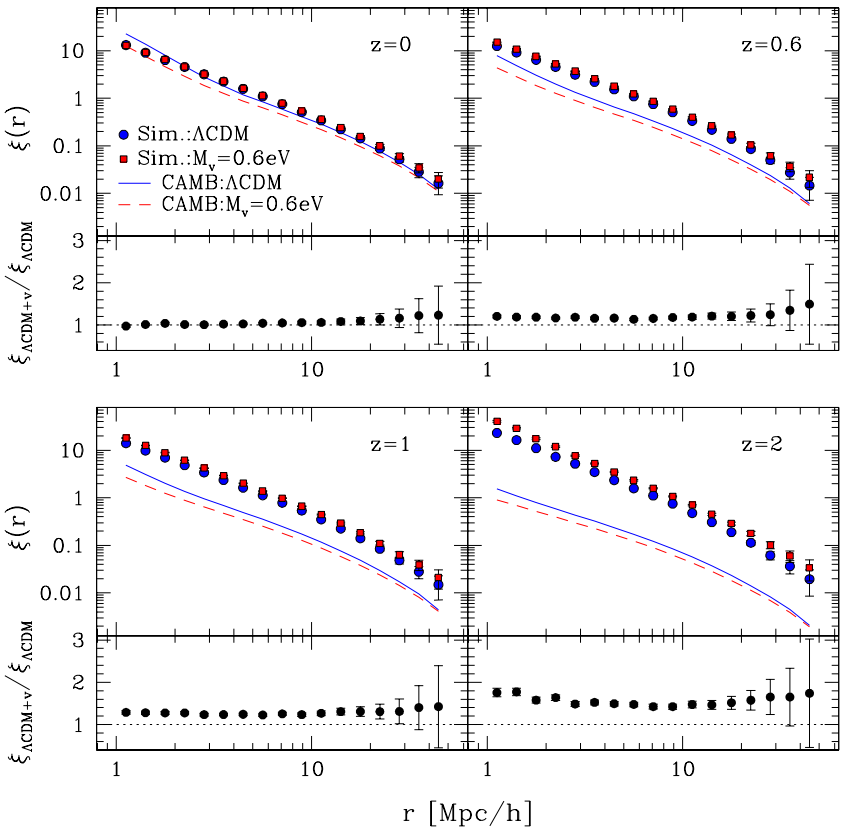

Figure 39: DM halo mass function (MF) as a function of Σ and redshift. Real space two-point auto-correlation function of the DM haloes in the ΛCDM N-body simulation (blue circles) and in the simulation with $\Sigma = 0.6$ eV (red squares). The blue and red lines show the DM correlation function computed using the CAMB matter power spectrum with $\Sigma = 0$ and $\Sigma = 0.6$ eV, respectively. The bottom panels show the ratio between the halo correlation function extracted from the simulations with and without massive neutrinos.

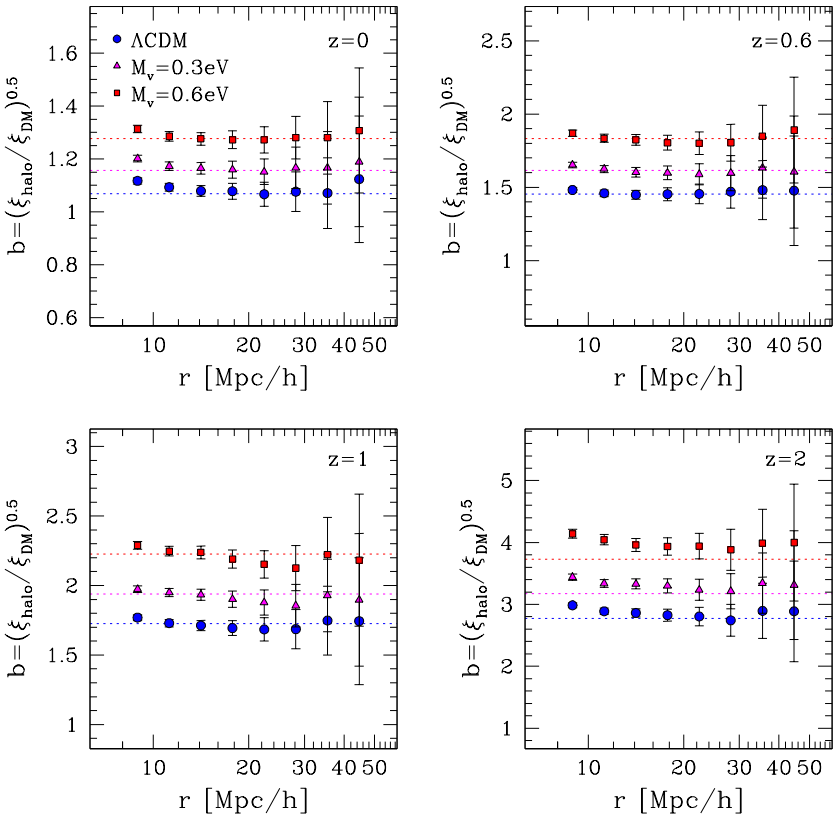

Figure 40: Real space two-point auto-correlation function of the DM haloes in the ΛCDM N-body simulation (blue circles) and in the simulation with $\Sigma = 0.6$ eV (red squares). The blue and red lines show the DM correlation function computed using the CAMB matter power spectrum with $\Sigma = 0$ and $\Sigma = 0.6$ eV, respectively. The bottom panels show the ratio between the halo correlation function extracted from the simulations with and without massive neutrinos.

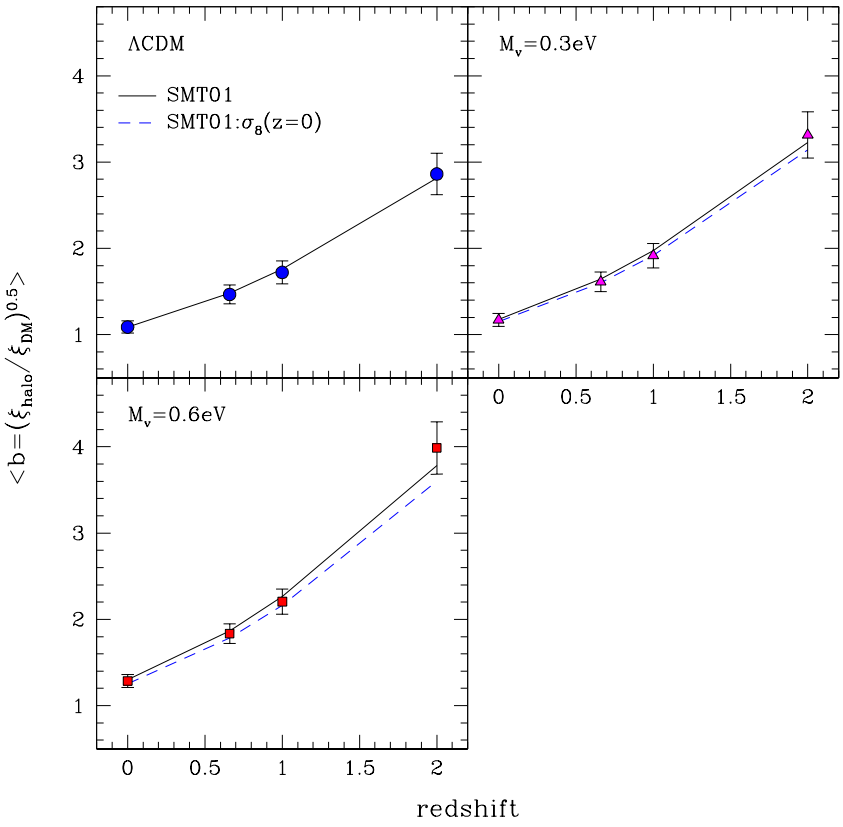

Figure 41: Mean bias (averaged in $10 < r\,[\mathrm{Mpc}/h] < 50$) as a function of redshift compared with the theoretical predictions of [824]. Here the dashed lines represent the theoretical expectations for a ΛCDM cosmology renormalized with the σ_8 value of the simulations with a massive neutrino component.

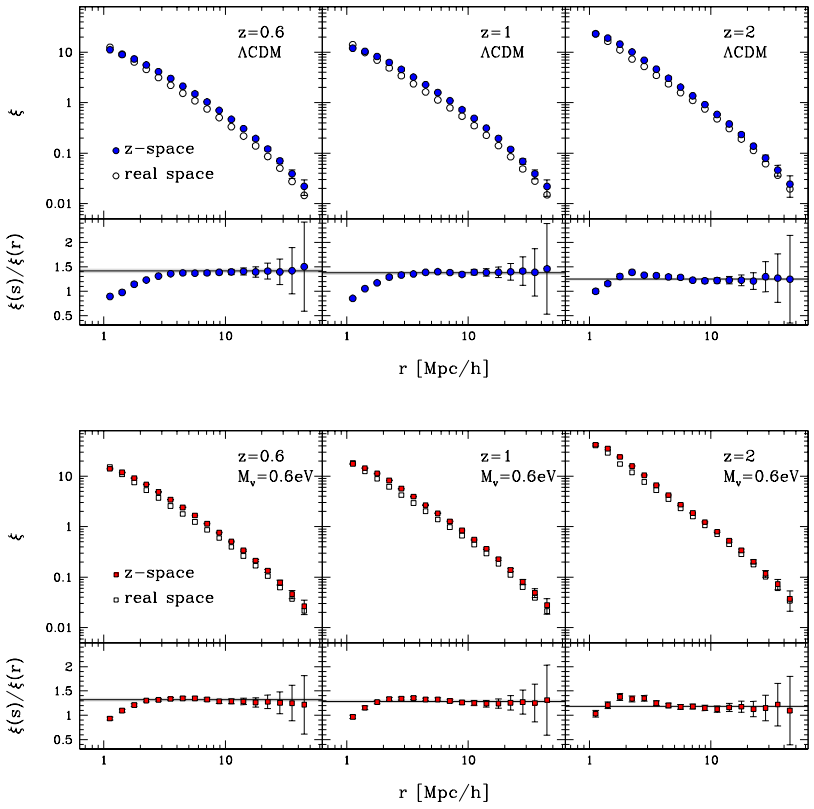

Figure 42: Two-point auto-correlation function in real and redshift space of the DM-haloes in the ΛCDM N-body simulation (blue circles) and in the simulation with $\Sigma = 0.6$ eV (red squares). The bottom panels show the ratio between them, compared with the theoretical expectation.

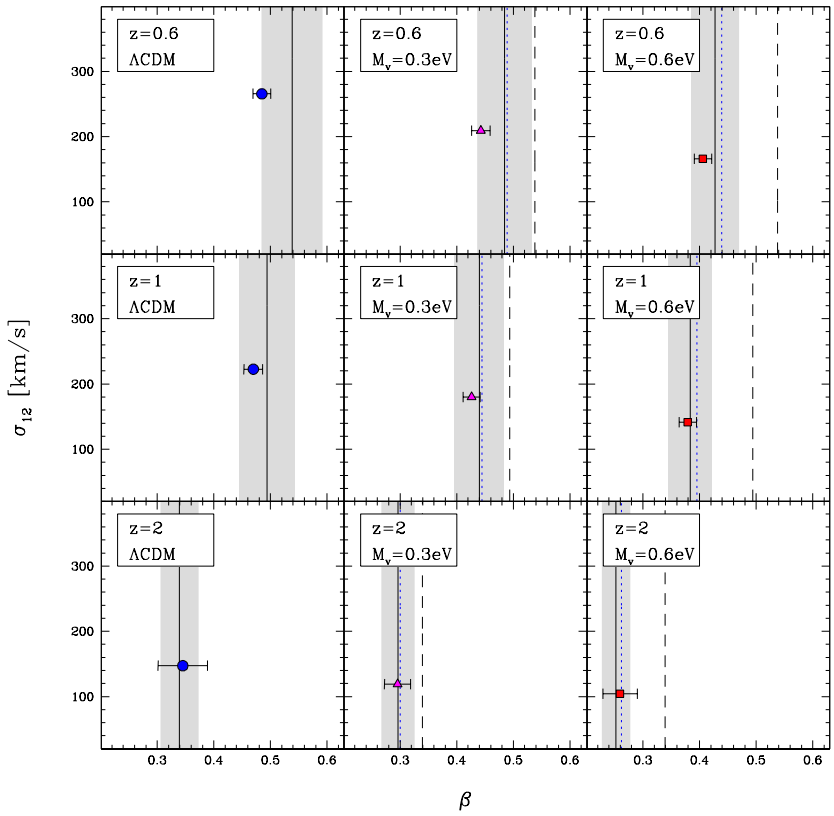

Figure 43: Best-fit values of β-σ_{12}, as a function of Σ and redshift (points), compared with the theoretical prediction (grey shaded area). The blue dotted lines show the theoretical prediction for $\Sigma = 0$ and with $\sigma_8(z = 0)$.

neutrino fluid. As a consequence, when a coupling between dark energy and neutrinos is active, the amount of dark energy and its equation of state today are strictly connected to the present value of the neutrino mass.

The interaction between neutrinos and dark energy is a nice and concrete example of the significant imprint that dynamical coupled dark energy can leave on observables and in particular on structure formation and on the cosmic microwave background. This is due to the fact that the coupling, playing a role only after neutrinos become non-relativistic, can reach relatively high values as compared to gravitational attraction. Typical values of β are order $50 \div 100$ or even more such that even the small fraction of cosmic energy density in neutrinos can have a substantial influence on the time evolution of the quintessence field. During this time the fifth force can be of order $10^2 \div 10^4$ times stronger than gravity. The neutrino contribution to the gravitational potential influences indirectly also dark matter and structure formation, as well as CMB, via the Integrated Sachs–Wolfe effect and the nonlinear Rees–Sciama effect, which is non-negligible at the scales where neutrinos form stable lumps. Furthermore, backreaction effects can substantially modify the growth of large scale neutrino lumps, with effects which are much larger than in the dark matter case. The presence of a fifth force due to an interaction between neutrinos and dark energy can lead to remarkably peculiar differences with respect to a cosmological constant scenario.

Here, we just recall some of the typical features that can arise when such an interaction is active:

- existence of very large structures, order $10 \div 500$ Mpc [12, 668, 963, 962, 727];
- enhanced ISW effect, drastically reduced when taking into account nonlinearities [727]: information on the gravitational potential is a good mean to constrain the range of allowed values for the coupling β;
- large-scale anisotropies and enhanced peculiar velocities [947, 69];
- the influence of the gravitational potential induced by the neutrino inhomogeneities can affect BAO in the dark-matter spectra [179].

Investigation of structure formation at very large scales (order $1 \div 100$ Mpc) as well as cross correlation with CMB are crucial in order to disentangle coupled neutrino-quintessence cosmologies from a cosmological constant scenario. Detection of a population of very large-scale structures could pose serious difficulties to the standard framework and open the way to the existence of a new cosmological interaction stronger than gravity.

2.10 Unified Dark Matter

The appearance of two unknown components in the standard cosmological model, dark matter and dark energy, has prompted discussion of whether they are two facets of a single underlying dark component. This concept goes under the name of quartessence [615], or unified dark matter (UDM). *A priori* this is attractive, replacing two unknown components with one, and in principle it might explain the 'why now?' problem of why the energy densities of the two components are similar (also referred to as the coincidence problem). Many UDM models are characterized by a sound speed, whose value and evolution imprints oscillatory features on the matter power spectrum, which may be detectable through weak lensing or BAO signatures with Euclid.

The field is rich in UDM models [see 128, for a review and for references to the literature]. The models can grow structure, as well as providing acceleration of the universe at late times. In many cases, these models have a non-canonical kinetic term in the Lagrangian, e.g., an arbitrary function of the square of the time derivative of the field in a homogeneous and isotropic background.

Early models with acceleration driven by kinetic energy [k-inflation 60, 384, 154] were generalized to more general Lagrangians [k-essence; e.g., 61, 62, 795]. For UDM, several models have been investigated, such as the generalized Chaplygin gas [488, 123, 137, 979, 741], although these may be tightly constrained due to the finite sound speed [e.g. 38, 124, 784, 985]. Vanishing sound speed models however evade these constraints [e.g., the silent Chaplygin gas of 50]. Other models consider a single fluid with a two-parameter equation of state [e.g 74]), models with canonical Lagrangians but a complex scalar field [55], models with a kinetic term in the energy-momentum tensor [379, 234], models based on a DBI action [236], models which violate the weak equivalence principle [375] and models with viscosity [321]. Finally, there are some models which try to unify inflation as well as dark matter and dark energy [206, 688, 572, 575, 430].

A requirement for UDM models to be viable is that they must be able to cluster to allow structure to form. A generic feature of the UDM models is an effective sound speed, which may become significantly non-zero during the evolution of the universe, and the resulting Jeans length may then be large enough to inhibit structure formation. The appearance of this sound speed leads to observable consequences in the CMB as well, and generally speaking the speed needs to be small enough to allow structure formation and for agreement with CMB measurements. In the limit of zero sound speed, the standard cosmological model is recovered in many models. Generally the models require fine-tuning, although some models have a fast transition between a dark matter only behavior and ΛCDM. Such models [729] can have acceptable Jeans lengths even if the sound speed is not negligible.

2.10.1 Theoretical background

An action which is applicable for most UDM models, with a single scalar field φ, is

$$S = \int \mathrm{d}^4x\sqrt{-g}\left[\frac{R}{2} + \mathcal{L}(\varphi, X)\right], \tag{2.10.1}$$

where

$$X \equiv -\frac{1}{2}\nabla_\mu\varphi\nabla^\mu\varphi \tag{2.10.2}$$

and ∇ indicates covariant differentiation. This leads to an energy density which is $\rho = 2X\,\partial p/\partial X - p$, and hence an equation-of-state parameter $w \equiv p/\rho$ (in units of $c = 1$) given by

$$w = \frac{p}{2X\,\partial p/\partial X - p}, \tag{2.10.3}$$

and $p = \mathcal{L}$. A full description of the models investigated and Lagrangians considered is beyond the scope of this work; the reader is directed to the review by [128] for more details. Lagrangians of the form

$$\mathcal{L}(\varphi, X) = f(\varphi)g(X) - V(\varphi), \tag{2.10.4}$$

where $g(X)$ is a Born–Infeld kinetic term, were considered in a Euclid-like context by [201], and models of this form can avoid a strong ISW effect which is often a problem for UDM models [see 127, and references therein]. This model is parameterized by a late-time sound speed, c_∞, and its influence on the matter power spectrum is illustrated in Figure 44. For zero sound speed ΛCDM is recovered.

2.10.2 Euclid observables

Of interest for Euclid are the weak lensing and BAO signatures of these models, although the supernova Hubble diagram can also be used [885]. The observable effects come from the power

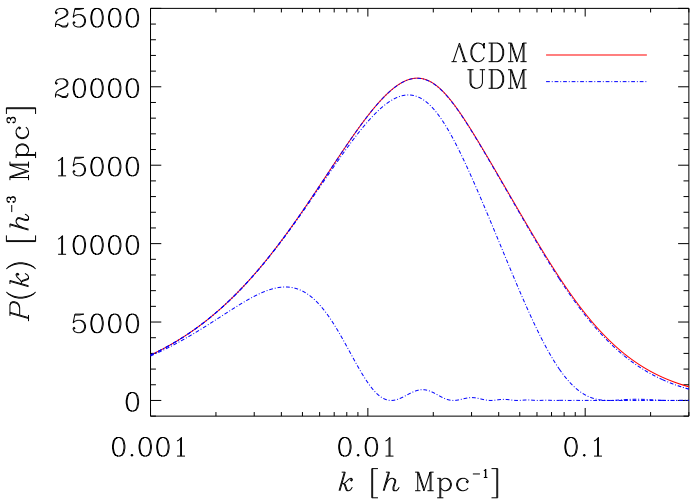

Figure 44: The $z = 0$ matter power spectrum arising in UDM models with a Lagrangian given by Eq. (2.10.4). ΛCDM is solid, and UDM models with $c_\infty = 10^{-1}, 10^{-2}, 10^{-3}$ are shown from bottom to top. Image reproduced by permission from [201].

spectrum and the evolution of the equation-of-state parameter of the unified fluid, which affects distance measurements. The observational constraints of the generalized Chaplygin gas have been investigated [706], with the model already constrained to be close to ΛCDM with SDSS data and the CMB. The effect on BAO measurements for Euclid has yet to be calculated, but the weak lensing effect has been considered for non-canonical UDM models [202]. The change in shape and oscillatory features introduced in the power spectrum allow the sound speed parameter to be constrained very well by Euclid, using 3D weak lensing [427, 506] with errors $\sim 10^{-5}$ [see also 198].

2.11 Dark energy and dark matter

In Section 1.4, we have illustrated the possibility that dark energy, seen as a dynamical scalar field (quintessence), may interact with other components in the universe. When starting from an action such as Eq. (1.4.20), the species which interact with quintessence are characterized by a mass function that changes in time [514, 33, 35, 724]. Here, we consider the case in which the evolution of cold dark matter (CDM) particles depends on the evolution of the dark-energy scalar field. In this case the general framework seen in Section 1.4 is specified by the choice of the function $m_c = m_c(\phi)$. The coupling is not constrained by tests of the equivalence principle and solar system constraints, and can therefore be stronger than the coupling with baryons. Typical values of β presently allowed by observations (within current CMB data) are within the range $0 < \beta < 0.06$ at 95% CL for a constant coupling and an exponential potential, [114, 47, 35, 44], or possibly more if neutrinos are taken into account or more realistic time-dependent choices of the coupling are used [539, 531]. As mentioned in Section 1.4.4, this framework is generally referred to as 'coupled quintessence' (CQ). Various choices of couplings have been investigated in the literature, including constant β [33, 619, 35, 518, 414, 747, 748, 724] and varying couplings [76], with effects on Supernovæ, CMB and cross-correlation of the CMB and LSS [114, 47, 35, 44, 539, 531, 612].

The presence of a coupling (and therefore, of a fifth force acting among dark matter particles)

modifies the expansion of the universe, linear perturbations and most relevantly, structure formation. Coupled quintessence is a concrete model in which a non-negligible amount of dark energy is present at early times. The presence of such an early dark-energy component is accompanied specific features, as illustrated in Section 1.4 for a general framework:

1. a fifth force $\nabla[\Phi_\alpha + \beta\phi]$ with an effective $\tilde{G}_\alpha = G_N[1 + 2\beta^2(\phi)]$;
2. a velocity-dependent term $\tilde{H}\mathbf{v}_\alpha \equiv H\left(1 - \beta(\phi)\frac{\dot{\phi}}{H}\right)\mathbf{v}_\alpha$;
3. a time-dependent mass for each particle α, evolving according to Eq. (1.4.25).

All these effects, and in particular the first two, contribute significantly to structure formation. Note that the second and third terms are not independent of each other as they are a direct consequence of momentum conservation. Depending on the function $m_c(\phi)$, and therefore $\beta(\phi)$, the first two terms can partially balance: the fifth force increases gravitational attraction whilst the velocity-dependent term, if the CDM mass decreases with time, tries to dilute the concentration of the virialized haloes. In particular, a striking difference between constant and variable-coupling models concerning the interplay of all these three effects has been highlighted in [76]: whilst for constant couplings only the latter two effects can alter the virial equilibrium of an already-collapsed object, for the case of a variable coupling the time evolution of the effective gravitational constant can also modify the virial status of a halo, and can either enhance or counteract the effect of reducing halo concentrations (for decreasing and increasing couplings, respectively). Nonlinear evolution within coupled quintessence cosmologies has been addressed using various methods of investigation, such as spherical collapse [611, 962, 618, 518, 870, 3, 129] and alternative semi-analytic methods [787, 45]. N-body and hydro-simulations have also been done [604, 79, 76, 77, 80, 565, 562, 75, 980].

We list here briefly the main observable features typical of this class of models:

- enhanced ISW effect [33, 35, 612]; such effects may be partially reduced when taking into account nonlinearities, as described in [727];
- increase in the number counts of massive clusters at high redshift [77];
- scale-dependent bias between baryons and dark matter, which behave differently if only dark matter is coupled to dark energy [79, 75];
- less steep inner core halo profiles (depending on the interplay between fifth force and velocity-dependent terms) [79, 76, 565, 562, 75];
- lower concentration of the halos [79, 76, 562];
- voids are emptier when a coupling is active [80].

As discussed in subsection 1.6.1, when a variable coupling $\beta(\phi)$ is active the relative balance of the fifth-force and other dynamical effects depends on the specific time evolution of the coupling strength. Under such conditions, certain cases may also lead to the opposite effect of larger halo inner overdensities and higher concentrations, as in the case of a steeply growing coupling function [see 76]. Alternatively, the coupling can be introduced by choosing directly a covariant stress-energy tensor, treating dark energy as a fluid in the absence of a starting action [619, 916, 193, 794, 915, 613, 387, 192, 388]. For an illustration of nonlinear effects in the presence of a coupling see Section 1.6.

2.12 Ultra-light scalar fields

Ultra-light scalar fields arise generically in high energy physics, most commonly as axions or other axion-like particles (ALPs). They are the Pseudo-Goldstone bosons (PGBs) of spontaneously broken symmetries. Their mass remains protected to all loop orders by a shift symmetry, which is only weakly broken to give the fields a mass and potential, through non perturbative effects. Commonly these effects are presumed to be caused by instantons, as in the case of the QCD axion, but the potential can also be generated in other ways that give potentials that are useful, for example, in the study of quintessence [705]. Here we will be considering a general scenario, motivated by the suggestions of [63] and [452], where an ultralight scalar field constitutes some fraction of the dark matter, and we make no detailed assumptions about its origin.

Axions arise generically in string theory [871]. They are similar to the well known QCD axion [715, 873, 872, 315, 742, 866, 911, 2, 316, 908, 932], and their cosmology has been extensively studied [see, for example, 84]. String axions are the Kaluza–Klein zero modes of anti-symmetric tensor fields, the number of which is given by the number of closed cycles in the compact space: for example a two-form such as B_{MN}[16] has a number of zero modes coming from the number of closed two-cycles. In any realistic compactification giving rise to the Standard Model of particle physics the number of closed cycles will typically be in the region of hundreds. Since such large numbers of these particles are predicted by String Theory, we are motivated to look for their general properties and resulting cosmological phenomenology.

The properties of the axion θ are entirely determined by its potential U, whose specific form depends on details in string theory that will not concern us, and two parameters in the four-dimensional Lagrangian

$$\mathcal{L} = \frac{f_a^2}{2}(\partial\theta)^2 - \Lambda^4 U(a), \tag{2.12.1}$$

where f_a is the scale at which the Peccei–Quinn-like symmetry – an additional global $U(1)$ symmetry – is broken, also referred to as the axion decay constant, and Λ is the overall scale of the potential. In terms of the canonically normalized field $\phi = f_a\theta$, we find that the mass is given by

$$m = \frac{\Lambda^2}{f_a}. \tag{2.12.2}$$

The values of these parameters are determined by the action S of the non-perturbative physics that generates the potential for a given axion, and it was argued in [63] that this scales with the volume/area of the closed cycle giving rise to that axion, $S \sim A$. f_a and S are related by

$$f_a \sim \frac{M_{\rm pl}}{S}. \tag{2.12.3}$$

f_a is typically of order 10^{16} GeV and can be considered constant for all string axions [871]. However, the mass of each axion depends exponentially on S from

$$\Lambda^4 = \mu^4 e^{-S}, \tag{2.12.4}$$

where μ sets the scale of the non-perturbative physics (essentially, the Planck Scale in the string case), and so, as S varies from axion to axion depending on the cycle areas in the compact space, we expect axion masses to evenly distribute on a logarithmic mass scale all the way down to the Hubble scale today, $H_0 \sim 10^{-33}$ eV [63].

There will be a small thermal population of ALPs, but the majority of the cosmological population will be cold and non-thermally produced. Production of cosmological ALPs proceeds by the

[16] B_{MN} is the antisymmetric partner of the metric, which in heterotic string theory gives rise to the model-independent axion. The indices M, N run over the spacetime dimensions, $0, \ldots, D-1$.

vacuum realignment mechanism. When the Peccei–Quinn-like $U(1)$ symmetry is spontaneously broken at the scale f_a the ALP acquires a vacuum expectation value, the misalignment angle θ_i, uncorrelated across different causal horizons. However, provided that inflation occurs after symmetry breaking, and with a reheat temperature $T \lesssim f_a$, then the field is homogenized over our entire causal volume. This is the scenario we will consider. The field θ is a PGB and evolves according to the potential U acquired at the scale μ. However, a light field will be frozen at θ_i until the much later time when the mass overcomes the Hubble drag and the field begins to roll towards the minimum of the potential, in exact analogy to the minimum of the instanton potential restoring $\mathcal{CP}$ invariance in the Peccei-Quinn mechanism for the QCD axion. Coherent oscillations about the minimum of U lead to the production of the weakly coupled ALPs, and it is the value of the misalignment angle that determines the cosmological density in ALPs [579, 431, 826].

The underlying shift symmetry restricts U to be a periodic function of θ for true axions, but since in the expansion all couplings will be suppressed by the high scale f_a, and the specific form of U is model-dependent, we will make the simplification to consider only the quadratic mass term as relevant in the cosmological setting, though some discussion of the effects of anharmonicites will be made. In addition, [705] have constructed non-periodic potentials in string theory.

Scalar fields with masses in the range 10^{-33} eV $< m < 10^{-22}$ eV are also well-motivated dark matter candidates independently of their predicted existence in string theory, and constitute what Hu has dubbed "fuzzy cold dark matter", or FCDM [452]. The Compton wavelength of the particles associated with ultra-light scalar fields, $\lambda_c = 1/m$ in natural units, is of the size of galaxies or clusters of galaxies, and so the uncertainty principle prevents localization of the particles on any smaller scale. This naturally suppresses formation of structure and serves as a simple solution to the problem of "cuspy halos" and the large number of dwarf galaxies, which are not observed and are otherwise expected in the standard picture of CDM. Sikivie has argued [827] that axion dark matter fits the observed caustics in dark matter profiles of galaxies, which cannot be explained by ordinary dust CDM.

The large phase space density of ultralight scalar fields causes them to form Bose–Einstein condensates [see 828, and references therein] and allows them to be treated as classical fields in a cosmological setting. This could lead to many interesting, and potentially observable phenomena, such as formation of vortices in the condensate, which may effect halo mass profiles [829, 484], and black hole super radiance [63, 64, 772], which could provide direct tests of the "string axiverse" scenario of [63]. In this summary we will be concerned with the large-scale indirect effects of ultra-light scalar fields on structure formation via the matter power spectrum in a cosmology where a fraction $f = \Omega_a/\Omega_m$ of the dark matter is made up of such a field, with the remaining dark matter a mixture of any other components but for simplicity we will here assume it to be CDM so that $(1-f)\Omega_m = \Omega_c$.

If ALPs exist in the high energy completion of the standard model of particle physics, and are stable on cosmological time scales, then regardless of the specifics of the model [882] have argued that on general statistical grounds we indeed expect a scenario where they make up an order one fraction of the CDM, alongside the standard WIMP candidate of the lightest supersymmetric particle. However, it must be noted that there are objections when we consider a population of light fields in the context of inflation [605, 606]. The problem with these objections is that they make some assumptions about what we mean by "fine tuning" of fundamental physical theories, which is also related to the problem of finding a measure on the landscape of string theory and inflation models [see, e.g., 583], the so-called "Goldilocks problem." Addressing these arguments in any detail is beyond the scope of this summary.

We conclude with a summary of the most important equations and properties of ultra-light scalar fields.

- In conformal time and in the synchronous gauge with scalar perturbation h as defined in [599], a scalar field with a quadratic potential evolves according to the following equations

for the homogeneous, $\phi_0(\tau)$, and first order perturbation, $\phi_1(\tau, \vec{k})$, components

$$\ddot{\phi}_0 + 2\mathcal{H}\dot{\phi}_o + m^2 a^2 \phi_0 = 0, \tag{2.12.5}$$

$$\ddot{\phi}_1 + 2\mathcal{H}\dot{\phi}_1 + (m^2 a^2 + k^2)\phi_1 = -\frac{1}{2}\dot{\phi}_0 \dot{h}; \tag{2.12.6}$$

- In cosmology we are interested in the growth of density perturbations in the dark matter, and how they effect the expansion of the universe and the growth of structure. The energy-momentum tensor for a scalar field is

$$T^{\mu}{}_{\nu} = \phi^{;\mu}\phi_{;\nu} - \frac{1}{2}(\phi^{;\alpha}\phi_{;\alpha} + 2V)\delta^{\mu}_{\nu} \tag{2.12.7}$$

which to first order in the perturbations has the form of a perfect fluid and so we find the density and pressure components in terms of ϕ_0, ϕ_1,

$$\rho_a = \frac{a^{-2}}{2}\dot{\phi}_0^2 + \frac{m^2}{2}\phi_0^2, \tag{2.12.8}$$

$$\delta\rho_a = a^{-2}\dot{\phi}_0\dot{\phi}_1 + m^2\phi_0\phi_1, \tag{2.12.9}$$

$$P_a = \frac{a^{-2}}{2}\dot{\phi}_0^2 - \frac{m^2}{2}\phi_0^2, \tag{2.12.10}$$

$$\delta P_a = a^{-2}\dot{\phi}_0\dot{\phi}_1 - m^2\phi_0\phi_1, \tag{2.12.11}$$

$$(\rho + P)\theta_a = a^{-2}k^2\dot{\phi}_0\phi_1; \tag{2.12.12}$$

- The scalar field receives an initial value after symmetry breaking and at early times it remains frozen at this value by the Hubble drag. A frozen scalar field behaves as a cosmological constant; once it begins oscillating it will behave as matter. A field begins oscillating when

$$H(t) < m; \tag{2.12.13}$$

- Do oscillations begin in the radiation or matter dominated era? The scale factor at which oscillations begin, $a_{\rm osc}$, is given by

$$\begin{aligned} a_{\rm osc} &= \left(\frac{t_{\rm eq}}{t_0}\right)^{1/6}\left(\frac{1}{mt_0}\right)^{1/2}, \qquad m \gtrsim 10^{-27}{\rm eV}, \\ a_{\rm osc} &= \left(\frac{1}{mt_0}\right)^{2/3}, \qquad m \lesssim 10^{-27}{\rm eV}; \end{aligned} \tag{2.12.14}$$

- If oscillations begin in the matter-dominated era then the epoch of equality will not be the same as that inferred from the matter density today. Only CDM will contribute to the matter density at equality, so that the scale factor of equality is given by

$$a_{\rm eq} \simeq \frac{\Omega_r}{\Omega_m}\frac{1}{(1-f)}; \tag{2.12.15}$$

- The energy density today in such an ultralight field can be estimated from the time when oscillations set in and depends on its initial value as

$$\Omega_a = \frac{1}{6}\left(\frac{1}{t_0}\right)^2 \phi_0(t_i)^2, \tag{2.12.16}$$

while fields that begin oscillations in the radiation era also have a mass dependence in the final density as $\sim m^{1/2}$;

- In the context of generalized dark matter [447] we can see the effect of the Compton scale of these fields through the fluid dynamics of the classical field. The sound speed of a field with momentum k and mass m at a time when the scale factor of the FLRW metric is a is given by

$$c_s^2 = \frac{k^2}{4m^2a^2}, \quad k < 2ma,$$
$$c_s^2 = 1, \quad k > 2ma. \tag{2.12.17}$$

  On large scales the pressure becomes negligible, the sound speed goes to zero and the field behaves as ordinary dust CDM and will collapse under gravity to form structure. However on small scales, set by λ_c, the sound speed becomes relativistic, suppressing the formation of structure;

- This scale-dependent sound speed will affect the growth of overdensities, so we ask: are the perturbations on a given scale at a given time relativistic? The scale

$$k_R = ma(t) \tag{2.12.18}$$

  separates the two regimes. On small scales: $k > k_R$ the sound speed is relativistic. Structure formation is suppressed in modes that entered the horizon whilst relativistic.

- Time dependence of the scale k_R and the finite size of the horizon mean that suppression of structure formation will accumulate on scales larger than k_R. For the example of ultralight fields that began oscillations in the matter-dominated regime, we calculate that suppression of structure begins at a scale

$$k_m \sim \left(\frac{m}{10^{-33}\ \mathrm{eV}}\right)^{1/3} \left(\frac{100\ \mathrm{km\ s^{-1}}}{c}\right) h\ \mathrm{Mpc}^{-1}, \tag{2.12.19}$$

  which is altered to $k_m \sim m^{1/2}$ for heavier fields that begin oscillations in the radiation era [37];

- The suppression leads to steps in the matter power spectrum, the size of which depends on f. The amount of suppression can be estimated, following [37], as

$$S(a) = \left(\frac{a_{\mathrm{osc}}}{a}\right)^{2(1-1/4(-1+\sqrt{25-24f}))}. \tag{2.12.20}$$

  As one would expect, a larger f gives rise to greater suppression of structure, as do lighter fields that free-stream on larger scales.

Numerical solutions to the perturbation equations indeed show that the effect of ultralight fields on the growth of structure is approximately as expected, with steps in the matter power spectrum appearing. However, the fits become less reliable in some of the most interesting regimes where the field begins oscillations around the epoch of equality, and suppression of structure occurs near the turnover of the power spectrum, and also for the lightest fields that are still undergoing the transition from cosmological constant to matter-like behavior today [632]. These uncertainties are caused by the uncertainty in the background expansion during such an epoch. In both cases a change in the expansion rate away from the expectation of the simplest ΛCDM model is expected. During matter and radiation eras the scale factor grows as $a \sim \tau^p$ and p can be altered away from the ΛCDM expectation by $\mathcal{O}(10)\%$ by oscillations caused during the scalar field transition,

which can last over an order of magnitude in scale factor growth, before returning to the expected behavior when the scalar field is oscillating sufficiently rapidly and behaves as CDM.

The combined CMB-large scale structure likelihood analysis of [37] has shown that ultralight fields with mass around $10^{-30} - 10^{-24}$ eV might account for up to 10% of the dark matter abundance.

2.12.1 Requirements

Ultralight fields are similar in many ways to massive neutrinos [37], the major difference being that their non-thermal production breaks the link between the scale of suppression, k_m, and the fraction of dark matter, f_{ax}, through the dependence of f_{ax} on the initial field value ϕ_i. Therefore an accurate measurement of the matter power spectrum in the low-k region where massive neutrinos corresponding to the WMAP limits on Ω_ν are expected to suppress structure will determine whether the expected relationship between Ω_ν and k_m holds. These measurements will limit the abundance of ultralight fields that begin oscillations in the matter-dominated era.

Another powerful test of the possible abundance of ultralight fields beginning oscillations in the matter era will be an accurate measure of the position of the turn over in the matter power spectrum, since this gives a handle on the species present at equality. Ultralight fields with masses in the regime such that they begin oscillations in the radiation-dominated era may suppress structure at scales where the BAO are relevant, and thus distort them. An accurate measurement of the BAO that fits the profile in $P(k)$ expected from standard ΛCDM would place severe limits on ultralight fields in this mass regime.

Recently, [633] showed that with current and next generation galaxy surveys alone it should be possible to unambiguously detect a fraction of dark matter in axions of the order of 1% of the total. Furthermore, they demonstrated that the tightest constraints on the axion fraction f_{ax} come from weak lensing; when combined with a galaxy redshift survey, constraining f_{ax} to 0.1% should be possible, see Figure 45. The strength of the weak lensing constraint depends on the photometric redshift measurement, i.e., on tomography. Therefore, lensing tomography will allow Euclid – through the measurement of the growth rate – to resolve the redshift evolution of the axion suppression of small scale convergence power. Further details can be found in [633].

Finally, the expected suppression of structure caused by ultralight fields should be properly taken into account in N-body simulations. The nonlinear regime of $P(k)$ needs to be explored further both analytically and numerically for cosmologies containing exotic components such as ultralight fields, especially to constrain those fields which are heavy enough such that k_m occurs around the scale where nonlinearities become significant, i.e., those that begin oscillation deep inside the radiation-dominated regime. For lighter fields the effects in the nonlinear regime should be well-modelled by using the linear $P(k)$ for N-body input, and shifting the other variables such as Ω_c accordingly.

2.13 Dark-matter surrogates in theories of modified gravity

2.13.1 Extra fields in modified gravity

The idea that the dark universe may be a signal of modified gravity has led to the development of a plethora of theories. From polynomials in curvature invariants, preferred reference frames, UV and IR modifications and extra dimensions, all lead to significant modifications to the gravitational sector. A universal feature that seems to emerge in such theories is the existence of fields that may serve as a proxy to dark matter. This should not be unexpected. On a case by case basis, one can see that modifications to gravity generically lead to extra degrees of freedom.

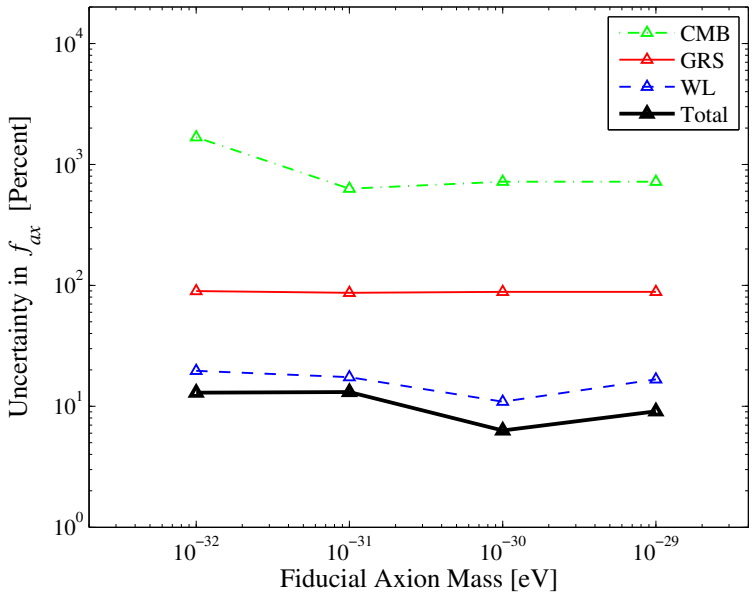

Figure 45: Marginalized uncertainty in f_{ax} for CMB (green), a galaxy redshift survey (red), weak lensing (blue) and the total (black) evaluated for four different fiducial axion masses, for the cosmology ΛCDM+f_{ax}+ν. Image reproduced by permission from [633], copyright by APS.

For example, polynomials in curvature invariants lead to higher-derivative theories which inevitably imply extra (often unstable) solutions that can play the role of dark matter. This can be made patently obvious when mapping such theories onto the Einstein frame with an addition scalar field (Scalar-Tensor theories). Einstein-Aether theories [989] explicitly introduce an extra time-like vector field. The time-like constraint locks the background, leading to modifications to the background expansion; perturbations in the vector field can, under certain conditions, lead to growth of structure, mimicking the effect of pressureless dark matter. The vector field plays the same role in TeVeS [117], where two extra fields are introduced to modify the gravitational dynamics. And the same effects come into play in bigravity models [83] where two metrics are explicitly introduced – the scalar modes of the second metric can play the role of dark matter.

In what follows we briefly focus on three of the above cases where extra gravitational degrees of freedom play the role of dark matter: Einstein-Aether models, TeVeS models and bigravity models. We will look at the Einstein-Aether model more carefully and then briefly discuss the other two cases.

2.13.2 Vector dark matter in Einstein-Aether models

As we have seen in a previous section, Einstein-Aether models introduce a time-like vector field A^a into gravitational dynamics. The four vector A^a can be expanded as $A^\mu = (1+\epsilon X, \epsilon\partial^j Z) = (1+\epsilon X, \frac{\epsilon}{a^2}\partial_j Z)$ [989]. In Fourier space we have $A^\mu = (1-\epsilon\Psi, i\frac{\epsilon}{a}k_j V)$, where, for computational convenience, we have defined $V \equiv Z/a$ and have used the fact that the constraint fixes $X = -\Psi$.

The evolution equation for the perturbation in the vector field becomes (where primes denote

derivatives with respect to conformal time)

$$\begin{aligned} 0 = {} & c_1[V'' + k^2 V + 2\mathcal{H}V' + 2\mathcal{H}^2 V + \Psi' + \Phi' + 2\mathcal{H}\Psi] \\ & + c_2[k^2 V + 6\mathcal{H}^2 V - 3\frac{a''}{a}V + 3\Phi' + 3\mathcal{H}\Psi] \\ & + c_3[k^2 V + 2\mathcal{H}^2 V - \frac{a''}{a}V + \Phi' + \mathcal{H}\Psi] \\ & + \frac{F_{KK}}{F_K}[-K^\epsilon \alpha\mathcal{H} - K^{0'}(-c_1(V' + \Psi) + 3c_2\mathcal{H}V + c_3\mathcal{H}V)]. \end{aligned} \tag{2.13.1}$$

The perturbation in the vector field is sourced by the two gravitational potentials Φ and Ψ and will in turn source them through Einstein's equations. The Poisson equation takes the form

$$\begin{aligned} k^2\Phi = {} & -\frac{1}{2}F_K c_1 k^2[V' + \Psi + (3 + 2\tilde{c}_3)\mathcal{H}V] \\ & - 4\pi G a^2 \sum_a (\bar{\rho}_a\delta_a + 3(\bar{\rho}_a + \bar{P}_a)\mathcal{H}\frac{\theta_a}{k^2}). \end{aligned} \tag{2.13.2}$$

To understand why the vector field can play the role of dark matter it is instructive to study the effect of the vector field during matter domination. It should give us a sense of how in the generalized Einstein-Aether case, the growth of structure is affected. Let us consider the simplest case in which the the dominant remaining contribution to the energy density is baryonic, treated as a pressureless perfect fluid with energy-momentum tensor $\mathbf{T}$ and let us introduce the variable $V' \equiv E$. For ease of illustration we will initially consider only the case where V is described by a growing monomial, i.e. $V = V_0(\eta/\eta_0)^p$. During the matter era we have

$$a^2\delta T^0{}_0 \simeq -l_E\xi(k)k^2\eta^{5+p-6n} \tag{2.13.3}$$

$$k^2(\Psi - \Phi) \simeq -l_S\xi(k)k^2\eta^{5+p-6n} \tag{2.13.4}$$

with $l_E \equiv -(c_1(2+p)n + 2\alpha(1-2n)n)$, $l_S \equiv -(c_1 + c_3)n(6n - p - 10)$, and

$$\xi(k) \sim \gamma V_0(k)\eta_0^{-p}k_{\rm hub}^{6-6n}\left[3\alpha\Omega_m\left(\frac{H_0}{M}\right)^2\right]^{n-1}, \tag{2.13.5}$$

where $k_{\rm hub} \equiv 1/\eta_{\rm today}$. Hence, the vector field affects our evolution equations for the matter and metric perturbations only through its contribution to the energy density and its anisotropic stress. On large scales, $k\eta \ll 1$, and assuming adiabatic initial conditions for the fields δ, Φ and θ, this leads to

$$\delta = C_1(k) + \frac{6l_S\xi(k)}{(10 + p - 6n)}\eta^{5+p-6n}, \tag{2.13.6}$$

where C_1 is a constant of integration and we have omitted the decaying mode. Therefore, even before horizon crossing, the anisotropic stress term due to the vector field can influence the time evolution of the baryon density contrast.

On small scales ($k\eta \gg 1$), we find

$$\delta(k,\eta) = C_2(k)\eta^2 + \frac{(\frac{1}{2}l_E + l_S)}{(5 + p - 6n)(10 + p - 6n)}\xi(k)(k\eta)^2\eta^{5+p-6n}, \tag{2.13.7}$$

where $C_2(k)$ is a constant of integration. Hence, for sub-horizon modes, the influence of the vector field on the evolution of δ is a combination of the effect of the energy density and anisotropic stress contributions though both, in this limit, result in the same contributions to the scale dependence and time evolution of the density contrast. The net effect is that, for particular choices of parameters in the action, the perturbations in the vector field can enhance the growth of the baryon density contrast, very much along the lines of dark matter in the dark matter dominated scenario.

2.13.3 Scalar and tensors in TeVeS

We have already come across the effect of the extra fields of TeVeS. Recall that, in TeVeS, as well as a metric (tensor) field, there is a time-like vector field and a scalar field both of which map the two frames on to each other. While at the background level the extra fields contribute to modifying the overall dynamics, they do not contribute significantly to the overall energy density. This is not so at the perturbative level. The field equations for the scalar modes of all three fields can be found in the conformal Newtonian gauge in [841]. While the perturbations in the scalar field will have a negligible effect, the space-like perturbation in the vector field has an intriguing property: it leads to growth. [318] have shown that the growing vector field feeds into the Einstein equations and gives rise to a growing mode in the gravitational potentials and in the baryon density. Thus, baryons will be aided by the vector field leading to an effect akin to that of pressureless dark matter. The effect is very much akin to that of the vector field in Einstein-Aether models – in fact it is possible to map TeVeS models onto a specific subclass of Einstein-Aether models. Hence the discussion above for Einstein-Aether scenarios can be used in the case of TeVeS.

2.13.4 Tensor dark matter in models of bigravity

In bigravity theories [83], one considers two metrics: a dynamical metric $g_{\mu\nu}$ and a background metric, $\tilde{g}_{\alpha\beta}$. As in TeVeS, the dynamical metric is used to construct the energy-momentum tensor of the non-gravitational fields and is what is used to define the geodesic equations of test particles. The equations that define its evolution are usually not the Einstein field equations but may be defined in terms of the background metric.

Often one has that $\tilde{g}_{\alpha\beta}$ is dynamical, with a corresponding term in the gravitational action. It then becomes necessary to link $\tilde{g}_{\alpha\beta}$ to $g_{\mu\nu}$ with the background metric determining the field equations of the dynamical metric through a set of interlinked field equations. In bigravity models both metrics are used to build the Einstein–Hilbert action even though only one of them couples to the matter content. A complete action is of the form

$$S = \frac{1}{16\pi G}\int \mathrm{d}^4x \left[\sqrt{-g}(R-2\Lambda) + \sqrt{-\tilde{g}}(\tilde{R}-2\tilde{\Lambda}) - \sqrt{-\tilde{g}}\frac{1}{\ell^2}(\tilde{g}^{-1})^{\alpha\beta}g_{\alpha\beta}\right], \tag{2.13.8}$$

where Λ and $\tilde{\Lambda}$ are two cosmological constant terms and ℓ^2 defines the strength of the linking term between the two actions. The cosmological evolution of perturbations in these theories has been worked out in some detail. It turns out that perturbations in the auxiliary field can be rewritten in the form of a generalized dark matter fluid [453] with fluid density, momentum, pressure and shear that obey evolution equations which are tied to the background evolution. As a result, it is possible to work out cosmological observables such as perturbations in the CMB and large scale structure. If we restrict ourselves to a regime in which $\tilde{\rho}$ simply behaves as dark matter, then the best-fit bimetric model will be entirely indistinguishable from the standard CDM scenario.

2.14 Outlook

Dark matter dominates the matter content of the universe, and only through astrophysical and cosmological observations can the nature of dark matter on large scales be determined. In this review, we have discussed a number of observational techniques available to Euclid: dark matter mapping, complementarity with other astronomical observations (e.g., X-ray and CMB experiments); cluster and galaxy scale dark matter halo mapping; and power spectrum analyses. The techniques described will allow Euclid to constrain a variety of dark matter candidates and their microphysical properties. We have discussed Warm Dark Matter scenarios, axion-like dark matter, scalar field

dark matter models (as well as the possible interactions between dark energy and scattering with ordinary matter) and massive neutrinos (the only known component of dark matter).

Here, we briefly list the main dark matter constraints so far forecasted for Euclid:

- The weak lensing power spectrum from Euclid will be able to constrain warm dark matter particle mass to about $m_{\rm WDM} > 2$ keV [630];
- The galaxy power spectrum, with priors from Planck (primary CMB only), will yield an error on the sum of neutrino masses Σ of 0.04 eV (see Table 18; [211]);
- Euclid's weak lensing should also yield an error on Σ of 0.05 eV [507];
- [480] have shown that weak gravitational lensing from Euclid data will be able to determine neutrino hierarchy (if $\Sigma < 0.13$);
- The forecasted errors on the effective number of neutrino species $N_{\nu,\rm eff}$ for Euclid (with a Planck prior) are ± 0.1 [for weak lensing 507] and ± 0.086 [for galaxy clustering 211];
- The sound speed of unified dark energy-dark matter can be constrained with errors $\sim 10^{-5}$ by using 3D weak lensing [202];
- Recently, [633] showed that with current and next generation galaxy surveys alone it should be possible to unambiguously detect a fraction of dark matter in axions of the order of 1% of the total;

We envisage a number of future scenarios, all of which give Euclid an imperative to confirm or identify the nature of dark matter. In the event that a dark matter candidate is discovered in direct detection experiments or an accelerator (e.g. LHC) a primary goal for Euclid will be to confirm, or refute, the existence of this particle on large scales. In the event that no discovery is made directly, then astronomical observations will remain our only way to determine the nature of dark matter.

Part 3: Initial Conditions

3.1 Introduction

The exact origin of the primordial perturbations that seeded the formation of the large-scale structure in the universe is still unknown. Our current understanding of the initial conditions is based on inflation, a phase of accelerated expansion preceding the standard evolution of the universe [416, 861, 863, 791]. In particular, inflation explains why the universe is so precisely flat, homogeneous and isotropic. During this phase, scales much smaller than the Hubble radius are inflated to super-horizon sizes, so that regions appearing today as causally disconnected were in fact very close in the past. This mechanism is also at the origin of the cosmic large-scale structure. Vacuum quantum fluctuations of any light field present during inflation are amplified by the accelerated expansion and *freeze-out* on super-Hubble scales acquiring a quasi-scale invariant spectrum [675, 425, 863, 417, 86].

From the early development of inflation, the simplest proposal based on a weakly-coupled single field rolling along its potential [576, 20] has gained strength and many models have been built based on this picture (see for instance [581] for a review). Although some inflationary potentials are now excluded by current data (see for instance [525]), this scenario has been extremely successful in passing many observational tests: it predicts perfectly adiabatic and almost Gaussian fluctuations with a quasi scale-invariant spectrum and a small amount of gravitational waves.

While current data have ruled out some classes of inflationary models, the next qualitative step forward is investigating the physics responsible for inflation: we still lack a complete understanding of the high energy physics describing it. In fact, most likely the physics of inflation is far out of reach of terrestrial experiments, many orders of magnitude larger than the center-of-mass energy at the Large Hadron Collider (LHC). Thus, cosmological tests of inflation offer a unique opportunity to learn about ultra-high energy physics. We can do this by targeting observations which directly probe the dynamics of inflation. One route is to accurately measure the shape of the primordial power spectrum of scalar perturbations produced during the phase of accelerated expansion, which is directly related to the shape of the inflaton potential, and to constrain the amplitude of the corresponding stochastic gravitational-wave background, which is related instead to the energy-scale of inflation.

A complementary approach is offered by constraining – or exploring – how much the distribution of primordial density perturbations departs from Gaussian statistics and purely adiabatic fluctuations. Indeed, future large-scale structure surveys like Euclid can probe these features with an unprecedented accuracy, thus providing a way to test aspects of inflationary physics that are not easily accessible otherwise. Non-Gaussianity is a very sensitive probe of self-couplings and interactions between the fields generating the primordial perturbations, whereas the presence of isocurvature modes can teach us about the number of fields present during inflation and their role in reheating and generating the matter in the universe.

Furthermore, non-minimal scenarios or proposals even radically different from single-field inflation are still compatible with the data. In order to learn something about the physics of the early universe we need to rule out or confirm the conventional slow-roll scenario and possibly discriminate between non-conventional models. Non-Gaussianities and isocurvature perturbations currently represent the best tools that we have to accomplish this task. Any deviation from the conventional Gaussian and adiabatic initial perturbations would represent important breakthroughs in our understanding of the early universe. In this section we are going to review what we can learn by constraining the initial conditions with a large-scale structure survey like Euclid.

3.2 Constraining inflation

The spectrum of cosmological perturbations represents an important source of information on the early universe. During inflation scalar (compressional) and tensor (purely gravitational) fluctuations are produced. The shape and the amplitude of the power spectrum of scalar fluctuations can be related to the dynamics of the inflationary phase, providing a window on the inflaton potential. Inflation generically predicts a deviation from a purely scale-invariant spectrum. Together with future CMB experiments such as Planck, Euclid will improve our constraints on the scalar spectral index and its running, helping to pin down the model of inflation.

3.2.1 Primordial perturbations from inflation

It is convenient to describe primordial perturbations using the curvature perturbation on uniform density hypersurfaces ζ introduced in [86]. An important property of this quantity is that for adiabatic perturbations – i.e., in absence of isocurvature perturbations, discussed in Section 3.5 – it remains constant on super-Hubble scales, allowing us to connect the early inflationary phase to the late-time universe observations, regardless of the details of reheating. In a gauge where the energy density of the inflaton vanishes, we can define ζ from the spatial part of the metric (assuming a flat FRW universe), as [781, 616]

$$g_{ij} = a^2(t) \exp(2\zeta)\, \delta_{ij} \,. \tag{3.2.1}$$

This definition, where ζ enters the metric in the exponential form, has the advantage that it is valid also beyond linear order and can be consistently used when discussing non-Gaussian fluctuations, such as in Section 3.3.

The power spectrum of primordial perturbations is given by

$$\langle \zeta_{\mathbf{k}} \zeta_{\mathbf{k}'} \rangle = (2\pi)^3 \delta(\mathbf{k} + \mathbf{k}') P_\zeta(k) \,, \tag{3.2.2}$$

where $\langle \ldots \rangle$ denotes the average over an ensemble of realizations. It is useful to define a dimensionless spectrum as $\mathcal{P}_s(k) \equiv \frac{k^3}{2\pi^2} P_\zeta(k)$, where the index s stands for scalar, to distinguish it from the spectrum of tensor perturbations, defined below. The deviation from scale-invariance of the scalar spectrum is characterized by the spectral index n_s, defined by (see, for instance, [570])

$$n_s \equiv 1 + \frac{d \ln \mathcal{P}_s}{d \ln k} \,, \tag{3.2.3}$$

where $n_s = 1$ denotes a purely scale-invariant spectrum. We also define the running of the spectral index α_s as

$$\alpha_s \equiv \frac{dn_s}{d \ln k} \,. \tag{3.2.4}$$

These quantities are taken at a particular pivot scale. For our analysis we chose it to be $k_* \equiv 0.05$ Mpc^{-1}. Thus, with these definitions the power spectrum can be written as

$$P_\zeta(k) = \frac{2\pi^2}{k^3} A_s(k_*) (k/k_*)^{n_s(k_*) - 1 + \frac{1}{2}\alpha_s(k_*) \ln(k/k_*)} \,, \tag{3.2.5}$$

where A_s is the normalization parameterising the amplitude of the fluctuations.

During inflation tensor modes are also generated. They are described by the gauge invariant metric perturbation h_{ij}, defined from the spatial part of the metric as

$$g_{ij} = a^2(t) \left(\delta_{ij} + h_{ij}\right) \,, \quad h^j_{i,j} = 0 = h^i_i \,. \tag{3.2.6}$$

Each mode has 2 polarizations, h_+ and $h_\times$, each with power spectrum given by

$$\langle h_{\mathbf{k}} h_{\mathbf{k}'} \rangle = (2\pi)^3 \delta(\mathbf{k}+\mathbf{k}') P_h(k)\,. \tag{3.2.7}$$

Defining the dimensionless power spectrum of tensor fluctuations as $\mathcal{P}_t(k) \equiv 2\frac{k^3}{2\pi^2}P_h(k)$, where the factor of 2 comes from the two polarizations, it is convenient to define the ratio of tensor to scalar fluctuations as

$$r \equiv \mathcal{P}_t(k_*)/\mathcal{P}_s(k_*)\,. \tag{3.2.8}$$

The form of the power spectrum given in Eq. (3.2.5) approximates very well power spectra of perturbations generated by slow-roll models. In particular, the spectrum of scalar fluctuations is given in terms of the Hubble rate H and the first slow-roll parameter $\epsilon \equiv -\dot{H}/H^2$, both evaluated at the time when the comoving scale k crosses the Hubble radius during inflation,

$$\mathcal{P}_s(k) = \left.\frac{1}{8\pi^2\epsilon}\frac{H^2}{M_{\rm Pl}^2}\right|_{k=aH}\,. \tag{3.2.9}$$

During slow-roll, ϵ is related to the first derivative of the inflaton potential $V(\phi)$, $\epsilon \approx \frac{M_{\rm Pl}^2}{2}\left(\frac{V'}{V}\right)^2$, where the prime denotes differentiation with respect to ϕ. As H and ϵ vary slowly during inflation, this spectrum is almost scale-invariant. Indeed, the scalar spectral index n_s in Eq. (3.2.3) reads

$$n_s = 1 - 6\epsilon + 2\eta_V\,, \tag{3.2.10}$$

where the second slow-roll parameter $\eta_V \equiv M_{\rm Pl}^2\frac{V''}{V}$ must be small for inflation to yield a sufficient number of e-foldings. The running of the spectral index defined in Eq. (3.2.4) is even smaller, being second-order in the slow-roll parameters. It is given by $\alpha_s = 16\epsilon\eta_V - 24\epsilon^2 - 2\xi_V$ where we have introduced the third slow-roll parameter $\xi_V \equiv M_{\rm Pl}^4\frac{V'V'''}{V^2}$.

The spectrum of tensor fluctuations is given by

$$\mathcal{P}_t(k) = \left.\frac{2}{\pi^2}\frac{H^2}{M_{\rm Pl}^2}\right|_{k=aH}\,, \tag{3.2.11}$$

which shows that the ratio of tensor to scalar fluctuations in Eq. (3.2.8) is simply related to the first slow-roll parameter by $r = 16\epsilon$.

As a fiducial model, in the next section we will consider chaotic inflation [577], based on the quadratic inflaton potential $V = \frac{1}{2}m^2\phi^2$. In this case, the first two slow-roll parameters are both given in terms of the value of the inflaton field at Hubble crossing ϕ or, equivalently, in terms of number of e-folds from Hubble crossing to the end of inflation N, as $\epsilon = \eta_V = 2M_{\rm Pl}^2/\phi^2 = 1/2N$, while $\xi_V = 0$. This implies

$$n_s = 1 - 2/N_*\,, \quad r = 8/N_*\,, \quad \alpha_s = -2/N_*^2\,, \tag{3.2.12}$$

where the star denotes Hubble crossing of the pivot scale k_*. Choosing $N_* = 62.5$, this yields $n_s = 0.968$, $r = 0.128$ and $\alpha_s = 0$ as our fiducial model.

3.2.2 Forecast constraints on the power spectrum

We will now study how much Euclid will help in improving the already very tight constraints on the power spectrum given by the Planck satellite. Let us start discussing the forecast for Planck. We assume 2.5 years (5 sky surveys) of multiple CMB channel data, with instrument characteristics for the different channels listed in Table 19. We take the detector sensitivities and the values of the full width half maximum from the Planck "Blue Book" [735]. In this analysis we use three

Table 19: Instrument specifics for the Planck satellite with 30 months of integration.

Channel Frequency (GHz)	70	100	143
Resolution (arcmin)	14	10	7.1
Sensitivity - intensity (μK)	8.8	4.7	4.1
Sensitivity - polarization (μK)	12.5	7.5	7.8

channels for Planck mock data and we assume that the other channels are used for foreground removal and thus do not provide cosmological information.

For a nearly full-sky CMB experiment (we use $f_{\rm sky} = 0.75$), the likelihood $\mathcal{L}$ can be approximated by [923]

$$-2\ln\mathcal{L} = \sum_{\ell=\ell_{\rm min}}^{\ell_{\rm max}} (2\ell+1) f_{\rm sky} \left[-3 + \frac{\hat{C}_\ell^{BB}}{C_\ell^{BB}} + \ln\left(\frac{C_\ell^{BB}}{\hat{C}_\ell^{BB}}\right) + \frac{\hat{C}_\ell^{TT} C_\ell^{EE} + \hat{C}_\ell^{EE} C_\ell^{TT} - 2\hat{C}_\ell^{TE} C_\ell^{TE}}{C_\ell^{TT} C_\ell^{EE} - (C_\ell^{TE})^2} + \ln\left(\frac{C_\ell^{TT} C_\ell^{EE} - (C_\ell^{TE})^2}{\hat{C}_\ell^{TT} \hat{C}_\ell^{EE} - (\hat{C}_\ell^{TE})^2}\right) \right], \tag{3.2.13}$$

where we assume $l_{\rm min} = 3$ and $l_{\rm max} = 2500$. Here, C_ℓ is the sum of the model-dependent theoretical power spectrum $C_\ell^{\rm theory}$ and of the noise spectrum N_ℓ, which we assume perfectly known. The mock data $\hat{C}_\ell$ is C_ℓ for the fiducial model, with $C_\ell^{\rm theory}$ calculated using the publicly available code CAMB [559] and N_ℓ calculated assuming a Gaussian beam. We use the model described in [923, 109] to propagate the effect of polarization foreground residuals into the estimated uncertainties on the cosmological parameters. For simplicity, in our simulation we consider only the dominating components in the frequency bands that we are using, i.e., the synchrotron and dust signals. The fraction of the residual power spectra are all assumed to be 5%.

Let us turn now to the Euclid forecast based on the spectroscopic redshift survey. We will model the galaxy power spectrum in redshift space as ([485, 711, 713]; see also discussion in Section 1.7.3)

$$P_g(k,z,\mu) = \left(b + f_g\mu^2\right)^2 G^2(z) P_{\rm matter}(k; z=0) e^{-k^2\mu^2\sigma_r^2}, \tag{3.2.14}$$

where μ is the cosine of the angle between the wavenumber $\mathbf{k}$ and the line of sight, $G(z)$ is the linear growth factor defined in Eq. (1.3.21), $f_g \equiv d\ln G/d\ln a$ is the linear growth rate (see Eq. (1.3.22)) and $P_{\rm matter}(k; z=0)$ is the matter power spectrum at redshift 0. The term $f_g\mu^2$ comes for the redshift distortions due to the large-scale peculiar velocity field [485], which is correlated with the matter density field. The factor $e^{-k^2\mu^2\sigma_r^2}$ accounts for the radial smearing due to the redshift distortions that are uncorrelated with the large-scale structure. We consider two contributions. The first is due to the redshift uncertainty of the spectroscopic galaxy samples. Assuming a typical redshift uncertainty $\sigma_z = 0.001(1+z)$, this turns into a contribution to σ_r given by $\partial r/\partial z\, \sigma_z = H^{-1}\sigma_z$, where $r(z) = \int_0^z c dz'/H(z')$ is the comoving distance of a flat FRW universe and H is the Hubble parameter as a function of the redshift. The second contribution comes from the Doppler shift due to the virialized motion of galaxies within clusters, which typically have a pairwise velocity dispersion v_p of the order of few hundred kilometers per second. This term can be parameterized as $\frac{v_p}{\sqrt{2}} H^{-1}(1+z)$ [713]. Taking the geometric mean of the two contributions, we obtain

$$\sigma_r^2 = \frac{(1+z)^2}{H^2}\left(10^{-6} + v_p^2/2\right), \tag{3.2.15}$$

where the two velocities in the parenthesis contribute roughly the same. Practically neither the redshift measurement nor the virialized virialized motion of galaxies can be precisely quantified. In

particular, the radial smearing due to peculiar velocity is not necessarily close to Gaussian. Thus, Eq. (3.2.14) should not be used for wavenumbers $k > \frac{H(z)}{v_p(1+z)}$, where the radial smearing effect is important.

On large scales the matter density field has, to a very good approximation, Gaussian statistics and uncorrelated Fourier modes. Under the assumption that the positions of observed galaxies are generated by a random Poissonian point process, the band-power uncertainty is given by ([883]; see also Eq. (1.7.26) in Section 1.7.3)

$$\Delta P_g = \left[\frac{2(2\pi)^3}{(2\pi k^2\, dk\, d\mu)(4\pi r^2 f_{\rm sky}\, dr)}\right]^{1/2} \left(P_g + \frac{1}{\bar{n}}\right). \tag{3.2.16}$$

Here $f_{\rm sky}$ is the observed fraction of sky, r the comoving distance defined above, and $\bar{n}$ is the expected number density of galaxies that can be used.

Finally, we ignore the band-band correlations and write the likelihood as

$$-2\ln\mathcal{L} = \sum_{k,\mu,z\ \text{bins}} \left(\frac{P_g^{\rm model} - P_g^{\rm fiducial}}{\Delta P_g^{\rm fiducial}}\right)^2. \tag{3.2.17}$$

To produce the mock data we use a fiducial ΛCDM model with $\Omega_c h^2 = 0.1128$, $\Omega_b h^2 = 0.022$, $h = 0.72$, $\sigma_8 = 0.8$ and $\tau = 0.09$, where τ is the reionization optical depth. As mentioned above, we take the fiducial value for the spectral index, running and tensor to scalar ratio, defined at the pivot scale $k_* = 0.05\,{\rm Mpc}^{-1}$, as given by chaotic inflation with quadratic potential, i.e., $n_s = 0.968$, $\alpha_s = 0$ and $r = 0.128$. We have checked that for Planck data r is almost orthogonal to n_s and α_s. Therefore our result is not sensitive to the fiducial value of r.

The fiducial Euclid spectroscopically selected galaxies are split into 14 redshift bins. The redshift ranges and expected numbers of observed galaxies per unit volume $\bar{n}_{\rm obs}$ are taken from [551] and shown in the third column of Table 3 in Section 1.8.2 ($n_2(z)$). The number density of galaxies that can be used is $\bar{n} = \varepsilon\bar{n}_{\rm obs}$, where ε is the fraction of galaxies with measured redshift. The boundaries of the wavenumber range used in the analysis, labeled $k_{\rm min}$ and $k_{\rm max}$, vary in the ranges $(0.00435-0.00334)h$ Mpc^{-1} and $(0.16004-0.23644)h$ Mpc^{-1} respectively, for $0.7 \le z \le 2$. The IR cutoff $k_{\rm min}$ is chosen such that $k_{\rm min} r = 2\pi$, where r is the comoving distance of the redshift slice. The UV cutoff is the smallest between $\frac{H}{v_p(1+z)}$ and $\frac{\pi}{2R}$. Here R is chosen such that the r.m.s. linear density fluctuation of the matter field in a sphere with radius R is 0.5. In each redshift bin we use 30 k-bins uniformly in $\ln k$ and 20 uniform μ-bins.

For the fiducial value of the bias, in each of the 14 redshift bins of width $\Delta z = 0.1$ in the range $(0.7-2)$, we use those derived from [698], i.e. (1.083, 1.125, 1.104, 1.126, 1.208, 1.243, 1.282, 1.292, 1.363, 1.497, 1.486, 1.491, 1.573, 1.568), and we assume that v_p is redshift dependent choosing $v_p = 400$ km/s as the fiducial value in each redshift bin. Then we marginalize over b and v_p in the 14 redshift bins, for a total of 28 nuisance parameters.

In these two cases, we consider the forecast constraints on eight cosmological parameters, i.e., $\Omega_b h^2$, $\Omega_c h^2$, θ, τ, $\ln A_s$, n_s, α_s, and r. Here θ is the angle subtended by the sound horizon on the last scattering surface, rescaled by a factor 100. We use the publicly available code CosmoMC [558] to perform Markov Chain Monte Carlo calculation. The nuisance parameters are marginalized over in the final result. The marginalized 68.3% confidence level (CL) constraints on cosmological parameters for Planck forecast only, and Planck and Euclid forecast are listed in the second and third columns of Table 20, respectively.

Euclid can improve the 'figure of merit' on the n_s-α_s plane by a factor of 2.2, as shown in the left panel of Figure 46. Because the bias is unknown, the LSS data do not directly measure A_s or σ_8. However, Euclid can measure Ω_m to a much better accuracy, which can break the degeneracy

Table 20: Cosmological parameters

parameter	Planck constraint	Planck + Euclid constraint
$\Omega_b h^2$	$0.02227^{+0.00011}_{-0.00011}$	$0.02227^{+0.00008}_{-0.00008}$
$\Omega_c h^2$	$0.1116^{+0.0008}_{-0.0008}$	$0.1116^{+0.0002}_{-0.0002}$
θ	$1.0392^{+0.0002}_{-0.0002}$	$1.0392^{+0.0002}_{-0.0002}$
$\tau_{\rm re}$	$0.085^{+0.004}_{-0.004}$	$0.085^{+0.003}_{-0.003}$
n_s	$0.966^{+0.003}_{-0.003}$	$0.966^{+0.002}_{-0.002}$
α_s	$-0.000^{+0.005}_{-0.005}$	$-0.000^{+0.003}_{-0.003}$
$\ln(10^{10} A_s)$	$3.078^{+0.009}_{-0.009}$	$3.077^{+0.006}_{-0.006}$
r	$0.128^{+0.018}_{-0.018}$	$0.127^{+0.019}_{-0.018}$
Ω_m	$0.271^{+0.005}_{-0.004}$	$0.271^{+0.001}_{-0.001}$
σ_8	$0.808^{+0.005}_{-0.005}$	$0.808^{+0.003}_{-0.003}$
h	$0.703^{+0.004}_{-0.004}$	$0.703^{+0.001}_{-0.001}$

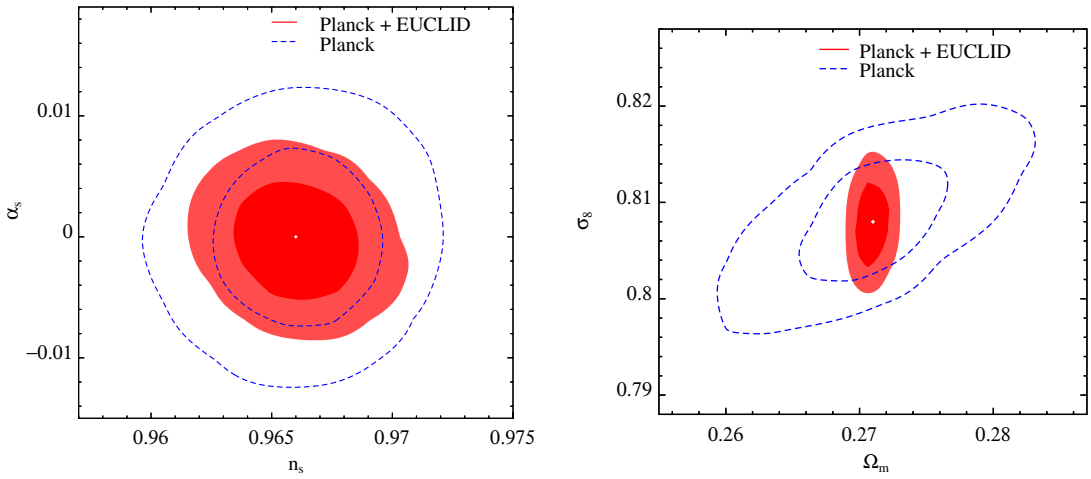

Figure 46: The marginalized likelihood contours (68.3% and 95.4% CL) for Planck forecast only (blue dashed lines) and Planck plus Euclid pessimistic (red filled contours). The white points correspond to the fiducial model.

between Ω_m and σ_8 that one typically finds using CMB data alone. This is shown in the right panel of Figure 46.

A more extensive and in depth analysis of what constraints on inflationary models a survey like Euclid can provide is presented in [460]. In particular they find that for models where the primordial power spectrum is not featureless (i.e., close to a power law with small running) a survey like Euclid will be crucial to detect and measure features. Indeed, what we measure with the CMB is the angular power spectrum of the anisotropies in the 2-D multipole space, which is a projection of the power spectrum in the 3-D momentum space. Features at large ℓ's and for small width in momentum space get smoothed during this projection but this does not happen for large-scale structure surveys. The main limitation on the width of features measured using large-scale structure comes from the size of the volume of the survey: the smallest detectable feature being of the order of the inverse cubic root of this volume and the error being determined by number of modes contained in this volume. Euclid, with the large volume surveyed and the sheer number of modes that are sampled and cosmic variance dominated offers a unique opportunity to probe inflationary models where the potential is not featureless. In addition the increased statistical power would enable us to perform a Bayesian model selection on the space of inflationary models (e.g., [334, 691] and references therein).

3.3 Probing the early universe with non-Gaussianities

The workhorse for primordial non-Gaussianity has been so far the "local model" [781, 376, 924, 524, 93]:

$$\Phi = \phi + f_{\rm NL}\left(\phi^2 - \langle\phi^2\rangle\right). \tag{3.3.1}$$

Here ϕ is a Gaussian random field while Φ denotes Bardeen's gauge-invariant potential, which, on sub-Hubble scales reduces to the usual Newtonian peculiar gravitational potential, up to a minus sign. On large scales it is related to the conserved variable ζ by

$$\zeta = \frac{5+3w}{3+3w}\Phi\,, \tag{3.3.2}$$

where w is the equation of state of the dominant component in the universe. The amount of primordial non-Gaussianity is quantified by the nonlinearity parameter $f_{\rm NL}$. Note that, since $\Phi \simeq \phi \simeq 10^{-5}$, $f_{\rm NL} \sim 100$ corresponds to relative non-Gaussian corrections of order 10^{-3}. While ζ is constant on large scales, Φ is not. For this reason, in the literature there are two conventions for Eq. (3.3.1): the large-scale structure (LSS) and the cosmic microwave background (CMB) one. In the LSS convention, Φ is linearly extrapolated at $z = 0$; in the CMB convention Φ is instead primordial: thus $f_{\rm NL}^{\rm LSS} = g(z=\infty)/g(0) f_{\rm NL}^{\rm CMB} \sim 1.3\, f_{\rm NL}^{\rm CMB}$, where $g(z)$ denotes the linear growth suppression factor relative to an Einstein–de Sitter universe. In the past few years it has become customary to always report $f_{\rm NL}^{\rm CMB}$ values even though, for simplicity as it will be clear below, one carries out the calculations with $f_{\rm NL}^{\rm LSS}$.

In this section we review the theoretical motivations and implications for looking into primordial non-Gaussianity; the readers less theoretically oriented can go directly to Section 3.4.

3.3.1 Local non-Gaussianity

The non-Gaussianities generated in the conventional scenario of inflation (single-field with standard kinetic term, in slow-roll, initially in the Bunch–Davies vacuum) are predicted to be extremely small. Earlier calculations showed that $f_{\rm NL}$ would be of the order of the slow-roll parameters [781, 353, 376]. More recently, with an exact calculation [616] confirmed this result and showed that the dominant contribution to non-Gaussianity comes from gravitational interaction and it is

thus independent of the inflaton potential. More precisely, in the squeezed limit, i.e. when one of the modes is much smaller than the other two, the bispectrum of the primordial perturbation ζ is given by

$$B_\zeta(k_1 \ll k_2, k_3) = 4 f_{\rm NL}^{\rm local} P_\zeta(k_2) P_\zeta(k_3)\,, \tag{3.3.3}$$

where $f_{\rm NL}^{\rm local}$ is proportional to the tilt of scalar fluctuations, $f_{\rm NL}^{\rm local} = -(5/12)(n_s - 1)$, a value much too small to be observable. Thus, any deviation from this prediction would rule out a large class of models based on the simplest scenario.

Furthermore, [264] showed that irrespective of slow-roll and of the particular inflaton Lagrangian or dynamics, in single-field inflation, or more generally when only adiabatic fluctuations are present, there exists a consistency relation involving the 3-point function of scalar perturbations in the squeezed limit (see also [806, 226, 227]). In this limit, when the short wavelength modes are inside the Hubble radius during inflation, the long mode is far out of the horizon and its only effect on the short modes is to rescale the unperturbed history of the universe. This implies that the 3-point function is simply proportional to the 2-point function of the long wavelength modes times the 2-point function of the short wavelength mode times its deviation from scale invariance. In terms of local non-Gaussianity this translates into the same $f_{\rm NL}^{\rm local}$ found in [616]. Thus, a convincing detection of local non-Gaussianity would rule out all classes of inflationary single-field models.

To overcome the consistency relation and produce large local non-Gaussianity one can go beyond the single-field case and consider scenarios where a second field plays a role in generating perturbations. In this case, because of non-adiabatic fluctuations, scalar perturbations can evolve outside the horizon invalidating the argument of the consistency relation and possibly generating a large $f_{\rm NL}^{\rm local}$ as in [582]. The curvaton scenario is one of such mechanisms. The curvaton is a light scalar field that acquires scale-invariant fluctuations during inflation and decays after inflation but well before nucleosynthesis [661, 664, 598, 342]. During the decay it dominates the universe affecting its expansion history thus imprints its perturbations on super-horizon scales. The way the expansion history depends on the value of the curvaton field at the end of the decay can be highly nonlinear, leading to large non-Gaussianity. Indeed, the nonlinear parameter $f_{\rm NL}^{\rm local}$ is inversely proportional to the curvaton abundance before the decay [597].

Models exists where both curvaton and inflaton fluctuations contribute to cosmological perturbations [545]. Interestingly, curvaton fluctuations could be negligible in the 2-point function but detectable through their non-Gaussian signature in the 3-point function, as studied in [155]. We shall come back on this point when discussing isocurvature perturbations. Other models generating local non-Gaussianities are the so called modulated reheating models, in which one light field modulates the decay of the inflaton field [329, 515]. Indeed, non-Gaussianity could be a powerful window into the physics of reheating and preheating, the phase of transition from inflation to the standard radiation dominated era (see e.g., [148, 222]).

In the examples above only one field is responsible for the dynamics of inflation, while the others are spectators. When the inflationary dynamics is dominated by several fields along the ~ 60 e-foldings of expansion from Hubble crossing to the end of inflation we are truly in the multi-field case. For instance, a well-studied model is double inflation with two massive non-interacting scalar fields [739]. In this case, the overall expansion of the universe is affected by each of the field while it is in slow-roll; thus, the final non-Gaussianity is slow-roll suppressed, as in single field inflation [768, 19, 926].

Because the slow-roll conditions are enforced on the fields while they dominate the inflationary dynamics, it seems difficult to produce large non-Gaussianity in multi-field inflation; however, by tuning the initial conditions it is possible to construct models leading to an observable signal (see [191, 876]). Non-Gaussianity can be also generated at the end of inflation, where large-scale perturbations may have a nonlinear dependence on the non-adiabatic modes, especially if there is an abrupt change in the equation of state (see e.g., [126, 596]). Hybrid models [580], where inflation

is ended by a tachyonic instability triggered by a waterfall field decaying in the true vacuum, are natural realizations of this mechanism [343, 88].

3.3.2 Shapes: what do they tell us?

As explained above, local non-Gaussianity is expected for models where nonlinearities develop outside the Hubble radius. However, this is not the only type of non-Gaussianity. Single-field models with derivative interactions yield a negligible 3-point function in the squeezed limit, yet leading to possibly observable non-Gaussianities. Indeed, as the interactions contain time derivatives and gradients, they vanish outside the horizon and are unable to produce a signal in the squeezed limit. Correlations will be larger for other configurations, for instance between modes of comparable wavelength. In order to study the observational signatures of these models we need to go beyond the local case and study the *shape* of non-Gaussianity [70].

Because of translational and rotational invariance, the 3-point function is characterized by a function of the modulus of the three wave-vectors, also called the bispectrum $B_\zeta(k_1, k_2, k_3)$, defined as

$$\langle \zeta_{\mathbf{k_1}} \zeta_{\mathbf{k_2}} \zeta_{\mathbf{k_3}} \rangle = (2\pi)^3 \delta(\mathbf{k_1} + \mathbf{k_2} + \mathbf{k_3}) B_\zeta(k_1, k_2, k_3)\,. \tag{3.3.4}$$

Relaxing the assumption of a local $f_{\rm NL}$, this function is a rich object which can contain a wealth of information, depending on the size and shape of the triangle formed by k_1, k_2 and k_3. Indeed, the dependence of the bispectrum on configuration in momentum space is related to the particular inflationary model generating it. Namely, each third-order operator present in the field action gives rise to a particular shape of the bispectrum.

An example of models containing large derivative interactions has been proposed by [830, 25]. Based on the Dirac–Born–Infeld Lagrangian, $\mathcal{L} = f(\phi)^{-1}\sqrt{1 - f(\phi)X} + V(\phi)$, with $X = -g^{\mu\nu}\partial_\mu\phi\partial_\nu\phi$, it is called DBI inflation. This Lagrangian is string theory-motivated and ϕ describes the low-energy radial dynamics of a D3-brane in a warped throat: $f(\phi)^{-1}$ is the warped brane tension and $V(\phi)$ the interaction field potential. In this model the non-Gaussianity is dominated by derivative interactions of the field perturbations so that we do not need to take into account mixing with gravity. An estimate of the non-Gaussianity is given by the ratio between the third-order and the second order Lagrangians, respectively $\mathcal{L}_3$ and $\mathcal{L}_2$, divided by the amplitude of scalar fluctuations. This gives $f_{\rm NL} \sim (\mathcal{L}_3/\mathcal{L}_2)\Phi^{-1} \sim -1/c_s^2$, where $c_s^2 = [1 + 2X(\partial^2\mathcal{L}/\partial X^2)/(\partial\mathcal{L}/\partial X)]^{-1} < 1$ is the speed of sound of linear fluctuations and we have assumed that this is small, as it is the case for DBI inflation. Thus, the non-Gaussianity can be quite large if $c_s \ll 1$.

However, this signal vanishes in the squeezed limit due to the derivative interactions. More precisely, the particular momentum configuration of the bispectrum is very well described by

$$B_\zeta(k_1, k_2, k_3) = 6 f_{\rm NL}^{\rm equil} \left(\frac{P_\zeta(k_1)P_\zeta(k_2)}{2} + \frac{[P_\zeta(k_1)P_\zeta(k_2)P_\zeta(k_3)]^{\frac{2}{3}}}{3} - P_\zeta(k_1)^{\frac{1}{3}} P_\zeta(k_2)^{\frac{2}{3}} P_\zeta(k_3) + 5 \text{ perms.} \right), \tag{3.3.5}$$

where, up to numerical factors of order unity, $f_{\rm NL}^{\rm equil} \simeq -1/c_s^2$. The function of momenta inside the parenthesis is the *equilateral* shape [260], a *template* used to approximate a large class of inflationary models. It is defined in such a way as to be factorisable, maximized for equilateral configurations and vanishing in the squeezed limit faster than the local shape, see Eq. (3.3.3).

To compare two shapes F_1 and F_2, it is useful to define a 3-dimensional scalar product between them as [70]

$$F_1 \cdot F_2 = \sum F_1(k_1, k_2, k_3) F_2(k_1, k_2, k_3) / (P_\zeta(k_1)P_\zeta(k_2)P_\zeta(k_3))\,, \tag{3.3.6}$$

where the sum is over all configurations forming a triangle. Then, $\cos\theta = F_1 \cdot F_2 / \sqrt{(F_1 \cdot F_1)(F_2 \cdot F_2)}$ defines a quantitative measure of how much two shapes "overlap" and their signal is correlated. The cosine is small between the local and equilateral shapes. Two shapes with almost vanishing cosine are said to be orthogonal and any estimator developed to be sensitive to a particular shape will be completely blind to its orthogonal one. Note that the observable signal could actually be a combination of different shapes. For instance, multi-field models base on the DBI action [543] can generate a linear combination of local and equilateral non-Gaussianities [763].

The interplay between theory and observations, reflected in the relation between derivative interactions and the shape of non-Gaussianity, has motivated the study of inflation according to a new approach, the *effective field theory of inflation* ([228]; see also [951]). Inflationary models can be viewed as effective field theories in presence of symmetries. Once symmetries are defined, the Lagrangian will contain each possible operator respecting such symmetries. As each operator leads to a particular non-Gaussian signal, constraining non-Gaussianity directly constrains the coefficients in front of these operators, similarly to what is done in high-energy physics with particle accelerators. For instance, the operator $\mathcal{L}_3$ discussed in the context of DBI inflation leads to non-Gaussianity controlled by the speed of sound of linear perturbations. This operator can be quite generic in single field models. Current constraints on non-Gaussianity allow to constrain the speed of sound of the inflaton field during inflation to be $c_s \geq 0.01$ [228, 814]. Another well-studied example is ghost inflation [57], based on the ghost condensation, a model proposed by [56] to modify gravity in the infrared. This model is motivated by shift symmetry and exploits the fact that in the limit where this symmetry is exact, higher-derivative operators play an important role in the dynamics, generating large non-Gaussianity with approximately equilateral shape.

Following this approach has allowed to construct operators or combination of operators leading to new shapes, orthogonal to the equilateral one. An example of such a shape is the *orthogonal* shape proposed in [814]. This shape is generated by a particular combination of two operators already present in DBI inflation. It is peaked both on equilateral-triangle configurations and on flattened-triangle configurations (where the two lowest-k sides are equal exactly to half of the highest-k side) – the sign in this two limits being opposite. The orthogonal and equilateral are not an exhaustive list. For instance, [258] have shown that the presence in the inflationary theory of an approximate Galilean symmetry (proposed by [686] in the context of modified gravity) generates third-order operators with two derivatives on each field. A particular combination of these operators produces a shape that is approximately orthogonal to the three shapes discussed above.

Non-Gaussianity is also sensitive to deviations from the initial adiabatic Bunch–Davies vacuum of inflaton fluctuations. Indeed, considering excited states over it, as done in [226, 444, 653], leads to a shape which is maximized in the collinear limit, corresponding to enfolded or squashed triangles in momentum space, although one can show that this shape can be written as a combination of the equilateral and orthogonal ones [814].

3.3.3 Beyond shapes: scale dependence and the squeezed limit

There is a way out to generate large non-Gaussianity in single-field inflation. Indeed, one can temporarily break scale-invariance, for instance by introducing features in the potential as in [225]. This can lead to large non-Gaussianity typically associated with scale-dependence. These signatures could even teach us something about string theory. Indeed, in axion monodromy, a model recently proposed by [831] based on a particular string compactification mechanism, the inflaton potential is approximately linear, but periodically modulated. These modulations lead to tiny oscillations in the power spectrum of cosmological fluctuations and to large non-Gaussianity (see for instance [366]).

This is not the only example of scale dependence. While in general the amplitude of the non-

Gaussianity signal is considered constant, there are several models, beside the above example, which predict a scale-dependence. For example models like the Dirac–Born–Infeld (DBI) inflation, e.g., [25, 223, 224, 111] can be characterized by a primordial bispectrum whose amplitude varies significantly over the range of scales accessible by cosmological probes.

In view of measurements from observations it is also worth considering the so-called squeezed limit of non-Gaussianity that is the limit in which one of the momenta is much smaller than the other two. Observationally this is because some probes (like, for example, the halo bias Section 3.4.2, accessible by large-scale structure surveys like Euclid) are sensitive to this limit. Most importantly, from the theoretical point of view, there are consistency relations valid in this limit that identify different classes of inflation, e.g., [262, 257] and references therein.

The scale dependence of non-gaussianity, the shapes of non-gaussianity and the behavior of the squeezed limit are all promising avenues, where the combination of CMB data and large-scale structure surveys such as Euclid can provide powerful constraints as illustrated, e.g., in [809, 690, 807].

3.3.4 Beyond inflation

As explained above, the search of non-Gaussianity could represent a unique way to rule out the simplest of the inflationary models and distinguish between different scenarios of inflation. Interestingly, it could also open up a window on new scenarios, alternative to inflation. There have been numerous attempts to construct models alternative to inflation able to explain the initial conditions of our universe. In order to solve the cosmological problems and generate large-scale primordial fluctuations, most of them require a phase during which observable scales today have exited the Hubble size. This can happen in bouncing cosmologies, in which the present era of expansion is preceded by a contracting phase. Examples are the pre-big bang [385] and the ekpyrotic scenario [498].

In the latter, the 4-d effective dynamics corresponds to a cosmology driven by a scalar field with a steep exponential potential $V(\phi) = \exp(-c\phi)$, with $c \gg 1$. Leaving aside the problem of the realization of the bounce, it has been shown that the adiabatic mode in this model generically leads to a steep blue spectrum for the curvature perturbations [595, 261]. Thus, at least a second field is required to generate an almost scale-invariant spectrum of perturbations [365, 263, 182, 528]. If two fields are present, both with exponential potentials and steepness coefficients c_1 and c_2, the non-adiabatic component has negative mass and acquires a quasi invariant spectrum of fluctuations with tilt $n_s - 1 = 4(c_1^{-2} + c_2^{-2})$, with $c_1, c_2 \gg 1$. Then one needs to convert the non-adiabatic fluctuation into curvature perturbation, similarly to what the curvaton mechanism does.

As the Hubble rate increases during the collapse, one expects nonlinearities in the fields to become more and more important, leading to non-Gaussianity in the produced perturbations. As nonlinearities grow larger on super-Hubble scales, one expects the signal to be of local type. The particular amplitude of the non-Gaussianity in the observable curvature perturbations depends on the conversion mechanism from the non-adiabatic mode to the observable perturbations. The tachyonic instability itself can lead to a phase transition to an ekpyrotic phase dominated by just one field ϕ_1. In this case [527] have found that $f_{\rm NL}^{\rm local} = -(5/12)c_1^2$. Current constraints on $f_{\rm NL}^{\rm local}$ (WMAP7 year data imposes $-10 < f_{\rm NL}^{\rm local} < 74$ at 95% confidence) gives an unacceptably large value for the scalar spectral index. In fact in this model, even for $f_{\rm NL} = -10$, $c_2 \simeq 5$ which implies a too large value of the scalar spectral index ($n_s - 1 > 0.17$) which is excluded by observations (recall that WMAP7 year data implies $n_s = 0.963 \pm 0.014$ at 68% confidence). Thus, one needs to modify the potential to accommodate a red spectrum or consider alternative conversion mechanisms to change the value of the generated non-Gaussianity [183, 554].

3.4 Primordial Non-Gaussianity and Large-Scale Structure

As we have seen, even the simplest inflationary models predict deviations from Gaussian initial conditions. Confirming or ruling out the simplest inflationary model is an important goal and in this section we will show how Euclid can help achieving this. Moreover, Euclid data (alone or in combination with CMB experiments like Planck) can be used to explore the primordial bispectrum and thus explore the interaction of the fields during inflation.

3.4.1 Constraining primordial non-Gaussianity and gravity from 3-point statistics

Contrary to CMB research which mainly probes the high-redshift universe, current studies of the LSS focus on data at much lower redshifts and are more heavily influenced by cosmic evolution. Even if the initial conditions were Gaussian, nonlinear evolution due to gravitational instability generates a non-zero bispectrum for the matter distribution. The first non-vanishing term in perturbation theory (e.g., [218]) gives

$$B(\vec{k}_1,\vec{k}_2,\vec{k}_3) = 2(P(k_1)P(k_2)J(\vec{k}_1,\vec{k}_2) + \text{cyclic permutations}) \tag{3.4.1}$$

where $J(\vec{k}_1,\vec{k}_2)$ is the gravitational instability "kernel" which depends very weakly on cosmology and for an Einstein-de-Sitter universe assumes the form:

$$J(\vec{k}_1,\vec{k}_2) = \frac{5}{7} + \frac{\vec{k}_1\cdot\vec{k}_2}{2k_1k_2}\left(\frac{k_1}{k_2}+\frac{k_2}{k_1}\right) + \frac{2}{7}\left(\frac{\vec{k}_1\cdot\vec{k}_2}{k_1k_2}\right)^2 . \tag{3.4.2}$$

This kernel represents the "signature" of gravity as we know it on the large-scale structure of the universe. Either a modification of the gravitational law or the introduction of a coupling between dark matter and another component (say dark energy) would alter the bispectrum shape from the standard form. The volume covered by Euclid will enable us to exploit this.

It was recognized a decade ago [924] that the contribution to the matter bispectrum generated by gravitational instability is large compared to the fossil signal due to primordial non-Gaussianity and that the primordial signal "redshifts away" compared to the gravitational signal. In fact, primordial non-Gaussianity of the local type would affect the late-time dark matter density bispectrum with a contribution of the form

$$B^{f_{\rm NL}\,\rm local}(\vec{k}_1,\vec{k}_2,\vec{k}_3,z) = 2(f_{\rm NL}P(k_1)P(k_2)\frac{\mathcal{F}(\vec{k}_1,\vec{k}_2)}{D(z)/D(z=0)} + \text{cyclic permutations}). \tag{3.4.3}$$

where $D(z)$ is the linear growth function which in an Einstein–de Sitter universe goes like $(1+z)^{-1}$ and

$$\mathcal{F} = \frac{\mathcal{M}(k_3)}{\mathcal{M}(k_1)\mathcal{M}(k_2)}\,;\;\; \mathcal{M}(k) = \frac{2}{3}\frac{k^2T(k)}{H_0^2\Omega_{m,0}}\,, \tag{3.4.4}$$

$T(k)$ denoting the matter transfer function, H_0 the Hubble constant and $\Omega_{m,0}$ the matter density parameter. Clearly the contributions due to primordial non-Gaussianity and gravitational instability have different scale and redshift dependence and the two kernel shapes in configuration space are different, thus, making the two components, at least in principle and for high signal-to-noise, separable. This is particularly promising for high-redshift probes of the matter distribution like the 21-cm background which should simultaneously provide competing measures of $f_{\rm NL}$ and a test of the gravitational law [731]. Regrettably, these studies require using a long-wavelength radio telescope above the atmosphere (e.g., on the Moon) and will certainly come well after Euclid.

Galaxy surveys do not observe the dark matter distribution directly. However, dark matter halos are believed to host galaxy formation, and different galaxy types at different redshifts are expected to populate halos in disparate ways [610, 975]. A simple (and approximate) way to account for galaxy biasing is to assume that the overdensity in galaxy counts can be written as a truncated power expansion in terms of the mass overdensity (smoothed on some scale): $\delta_g(x) = b_1\delta_{\rm DM}(x) + b_2(\delta^2_{\rm DM} - \langle\delta^2_{\rm DM}\rangle)$. The linear and quadratic bias coefficient b_1 and b_2 are assumed to be scale-independent (although this assumption must break down at some point) but they can vary with redshift and galaxy type. Obviously, a quadratic bias will introduce non-Gaussianity even on an initially Gaussian field. In summary, for local non-Gaussianity and scale-independent quadratic bias we have [924]:

$$B(\vec{k}_1,\vec{k}_2,\vec{k}_3,z) = 2P(k_1)P(k_2)b_1(z)^3 \times \left[f_{\rm NL}\frac{\mathcal{F}(\vec{k}_1,\vec{k}_2)}{D(z)} + J(\vec{k}_1,\vec{k}_2) + \frac{b_2(z)}{2b_1(z)}\right] + \text{cyc.} \qquad (3.4.5)$$

Before the above expression can be compared against observations, it needs to be further complicated to account for redshift-space distortions and shot noise. Realistic surveys use galaxy redshifts as a proxy for distance, but gravitationally-induced peculiar velocities distort the redshift-space galaxy distribution. At the same time, the discrete nature of galaxies gives rise to corrections that should be added to the bispectrum computed in the continuous limit. We will not discuss these details here as including redshift space distortions and shot noise will not change the gist of the message.

From the observational point of view, it is important to note that photometric surveys are not well suited for extracting a primordial signal out of the galaxy bispectrum. Although in general they can cover larger volumes than spectroscopic surveys, the projection effects due to the photo-z smearing along the line-of-sight is expected to suppress significantly the sensitivity of the measured bispectrum to the shape of the primordial one (see e.g., [921]). [808] have shown that, if the evolution of the bias parameters is known a priori, spectroscopic surveys like Euclid would be able to give constraints on the $f_{\rm NL}$ parameter that are competitive with CMB studies. While the gravitationally-induced non-Gaussian signal in the bispectrum has been detected to high statistical significance (see, e.g., [925, 533] and references therein), the identification of nonlinear biasing (i.e., $b_2 \neq 0$) is still controversial, and there has been so far no detection of any extra (primordial) bispectrum contributions.

Of course, one could also consider higher-order correlations. One of the advantages of considering, e.g., the trispectrum is that, contrary to the bispectrum, it has very weak nonlinear growth [920], but it has the disadvantage that the signal is de-localized: the number of possible configurations grows fast with the dimensionality n of the n-point function!

Finally, it has been proposed to measure the level of primordial non-Gaussianity using Minkowski functionals applied either to the galaxy distribution or the weak lensing maps (see, e.g., [433, 679] and references therein). The potentiality of this approach compared to more traditional methods needs to be further explored in the near future.

3.4.2 Non-Gaussian halo bias

The discussion above neglects an important fact which went unnoticed until year 2008: the presence of small non-Gaussianity can have a large effect on the clustering of dark matter halos [272, 647]. The argument goes as follows. The clustering of the peaks in a Gaussian random field is completely specified by the field power spectrum. Thus, assuming that halos form out of linear density peaks, for Gaussian initial conditions the clustering of the dark matter halos is completely specified by the linear matter power spectrum. On the other hand, for a non-Gaussian field, the clustering of the peaks depends on all higher-order correlations, not just on the power spectrum. Therefore, for non-

Gaussian initial conditions, the clustering of dark matter halos depends on the linear bispectrum (and higher-order moments).

One can also understand the effect in the peak-background-split framework: overdense patches of the (linear) universe collapse to form dark matter halos if their overdensity lies above a critical collapse threshold. Short-wavelength modes define the overdense patches while the long-wavelength modes determine the spatial distribution of the collapsing ones by modulating their height above and below the critical threshold. In the Gaussian case, long- and short-wavelength modes are uncorrelated, yielding the well known linear, scale-independent peak bias. In the non-Gaussian case, however, long and short wavelength modes are coupled, yielding a different spatial pattern of regions that cross the collapse threshold.

In particular, for primordial non-Gaussianity of the local type, the net effect is that the halo distribution on very large scales relates to the underlying dark matter in a strongly scale-dependent fashion. For $k \lesssim 0.02\,h$ Mpc^{-1}, the effective linear bias parameter scales as k^{-2}. [272, 647, 392]. This is because the halo overdensity depends not only on the underlying matter density but also on the value of the auxiliary Gaussian potential ϕ [392].

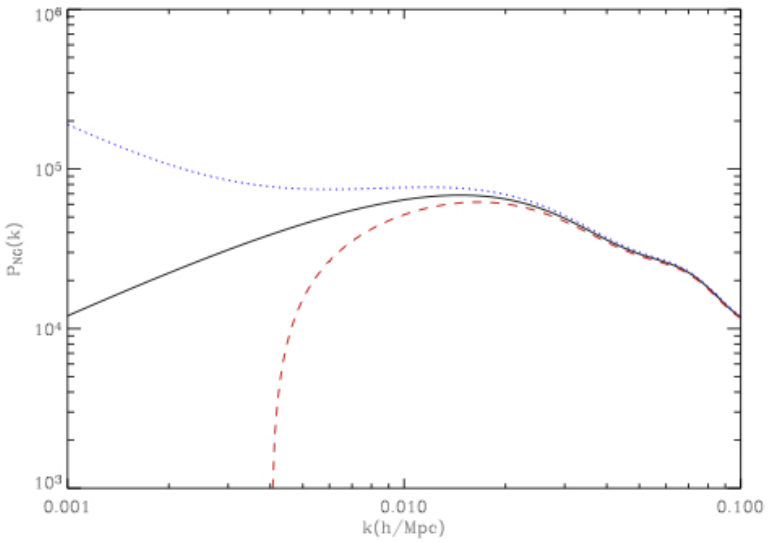

Figure 47: For illustration purposes this is the effect of a local $f_{\rm NL}$ of ± 50 on the $z = 0$ power spectrum of halos with mass above $10^{13}\,M_\odot$.

The presence of this effect is extremely important for observational studies as it allows to detect primordial non-Gaussianity from 2-point statistics of the galaxy distribution like the power spectrum. Combining current LSS data gives constraints on $f_{\rm NL}$ which are comparable to the CMB ones [842, 971]. Similarly, planned galaxy surveys are expected to progressively improve upon existing limits [210, 209, 393]. For example, Euclid could reach an error on $f_{\rm NL}$ of ~ 5 (see below for further details) which is comparable with the BPol forecast errors.

The scale dependence of the halo bias changes considering different shapes of primordial non-Gaussianity [799, 933]. For instance, orthogonal and folded models produce an effective bias that scales as k^{-1} while the scale dependence becomes extremely weak for equilateral models. Therefore, measurements of the galaxy power spectrum on the largest possible scales have the possibility to constrain the shape and the amplitude of primordial non-Gaussianity and thus shed new light on the dynamics of inflation.

On scales comparable with the Hubble radius, matter and halo clustering are affected by general-relativity effects: the Poisson equation gets a quadratic correction that acts effectively as a non-zero local $f_{\rm NL}$ [94, 731]. This contribution is peculiar to the inflationary initial conditions because it requires perturbations on super-horizon scales and it is mimicked in the halo bias by a local $f_{\rm NL} = -1.6$ [922]. This is at the level of detectability by a survey like Euclid.

3.4.3 Number counts of nonlinear structures

Even a small deviation from Gaussianity in the initial conditions can have a strong impact on those statistics which probe the tails of the linear density distribution. This is the case for the abundance of the most extreme nonlinear objects existing at a given cosmic epoch, massive dark matter halos and voids, as they correspond to the highest and lowest density peaks (the rarest events) in the underlying linear density field.

Thus small values of $f_{\rm NL}$ are potentially detectable by measuring the abundance of massive dark matter halos as traced by galaxies and galaxy clusters at $z \gtrsim 1$ [649]. This approach has recently received renewed attention (e.g., [591, 407, 730, 609, 275, 918, 732] and references therein) and might represent a promising tool for Euclid science. In Euclid, galaxy clusters at high redshift can be identified either by lensing studies or by building group catalogs based on the spectroscopic and photometric galaxy data. The main challenge here is to determine the corresponding halo mass with sufficient accuracy to allow comparison with the theoretical models.

While galaxy clusters form at the highest overdensities of the primordial density field and probe the high-density tail of the PDF, voids form in the low-density regions and thus probe the low-density tail of the PDF. Most of the volume of the evolved universe is underdense, so it seems interesting to pay attention to the distribution of underdense regions. For the derivation of the non-Gaussian void probability function one proceeds in parallel to the treatment for halos with the only subtlety that the critical threshold is not negative and that its numerical value depends on the precise definition of a void (and may depend on the observables used to find voids), e.g., [490]. Note that while a positive skewness ($f_{\rm NL} > 0$) boosts the number of halos at the high mass end (and slightly suppress the number of low-mass halos), it is a negative skewness that will increase the voids size distribution at the largest voids end (and slightly decrease it for small void sizes). In addition voids may probe slightly larger scales than halos, making the two approaches highly complementary.

Even though a number of observational techniques to detect voids in galaxy surveys have been proposed (see, e.g., [247] and references therein), the challenge here is to match the theoretical predictions to a particular void-identification criterion based on a specific galaxy sample. We envision that mock galaxy catalogs based on numerical simulations will be employed to calibrate these studies for Euclid.

3.4.4 Forecasts for Euclid

A number of authors have used the Fisher-matrix formalism to explore the potentiality of Euclid in determining the level and the shape of primordial non-Gaussianity [210, 209, 393]. In what follows, unless specifically mentioned, we will focus on the local type of non-Gaussianity which has been more widely studied so far.

The most promising avenue is exploiting the scale-dependent bias on very large scales in studies of galaxy clustering at the two-point level. Early Fisher forecasts for the Euclid redshift survey found that, for a fiducial model with $f_{\rm NL} = 0$, this gives a marginalized 1σ error on the nonlinearity parameter of $\Delta f_{\rm NL} \simeq 2$ [210, 209]. Forecasts based on the most recent specifics for the Euclid surveys (see Table 21) are presented in [393] and summarized in Table 22 below. Updated values of the galaxy number counts and of the efficiency in measuring spectroscopic redshifts correspond to

a marginalized 1σ error of $f_{\rm NL} \simeq 4-5$ (depending a little on the detailed assumptions of the Fisher matrix calculation), with a slightly better result obtained using the Euclid spectroscopic sample rather than the photometric one (complemented with multi-band ground-based photometry), at least for a fiducial value of $f_{\rm NL} = 0$ [393]. The forecast errors further improve by nearly a few per cent using Planck priors on the cosmological parameters determined with the power spectrum of CMB temperature anisotropies.

Table 21: Specifications of the surveys used in the Euclid forecasts given in Table 22. The redshift distributions of the different galaxy samples are as in Section 1.8.2 (see also [393]).

	Photometric survey	Spectroscopic survey
Surveyed area (deg^2)	15,000	15,000
Galaxy density (arcmin^{-2})	30	1.2
Median redshift	0.8	1.0
Number of redshift bins	12	12
Redshift uncertainty $\sigma_z/(1+z)$	0.05	0.001
Intrinsic ellipticity noise γ	-	0.247
Gaussian linear bias param.	$\sqrt{1+z}$	$\sqrt{1+z}$

The amplitude and shape of the matter power spectrum in the mildly nonlinear regime depend (at a level of a few per cent) on the level of primordial non-Gaussianity [877, 730, 392]. Measuring this signal with the Euclid weak-lensing survey gives $\Delta f_{\rm NL} \simeq 70$ (30 with Planck priors) [393]. On the other hand, counting nonlinear structures in terms of peaks in the weak-lensing maps (convergence or shear) should give limits in the same ballpark ([627] find $\Delta f_{\rm NL} = 13$ assuming perfect knowledge of all the cosmological parameters).

Finally, by combining lensing and angular power spectra (and accounting for all possible cross-correlations) one should achieve $\Delta f_{\rm NL} \simeq 5$ (4.5 with Planck priors) [393]. This matches what is expected from both the Planck mission and the proposed BPol satellite.

Note that the forecast errors on $f_{\rm NL}$ are somewhat sensitive to the assumed fiducial values of the galaxy bias. In our study we have adopted the approximation $b(z) = \sqrt{1+z}$ [753]. On the other hand, using semi-analytic models of galaxy formation, [698] found bias values which are nearly $10-15\%$ lower at all redshifts. Adopting this slightly different bias, the constraint on $f_{\rm NL}$ already degrades by 50% with respect to our fiducial case.

Euclid data can also be used to constrain the scale dependence of the nonlinearity parameter (see Table 23). To this purpose, we consider a local model of primordial non-Gaussianity where

$$f_{\rm NL} = f_{\rm NL}^{\rm (piv)} \cdot \left(\frac{k}{k_{\rm piv}}\right)^{n_{f_{\rm NL}}} , \tag{3.4.6}$$

with fiducial values $k_{\rm piv} = 0.02\,h$ Mpc^{-1}, $f_{\rm NL}^{\rm (piv)} = 30$, and $n_{f_{\rm NL}} = 0$. In this case, the combination of lensing and clustering data gives $\Delta\alpha_{\rm s,m} = 0.18$ (0.14 with Planck priors) and $\Delta f_{\rm NL}^{\rm (piv)} \simeq 9$ (7 with Planck priors) [393]. These constraints are similar to what is expected from future studies of the CMB bispectrum with Planck [809].

In the end, we briefly comment on how well Euclid data could constrain the amplitude of alternative forms of primordial non-Gaussianity than the local one. In particular, we consider the equilateral and orthogonal shapes introduced in Section 3.3.2. Table 22 summarizes the resulting constraints on the amplitude of the primordial bispectrum, $f_{\rm NL}$. The forecast errors from galaxy clustering grow larger and larger when one moves from the local to the orthogonal and finally to the equilateral model. This reflects the fact that the scale-dependent part of the galaxy bias for $k \to 0$ approximately scales as k^{-2}, k^{-1}, and k^0 for the local, orthogonal, and equilateral shapes,

Table 22: Forecast 1σ errors for the nonlinearity parameter $f_{\rm NL}$ based on two-point statistics (power spectra) of the Euclid redshift and weak-lensing surveys. Results are obtained using the Fisher-matrix formalism and marginalizing over eight cosmological parameters (Ω_Λ, Ω_m, Ω_b, h, n_s, σ_8, w_0, w_a) plus a large number of nuisance parameters to account for galaxy biasing, nonlinear redshift-space distortions and shot noise (see [393] for details). Results within parentheses include the forecast priors for the cosmological parameters from the power spectrum of CMB temperature anisotropies measured with the Planck satellite (note that no prior is assumed on $f_{\rm NL}$). The label "Galaxy clustering" refers to the anisotropic power spectrum $P(k_\parallel, k_\perp)$ for spectroscopic data and to the angular power spectrum C_ℓ for photometric data. The combined analysis of clustering and lensing data is based on angular power spectra and includes all possible cross-correlations between different redshift bins and probes. nonlinear power spectra are computed using the halo model. This introduces possible inaccuracies in the forecasts for weak lensing data in the equilateral and orthogonal shapes (see main text for details).

Bispectrum shape	local	orthogonal	equilateral
Fiducial $f_{\rm NL}$	0	0	0
Galaxy clustering (spectr. z)	4.1 (4.0)	54 (11)	220 (35)
Galaxy clustering (photom. z)	5.8 (5.5)	38 (9.6)	140 (37)
Weak lensing	73 (27)	9.6 (3.5)	34 (13)
Combined	4.7 (4.5)	4.0 (2.2)	16 (7.5)

Table 23: Forecast 1σ errors for a scale-dependent local model of primordial non-Gaussianity [393]. Details of the forecasts are as in the previous Table 22.

	$\Delta f_{\rm NL}^{\rm (piv)}$	$\Delta n_{f_{\rm NL}}$
Galaxy clustering (spectr. z)	9.3 (7.2)	0.28 (0.21)
Galaxy clustering (photom. z)	25 (18)	0.38 (0.26)
Weak lensing	134 (82)	0.66 (0.59)
Combined	8.9 (7.4)	0.18 (0.14)

respectively [799, 933, 802, 305, 306]. On the other hand, the lensing constraints (that, in this case, come from the very nonlinear scales) appear to get much stronger for the non-local shapes. A note of caution is in order here. In [393], the nonlinear matter power spectrum is computed using a halo model which has been tested against N-body simulations only for non-Gaussianity of the local type.[17] In consequence, the weak-lensing forecasts might be less reliable than in the local case (see the detailed discussion in [393]). This does not apply for the forecasts based on galaxy clustering which are always robust as they are based on the scale dependence of the galaxy bias on very large scales.

3.4.5 Complementarity

The CMB bispectrum is very sensitive to the shape of non-Gaussianity; halo bias and mass function, the most promising approaches to constrain $f_{\rm NL}$ with a survey like Euclid, are much less sensitive. However, it is the complementarity between CMB and LSS that matters. One could envision different scenarios. If non-Gaussianity is local with negative $f_{\rm NL}$ and CMB obtains a detection, then the halo bias approach should also give a high-significance detection (GR correction and primordial contributions add up), while if it is local but with positive $f_{\rm NL}$, the halo-bias approach could give a lower statistical significance as the GR correction contribution has the opposite sign. If CMB detects $f_{\rm NL}$ at the level of 10 and a form that is close to local, but halo bias does not

[17] Very few N-body simulations of the non-local models are currently available and none of them has very high spatial resolution.

detect it, then the CMB bispectrum is given by secondary effects (e.g., [620]). If CMB detects non-Gaussianity that is not of the local type, then halo bias can help discriminate between equilateral and enfolded shapes: if halo bias sees a signal, it indicates the enfolded type, and if halo bias does not see a signal, it indicates the equilateral type. Thus even a non-detection of the halo-bias effect, in combination with CMB constraints, can have an important discriminative power.

3.5 Isocurvature modes

At some time well after inflation but deep into the radiation era the universe is filled with several components. For instance, in the standard picture right before recombination there are four components: baryons, cold dark matter, photons and neutrinos. One can study the distribution of *super-Hubble* fluctuations between different species, which represent the initial conditions for the subsequent evolution. So far we have investigated mostly the adiabatic initial conditions; in this section we explore more generally the possibility of isocurvature initial conditions. Although CMB data are the most sensitive to constrain isocurvature perturbations, we discuss here the impact on Euclid results.

3.5.1 The origin of isocurvature perturbations

Let us denote by ρ_α the energy density of the component α. Perturbations are purely adiabatic when for each component α the quantity $\zeta_\alpha \equiv -3H\delta\rho_\alpha/\dot{\rho}_\alpha$ is the same [949, 617]. Let us consider for instance cold dark matter and photons. When fluctuations are adiabatic it follows that $\zeta_{\rm cdm} = \zeta_\gamma$. Using the energy conservation equation, $\dot{\rho}_\alpha = -3H(\rho_\alpha + p_\alpha)$ with $p_{\rm cdm} = 0$ and $p_\gamma = \rho_\gamma/3$, one finds that the density contrasts of these species are related by

$$\frac{\delta\rho_{\rm cdm}}{\rho_{\rm cdm}} = \frac{3}{4}\frac{\delta\rho_\gamma}{\rho_\gamma}\,. \tag{3.5.1}$$

Using that $n_{\rm cdm} \propto \rho_{\rm cdm}$ and $n_\gamma \propto \rho_\gamma^{3/4}$, this also implies that particle number ratios between these species is fixed, i.e., $\delta(n_{\rm cdm}/n_\gamma) = 0$.

When isocurvature perturbations are present, the condition described above is not satisfied.[18] In this case one can define a non-adiabatic or entropic perturbation between two components α and β as $\mathcal{S}_{\alpha,\beta} \equiv \zeta_\alpha - \zeta_\beta$, so that, for the example above one has

$$\mathcal{S}_{{\rm cdm},r} = \frac{\delta\rho_{\rm cdm}}{\rho_{\rm cdm}} - \frac{3}{4}\frac{\delta\rho_\gamma}{\rho_\gamma} = \frac{\delta(n_{\rm cdm}/n_\gamma)}{n_{\rm cdm} - n_\gamma}\,. \tag{3.5.2}$$

A sufficient condition for having purely adiabatic perturbations is that all the components in the universe were created by a single degree of freedom, such as during reheating after single field inflation.[19] Even if inflation has been driven by several fields, thermal equilibrium may erase isocurvature perturbations if it is established before any non-zero conserving quantum number was created (see [950]). Thus, a detection of non-adiabatic fluctuations would imply that severalvscalar fields where present during inflation *and* that either some ofvthe species were not in thermal equilibrium afterwards or that some non-zero conserving quantum number was created before thermal equilibrium.

[18] Strictly speaking, isocurvature perturbations are defined by the condition that their total energy density in the total comoving gauge vanishes, i.e., $\sum_\alpha \delta\rho_\alpha^{(\rm com.)} = 0$. Using the relativistic Poisson equation, one can verify that this implies that they do not contribute to the "curvature" potential.

[19] In this case in the flat gauge one finds, for each species α, $\zeta_\alpha = \zeta$, where ζ is the Bardeen curvature perturbation conserved on super-Hubble scales.

The presence of many fields is not unexpected. Indeed, in all the extension of the Standard Model scalar fields are rather ubiquitous. In particular, in String Theory dimensionless couplings are functions of moduli, i.e., scalar fields describing the compactification. Another reason to consider the relevant role of a second field other than the inflaton is that this can allow to circumvent the necessity of slow-roll (see, e.g., [331]) enlarging the possibility of inflationary models.

Departure from thermal equilibrium is one of the necessary conditions for the generation of baryon asymmetry and thus of the matter in the universe. Interestingly, the oscillations and decay of a scalar field requires departure from thermal equilibrium. Thus, baryon asymmetry can be generated by this process; examples are the decay of a right-handed sneutrino [419] or the [10] scenario. If the source of the baryon-number asymmetry in the universe is the condensation of a scalar field after inflation, one expects generation of baryon isocurvature perturbations [664]. This scalar field can also totally or partially generate adiabatic density perturbations through the curvaton mechanism.

In summary, given our ignorance about inflation, reheating, and the generation of matter in the universe, a discovery of the presence of isocurvature initial conditions would have radical implications on both the inflationary process and on the mechanisms of generation of matter in the universe.

Let us concentrate on the non-adiabatic perturbation between cold dark matter (or baryons, which are also non-relativistic) and radiation $\mathcal{S} = \mathcal{S}_{\mathrm{cdm},\gamma}$. Constraints on the amplitude of the non-adiabatic component are given in terms of the parameter α, defined at a given scale k_0, by $P_{\mathcal{S}} - P_\zeta \equiv \alpha - (1-\alpha)$, see e.g., [120, 113, 525]. As discussed in [542], adiabatic and entropy perturbations may be correlated. To measure the amplitude of the correlation one defines a cross-correlation coefficient, $\beta \equiv -P_{\mathcal{S},\zeta}/\sqrt{P_{\mathcal{S}} P_\zeta}$. Here $P_{\mathcal{S},\zeta}$ is the cross-correlation power-spectrum between $\mathcal{S}$ and ζ and for the definition of β we have adopted the sign convention of [525]. Observables, such as for instance the CMB anisotropies, depend on linear combinations of ζ and $\mathcal{S}$. Thus, constraints on α will considerably depend on the cross-correlation coefficient β (see for instance discussion in [403]).

If part of the cold dark matter is created out of equilibrium from a field other than the inflaton, totally uncorrelated isocurvature perturbations, with $\beta = 0$, are produced, as discussed for instance in [336, 582]. The axion is a well-known example of such a field. The axion is the Nambu–Goldstone boson associated with the [715] mechanism to solve the strong-CP problem in QCD. As it acquires a mass through QCD non-perturbative effects, when the Hubble rate drops below its mass the axion starts oscillating coherently, behaving as cold dark matter [742, 2, 316]. During inflation, the axion is practically massless and acquires fluctuations which are totally uncorrelated from photons, produced by the inflaton decay [805, 578, 579, 910]. As constraints on $\alpha_{\beta=0}$ are currently very strong (see e.g., [118, 526]), axions can only represent a small fraction of the total dark matter.

Totally uncorrelated isocurvature perturbations can also be produced in the curvaton mechanism, if the dark matter or baryons are created from inflation, before the curvaton decay, and remain decoupled from the product of curvaton reheating [546]. This scenario is ruled out if the curvaton is entirely responsible for the curvature perturbations. However, in models when the final curvature perturbation is a mix of the inflaton and curvaton perturbations [545], such an entropy contribution is still allowed.

When dark matter or baryons are produced solely from the curvaton decay, such as discussed by [597], the isocurvature perturbations are totally anti-correlated, with $\beta = -1$. For instance, some fraction of the curvaton decays to produce CDM particles or the out-of-equilibrium curvaton decay generates the primordial baryon asymmetry [419, 10].

If present, isocurvature fields are not constrained by the slow-roll conditions imposed on the inflaton field to drive inflation. Thus, they can be highly non-Gaussian [582, 126]. Even though negligible in the two-point function, their presence could be detected in the three-point function of the primordial curvature and isocurvature perturbations and their cross-correlations, as studied in [495, 546].

3.5.2 Constraining isocurvature perturbations

Even if pure isocurvature models have been ruled out, current observations allow for mixed adiabatic and isocurvature contributions (e.g., [267, 896, 525, 914]). As shown in [902, 40, 914, 544, 184, 847], the initial conditions issue is a very delicate problem: in fact, for current cosmological data, relaxing the assumption of adiabaticity reduces our ability to do precision cosmology since it compromises the accuracy of parameter constraints. Generally, allowing for isocurvature modes introduces new degeneracies in the parameter space which weaken constraints considerably.

The cosmic microwave background radiation (CMB), being our window on the early universe, is the preferred data set to learn about initial conditions. Up to now, however, the CMB temperature power spectrum alone, which is the CMB observable better constrained so far, has not been able to break the degeneracy between the nature of initial perturbations (i.e., the amount and properties of an isocurvature component) and cosmological parameters, e.g., [538, 902]. Even if the precision measurement of the CMB first acoustic peak at $\ell \simeq 220$ ruled out the possibility of a dominant isocurvature mode, allowing for isocurvature perturbations together with the adiabatic ones introduce additional degeneracies in the interpretation of the CMB data that current experiments could not break. Adding external data sets somewhat alleviates the issue for some degeneracy directions, e.g., [903, 120, 323]. As shown in [184], the precision polarization measurement of the next CMB experiments like Planck will be crucial to lift such degeneracies, i.e., to distinguish the effect of the isocurvature modes from those due to the variations of the cosmological parameters.

It is important to keep in mind that analyzing the CMB data with the prior assumption of purely adiabatic initial conditions when the real universe contains even a small isocurvature contribution, could lead to an incorrect determination of the cosmological parameters and on the inferred value of the sound horizon at radiation drag. The sound horizon at radiation drag is the standard ruler that is used to extract information about the expansion history of the universe from measurements of the baryon acoustic oscillations. Even for a CMB experiment like Planck, a small but non-zero isocurvature contribution, still allowed by Planck data, if ignored, can introduce a systematic error in the interpretation of the BAO signal that is comparable if not larger than the statistical errors. In fact, [621] shows that even a tiny amount of isocurvature perturbation, if not accounted for, could affect standard rulers calibration from CMB observations such as those provided by the Planck mission, affect BAO interpretation, and introduce biases in the recovered dark energy properties that are larger than forecast statistical errors from future surveys. In addition it will introduce a mismatch of the expansion history as inferred from CMB and as measured by BAO surveys. The mismatch between CMB predicted and the measured expansion histories has been proposed as a signature for deviations from a DM cosmology in the form of deviations from Einstein's gravity (e.g., [8, 476]), couplings in the dark sector (e.g., [589]) or time-evolving dark energy.

For the above reasons, extending on the work of [621], [208] adopted a general fiducial cosmology which includes a varying dark energy equation of state parameter and curvature. In addition to BAO measurements, in this case the information from the shape of the galaxy power spectrum are included and a joint analysis of a Planck-like CMB probe and a Euclid-type survey is considered. This allows one to break the degeneracies that affect the CMB and BAO combination. As a result, most of the cosmological parameter systematic biases arising from an incorrect assumption on the isocurvature fraction parameter $f_{\rm iso}$, become negligible with respect to the statistical errors. The combination of CMB and LSS gives a statistical error $\sigma(f_{\rm iso}) \sim 0.008$, even when curvature and a varying dark energy equation of state are included, which is smaller than the error obtained from CMB alone when flatness and cosmological constant are assumed. These results confirm the synergy and complementarity between CMB and LSS, and the great potential of future and planned galaxy surveys.

3.6 Summary and outlook

We have summarized aspects of the initial conditions for the growth of cosmological perturbations that Euclid will enable us to probe. In particular we have considered the shape of the primordial power spectrum and its connection to inflationary models, primordial non-Gaussianity and isocurvature perturbations.

A survey like Euclid will greatly improve our knowledge of the initial conditions for the growth of perturbations and will help shed light on the mechanism for the generation of primordial perturbations. The addition of Euclid data will improve the Planck satellite's cosmic microwave background constraints on parameters describing the shape of the primordial power spectrum by a factor of $2-3$.

Primordial non-Gaussianity can be tested by Euclid in three different and complementary ways: via the galaxy bispectrum, number counts of nonlinear structures and the non-Gaussian halo bias. These approaches are also highly competitive with and complementary to CMB constraints. In combination with Planck, Euclid will not only test a possible scale-dependence of non-Gaussianity but also its shape. The shape of non-Gaussianity is the key to constrain and classify possible deviations for the simplest single-field slow roll inflation.

Isocurvature modes affect the interpretation of large-scale structure clustering in two ways. The power spectrum shape is modified on small scales due to the extra perturbations although this effect however can be mimicked by scale-dependent bias. More importantly isocurvature modes can lead to an incorrect inferred value for the sound horizon at radiation drag from CMB data. This then predicts an incorrect location of the baryon acoustic feature. It is through this effect that Euclid BAO measurements improve constraints on isocurvature modes.

Part 4: Testing the Basic Cosmological Hypotheses

4.1 Introduction

The standard cosmological analyses implicitly make several assumptions, none of which are seriously challenged by current data. Nevertheless, Euclid offers the possibility of testing some of these basic hypotheses. Examples of the standard assumptions are that photon number is conserved, that the Copernican principle holds (i.e., we are not at a special place in the universe) and that the universe is homogeneous and isotropic, at least on large enough scales. These are the pillars on which standard cosmology is built, so it is important to take the opportunity offered by Euclid observations to test these basic hypotheses.

4.2 Transparency and Etherington Relation

The Etherington relation [352] implies that, in a cosmology based on a metric theory of gravity, distance measures are unique: the luminosity distance is $(1 + z)^2$ times the angular diameter distance. This is valid in any cosmological background where photons travel on null geodesics and where, crucially, photon number is conserved. There are several scenarios in which the Etherington relation would be violated: for instance we can have deviations from a metric theory of gravity, photons not travelling along unique null geodesics, variations of fundamental constants, etc. We follow here the approach of [65].

4.2.1 Violation of photon conservation

A change in the photon flux during propagation towards the Earth will affect the supernovae (SNe) luminosity distance measures $D_L(z)$ but not the determinations of the angular diameter distance. BAO will not be affected so $D_A(z)$ and $H(z)$ measurements from BAO could be combined with supernovae measurements of $D_L(z)$ to constrain deviations from photon number conservation. Photon conservation can be violated by simple astrophysical effects or by exotic physics. Amongst the former we find, for instance, attenuation due to interstellar dust, gas and/or plasmas. Most known sources of attenuation are expected to be clustered and can be typically constrained down to the 0.1% level [656, 663]. Unclustered sources of attenuation are however much more difficult to constrain. For example, grey dust [14] has been invoked to explain the observed dimming of Type Ia supernovae without resorting to cosmic acceleration. More exotic sources of photon conservation violation involve a coupling of photons to particles beyond the standard model of particle physics. Such couplings would mean that, while passing through the intergalactic medium, a photon could disappear or even (re)appear! Interacting with such exotic particles, modifying the apparent luminosity of sources. Recently, [65] considered the mixing of photons with scalars, known as axion-like particles, chameleons, and the possibility of mini-charged particles which have a tiny, and unquantized electric charge. In particular, the implications of these particles on the SN luminosity have been described in a number of publications [270, 665, 190, 16] and a detailed discussion of the proposed approach can be found in [100, 101, 66, 65].

Any systematic violations in photon conservation can then be interpreted as an opacity effect in the observed luminosity distance, parametrized through a generic opacity parameter, $\tau(z)$, as:

$$D^2_{L,\mathrm{obs}} = D^2_{L,\mathrm{true}} \exp[\tau(z)] \,.$$

Note that a negative $\tau(z)$ allows for apparent brightening of light sources, as would be the case, for example, if exotic particles were also emitted from the source and converted into photons along the line of sight [190]. Following [66] generic deviations from the Etherington relation can be parametrized as:

$$D_L(z) = D_A(z)(1+z)^{2+\epsilon}\,.$$

Forecast Euclid constraints are shown in Figure 48, taken from [65]. This assumes that Euclid is accompanied by a supernova sample with the characteristic of a Dark Energy Task Force stage IV survey

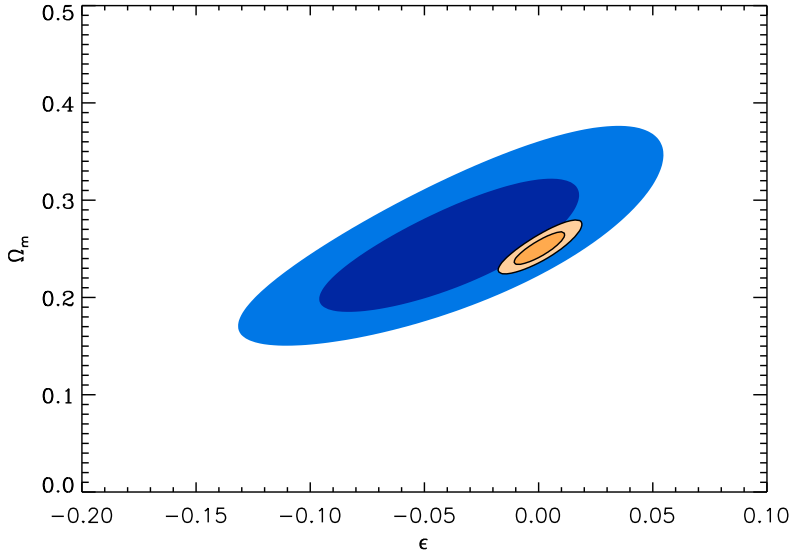

Figure 48: Constraints on possible violation of the Etherington relation in the form of deviations from a perfectly transparent universe ($\epsilon = 0$). Blue regions represent current constraints while orange are forecast Euclid constraints assuming it is accompanied by a Dark Energy Task Force stage IV supernovae sample.

For particular models of exotic matter-photon coupling, namely axion-like particles (ALPs), chameleons, and mini-charged particles (MCPs), the appropriate parameterization parametrization of $\tau(z)$ is used instead.

4.2.2 Axion-like particles

Axion-like particles (ALP) can arise from field theoretic extensions of the standard model as Goldstone bosons when a global shift symmetry, present in the high energy sector, is spontaneously broken. Interestingly, these fields also arise naturally in string theory (for a review see [871]). Chameleon scalar fields are another very interesting type of ALPs [169]. They were originally invoked to explain the current accelerated expansion of the universe with a quintessence field which can couple to matter without giving rise to large fifth forces or unacceptable violations of the weak equivalence principle. A chameleon model with only matter couplings will induce a coupling to photons.

The presence of ALPs will have an impact on observations of SNe if their observed light passes through (intergalactic) magnetic fields. The net effect depends on the ratio of the transition probability to the length travelled through a magnetic field, and a parameter A describing the

degree of thermalization of the initial flux ($A = 1$ means thermalized flux where the photon to ALP transition is compensated by the inverse ALP to photon, making the photon number constant). For the simplest ALP model $A = 2/3$, the present and forecast constraints are shown in Figure 49 taken from [65].

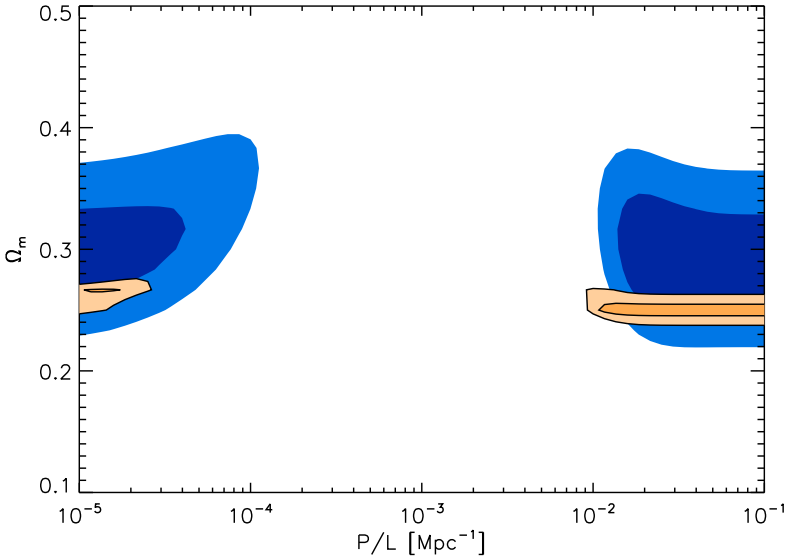

Figure 49: Constraints on the simplest Axion-like particles models. Blue regions represent current constraints while orange are forecast Euclid constraints assuming it is accompanied by a Dark Energy Task Force stage IV supernovae sample. Here P/L is the conversion probability per unit length and is the relevant parameter for $\tau(z)$ (see [65]).

4.2.3 Mini-charged particles

New particles with a small unquantized charge have been investigated in several extensions of the standard model [443, 105]. In particular, they arise naturally in extensions of the standard model which contain at least one additional U(1) hidden sector gauge group [443, 181]. The gauge boson of this additional U(1) is known as a hidden photon, and hidden sector particles, charged under the hidden U(1), get an induced electric charge proportional to the small mixing angle between the kinetic terms of the two photons. In string theory, such hidden U(1)s and the required kinetic mixing are a generic feature [5, 4, 311, 6, 402]. Hidden photons are not necessary however to explain mini-charged particles, and explicit brane-world scenarios have been constructed [105] where MCPs arise without the need for hidden photons.

More interestingly, [16, 395, 17] pointed out that photons propagating in a background magnetic field can actually pair-produce MCPs without the need for a second photon in the initial state. The opacity in this case is parametrized by $\kappa y(z)$ where y is the comoving distance to the source and κ encloses information on the MCP electric charge and the intervening magnetic field strength. Figure 50 shows current and forecast Euclid's constraints, taken from [65] assuming Euclid is accompanied by a supernova sample with the characteristic of a Dark Energy Task Force stage IV survey.

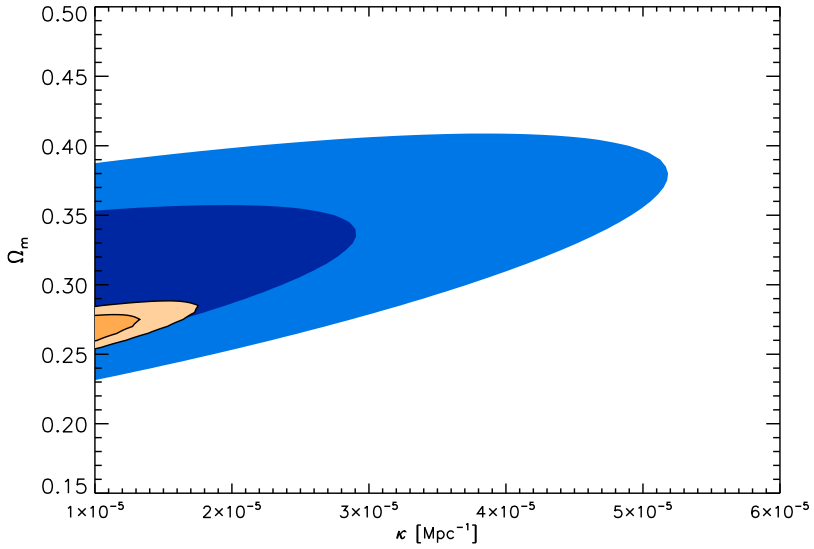

Figure 50: Constraints on MCP models. Blue regions represent current constraints while orange are forecast Euclid constraints assuming it is accompanied by a Dark Energy Task Force stage IV supernovae sample.

4.3 Beyond homogeneity and isotropy

The crucial ingredient that kickstarted dark energy research was the interpretation in 1998 of standard candle observations in terms of cosmic acceleration required to explain the data in the context of the FLRW metric. What we observe is however merely that distant sources ($z > 0.3$) are dimmer than we would predict in a matter-only universe calibrated through "nearby" sources. That is, we observe a different evolution of luminosity rather than directly an increase in the expansion rate. Can this be caused by a strong inhomogeneity rather than by an accelerating universe?

In addition, cosmic acceleration seems to be a recent phenomenon at least for standard dark-energy models, which gives rise to the coincidence problem. The epoch in which dark energy begins to play a role is close to the epoch in which most of the cosmic structures formed out of the slow linear gravitational growth. We are led to ask again: can the acceleration be caused by strong inhomogeneities rather than by a dark energy component?

Finally, one must notice that in all the standard treatment of dark energy one always assumes a perfectly isotropic expansion. Could it be that some of the properties of acceleration depends critically on this assumption?

In order to investigate these issues, in this section we explore radical deviations from homogeneity and isotropy and see how Euclid can test them.

4.3.1 Anisotropic models

In recent times, there has been a resurgent interest towards anisotropic cosmologies, classified in terms of Bianchi solutions to general relativity. This has been mainly motivated by hints of anomalies in the cosmic microwave background (CMB) distribution observed on the full sky by the WMAP satellite [288, 930, 268, 349]. While the CMB is very well described as a highly isotropic

(in a statistical sense) Gaussian random field, and the anomalies are *a posteriori* statistics and therefore their statistical significance should be corrected at least for the so-called *look elsewhere effect* (see, e.g., [740, 122] and references therein) recent analyses have shown that local deviations from Gaussianity in some directions (the so called cold spots, see [268]) cannot be excluded at high confidence levels. Furthermore, the CMB angular power spectrum extracted from the WMAP maps has shown in the past a quadrupole power lower than expected from the best-fit cosmological model [335]. Several explanations for this anomaly have been proposed (see, e.g., [905, 243, 297, 203, 408]) including the fact that the universe is expanding with different velocities along different directions. While deviations from homogeneity and isotropy are constrained to be very small from cosmological observations, these usually assume the non-existence of anisotropic sources in the late universe. Conversely, as suggested in [520, 519, 106, 233, 251], dark energy with anisotropic pressure acts as a late-time source of anisotropy. Even if one considers no anisotropic pressure fields, small departures from isotropy cannot be excluded, and it is interesting to devise possible strategies to detect them.

The effect of assuming an anisotropic cosmological model on the CMB pattern has been studied by [249, 89, 638, 601, 189, 516]. The Bianchi solutions describing the anisotropic line element were treated as small perturbations to a Friedmann–Robertson–Walker (FRW) background. Such early studies did not consider the possible presence of a non-null cosmological constant or dark energy and were upgraded recently by [652, 477].

One difficulty with the anisotropic models that have been shown to fit the large-scale CMB pattern, is that they have to be produced according to very unrealistic choices of the cosmological parameters. For example, the Bianchi VIIh template used in [477] requires an open universe, an hypothesis which is excluded by most cosmological observations. An additional problem is that an inflationary phase – required to explain a number of feature of the cosmological model – isotropizes the universe very efficiently, leaving a residual anisotropy that is negligible for any practical application. These difficulties vanish if an anisotropic expansion takes place only well after the decoupling between matter and radiation, for example at the time of dark energy domination [520, 519, 106, 233, 251].

Bianchi models are described by homogeneous and anisotropic metrics. If anisotropy is slight, the dynamics of any Bianchi model can be decomposed into an isotropic FRW background linearly perturbed to break isotropy; on the other side, homogeneity is maintained with respect to three Killing vector fields.

The geometry of Bianchi models is set up by the structure constants C^k_{ij}, defined by the commutators of (these) three Killing fields $\vec{\xi}_i$:

$$\left[\vec{\xi}_i, \vec{\xi}_j\right] = C^k_{ij}\vec{\xi}_k. \tag{4.3.1}$$

The structure constants are subject to the antisymmetry relation $C^k_{ij} = -C^k_{ji}$ and the Jacobi identities $C^a_{[bc}C^d_{e]a} = 0$. As a consequence, their attainable values are restricted to only four of the initial 27 necessary to describe a given space. In [340] these four values are dubbed as n_1, n_2, n_3 and a_1. The categorization of Bianchi models into different types relies on classifying the inequivalent sets of these four constants. In Table 24 the subclass of interest containing the FRW limit is shown. Bianchi types VIIh and IX contain the open and closed FRW model, respectively. Type VII_0 contains the flat FRW; types I and V are just particular subcases of the VII_0 and VIIh. In type I no vertical motions are allowed and the only extension with respect to the FRW case is that there are three different scale factors. The metric in general can be written as

$$g_{\mu\nu} = -n_\mu n_\nu + g_{ab}\xi^a_\mu \xi^b_\nu, \tag{4.3.2}$$

where g_{ab} is a 3×3 metric depending on t. It can be decomposed as $g_{ab} = e^{2\alpha}[e^{2\beta}]_{ab}$, where the first term represents the volumetric expansion and the second term includes the anisotropy.

Table 24: Bianchi models containing FRW limit and their structure constants.

Type	a	n_1	n_2	n_3
I	0	0	0	0
V	1	0	0	0
VII_0	0	0	1	1
VII_h	$\sqrt{h}$	0	1	1
IX	0	1	1	1

4.3.1.1 Late-time anisotropy

While deviations from homogeneity and isotropy are constrained to be very small from cosmological observations, these usually assume the non-existence of anisotropic sources in the late universe. The CMB provides very tight constraints on Bianchi models at the time of recombination [189, 516, 638] of order of the quadrupole value, i.e., $\sim 10^{-5}$. Usually, in standard cosmologies with a cosmological constant the anisotropy parameters scale as the inverse of the comoving volume. This implies an isotropization of the expansion from the recombination up to the present, leading to the typically derived constraints on the shear today, namely $\sim 10^{-9} \div 10^{-10}$. However, this is only true if the anisotropic expansion is not generated by any anisotropic source arising after decoupling, e.g., vector fields representing anisotropic dark energy [519].

As suggested in [520, 519, 106, 233, 251], dark energy with anisotropic pressure acts as a late-time source of anisotropy. An additional problem is that an inflationary phase – required to explain a number of feature of the cosmological model – isotropizes the universe very efficiently, leaving a residual anisotropy that is negligible for any practical application. These difficulties vanish if an anisotropic expansion takes place only well after the decoupling between matter and radiation, for example at the time of dark energy domination [520, 519, 106, 233, 251].

For example, the effect of cosmic parallax [749] has been recently proposed as a tool to assess the presence of an anisotropic expansion of the universe. It is essentially the change in angular separation in the sky between far-off sources, due to an anisotropic expansion.

A common parameterization of an anisotropically distributed dark energy component is studied in a class of Bianchi I type, where the line element is

$$\mathrm{d}s^2 = -\mathrm{d}t^2 + a^2(t)\,\mathrm{d}x^2 + b^2(t)\,\mathrm{d}y^2 + c^2(t)\,\mathrm{d}z^2\,. \tag{4.3.3}$$

The expansion rates in the three Cartesian directions x, y and z are defined as $H_X = \dot{a}/a$, $H_Y = \dot{b}/b$ and $H_Z = \dot{c}/c$, where the dot denotes the derivative with respect to coordinate time. In these models they differ from each other, but in the limit of $H_X = H_Y = H_Z$ the flat FRW isotropic expansion is recovered. Among the Bianchi classification models the type I exhibits flat geometry and no overall vorticity; conversely, shear components $\Sigma_{X,Y,Z} = H_{X,Y,Z}/H - 1$ are naturally generated, where H is the expansion rate of the average scale factor, related to the volume expansion as $H = \dot{A}/A$ with $A = (abc)^{1/3}$.

The anisotropic expansion is caused by the anisotropically stressed dark energy fluid whenever its energy density contributes to the global energy budget. If the major contributions to the overall budget come from matter and dark energy, as after recombination, their energy-momentum tensor can be parametrized as:

$$T^{\mu}_{(m)\nu} = \mathrm{diag}(-1, w_m, w_m, w_m)\rho_m \tag{4.3.4}$$

$$T^{\mu}_{(\mathrm{DE})\nu} = \mathrm{diag}(-1, w, w+3\delta, w+3\gamma)\rho_{\mathrm{DE}}\,, \tag{4.3.5}$$

respectively, where w_m and w are the equation of state parameters of matter and dark energy and the skewness parameters δ and γ can be interpreted as the difference of pressure along the x and

y and z axis. Note that the energy-momentum tensor (4.3.5) is the most general one compatible with the metric (4.3.3) [519]. Two quantities are introduced to define the degree of anisotropic expansion:

$$\begin{aligned} R &\equiv (\dot{a}/a - \dot{b}/b)/H &&= \Sigma_x - \Sigma_y\,, \\ S &\equiv (\dot{a}/a - \dot{c}/c)/H &&= 2\Sigma_x + \Sigma_y\,. \end{aligned} \tag{4.3.6}$$

Considering the generalized Friedmann equation, the continuity equations for matter and dark energy and no coupling between the two fluids, the derived autonomous system reads [520, 519]:

$$\begin{aligned} U' =& U(U-1)[\gamma(3+R-2S) + \delta(3-2R+S) + 3(w-w_m)] \\ S' =& \frac{1}{6}(9-R^2+RS-S^2)\big\{S[U(\delta+\gamma+w-w_m)+w_m-1]-6\,\gamma\,U\big\} \\ R' =& \frac{1}{6}(9-R^2+RS-S^2)\big\{R[U(\delta+\gamma+w-w_m)+w_m-1]-6\,\delta\,U\big\}, \end{aligned} \tag{4.3.7}$$

where $U \equiv \rho_{\rm DE}/(\rho_{\rm DE}+\rho_m)$ and the derivatives are taken with respect to $\log(A)/3$. System (4.3.7) exhibits many different fixed points, defined as the solutions of the system $S' = R' = U' = 0$. Beside the Einstein–de Sitter case ($R_* = S_* = U_* = 0$), the most physically interesting for our purposes are the dark energy dominated solution

$$R_* = \frac{6\delta}{\delta+\gamma+w-1}\,, \quad S_* = \frac{6\gamma}{\delta+\gamma+w-1}\,, \quad U_* = 1\,, \tag{4.3.8}$$

and the scaling solution

$$R_* = \frac{3\delta(\delta+\gamma+w)}{2(\delta^2-\delta\gamma+\gamma^2)}\,, \quad S_* = \frac{3\gamma(\delta+\gamma+w)}{2(\delta^2-\delta\gamma+\gamma^2)}\,, \quad U_* = \frac{w+\gamma+\delta}{w^2-3(\gamma-\delta)^2+2w(\gamma+\delta)}\,, \tag{4.3.9}$$

in which $\rho_{\rm DE}/\rho_m = $ const., i.e., the fractional dark energy contribution to the total energy density is constant.

Anisotropic distribution of sources in Euclid survey might constrain the anisotropy at present, when the dark energy density is of order 74%, hence not yet in the final dark energy dominant attractor phase (4.3.8).

4.3.2 Late-time inhomogeneity

Inhomogeneity is relatively difficult to determine, as observations are typically made on our past light cone, but some methods exist (e.g., [242, 339, 600]). However, homogeneity may be tested by exploring the interior of the past light cone by using the fossil record of galaxies to probe along the past world line of a large number of galaxies [428]. One can use the average star formation rate at a fixed lookback time as a diagnostic test for homogeneity. The lookback time has two elements to it – the lookback time of the emission of the light, plus the time along the past world line. The last of these can be probed using the integrated stellar spectra of the galaxies, using a code such as VESPA [890], and this is evidently dependent only on atomic and nuclear physics, independent of homogeneity. The lookback time can also be computed, surprisingly simply, without assuming homogeneity from [428]

$$\Delta t = \int_0^z \frac{dz'}{(1+z')H_r(z')}\,, \tag{4.3.10}$$

where H_r is the radial Hubble constant. In principle, this can be obtained from radial BAOs, assuming early-time homogeneity so that the physical BAO scale is fixed. The spectroscopic part of Euclid could estimate both the star formation histories from stacked spectra, and the radial expansion rate.

4.3.3 Inhomogeneous models: Large voids

Nonlinear inhomogeneous models are traditionally studied either with higher-order perturbation theory or with N-body codes. Both approaches have their limits. A perturbation expansion obviously breaks down when the perturbations are deeply in the nonlinear regime. N-body codes, on the other hand, are intrinsically Newtonian and, at the moment, are unable to take into account full relativistic effects. Nevertheless, these codes can still account for the general relativistic behavior of gravitational collapse in the case of inhomogeneous large void models, as shown recently in [30], where the growth of the void follows the full nonlinear GR solution down to large density contrasts (of order one).

A possibility to make progress is to proceed with the most extreme simplification: radial symmetry. By assuming that the inhomogeneity is radial (i.e., we are at the center of a large void or halo) the dynamical equations can be solved exactly and one can make definite observable predictions.

It is however clear from the start that these models are highly controversial, since the observer needs to be located at the center of the void with a tolerance of about few percent of the void scale radius, see [141, 242], disfavoring the long-held Copernican principle (CP). Notwithstanding this, the idea that we live near the center of a huge void is attractive for another important reason: a void creates an apparent acceleration field that could in principle match the supernovae observations [891, 892, 220, 474]. Since we observe that nearby SN Ia recede faster than the $H(z)$ predicted by the Einstein–de Sitter universe, we could assume that we live in the middle of a huge spherical region which is expanding faster because it is emptier than the outside. The transition redshift z_e, i.e., the void edge, should be located around $0.3-0.5$, the value at which in the standard interpretation we observe the beginning of acceleration.

The consistent way to realize such a spherical inhomogeneity has been studied since the 1930s in the relativistic literature: the Lemaître–Tolman–Bondi (LTB) metric. This is the generalization of a FLRW metric in which the expansion factor along the radial coordinate r is different relative to the surface line element $\mathrm{d}\Omega^2 = \mathrm{d}\theta^2 + \sin^2\theta\,\mathrm{d}\phi^2$. If we assume the inhomogeneous metric (this subsection follows closely the treatment in [49])

$$\mathrm{d}s^2 = -\mathrm{d}t^2 + X^2(t,r)\,\mathrm{d}r^2 + R^2(t,r)\,\mathrm{d}\Omega^2\,, \tag{4.3.11}$$

and solve the $(0,1)$ Einstein equation for a fluid at rest we find that the LTB metric is given by

$$\mathrm{d}s^2 = -\mathrm{d}t^2 + \frac{[R'(t,r)]^2}{1+\beta(r)}\mathrm{d}r^2 + R^2(t,r)\mathrm{d}\Omega^2\,, \tag{4.3.12}$$

where $R(t,r), \beta(r)$ are arbitrary functions. Here primes and dots refer to partial space and time derivatives, respectively. The function $\beta(r)$ can be thought of as a position-dependent spatial curvature. If R is factorized so that $R(t,r) = a(t)f(r)$ and $\beta(r) = -Kf^2(r)$, then we recover the FLRW metric (up to a redefinition of r: from now on when we seek the FLRW limit we put $R = a(t)r$ and $\beta = -Kr^2$). Otherwise, we have a metric representing a spherical inhomogeneity centered on the origin. An observer located at the origin will observe an isotropic universe. We can always redefine r at the present time to be $R_0 \equiv R(t_0, r) = r$, so that the metric is very similar to a FLRW today.

Considering the infinitesimal radial proper length $D_{||} = R'\mathrm{d}r/\sqrt{1+\beta}$, we can define the *radial Hubble function* as

$$H_{||} \equiv \dot{D}_{||}/D_{||} = \dot{R}'/R'\,, \tag{4.3.13}$$

and similarly the *transverse Hubble function*:

$$H_{\perp} = \dot{R}/R\,. \tag{4.3.14}$$

Of course the two definitions coincide for the FLRW metric. The non-vanishing components of the Ricci tensor for the LTB metric are

$$R_0^0 = \frac{2\ddot{R}}{R} + \frac{\ddot{R}'}{R'}\,, \tag{4.3.15}$$

$$R_1^1 = \frac{2\dot{R}\dot{R}' + R\ddot{R}' - \beta'}{RR'}\,, \tag{4.3.16}$$

$$R_2^2 = R_3^3 = \frac{\dot{R}^2 - \beta}{R^2} + \frac{\dot{R}\dot{R}' + R'\ddot{R} - \beta'/2}{RR'}\,. \tag{4.3.17}$$

In terms of the two Hubble functions, we find that the Friedmann equations for the pressureless matter density $\rho_m(t,r)$ are given by [28]

$$H_\perp^2 + 2H_{||}H_\perp - \frac{\beta}{R^2} - \frac{\beta'}{RR'} = 8\pi G\rho_m\,, \tag{4.3.18}$$

$$6\frac{\ddot{R}}{R} + 2H_\perp^2 - 2\frac{\beta}{R^2} - 2H_{||}H_\perp + \frac{\beta'}{RR'} = -8\pi G\rho_m\,. \tag{4.3.19}$$

Adding Eqs. (4.3.18) and (4.3.19), it follows that $2R\ddot{R} + \dot{R}^2 = \beta$. Integrating this equation, we obtain a Friedmann-like equation

$$H_\perp^2 = \frac{\alpha(r)}{R^3} + \frac{\beta(r)}{R^2}\,, \tag{4.3.20}$$

where $\alpha(r)$ is a free function that we can use along with $\beta(r)$ to describe the inhomogeneity. From this we can define an effective density parameter $\Omega_m^{(0)}(r) = \Omega_m(r,t_0)$ today:

$$\Omega_m^{(0)}(r) \equiv \frac{\alpha(r)}{R_0^3 H_{\perp 0}^2}\,, \tag{4.3.21}$$

where $R_0 \equiv R(r,t_0) = r$, $H_{\perp 0} \equiv H_\perp(r,t_0)$ (the superscript (0) denotes the present value) and an effective spatial curvature

$$\Omega_K^{(0)}(r) = 1 - \Omega_m^{(0)}(r) = \frac{\beta(r)}{R_0^2 H_{\perp 0}^2}\,. \tag{4.3.22}$$

Hence, we see that the initial condition at some time t_0 (which here we take as the present time) must specify two free functions of r, for instance $\alpha(r), \beta(r)$ or $\Omega_m^{(0)}(r), H_{\perp 0}(r)$. The latter choice shows that the inhomogeneity can be in the matter distribution or in the expansion rate or in both. This freedom can be used to fit simultaneously for any expansion rate (and therefore luminosity and angular diameter distances [771]) and for any source number density [681].

If one imposes the additional constraint that the age of the universe is the same for every observer, then only one free function is left [380]. The same occurs if one chooses $\Omega_m^{(0)}(r) =$ constant (notice that this is different from $\rho_m^{(0)}(r) =$ constant, which is another possible choice), i.e., if the matter density fraction is assumed homogeneous today (and only today) [341]. The choice of a homogeneous universe age guarantees against the existence of diverging inhomogeneities in the past. However, there is no compelling reason to impose such restrictions.

Eq. (4.3.20) is the classical cycloid equation whose solution for $\beta > 0$ is given parametrically by

$$R(r,\eta) = \frac{\alpha(r)}{2\beta(r)}(\cosh\eta - 1) = \frac{R_0\Omega_m^{(0)}(r)}{2[1-\Omega_m^{(0)}(r)]}(\cosh\eta - 1)\,, \tag{4.3.23}$$

$$t(r,\eta) - t_B(r) = \frac{\alpha(r)}{2\beta^{3/2}(r)}(\sinh\eta - \eta) = \frac{\Omega_m^{(0)}(r)}{2[1-\Omega_m^{(0)}(r)]^{3/2}H_{\perp 0}}(\sinh\eta - \eta)\,, \tag{4.3.24}$$

where $t_B(r) = t(r, \eta = 0)$ is the inhomogeneous "big-bang" time, i.e., the time for which $\eta = 0$ and $R = 0$ for a point at comoving distance r. This can be put to zero in all generality by a redefinition of time. The "time" variable η is defined by the relation

$$\eta = \int_0^t \frac{\beta(r)^{1/2}}{R(\tilde{t}, r)} \mathrm{d}\tilde{t} \,. \tag{4.3.25}$$

Notice that the "time" η that corresponds to a given t depends on r; so $R(r, t)$ is found by solving numerically $\eta(t, r)$ from Eq. (4.3.24) and then substituting $R[r, \eta(r, t)]$. The present epoch $\eta_0(r)$ is defined by the condition $R = R_0$. In the problem [10.2] we will derive the age of the universe $t_{\rm age}(r) = t(r, \eta_0) - t_B(r)$ in terms of $\Omega_m^{(0)}, H_{\perp 0}$. For $\beta < 0$ the η functions in Eqs. (4.3.23–4.3.24) become $(1 - \cos\eta)$ and $(\eta - \sin\eta)$ for R and t, respectively, while for $\beta = 0$ they are $\eta^2/2$ and $\eta^3/6$: we will not consider these cases further.

As anticipated, since we need to have a faster expansion inside some distance to mimic cosmic acceleration, we need to impose to our solution the structure of a void. An example of the choice of $\Omega_m^{(0)}(r) \equiv \Omega_m(r, t_0), h^{(0)}(r) \equiv H_{\perp 0}/(100 \text{ km s}^{-1} \text{ Mpc}^{-1})$ is [380]

$$\Omega_m^{(0)}(r) = \Omega_{\rm out} + (\Omega_{\rm in} - \Omega_{\rm out}) f(r, r_0, \Delta) \,, \tag{4.3.26}$$

$$h^{(0)}(r) = h_{\rm out} + (h_{\rm in} - h_{\rm out}) f(r, r_0, \Delta) \,, \tag{4.3.27}$$

with

$$f(r, r_0, \Delta) = \frac{1 - \tanh[(r - r_0)/2\Delta]}{1 + \tanh(r_0/2\Delta)} \,, \tag{4.3.28}$$

representing the transition function of a shell of radius r_0 and thickness Δ. The six constants $\Omega_{\rm in}, \Omega_{\rm out}, h_{\rm in}, h_{\rm out}, r_0, \Delta$ completely fix the model. If $h_{\rm in} > h_{\rm out}$ we can mimic the accelerated expansion.

In order to compare the LTB model to observations we need to generalize two familiar concepts: redshift and luminosity distance. The redshift can be calculated through the equation [27]

$$\frac{\mathrm{d}z}{\mathrm{d}r} = (1 + z) \frac{\dot{R}'}{\sqrt{1 + \beta}} \,, \tag{4.3.29}$$

where $R(t, r)$ must be calculated on the trajectory $t_p(r)$ and we must impose $z(r = 0) = 0$. Every LTB function, e.g., $H_\perp(t, r), R(t, r)$ etc. can be converted into line-of-sight functions of redshift by evaluating the arguments $r_p(z), t_p(z)$ along the past light cone.

The proper area of an infinitesimal surface at $r, t =$ constant is given by $A = R^2(r, t) \sin\theta \, \mathrm{d}\theta \, \mathrm{d}\phi$. The angular diameter distance is the square root of $A/(\sin\theta \, \mathrm{d}\theta \, \mathrm{d}\phi)$ so that $d_A(z) = R(t_p(z), r_p(z))$. Since the Etherington duality relation $d_L = (1 + z)^2 d_A$ remains valid in inhomogeneous models, we have [530]

$$d_L(z) = (1 + z)^2 R(t_p(z), r_p(z)) \,. \tag{4.3.30}$$

This clearly reduces to $d_L = (1+z)r(z)$ in the FLRW background. Armed with these observational tools, we can compare any LTB model to the observations.

Besides matching the SN Ia Hubble diagram, we do not want to spoil the CMB acoustic peaks and we also need to impose a local density $\Omega_{\rm in}$ near $0.1-0.3$, a flat space outside (to fulfil inflationary predictions), i.e., $\Omega_{\rm out} = 1$, and finally the observed local Hubble value $h_{\rm in} \approx 0.7 \pm 0.1$. The CMB requirement can be satisfied by a small value of $h_{\rm out}$, since we know that to compensate for $\Omega_{\rm out} = 1$ we need a small Hubble rate (remember that the CMB essentially constrains $\Omega_m^{(0)} h^2$). This fixes $h_{\rm out} \approx 0.5$. So we are left with only r_0 and Δ to be constrained by SN Ia. As anticipated we expect r_0 to be near $z = 0.5$, which in the standard ΛCDM model gives a distance $r(z) \approx 2$ Gpc. An analysis using SN Ia data [382] finds that $r_0 = 2.3 \pm 0.9$ Gpc and $\Delta/r_0 > 0.2$. Interestingly, a "cold spot" in the CMB sky could be attributed to a void of comparable size [269, 642].

There are many more constraints one can put on such large inhomogeneities. Matter inside the void moves with respect to CMB photons coming from outside. So the hot intracluster gas will scatter the CMB photons with a large peculiar velocity and this will induce a strong kinematic Sunyaev–Zel'dovich effect [381]. Moreover, secondary photons scattered towards us by reionized matter inside the void should also distort the black-body spectrum due to the fact that the CMB radiation seen from anywhere in the void (except from the center) is anisotropic and therefore at different temperatures [197]. These two constraints require the voids not to exceed 1 or 2 Gpc, depending on the exact modelling and are therefore already in mild conflict with the fit to supernovae.

Moreover, while in the FLRW background the function $H(z)$ fixes the comoving distance $\chi(z)$ up to a constant curvature (and consequently also the luminosity and angular diameter distances), in the LTB model the relation between $\chi(z)$ and $H_\perp(z)$ or $H_\parallel(z)$ can be arbitrary. That is, one can choose the two spatial free functions to be for instance $H_\perp(r,0)$ and $R(r,0)$, from which the line-of-sight values $H_\perp(z)$ and $\chi(z)$ would also be arbitrarily fixed. This shows that the "consistency" FLRW relation between $\chi(z)$ and $H(z)$ is violated in the LTB model, and in general in any strongly inhomogeneous universe.

Further below we discuss how this consistency test can be exploited by Euclid to test for large-scale inhomogeneities. Recently, there has been an implementation of LTB models in large-scale structure N-body simulations [30], where inhomogeneities grow in the presence of a large-scale void and seen to follow the predictions of linear perturbation theory.

An interesting class of tests on large-scale inhomogeneities involve probes of the growth of structure. However, progress in making theoretical predictions has been hampered by the increased complexity of cosmological perturbation theory in the LTB spacetime, where scalar and tensor perturbations couple, see for example [241]. Nevertheless, a number of promising tests of large-scale inhomogeneity using the growth of structure have been proposed. [29] used N-body simulations to modify the Press–Schechter halo mass function, introducing a sensitive dependence on the background shear. The shear vanishes in spatially-homogeneous models, and so a direct measurement of this quantity would put stringent constraints on the level of background inhomogeneity, independent of cosmological model assumptions. Furthermore, recent upper limits from the ACT and SPT experiments on the linear, all-sky kinematic Sunyaev–Zel'dovich signal at $\ell = 3000$, a probe of the peculiar velocity field, appear to put strong constraints on voids [986]. This result depends sensitively on theoretical uncertainties on the matter power spectrum of the model, however.

Purely geometric tests involving large-scale structure have been proposed, which neatly sidestep the perturbation theory issue. The Baryon Acoustic Oscillations (BAO) measure a preferred length scale, $d(z)$, which is a combination of the acoustic length scale, l, set at matter-radiation decoupling, and projection effects due to the geometry of the universe, characterized by the volume distance, $D_V(z)$. In general, the volume distance in an LTB model will differ significantly from that in the standard model, even if the two predict the same SN Ia Hubble diagram and CMB power spectrum. Assuming that the LTB model is almost homogeneous around the decoupling epoch, l may be inferred from CMB observations, allowing the purely geometric volume distance to be reconstructed from BAO measurements. It has been shown by [990] that, based on these considerations, recent BAO measurements effectively rule out giant void models, independent of other observational constraints.

The tests discussed so far have been derived under the assumption of a homogeneous Big Bang (equivalent to making a particular choice of the bang time function). Allowing the Big Bang to be inhomogeneous considerably loosens or invalidates some of the constraints from present data. It has been shown [187] that giant void models with inhomogeneous bang times can be constructed to fit the SN Ia data, WMAP small-angle CMB power spectrum, and recent precision measurements of h simultaneously. This is contrary to claims by, e.g., [767], that void models are ruled out

by this combination of observables. However, the predicted kinematic Sunyaev–Zel'dovich signal in such models was found to be severely incompatible with existing constraints. When taken in combination with other cosmological observables, this also indicates a strong tension between giant void models and the data, effectively ruling them out.

4.3.4 Inhomogeneous models: Backreaction

In general, we would like to compute directly the impact of the inhomogeneities, without requiring an exact and highly symmetric solution of Einstein's equations like FLRW or even LTB. Unfortunately there is no easy way to approach this problem. One ansatz tries to construct average quantities that follow equations similar to those of the traditional FLRW model, see e.g., [185, 751, 752, 186]. This approach is often called *backreaction* as the presence of the inhomogeneities acts on the background evolution and changes it. In this framework, it is possible to obtain a set equations, often called Buchert equations, that look surprisingly similar to the Friedmann equations for the averaged scale factor $a_{\mathcal{D}}$, with extra contributions:

$$3\left(\frac{\dot{a}_{\mathcal{D}}}{a_{\mathcal{D}}}\right)^2 - 8\pi G\left\langle\varrho\right\rangle_{\mathcal{D}} - \Lambda = -\frac{\left\langle\mathcal{R}\right\rangle_{\mathcal{D}} + \mathcal{Q}_{\mathcal{D}}}{2}\,, \tag{4.3.31}$$

$$3\frac{\ddot{a}_{\mathcal{D}}}{a_{\mathcal{D}}} + 4\pi G\left\langle\varrho\right\rangle_{\mathcal{D}} - \Lambda = \mathcal{Q}_{\mathcal{D}}\,, \tag{4.3.32}$$

Here $\mathcal{R}$ is the 3-Ricci scalar of the spatial hypersurfaces and $\mathcal{Q}$ is given by

$$\mathcal{Q}_{\mathcal{D}} = \frac{2}{3}\left\langle\left(\theta - \left\langle\theta\right\rangle_{\mathcal{D}}\right)^2\right\rangle_{\mathcal{D}} - 2\left\langle\sigma^2\right\rangle_{\mathcal{D}}\,, \tag{4.3.33}$$

i.e., it is a measure of the variance the expansion rate θ and of the shear σ_{ij}. We see that this quantity, if it is positive, can induce an accelerated growth of $a_{\mathcal{D}}$, which suggests that observers would conclude that the universe is undergoing accelerated expansion.

However, it is not possible to directly link this formalism to observations. A first step can be done by imposing by hand an effective, average geometry with the help of a template metric that only holds on average. The probably simplest first choice is to impose on each spatial hypersurface a spatial metric with constant curvature, by imagining that the inhomogeneities have been smoothed out. But in general the degrees of freedom of this metric (scale factor and spatial curvature) will not evolve as in the FLRW case, since the evolution is given by the full, inhomogeneous universe, and we would not expect that the smoothing of the inhomogeneous universe follows exactly the evolution that we would get for a smooth (homogeneous) universe. For example, the average curvature could grow over time, due to the collapse of overdense structure and the growth (in volume) of the voids. Thus, unlike in the FRLW case, the average curvature in the template metric should be allowed to evolve. This is the case that was studied in [547].

While the choice of template metric and the Buchert equations complete the set of equations, there are unfortunately further choices that need to be made. Firstly, although there is an integrability condition linking the evolution of $\left\langle\mathcal{R}\right\rangle_{\mathcal{D}}$ and $\mathcal{Q}_{\mathcal{D}}$ and in addition a consistency requirement that the effective curvature $\kappa(t)$ in the metric is related to $\left\langle\mathcal{R}\right\rangle_{\mathcal{D}}$, we still need to impose an overall evolution by hand as it was not yet possible to compute this from first principles. Larena assumed a scaling solution $\left\langle\mathcal{R}\right\rangle_{\mathcal{D}} \propto a_{\mathcal{D}}^n$, with n a free exponent. In a dark energy context, this scaling exponent n corresponds to an effective dark energy with $w_{\mathcal{D}} = -(n+3)/3$, but in the backreaction case with the template metric the geometry is different from the usual dark energy case. A perturbative analysis [569] found $n = -1$, but of course this only an indication of the possible behavior as the situation is essentially non-perturbative.

The second choice concerns the computation of observables. [547] studied distances to supernovae and the CMB peak position, effectively another distance. The assumption taken was that

distances could be computed within the averaged geometry as if this was the true geometry, by integrating the equation of radial null geodesics. In other words, the effective metric was taken to be the one that describes distances correctly. The resulting constraints are shown in Figure 51. We see that the leading perturbative mode ($n = 1$) is marginally consistent with the constraints. These contours should be regarded as an indication of what kind of backreaction is needed if it is to explain the observed distance data.

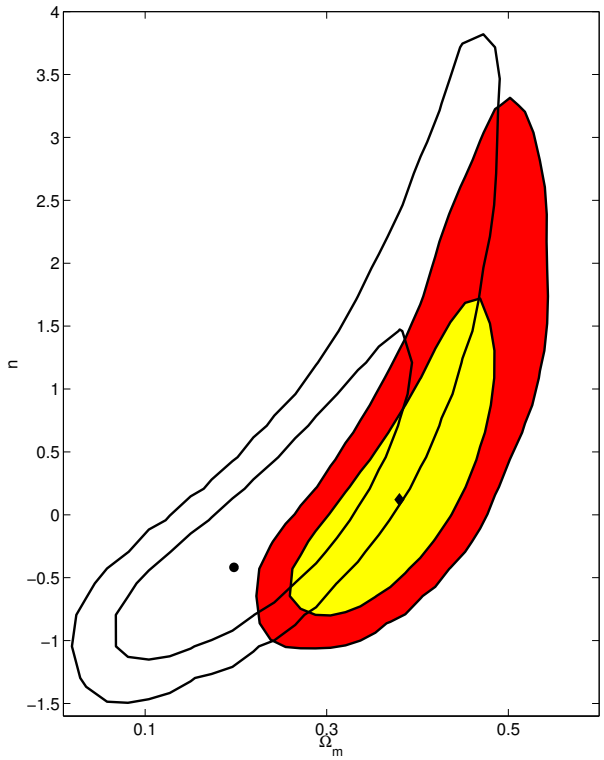

Figure 51: Supernovae and CMB constraints in the ($\Omega_m^{\mathcal{D}_0}$,n) plane for the averaged effective model with zero Friedmannian curvature (filled ellipses) and for a standard flat FLRW model with a quintessence field with constant equation of state $w = -(n + 3)/3$ (black ellipses). The disk and diamond represent the absolute best-fit models respectively for the standard FLRW model and the averaged effective model.

One interesting point, and maybe the main point in light of the discussion in the following section, is that the averaged curvature needs to become necessarily large at late times due to the link between it and the backreaction term $\mathcal{Q}$, in order to explain the data. Just as in the case of a huge void, this effective curvature makes the backreaction scenario testable to some degree with future large surveys like Euclid.

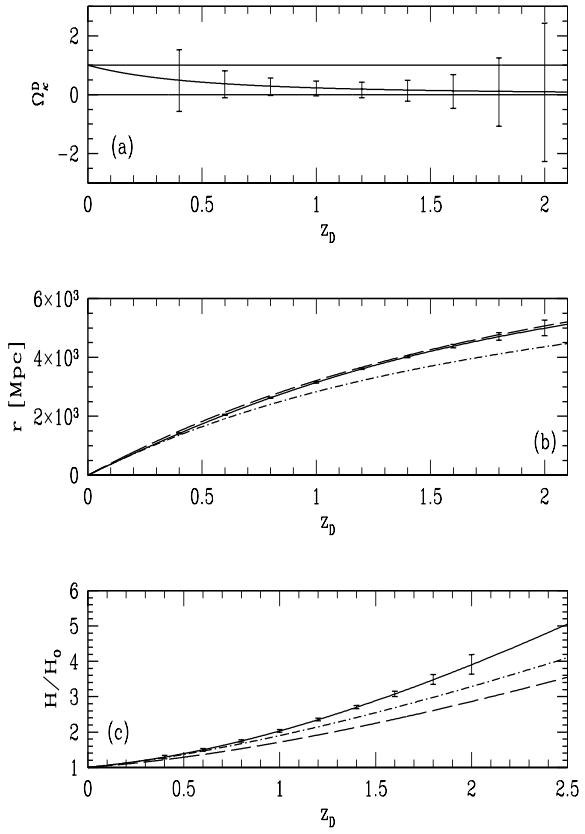

Figure 52: *Upper panel:* Evolution of $\Omega_k(z_{\mathcal{D}})$ as a function of redshift for the absolute best-fit averaged model represented by the diamond in Figure 51. One can see that all positively curved FLRW models ($\Omega_{k,0} < 0$) and only highly negatively curved FLRW models ($\Omega_{k,0} > 0.5$) can be excluded by the estimation of $\Omega_k(z_{\mathcal{D}})$. *Central panel:* Evolution of the coordinate distance for the best-fit averaged model (solid line), for a ΛCDM model with $\Omega_{m,0} = 0.277$, $\Omega_\Lambda = 0.735$ and $H_0 = 73$ km/s/Mpc (dashed line), and for the FLRW model with the same parameters as the best-fit averaged model (dashed-dotted line). *Lower panel:* Evolution of the Hubble parameter H/H_0 for the best-fit averaged model (solid line), the FLRW model with the same parameters as the averaged best-fit model (dashed-dotted line), and for the same ΛCDM model as in the central panel (dashed line). The error bars in all panels correspond to the expectations for future large surveys like Euclid.

4.4 Reconstructing the global curvature at different redshifts

Clarkson et al. [240] presented an observational test for the Copernican principle which relies on the consistency relation between expansion rate and angular diameter distance. Here we discuss the implications for Euclid.

Let us recall that the angular diameter distance in a FLRW model can be written as:

$$D_A(z) = \frac{1}{1+z}\frac{1}{H_0\sqrt{-\Omega_K^{(0)}}}\sin\left(\sqrt{-\Omega_K^{(0)}}\int_0^z dz'\frac{H_0}{H(z')}\right). \tag{4.4.1}$$

where $\Omega_K^{(0)}$ is the curvature parameter *today*.

We can invert the last equation to obtain an expression for the curvature parameter that depends on the Hubble parameter H and comoving angular diameter distance $D(z) = (1+z)\,D_A(z)$ only, see [240]:

$$\Omega_K^{(0)} = \frac{\left[H(z)\,D'(z)\right]^2 - 1}{\left[H_0 D(z)\right]^2} \tag{4.4.2}$$

where here the prime refers to the derivative with respect the redshift. Then Eq. (4.4.2) tells us how the curvature parameter can be measured from the distance and the Hubble rate observations, in a model-independent way.

The idea is then to measure the curvature parameter $\Omega_K^{(0)}$ at different redshifts. Let us consider again Eq. (4.4.2); if we are in a FLRW universe then $\Omega_K^{(0)}$ should be independent of redshift, i.e., its derivative with respect to z should be zero

$$\mathcal{C}(z) = \frac{\mathrm{d}\Omega_K^{(0)}}{\mathrm{d}z} = 0\,. \tag{4.4.3}$$

If it happens that $\mathcal{C}(z) \neq 0$ even at a single redshift then this means the large-scale universe is not homogeneous.

A possible test to measure $\Omega_K^{(0)}$ at various redshifts is provided by baryon acoustic oscillations. Observing the features of BAO in the galaxy power spectrum in both angular (orthogonal to the line of sight $L_\perp$) and radial direction (along the line of sight $L_\parallel$) allows us to measure with a great accuracy both $D_A(z)$ and $H(z)$, respectively.

If the geometry is not FLRW, then the standard BAO will be deformed in three different ways:

1. The sound horizon scale, which is the characteristic ruler, will be different in the $\perp$ and $\parallel$ directions and it will be also different from that for the FLRW universe.
2. Even if the sound horizon were isotropic at decoupling, the subsequent expansion in the $\perp$ and $\parallel$ directions will be different just because they will be governed by two distinct Hubble parameters: $H_\perp$ and $H_\parallel$.
3. The redshift distortion parameter will be different because it will depend on the background expansion.

Also the growth factor will be modified, perhaps in a scale dependent way. If the true underlying model is radically inhomogeneous, but we assume a FLRW in interpreting the observations, the derived cosmological parameters will be biased (or unphysical) and the parameters derived from BAO data will be different from those measured by SN Ia and/or lensing. As argued also in different contexts, a mismatch on the value of one of more parameters may indicate that we are assuming a wrong model.

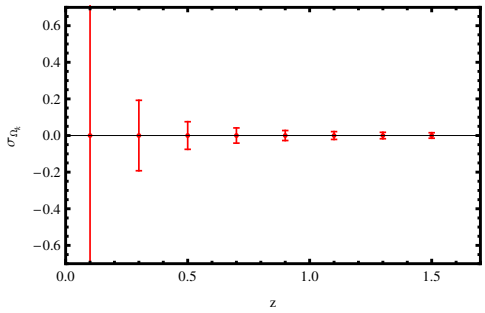

Figure 53: Relative errors on Ω_K for our benchmark survey for different redshifts.

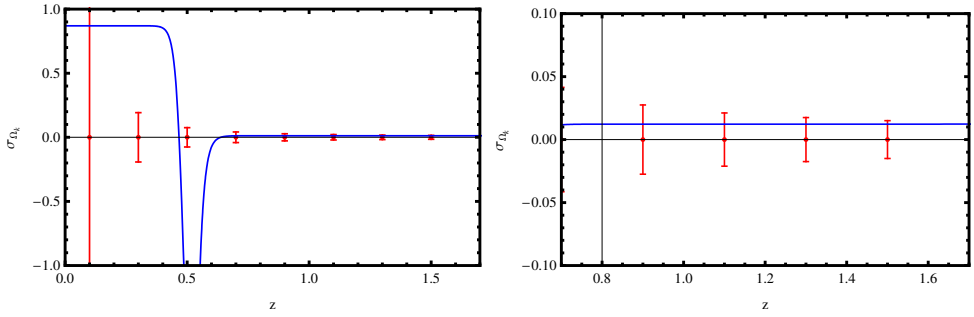

Figure 54: *Left:* same as Figure 53 but now with superimposed the prediction for the Lemaître–Tolman–Bondi model considered by [380]. *Right:* zoom in the high-redshift range.

We show here the sensitivity that can be reached with an experiment like Euclid for the curvature parameter $\Omega_K^{(0)}$ (Amendola and Sapone, in preparation). We choose a redshift survey with a depth of $z = 1.6$ and consider different redshift bins.

In Figure 53 we show the first 1σ absolute errors on the curvature parameter for different redshift bins that can be obtained measuring the Hubble parameter and the angular diameter distance. In obtaining these errors we used Fisher-based forecasts for the radial and angular BAO signal following [815, 338], as discussed in Section 1.7.3.

The sensitivity that can be reached with an experiment like Euclid is extremely high; we can measure the curvature parameter better than 0.02 at redshift of the order of $z \simeq 1$. This will allow us to discriminate between FLRW and averaged cosmology as for example illustrated in Figure 54.

An alternative to measuring the global curvature is to measure the shear of the background geometry. If there is a large inhomogeneous void then a congruence of geodesics will not only expand but also suffer shear [382]. The amount of shear will depend on the width and magnitude of the transition between the interior of the void and the asymptotic Einstein–de Sitter universe. Normalizing the shear w.r.t. the overall expansion, one finds [382]

$$\varepsilon = \frac{H_\perp(z) - H_{||}(z)}{2H_\perp + H_{||}} \simeq \frac{1 - H_{||}(z)\,\partial_z\Big[(1+z)\,D_A(z)\Big]}{3H_{||}(z)D_A(z) + 2\Big(1 - H_{||}(z)\,\partial_z\Big[(1+z)\,D_A(z)\Big]\Big)}\,. \tag{4.4.4}$$

Clearly, in homogeneous FRW universes the shear vanishes identically since $H_\perp = H_{||} = H$. Also note that the function $H_{||}(z)D_A(z)$ is nothing but the Alcock–Paczynski factor, which is normally used as a geometric test for the existence of vacuum energy in ΛCDM FRW models.

4.5 Speculative avenues: non-standard models of primordial fluctuations

In this section we explore other non-conventional scenarios that challenge our understanding of the universe. Here we present models that include mechanisms for primordial anisotropy in the fluctuation spectrum, due to spacetime non-commutativity, to inflationary vector fields or to super-horizon fluctuations. Since inflation can occur at high energies for which we lack robust direct experimental probes, it is reasonable to pay attention on possible deviations from some standard properties of low energy physics. We review these here and point out possible observables for the Euclid project.

4.5.1 Probing the quantum origin of primordial fluctuations

Conventionally, the 2-point correlation function of a random variable $X(\vec{k},t)$ is regarded as a classical object, related to the power spectrum P_X via the relation

$$\langle X(\vec{k},t)X(\vec{k}',t)\rangle = (2\pi)^3\delta(\vec{k}-\vec{k}')P_X(k)\ , \tag{4.5.1}$$

where $k=|\vec{k}|$.

When we look at $X(\vec{k},t)$ in terms of a *quantum field* in momentum space, we need to reinterpret the average $\langle\ldots\rangle$ as the expectation value of the 2-point function over a determined quantum state. This raises several issues that are usually ignored in a classical analysis. For instance, the value of the expectation value depends in the algebra of the annihilation and creation operators that compose the field operator. Any non-trivial algebra such as a non-commutative one, leads to non-trivial power spectra. Also, the quantum expectation value depends on the state of the field, and different choices can lead to radically different results.

Suppose that $\varphi(\vec{x},t)$ represents a perturbation propagating on an inflationary background. Upon quantization, we have

$$\hat{\varphi}(\vec{x},t) = (2\pi)^{-3/2}\int \mathrm{d}^3k\left[\varphi_k(t)\hat{a}_{\vec{k}}\,e^{i\vec{k}\cdot t} + \varphi_k^*(t)\hat{a}_{\vec{k}}^\dagger\,e^{-i\vec{k}\cdot t}\right]\ , \tag{4.5.2}$$

where $\hat{a}_{\vec{k}}$ is the usual annihilation operator. When calculated in the limit $\vec{k}\to\vec{k}'$, the expectation value of the two-point function in coordinate space diverges, signalling the breakdown of the theory at short distances. From the quantum field theory perspective, this means that the expectation value needs to be regularized in the ultraviolet (UV). It has been argued that this has in specific scenarios sizeable effects on the observable spectrum – see e.g., [15], see however e.g., [324] for a contrary viewpoint.

In addition to UV divergences, there are infrared (IR) ones in long-range correlations. Usually, one tames these by putting the universe in a box and cutting off super-horizon correlations. However, several authors have recently proposed more sensible IR regulating techniques, see e.g., [394, 523]. Very natural ways to obtain IR finite results are to take into account the presence of tiny spatial curvature or a pre-inflationary phase which alters the initial conditions [479, 523]. In principle these regularizations will leave an imprint in the large-scale structure data, in the case that regularization scale is not too far beyond the present horizon scale. If this pre-inflationary phase is characterized by modified field theory, such as modified dispersion relations or lower dimensional effective gravity, the scalar and tensor power spectra show a modification whose magnitude is model-dependent, see e.g., [770].

The two-point function of a scalar field is constructed from basic quantum field theory, according to a set of rules determined in the context of relativistic quantum mechanics. In particular, the

usual commutation rules between position and momentum are promoted to commutation rules between the field and its canonical conjugate. A modification of the fundamental quantum mechanical commutation rules can easily be generalized to field theory. The most popular case is represented by non-commutative geometry, which implies that coordinate operators do not commute, i.e.,

$$[\hat{x}^\mu, \hat{x}^\nu] = i\theta^{\mu\nu}\,, \tag{4.5.3}$$

where $\theta^{\mu\nu}$ is an anti-symmetric matrix, usually taken to be constant, see e.g., [846, 250]. There are many fundamental theories that phenomenologically reduce to an ordinary field theory over a non-commutative manifold, from string theory to quantum gravity. It is therefore important to consider the possibility that non-commutative effects took place during the inflationary era and try to extract some prediction.

One can construct models where the inflationary expansion of the universe is driven by non-commutative effects, as in [24, 769]. In this kind of models, there is no need for an inflaton field and non-commutativity modifies the equation of state in the radiation-dominated universe in a way that it generates a quasi-exponential expansion. The initial conditions are thermal and not determined by a quantum vacuum. For the model proposed in [24], the predictions for the power spectra have been worked out in [517]. Here, Brandenberger and Koh find that the spectrum of fluctuations is nearly scale invariant, and shows a small red tilt, the magnitude of which is different from what is obtained in a usual inflationary model with the same expansion rate.

On the other hand, non-commutativity could introduce corrections to standard inflation. Such a, perhaps less radical approach, consists in assuming the usual inflaton-driven background, where scalar and tensor perturbations propagate with a Bunch and Davies vacuum as initial condition, but are subjected to non-commutativity at short distance. It turns out that the power spectrum is modified according to (see e.g., [522], and references therein)

$$P = P_0\, e^{H\vec{\theta}\cdot\vec{k}}\,, \tag{4.5.4}$$

where H is the Hubble parameter, P_0 is the usual commutative spectrum, and $\vec{\theta}$ is the vector formed by the θ^{0i} components of $\theta^{\mu\nu}$. This prediction can be obtained by using a deformation of statistics in non-commutative spacetime on the usual inflationary computation. It can be also derived in an alternative way beginning from an effective deformation of the Heisenberg algebra of the inflaton field. The most important aspect of the result is that the spectrum becomes direction-dependent. The perturbations thus distinguish a preferred direction given by the vector $\vec{\theta}$ that specifies the non-commutativity between space and time.

Furthermore, it is interesting that the violation of isotropy can also violate parity. This could provide what seems a quite unique property of possible signatures in the CMB and large-scale structure. However, there is also an ambiguity with the predictions of the simplest models, which is related to interpretations of non-commuting quantum observables at the classical limit. This is evident from the fact that one has to consider an effectively imaginary $\vec{\theta}$ in the above formula (4.5.4). Reality of physical observables requires the odd parity part of the spectrum (4.5.4) to be imaginary. The appearance of this imaginary parameter $\vec{\theta}$ into the theory may signal the unitary violation that has been reported in theories of time-space non-commutativity. It is known that the Seiberg–Witten map to string theory applies only for space-space non-commutativity [810]. Nevertheless, the phenomenological consequence that the primordial fluctuations can distinguish handedness, seems in principle a physically perfectly plausible – though speculative – possibility, and what ultimately renders it very interesting is that we can test by cosmological observations. Thus, while lacking the completely consistent and unique non-commutative field theory, we can parametrize the ambiguity by a phenomenological parameter whose correct value is left to be determined observationally. The parameter $\alpha \in [0, 1]$ can be introduced [522] to quantify the

relative amplitude of odd and even contributions in such a way that $P = \alpha P^+ + i(1-\alpha)P^-$, where $P^\pm = (P(\vec{k}) \pm P(-\vec{k}))/2$.

The implications of the anisotropic power spectra, such as (4.5.4), for the large-scale structure measurements, is discussed below in Section 4.5.3. Here we proceed to analyse some consequences of the non-commutativity relation (4.5.3) to the higher order correlations of cosmological perturbations. We find that they can violate both isotropy and parity symmetry of the FRW background. In particular, the latter effect persists also in the case $\alpha = 1$. This case corresponds to the prescription in [18] and in the remainder of this subsection we restrict to this case for simplicity. Thus, even when we choose this special prescription where the power spectrum is even, higher order correlations will violate parity. This realizes the possibility of an odd bispectrum that was recently contemplated upon in [489].

More precisely, the functions B defined in Eq. (3.3.4) for the three-point function of the curvature perturbation can be shown to have the form

$$\begin{aligned} B_\Phi(\vec{k}_1, \vec{k}_2, \vec{k}_3) = {} & 2\cos\left(\vec{k}_1 \wedge \vec{k}_2\right)\Big(\cosh(2H\vec{\theta}\cdot\vec{k}_3)P_0(\vec{k}_1)P_0(\vec{k}_2)f_s(\vec{k}_3) + 2\,\text{perm.}\Big) \\ & - 2i\sin\left(\vec{k}_1 \wedge \vec{k}_2\right)\Big(\sinh(2H\vec{\theta}\cdot\vec{k}_3)P_0(\vec{k}_1)P_0(\vec{k}_2)f_s(\vec{k}_3) + 2\,\text{perm.}\Big)\,, \end{aligned} \tag{4.5.5}$$

where the function $f_s(k)$ is

$$f_s(k) = \frac{N''}{2N'^2}\left(1 + n_{f_{\rm NL},0}\,\ln\frac{k}{k_p}\right)\,, \tag{4.5.6}$$

k_p being a pivot scale and primes denoting derivatives with respect to the inflaton field. The quantity $n_{f_{\rm NL},0}$ is the scale dependence in the commutative case explicitly given by

$$n_{f_{\rm NL},0} = \frac{N'}{N''}\left(-3\eta + \frac{V'''}{3H^2}\right)\,. \tag{4.5.7}$$

The spatial components of the non-commutativity matrix θ_{ij} enter the bispectrum through the phase $\vec{k}_1 \wedge \vec{k}_2 = k_1^i k_2^j\,\theta_{ij}$. They do not appear in the results for the spectrum and therefore affect only the non-Gaussian statistics of primordial perturbations.

We now focus on this part in the following only and set all components of $\vec{\theta}$ equal to zero. This gives

$$f_{{\rm NL},\theta} = \frac{5}{3}\cos\left(\vec{k}_1 \wedge \vec{k}_2\right)\frac{P_0(k_1)P_0(k_2)f_s(k_3) + 2\,\text{perm.}}{P_0(k_1)P_0(k_2) + 2\,\text{perm.}}\,, \tag{4.5.8}$$

where the only contribution from the non-commutativity is the pre-factor involving the wedge product. This affects the scale dependence of $n_{f_{{\rm NL},\theta}}$ and can hence be constrained observationally. For example, computing the scale-dependence for shape preserving variations of the momentum space triangle, $\vec{k}_i \to \lambda\vec{k}_i$, defined as

$$n_{f_{{\rm NL},\theta}} = \left.\frac{\partial \ln|f_{{\rm NL},\theta}(\lambda\vec{k}_1, \lambda\vec{k}_2, \lambda\vec{k}_3)|}{\partial \ln\lambda}\right|_{\lambda=1}\,, \tag{4.5.9}$$

we find, in the present case

$$n_{f_{{\rm NL},\theta}} = -2k_1^i k_2^j\theta_{ij}\tan(k_1^i k_2^j\theta_{ij}) + n_{f_{\rm NL},0}\,, \tag{4.5.10}$$

where $n_{f_{\rm NL},0}$ given by (4.5.7) is the result in the commuting case. The part dependent on θ_{ij} arises purely from non-commutative features. The Euclid data can be used to constrain the scale dependence of the nonlinearity parameter $f_{{\rm NL},\theta}$, and the scale dependence could therefore place interesting bounds on θ_{ij}. We note however that the amplitude of the nonlinearity is not enhanced by

the purely spatial non-commutativity, but is given by the underlying inflationary model. The amplitude on the other hand is exponentially enhanced by the possible timespace non-commutativity.

Moreover, it is worth noting that the result (4.5.10) depends on the wave vectors $\vec{k}_1$ and $\vec{k}_2$ and hence on the shape of the momentum space triangle. This is in contrast with the commutative case, where the scale dependence is given by the same result (4.5.7)for all shape preserving variations, $\vec{k}_i \to \lambda\vec{k}_i$, regardless of triangle shape. This allows, in principle, to distinguish between the contributions arising from the non-commutative properties of the theory and from the standard classical inflationary physics or gravitational clustering.

To recapitulate, parity violations in the statistics of large-scale structures would be a smoking gun signature of timespace non-commutativity at work during inflation. Moreover, purely spatial non-commutativity predicts peculiar features in the higher order correlations of the perturbations, and in particular these can be most efficiently detected by combining information of the scale- and shape-dependence of non-Gaussianity. As discussed earlier in this document, this information is extractable from the Euclid data.

4.5.2 Early-time anisotropy

Besides the non-commutative effects seen in the previous section, anisotropy can be generated by the presence of anisotropic fields at inflation. Such could be spinors, vectors or higher order forms which modify the properties of fluctuations in a direction-dependent way, either directly through perturbation dynamics or by causing the background to inflate slightly anisotropically. The most common alternative is vector fields (see Section 4.5.2.1). Whereas a canonical scalar field easily inflates the universe if suitable initial conditions are chosen, it turns out that it much less straightforward to construct vector field alternatives. In particular, one must maintain a sufficient level of isotropy of the universe, achieve slow roll and keep perturbations stable. Approaches to deal with the anisotropy have been based on a "triad" of three identical vectors aligned with the three axis [59], a large number of randomly oriented fields averaging to isotropy [401], time-like [521] or sub-dominant [313] fields. There are many variations of inflationary scenarios involving vector fields, and in several cases the predictions of the primordial spectra of perturbations have been worked out in detail, see e.g., [946]. The generic prediction is that the primordial perturbation spectra become statistically anisotropic, see e.g., [7].

Anisotropy could be also regarded simply as a trace of the initial conditions set before inflation. One then assumes that inflation has lasted just about the 60 e-folds so that the largest observable scales were not yet smoothed out, or isotropized, by the early inflationary expansion [734]. Such a scenario can also be linked to various speculative ideas of pre-inflationary physics such as gravitational tunnelling into an anisotropic universe, see e.g., [9].

Also in this case the interest in such possibilities has been stimulated by several anomalies observed in the temperature WMAP maps, see [254] for a recent review (some of them were also present in the COBE maps). Their statistical evidence is quite robust w.r.t. the increase of the signal-to-noise ratio over the years of the WMAP mission and to independent tests by the international scientific community, although the a posteriori choice of statistics could make their interpretation difficult, see [122]. Apart from those already mentioned in Section 4.3.1, these anomalies include an alignment between the harmonic quadrupole and octupole modes in the temperature anisotropies [288], an asymmetric distribution of CMB power between two hemispheres, or dipole asymmetry [350], the lack of power of the temperature two-point correlation function on large angular scales ($> 60°$), asymmetries in the even vs. odd multipoles of the CMB power spectra (parity symmetry breaking), both at large [503, 409] and intermediate angular scales [122]. Some of the anomalies could be connected among each other, e.g., the CMB parity breaking has been recently linked to the lack of large-scale power [628, 253, 504].

4.5.2.1 Vector field models

Various inflationary models populated by vector fields can be described with a Lagrangian of the following form

$$L_{\rm vector} = -\frac{1}{4} f(\varphi) F_{\mu\nu} F^{\mu\nu} + \frac{1}{2} m^2 B_\mu B^\mu \,, \tag{4.5.11}$$

where $F_{\mu\nu} \equiv \partial_\mu B_\nu - \partial_\nu B_\mu$, and $f(\varphi)$ is a suitable function of the inflaton field. A Lagrangian containing just the standard kinetic term $F_{\mu\nu}F^{\mu\nu}$ would be conformally invariant thus preventing fluctuations of the vector field B_μ to be excited on super-horizon scales. Contrary to the case of a light scalar field, large-scale primordial perturbations of the vector field can be generated during inflation if the vector field is sufficiently massive (with $m^2 \approx -2H^2$). This Lagrangian includes the case of a massive (curvaton) vector field (when $f \equiv 1$) studied by [312, 313] and where the mass of the vector field is acquired via a non-minimal coupling to gravity to break conformal invariance. For some of these models there are actually some instability issues about the evolution of the primordial longitudinal perturbation modes of the vector field [435, 434]. The models with varying kinetic function (when $f(\varphi)$ is switched on) allows to overcome these difficulties, since in this case the longitudinal mode is gauged away. They have been studied in various contexts (e.g., [973, 314]). The Ackerman–Carroll–Wise models, [7], employ a different Lagrangian of the form $L_{\rm vector} = -\frac{1}{4}F_{\mu\nu}F^{\mu\nu} + \lambda(B^\mu B_\mu - m^2)$, so that the norm of the vector field is fixed by the Lagrangian multiplier λ. In these models (where inflation is driven by an inflaton field) the main effect of the vector field is a slightly anisotropic background evolution described by a metric, with $c(t) = b(t)$) with a backreaction on the inflaton field fluctuations, rather than the vector field perturbations themselves. Another possibility that has been explored is based on a non-Abelian gauge $SU(2)$ vector multiplet [92, 91], providing a realistic model of gauge interactions neglected so far.

A general prediction from all these scenarios is that the power spectrum of primordial perturbations can be written as

$$P(\mathbf{k}) = P(k)\left[1 + g(k)(\hat{\mathbf{k}}\cdot\hat{\mathbf{n}})^2\right] \,, \tag{4.5.12}$$

where $g(k)$ is the amplitude of the rotational invariance breaking (statistical isotropy breaking) induced by a preferred direction $\mathbf{n}$. Thus, the power spectrum is not just a function of k but it depends on the wave vector $\mathbf{k}$. Usually the preferred direction is related to the vector fields $n^i \propto B^i$ while the amplitude is related to the contribution of the vector field perturbations to the total curvature perturbation $g \sim P_{\zeta_B}/P_\zeta$.

However, beyond the various concrete realizations, the expression (4.5.12), first introduced in [7], provides a robust and useful way to study observable consequences of a preferred direction during inflation and also a practical template for comparison with observations (see below). Usually the amplitude $g(k)$ is set to a constant g_*. A generalization of the above parametrization is $P(\mathbf{k}) = P(k)\left[1 + \sum_{LM} g_{\rm LM}(k) Y_{LM}(\hat{\mathbf{k}})\right]$, where $Y_{\rm LM}(\hat{\mathbf{k}})$ are spherical harmonics with only even multipoles $L \geq 2$ [746]. Interestingly enough, inflationary models with vector fields can also generate higher-order correlators, such as bispetrum and trispectrum, which display anisotropic features as well (e.g., [973, 492, 92, 91]).

4.5.2.2 Modulated perturbations

The alignment of low CMB multipoles and the hemispherical power asymmetry observed in the CMB anisotropies can find an explanation in some models where the primordial gravitational perturbation is the result of fluctuations within our Hubble volume, modulated by super-horizon fluctuations. The primordial gravitational perturbation can thus be thought of as a product of two

fields $\Phi_1(\mathbf{x})$ and $\Phi_2(\mathbf{x})$ ([333], and references therein)

$$\Phi(\mathbf{x}) = \Phi_1(\mathbf{x})\,[1 + \Phi_2(\mathbf{x})]\ , \tag{4.5.13}$$

with $\Phi_2(\mathbf{x})$ where $\Phi_2(\mathbf{x})$ has only super-horizon fluctuations, so that within a given Hubble volume it takes a fixed value, while $\Phi_1(\mathbf{x})$ has sub-horizon stochastic fluctuations within that volume. The result is that an observer within our Hubble volume would see broken statistical homogeneity from the modulation on large scales of $\Phi_1(\mathbf{x})$, and also broken statistical isotropy from the gradient of the modulating field $\Phi_2(\mathbf{x})$. The dipole modulation $\delta T(\hat{\mathbf{p}})/T = S(\hat{\mathbf{p}})\,[1 + A(\hat{\mathbf{p}} \cdot \hat{\mathbf{n}})]$ used for CMB by, e.g., [348] and [423] (or for LSS [437]) to explain the hemispherical asymmetry falls within the parametrization of Eq. (4.5.13). A scenario with a dipole modulation has been realized in some concrete and detailed models, such as those involving adiabatic and isocurvature modulating perturbations from a curvaton field [346, 345].

4.5.3 Current and future constraints from CMB and LSS on an anisotropic power spectrum

Groeneboom and Eriksen [405], using WMAP5 year data (up to multipoles $\ell = 400$), claimed a detection of a quadrupolar power spectrum of the form of Eq. (4.5.12) at more than 3σ ($g_* = 0.15 \pm 0.039$) with preferred direction $(l, b) = (110°, 10°)$. Subsequently this result has been put under further check. [423] confirmed this effect at high statistical significance, pointing out however that beam asymmetries could be a strong contaminant (see also [424]). The importance of this systematic effect is somewhat debated: [404], including polarization and beam asymmetries analysis excluded that the latter can be responsible for the observed effect. Their claim is a 9σ detection with $g_* = 0.29 \pm 0.031$. However, the preferred direction shifted much closer to the ecliptic poles, which is probably an indication that some unknown systematic is involved and must be corrected in order to obtain true constraints on any primordial modulation. Foregrounds and noise are disfavored as possible systematic effects [122, 405]. Thus the cause of this kind of asymmetry is not definitely known. Planck should be able to detect a power quadrupole as small as 2% (at 3σ) [746, 405, 404]. It is of course desirable to test this (and other anisotropic effects) with other techniques.

What about large-scale structure surveys? Up to now there are just a few analyses testing anisotropies in large-scale structure surveys, but all of them have been crucial, indicating that large-scale structure surveys such as Euclid offer a promising avenue to constrain these features.

Hirata [437] used high-redshift quasars from the Sloan Digital Sky Survey to rule out the simplest version of dipole modulation of the primordial power spectrum. In comparison the Planck mission using the CMB hemispherical asymmetry would only marginally distinguish it from the standard case [348]. The constraints obtained by high-redshift quasars require an amplitude for the dipole modulation 6 times smaller than the one required by CMB. This would disfavor the simple curvaton spatial gradient scenario [346] proposed to generate this dipole modulation. Only a curvaton scenario with a non-negligible fraction of isocurvature perturbations at late times could avoid this constraint from current high-redshift quasars [345].

Pullen and Hirata [745] considered a sample of photometric luminous red galaxies from the SDSS survey to assess the quadrupole anisotropy in the primordial power spectrum of the type described by Eq. (4.5.12). The sample is divided into eight redshift slices (from $z = 0.2$ up to $z = 0.6$), and within each slice the galaxy angular power spectrum is analysed. They also accounted for possible systematic effects (such as a modulation of the signal and noise due to a slow variation of the photometric calibration errors across the survey) and redshift-space distortion effects. In this case

[745]

$$C_g(\mathbf{n},\mathbf{n}') = \langle \delta_g(\mathbf{n})\delta_g(\mathbf{n}')\rangle = \sum_l \frac{2l+1}{4\pi} C_{g,l} P_l(\mathbf{n}\cdot\mathbf{n}') + \sum_{LM}\sum_{lml'm'} D^{LM}_{g,ll'} X^{LM}_{lml'm'} R_{lm}(\mathbf{n}) R_{l'm'}(\mathbf{n}') \,. \tag{4.5.14}$$

Here, the set of $C_{g,l}$s are given by the usual galaxy angular power spectrum for the case of statistical isotropy. Statistical anisotropy produces the second term

$$D^{LM}_{g,ll'} = \mathrm{i}^{l-l'} \frac{2}{\pi} \int_0^\infty \mathrm{d}k\, k^2 P_g(k) g_{LM} W_l(k) W_{l'}(k) \,, \tag{4.5.15}$$

where $X^{LM}_{lml'm'}$ are geometric coefficients related to Wigner $3-j$ symbols, R denotes the real spherical harmonics (see Eqs. (3) and (13) of [746] for more details), $P_g(k) = b_g^2 P(k)$ is the isotropic galaxy power spectrum and $W_l(k) = \int \mathrm{d}\chi f(\chi) j_l(k\chi)$ is the window function (χ is the comoving distance, and $f(\chi)$ is the selection function, i.e., the normalized redshift distribution for a redshift slice).

Assuming the same preferred direction singled out by [405], they derive a constraint on the anisotropy amplitude $g_* = 0.006 \pm 0.036$ (1σ), thus finding no evidence for anisotropy. Marginalizing over $\mathbf{n}$ with a uniform prior they find $-0.41 < g_* < 0.38$ at 95% C.L. These results could confirm that the signal seen in CMB data is of systematic nature. However, it must be stressed that CMB and LSS analyses probe different scales, and in general the amplitude of the anisotropy is scale dependent $g = g(k)$, as in the model proposed in [345]. An estimate for what an experiment like Euclid can achieve is to consider how the uncertainty in g_* scale in terms of number of modes measured and the number of redshift slices. Following the arguments of [745], the uncertainty will scale roughly as $\ell_{\rm max}^{-1} N_z^{-1/2}$, where $\ell_{\rm max}$ is the maximum multipole at which the galaxy angular power spectrum is probed, and N_z is the number of redshift slices. Considering that the redshift survey of Euclid will cover redshifts $0.4 < z < 2$, there is an increase by a factor of 3 in distance of the survey and hence a factor 3 increase in $l_{\rm max}$ ($l_{\rm max} \sim k_{\rm max}\chi(z)$, see the expression for the selection function after Eq. (4.5.15)). Taking $k_{\rm max} = 0.2h\,{\rm Mpc}^{-1}$ the effective number of redshift slices is also increased of a factor of ~ 3 ($N_z \sim k_{\rm max}\,\Delta\chi/\pi$, with $\Delta\chi$ the radial width of the survey). Therefore, one could expect that for a mission like Euclid one can achieve an uncertainty (at 1σ) $\sigma_{g_*} \sim 10^{-3} - 10^{-2}$ or $\sigma_{g_*} \sim 10^{-2}$, for a fixed anisotropy axis or marginalizing over $\mathbf{n}$, respectively. This will be competitive with Planck measurements and highly complementary to it [702, 409]. Notice that these constraints apply to an analysis of the galaxy angular power spectrum. An analysis of the 3-dimensional power spectrum $P(\mathbf{k})$ could improve the sensitivity further. In this case the uncertainty would scale as $\Delta g_* \sim N_{\rm modes}^{-1/2}$, where $N_{\rm modes}$ is the number of independent Fourier modes.

Part 5: Statistical Methods for Performance Forecasts

5.1 Introduction

As cosmology becomes nowadays increasingly dominated by results emerging from large-scale observational programmes, it is imperative to be able to justify that resources are being deployed as effectively as possible. In recent years it has become standard to quantify the expected outcome of cosmological surveys to enable comparison, a procedure exemplified by the Figure of Merit (FoM) introduced by [470] and later used in the influential Dark Energy Task Force (DETF) report about dark-energy surveys [21, 22].

The idea is to be able to capture in one single number the scientific return of a future mission, in order to be able to rank competing proposals and to forecast their ability to answer relevant scientific questions, such as: is dark energy a cosmological constant or does it evolve with time? Is it an expression of modified gravity? How well can a time-evolution of dark energy be constrained?

Encapsulating the entire value of a proposed cosmological survey in one single number is of course highly reductive, and the ensuing conclusions should therefore be taken with a large grain of salt. Having said that, work in recent years has focused on attempts to devise Figures of Merit (FoMs) that represent in an increasingly realistic way future missions. It is perhaps obvious that, to a certain extent, the assessment of a future probe will depend on the scientific question one is most interested in: parameter constraints, model selection, robustness to systematics are but a few examples of the different levels on which a proposed mission can be evaluated and optimized.

This part gives an overview of some of the approaches recently adopted in the field, and used elsewhere in this document to produce forecasts for Euclid. Useful references and background material to some of the concepts discussed below are: [897, 439] for an introduction to Bayesian methods in cosmology, [839, 607] for introductions to the Bayesian approach in data analysis, [396] for an introduction to Markov Chain Monte Carlo (MCMC) methods.

5.2 Predicting the science return of a future experiment

We consider a toy Gaussian linear model in order to illustrate the different approaches to performance forecast. We notice that, although motivated by computational simplicity and the ability to obtain analytical results, a Gaussian model is actually a fairly close representation of many cases of interest. In Figure 55 we illustrate this point by plotting the parameter constraints expected from a Euclid-like survey and the corresponding Gaussian approximation in the Fisher-matrix approach to the likelihood (described below). In these cases, it seem clear that the Gaussian model captures fairly well the full probability distribution. Another example shown in Figure 56 are cosmological constraints from WMAP and SDSS data, where a Gaussian approximation to the likelihood (so-called Laplace approximation) is seen to give an excellent description of the full distribution obtained numerically via MCMC.

5.2.1 The Gaussian linear model

Suppose we have N cosmological probes, whose likelihood function is assumed to be a multi-dimensional Gaussian, given by: L_i $(i = 1, \ldots, N)$, i.e.,

$$\mathcal{L}_i(\Theta) \equiv p(D_i|\Theta) = \mathcal{L}_0^i \exp\left(-\frac{1}{2}(\mu_i - \Theta)^t L_i (\mu_i - \Theta)\right). \tag{5.2.1}$$

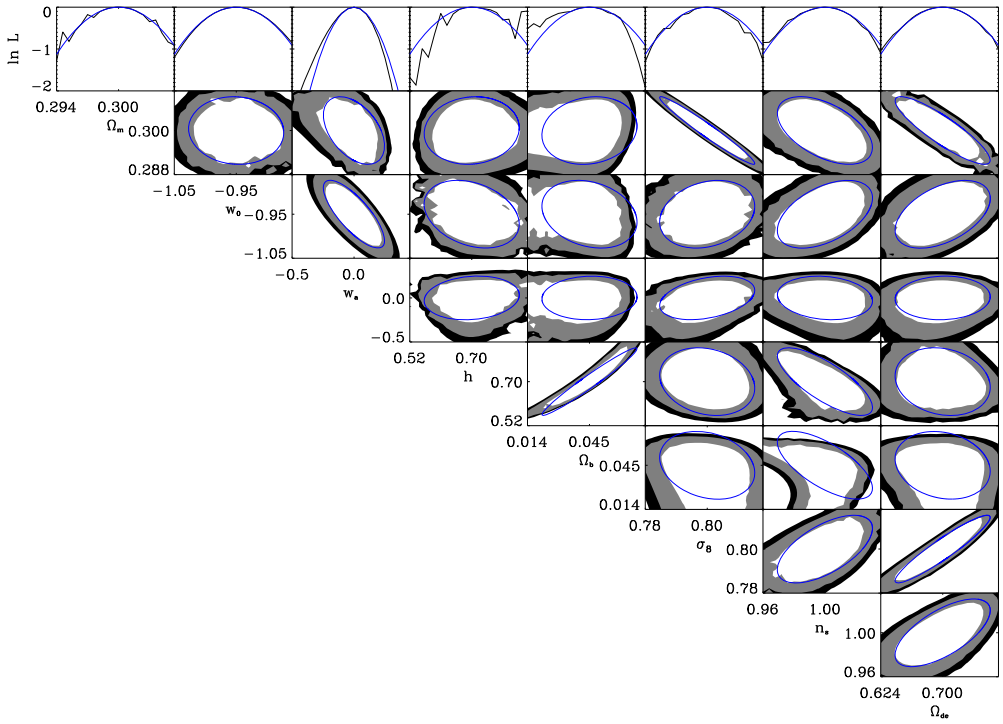

Figure 55: Projected cosmological 8-parameter space for a 20,000 square degrees, median redshift of $z = 0.8$, 10 bin tomographic cosmic shear survey. Specifications are based on Euclid Yellow book [550] as this figure is representative of a method, rather than on forecast analysis; the discussion is still valid with more updated [551] Euclid specifications. The upper panel shows the 1D parameter constraints using analytic marginalization (black) and the Gaussian approximation (Fisher matrix, blue, dark grey). The other panels show the 2D parameter constraints. Grey contours are 1- 2- and 3-σ levels using analytic marginalization over the extra parameters, solid blue ellipses are the 1-σ contours using the Fisher-matrix approximation to the projected likelihood surface, solid red ellipses are the 1-σ fully marginalized. Image reproduced by permission from [878].

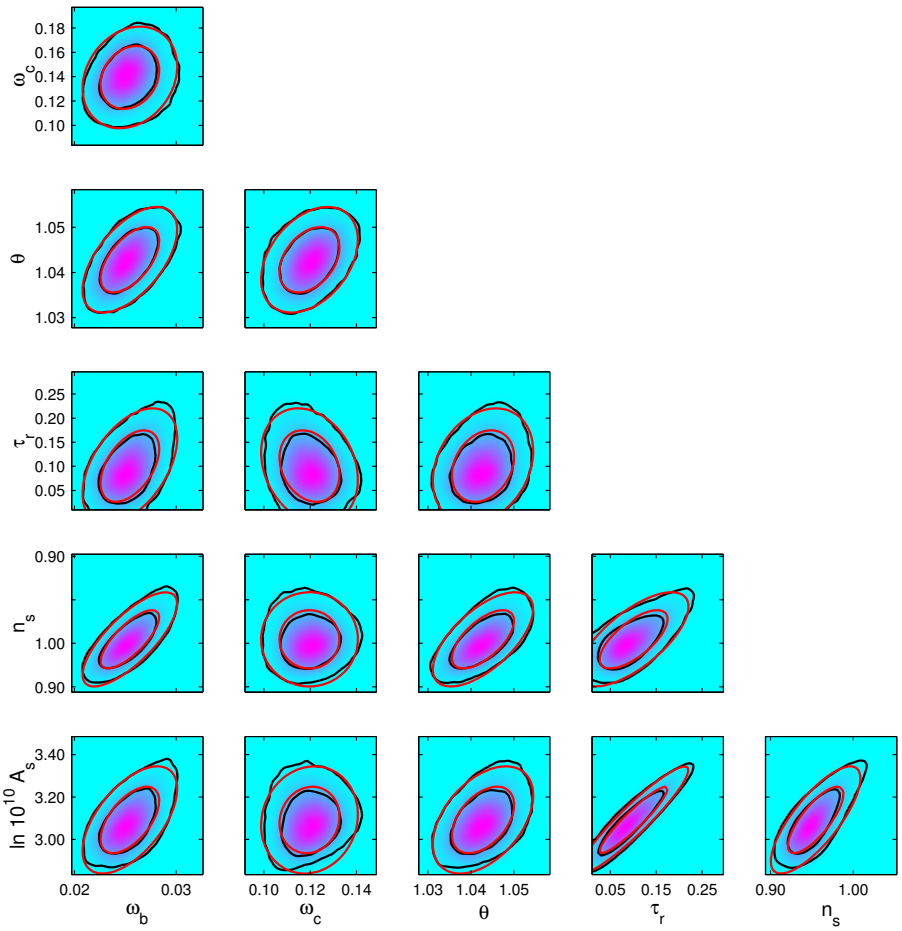

Figure 56: Gaussian approximation (Laplace approximation) to a 6-dimensional posterior distribution for cosmological parameters, from WMAP1 and SDSS data. For all couples of parameters, panels show contours enclosing 68% and 95% of joint probability from $2 \cdot 10^5$ MC samples (black contours), along with the Laplace approximation (red ellipses). It is clear that the Laplace approximation captures the bulk of the posterior volume in parameter space in this case where there is little non-Gaussianity in the posterior PDF. Image reproduced from 2005 preprint of [894].

where Θ are the parameters one is interested in constraining, D_i are the available data from probe i and μ_i is the location of the maximum likelihood value in parameter space. The matrix L_i is the inverse of the covariance matrix of the parameters.

The posterior distribution for the parameters from each probe, $p(\Theta|D_i)$, is obtained by Bayes' theorem as

$$p(\Theta|D_i) = \frac{p(\Theta)p(D_i|\Theta)}{p(D_i)}, \tag{5.2.2}$$

where and $p(\Theta)$ is the prior and $p(D_i)$ is a normalizing constant (the Bayesian evidence). If we assume a Gaussian prior centered on the origin with inverse covariance matrix Σ, the posterior from each probe is also a Gaussian, with inverse covariance matrix

$$F_i = L_i + \Sigma \quad (i = 1, \ldots, N) \tag{5.2.3}$$

and posterior mean

$$\overline{\mu}_i = F_i^{-1}(L_i\mu_i). \tag{5.2.4}$$

Tighter constraints on the parameters can be usually obtained by combining all available probes together (provided there are no systematics, see below). If we combine all probes together, we obtain a Gaussian posterior with inverse covariance matrix

$$F = \sum_{i=1}^{N} L_i + \Sigma \tag{5.2.5}$$

and mean

$$\overline{\mu} = F^{-1} \sum_{i=1}^{N} L_i\mu_i. \tag{5.2.6}$$

Notice that the precision of the posterior (i.e., the inverse covariance matrix) does not depend on the degree of overlap of the likelihoods from the individual probes. This is a property of the Gaussian linear model.

For future reference, it is also useful to write down the general expression for the Bayesian evidence. For a normal prior $p(\Theta) \sim \mathcal{N}(\theta_\pi, \Sigma)$ and a likelihood

$$\mathcal{L}(\Theta) = \mathcal{L}_0 \exp\left(-\frac{1}{2}(\theta_0 - \Theta)^t L(\theta_0 - \Theta)\right), \tag{5.2.7}$$

the evidence for data d is given by

$$p(d) \equiv \int \mathrm{d}\Theta p(d|\Theta)p(\Theta) = \mathcal{L}_0 \frac{|\Sigma|^{1/2}}{|F|^{1/2}} \exp\left[-\frac{1}{2}\left(\theta_0^t L\theta_0 + \theta_\pi^t \Sigma\theta_\pi - \overline{\theta}^t F\overline{\theta}\right)\right], \tag{5.2.8}$$

where F is given by Eq. (5.2.5) with $N = 1$ and $\overline{\theta} = F^{-1}L\theta_0$.

5.2.2 Fisher-matrix error forecast

A general likelihood function for a future experiment (subscript i) can be Taylor-expanded around its maximum-likelihood value, μ_i. By definition, at the maximum the first derivatives vanish, and the shape of the log-likelihood in parameter space is approximated by the Hessian matrix H_i,

$$\ln \mathcal{L}_i(\Theta) \approx \ln \mathcal{L}_i(\mu_i) + \frac{1}{2}(\Theta - \mu_i)^t H_i(\Theta - \mu_i), \tag{5.2.9}$$

where H_i is given by

$$(H_i)_{\alpha\beta} \equiv \frac{\partial^2 \ln \mathcal{L}_i}{\partial\Theta_\alpha \partial\Theta_\beta}\Big|_{\mu_i}, \tag{5.2.10}$$

and the derivatives are evaluated at the maximum-likelihood point. By taking the expectation of equation (5.2.9) with respect to many data realizations, we can replace the maximum-likelihood value μ_i with the true value, Θ_*, as the maximum-likelihood estimate is unbiased (in the absence of systematics), i.e., $\langle \mu_i \rangle = \Theta_*$. We then define the Fisher information matrix as the expectation value of the Hessian,

$$F_i \equiv \langle H_i \rangle. \tag{5.2.11}$$

The inverse of the Fisher matrix, F^{-1}, is an estimate of the covariance matrix for the parameters, and it describes how fast the log-likelihood falls (on average) around the maximum likelihood value, and we recover the Gaussian expression for the likelihood, Eq. (5.2.1), with the maximum likelihood value replaced by the true value of the parameters and the inverse covariance matrix given by the Fisher matrix, $L_i = F_i^{-1}$ [496]. In general, the derivatives depend on where in parameter space we take them (except for the simple case of linear models), hence it is clear that F_i is a function of the fiducial parameters.

Once we have the Fisher matrix, we can give estimates for the accuracy on the parameters from a future measurement, by computing the posterior as in Eq. (5.2.2). If we are only interested in a subset of the parameters, then we can marginalize easily over the others: computing the Gaussian integral over the unwanted parameters is the same as inverting the Fisher matrix, dropping the rows and columns corresponding to those parameters (keeping only the rows and columns containing the parameters of interest) and inverting the smaller matrix back. The result is the marginalized Fisher matrix $\mathcal{F}_i$. For example, the 1σ error for parameter α from experiment i, marginalized over all other parameters, is simply given by $\sigma_\alpha = \sqrt{(F_i^{-1})_{\alpha\alpha}}$.

It remains to compute the Fisher matrix for the future experiment. This can be done analytically for the case where the likelihood function is approximately Gaussian in the data, which is a good approximation for many applications of interest. We can write for the log-likelihood (in the following, we drop the subscript i denoting the experiment under consideration for simplicity of notation)

$$-2\ln\mathcal{L} = \ln|C| + (D-\mu)^t C^{-1}(D-\mu), \tag{5.2.12}$$

where D are the (simulated) data that would be observed by the experiment and in general both the mean μ and covariance matrix C may depend on the parameters Θ we are trying to estimate. The expectation value of the data corresponds to the true mean, $\langle D \rangle = \mu$, and similarly the expectation value of the data matrix $\Delta \equiv (D-\mu)^t(D-\mu)$ is equal to the true covariance, $\langle \Delta \rangle = C$. Then it can be shown (see e.g. [884]) that the Fisher matrix is given by

$$F_{\alpha\beta} = \frac{1}{2}\mathrm{tr}\left[A_\alpha A_\beta + C^{-1}\langle \Delta_{,\alpha\beta}\rangle\right], \tag{5.2.13}$$

where $A_\alpha \equiv C^{-1}C_{,\alpha}$ and the comma denotes a derivative with respect to the parameters, for example $C_{,\alpha} \equiv \partial C/\partial\Theta_\alpha$. The fact that this expression depends only on *expectation values* and not on the particular data realization means that the Fisher matrix can be computed from knowledge of the noise properties of the experiment without having to go through the step of actually generating any simulated data. The specific form of the Fisher matrix then becomes a function of the type of observable being considered and of the experimental parameters.

Explicit expressions for the Fisher matrix for cosmological observables can be found in [884] for cosmic microwave background data, in [880] for the matter power spectrum from galaxy redshift surveys (applied to baryonic acoustic oscillations in [815] and in [454] for weak lensing. These approaches have been discussed in Section 1.7. A useful summary of Fisher matrix technology is

given in the Dark Energy Task Force report [21] and in [919]. A useful numerical package which includes several of the a bove calculations is the publicly available Matlab code[20] FISHER4CAST [99, 98]. Attempts to include systematic errors modelling in this framework can be found in [508, 878, 505].

5.2.3 Figure of merits

It has become customary to describe the statistical power of a future dark energy probe by the inverse area enclosed by the 68% covariance ellipse marginalized down to the dark-energy parameter space. This measure of statistical performance for probe i (widely known as the DETF FoM [21, 470]) is usually defined (up to multiplicative constants) as

$$\mathrm{FoM} = |F_i|^{-1/2}\,, \tag{5.2.14}$$

where the Fisher matrix F_i is given in Eq. (5.2.11). [21] suggested to use the inverse area of the 95% error ellipse of $w_0 - w_a$ (where w_0 and w_a are defined in [584], [229]). This definition was inspired by [470]. In [22] it is suggested to model $w(a)$ as piecewise constant values of $w(a)$ defined in many small redshift bins ($\Delta a = 0.025$). The suggestion is then to apply a principal component approach [468] in order to understand the redshifts at which each experiment has the power to constrain w.

A closely related but more statistically motivated measure of the information gain is the Kullback–Leibler divergence (KL) between the posterior and the prior, representing the information gain obtained when upgrading the prior to the posterior via Bayes' theorem:

$$D_{\mathrm{KL}} \equiv \int p(\Theta|D) \ln \frac{p(\Theta|D)}{p(\Theta)} d\Theta. \tag{5.2.15}$$

The KL divergence measures the relative entropy between the two distributions: it is a dimensionless quantity which expressed the information gain obtained via the likelihood. For the Gaussian likelihood and prior introduced above, the information gain (w.r.t. the prior Σ) from the combination of all probes is given by [900]

$$D_{\mathrm{KL}} = \frac{1}{2}\left(\ln|F| - \ln|\Sigma| - \mathrm{tr}[1 - \Sigma F^{-1}]\right). \tag{5.2.16}$$

A discussion of other, alternative FoMs (D-optimality, A-optimality) can be found in [96]. In [939] a different FoM for dark energy is suggested. For a set of DE parameters Θ, the FoM is defined as $\mathrm{FoM} = 1/\sqrt{\mathrm{Cov}(\Theta)}$, where $Cov(\Theta)$ is the covariance matrix of Θ. This definition is more flexible since one can use it for any DE parametrization [945].

Given that Euclid can constrain both the expansion history and the growth of structure, it is also useful to introduce a new FoM for the growth of perturbations. Similarly to the DETF FoM, one can define this new FoM as the inverse area of the 95% error ellipse of $\Omega_m - \gamma$, where γ is the growth index, defined starting from the growth rate $f_G(z) \equiv \frac{d\ln G(z)}{d\ln a} = \Omega_m^\gamma$, or as $1/\sqrt{Cov(w_0, w_a, \gamma)}$ or similar variants [614, 308]. Instead of γ, other parameters describing the growth can also be employed.

A FoM targeted at evaluating the robustness of a future probe to potential systematic errors has been introduced in [625]. The robustness of a future probe is defined via the degree of overlap between the posterior distribution from that probe and the posterior from other, existing probes. The fundamental notion is that maximising statistical power (e.g., by designing a future probe to deliver orthogonal constraints w.r.t. current probes) will in general reduce its robustness (by

[20] Available from http://www.cosmology.org.za

increasing the probability of an incompatible results, for example because of systematic bias). Thus in evaluating the strength of a probe, both its statistical power and its resilience to plausible systematics ought to be considered.

5.2.4 The Bayesian approach

When considering the capabilities of future experiments, it is common stance to predict their performance in terms of constraints on relevant parameters, assuming a fiducial point in parameter space as the true model (often, the current best-fit model), as explained above. While this is a useful indicator for parameter inference tasks, many questions in cosmology fall rather in the model comparison category. Dark energy is a case in point, where the science driver for many future probes (including Euclid) is to detect possible departures from a cosmological constant, hence to gather evidence in favor of an evolving dark-energy model. Therefore, it is preferable to assess the capabilities of future experiments by their ability to answer model selection questions.

The procedure is as follows (see [677] for details and the application to dark-energy scenarios). At every point in parameter space, mock data from the future observation are generated and the Bayes factor between the competing models is computed, for example between an evolving dark energy and a cosmological constant. Then one delimits in parameter space the region where the future data would *not* be able to deliver a clear model comparison verdict, for example $|\ln B_{01}| < 5$ (evidence falling short of the "strong" threshold). Here, B_{01} is the Bayes factor, which is formed from the ratio of the Bayesian evidences of the two models being considered:

$$B_{01} = \frac{p(d|\mathcal{M}_0)}{p(d|\mathcal{M}_1)}, \tag{5.2.17}$$

where the Bayesian evidence is the average of the likelihood under the prior in each model (denoted by a subscript m):

$$p(d|\mathcal{M}_m) = \int \mathrm{d}\Theta_m p(d|\Theta_m, \mathcal{M}_m) p(\Theta_m|\mathcal{M}_m). \tag{5.2.18}$$

The Bayes factor updates the prior probability ratio of the models to the posterior one, indicating the extent to which the data have modified one's original view on the relative probabilities of the two models. The experiment with the smallest "model-confusion" volume in parameter space is to be preferred, since it achieves the highest discriminative power between models. An application of a related technique to the spectral index from the Planck satellite is presented in [704, 703].

Alternatively, we can investigate the full probability distribution for the Bayes factor from a future observation. This allows to make probabilistic statements regarding the outcome of a future model comparison, and in particular to quantify the probability that a new observation will be able to achieve a certain level of evidence for one of the models, given current knowledge. This technique is based on the *predictive distribution* for a future observation, which gives the expected posterior for an observation with a certain set of experimental capabilities (further details are given in [895]). This method is called PPOD, for *predictive posterior odds distribution* and can be useful in the context of experiment design and optimization

Hybrid approaches have also been attempted, i.e., to defined model-selection oriented FoMs while working in the Fisher-matrix framework, such as the expected Bayesian evidence ratio [429, 31].

The most general approach to performance forecasting involves the use of a suitably defined utility function, and it has recently been presented in [899]. Consider the different levels of uncertainty that are relevant when predicting the probability of a certain model selection outcome from a future probe, which can be summarized as follows:

- **Level 1:** current uncertainty about the correct model (e.g., is it a cosmological constant or a dark-energy model?).

- **Level 2:** present-day uncertainty in the value of the cosmological parameters for a given model (e.g., present error on the dark-energy equation of state parameters assuming an evolving dark-energy model).

- **Level 3:** realization noise, which will be present in future data even when assuming a model and a fiducial choice for its parameters.

The commonly-used Fisher matrix forecast ignores the uncertainty arising from Levels 1 and 2, as it assumes a fiducial model (Level 1) and fiducial parameter values (Level 2). It averages over realization noise (Level 3) in the limit of an infinite number of realizations. Clearly, the Fisher matrix procedure provides a very limited assessment of what we can expect for the scientific return of a future probe, as it ignores the uncertainty associated with the choice of model and parameter values.

The Bayesian framework allows improvement on the usual Fisher matrix error forecast thanks to a general procedure which fully accounts for all three levels of uncertainty given above. Following [590], we think of future data D_f as *outcomes*, which arise as consequence of our choice of experimental parameters e (*actions*). For each action and each outcome, we define a utility function $\mathcal{U}(D_f, e)$. Formally, the utility only depends on the future data realization D_f. However, as will become clear below, the data D_f are realized from a fiducial model and model parameter values. Therefore, the utility function implicitly depends on the assumed model and parameters from which the data D_f are generated. The best action is the one that maximizes the expected utility, i.e., the utility averaged over possible outcomes:

$$\mathcal{EU}(e) \equiv \int \mathrm{d}D_f p(D_f|e,d)\mathcal{U}(D_f,e). \tag{5.2.19}$$

Here, $p(D_f|e,d)$ is the predictive distribution for the future data, conditional on the experimental setup (e) and on current data (d). For a single fixed model the predictive distribution is given by

$$\begin{aligned} p(D_f|e,d) &= \int \mathrm{d}\Theta\, p(D_f,\Theta|e,d) \\ &= \int \mathrm{d}\Theta\, p(D_f|\Theta,e,d)p(\Theta|e,d) \\ &= \int \mathrm{d}\Theta\, p(D_f|\Theta,e)p(\Theta|d)\,, \end{aligned} \tag{5.2.20}$$

where the last line follows because $p(D_f|\Theta,e,d) = p(D_f|\Theta,e)$ (conditioning on current data is irrelevant once the parameters are given) and $p(\Theta|e,d) = p(\Theta|d)$ (conditioning on future experimental parameters is irrelevant for the present-day posterior). So we can predict the probability distribution for future data D_f by averaging the likelihood function for the future measurement (Level 3 uncertainty) over the current posterior on the parameters (Level 2 uncertainty). The expected utility then becomes

$$\mathcal{EU}(e) = \int \mathrm{d}\Theta p(\Theta|o,d) \int \mathrm{d}D_f p(D_f|\Theta,e)\mathcal{U}(D_f,e)\,. \tag{5.2.21}$$

So far, we have tacitly assumed that only one model was being considered for the data. In practice, there will be several models that one is interested in testing (Level 1 uncertainty), and typically there is uncertainty over which one is best. This is in fact one of the main motivations for designing a new dark energy probe. If M models $\{\mathcal{M}_1,\ldots,\mathcal{M}_M\}$ are being considered, each one with parameter vector Θ_m ($m = 1,\ldots,M$), the current posterior can be further extended in terms

of model averaging (Level 1), weighting each model by its current model posterior probability, $p(\mathcal{M}_m|d)$, obtaining from Eq. (5.2.21) the model-averaged expected utility

$$\mathcal{EU}(e) = \sum_{m=1}^{M} p(\mathcal{M}_m|d) \int \mathrm{d}\Theta_m p(\Theta_m|d,\mathcal{M}_m) \times \int \mathrm{d}D_f p(D_f|\Theta_m, e, \mathcal{M}_m)\mathcal{U}(D_f, e, \mathcal{M}_m)\,. \tag{5.2.22}$$

This expected utility is the most general definition of a FoM for a future experiment characterized by experimental parameters e. The usual Fisher matrix forecast is recovered as a special case of Eq. (5.2.22), as are other *ad hoc* FoMs that have been defined in the literature. Therefore Eq. (5.2.22) gives us a formalism to define in all generality the scientific return of a future experiment. This result clearly accounts for all three levels of uncertainty in making our predictions: the utility function $\mathcal{U}(D_f, e, \mathcal{M}_m)$ (to be specified below) depends on the future data realization, D_f, (Level 3), which in turn is a function of the fiducial parameters value, Θ_m, (Level 2), and is averaged over present-day model probabilities (Level 1).

This approach is used in [899] to define two model-selection oriented Figures of Merit: the decisiveness $\mathcal{D}$, which quantifies the probability that a probe will deliver a decisive result in favor or against the cosmological constant, and the expected strength of evidence, $\mathcal{E}$, that returns a measure of the expected power of a probe for model selection.

5.3 Survey design and optimization

Although the topic of survey design is still in its infancy, the basic idea is to carry out an optimization of survey parameters (such as for example choice of targets, depth of field, number of spectroscopic fibers, etc.) in order to identify the configuration that is more likely to return a high FoM for the scientific question being considered. Example of this approach applied to dark-energy parameters can be found in [96, 707, 708, 103], while [590] discussed a more general methodology. In [96] a method is defined to optimize future surveys, in the framework of Bayesian statistics and without necessarily assuming a dark-energy model. In [103], [707] and [708] this method is used to produce forecasts for future weak lensing and galaxy redshift surveys.

The optimization process is carried out subject to constraints, such as for example design parameter ranges and/or cost constraints. This is generally a numerically complex and computationally expensive procedure. It typically requires to explore the design parameters space (e.g., via MCMC), generating at each point a set of pseudo-data that are analysed as real data would, in order to compute their FoM. Then the search algorithm moves on to maximize the FoM.

In order to carry out the optimization procedure, it might be useful to adopt a principal component analysis (PCA) to determine a suitable parametrization of $w(z)$ [468, 838]. The redshift range of the survey can be split into N bins, with the equation of state taking on a value w_i in the i-th bin:

$$w(z) = \sum_{i=1}^{N} w_i b_i(z)\,. \tag{5.3.1}$$

where the basis functions b_i are top-hats of value 1 inside the bin, and 0 elsewhere. If F is the Fisher matrix for the N parameters w_i, one can diagonalize it by writing $F = W^T \Lambda W$, where Λ is a diagonal matrix, and the rows of W are the eigenvectors $e_i(z)$ or the so-called principal components. These define a new basis (in which the new coefficients α_i are uncorrelated) so the

equation of state can be written as

$$w(z) = \sum_{i=1}^{N} \alpha_i e_i(z)\,. \tag{5.3.2}$$

The diagonal elements of Λ are the eigenvalues λ_i and define the variance of the new parameters, $\sigma^2(\alpha_i) = 1/\lambda_i$.

One can now reconstruct $w(z)$ by keeping only a certain number of the most accurately determined modes, i.e., the ones with largest eigenvalues. The optimal number of modes to retain can be estimated by minimizing the risk, defined as the sum of the bias squared (how much the reconstructed equation of state departs from the true one by neglecting the more noisy modes) plus the variance of the estimate [468].

5.4 Future activities and open challenges

As outlined in the previous sections, several approaches are available to capture the expected scientific performance of Euclid. As part of future theoretical activities, it will be necessary to build on the above concepts in order to obtain a realistic assessment of the science return of Euclid. Operationally, this means that the following tasks will need to be carried out:

- Estimation of likelihood contours around the maximum likelihood peak beyond the Fisher matrix approach. We envisage here a programme where simulated mock data will be generated and then used to blindly reconstruct the likelihood surface to sufficient accuracy.

- Estimation of Bayesian posterior distributions and assessment of impact of various priors. Bayesian inference is a mature field in cosmology and we now have at our disposal a number of efficient and reliable numerical algorithms based on Markov Chain Monte Carlo or nested sampling methods.

- Comparison of Bayesian inferences with inferences based on profile likelihoods. Discrepancies might occur in the presence of large "volume effects" arising from insufficiently constraining data sets and highly multi-modal likelihoods [898]. Based on our experience so far, this is unlikely to be a problem for most of the statistical quantities of interest here but we recommend to check this explicitly for the more complicated distributions.

- Investigation of the coverage properties of Bayesian credible and frequentist confidence intervals. Coverage of intervals is a fundamental property in particle physics, but rarely discussed in the cosmological setting. We recommend a careful investigation of coverage from realistically simulated data sets (as done recently in [626]). Fast neural networks techniques might be required to speed up the inference step by several orders of magnitude in order to make this kind of studies computationally feasible [822, 174].

- Computation of the Bayesian evidence to carry out Bayesian model selection [897, 677]. Algorithms based on nested sampling, and in particular, MultiNest [362], seem to be ideally suited to this task, but other approaches are available, as well, such as population Monte Carlo [502] and semi-analytical ones [894, 429]. A robust Bayesian model selection will require a careful assessment of the impact of priors. Furthermore, the outcome of Bayesian model selection is dependent on the chosen parametrization if different nonlinearly related reparametrizations can equally plausibly be chosen from physical consideration (relevant examples include parametrizations of the isocurvature fraction [119], the tensor-to-scalar ratio [710] and the inflaton potential [634]). It will be important to cross check results with

frequentist hypothesis testing, as well. The notion of Bayesian doubt, introduced in [624], can also be used to extend the power of Bayesian model selection to the space of unknown models in order to test our paradigm of a ΛCDM cosmological model.

- Bayesian model averaging [571, 709] can also be used to obtain final inferences parameters which take into account the residual model uncertainty. Due to the concentration of probability mass onto simpler models (as a consequence of Occam's razor), Bayesian model averaging can lead to tighter parameter constraints than non-averaged procedures, for example on the curvature parameter [917].

Acknowledgments

It is a pleasure to thank the Euclid theory science working group, all science working group members, the Euclid Consortium Board and the whole Euclid consortium for fruitful discussions. We also kindly thank Rene Laureijs, Ana Heras, Philippe Gondoin, Ludovic Duvet and Marc Sauvage for their continuous work and support, and Thomas Buchert for comments on the draft.

References

[1] Abazajian, K., Switzer, E.R., Dodelson, S., Heitmann, K. and Habib, S., "Nonlinear cosmological matter power spectrum with massive neutrinos: The halo model", *Phys. Rev. D*, **71**, 043507 (2005). [DOI], [ADS], [arXiv:astro-ph/0411552]. (Cited on page 142.)

[2] Abbott, L.F. and Sikivie, P., "A cosmological bound on the invisible axion", *Phys. Lett. B*, **120**, 133–136 (1983). [DOI], [ADS]. (Cited on pages 154 and 181.)

[3] Abdalla, E., Abramo, L.R., Sodré Jr, L. and Wang, B., "Signature of the interaction between dark energy and dark matter in galaxy clusters", *Phys. Lett. B*, **673**, 107–110 (2009). [DOI], [arXiv:0710.1198 [astro-ph]]. (Cited on pages 34, 66, and 153.)

[4] Abel, S.A., Goodsell, M.D., Jaeckel, J., Khoze, V.V. and Ringwald, A., "Kinetic mixing of the photon with hidden U(1)s in string phenomenology", *J. High Energy Phys.*, **2008**(07), 124 (2008). [DOI], [ADS], [arXiv:0803.1449 [hep-ph]]. (Cited on page 186.)

[5] Abel, S.A., Jaeckel, J., Khoze, V.V. and Ringwald, A., "Illuminating the hidden sector of string theory by shining light through a magnetic field", *Phys. Lett. B*, **666**, 66–70 (2008). [DOI], [ADS], [arXiv:hep-ph/0608248]. (Cited on page 186.)

[6] Abel, S.A. and Schofield, B.W., "Brane-antibrane kinetic mixing, millicharged particles and SUSY breaking", *Nucl. Phys. B*, **685**, 150–170 (2004). [DOI], [ADS], [arXiv:hep-th/0311051]. (Cited on page 186.)

[7] Ackerman, L., Carroll, S.M. and Wise, M.B., "Imprints of a primordial preferred direction on the microwave background", *Phys. Rev. D*, **75**, 083502 (2007). [DOI], [ADS], [arXiv:astro-ph/0701357]. (Cited on pages 203 and 204.)

[8] Acquaviva, V. and Verde, L., "Observational signatures of Jordan–Brans–Dicke theories of gravity", *J. Cosmol. Astropart. Phys.*, **2007**(12), 001 (2007). [DOI], [ADS], [arXiv:0709.0082]. (Cited on page 182.)

[9] Adamek, J., Campo, D. and Niemeyer, J.C., "Anisotropic Kantowski-Sachs Universe from Gravitational Tunneling and its Observational Signatures", *Phys. Rev. D*, **82**, 086006 (2010). [DOI], [arXiv:1003.3204 [hep-th]]. (Cited on page 203.)

[10] Affleck, I. and Dine, M., "A new mechanism for baryogenesis", *Nucl. Phys. B*, **249**, 361–380 (1985). [DOI], [ADS]. (Cited on page 181.)

[11] Afshordi, N., Geshnizjani, G. and Khoury, J., "Do observations offer evidence for cosmological-scale extra dimensions?", *J. Cosmol. Astropart. Phys.*, **2009**(08), 030 (2009). [DOI], [arXiv:0812.2244 [astro-ph]]. (Cited on pages 47, 75, and 85.)

[12] Afshordi, N., Zaldarriaga, M. and Kohri, K., "On the stability of Dark Energy with Mass-Varying Neutrinos", *Phys. Rev. D*, **72**, 065024 (2005). [DOI], [arXiv:astro-ph/0506663]. (Cited on pages 34, 143, and 150.)

[13] Aguilar-Arevalo, A.A. et al. (MiniBooNE Collaboration), "Search for Electron Neutrino Appearance at the $\Delta m^2 \sim 1\mathrm{eV}^2$ Scale", *Phys. Rev. Lett.*, **98**, 231801 (2007). [DOI], [ADS], [arXiv:0704.1500 [hep-ex]]. (Cited on page 136.)

[14] Aguirre, A.N., "Intergalactic Dust and Observations of Type Ia Supernovae", *Astrophys. J.*, **525**, 583–593 (1999). [DOI], [ADS], [arXiv:astro-ph/9904319]. (Cited on page 184.)

[15] Agulló, I., Navarro-Salas, J., Olmo, G.J. and Parker, L., "Revising the observable consequences of slow-roll inflation", *Phys. Rev. D*, **81**, 043514 (2010). [DOI], [ADS], [arXiv:0911.0961 [hep-th]]. (Cited on page 200.)

[16] Ahlers, M., "Hubble diagram as a probe of minicharged particles", *Phys. Rev. D*, **80**, 023513 (2009). [DOI], [ADS], [arXiv:0904.0998 [hep-ph]]. (Cited on pages 184 and 186.)

[17] Ahlers, M., Gies, H., Jaeckel, J., Redondo, J. and Ringwald, A., "Laser experiments explore the hidden sector", *Phys. Rev. D*, **77**, 095001 (2008). [DOI], [ADS], [arXiv:0711.4991 [hep-ph]]. (Cited on page 186.)

[18] Akofor, E., Balachandran, A.P., Jo, S.G., Joseph, A. and Qureshi, B.A., "Direction-dependent CMB power spectrum and statistical anisotropy from noncommutative geometry", *J. High Energy Phys.*, **2008**(05), 092 (2008). [DOI], [ADS], [arXiv:0710.5897 [astro-ph]]. (Cited on page 202.)

[19] Alabidi, L. and Lyth, D.H., "Inflation models and observation", *J. Cosmol. Astropart. Phys.*, **2006**(05), 016 (2006). [DOI], [ADS], [arXiv:astro-ph/0510441]. (Cited on page 170.)

[20] Albrecht, A. and Steinhardt, P.J., "Cosmology for Grand Unified Theories with Radiatively Induced Symmetry Breaking", *Phys. Rev. Lett.*, **48**, 1220–1223 (1982). [DOI], [ADS]. (Cited on page 163.)

[21] Albrecht, A. et al., *Report of the Dark Energy Task Force*, (NSF, Arlington, VA, 2006). [ADS], [arXiv:astro-ph/0609591]. Online version (accessed 16 August 2013): http://www.nsf.gov/mps/ast/detf.jsp. (Cited on pages 96, 207, and 212.)

[22] Albrecht, A. et al., "Findings of the Joint Dark Energy Mission Figure of Merit Science Working Group", *arXiv*, e-print, (2009). [ADS], [arXiv:0901.0721 [astro-ph.IM]]. (Cited on pages 100, 207, and 212.)

[23] Alcock, C. et al., "The MACHO Project: Microlensing Results from 5.7 Years of Large Magellanic Cloud Observations", *Astrophys. J.*, **542**, 281–307 (2000). [DOI], [ADS], [arXiv:astro-ph/0001272]. (Cited on page 122.)

[24] Alexander, S., Brandenberger, R.H. and Magueijo, J., "Noncommutative inflation", *Phys. Rev. D*, **67**, 081301 (2003). [DOI], [ADS], [arXiv:hep-th/0108190]. (Cited on page 201.)

[25] Alishahiha, M., Silverstein, E. and Tong, D., "DBI in the sky: Non-Gaussianity from inflation with a speed limit", *Phys. Rev. D*, **70**, 123505 (2004). [DOI], [ADS], [arXiv:hep-th/0404084]. (Cited on pages 171 and 173.)

[26] Allen, S.W., Rapetti, D.A., Schmidt, R.W., Ebeling, H., Morris, R.G. and Fabian, A.C., "Improved constraints on dark energy from Chandra X-ray observations of the largest relaxed galaxy clusters", *Mon. Not. R. Astron. Soc.*, **383**, 879–896 (2008). [DOI], [ADS], [arXiv:0706.0033]. (Cited on page 129.)

[27] Alnes, H. and Amarzguioui, M., "CMB anisotropies seen by an off-center observer in a spherically symmetric inhomogeneous universe", *Phys. Rev. D*, **74**, 103520 (2006). [DOI], [ADS], [arXiv:astro-ph/0607334]. (Cited on page 193.)

[28] Alnes, H., Amarzguioui, M. and Groen, O., "Inhomogeneous alternative to dark energy?", *Phys. Rev. D*, **73**, 083519 (2006). [DOI], [ADS], [arXiv:astro-ph/0512006]. (Cited on page 192.)

[29] Alonso, D., García-Bellido, J., Haugbølle, T. and Knebe, A., "Halo abundances and shear in void models", *Phys. Dark Universe*, **1**, 24–31 (2012). [DOI], [ADS], [arXiv:1204.3532 [astro-ph.CO]]. (Cited on page 194.)

[30] Alonso, D., García-Bellido, J., Haugbølle, T. and Vicente, J., "Large scale structure simulations of inhomogeneous Lemaître-Tolman-Bondi void models", *Phys. Rev. D*, **82**, 123530 (2010). [DOI], [ADS], [arXiv:1010.3453 [astro-ph.CO]]. (Cited on pages 191 and 194.)

[31] Amara, A. and Kitching, T.D., "Figures of Merit for Testing Standard Models: Application to Dark Energy Experiments in Cosmology", *Mon. Not. R. Astron. Soc.*, **413**, 1505–1514 (2010). [DOI], [ADS], [arXiv:1009.3274 [astro-ph.CO]]. (Cited on page 213.)

[32] Amarzguioui, M., Elgarøy, Ø., Mota, D.F. and Multamäki, T., "Cosmological constraints on $f(R)$ gravity theories within the Palatini approach", *Astron. Astrophys.*, **454**, 707–714 (2006). [DOI], [arXiv:astro-ph/0510519 [astro-ph]]. (Cited on pages 40 and 68.)

[33] Amendola, L., "Coupled quintessence", *Phys. Rev. D*, **62**, 043511 (2000). [DOI], [arXiv:astro-ph/9908023]. (Cited on pages 32, 34, 38, 66, 91, 113, 152, and 153.)

[34] Amendola, L., "Perturbations in a coupled scalar field cosmology", *Mon. Not. R. Astron. Soc.*, **312**, 521–530 (2000). [DOI], [ADS], [arXiv:astro-ph/9906073]. (Cited on page 34.)

[35] Amendola, L., "Linear and nonlinear perturbations in dark energy models", *Phys. Rev. D*, **69**, 103524 (2004). [DOI], [arXiv:astro-ph/0311175]. (Cited on pages 32, 34, 66, 152, and 153.)

[36] Amendola, L., Baldi, M. and Wetterich, C., "Quintessence cosmologies with a growing matter component", *Phys. Rev. D*, **78**, 023015 (2008). [DOI], [arXiv:0706.3064 [astro-ph]]. (Cited on pages 34, 67, and 143.)

[37] Amendola, L. and Barbieri, R., "Dark matter from an ultra-light pseudo-Goldsone-boson", *Phys. Lett. B*, **642**, 192–196 (2006). [DOI], [ADS], [arXiv:hep-ph/0509257]. (Cited on pages 157 and 158.)

[38] Amendola, L., Finelli, F., Burigana, C. and Carturan, D., "WMAP and the generalized Chaplygin gas", *J. Cosmol. Astropart. Phys.*, **2003**(07), 005 (2003). [DOI], [ADS], [arXiv:astro-ph/0304325]. (Cited on page 151.)

[39] Amendola, L., Gannouji, R., Polarski, D. and Tsujikawa, S., "Conditions for the cosmological viability of $f(R)$ dark energy models", *Phys. Rev. D*, **75**, 083504 (2007). [DOI], [ADS], [arXiv:gr-qc/0612180]. (Cited on pages 41 and 42.)

[40] Amendola, L., Gordon, C., Wands, D. and Sasaki, M., "Correlated Perturbations from Inflation and the Cosmic Microwave Background", *Phys. Rev. Lett.*, **88**, 211302 (2002). [DOI], [ADS], [arXiv:astro-ph/0107089]. (Cited on page 182.)

[41] Amendola, L., Kunz, M. and Sapone, D., "Measuring the dark side (with weak lensing)", *J. Cosmol. Astropart. Phys.*, **2008**(04), 013 (2008). [DOI], [arXiv:0704.2421 [astro-ph]]. (Cited on pages 25, 60, 85, 86, and 108.)

[42] Amendola, L., Pettorino, V., Quercellini, C. and Vollmer, A., "Testing coupled dark energy with next-generation large-scale observations", *Phys. Rev. D*, **85**, 103008 (2011). [DOI], [ADS], [arXiv:1111.1404 [astro-ph.CO]]. (Cited on pages 34, 91, 113, 114, and 115.)

[43] Amendola, L., Polarski, D. and Tsujikawa, S., "Are $f(R)$ Dark Energy Models Cosmologically Viable?", *Phys. Rev. Lett.*, **98**, 131302 (2007). [DOI], [ADS], [arXiv:astro-ph/0603703]. (Cited on pages 40, 41, and 110.)

[44] Amendola, L. and Quercellini, C., "Tracking and coupled dark energy as seen by the Wilkinson Microwave Anisotropy Probe", *Phys. Rev. D*, **68**, 023514 (2003). [DOI], [ADS], [arXiv:astro-ph/0303228]. (Cited on pages 34, 91, 96, and 152.)

[45] Amendola, L. and Quercellini, C., "Skewness as a Test of the Equivalence Principle", *Phys. Rev. Lett.*, **92**, 181102 (2004). [DOI], [ADS], [arXiv:astro-ph/0403019]. (Cited on pages 34, 35, 66, and 153.)

[46] Amendola, L., Quercellini, C. and Giallongo, E., "Constraints on perfect fluid and scalar field dark energy models from future redshift surveys", *Mon. Not. R. Astron. Soc.*, **357**, 429–439 (2005). [DOI], [ADS], [arXiv:astro-ph/0404599]. (Cited on page 81.)

[47] Amendola, L., Quercellini, C., Tocchini-Valentini, D. and Pasqui, A., "Cosmic Microwave Background as a Gravity Probe", *Astrophys. J. Lett.*, **583**, L53–L56 (2003). [DOI], [ADS], [arXiv:astro-ph/0205097]. (Cited on pages 34 and 152.)

[48] Amendola, L. and Tsujikawa, S., "Phantom crossing, equation-of-state singularities, and local gravity constraints in $f(R)$ models", *Phys. Lett. B*, **660**, 125–132 (2008). [DOI], [ADS], [arXiv:0705.0396]. (Cited on page 41.)

[49] Amendola, L. and Tsujikawa, S., *Dark Energy: Theory and Observations*, (Cambridge University Press, Cambridge; New York, 2010). [Google Books]. (Cited on pages 27, 39, and 191.)

[50] Amendola, L., Waga, I. and Finelli, F., "Observational constraints on silent quartessence", *J. Cosmol. Astropart. Phys.*, **2005**(11), 009 (2005). [DOI], [ADS], [arXiv:astro-ph/0509099]. (Cited on page 151.)

[51] Amsler, C. et al. (Particle Data Group), "Review of Particle Physics", *Phys. Lett. B*, **667**, 1–6 (2008). [DOI]. (Cited on page 123.)

[52] André, P. et al. (PRISM Collaboration), "PRISM (Polarized Radiation Imaging and Spectroscopy Mission): A White Paper on the Ultimate Polarimetric Spectro-Imaging of the Microwave and Far-Infrared Sky", *arXiv*, e-print, (2013). [ADS], [arXiv:1306.2259 [astro-ph.CO]]. (Cited on page 56.)

[53] Appleby, S. and Battye, R., "Do consistent $F(R)$ models mimic general relativity plus Λ?", *Phys. Lett. B*, **654**, 7–12 (2007). [DOI], [ADS], [arXiv:0705.3199]. (Cited on page 41.)

[54] Appleby, S.A. and Weller, J., "Parameterizing scalar-tensor theories for cosmological probes", *J. Cosmol. Astropart. Phys.*, **2010**(12), 006 (2010). [DOI], [arXiv:1008.2693 [astro-ph.CO]]. (Cited on pages 34 and 68.)

[55] Arbey, A., "Dark fluid: A complex scalar field to unify dark energy and dark matter", *Phys. Rev. D*, **74**, 043516 (2006). [DOI], [ADS], [arXiv:astro-ph/0601274]. (Cited on page 151.)

[56] Arkani-Hamed, N.A., Cheng, H.S., Luty, M.A. and Mukohyama, S., "Ghost condensation and a consistent infrared modification of gravity", *J. High Energy Phys.*, **2004**(05), 074 (2004). [DOI], [ADS], [arXiv:hep-th/0312099]. (Cited on pages 69 and 172.)

[57] Arkani-Hamed, N., Creminelli, P., Mukohyama, S. and Zaldarriaga, M., "Ghost inflation", *J. Cosmol. Astropart. Phys.*, **2004**(04), 001 (2004). [DOI], [ADS], [arXiv:hep-th/0312100]. (Cited on page 172.)

[58] Arkani-Hamed, N., Dimopoulos, S., Dvali, G. and Gabadadze, G., "Non-local modification of gravity and the cosmological constant problem", *arXiv*, e-print, (2002). [ADS], [arXiv:hep-th/0209227]. (Cited on pages 43 and 45.)

[59] Armendariz-Picon, C., "Could dark energy be vector-like?", *J. Cosmol. Astropart. Phys.*, **2004**(07), 007 (2004). [DOI], [ADS], [arXiv:astro-ph/0405267 [astro-ph]]. (Cited on page 203.)

[60] Armendariz-Picon, C., Damour, T. and Mukhanov, V.F., "k-Inflation", *Phys. Lett. B*, **458**, 209–218 (1999). [DOI], [ADS], [arXiv:hep-th/9904075]. (Cited on page 151.)

[61] Armendariz-Picon, C., Mukhanov, V.F. and Steinhardt, P.J., "A dynamical solution to the problem of a small cosmological constant and late-time cosmic acceleration", *Phys. Rev. Lett.*, **85**, 4438–4441 (2000). [DOI], [arXiv:astro-ph/0004134]. (Cited on pages 30, 51, and 151.)

[62] Armendariz-Picon, C., Mukhanov, V.F. and Steinhardt, P.J., "Essentials of k-essence", *Phys. Rev. D*, **63**, 103510 (2001). [DOI], [ADS], [arXiv:astro-ph/0006373]. (Cited on pages 30 and 151.)

[63] Arvanitaki, A., Dimopoulos, S., Dubovsky, S., Kaloper, N. and March-Russell, J., "String Axiverse", *Phys. Rev. D*, **81**, 123530 (2010). [DOI], [ADS], [arXiv:0905.4720]. (Cited on pages 154 and 155.)

[64] Arvanitaki, A. and Dubovsky, S., "Exploring the string axiverse with precision black hole physics", *Phys. Rev. D*, **83**, 044026 (2011). [DOI], [ADS], [arXiv:1004.3558 [hep-th]]. (Cited on page 155.)

[65] Avgoustidis, A., Burrage, C., Redondo, J., Verde, L. and Jimenez, R., "Constraints on cosmic opacity and beyond the standard model physics from cosmological distance measurements", *J. Cosmol. Astropart. Phys.*, **2010**(10), 024 (2010). [DOI], [ADS], [arXiv:1004.2053 [astro-ph.CO]]. (Cited on pages 184, 185, and 186.)

[66] Avgoustidis, A., Verde, L. and Jimenez, R., "Consistency among distance measurements: transparency, BAO scale and accelerated expansion", *J. Cosmol. Astropart. Phys.*, **2009**(06), 012 (2009). [DOI], [ADS], [arXiv:0902.2006 [astro-ph.CO]]. (Cited on pages 184 and 185.)

[67] Avila-Reese, V., Colín, P., Valenzuela, O., D'Onghia, E. and Firmani, C., "Formation and Structure of Halos in a Warm Dark Matter Cosmology", *Astrophys. J.*, **559**, 516–530 (2001). [DOI], [ADS], [arXiv:astro-ph/0010525]. (Cited on page 124.)

[68] Axelsson, M.J., Hansen, F.K., Koivisto, T. and Mota, D.F., "CMB Anomalies from Imperfect Dark Energy: Confrontation with the Data", *arXiv*, e-print, (2011). [ADS], [arXiv:1109.2778 [astro-ph.CO]]. (Cited on page 25.)

[69] Ayaita, Y., Weber, M. and Wetterich, C., "Peculiar Velocity Anomaly from Forces Beyond Gravity?", *arXiv*, e-print, (2009). [ADS], [arXiv:0908.2903 [astro-ph.CO]]. (Cited on page 150.)

[70] Babich, D., Creminelli, P. and Zaldarriaga, M., "The shape of non-Gaussianities", *J. Cosmol. Astropart. Phys.*, **2004**(08), 009 (2004). [DOI], [ADS], [arXiv:astro-ph/0405356]. (Cited on page 171.)

[71] Babichev, E., Mukhanov, V.F. and Vikman, A., "k-Essence, superluminal propagation, causality and emergent geometry", *J. High Energy Phys.*, **2008**(02), 101 (2008). [DOI], [ADS], [arXiv:0708.0561 [hep-th]]. (Cited on page 30.)

[72] Bacon, D.J. and Taylor, A.N., "Mapping the 3D dark matter potential with weak shear", *Mon. Not. R. Astron. Soc.*, **344**, 1307–1326 (2003). [DOI], [ADS], [arXiv:astro-ph/0212266]. (Cited on page 130.)

[73] Baker, T., Ferreira, P.G. and Skordis, C., "The parameterized post-Friedmann framework for theories of modified gravity: Concepts, formalism, and examples", *Phys. Rev. D*, **87**, 024015 (2013). [DOI], [ADS], [arXiv:1209.2117 [astro-ph.CO]]. (Cited on pages 61 and 62.)

[74] Balbi, A., Bruni, M. and Quercellini, C., "ΛαDM: Observational constraints on unified dark matter with constant speed of sound", *Phys. Rev. D*, **76**, 103519 (2007). [DOI], [ADS], [arXiv:astro-ph/0702423]. (Cited on page 151.)

[75] Baldi, M., "Clarifying the effects of interacting dark energy on linear and non-linear structure formation processes", *Mon. Not. R. Astron. Soc.*, **414**, 116–128 (2011). [DOI], [ADS], [arXiv:1012.0002 [astro-ph.CO]]. (Cited on pages 34, 66, 72, and 153.)

[76] Baldi, M., "Time-dependent couplings in the dark sector: from background evolution to non-linear structure formation", *Mon. Not. R. Astron. Soc.*, **411**, 1077–1103 (2011). [DOI], [ADS], [arXiv:1005.2188 [astro-ph.CO]]. (Cited on pages 34, 66, 67, 72, 152, and 153.)

[77] Baldi, M. and Pettorino, V., "High-z massive clusters as a test for dynamical coupled dark energy", *Mon. Not. R. Astron. Soc.*, **412**, L1–L5 (2011). [DOI], [ADS], [arXiv:1006.3761 [astro-ph.CO]]. (Cited on pages 34, 66, 72, and 153.)

[78] Baldi, M., Pettorino, V., Amendola, L. and Wetterich, C., "Oscillating non-linear large-scale structures in growing neutrino quintessence", *Mon. Not. R. Astron. Soc.*, **418**, 214–229 (2011). [DOI], [ADS], [arXiv:1106.2161 [astro-ph.CO]]. (Cited on page 34.)

[79] Baldi, M., Pettorino, V., Robbers, G. and Springel, V., "Hydrodynamical N-body simulations of coupled dark energy cosmologies", *Mon. Not. R. Astron. Soc.*, **403**, 1684–1702 (2010). [DOI], [ADS]. (Cited on pages 34, 59, 66, and 153.)

[80] Baldi, M. and Viel, M., "The impact of coupled dark energy cosmologies on the high-redshift intergalactic medium", *Mon. Not. R. Astron. Soc.*, **409**, L89–L93 (2010). [DOI], [ADS], [arXiv:1007.3736 [astro-ph.CO]]. (Cited on pages 34, 66, and 153.)

[81] Ballinger, W.E., Peacock, J.A. and Heavens, A.F., "Measuring the cosmological constant with redshift surveys", *Mon. Not. R. Astron. Soc.*, **282**, 877–888 (1996). [ADS], [arXiv:astro-ph/9605017]. (Cited on page 81.)

[82] Baltz, E.A. and Murayama, H., "Gravitino warm dark matter with entropy production", *J. High Energy Phys.*, **2003**(05), 067 (2003). [DOI], [arXiv:astro-ph/0108172]. (Cited on page 135.)

[83] Bañados, M., Ferreira, P.G. and Skordis, C., "Eddington-Born-Infeld gravity and the large scale structure of the Universe", *Phys. Rev. D*, **79**, 063511 (2009). [DOI], [ADS], [arXiv:0811.1272]. (Cited on pages 52, 159, and 161.)

[84] Banks, T. and Dine, M., "The Cosmology of String Theoretic Axions", *Nucl. Phys. B*, **505**, 445–460 (1997). [DOI], [ADS], [arXiv:hep-th/9608197]. (Cited on page 154.)

[85] Bardeen, J.M., Bond, J.R., Kaiser, N. and Szalay, A.S., "The Statistics of Peaks of Gaussian Random Fields", *Astrophys. J.*, **304**, 15–61 (1986). [DOI]. (Cited on page 78.)

[86] Bardeen, J.M., Steinhardt, P.J. and Turner, M.S., "Spontaneous creation of almost scale-free density perturbations in an inflationary universe", *Phys. Rev. D*, **28**, 679–693 (1983). [DOI], [ADS]. (Cited on pages 163 and 164.)

[87] Barkana, R., Haiman, Z. and Ostriker, J.P., "Constraints on Warm Dark Matter from Cosmological Reionization", *Astrophys. J.*, **558**, 482–496 (2001). [DOI], [ADS], [arXiv:astro-ph/0102304]. (Cited on page 124.)

[88] Barnaby, N. and Cline, J.M., "Non-Gaussian and nonscale-invariant perturbations from tachyonic preheating in hybrid inflation", *Phys. Rev. D*, **73**, 106012 (2006). [DOI], [ADS], [arXiv:astro-ph/0601481]. (Cited on page 171.)

[89] Barrow, J.D., Juszkiewicz, R. and Sonoda, D.H., "Universal rotation: how large can it be?", *Mon. Not. R. Astron. Soc.*, **213**, 917–943 (1985). [ADS]. (Cited on page 188.)

[90] Bartelmann, M., Narayan, R., Seitz, S. and Schneider, P., "Maximum Likelihood Cluster Reconstruction", *Astrophys. J. Lett.*, **464**, L115 (1996). [DOI], [ADS], [arXiv:astro-ph/9601011]. (Cited on page 130.)

[91] Bartolo, N., Dimastrogiovanni, E., Matarrese, S. and Riotto, A., "Anisotropic Bispectrum of Curvature Perturbations from Primordial Non-Abelian Vector Fields", *J. Cosmol. Astropart. Phys.*, **2009**(10), 015 (2009). [DOI], [ADS], [arXiv:0906.4944 [astro-ph.CO]]. (Cited on page 204.)

[92] Bartolo, N., Dimastrogiovanni, E., Matarrese, S. and Riotto, A., "Anisotropic trispectrum of curvature perturbations induced by primordial non-Abelian vector fields", *J. Cosmol. Astropart. Phys.*, **2009**(11), 028 (2009). [DOI], [ADS], [arXiv:0909.5621 [astro-ph.CO]]. (Cited on page 204.)

[93] Bartolo, N., Komatsu, E., Matarrese, S. and Riotto, A., "Non-Gaussianity from inflation: theory and observations", *Phys. Rep.*, **402**, 103–266 (2004). [DOI], [ADS], [arXiv:astro-ph/0406398]. (Cited on page 169.)

[94] Bartolo, N., Matarrese, S. and Riotto, A., "Signatures of primordial non-Gaussianity in the large-scale structure of the universe", *J. Cosmol. Astropart. Phys.*, **2005**(10), 010 (2005). [DOI], [ADS], [arXiv:astro-ph/0501614]. (Cited on page 177.)

[95] Basse, T., Bjælde, O.E. and Wong, Y.Y.Y., "Spherical collapse of dark energy with an arbitrary sound speed", *J. Cosmol. Astropart. Phys.*, **2011**(10), 038 (2011). [DOI], [ADS], [arXiv:1009.0010 [astro-ph.CO]]. (Cited on page 69.)

[96] Bassett, B.A., "Optimising cosmological surveys in a crowded market", *Phys. Rev. D*, **71**, 083517 (2005). [DOI], [ADS], [arXiv:astro-ph/0407201]. (Cited on pages 212 and 215.)

[97] Bassett, B.A., Corasaniti, P.S. and Kunz, M., "The essence of quintessence and the cost of compression", *Astrophys. J.*, **617**, L1–L4 (2004). [DOI], [arXiv:astro-ph/0407364]. (Cited on page 20.)

[98] Bassett, B.A., Fantaye, Y., Hlozek, R. and Kotze, J., "Fisher4Cast Users' Manual", *arXiv*, e-print, (2009). [arXiv:0906.0974 [astro-ph.IM]]. (Cited on page 212.)

[99] Bassett, B.A., Fantaye, Y., Hlozek, R. and Kotze, J., "Fisher Matrix Preloaded – Fisher4Cast", *Int. J. Mod. Phys. D*, **20**, 2559–2598 (2011). [DOI], [ADS], [arXiv:0906.0993 [astro-ph.CO]]. (Cited on page 212.)

[100] Bassett, B.A. and Kunz, M., "Cosmic Acceleration versus Axion-Photon Mixing", *Astrophys. J.*, **607**, 661–664 (2004). [DOI], [ADS], [arXiv:astro-ph/0311495]. (Cited on page 184.)

[101] Bassett, B.A. and Kunz, M., "Cosmic distance-duality as a probe of exotic physics and acceleration", *Phys. Rev. D*, **69**, 101305 (2004). [DOI], [ADS], [arXiv:astro-ph/0312443]. (Cited on page 184.)

[102] Bassett, B.A., Kunz, M., Silk, J. and Ungarelli, C., "A late-time transition in the cosmic dark energy?", *Mon. Not. R. Astron. Soc.*, **336**, 1217–1222 (2002). [DOI], [arXiv:astro-ph/0203383 [astro-ph]]. (Cited on pages 28 and 74.)

[103] Bassett, B.A., Parkinson, D. and Nichol, R.C., "Designer Cosmology", *Astrophys. J.*, **626**, L1–L4 (2005). [DOI], [arXiv:astro-ph/0409266]. (Cited on page 215.)

[104] Bassett, B.A., Tsujikawa, S. and Wands, D., "Inflation dynamics and reheating", *Rev. Mod. Phys.*, **78**, 537–589 (2006). [DOI], [ADS], [arXiv:astro-ph/0507632]. (Cited on page 28.)

[105] Batell, B. and Gherghetta, T., "Localized U(1) gauge fields, millicharged particles, and holography", *Phys. Rev. D*, **73**, 045016 (2006). [DOI], [ADS], [arXiv:hep-ph/0512356]. (Cited on page 186.)

[106] Battye, R.A. and Moss, A., "Anisotropic perturbations due to dark energy", *Phys. Rev. D*, **74**, 041301 (2006). [DOI], [ADS], [arXiv:astro-ph/0602377]. (Cited on pages 188 and 189.)

[107] Battye, R.A. and Pearson, J.A., "Effective action approach to cosmological perturbations in dark energy and modified gravity", *J. Cosmol. Astropart. Phys.*, **2012**(07), 019 (2012). [DOI], [ADS], [arXiv:1203.0398 [hep-th]]. (Cited on page 63.)

[108] Baugh, C.M., Lacey, C.G., Frenk, C.S., Granato, G.L., Silva, L., Bressan, A., Benson, A.J. and Cole, S., "Can the faint submillimetre galaxies be explained in the Λ cold dark matter model?", *Mon. Not. R. Astron. Soc.*, **356**, 1191–1200 (2005). [DOI], [arXiv:astro-ph/0406069 [astro-ph]]. (Cited on page 91.)

[109] Baumann, D. et al. (Inflation Working Group), "Probing Inflation with CMB Polarization", in Dodelson, S. et al., eds., *CMB Polarization Workshop: Theory and Foregrounds: CMBPol Mission Concept Study*, Workshop held at Fermilab in Batavia, IL, USA, 23 – 26 June 2008, AIP Conference Proceedings, 1141, pp. 10–120, (American Institute of Physics, Melville, NY, 2009). [DOI], [ADS], [arXiv:0811.3919 [astro-ph]]. (Cited on page 166.)

[110] Bean, R., Bernat, D., Pogosian, L., Silvestri, A. and Trodden, M., "Dynamics of linear perturbations in $f(R)$ gravity", *Phys. Rev. D*, **75**, 064020 (2007). [DOI], [ADS], [arXiv:astro-ph/0611321]. (Cited on page 41.)

[111] Bean, R., Chen, X., Peiris, H. and Xu, J., "Comparing Infrared Dirac-Born-Infeld Brane Inflation to Observations", *Phys. Rev. D*, **77**, 023527 (2008). [DOI], [arXiv:0710.1812 [hep-th]]. (Cited on page 173.)

[112] Bean, R. and Dore, O., "Probing dark energy perturbations: The Dark energy equation of state and speed of sound as measured by WMAP", *Phys. Rev. D*, **69**, 083503 (2004). [DOI], [arXiv:astro-ph/0307100 [astro-ph]]. (Cited on page 37.)

[113] Bean, R., Dunkley, J. and Pierpaoli, E., "Constraining isocurvature initial conditions with WMAP 3-year data", *Phys. Rev. D*, **74**, 063503 (2006). [DOI], [ADS], [arXiv:astro-ph/0606685]. (Cited on page 181.)

[114] Bean, R., Flanagan, É.É., Laszlo, I. and Trodden, M., "Constraining Interactions in Cosmology's Dark Sector", *Phys. Rev. D*, **78**, 123514 (2008). [DOI], [arXiv:0808.1105 [astro-ph]]. (Cited on pages 34 and 152.)

[115] Bean, R. and Tangmatitham, M., "Current constraints on the cosmic growth history", *Phys. Rev. D*, **81**, 083534 (2010). [DOI], [arXiv:1002.4197 [astro-ph.CO]]. (Cited on pages 25 and 63.)

[116] Bekenstein, J.D., "The relation between physical and gravitational geometry", *Phys. Rev. D*, **48**, 3641–3647 (1993). [DOI], [arXiv:gr-qc/9211017]. (Cited on page 50.)

[117] Bekenstein, J.D., "Relativistic gravitation theory for the MOND paradigm", *Phys. Rev. D*, **70**, 083509 (2004). [DOI], [arXiv:astro-ph/0403694]. (Cited on page 159.)

[118] Beltrán, M., García-Bellido, J. and Lesgourgues, J., "Isocurvature bounds on axions revisited", *Phys. Rev. D*, **75**, 103507 (2007). [DOI], [ADS], [arXiv:hep-ph/0606107]. (Cited on page 181.)

[119] Beltrán, M., García-Bellido, J., Lesgourgues, J., Liddle, A.R. and Slosar, A., "Bayesian model selection and isocurvature perturbations", *Phys. Rev. D*, **71**, 063532 (2005). [DOI], [arXiv:astro-ph/0501477 [astro-ph]]. (Cited on page 216.)

[120] Beltrán, M., García-Bellido, J., Lesgourgues, J. and Riazuelo, A., "Bounds on cold dark matter and neutrino isocurvature perturbations from CMB and LSS data", *Phys. Rev. D*, **70**, 103530 (2004). [DOI], [ADS], [arXiv:astro-ph/0409326]. (Cited on pages 181 and 182.)

[121] Bennett, C.L. et al., "First-Year Wilkinson Microwave Anisotropy Probe (WMAP) Observations: Preliminary Maps and Basic Results", *Astrophys. J. Suppl. Ser.*, **148**, 1–27 (2003). [DOI], [ADS], [arXiv:astro-ph/0302207]. (Cited on page 85.)

[122] Bennett, C.L. et al., "Seven-Year Wilkinson Microwave Anisotropy Probe (WMAP) Observations: Are There Cosmic Microwave Background Anomalies?", *Astrophys. J. Suppl. Ser.*, **192**, 17 (2011). [DOI], [ADS], [arXiv:1001.4758 [astro-ph.CO]]. (Cited on pages 188, 203, and 205.)

[123] Bento, M.C., Bertolami, O. and Sen, A.A., "Generalized Chaplygin gas, accelerated expansion, and dark-energy-matter unification", *Phys. Rev. D*, **66**, 043507 (2002). [DOI], [ADS], [arXiv:gr-qc/0202064]. (Cited on page 151.)

[124] Bento, M.C., Bertolami, O. and Sen, A.A., "Letter: Generalized Chaplygin Gas Model: Dark Energy-Dark Matter Unification and CMBR Constraints", *Gen. Relativ. Gravit.*, **35**, 2063–2069 (2003). [DOI], [ADS], [arXiv:gr-qc/0305086]. (Cited on page 151.)

[125] Bernardeau, F., Bonvin, C. and Vernizzi, F., "Full-sky lensing shear at second order", *Phys. Rev. D*, **81**, 083002 (2010). [DOI], [arXiv:0911.2244 [astro-ph.CO]]. (Cited on page 76.)

[126] Bernardeau, F. and Uzan, J.-P., "Non-Gaussianity in multifield inflation", *Phys. Rev. D*, **66**, 103506 (2002). [DOI], [ADS], [arXiv:hep-ph/0207295]. (Cited on pages 170 and 181.)

[127] Bertacca, D., Bartolo, N., Diaferio, A. and Matarrese, S., "How the scalar field of unified dark matter models can cluster", *J. Cosmol. Astropart. Phys.*, **2008**(10), 023 (2008). [DOI], [ADS], [arXiv:0807.1020]. (Cited on page 151.)

[128] Bertacca, D., Bartolo, N. and Matarrese, S., "Unified Dark Matter Scalar Field Models", *Adv. Astron.*, **2010**, 904379 (2010). [DOI], [ADS], [arXiv:1008.0614 [astro-ph.CO]]. (Cited on pages 150 and 151.)

[129] Bertolami, O., Pedro, F.G. and Le Delliou, M., "The Abell Cluster A586 and the Equivalence Principle", *Gen. Relativ. Gravit.*, **41**, 2839–2846 (2009). [DOI], [arXiv:0705.3118 [astro-ph]]. (Cited on pages 34, 66, and 153.)

[130] Bertotti, B., Iess, L. and Tortora, P., "A test of general relativity using radio links with the Cassini spacecraft", *Nature*, **425**, 374–376 (2003). [DOI]. (Cited on page 33.)

[131] Bertschinger, E. and Zukin, P., "Distinguishing modified gravity from dark energy", *Phys. Rev. D*, **78**, 024015 (2008). [DOI], [arXiv:0801.2431 [astro-ph]]. (Cited on pages 63 and 111.)

[132] Beynon, E., Bacon, D.J. and Koyama, K., "Weak lensing predictions for modified gravities at non-linear scales", *Mon. Not. R. Astron. Soc.*, **403**, 353–362 (2010). [DOI], [ADS], [arXiv:0910.1480]. (Cited on page 86.)

[133] Bezrukov, F. and Shaposhnikov, M., "The Standard Model Higgs boson as the inflaton", *Phys. Lett. B*, **659**, 703–706 (2008). [DOI], [ADS], [arXiv:0710.3755 [hep-th]]. (Cited on page 56.)

[134] Bi, H. and Davidsen, A.F., "Evolution of Structure in the Intergalactic Medium and the Nature of the Lyα Forest", *Astrophys. J.*, **479**, 523 (1997). [DOI], [ADS], [arXiv:astro-ph/9611062]. (Cited on page 122.)

[135] Bi, X.-J., Feng, B., Li, H. and Zhang, X., "Cosmological evolution of interacting dark energy models with mass varying neutrinos", *Phys. Rev. D*, **72**, 123523 (2005). [DOI], [arXiv:hep-ph/0412002]. (Cited on pages 34 and 143.)

[136] Biermann, P.L. and Munyaneza, F., "Dark matter and sterile neutrinos", in Kleinert, H., Jantzen, R.T. and Ruffini, R., eds., *The Eleventh Marcel Grossmann Meeting: On recent developments in theoretical and experimental general relativity, gravitation, and relativistic field theories*, Proceedings of the MG11 Meeting on General Relativity held in Berlin, Germany, 23 – 29 July 2006, pp. 291–308, (World Scientific, Singapore; River Edge, 2008). [DOI], [ADS], [arXiv:astro-ph/0702173]. (Cited on page 133.)

[137] Bilić, N., Tupper, G.B. and Viollier, R.D., "Unification of dark matter and dark energy: the inhomogeneous Chaplygin gas", *Phys. Lett. B*, **535**, 17–21 (2002). [DOI], [ADS], [arXiv:astro-ph/0111325]. (Cited on page 151.)

[138] Binétruy, P., "Models of dynamical supersymmetry breaking and quintessence", *Phys. Rev. D*, **60**, 063502 (1999). [DOI], [ADS], [arXiv:hep-ph/9810553]. (Cited on page 28.)

[139] Bjælde, O.E., Brookfield, A.W., van de Bruck, C., Hannestad, S., Mota, D.F., Schrempp, L. and Tocchini-Valentini, D., "Neutrino Dark Energy – Revisiting the Stability Issue", *J. Cosmol. Astropart. Phys.*, **2008**(01), 026 (2008). [DOI], [arXiv:0705.2018 [astro-ph]]. (Cited on pages 34 and 143.)

[140] Blake, C.A., Abdalla, F.B., Bridle, S.L. and Rawlings, S., "Cosmology with the Square Kilometre Array", *New Astron. Rev.*, **48**, 1063–1077 (2004). [DOI], [arXiv:astro-ph/0409278 [astro-ph]]. (Cited on page 117.)

[141] Blomqvist, M. and Mörtsell, E., "Supernovae as seen by off-center observers in a local void", *J. Cosmol. Astropart. Phys.*, **2010**(05), 006 (2010). [DOI], [ADS], [arXiv:0909.4723 [astro-ph.CO]]. (Cited on page 191.)

[142] Bloomfield, J.K., Flanagan, É.É., Park, M. and Watson, S., "Dark energy or modified gravity? An effective field theory approach", *J. Cosmol. Astropart. Phys.*, **2013**(08), 010 (2013). [DOI], [ADS], [arXiv:1211.7054 [astro-ph.CO]]. (Cited on page 63.)

[143] Bode, P., Ostriker, J.P. and Turok, N., "Halo Formation in Warm Dark Matter Models", *Astrophys. J.*, **556**, 93–107 (2001). [DOI], [ADS], [arXiv:astro-ph/0010389]. (Cited on pages 124, 133, and 135.)

[144] Boehmer, C.G., Caldera-Cabral, G., Chan, N., Lazkoz, R. and Maartens, R., "Quintessence with quadratic coupling to dark matter", *Phys. Rev. D*, **81**, 083003 (2010). [DOI], [arXiv:0911.3089 [gr-qc]]. (Cited on page 34.)

[145] Boehmer, C.G., Caldera-Cabral, G., Lazkoz, R. and Maartens, R., "Dynamics of dark energy with a coupling to dark matter", *Phys. Rev. D*, **78**, 023505 (2008). [DOI], [arXiv:0801.1565 [gr-qc]]. (Cited on page 34.)

[146] Boisseau, B., Esposito-Farèse, G., Polarski, D. and Starobinsky, A.A., "Reconstruction of a scalar-tensor theory of gravity in an accelerating universe", *Phys. Rev. Lett.*, **85**, 2236 (2000). [DOI], [arXiv:gr-qc/0001066]. (Cited on page 34.)

[147] Bond, J.R., Cole, S., Efstathiou, G. and Kaiser, N., "Excursion set mass functions for hierarchical Gaussian fluctuations", *Astrophys. J.*, **379**, 440–460 (1991). [DOI], [ADS]. (Cited on page 68.)

[148] Bond, J.R., Frolov, A.V., Huang, Z. and Kofman, L., "Non-Gaussian Curvature Spikes from Chaotic Billiards in Inflation Preheating", *Phys. Rev. Lett.*, **103**, 071301 (2009). [DOI], [ADS], [arXiv:0903.3407 [astro-ph.CO]]. (Cited on page 170.)

[149] Bonometto, S.A., Casarini, L., Macciò, A.V. and Stinson, G., "High precision spectra at large redshift for dynamical DE cosmologies", *J. Phys.: Conf. Ser.*, **259**, 012025 (2010). [DOI], [arXiv:1009.2964 [astro-ph.CO]]. (Cited on page 104.)

[150] Bonvin, C., "Effect of Peculiar Motion in Weak Lensing", *Phys. Rev. D*, **78**, 123530 (2008). [DOI], [arXiv:0810.0180 [astro-ph]]. (Cited on pages 75 and 76.)

[151] Borgani, S. and Masiero, A., "Dark Matter and the Scale of SUSY Breaking", *arXiv*, e-print, (1997). [ADS], [arXiv:hep-ph/9701417]. (Cited on page 135.)

[152] Borgani, S., Rosati, P., Sartoris, B., Tozzi, P. and Giacconi, R. (WFXT Team), "Astrophysics and cosmology with galaxy clusters: the WFXT perspective", *Mem. Soc. Astron. Ital. Suppl.*, **17**, 36 (2011). [ADS], [arXiv:1010.6213 [astro-ph.CO]]. (Cited on page 129.)

[153] Borriello, A. and Salucci, P., "The dark matter distribution in disc galaxies", *Mon. Not. R. Astron. Soc.*, **323**, 285–292 (2001). [DOI], [ADS], [arXiv:astro-ph/0001082]. (Cited on page 124.)

[154] Bose, N. and Majumdar, A.S., "Unified model of k-inflation, dark matter, and dark energy", *Phys. Rev. D*, **80**, 103508 (2009). [DOI], [ADS], [arXiv:0907.2330 [astro-ph.CO]]. (Cited on page 151.)

[155] Boubekeur, L. and Lyth, D.H., "Detecting a small perturbation through its non-Gaussianity", *Phys. Rev. D*, **73**, 021301 (2006). [DOI], [ADS], [arXiv:astro-ph/0504046]. (Cited on page 170.)

[156] Bourassa, R.R. and Kantowski, R., "The theory of transparent gravitational lenses", *Astrophys. J.*, **195**, 13–21 (1975). [DOI], [ADS]. (Cited on page 124.)

[157] Bourliot, F., Ferreira, P.G., Mota, D.F. and Skordis, C., "Cosmological behavior of Bekenstein's modified theory of gravity", *Phys. Rev. D*, **75**, 063508 (2007). [DOI], [ADS], [arXiv:astro-ph/0611255]. (Cited on page 51.)

[158] Bowen, R., Hansen, S.H., Melchiorri, A., Silk, J. and Trotta, R., "The Impact of an Extra Background of Relativistic Particles on the Cosmological Parameters derived from Microwave Background Anisotropies", *Mon. Not. R. Astron. Soc.*, **334**, 760 (2002). [DOI], [arXiv:astro-ph/0110636]. (Cited on page 139.)

[159] Boyanovsky, D., de Vega, H.J. and Sanchez, N., "Constraints on dark matter particles from theory, galaxy observations and N-body simulations", *Phys. Rev. D*, **77**, 043518 (2008). [DOI], [arXiv:0710.5180 [astro-ph]]. (Cited on page 133.)

[160] Boyarsky, A., Lesgourgues, J., Ruchayskiy, O. and Viel, M., "Realistic sterile neutrino dark matter with keV mass does not contradict cosmological bounds", *Phys. Rev. Lett.*, **102**, 201304 (2009). [DOI], [arXiv:0812.3256 [hep-ph]]. (Cited on page 136.)

[161] Boyarsky, A., Neronov, A., Ruchayskiy, O. and Shaposhnikov, M., "The masses of active neutrinos in the νMSM from X-ray astronomy", *JETP Lett.*, **83**, 133–135 (2006). [DOI], [arXiv:hep-ph/0601098]. (Cited on page 136.)

[162] Bradač, M., Allen, S.W., Treu, T., Ebeling, H., Massey, R., Morris, R.G., von der Linden, A. and Applegate, D., "Revealing the Properties of Dark Matter in the Merging Cluster MACS J0025.4-1222", *Astrophys. J.*, **687**, 959–967 (2008). [DOI], [ADS], [arXiv:0806.2320 [astro-ph]]. (Cited on page 132.)

[163] Bradač, M., Schneider, P., Lombardi, M. and Erben, T., "Strong and weak lensing united", *Astron. Astrophys.*, **437**, 39–48 (2005). [DOI], [ADS]. (Cited on page 130.)

[164] Bradač, M. et al., "Strong and Weak Lensing United. III. Measuring the Mass Distribution of the Merging Galaxy Cluster 1ES 0657-558", *Astrophys. J.*, **652**, 937–947 (2006). [DOI], [ADS], [arXiv:astro-ph/0608408]. (Cited on pages 130 and 132.)

[165] Branchini, E., Plionis, M. and Sciama, D.W., "Reconstructing Positions and Peculiar Velocities of Galaxy Clusters within 25,000 Kilometers per Second: The Bulk Velocity", *Astrophys. J. Lett.*, **461**, L17 (1996). [DOI], [ADS], [arXiv:astro-ph/9512055]. (Cited on page 84.)

[166] Brandbyge, J. and Hannestad, S., "Grid based linear neutrino perturbations in cosmological N-body simulations", *J. Cosmol. Astropart. Phys.*, **2009**(05), 002 (2009). [DOI], [ADS], [arXiv:0812.3149]. (Cited on page 142.)

[167] Brandbyge, J., Hannestad, S., Haugbølle, T. and Thomsen, B., "The effect of thermal neutrino motion on the non-linear cosmological matter power spectrum", *J. Cosmol. Astropart. Phys.*, **2008**(08), 020 (2008). [DOI], [ADS], [arXiv:0802.3700]. (Cited on page 142.)

[168] Brandbyge, J., Hannestad, S., Haugbølle, T. and Wong, Y.Y.Y., "Neutrinos in non-linear structure formation – the effect on halo properties", *J. Cosmol. Astropart. Phys.*, **2010**(09), 014 (2010). [DOI], [ADS], [arXiv:1004.4105 [astro-ph.CO]]. (Cited on page 142.)

[169] Brax, P., Burrage, C., Davis, A.-C., Seery, D. and Weltman, A., "Higgs production as a probe of chameleon dark energy", *Phys. Rev. D*, **81**, 103524 (2010). [DOI], [ADS], [arXiv:0911.1267 [hep-ph]]. (Cited on page 185.)

[170] Brax, P.H. and Martin, J., "Quintessence and supergravity", *Phys. Lett. B*, **468**, 40–45 (1999). [DOI], [ADS], [arXiv:astro-ph/9905040]. (Cited on page 29.)

[171] Brax, P., van de Bruck, C., Davis, A.-C., Khoury, J. and Weltman, A., "Detecting dark energy in orbit: The cosmological chameleon", *Phys. Rev. D*, **70**, 123518 (2004). [DOI], [arXiv:astro-ph/0408415]. (Cited on page 35.)

[172] Brax, P., van de Bruck, C., Davis, A.-C. and Shaw, D.J., "$f(R)$ gravity and chameleon theories", *Phys. Rev. D*, **78**, 104021 (2008). [DOI], [arXiv:0806.3415 [astro-ph]]. (Cited on page 35.)

[173] Brax, P., van de Bruck, C., Mota, D.F., Nunes, N.J. and Winther, H.A., "Chameleons with field-dependent couplings", *Phys. Rev. D*, **82**, 083503 (2010). [DOI], [arXiv:1006.2796 [astro-ph.CO]]. (Cited on page 35.)

[174] Bridges, M., Cranmer, K., Feroz, F., Hobson, M., Ruiz de Austri, R. and Trotta, R., "A coverage study of the CMSSM based on ATLAS sensitivity using fast neural networks techniques", *J. High Energy Phys.*, **2011**(03), 012 (2011). [DOI], [ADS], [arXiv:1011.4306 [hep-ph]]. (Cited on page 216.)

[175] Broadhurst, T.J., Taylor, A.N. and Peacock, J.A., "Mapping cluster mass distributions via gravitational lensing of background galaxies", *Astrophys. J.*, **438**, 49–61 (1995). [DOI], [ADS], [arXiv:astro-ph/9406052]. (Cited on pages 75 and 77.)

[176] Brookfield, A.W., van de Bruck, C. and Hall, L.M.H., "New interactions in the dark sector mediated by dark energy", *Phys. Rev. D*, **77**, 043006 (2008). [DOI], [arXiv:0709.2297 [astro-ph]]. (Cited on page 33.)

[177] Brookfield, A.W., van de Bruck, C., Mota, D.F. and Tocchini-Valentini, D., "Cosmology of mass-varying neutrinos driven by quintessence: Theory and observations", *Phys. Rev. D*, **73**, 083515 (2006). [DOI], [arXiv:astro-ph/0512367]. (Cited on pages 34 and 143.)

[178] Brookfield, A.W., van de Bruck, C., Mota, D.F. and Tocchini-Valentini, D., "Cosmology with massive neutrinos coupled to dark energy", *Phys. Rev. Lett.*, **96**, 061301 (2006). [DOI], [arXiv:astro-ph/0503349]. (Cited on pages 34 and 143.)

[179] Brouzakis, N., Pettorino, V., Tetradis, N. and Wetterich, C., "Nonlinear matter spectra in growing neutrino quintessence", *J. Cosmol. Astropart. Phys.*, **2011**(03), 049 (2011). [DOI], [ADS], [arXiv:1012.5255 [astro-ph.CO]]. (Cited on pages 34, 73, 143, and 150.)

[180] Brouzakis, N., Tetradis, N. and Wetterich, C., "Neutrino Lumps in Quintessence Cosmology", *Phys. Lett. B*, **665**, 131–134 (2008). [DOI], [arXiv:0711.2226 [astro-ph]]. (Cited on page 73.)

[181] Brümmer, F., Jaeckel, J. and Khoze, V.V., "Magnetic mixing – electric minicharges from magnetic monopoles", *J. High Energy Phys.*, **2009**(06), 037 (2009). [DOI], [ADS], [arXiv:0905.0633 [hep-ph]]. (Cited on page 186.)

[182] Buchbinder, E.I., Khoury, J. and Ovrut, B.A., "New ekpyrotic cosmology", *Phys. Rev. D*, **76**, 123503 (2007). [DOI], [ADS], [arXiv:hep-th/0702154]. (Cited on page 173.)

[183] Buchbinder, E.I., Khoury, J. and Ovrut, B.A., "Non-Gaussianities in New Ekpyrotic Cosmology", *Phys. Rev. Lett.*, **100**, 171302 (2008). [DOI], [ADS], [arXiv:0710.5172 [hep-th]]. (Cited on page 173.)

[184] Bucher, M., Moodley, K. and Turok, N., "Constraining Isocurvature Perturbations with Cosmic Microwave Background Polarization", *Phys. Rev. Lett.*, **87**, 191301 (2001). [DOI], [ADS], [arXiv:astro-ph/0012141]. (Cited on page 182.)

[185] Buchert, T., "On Average Properties of Inhomogeneous Fluids in General Relativity: Dust Cosmologies", *Gen. Relativ. Gravit.*, **32**, 105–125 (2000). [DOI], [arXiv:gr-qc/9906015 [gr-qc]]. (Cited on page 195.)

[186] Buchert, T., "Dark energy from structure: a status report", *Gen. Relativ. Gravit.*, **40**, 467–527 (2008). [DOI], [ADS], [arXiv:0707.2153 [gr-qc]]. (Cited on page 195.)

[187] Bull, P., Clifton, T. and Ferreira, P.G., "Kinematic Sunyaev-Zel'dovich effect as a test of general radial inhomogeneity in Lemaître-Tolman-Bondi cosmology", *Phys. Rev. D*, **85**, 024002 (2012). [DOI], [arXiv:1108.2222 [astro-ph.CO]]. (Cited on page 194.)

[188] Bullock, J.S., "Notes on the Missing Satellites Problem", *arXiv*, e-print, (2010). [ADS], [arXiv:1009.4505 [astro-ph.CO]]. (Cited on page 133.)

[189] Bunn, E.F., Ferreira, P.G. and Silk, J., "How Anisotropic is Our Universe?", *Phys. Rev. Lett.*, **77**, 2883–2886 (1996). [DOI], [ADS], [arXiv:astro-ph/9605123]. (Cited on pages 188 and 189.)

[190] Burrage, C., "Supernova brightening from chameleon-photon mixing", *Phys. Rev. D*, **77**, 043009 (2008). [DOI], [ADS], [arXiv:0711.2966]. (Cited on pages 184 and 185.)

[191] Byrnes, C.T., Choi, K.-Y. and Hall, L.M.H., "Conditions for large non-Gaussianity in two-field slow-roll inflation", *J. Cosmol. Astropart. Phys.*, **2008**(10), 008 (2008). [DOI], [ADS], [arXiv:0807.1101]. (Cited on page 170.)

[192] Caldera-Cabral, G., Maartens, R. and Schaefer, B.M., "The Growth of Structure in Interacting Dark Energy Models", *J. Cosmol. Astropart. Phys.*, **2009**(07), 027 (2009). [DOI], [arXiv:0905.0492 [astro-ph.CO]]. (Cited on pages 34, 67, and 153.)

[193] Caldera-Cabral, G., Maartens, R. and Ureña-López, L.A., "Dynamics of interacting dark energy", *Phys. Rev. D*, **79**, 063518 (2009). [DOI], [arXiv:0812.1827 [gr-qc]]. (Cited on pages 34, 67, and 153.)

[194] Caldwell, R., Cooray, A. and Melchiorri, A., "Constraints on a new post-general relativity cosmological parameter", *Phys. Rev. D*, **76**, 023507 (2007). [DOI], [arXiv:astro-ph/0703375]. (Cited on page 25.)

[195] Caldwell, R.R., Dave, R. and Steinhardt, P.J., "Cosmological Imprint of an Energy Component with General Equation of State", *Phys. Rev. Lett.*, **80**, 1582–1585 (1998). [DOI], [ADS], [arXiv:astro-ph/9708069]. (Cited on page 27.)

[196] Caldwell, R.R. and Linder, E.V., "Limits of Quintessence", *Phys. Rev. Lett.*, **95**, 141301 (2005). [DOI], [ADS], [arXiv:astro-ph/0505494]. (Cited on page 28.)

[197] Caldwell, R.R. and Stebbins, A., "A Test of the Copernican Principle", *Phys. Rev. Lett.*, **100**, 191302 (2008). [DOI], [ADS], [arXiv:0711.3459]. (Cited on page 194.)

[198] Camera, S., Bertacca, D., Diaferio, A., Bartolo, N. and Matarrese, S., "Weak lensing signal in Unified Dark Matter models", *Mon. Not. R. Astron. Soc.*, **399**, 1995–2003 (2009). [DOI], [arXiv:0902.4204 [astro-ph.CO]]. (Cited on page 152.)

[199] Camera, S., Diaferio, A. and Cardone, V.F., "Testing a Phenomenologically Extended DGP Model with Upcoming Weak Lensing Surveys", *J. Cosmol. Astropart. Phys.*, **2011**(01), 029 (2011). [DOI], [arXiv:1101.2560 [astro-ph.CO]]. (Cited on pages 85 and 120.)

[200] Camera, S., Diaferio, A. and Cardone, V.F., "Tomography from the Next Generation of Cosmic Shear Experiments for Viable $f(R)$ Models", *J. Cosmol. Astropart. Phys.*, **2011**(07), 016 (2011). [DOI], [arXiv:1104.2740 [astro-ph.CO]]. (Cited on page 110.)

[201] Camera, S., Kitching, T.D., Heavens, A.F., Bertacca, D. and Diaferio, A., "Measuring unified dark matter with 3D cosmic shear", *Mon. Not. R. Astron. Soc.*, **415**, 399–409 (2010). [DOI], [ADS], [arXiv:1002.4740 [astro-ph.CO]]. (Cited on pages 151 and 152.)

[202] Camera, S., Kitching, T.D., Heavens, A.F., Bertacca, D. and Diaferio, A., "Measuring unified uark matter with 3D cosmic shear", *Mon. Not. R. Astron. Soc.*, **415**, 399–409 (2011). [DOI], [ADS], [arXiv:1002.4740 [astro-ph.CO]]. (Cited on pages 152 and 162.)

[203] Campanelli, L., Cea, P. and Tedesco, L., "Cosmic microwave background quadrupole and ellipsoidal universe", *Phys. Rev. D*, **76**, 063007 (2007). [DOI], [ADS], [arXiv:0706.3802]. (Cited on page 188.)

[204] Capozziello, S., "Curvature Quintessence", *Int. J. Mod. Phys. D*, **11**, 483–491 (2002). [DOI], [ADS], [arXiv:gr-qc/0201033]. (Cited on page 40.)

[205] Capozziello, S., Nesseris, S. and Perivolaropoulos, L., "Reconstruction of the scalar–tensor Lagrangian from a ΛCDM background and Noether symmetry", *J. Cosmol. Astropart. Phys.*, **2007**(12), 009 (2007). [DOI], [ADS], [arXiv:0705.3586 [astro-ph]]. (Cited on page 34.)

[206] Capozziello, S., Nojiri, S. and Odintsov, S.D., "Unified phantom cosmology: Inflation, dark energy and dark matter under the same standard", *Phys. Lett. B*, **632**, 597–604 (2006). [DOI], [ADS], [arXiv:hep-th/0507182]. (Cited on page 151.)

[207] Cappelluti, N. et al., "eROSITA on SRG: A X-ray all-sky survey mission", *Mem. Soc. Astron. Ital. Suppl.*, **17**, 159–164 (2011). [arXiv:1004.5219 [astro-ph.IM]]. URL (accessed 11 June 2013): `http://sait.oat.ts.astro.it/MSAIS/17/PDF/159.pdf`. (Cited on page 129.)

[208] Carbone, C., Mangilli, A. and Verde, L., "Isocurvature modes and Baryon Acoustic Oscillations II: gains from combining CMB and Large Scale Structure", *J. Cosmol. Astropart. Phys.*, **2011**(09), 028 (2011). [DOI], [ADS], [arXiv:1107.1211 [astro-ph.CO]]. (Cited on page 182.)

[209] Carbone, C., Mena, O. and Verde, L., "Cosmological parameters degeneracies and non-Gaussian halo bias", *J. Cosmol. Astropart. Phys.*, **2010**(07), 020 (2010). [DOI], [ADS], [arXiv:1003.0456 [astro-ph.CO]]. (Cited on pages 176 and 177.)

[210] Carbone, C., Verde, L. and Matarrese, S., "Non-Gaussian Halo Bias and Future Galaxy Surveys", *Astrophys. J. Lett.*, **684**, L1–L4 (2008). [DOI], [ADS], [arXiv:0806.1950]. (Cited on pages 176 and 177.)

[211] Carbone, C., Verde, L., Wang, Y. and Cimatti, A., "Neutrino constraints from future nearly all-sky spectroscopic galaxy surveys", *J. Cosmol. Astropart. Phys.*, **2011**(03), 030 (2011). [DOI], [ADS], [arXiv:1012.2868 [astro-ph.CO]]. (Cited on pages 138, 140, 141, and 162.)

[212] Carroll, S.M., Duvvuri, V., Trodden, M. and Turner, M.S., "Is cosmic speed-up due to new gravitational physics?", *Phys. Rev. D*, **70**, 043528 (2004). [DOI], [ADS], [arXiv:astro-ph/0306438]. (Cited on page 40.)

[213] Carroll, S.M., Sawicki, I., Silvestri, A. and Trodden, M., "Modified-source gravity and cosmological structure formation", *New J. Phys.*, **8**, 323 (2006). [DOI], [ADS], [arXiv:astro-ph/0607458]. (Cited on page 41.)

[214] Carturan, D. and Finelli, F., "Cosmological effects of a class of fluid dark energy models", *Phys. Rev. D*, **68**, 103501 (2003). [DOI], [ADS], [arXiv:astro-ph/0211626]. (Cited on page 37.)

[215] Casarini, L., La Vacca, G., Amendola, L., Bonometto, S.A. and Macciò, A.V., "Non-linear weak lensing forecasts", *J. Cosmol. Astropart. Phys.*, **2011**(03), 026 (2011). [DOI], [ADS], [arXiv:1102.3877 [astro-ph.CO]]. (Cited on pages 103 and 104.)

[216] Casas, J.A., García-Bellido, J. and Quirós, M., "On the gravity theories and cosmology from strings", *Nucl. Phys. B*, **361**, 713–728 (1991). [DOI]. (Cited on page 34.)

[217] Casas, J.A., García-Bellido, J. and Quirós, M., "Scalar–tensor theories of gravity with ϕ-dependent masses", *Class. Quantum Grav.*, **9**, 1371–1384 (1992). [DOI]. (Cited on page 34.)

[218] Catelan, P., Lucchin, F., Matarrese, S. and Moscardini, L., "Eulerian perturbation theory in non-flat universes: second-order approximation", *Mon. Not. R. Astron. Soc.*, **276**, 39–56 (1995). [ADS], [arXiv:astro-ph/9411066]. (Cited on page 174.)

[219] Catena, R., Pietroni, M. and Scarabello, L., "Einstein and Jordan frames reconciled: a frame-invariant approach to scalar-tensor cosmology", *Phys. Rev. D*, **76**, 084039 (2007). [DOI], [arXiv:astro-ph/0604492]. (Cited on pages 35 and 39.)

[220] Célérier, M.-N., "Do we really see a cosmological constant in the supernovae data?", *Astron. Astrophys.*, **353**, 63–71 (2000). [ADS], [arXiv:astro-ph/9907206]. (Cited on page 191.)

[221] Cembranos, J.A.R., Feng, J.L., Rajaraman, A. and Takayama, F., "Superweakly Interacting Massive Particle Solutions to Small Scale Structure Problems", *Phys. Rev. Lett.*, **95**, 181301 (2005). [DOI]. (Cited on page 135.)

[222] Chambers, A., Nurmi, S. and Rajantie, A., "Non-Gaussianity from resonant curvaton decay", *J. Cosmol. Astropart. Phys.*, **2010**(01), 012 (2010). [DOI], [ADS], [arXiv:0909.4535 [astro-ph.CO]]. (Cited on page 170.)

[223] Chen, X., "Inflation from warped space", *J. High Energy Phys.*, **2005**(08), 045 (2005). [DOI], [arXiv:hep-th/0501184 [hep-th]]. (Cited on page 173.)

[224] Chen, X., "Running non-Gaussianities in Dirac-Born-Infeld inflation", *Phys. Rev. D*, **72**, 123518 (2005). [DOI], [arXiv:astro-ph/0507053 [astro-ph]]. (Cited on page 173.)

[225] Chen, X., Easther, R. and Lim, E.A., "Large non-Gaussianities in single-field inflation", *J. Cosmol. Astropart. Phys.*, **2007**(06), 023 (2007). [DOI], [ADS], [arXiv:astro-ph/0611645]. (Cited on page 172.)

[226] Chen, X., Huang, M.-X., Kachru, S. and Shiu, G., "Observational signatures and non-Gaussianities of general single-field inflation", *J. Cosmol. Astropart. Phys.*, **2007**(01), 002 (2007). [DOI], [ADS], [arXiv:hep-th/0605045]. (Cited on pages 170 and 172.)

[227] Cheung, C., Fitzpatrick, A.L., Kaplan, J. and Senatore, L., "On the consistency relation of the three-point function in single-field inflation", *J. Cosmol. Astropart. Phys.*, **2008**(02), 021 (2008). [DOI], [ADS], [arXiv:0709.0295 [hep-th]]. (Cited on page 170.)

[228] Cheung, C., Fitzpatrick, A.L., Kaplan, J., Senatore, L. and Creminelli, P., "The effective field theory of inflation", *J. High Energy Phys.*, **2008**(03), 014 (2008). [DOI], [ADS], [arXiv:0709.0293 [hep-th]]. (Cited on pages 69 and 172.)

[229] Chevallier, M. and Polarski, D., "Accelerating universes with scaling dark matter", *Int. J. Mod. Phys. D*, **10**, 213–224 (2001). [DOI], [arXiv:gr-qc/0009008 [gr-qc]]. (Cited on pages 20, 89, and 212.)

[230] Chiba, T., "$1/R$ gravity and scalar-tensor gravity", *Phys. Lett. B*, **575**, 1–3 (2003). [DOI], [ADS], [arXiv:astro-ph/0307338]. (Cited on pages 40 and 110.)

[231] Chiba, T., Dutta, S. and Scherrer, R.J., "Slow-roll k-essence", *Phys. Rev. D*, **80**, 043517 (2009). [DOI], [arXiv:0906.0628 [astro-ph.CO]]. (Cited on page 19.)

[232] Chiba, T., Siino, M. and Yamaguchi, M., "Slow-roll Extended Quintessence", *Phys. Rev. D*, **81**, 083530 (2010). [DOI], [arXiv:1002.2986 [astro-ph.CO]]. (Cited on page 19.)

[233] Chimento, L.P. and Forte, M., "Anisotropic k-essence cosmologies", *Phys. Rev. D*, **73**, 063502 (2006). [DOI], [ADS], [arXiv:astro-ph/0510726]. (Cited on pages 188 and 189.)

[234] Chimento, L.P. and Forte, M., "Unified model of baryonic matter and dark components", *Phys. Lett. B*, **666**, 205–211 (2008). [DOI], [ADS], [arXiv:0706.4142]. (Cited on page 151.)

[235] Chimento, L.P., Jakubi, A.S., Pavon, D. and Zimdahl, W., "Interacting quintessence solution to the coincidence problem", *Phys. Rev. D*, **67**, 083513 (2003). [DOI], [arXiv:astro-ph/0303145]. (Cited on page 34.)

[236] Chimento, L.P., Lazkoz, R. and Sendra, I., "DBI models for the unification of dark matter and dark energy", *Gen. Relativ. Gravit.*, **42**, 1189–1209 (2010). [DOI], [ADS], [arXiv:0904.1114 [astro-ph.CO]]. (Cited on page 151.)

[237] Chimento, L.P. and Pavon, D., "Dual interacting cosmologies and late accelerated expansion", *Phys. Rev. D*, **73**, 063511 (2006). [DOI], [arXiv:gr-qc/0505096]. (Cited on page 34.)

[238] Choudhury, T.R., Srianand, R. and Padmanabhan, T., "Semianalytic Approach to Understanding the Distribution of Neutral Hydrogen in the Universe: Comparison of Simulations with Observations", *Astrophys. J.*, **559**, 29–40 (2001). [DOI], [ADS], [arXiv:astro-ph/0012498]. (Cited on page 122.)

[239] Cimatti, A. et al., "SPACE: the spectroscopic all-sky cosmic explorer", *Exp. Astron.*, **23**, 39–66 (2009). [DOI], [ADS], [arXiv:0804.4433]. (Cited on page 15.)

[240] Clarkson, C., Bassett, B. and Lu, T.H.-C., "A General Test of the Copernican Principle", *Phys. Rev. Lett.*, **101**, 011301 (2008). [DOI], [ADS], [arXiv:0712.3457]. (Cited on page 198.)

[241] Clarkson, C., Clifton, T. and February, S., "Perturbation theory in Lemaître-Tolman-Bondi cosmology", *J. Cosmol. Astropart. Phys.*, **2009**(06), 025 (2009). [DOI], [arXiv:0903.5040 [astro-ph.CO]]. (Cited on page 194.)

[242] Clarkson, C. and Maartens, R., "Inhomogeneity and the foundations of concordance cosmology", *Class. Quantum Grav.*, **27**, 124008 (2010). [DOI], [ADS], [arXiv:1005.2165 [astro-ph.CO]]. (Cited on pages 190 and 191.)

[243] Cline, J.M., Crotty, P. and Lesgourgues, J., "Does the small CMB quadrupole moment suggest new physics?", *J. Cosmol. Astropart. Phys.*, **2003**(09), 010 (2003). [DOI], [ADS], [arXiv:astro-ph/0304558]. (Cited on page 188.)

[244] Clowe, D., Bradač, M., Gonzalez, A.H., Markevitch, M., Randall, S.W., Jones, C. and Zaritsky, D., "A Direct Empirical Proof of the Existence of Dark Matter", *Astrophys. J. Lett.*, **648**, L109–L113 (2006). [DOI], [ADS], [arXiv:astro-ph/0608407]. (Cited on pages 124 and 132.)

[245] Clowe, D. et al., "Weak lensing mass reconstructions of the ESO Distant Cluster Survey", *Astron. Astrophys.*, **451**, 395–408 (2006). [DOI], [ADS], [arXiv:astro-ph/0511746]. (Cited on page 130.)

[246] Coc, A., Vangioni-Flam, E., Cassé, M. and Rabiet, M., "Constraints on Ω_b from nucleosynthesis of ^{7}Li in the standard big bang model", *Phys. Rev. D*, **65**, 043510 (2002). [DOI], [ADS], [arXiv:astro-ph/0111077]. (Cited on page 122.)

[247] Colberg, J.M. et al., "The Aspen-Amsterdam void finder comparison project", *Mon. Not. R. Astron. Soc.*, **387**, 933–944 (2008). [DOI], [ADS], [arXiv:0803.0918]. (Cited on page 177.)

[248] Colin, P., Avila-Reese, V. and Valenzuela, O., "Substructure and halo density profiles in a Warm Dark Matter Cosmology", *Astrophys. J.*, **542**, 622–630 (2000). [DOI], [arXiv:astro-ph/0004115]. (Cited on page 133.)

[249] Collins, C.B. and Hawking, S.W., "The rotation and distortion of the Universe", *Mon. Not. R. Astron. Soc.*, **162**, 307 (1973). [ADS]. (Cited on page 188.)

[250] Connes, A., *Géométrie non commutative*, (InterEditions, Paris, 1990). (Cited on page 201.)

[251] Cooray, A., Holz, D.E. and Caldwell, R., "Measuring dark energy spatial inhomogeneity with supernova data", *J. Cosmol. Astropart. Phys.*, **2010**(11), 015 (2010). [DOI], [ADS], [arXiv:0812.0376 [astro-ph]]. (Cited on pages 188 and 189.)

[252] Copeland, E.J., Liddle, A.R. and Wands, D., "Exponential potentials and cosmological scaling solutions", *Phys. Rev. D*, **57**, 4686–4690 (1998). [DOI], [arXiv:gr-qc/9711068]. (Cited on page 19.)

[253] Copi, C.J., Huterer, D., Schwarz, D.J. and Starkman, G.D., "Uncorrelated universe: Statistical anisotropy and the vanishing angular correlation function in WMAP years 1–3", *Phys. Rev. D*, **75**, 023507 (2007). [DOI], [ADS], [arXiv:astro-ph/0605135]. (Cited on page 203.)

[254] Copi, C.J., Huterer, D., Schwarz, D.J. and Starkman, G.D., "Large-Angle Anomalies in the CMB", *Adv. Astron.*, **2010**, 847541 (2010). [DOI], [ADS], [arXiv:1004.5602 [astro-ph.CO]]. (Cited on page 203.)

[255] Corasaniti, P.S. and Melchiorri, A., "Testing cosmology with cosmic sound waves", *Phys. Rev. D*, **77**, 103507 (2008). [DOI], [arXiv:0711.4119 [astro-ph]]. (Cited on page 118.)

[256] Courteau, S., Willick, J.A., Strauss, M.A., Schlegel, D. and Postman, M., "Shellflow. I. The Convergence of the Velocity Field at 6000 Kilometers Per Second", *Astrophys. J.*, **544**, 636–640 (2000). [DOI], [ADS], [arXiv:astro-ph/0002420]. (Cited on page 84.)

[257] Creminelli, P., D'Amico, G., Musso, M. and Noreña, J., "The (not so) squeezed limit of the primordial 3-point function", *J. Cosmol. Astropart. Phys.*, **2011**(11), 038 (2011). [DOI], [ADS], [arXiv:1106.1462 [astro-ph.CO]]. (Cited on page 173.)

[258] Creminelli, P., D'Amico, G., Noreña, J., Senatore, L. and Vernizzi, F., "Spherical collapse in quintessence models with zero speed of sound", *J. Cosmol. Astropart. Phys.*, **2010**(03), 027 (2010). [DOI], [ADS], [arXiv:0911.2701 [astro-ph.CO]]. (Cited on pages 69, 70, 110, and 172.)

[259] Creminelli, P., D'Amico, G., Noreña, J. and Vernizzi, F., "The effective theory of quintessence: the $w < -1$ side unveiled", *J. Cosmol. Astropart. Phys.*, **2009**(02), 018 (2009). [DOI], [ADS], [arXiv:0811.0827]. (Cited on page 69.)

[260] Creminelli, P., Luty, M.A., Nicolis, A. and Senatore, L., "Starting the Universe: stable violation of the null energy condition and non-standard cosmologies", *J. High Energy Phys.*, **2006**(12), 080 (2006). [DOI], [ADS], [arXiv:hep-th/0606090]. (Cited on pages 69 and 171.)

[261] Creminelli, P., Nicolis, A. and Zaldarriaga, M., "Perturbations in bouncing cosmologies: Dynamical attractor versus scale invariance", *Phys. Rev. D*, **71**, 063505 (2005). [DOI], [ADS], [arXiv:hep-th/0411270]. (Cited on page 173.)

[262] Creminelli, P., Noreña, J. and Simonović, M., "Conformal consistency relations for single-field inflation", *J. Cosmol. Astropart. Phys.*, **2012**(07), 052 (2012). [DOI], [ADS], [arXiv:1203.4595 [hep-th]]. (Cited on page 173.)

[263] Creminelli, P. and Senatore, L., "A smooth bouncing cosmology with scale invariant spectrum", *J. Cosmol. Astropart. Phys.*, **2007**(11), 010 (2007). [DOI], [ADS], [arXiv:hep-th/0702165]. (Cited on page 173.)

[264] Creminelli, P. and Zaldarriaga, M., "A single-field consistency relation for the three-point function", *J. Cosmol. Astropart. Phys.*, **2004**(10), 006 (2004). [DOI], [ADS], [arXiv:astro-ph/0407059]. (Cited on page 170.)

[265] Cremonesi, O., "Neutrino masses and Neutrinoless Double Beta Decay: Status and expectations", *arXiv*, e-print, (2010). [ADS], [arXiv:1002.1437 [hep-ex]]. (Cited on page 137.)

[266] Crittenden, R., Majerotto, E. and Piazza, F., "Measuring deviations from a cosmological constant: a field-space parameterization", *Phys. Rev. Lett.*, **98**, 251301 (2007). [DOI], [arXiv:astro-ph/0702003]. (Cited on page 19.)

[267] Crotty, P., García-Bellido, J., Lesgourgues, J. and Riazuelo, A., "Bounds on isocurvature perturbations from CMB and LSS data", *Phys. Rev. Lett.*, **91**, 171301 (2003). [DOI], [arXiv:astro-ph/0306286]. (Cited on page 182.)

[268] Cruz, M., Martínez-González, E., Vielva, P. and Cayón, L., "Detection of a non-Gaussian spot in WMAP", *Mon. Not. R. Astron. Soc.*, **356**, 29–40 (2005). [DOI], [ADS], [arXiv:astro-ph/0405341]. (Cited on pages 187 and 188.)

[269] Cruz, M., Martínez-González, E., Vielva, P., Diego, J.M., Hobson, M. and Turok, N., "The CMB cold spot: texture, cluster or void?", *Mon. Not. R. Astron. Soc.*, **390**, 913–919 (2008). [DOI], [ADS], [arXiv:0804.2904]. (Cited on page 193.)

[270] Csáki, C., Kaloper, N. and Terning, J., "Dimming Supernovae without Cosmic Acceleration", *Phys. Rev. Lett.*, **88**, 161302 (2002). [DOI], [ADS], [arXiv:hep-ph/0111311]. (Cited on page 184.)

[271] da Costa, L.N., Bernardi, M., Alonso, M.V., Wegner, G., Willmer, C.N.A., Pellegrini, P.S., Maia, M.A.G. and Zaroubi, S., "Redshift-Distance Survey of Early-Type Galaxies: Dipole of the Velocity Field", *Astrophys. J. Lett.*, **537**, L81–L84 (2000). [DOI], [ADS], [arXiv:astro-ph/9912225]. (Cited on page 84.)

[272] Dalal, N., Doré, O., Huterer, D. and Shirokov, A., "Imprints of primordial non-Gaussianities on large-scale structure: Scale-dependent bias and abundance of virialized objects", *Phys. Rev. D*, **77**, 123514 (2008). [DOI], [ADS], [arXiv:0710.4560]. (Cited on pages 175 and 176.)

[273] Dalcanton, J.J. and Hogan, C.J., "Halo Cores and Phase-Space Densities: Observational Constraints on Dark Matter Physics and Structure Formation", *Astrophys. J.*, **561**, 35–45 (2001). [DOI], [ADS], [arXiv:astro-ph/0004381]. (Cited on page 124.)

[274] Daly, R.A. and Djorgovski, S.G., "A Model-Independent Determination of the Expansion and Acceleration Rates of the Universe as a Function of Redshift and Constraints on Dark Energy", *Astrophys. J.*, **597**, 9–20 (2003). [DOI], [ADS], [arXiv:astro-ph/0305197]. (Cited on page 20.)

[275] D'Amico, G., Musso, M., Noreña, J. and Paranjape, A., "An Improved Calculation of the Non-Gaussian Halo Mass Function", *arXiv*, e-print, (2010). [ADS], [arXiv:1005.1203 [astro-ph.CO]]. (Cited on page 177.)

[276] Damour, T., Gibbons, G.W. and Gundlach, C., "Dark matter, time-varying G, and a dilaton field", *Phys. Rev. Lett.*, **64**, 123–126 (1990). [DOI]. (Cited on page 34.)

[277] Daniel, S.F. and Linder, E.V., "Confronting general relativity with further cosmological data", *Phys. Rev. D*, **82**, 103523 (2010). [DOI], [arXiv:1008.0397 [astro-ph.CO]]. (Cited on pages 25 and 63.)

[278] Daniel, S.F., Linder, E.V., Smith, T.L., Caldwell, R.R., Cooray, A., Leauthaud, A. and Lombriser, L., "Testing general relativity with current cosmological data", *Phys. Rev. D*, **81**, 123508 (2010). [DOI], [ADS], [arXiv:1002.1962 [astro-ph.CO]]. (Cited on page 25.)

[279] Das, S., Corasaniti, P.S. and Khoury, J., "Superacceleration as the signature of a dark sector interaction", *Phys. Rev. D*, **73**, 083509 (2006). [DOI], [arXiv:astro-ph/0510628]. (Cited on pages 34 and 38.)

[280] Das, S. and Weiner, N., "Late forming dark matter in theories of neutrino dark energy", *Phys. Rev. D*, **84**, 123511 (2011). [DOI], [ADS], [arXiv:astro-ph/0611353]. (Cited on pages 34 and 143.)

[281] Davis, A.-C., Li, B., Mota, D.F. and Winther, H.A., "Structure Formation in the Symmetron Model", *arXiv*, e-print, (2011). [arXiv:1108.3081 [astro-ph.CO]]. (Cited on page 68.)

[282] Davis, A.-C., Lim, E.A., Sakstein, J. and Shaw, D., "Modified Gravity Makes Galaxies Brighter", *arXiv*, e-print, (2011). [arXiv:1102.5278 [astro-ph.CO]]. (Cited on page 35.)

[283] Davis, M. and Huchra, J., "A survey of galaxy redshifts. III. The density field and the induced gravity field", *Astrophys. J.*, **254**, 437–450 (1982). [DOI], [ADS]. (Cited on page 85.)

[284] De Bernardis, F., Martinelli, M., Melchiorri, A., Mena, O. and Cooray, A., "Future weak lensing constraints in a dark coupled universe", *arXiv*, e-print, (2011). [arXiv:1104.0652 [astro-ph.CO]]. (Cited on page 113.)

[285] De Bernardis, F., Pagano, L., Serra, P., Melchiorri, A. and Cooray, A., "Anisotropies in the cosmic neutrino background after Wilkinson Microwave Anisotropy Probe five-year data", *J. Cosmol. Astropart. Phys.*, **2008**(06), 013 (2008). [DOI], [ADS], [arXiv:0804.1925 [astro-ph]]. (Cited on page 139.)

[286] de Blok, W.J.G., McGaugh, S.S., Bosma, A. and Rubin, V.C., "Mass Density Profiles of Low Surface Brightness Galaxies", *Astrophys. J. Lett.*, **552**, L23–L26 (2001). [DOI], [ADS], [arXiv:astro-ph/0103102]. (Cited on page 124.)

[287] de Felice, A., Mukohyama, S. and Tsujikawa, S., "Density perturbations in general modified gravitational theories", *Phys. Rev. D*, **82**, 023524 (2010). [DOI], [ADS], [arXiv:1006.0281 [astro-ph.CO]]. (Cited on page 43.)

[288] de Oliveira-Costa, A., Tegmark, M., Zaldarriaga, M. and Hamilton, A., "Significance of the largest scale CMB fluctuations in WMAP", *Phys. Rev. D*, **69**, 063516 (2004). [DOI], [ADS], [arXiv:astro-ph/0307282]. (Cited on pages 187 and 203.)

[289] de Putter, R., Zahn, O. and Linder, E.V., "CMB lensing constraints on neutrinos and dark energy", *Phys. Rev. D*, **79**, 065033 (2009). [DOI], [ADS], [arXiv:0901.0916 [astro-ph.CO]]. (Cited on page 138.)

[290] de Rham, C., Dvali, G., Hofmann, S., Khoury, J., Pujolàs, O., Redi, M. and Tolley, A.J., "Cascading Gravity: Extending the Dvali-Gabadadze-Porrati Model to Higher Dimension", *Phys. Rev. Lett.*, **100**, 251603 (2008). [DOI], [ADS], [arXiv:0711.2072 [hep-th]]. (Cited on page 46.)

[291] de Rham, C. and Gabadadze, G., "Generalization of the Fierz-Pauli Action", *Phys. Rev. D*, **82**, 044020 (2010). [DOI], [arXiv:1007.0443 [hep-th]]. (Cited on page 46.)

[292] de Rham, C., Gabadadze, G. and Tolley, A.J., "Resummation of Massive Gravity", *Phys. Rev. Lett.*, **106**, 231101 (2011). [DOI], [ADS], [arXiv:1011.1232 [hep-th]]. (Cited on page 46.)

[293] de Rham, C., Hofmann, S., Khoury, J. and Tolley, A.J., "Cascading Gravity and Degravitation", *J. Cosmol. Astropart. Phys.*, **2008**(02), 011 (2008). [DOI], [arXiv:0712.2821 [hep-th]]. (Cited on pages 45 and 46.)

[294] de Rham, C., Khoury, J. and Tolley, A.J., "Cascading Gravity is Ghost Free", *Phys. Rev. D*, **81**, 124027 (2010). [DOI], [arXiv:1002.1075 [hep-th]]. (Cited on page 46.)

[295] de Rham, C. and Tolley, A.J., "DBI and the Galileon reunited", *J. Cosmol. Astropart. Phys.*, **2010**(05), 015 (2010). [DOI], [arXiv:1003.5917 [hep-th]]. (Cited on page 44.)

[296] Debattista, V.P., Moore, B., Quinn, T., Kazantzidis, S., Maas, R., Mayer, L., Read, J. and Stadel, J., "The Causes of Halo Shape Changes Induced by Cooling Baryons: Disks versus Substructures", *Astrophys. J.*, **681**, 1076–1088 (2008). [DOI], [ADS], [arXiv:0707.0737]. (Cited on page 126.)

[297] DeDeo, S., Caldwell, R.R. and Steinhardt, P.J., "Effects of the sound speed of quintessence on the microwave background and large scale structure", *Phys. Rev. D*, **67**, 103509 (2003). [DOI], [ADS], [arXiv:astro-ph/0301284]. (Cited on page 188.)

[298] Deffayet, C., Dvali, G.R. and Gabadadze, G., "Accelerated universe from gravity leaking to extra dimensions", *Phys. Rev. D*, **65**, 044023 (2002). [DOI], [arXiv:astro-ph/0105068 [astro-ph]]. (Cited on page 44.)

[299] Deffayet, C., Dvali, G.R., Gabadadze, G. and Vainshtein, A.I., "Nonperturbative continuity in graviton mass versus perturbative discontinuity", *Phys. Rev. D*, **65**, 044026 (2002). [DOI], [arXiv:hep-th/0106001 [hep-th]]. (Cited on page 48.)

[300] Deffayet, C., Gao, X., Steer, D.A. and Zahariade, G., "From k-essence to generalized Galileons", *Phys. Rev. D*, **84**, 064039 (2011). [DOI], [ADS], [arXiv:1103.3260 [hep-th]]. (Cited on page 45.)

[301] Dekel, A., Eldar, A., Kolatt, T., Yahil, A., Willick, J.A., Faber, S.M., Courteau, S. and Burstein, D., "POTENT Reconstruction from Mark III Velocities", *Astrophys. J.*, **522**, 1–38 (1999). [DOI], [ADS], [arXiv:astro-ph/9812197]. (Cited on page 84.)

[302] del Campo, S., Herrera, R., Olivares, G. and Pavon, D., "Interacting models of soft coincidence", *Phys. Rev. D*, **74**, 023501 (2006). [DOI], [arXiv:astro-ph/0606520]. (Cited on page 34.)

[303] Dent, T., Stern, S. and Wetterich, C., "Unifying cosmological and recent time variations of fundamental couplings", *Phys. Rev. D*, **78**, 103518 (2008). [DOI], [arXiv:0808.0702 [hep-ph]]. (Cited on page 33.)

[304] Dent, T., Stern, S. and Wetterich, C., "Time variation of fundamental couplings and dynamical dark energy", *J. Cosmol. Astropart. Phys.*, **2009**(01), 038 (2009). [DOI], [arXiv:0809.4628 [hep-ph]]. (Cited on page 33.)

[305] Desjacques, V., Jeong, D. and Schmidt, F., "Accurate predictions for the scale-dependent galaxy bias from primordial non-Gaussianity", *Phys. Rev. D*, **84**, 061301 (2011). [DOI], [ADS], [arXiv:1105.3476 [astro-ph.CO]]. (Cited on page 179.)

[306] Desjacques, V., Jeong, D. and Schmidt, F., "Non-Gaussian Halo Bias Re-examined: Mass-dependent Amplitude from the Peak-Background Split and Thresholding", *Phys. Rev. D*, **84**, 063512 (2011). [DOI], [ADS], [arXiv:1105.3628 [astro-ph.CO]]. (Cited on page 179.)

[307] Di Porto, C. and Amendola, L., "Observational constraints on the linear fluctuation growth rate", *Phys. Rev. D*, **77**, 083508 (2008). [DOI], [arXiv:0707.2686 [astro-ph]]. (Cited on pages 90, 99, and 100.)

[308] Di Porto, C., Amendola, L. and Branchini, E., "Growth factor and galaxy bias from future redshift surveys: a study on parametrizations", *Mon. Not. R. Astron. Soc.*, **419**, 985–997 (2012). [DOI], [ADS], [arXiv:1101.2453]. (Cited on pages 81, 89, and 212.)

[309] Diaz-Rivera, L.M., Samushia, L. and Ratra, B., "Inflation and accelerated expansion tensor-vector-scalar cosmological solutions", *Phys. Rev. D*, **73**, 083503 (2006). [DOI], [ADS], [arXiv:astro-ph/0601153]. (Cited on page 51.)

[310] Diemand, J. and Moore, B., "The structure and evolution of cold dark matter halos", *arXiv*, e-print, (2009). [arXiv:0906.4340 [astro-ph.CO]]. (Cited on page 133.)

[311] Dienes, K.R., Kolda, C. and March-Russell, J., "Kinetic mixing and the supersymmetric gauge hierarchy", *Nucl. Phys. B*, **492**, 104–118 (1997). [DOI], [ADS], [arXiv:hep-ph/9610479]. (Cited on page 186.)

[312] Dimopoulos, K., "Can a vector field be responsible for the curvature perturbation in the Universe?", *Phys. Rev. D*, **74**, 083502 (2006). [DOI], [ADS], [arXiv:hep-ph/0607229]. (Cited on page 204.)

[313] Dimopoulos, K. and Karčiauskas, M., "Non-minimally coupled vector curvaton", *J. High Energy Phys.*, **2008**(07), 119 (2008). [DOI], [ADS], [arXiv:0803.3041 [hep-th]]. (Cited on pages 203 and 204.)

[314] Dimopoulos, K., Karčiauskas, M. and Wagstaff, J.M., "Vector curvaton with varying kinetic function", *Phys. Rev. D*, **81**, 023522 (2010). [DOI], [ADS], [arXiv:0907.1838 [hep-ph]]. (Cited on page 204.)

[315] Dine, M., "A simple solution to the strong CP problem with a harmless axion", *Phys. Lett. B*, **104**, 199–202 (1981). [DOI]. (Cited on page 154.)

[316] Dine, M. and Fischler, W., "The not-so-harmless axion", *Phys. Lett. B*, **120**, 137–141 (1983). [DOI], [ADS]. (Cited on pages 154 and 181.)

[317] Dodelson, S., *Modern Cosmology*, (Academic Press, London; Burlington, MA, 2003). [Google Books]. (Cited on page 78.)

[318] Dodelson, S. and Liguori, M., "Can Cosmic Structure form without Dark Matter?", *Phys. Rev. Lett.*, **97**, 231301 (2006). [DOI], [ADS], [arXiv:astro-ph/0608602]. (Cited on pages 51, 52, 53, and 161.)

[319] Dolgov, A.D. and Kawasaki, M., "Can modified gravity explain accelerated cosmic expansion?", *Phys. Lett. B*, **573**, 1–4 (2003). [DOI], [ADS], [arXiv:astro-ph/0307285]. (Cited on pages 40 and 41.)

[320] Dossett, J.N., Ishak, M. and Moldenhauer, J., "Testing general relativity at cosmological scales: Implementation and parameter correlations", *Phys. Rev. D*, **84**, 123001 (2011). [DOI], [ADS], [arXiv:1109.4583 [astro-ph.CO]]. (Cited on page 63.)

[321] Dou, X. and Meng, X.-H., "Bulk Viscous Cosmology: Unified Dark Matter", *Adv. Astron.*, **2011**, 829340 (2011). [DOI], [ADS], [arXiv:1012.3045 [astro-ph.CO]]. (Cited on page 151.)

[322] Douspis, M., Zolnierowski, Y., Blanchard, A. and Riazuelo, A., "What can we learn about dark energy evolution?", *arXiv*, e-print, (2006). [arXiv:astro-ph/0602491]. (Cited on page 20.)

[323] Dunkley, J., Bucher, M., Ferreira, P.G., Moodley, K. and Skordis, C., "Measuring the Geometry of the Universe in the Presence of Isocurvature Modes", *Phys. Rev. Lett.*, **95**, 261303 (2005). [DOI], [ADS], [arXiv:astro-ph/0507473]. (Cited on page 182.)

[324] Durrer, R., Marozzi, G. and Rinaldi, M., "Adiabatic renormalization of inflationary perturbations", *Phys. Rev. D*, **80**, 065024 (2009). [DOI], [ADS], [arXiv:0906.4772 [astro-ph.CO]]. (Cited on page 200.)

[325] Dutta, S. and Scherrer, R.J., "Hilltop quintessence", *Phys. Rev. D*, **78**, 123525 (2008). [DOI], [arXiv:0809.4441 [astro-ph]]. (Cited on page 19.)

[326] Dvali, G.R., Gabadadze, G. and Porrati, M., "4D gravity on a brane in 5D Minkowski space", *Phys. Lett. B*, **485**, 208–214 (2000). [DOI], [arXiv:hep-th/0005016 [hep-th]]. (Cited on page 43.)

[327] Dvali, G., Gabadadze, G. and Shifman, M., "Diluting cosmological constant via large distance modification of gravity", *arXiv*, e-print, (2002). [arXiv:hep-th/0208096]. (Cited on pages 43 and 45.)

[328] Dvali, G., Gabadadze, G. and Shifman, M., "Diluting cosmological constant in infinite volume extra dimensions", *Phys. Rev. D*, **67**, 044020 (2003). [DOI], [arXiv:hep-th/0202174]. (Cited on pages 43 and 45.)

[329] Dvali, G., Gruzinov, A. and Zaldarriaga, M., "New mechanism for generating density perturbations from inflation", *Phys. Rev. D*, **69**, 023505 (2004). [DOI], [ADS], [arXiv:astro-ph/0303591]. (Cited on page 170.)

[330] Dvali, G., Hofmann, S. and Khoury, J., "Degravitation of the cosmological constant and graviton width", *Phys. Rev. D*, **76**, 084006 (2007). [DOI], [arXiv:hep-th/0703027]. (Cited on pages 43 and 45.)

[331] Dvali, G. and Kachru, S., "New Old Inflation", *arXiv*, e-print, (2003). [ADS], [arXiv:hep-th/0309095]. (Cited on page 181.)

[332] Dvali, G. and Turner, M.S., "Dark Energy as a Modification of the Friedmann Equation", *arXiv*, e-print, (2003). [ADS], [arXiv:astro-ph/0301510]. (Cited on page 85.)

[333] Dvorkin, C., Peiris, H.V. and Hu, W., "Testable polarization predictions for models of CMB isotropy anomalies", *Phys. Rev. D*, **77**, 063008 (2008). [DOI], [ADS], [arXiv:0711.2321]. (Cited on page 205.)

[334] Easther, R. and Peiris, H.V., "Bayesian Analysis of Inflation II: Model Selection and Constraints on Reheating", *Phys. Rev. D*, **85**, 103533 (2012). [DOI], [arXiv:1112.0326 [astro-ph.CO]]. (Cited on page 169.)

[335] Efstathiou, G., "A maximum likelihood analysis of the low cosmic microwave background multipoles from the Wilkinson Microwave Anisotropy Probe", *Mon. Not. R. Astron. Soc.*, **348**, 885–896 (2004). [DOI], [ADS], [arXiv:astro-ph/0310207]. (Cited on page 188.)

[336] Efstathiou, G. and Bond, J.R., "Isocurvature cold dark matter fluctuations", *Mon. Not. R. Astron. Soc.*, **218**, 103–121 (1986). [ADS]. (Cited on page 181.)

[337] Eisenstein, D.J. and Hu, W., "Power Spectra for Cold Dark Matter and its Variants", *Astrophys. J.*, **511**, 5–15 (1999). [DOI], [arXiv:astro-ph/9710252]. (Cited on pages 82, 101, and 107.)

[338] Eisenstein, D.J., Seo, H.-J. and White, M., "On the Robustness of the Acoustic Scale in the Low-Redshift Clustering of Matter", *Astrophys. J.*, **664**, 660–674 (2007). [DOI], [arXiv:astro-ph/0604361 [astro-ph]]. (Cited on pages 82, 83, and 199.)

[339] Ellis, G.F.R., "Inhomogeneity effects in cosmology", *Class. Quantum Grav.*, **28**, 164001 (2011). [DOI], [ADS], [arXiv:1103.2335 [astro-ph.CO]]. (Cited on page 190.)

[340] Ellis, G.F.R. and MacCallum, M.A.H., "A class of homogeneous cosmological models", *Commun. Math. Phys.*, **12**, 108–141 (1969). [DOI], [ADS]. (Cited on page 188.)

[341] Enqvist, K., "Lemaitre–Tolman–Bondi model and accelerating expansion", *Gen. Relativ. Gravit.*, **40**, 451–466 (2008). [DOI], [ADS], [arXiv:0709.2044]. (Cited on page 192.)

[342] Enqvist, K. and Sloth, M.S., "Adiabatic CMB perturbations in pre-Big-Bang string cosmology", *Nucl. Phys. B*, **626**, 395–409 (2002). [DOI], [ADS], [arXiv:hep-ph/0109214]. (Cited on page 170.)

[343] Enqvist, K. and Väihkönen, A., "Non-Gaussian perturbations in hybrid inflation", *J. Cosmol. Astropart. Phys.*, **2004**(09), 006 (2004). [DOI], [ADS], [arXiv:hep-ph/0405103]. (Cited on page 171.)

[344] Erdoğdu, P. et al., "The dipole anisotropy of the 2 Micron All-Sky Redshift Survey", *Mon. Not. R. Astron. Soc.*, **368**, 1515–1526 (2006). [DOI], [ADS], [arXiv:astro-ph/0507166]. (Cited on page 85.)

[345] Erickcek, A.L., Hirata, C.M. and Kamionkowski, M., "A scale-dependent power asymmetry from isocurvature perturbations", *Phys. Rev. D*, **80**, 083507 (2009). [DOI], [ADS], [arXiv:0907.0705 [astro-ph.CO]]. (Cited on pages 205 and 206.)

[346] Erickcek, A.L., Kamionkowski, M. and Carroll, S.M., "A hemispherical power asymmetry from inflation", *Phys. Rev. D*, **78**, 123520 (2008). [DOI], [ADS], [arXiv:0806.0377]. (Cited on page 205.)

[347] Erickson, J.K., Caldwell, R.R., Steinhardt, P.J., Armendariz-Picon, C. and Mukhanov, V.F., "Measuring the Speed of Sound of Quintessence", *Phys. Rev. Lett.*, **88**, 121301 (2002). [DOI], [ADS], [arXiv:astro-ph/0112438]. (Cited on page 37.)

[348] Eriksen, H.K., Banday, A.J., Górski, K.M., Hansen, F.K. and Lilje, P.B., "Hemispherical Power Asymmetry in the Three-Year Wilkinson Microwave Anisotropy Probe Sky Maps", *Astrophys. J.*, **660**, L81–L84 (2007). [DOI], [arXiv:astro-ph/0701089]. (Cited on page 205.)

[349] Eriksen, H.K., Hansen, F.K., Banday, A.J., Górski, K.M. and Lilje, P.B., "Asymmetries in the Cosmic Microwave Background Anisotropy Field", *Astrophys. J.*, **605**, 14–20 (2004). [DOI], [ADS]. (Cited on page 187.)

[350] Eriksen, H.K., Hansen, F.K., Banday, A.J., Górski, K.M. and Lilje, P.B., "Erratum: 'Asymmetries in the Cosmic Microwave Background Anisotropy Field' (ApJ, 605, 14 [2004])", *Astrophys. J.*, **609**, 1198–1199 (2004). [DOI], [ADS]. (Cited on page 203.)

[351] Esposito-Farèse, G. and Polarski, D., "Scalar-tensor gravity in an accelerating universe", *Phys. Rev. D*, **63**, 063504 (2001). [DOI], [arXiv:gr-qc/0009034]. (Cited on pages 35 and 39.)

[352] Etherington, I.M.H., "The Definition of Distance in General Relativity", *Philos. Mag.*, **15**, 761–773 (1933). [DOI], [ADS]. (Cited on page 184.)

[353] Falk, T., Rangarajan, R. and Srednicki, M., "The angular dependence of the three-point correlation function of the cosmic microwave background radiation as predicted by inflationary cosmologies", *Astrophys. J. Lett.*, **403**, L1–L3 (1993). [DOI], [ADS], [arXiv:astro-ph/9208001]. (Cited on page 169.)

[354] Faraoni, V., "Inflation and quintessence with nonminimal coupling", *Phys. Rev. D*, **62**, 023504 (2000). [DOI], [arXiv:gr-qc/0002091]. (Cited on page 34.)

[355] Faraoni, V., "Solar system experiments do not yet veto modified gravity models", *Phys. Rev. D*, **74**, 023529 (2006). [DOI], [ADS], [arXiv:gr-qc/0607016]. (Cited on pages 40 and 41.)

[356] Fardon, R., Nelson, A.E. and Weiner, N., "Dark Energy from Mass Varying Neutrinos", *J. Cosmol. Astropart. Phys.*, **2004**(10), 005 (2004). [DOI], [arXiv:astro-ph/0309800]. (Cited on pages 34 and 143.)

[357] Farrar, G.R. and Peebles, P. James E., "Interacting Dark Matter and Dark Energy", *Astrophys. J.*, **604**, 1–11 (2004). [DOI], [arXiv:astro-ph/0307316]. (Cited on page 34.)

[358] Faulkner, T., Tegmark, M., Bunn, E.F. and Mao, Y., "Constraining $f(R)$ gravity as a scalar-tensor theory", *Phys. Rev. D*, **76**, 063505 (2007). [DOI], [ADS], [arXiv:astro-ph/0612569]. (Cited on page 41.)

[359] Feldman, H.A., Kaiser, N. and Peacock, J.A., "Power-spectrum analysis of three-dimensional redshift surveys", *Astrophys. J.*, **426**, 23–37 (1994). [DOI], [ADS], [arXiv:astro-ph/9304022]. (Cited on page 81.)

[360] Feng, B., Wang, X.-L. and Zhang, X.-M., "Dark energy constraints from the cosmic age and supernova", *Phys. Lett. B*, **607**, 35–41 (2005). [DOI], [arXiv:astro-ph/0404224 [astro-ph]]. (Cited on page 37.)

[361] Feng, J.L., Kaplinghat, M. and Yu, H.-B., "Halo-Shape and Relic-Density Exclusions of Sommerfeld-Enhanced Dark Matter Explanations of Cosmic Ray Excesses", *Phys. Rev. Lett.*, **104**, 151301 (2010). [DOI], [ADS], [arXiv:0911.0422 [hep-ph]]. (Cited on page 132.)

[362] Feroz, F. and Hobson, M.P., "Multimodal nested sampling: an efficient and robust alternative to Markov Chain Monte Carlo methods for astronomical data analyses", *Mon. Not. R. Astron. Soc.*, **384**, 449–463 (2008). [DOI], [ADS], [arXiv:0704.3704]. (Cited on page 216.)

[363] Ferreira, P.G. and Skordis, C., "The linear growth rate of structure in Parametrized Post Friedmannian Universes", *Phys. Rev. D*, **81**, 104020 (2010). [DOI], [arXiv:1003.4231 [astro-ph.CO]]. (Cited on pages 23, 25, and 26.)

[364] Ferreira, P.G., Skordis, C. and Zunckel, C., "Dark Matter, Modified Gravity and the Mass of the Neutrino", *Phys. Rev. D*, **78**, 044043 (2008). [DOI], [arXiv:0806.0116 [astro-ph]]. (Cited on page 52.)

[365] Finelli, F., "A contracting universe driven by two scalar fields", *Phys. Lett. B*, **545**, 1–7 (2002). [DOI], [ADS], [arXiv:hep-th/0206112]. (Cited on page 173.)

[366] Flauger, R., McAllister, L., Pajer, E., Westphal, A. and Xu, G., "Oscillations in the CMB from axion monodromy inflation", *J. Cosmol. Astropart. Phys.*, **2010**(06), 009 (2010). [DOI], [ADS], [arXiv:0907.2916 [hep-th]]. (Cited on page 172.)

[367] Francis, M.J., Lewis, G.F. and Linder, E.V., "Can Early Dark Energy be Detected in Non-Linear Structure?", *Mon. Not. R. Astron. Soc.*, **394**, 605–614 (2008). [DOI], [arXiv:0808.2840 [astro-ph]]. (Cited on page 64.)

[368] Francis, M.J., Lewis, G.F. and Linder, E.V., "Halo mass functions in early dark energy cosmologies", *Mon. Not. R. Astron. Soc.*, **393**, L31–L35 (2008). [DOI], [arXiv:0810.0039 [astro-ph]]. (Cited on page 74.)

[369] Frenk, C.S., White, S.D.M., Efstathiou, G. and Davis, M., "Galaxy clusters and the amplitude of primordial fluctuations", *Astrophys. J.*, **351**, 10–21 (1990). [DOI], [ADS]. (Cited on page 122.)

[370] Frieman, J.A., Hill, C.T., Stebbins, A. and Waga, I., "Cosmology with Ultralight Pseudo Nambu-Goldstone Bosons", *Phys. Rev. Lett.*, **75**, 2077–2080 (1995). [DOI], [ADS], [arXiv:astro-ph/9505060]. (Cited on page 29.)

[371] Fry, J.N. and Gaztanaga, E., "Biasing and hierarchical statistics in large-scale structure", *Astrophys. J.*, **413**, 447–452 (1993). [DOI], [ADS], [arXiv:astro-ph/9302009]. (Cited on page 83.)

[372] Fu, X., Wu, P. and Yu, H., "The growth of linear perturbations in the DGP model", *Phys. Lett. B*, **677**, 12–15 (2009). [DOI], [arXiv:0905.1735 [gr-qc]]. (Cited on pages 90 and 91.)

[373] Fukuda, Y. et al. (Super-Kamiokande Collaboration), "Evidence for Oscillation of Atmospheric Neutrinos", *Phys. Rev. Lett.*, **81**, 1562–1567 (1998). [DOI], [ADS], [arXiv:hep-ex/9807003]. (Cited on page 136.)

[374] Fukugita, M. and Yanagida, T., "Barygenesis without grand unification", *Phys. Lett. B*, **174**, 45–47 (1986). [DOI], [ADS]. (Cited on page 137.)

[375] Füzfa, A. and Alimi, J.-M., "Toward a unified description of dark energy and dark matter from the abnormally weighting energy hypothesis", *Phys. Rev. D*, **75**, 123007 (2007). [DOI], [ADS], [arXiv:astro-ph/0702478]. (Cited on page 151.)

[376] Gangui, A., Lucchin, F., Matarrese, S. and Mollerach, S., "The three-point correlation function of the cosmic microwave background in inflationary models", *Astrophys. J.*, **430**, 447–457 (1994). [DOI], [ADS], [arXiv:astro-ph/9312033]. (Cited on page 169.)

[377] Gannouji, R., Moraes, B., Mota, D.F., Polarski, D., Tsujikawa, S. and Winther, H.A., "Chameleon dark energy models with characteristic signatures", *Phys. Rev. D*, **82**, 124006 (2010). [DOI], [ADS], [arXiv:1010.3769 [astro-ph.CO]]. (Cited on page 34.)

[378] Gannouji, R., Moraes, B. and Polarski, D., "The growth of matter perturbations in $f(R)$ models", *J. Cosmol. Astropart. Phys.*, **2009**(02), 034 (2009). [DOI], [arXiv:0809.3374 [astro-ph]]. (Cited on pages 90 and 91.)

[379] Gao, C., Kunz, M., Liddle, A.R. and Parkinson, D., "Unified dark energy and dark matter from a scalar field different from quintessence", *Phys. Rev. D*, **81**, 043520 (2010). [DOI], [ADS], [arXiv:0912.0949 [astro-ph.CO]]. (Cited on page 151.)

[380] García-Bellido, J. and Haugbølle, T., "Confronting Lemaitre–Tolman–Bondi models with observational cosmology", *J. Cosmol. Astropart. Phys.*, **2008**(04), 003 (2008). [DOI], [ADS], [arXiv:0802.1523 [astro-ph]]. (Cited on pages 192, 193, and 199.)

[381] García-Bellido, J. and Haugbølle, T., "Looking the void in the eyes – the kinematic Sunyaev–Zeldovich effect in Lemaître–Tolman–Bondi models", *J. Cosmol. Astropart. Phys.*, **2008**(09), 016 (2008). [DOI], [arXiv:0807.1326 [astro-ph]]. (Cited on page 194.)

[382] García-Bellido, J. and Haugbølle, T., "The radial BAO scale and Cosmic Shear, a new observable for Inhomogeneous Cosmologies", *J. Cosmol. Astropart. Phys.*, **2009**(09), 028 (2009). [DOI], [arXiv:0810.4939 [astro-ph]]. (Cited on pages 193 and 199.)

[383] García-Bellido, J., Rubio, J., Shaposhnikov, M. and Zenhäusern, D., "Higgs-dilaton cosmology: From the early to the late Universe", *Phys. Rev. D*, **84**, 123504 (2011). [DOI], [ADS], [arXiv:1107.2163 [hep-ph]]. (Cited on page 56.)

[384] Garriga, J. and Mukhanov, V.F., "Perturbations in k-inflation", *Phys. Lett. B*, **458**, 219–225 (1999). [DOI], [ADS], [arXiv:hep-th/9904176]. (Cited on page 151.)

[385] Gasperini, M. and Veneziano, G., "Pre-big-bang in string cosmology", *Astropart. Phys.*, **1**, 317–339 (1993). [DOI], [ADS], [arXiv:hep-th/9211021]. (Cited on page 173.)

[386] Gavazzi, R. and Soucail, G., "Weak lensing survey of galaxy clusters in the CFHTLS Deep", *Astron. Astrophys.*, **462**, 459–471 (2007). [DOI], [ADS], [arXiv:astro-ph/0605591]. (Cited on page 130.)

[387] Gavela, M.B., Hernández, D., Lopez Honorez, L., Mena, O. and Rigolin, S., "Dark coupling", *J. Cosmol. Astropart. Phys.*, **2009**(07), 034 (2009). [DOI], [arXiv:0901.1611 [astro-ph]]. (Cited on pages 34, 67, and 153.)

[388] Gavela, M.B., Lopez Honorez, L., Mena, O. and Rigolin, S., "Dark Coupling and Gauge Invariance", *J. Cosmol. Astropart. Phys.*, **2010**(11), 044 (2010). [DOI], [arXiv:1005.0295 [astro-ph.CO]]. (Cited on pages 34, 67, and 153.)

[389] Geach, J.E. et al., "Empirical Hα emitter count predictions for dark energy surveys", *Mon. Not. R. Astron. Soc.*, **402**, 1330–1338 (2010). [DOI], [ADS], [arXiv:0911.0686 [astro-ph.CO]]. (Cited on page 88.)

[390] Giacconi, R. et al., "Galaxy clusters and the cosmic cycle of baryons across cosmic times", in *Astro2010: The Astronomy and Astrophysics Decadal Survey – Science White Papers*, 90, (National Academy of Sciences, Washington, DC, 2009). [ADS], [arXiv:0902.4857 [astro-ph.CO]]. URL (accessed 6 June 2013): http://sites.nationalacademies.org/bpa/BPA_050603. (Cited on page 129.)

[391] Giannantonio, T., "Constraints on dark energy and modified gravity from the ISW effect", *Nucl. Phys. B (Proc. Suppl.)*, **194**, 224–229 (2009). [DOI]. (Cited on page 35.)

[392] Giannantonio, T. and Porciani, C., "Structure formation from non-Gaussian initial conditions: Multivariate biasing, statistics, and comparison with N-body simulations", *Phys. Rev. D*, **81**, 063530 (2010). [DOI], [ADS], [arXiv:0911.0017 [astro-ph.CO]]. (Cited on pages 176 and 178.)

[393] Giannantonio, T., Porciani, C., Carron, J., Amara, A. and Pillepich, A., "Constraining primordial non-Gaussianity with future galaxy surveys", *Mon. Not. R. Astron. Soc.*, **422**, 2854–2877 (2012). [DOI], [ADS], [arXiv:1109.0958 [astro-ph.CO]]. (Cited on pages 176, 177, 178, and 179.)

[394] Giddings, S.B. and Sloth, M.S., "Semiclassical relations and IR effects in de Sitter and slow-roll space-times", *J. Cosmol. Astropart. Phys.*, **2011**(01), 023 (2011). [DOI], [ADS], [arXiv:1005.1056 [hep-th]]. (Cited on page 200.)

[395] Gies, H., Jaeckel, J. and Ringwald, A., "Polarized Light Propagating in a Magnetic Field as a Probe for Millicharged Fermions", *Phys. Rev. Lett.*, **97**, 140402 (2006). [DOI], [ADS], [arXiv:hep-ph/0607118]. (Cited on page 186.)

[396] Gilks, W.R., Richardson, S. and Spiegelhalter, D.J., eds., *Markov Chain Monte Carlo in Practice*, Interdisciplinary Statistics, (Chapman & Hall, Boca Raton; London, 1996). [Google Books]. (Cited on page 207.)

[397] Giovanelli, R., Haynes, M.P., Freudling, W., da Costa, L.N., Salzer, J.J. and Wegner, G., "Peculiar Velocity Dipoles of Field Galaxies", *Astrophys. J. Lett.*, **505**, L91–L94 (1998). [DOI], [ADS], [arXiv:astro-ph/9807274]. (Cited on page 84.)

[398] Giovanelli, R., Haynes, M.P., Salzer, J.J., Wegner, G., da Costa, L.N. and Freudling, W., "The Motions of Clusters of Galaxies and the Dipoles of the Peculiar Velocity Field", *Astron. J.*, **116**, 2632–2643 (1998). [DOI], [ADS], [arXiv:astro-ph/9808158]. (Cited on page 84.)

[399] Gnedin, O.Y. and Ostriker, J.P., "Limits on Collisional Dark Matter from Elliptical Galaxies in Clusters", *Astrophys. J.*, **561**, 61–68 (2001). [DOI], [ADS], [arXiv:astro-ph/0010436]. (Cited on page 131.)

[400] Goldhaber, A.S. and Nieto, M.M., "Photon and graviton mass limits", *Rev. Mod. Phys.*, **82**, 939–979 (2010). [DOI], [arXiv:0809.1003 [hep-ph]]. (Cited on page 46.)

[401] Golovnev, A., Mukhanov, V.F. and Vanchurin, V., "Vector Inflation", *J. Cosmol. Astropart. Phys.*, **2008**(06), 009 (2008). [DOI], [arXiv:0802.2068 [astro-ph]]. (Cited on page 203.)

[402] Goodsell, M., Jaeckel, J., Redondo, J. and Ringwald, A., "Naturally light hidden photons in LARGE volume string compactifications", *J. High Energy Phys.*, **2009**(11), 027 (2009). [DOI], [ADS], [arXiv:0909.0515 [hep-ph]]. (Cited on page 186.)

[403] Gordon, C. and Lewis, A., "Observational constraints on the curvaton model of inflation", *Phys. Rev. D*, **67**, 123513 (2003). [DOI], [ADS], [arXiv:astro-ph/0212248]. (Cited on page 181.)

[404] Groeneboom, N.E., Ackerman, L., Wehus, I.K. and Eriksen, H.K., "Bayesian Analysis of an Anisotropic Universe Model: Systematics and Polarization", *Astrophys. J.*, **722**, 452–459 (2010). [DOI], [ADS], [arXiv:0911.0150 [astro-ph.CO]]. (Cited on page 205.)

[405] Groeneboom, N.E. and Eriksen, H.K., "Bayesian Analysis of Sparse Anisotropic Universe Models and Application to the Five-Year WMAP Data", *Astrophys. J.*, **690**, 1807–1819 (2009). [DOI], [ADS], [arXiv:0807.2242]. (Cited on pages 205 and 206.)

[406] Grossi, M. and Springel, V., "The impact of Early Dark Energy on non-linear structure formation", *Mon. Not. R. Astron. Soc.*, **394**, 1559–1574 (2009). [DOI], [arXiv:0809.3404 [astro-ph]]. (Cited on page 64.)

[407] Grossi, M., Verde, L., Carbone, C., Dolag, K., Branchini, E., Iannuzzi, F., Matarrese, S. and Moscardini, L., "Large-scale non-Gaussian mass function and halo bias: tests on N-body simulations", *Mon. Not. R. Astron. Soc.*, **398**, 321–332 (2009). [DOI], [ADS], [arXiv:0902.2013 [astro-ph.CO]]. (Cited on page 177.)

[408] Gruppuso, A., "Complete statistical analysis for the quadrupole amplitude in an ellipsoidal universe", *Phys. Rev. D*, **76**, 083010 (2007). [DOI], [ADS], [arXiv:0705.2536]. (Cited on page 188.)

[409] Gruppuso, A., Finelli, F., Natoli, P., Paci, F., Cabella, P., de Rosa, A. and Mandolesi, N., "New constraints on parity symmetry from a re-analysis of the WMAP-7 low-resolution power spectra", *Mon. Not. R. Astron. Soc.*, **411**, 1445–1452 (2011). [DOI], [ADS], [arXiv:1006.1979 [astro-ph.CO]]. (Cited on pages 203 and 206.)

[410] Gu, J.-A., "Cosmological and Solar-System Tests of $f(R)$ Modified Gravity", *Int. J. Mod. Phys. D*, **20**, 1357–1362 (2011). [DOI], [ADS], [arXiv:1009.3488 [astro-ph.CO]]. (Cited on page 110.)

[411] Gubitosi, G., Piazza, F. and Vernizzi, F., "The effective field theory of dark energy", *J. Cosmol. Astropart. Phys.*, **2013**(02), 032 (2013). [DOI], [ADS], [arXiv:1210.0201 [hep-th]]. (Cited on page 63.)

[412] Gudnason, S.B., Kouvaris, C. and Sannino, F., "Dark matter from new technicolor theories", *Phys. Rev. D*, **74**, 095008 (2006). [DOI]. (Cited on page 123.)

[413] Gunn, J.E. and Gott III, J.R., "On the Infall of Matter Into Clusters of Galaxies and Some Effects on Their Evolution", *Astrophys. J.*, **176**, 1–19 (1972). [DOI], [ADS]. (Cited on page 68.)

[414] Guo, Z.-K., Ohta, N. and Tsujikawa, S., "Probing the Coupling between Dark Components of the Universe", *Phys. Rev. D*, **76**, 023508 (2007). [DOI], [arXiv:astro-ph/0702015]. (Cited on pages 34 and 152.)

[415] Gurovich, V.T. and Starobinsky, A.A., "Quantum effects and regular cosmological models", *J. Exp. Theor. Phys.*, **50**, 844–852 (1979). [ADS]. (Cited on page 110.)

[416] Guth, A.H., "Inflationary universe: A possible solution to the horizon and flatness problems", *Phys. Rev. D*, **23**, 347–356 (1981). [DOI], [ADS]. (Cited on page 163.)

[417] Guth, A.H. and Pi, S.-Y., "Fluctuations in the new inflationary universe", *Phys. Rev. Lett.*, **49**, 1110–1113 (1982). [DOI], [ADS]. (Cited on page 163.)

[418] Guzzo, L. et al., "A test of the nature of cosmic acceleration using galaxy redshift distortions", *Nature*, **451**, 541–544 (2008). [DOI], [ADS], [arXiv:0802.1944]. (Cited on page 81.)

[419] Hamaguchi, K., Murayama, H. and Yanagida, T., "Leptogenesis from an $\tilde{\text{N}}$-dominated early universe", *Phys. Rev. D*, **65**, 043512 (2002). [DOI], [ADS], [arXiv:hep-ph/0109030]. (Cited on page 181.)

[420] Hamilton, A.J.S., "Measuring Omega and the real correlation function from the redshift correlation function", *Astrophys. J. Lett.*, **385**, L5–L8 (1992). [DOI], [ADS]. (Cited on page 83.)

[421] Hannestad, S., Ringwald, A., Tu, H. and Wong, Y.Y.Y., "Is it possible to tell the difference between fermionic and bosonic hot dark matter?", *J. Cosmol. Astropart. Phys.*, **2005**(09), 014 (2005). [DOI], [ADS], [arXiv:astro-ph/0507544]. (Cited on page 142.)

[422] Hannestad, S., Tu, H. and Wong, Y.Y., "Measuring neutrino masses and dark energy with weak lensing tomography", *J. Cosmol. Astropart. Phys.*, **2006**(06), 025 (2006). [DOI], [ADS], [arXiv:astro-ph/0603019]. (Cited on page 142.)

[423] Hanson, D. and Lewis, A., "Estimators for CMB statistical anisotropy", *Phys. Rev. D*, **80**, 063004 (2009). [DOI], [ADS], [arXiv:0908.0963 [astro-ph.CO]]. (Cited on page 205.)

[424] Hanson, D., Lewis, A. and Challinor, A., "Asymmetric beams and CMB statistical anisotropy", *Phys. Rev. D*, **81**, 103003 (2010). [DOI], [ADS], [arXiv:1003.0198 [astro-ph.CO]]. (Cited on page 205.)

[425] Hawking, S.W., "The development of irregularities in a single bubble inflationary universe", *Phys. Lett. B*, **115**, 295–297 (1982). [DOI], [ADS]. (Cited on page 163.)

[426] Hearin, A.P. and Zentner, A.R., "The Influence of Galaxy Formation Physics on Weak Lensing Tests of General Relativity", *J. Cosmol. Astropart. Phys.*, **2009**(04), 032 (2009). [DOI], [arXiv:0904.3334 [astro-ph.CO]]. (Cited on page 104.)

[427] Heavens, A., "3D weak lensing", *Mon. Not. R. Astron. Soc.*, **343**, 1327–1334 (2003). [DOI], [ADS], [arXiv:astro-ph/0304151]. (Cited on page 152.)

[428] Heavens, A.F., Jimenez, R. and Maartens, R., "Testing homogeneity with the fossil record of galaxies", *J. Cosmol. Astropart. Phys.*, **2011**(09), 035 (2011). [DOI], [ADS], [arXiv:1107.5910 [astro-ph.CO]]. (Cited on page 190.)

[429] Heavens, A.F., Kitching, T.D. and Verde, L., "On model selection forecasting, dark energy and modified gravity", *Mon. Not. R. Astron. Soc.*, **380**, 1029–1035 (2007). [DOI]. (Cited on pages 85, 120, 213, and 216.)

[430] Henriques, A.B., Potting, R. and Sá, P.M., "Unification of inflation, dark energy, and dark matter within the Salam-Sezgin cosmological model", *Phys. Rev. D*, **79**, 103522 (2009). [DOI], [ADS], [arXiv:0903.2014 [astro-ph.CO]]. (Cited on page 151.)

[431] Hertzberg, M.P., Tegmark, M. and Wilczek, F., "Axion Cosmology and the Energy Scale of Inflation", *Phys. Rev. D*, **78**, 083507 (2008). [DOI], [arXiv:0807.1726]. (Cited on page 155.)

[432] Heymans, C. et al., "The dark matter environment of the Abell 901/902 supercluster: a weak lensing analysis of the HST STAGES survey", *Mon. Not. R. Astron. Soc.*, **385**, 1431–1442 (2008). [DOI], [ADS], [arXiv:0801.1156]. (Cited on page 130.)

[433] Hikage, C., Coles, P., Grossi, M., Moscardini, L., Dolag, K., Branchini, E. and Matarrese, S., "The effect of primordial non-Gaussianity on the topology of large-scale structure", *Mon. Not. R. Astron. Soc.*, **385**, 1613–1620 (2008). [DOI], [ADS], [arXiv:0711.3603]. (Cited on page 175.)

[434] Himmetoglu, B., Contaldi, C.R. and Peloso, M., "Ghost instabilities of cosmological models with vector fields nonminimally coupled to the curvature", *Phys. Rev. D*, **80**, 123530 (2009). [DOI], [ADS], [arXiv:0909.3524 [astro-ph.CO]]. (Cited on page 204.)

[435] Himmetoglu, B., Contaldi, C.R. and Peloso, M., "Instability of Anisotropic Cosmological Solutions Supported by Vector Fields", *Phys. Rev. Lett.*, **102**, 111301 (2009). [DOI], [ADS], [arXiv:0809.2779]. (Cited on page 204.)

[436] Hinterbichler, K. and Khoury, J., "Symmetron Fields: Screening Long-Range Forces Through Local Symmetry Restoration", *Phys. Rev. Lett.*, **104**, 231301 (2010). [DOI], [arXiv:1001.4525 [hep-th]]. (Cited on page 48.)

[437] Hirata, C.M., "Constraints on cosmic hemispherical power anomalies from quasars", *J. Cosmol. Astropart. Phys.*, **2009**(09), 011 (2009). [DOI], [arXiv:0907.0703 [astro-ph.CO]]. (Cited on page 205.)

[438] Hisano, J., Kohri, K. and Nojiri, M.M., "Neutralino warm dark matter", *Phys. Lett. B*, **505**, 169–176 (2001). [DOI], [arXiv:hep-ph/0011216]. (Cited on page 135.)

[439] Hobson, M.P., Jaffe, A.H., Liddle, A.R., Mukherjee, P. and Parkinson, D., eds., *Bayesian Methods in Cosmology*, (Cambridge University Press, Cambridge; New York, 2010). [Google Books]. (Cited on page 207.)

[440] Hogan, C.J. and Dalcanton, J.J., "New dark matter physics: Clues from halo structure", *Phys. Rev. D*, **62**, 063511 (2000). [DOI], [ADS], [arXiv:astro-ph/0002330]. (Cited on page 124.)

[441] Hojjati, A., Pogosian, L. and Zhao, G.-B., "Testing gravity with CAMB and CosmoMC", *J. Cosmol. Astropart. Phys.*, **2011**(08), 005 (2011). [DOI], [ADS], [arXiv:1106.4543 [astro-ph.CO]]. (Cited on page 63.)

[442] Hojjati, A., Zhao, G.-B., Pogosian, L., Silvestri, A., Crittenden, R. and Koyama, K., "Cosmological tests of general relativity: A principal component analysis", *Phys. Rev. D*, **85**, 043508 (2012). [DOI], [ADS], [arXiv:1111.3960 [astro-ph.CO]]. (Cited on page 63.)

[443] Holdom, B., "Two U(1)'s and ϵ charge shifts", *Phys. Lett. B*, **166**, 196–198 (1986). [DOI], [ADS]. (Cited on page 186.)

[444] Holman, R. and Tolley, A.J., "Enhanced non-Gaussianity from excited initial states", *J. Cosmol. Astropart. Phys.*, **2008**(05), 001 (2008). [DOI], [ADS], [arXiv:0710.1302 [hep-th]]. (Cited on page 172.)

[445] Horndeski, G.W., "Second-order scalar-tensor field equations in a four-dimensional space", *Int. J. Theor. Phys.*, **10**, 363 (1974). [DOI]. (Cited on page 45.)

[446] Hrycyna, O. and Szydlowski, M., "Route to Lambda in conformally coupled phantom cosmology", *Phys. Lett. B*, **651**, 8–14 (2007). [DOI], [arXiv:0704.1651 [hep-th]]. (Cited on page 19.)

[447] Hu, W., "Structure Formation with Generalized Dark Matter", *Astrophys. J.*, **506**, 485–494 (1998). [DOI], [arXiv:astro-ph/9801234]. (Cited on page 157.)

[448] Hu, W., "Power Spectrum Tomography with Weak Lensing", *Astrophys. J. Lett.*, **522**, L21–L24 (1999). [DOI], [astro-ph/9904153]. (Cited on page 100.)

[449] Hu, W., "Weak lensing of the CMB: A harmonic approach", *Phys. Rev. D*, **62**, 043007 (2000). [DOI], [arXiv:astro-ph/0001303]. (Cited on page 79.)

[450] Hu, W., "Covariant linear perturbation formalism", *arXiv*, e-print, (2004). [arXiv:astro-ph/0402060]. (Cited on page 36.)

[451] Hu, W., "Crossing the phantom divide: Dark energy internal degrees of freedom", *Phys. Rev. D*, **71**, 047301 (2005). [DOI], [arXiv:astro-ph/0410680 [astro-ph]]. (Cited on page 37.)

[452] Hu, W., Barkana, R. and Gruzinov, A., "Fuzzy Cold Dark Matter: The Wave Properties of Ultralight Particles", *Phys. Rev. Lett.*, **85**, 1158–1161 (2000). [DOI], [arXiv:astro-ph/0003365]. (Cited on pages 154 and 155.)

[453] Hu, W., Eisenstein, D.J., Tegmark, M. and White, M., "Observationally determining the properties of dark matter", *Phys. Rev. D*, **59**, 023512 (1998). [DOI], [arXiv:astro-ph/9806362]. (Cited on page 161.)

[454] Hu, W. and Jain, B., "Joint Galaxy-Lensing Observables and the Dark Energy", *Phys. Rev. D*, **70**, 043009 (2004). [DOI], [arXiv:astro-ph/0312395]. (Cited on page 211.)

[455] Hu, W. and Keeton, C.R., "Three-dimensional mapping of dark matter", *Phys. Rev. D*, **66**, 063506 (2002). [DOI], [ADS], [arXiv:astro-ph/0205412]. (Cited on page 130.)

[456] Hu, W. and Sawicki, I., "Models of $f(R)$ cosmic acceleration that evade solar system tests", *Phys. Rev. D*, **76**, 064004 (2007). [DOI], [ADS], [arXiv:0705.1158]. (Cited on pages 41, 68, 91, 94, 95, and 110.)

[457] Hu, W. and Sawicki, I., "Parameterized post-Friedmann framework for modified gravity", *Phys. Rev. D*, **76**, 104043 (2007). [DOI], [arXiv:0708.1190 [astro-ph]]. (Cited on pages 30, 61, 62, and 86.)

[458] Hu, W. and Tegmark, M., "Weak Lensing: Prospects for Measuring Cosmological Parameters", *Astrophys. J. Lett.*, **514**, L65–L68 (1999). [DOI], [ADS], [arXiv:astro-ph/9811168]. (Cited on page 101.)

[459] Huang, Z., Bond, J.R. and Kofman, L., "Parameterizing and Measuring Dark Energy Trajectories from Late-Inflatons", *Astrophys. J.*, **726**, 64 (2011). [DOI], [arXiv:1007.5297 [astro-ph.CO]]. (Cited on page 19.)

[460] Huang, Z., Verde, L. and Vernizzi, F., "Constraining inflation with future galaxy redshift surveys", *J. Cosmol. Astropart. Phys.*, **2012**(04), 005 (2012). [DOI], [arXiv:1201.5955 [astro-ph.CO]]. (Cited on page 169.)

[461] Hudson, M.J., Smith, R.J., Lucey, J.R. and Branchini, E., "Streaming motions of galaxy clusters within 12 000 km s^{-1} – V. The peculiar velocity field", *Mon. Not. R. Astron. Soc.*, **352**, 61–75 (2004). [DOI], [ADS], [arXiv:astro-ph/0404386]. (Cited on page 84.)

[462] Huey, G. and Wandelt, B.D., "Interacting quintessence. The coincidence problem and cosmic acceleration", *Phys. Rev. D*, **74**, 023519 (2006). [DOI], [arXiv:astro-ph/0407196 [astro-ph]]. (Cited on page 38.)

[463] Hui, L., "Unitarity Bounds and the Cuspy Halo Problem", *Phys. Rev. Lett.*, **86**, 3467–3470 (2001). [DOI]. (Cited on page 131.)

[464] Hui, L., Nicolis, A. and Stubbs, C., "Equivalence principle implications of modified gravity models", *Phys. Rev. D*, **80**, 104002 (2009). [DOI], [arXiv:0905.2966 [astro-ph.CO]]. (Cited on page 35.)

[465] Huterer, D., "Weak lensing and dark energy", *Phys. Rev. D*, **65**, 063001 (2002). [DOI], [arXiv:astro-ph/0106399]. (Cited on page 103.)

[466] Huterer, D. and Linder, E.V., "Separating dark physics from physical darkness: Minimalist modified gravity vs. dark energy", *Phys. Rev. D*, **75**, 023519 (2007). [DOI], [arXiv:astro-ph/0608681]. (Cited on pages 23 and 26.)

[467] Huterer, D. and Peiris, H.V., "Dynamical behavior of generic quintessence potentials: Constraints on key dark energy observables", *Phys. Rev. D*, **75**, 083503 (2007). [DOI], [arXiv:astro-ph/0610427 [astro-ph]]. (Cited on page 29.)

[468] Huterer, D. and Starkman, G.D., "Parameterization of Dark-Energy Properties: A Principal-Component Approach", *Phys. Rev. Lett.*, **90**, 031301 (2003). [DOI], [arXiv:astro-ph/0207517]. (Cited on pages 20, 212, 215, and 216.)

[469] Huterer, D. and Takada, M., "Calibrating the Nonlinear Matter Power Spectrum: Requirements for Future Weak Lensing Surveys", *Astropart. Phys.*, **23**, 369–376 (2005). [DOI], [arXiv:astro-ph/0412142]. (Cited on page 103.)

[470] Huterer, D. and Turner, M.S., "Probing the dark energy: Methods and strategies", *Phys. Rev. D*, **64**, 123527 (2001). [DOI], [arXiv:astro-ph/0012510]. (Cited on pages 20, 207, and 212.)

[471] Hwang, J., "Cosmological perturbations in generalized gravity theories: Formulation", *Class. Quantum Grav.*, **7**, 1613–1631 (1990). [DOI]. (Cited on page 34.)

[472] Hwang, J., "Cosmological perturbations in generalized gravity theories: Solutions", *Phys. Rev. D*, **42**, 2601–2606 (1990). [DOI]. (Cited on page 34.)

[473] Hwang, J. and Noh, H., "Gauge-ready formulation of the cosmological kinetic theory in generalized gravity theories", *Phys. Rev. D*, **65**, 023512 (2002). [DOI], [arXiv:astro-ph/0102005]. (Cited on page 42.)

[474] Iguchi, H., Nakamura, T. and Nakao, K., "Is Dark Energy the Only Solution to the Apparent Acceleration of the Present Universe?", *Prog. Theor. Phys.*, **108**, 809–818 (2002). [DOI], [ADS], [arXiv:astro-ph/0112419]. (Cited on page 191.)

[475] Ilić, S., Kunz, M., Liddle, A.R. and Frieman, J.A., "Dark energy view of inflation", *Phys. Rev. D*, **81**, 103502 (2010). [DOI], [arXiv:1002.4196 [astro-ph.CO]]. (Cited on pages 54 and 55.)

[476] Ishak, M., Upadhye, A. and Spergel, D.N., "Probing cosmic acceleration beyond the equation of state: Distinguishing between dark energy and modified gravity models", *Phys. Rev. D*, **74**, 043513 (2006). [DOI], [ADS], [arXiv:astro-ph/0507184]. (Cited on page 182.)

[477] Jaffe, T.R., Hervik, S., Banday, A.J. and Górski, K.M., "On the Viability of Bianchi Type VII_h Models with Dark Energy", *Astrophys. J.*, **644**, 701–708 (2006). [DOI], [ADS], [arXiv:astro-ph/0512433]. (Cited on page 188.)

[478] Jain, B. and Khoury, J., "Cosmological Tests of Gravity", *Ann. Phys. (N.Y.)*, **325**, 1479–1516 (2010). [DOI], [arXiv:1004.3294 [astro-ph.CO]]. (Cited on pages 47 and 75.)

[479] Janssen, T.M. and Prokopec, T., "Regulating the infrared by mode matching: A massless scalar in expanding spaces with constant deceleration", *Phys. Rev. D*, **83**, 084035 (2011). [DOI], [ADS], [arXiv:0906.0666 [gr-qc]]. (Cited on page 200.)

[480] Jimenez, R., Kitching, T., Peña-Garay, C. and Verde, L., "Can we measure the neutrino mass hierarchy in the sky?", *J. Cosmol. Astropart. Phys.*, **2010**(05), 035 (2010). [DOI], [ADS], [arXiv:1003.5918 [astro-ph.CO]]. (Cited on pages 136, 137, 138, 139, 140, and 162.)

[481] Jing, Y.P., Zhang, P., Lin, W.P., Gao, L. and Springel, V., "The influence of baryons on the clustering of matter and weak lensing surveys", *Astrophys. J.*, **640**, L119–L122 (2006). [DOI], [arXiv:astro-ph/0512426]. (Cited on page 104.)

[482] Jungman, G., Kamionkowski, M. and Griest, K., "Supersymmetric dark matter", *Phys. Rep.*, **267**, 195–373 (1996). [DOI], [ADS], [arXiv:hep-ph/9506380]. (Cited on pages 122 and 124.)

[483] Juszkiewicz, R., Vittorio, N. and Wyse, R.F.G., "Local gravity and large-scale structure", *Astrophys. J.*, **349**, 408–414 (1990). [DOI], [ADS]. (Cited on page 84.)

[484] Kain, B. and Ling, H.Y., "Vortices in Bose-Einstein condensate dark matter", *Phys. Rev. D*, **82**, 064042 (2010). [DOI], [ADS], [arXiv:1004.4692 [hep-ph]]. (Cited on page 155.)

[485] Kaiser, N., "Clustering in real space and in redshift space", *Mon. Not. R. Astron. Soc.*, **227**, 1–21 (1987). [ADS]. (Cited on pages 82, 83, and 166.)

[486] Kaiser, N. and Squires, G., "Mapping the dark matter with weak gravitational lensing", *Astrophys. J.*, **404**, 441–450 (1993). [DOI], [ADS]. (Cited on page 130.)

[487] Kallosh, R., Kratochvil, J., Linde, A., Linder, E.V. and Shmakova, M., "Observational bounds on cosmic doomsday", *J. Cosmol. Astropart. Phys.*, **2003**(10), 015 (2003). [DOI], [ADS], [arXiv:astro-ph/0307185]. (Cited on page 29.)

[488] Kamenshchik, A., Moschella, U. and Pasquier, V., "An alternative to quintessence", *Phys. Lett. B*, **511**, 265–268 (2001). [DOI], [ADS], [arXiv:gr-qc/0103004]. (Cited on page 151.)

[489] Kamionkowski, M. and Souradeep, T., "Odd-parity cosmic microwave background bispectrum", *Phys. Rev. D*, **83**, 027301 (2011). [DOI], [arXiv:1010.4304 [astro-ph.CO]]. (Cited on page 202.)

[490] Kamionkowski, M., Verde, L. and Jimenez, R., "The void abundance with non-Gaussian primordial perturbations", *J. Cosmol. Astropart. Phys.*, **2009**(01), 010 (2009). [DOI], [ADS], [arXiv:0809.0506]. (Cited on page 177.)

[491] Kaplinghat, M., Knox, L. and Song, Y.-S., "Determining Neutrino Mass from the Cosmic Microwave Background Alone", *Phys. Rev. Lett.*, **91**, 241301 (2003). [DOI], [ADS], [arXiv:astro-ph/0303344]. (Cited on page 138.)

[492] Karčiauskas, M., Dimopoulos, K. and Lyth, D.H., "Anisotropic non-Gaussianity from vector field perturbations", *Phys. Rev. D*, **80**, 023509 (2009). [DOI], [ADS], [arXiv:0812.0264]. (Cited on page 204.)

[493] Kashlinsky, A., Atrio-Barandela, F., Ebeling, H., Edge, A. and Kocevski, D., "A New Measurement of the Bulk Flow of X-Ray Luminous Clusters of Galaxies", *Astrophys. J. Lett.*, **712**, L81–L85 (2010). [DOI], [ADS], [arXiv:0910.4958 [astro-ph.CO]]. (Cited on page 84.)

[494] Kauffmann, G., White, S.D.M. and Guiderdoni, B., "The Formation and Evolution of Galaxies Within Merging Dark Matter Haloes", *Mon. Not. R. Astron. Soc.*, **264**, 201 (1993). (Cited on page 133.)

[495] Kawasaki, M., Nakayama, K., Sekiguchi, T., Suyama, T. and Takahashi, F., "Non-Gaussianity from isocurvature perturbations", *J. Cosmol. Astropart. Phys.*, **2008**(11), 019 (2008). [DOI], [ADS], [arXiv:0808.0009]. (Cited on page 181.)

[496] Kendall, M.G. and Stuart, A., *The advanced theory of statistics*, (C. Griffin, London, 1977), 4th edition. (Cited on page 211.)

[497] Khiabanian, H. and Dell'Antonio, I.P., "A Multiresolution Weak-Lensing Mass Reconstruction Method", *Astrophys. J.*, **684**, 794–803 (2008). [DOI], [ADS], [arXiv:0804.1809]. (Cited on page 130.)

[498] Khoury, J., Ovrut, B.A., Steinhardt, P.J. and Turok, N., "Ekpyrotic universe: Colliding branes and the origin of the hot big bang", *Phys. Rev. D*, **64**, 123522 (2001). [DOI], [ADS], [arXiv:hep-th/0103239]. (Cited on page 173.)

[499] Khoury, J. and Weltman, A., "Chameleon cosmology", *Phys. Rev. D*, **69**, 044026 (2004). [DOI], [arXiv:astro-ph/0309411 [astro-ph]]. (Cited on page 47.)

[500] Khoury, J. and Wyman, M., "N-Body Simulations of DGP and Degravitation Theories", *Phys. Rev. D*, **80**, 064023 (2009). [DOI], [arXiv:0903.1292 [astro-ph.CO]]. (Cited on page 68.)

[501] Kiakotou, A., Elgarøy, Ø. and Lahav, O., "Neutrino mass, dark energy, and the linear growth factor", *Phys. Rev. D*, **77**, 063005 (2008). [DOI], [ADS], [arXiv:0709.0253]. (Cited on page 82.)

[502] Kilbinger, M., Benabed, K., Cappe, O., Cardoso, J.-F., Fort, G., Prunet, S., Robert, C.P. and Wraith, D., "CosmoPMC: Cosmology Population Monte Carlo", *arXiv*, e-print, (2011). [ADS], [arXiv:1101.0950 [astro-ph.CO]]. (Cited on page 216.)

[503] Kim, J. and Naselsky, P., "Anomalous Parity Asymmetry of the Wilkinson Microwave Anisotropy Probe Power Spectrum Data at Low Multipoles", *Astrophys. J. Lett.*, **714**, L265–L267 (2010). [DOI], [ADS], [arXiv:1001.4613 [astro-ph.CO]]. (Cited on page 203.)

[504] Kim, J. and Naselsky, P., "Lack of Angular Correlation and Odd-parity Preference in Cosmic Microwave Background Data", *Astrophys. J.*, **739**, 79 (2011). [DOI], [ADS], [arXiv:1011.0377 [astro-ph.CO]]. (Cited on page 203.)

[505] Kitching, T.D., Amara, A., Abdalla, F.B., Joachimi, B. and Refregier, A., "Cosmological systematics beyond nuisance parameters: form-filling functions", *Mon. Not. R. Astron. Soc.*, **399**, 2107–2128 (2009). [DOI], [ADS], [arXiv:0812.1966]. (Cited on page 212.)

[506] Kitching, T.D., Heavens, A.F., Taylor, A.N., Brown, M.L., Meisenheimer, K., Wolf, C., Gray, M.E. and Bacon, D.J., "Cosmological constraints from COMBO-17 using 3D weak lensing", *Mon. Not. R. Astron. Soc.*, **376**, 771–778 (2007). [DOI], [ADS], [arXiv:astro-ph/0610284]. (Cited on page 152.)

[507] Kitching, T.D., Heavens, A.F., Verde, L., Serra, P. and Melchiorri, A., "Finding evidence for massive neutrinos using 3D weak lensing", *Phys. Rev. D*, **77**, 103008 (2008). [DOI], [ADS], [arXiv:0801.4565]. (Cited on pages 138, 139, and 162.)

[508] Kitching, T.D. and Taylor, A.N., "Path integral marginalization for cosmology: scale-dependent galaxy bias and intrinsic alignments", *Mon. Not. R. Astron. Soc.*, **410**, 1677–1686 (2011). [DOI], [ADS], [arXiv:1005.2063 [astro-ph.CO]]. (Cited on page 212.)

[509] Kleyna, J.T., Wilkinson, M.I., Evans, N.W. and Gilmore, G., "First Clear Signature of an Extended Dark Matter Halo in the Draco Dwarf Spheroidal", *Astrophys. J. Lett.*, **563**, L115–L118 (2001). [DOI], [ADS], [arXiv:astro-ph/0111329]. (Cited on page 124.)

[510] Klypin, A. and Holtzman, J., "Particle-Mesh code for cosmological simulations", *arXiv*, e-print, (1997). [arXiv:astro-ph/9712217]. (Cited on page 104.)

[511] Klypin, A.A., Kravtsov, A.V., Valenzuela, O. and Prada, F., "Where are the missing galactic satellites?", *Astrophys. J.*, **522**, 82–92 (1999). [DOI], [ADS], [arXiv:astro-ph/9901240]. (Cited on pages 124 and 133.)

[512] Klypin, A., Zhao, H. and Somerville, R.S., "ΛCDM-based Models for the Milky Way and M31. I. Dynamical Models", *Astrophys. J.*, **573**, 597–613 (2002). [DOI], [ADS], [arXiv:astro-ph/0110390]. (Cited on page 124.)

[513] Kocevski, D.D. and Ebeling, H., "On the Origin of the Local Group's Peculiar Velocity", *Astrophys. J.*, **645**, 1043–1053 (2006). [DOI], [ADS], [arXiv:astro-ph/0510106]. (Cited on page 85.)

[514] Kodama, H. and Sasaki, M., "Cosmological Perturbation Theory", *Prog. Theor. Phys. Suppl.*, **78**, 1–166 (1984). [DOI]. (Cited on pages 32 and 152.)

[515] Kofman, L., "Probing String Theory with Modulated Cosmological Fluctuations", *arXiv*, e-print, (2003). [ADS], [arXiv:astro-ph/0303614]. (Cited on page 170.)

[516] Kogut, A., Hinshaw, G. and Banday, A.J., "Limits to global rotation and shear from the COBE DMR four-year sky maps", *Phys. Rev. D*, **55**, 1901–1905 (1997). [DOI], [ADS], [arXiv:astro-ph/9701090]. (Cited on pages 188 and 189.)

[517] Koh, S. and Brandenberger, R.H., "Cosmological perturbations in non-commutative inflation", *J. Cosmol. Astropart. Phys.*, **2007**(06), 021 (2007). [DOI], [ADS], [arXiv:hep-th/0702217]. (Cited on page 201.)

[518] Koivisto, T., "Growth of perturbations in dark matter coupled with quintessence", *Phys. Rev. D*, **72**, 043516 (2005). [DOI], [arXiv:astro-ph/0504571]. (Cited on pages 34, 66, 152, and 153.)

[519] Koivisto, T. and Mota, D.F., "Accelerating Cosmologies with an Anisotropic Equation of State", *Astrophys. J.*, **679**, 1–5 (2008). [DOI], [ADS], [arXiv:0707.0279]. (Cited on pages 188, 189, and 190.)

[520] Koivisto, T. and Mota, D.F., "Anisotropic dark energy: dynamics of the background and perturbations", *J. Cosmol. Astropart. Phys.*, **2008**(06), 018 (2008). [DOI], [ADS], [arXiv:0801.3676]. (Cited on pages 188, 189, and 190.)

[521] Koivisto, T.S. and Mota, D.F., "Vector Field Models of Inflation and Dark Energy", *J. Cosmol. Astropart. Phys.*, **2008**(08), 021 (2008). [DOI], [arXiv:0805.4229 [astro-ph]]. (Cited on page 203.)

[522] Koivisto, T.S. and Mota, D.F., "CMB statistics in noncommutative inflation", *J. High Energy Phys.*, **2011**(02), 061 (2011). [DOI], [ADS], [arXiv:1011.2126 [astro-ph.CO]]. (Cited on page 201.)

[523] Koivisto, T.S. and Prokopec, T., "Quantum backreaction in evolving FLRW spacetimes", *Phys. Rev. D*, **83**, 044015 (2011). [DOI], [arXiv:1009.5510 [gr-qc]]. (Cited on page 200.)

[524] Komatsu, E. and Spergel, D.N., "Acoustic signatures in the primary microwave background bispectrum", *Phys. Rev. D*, **63**, 063002 (2001). [DOI], [ADS], [arXiv:astro-ph/0005036]. (Cited on page 169.)

[525] Komatsu, E. et al. (WMAP Collaboration), "Five-year Wilkinson Microwave Anisotropy Probe (WMAP) observations: cosmological interpretation", *Astrophys. J. Suppl. Ser.*, **180**, 330–376 (2009). [DOI], [ADS], [arXiv:0803.0547 [astro-ph]]. (Cited on pages 163, 181, and 182.)

[526] Komatsu, E. et al. (WMAP Collaboration), "Seven-year Wilkinson Microwave Anisotropy Probe (WMAP) Observations: Cosmological Interpretation", *Astrophys. J. Suppl. Ser.*, **192**, 18 (2011). [DOI], [ADS], [arXiv:1001.4538 [astro-ph.CO]]. (Cited on pages 19, 54, 83, 102, 103, 137, and 181.)

[527] Koyama, K., Mizuno, S., Vernizzi, F. and Wands, D., "Non-Gaussianities from ekpyrotic collapse with multiple fields", *J. Cosmol. Astropart. Phys.*, **2007**(11), 024 (2007). [DOI], [ADS], [arXiv:0708.4321 [hep-th]]. (Cited on page 173.)

[528] Koyama, K. and Wands, D., "Ekpyrotic collapse with multiple fields", *J. Cosmol. Astropart. Phys.*, **2007**(04), 008 (2007). [DOI], [ADS], [arXiv:hep-th/0703040]. (Cited on page 173.)

[529] Kravtsov, A.V., Gnedin, O.Y. and Klypin, A.A., "The Tumultuous Lives of Galactic Dwarfs and the Missing Satellites Problem", *Astrophys. J.*, **609**, 482–497 (2004). [DOI], [ADS], [arXiv:astro-ph/0401088]. (Cited on page 125.)

[530] Kristian, J. and Sachs, R.K., "Observations in Cosmology", *Astrophys. J.*, **143**, 379–399 (1966). [DOI], [ADS]. (Cited on page 193.)

[531] Kristiansen, J.R., La Vacca, G., Colombo, L.P.L., Mainini, R. and Bonometto, S.A., "Coupling between cold dark matter and dark energy from neutrino mass experiments", *New Astronomy*, **15**, 609–613 (2010). [DOI], [arXiv:0902.2737 [astro-ph.CO]]. (Cited on pages 34 and 152.)

[532] Kubo, J.M., Khiabanian, H., Dell'Antonio, I.P., Wittman, D. and Tyson, J.A., "Dark Matter Structures in the Deep Lens Survey", *Astrophys. J.*, **702**, 980–988 (2009). [DOI], [ADS], [arXiv:0809.5072]. (Cited on page 130.)

[533] Kulkarni, G.V., Nichol, R.C., Sheth, R.K., Seo, H.-J., Eisenstein, D.J. and Gray, A., "The three-point correlation function of luminous red galaxies in the Sloan Digital Sky Survey", *Mon. Not. R. Astron. Soc.*, **378**, 1196–1206 (2007). [DOI], [ADS], [arXiv:astro-ph/0703340]. (Cited on page 175.)

[534] Kunz, M., "The dark degeneracy: On the number and nature of dark components", *Phys. Rev. D*, **80**, 123001 (2009). [DOI], [arXiv:astro-ph/0702615 [astro-ph]]. (Cited on pages 20, 38, and 118.)

[535] Kunz, M., Amendola, L. and Sapone, D., "Dark Energy Phenomenology", *arXiv*, e-print, (2008). [arXiv:0806.1323 [astro-ph]]. (Cited on page 30.)

[536] Kunz, M. and Sapone, D., "Crossing the phantom divide", *Phys. Rev. D*, **74**, 123503 (2006). [DOI], [arXiv:astro-ph/0609040 [astro-ph]]. (Cited on pages 28, 36, 37, and 110.)

[537] Kunz, M. and Sapone, D., "Dark Energy versus Modified Gravity", *Phys. Rev. Lett.*, **98**, 121301 (2007). [DOI], [arXiv:astro-ph/0612452 [astro-ph]]. (Cited on pages 30, 39, and 59.)

[538] Kurki-Suonio, H., Muhonen, V. and Väliviita, J., "Correlated primordial perturbations in light of CMB and large scale structure data", *Phys. Rev. D*, **71**, 063005 (2005). [DOI], [ADS], [arXiv:astro-ph/0412439]. (Cited on page 182.)

[539] La Vacca, G., Kristiansen, J.R., Colombo, L.P.L., Mainini, R. and Bonometto, S.A., "Do WMAP data favor neutrino mass and a coupling between Cold Dark Matter and Dark Energy?", *J. Cosmol. Astropart. Phys.*, **2009**(04), 007 (2009). [DOI], [ADS], [arXiv:0902.2711 [astro-ph.CO]]. (Cited on pages 34 and 152.)

[540] Lahav, O., Lilje, P.B., Primack, J.R. and Rees, M.J., "Dynamical effects of the cosmological constant", *Mon. Not. R. Astron. Soc.*, **251**, 128–136 (1991). [ADS]. (Cited on pages 68, 71, and 90.)

[541] Landy, S.D. and Szalay, A.S., "Bias and variance of angular correlation functions", *Astrophys. J.*, **412**, 64–71 (1993). [DOI], [ADS]. (Cited on page 143.)

[542] Langlois, D., "Correlated adiabatic and isocurvature perturbations from double inflation", *Phys. Rev. D*, **59**, 123512 (1999). [DOI], [ADS], [arXiv:astro-ph/9906080]. (Cited on page 181.)

[543] Langlois, D., Renaux-Petel, S., Steer, D.A. and Tanaka, T., "Primordial Fluctuations and Non-Gaussianities in Multifield Dirac-Born-Infeld Inflation", *Phys. Rev. Lett.*, **101**, 061301 (2008). [DOI], [ADS], [arXiv:0804.3139 [hep-th]]. (Cited on page 172.)

[544] Langlois, D. and Riazuelo, A., "Correlated mixtures of adiabatic and isocurvature cosmological perturbations", *Phys. Rev. D*, **62**, 043504 (2000). [DOI], [ADS], [arXiv:astro-ph/9912497]. (Cited on page 182.)

[545] Langlois, D. and Vernizzi, F., "Mixed inflaton and curvaton perturbations", *Phys. Rev. D*, **70**, 063522 (2004). [DOI], [ADS], [arXiv:astro-ph/0403258]. (Cited on pages 170 and 181.)

[546] Langlois, D., Vernizzi, F. and Wands, D., "Non-linear isocurvature perturbations and non-Gaussianities", *J. Cosmol. Astropart. Phys.*, **2008**(12), 004 (2008). [DOI], [ADS], [arXiv:0809.4646]. (Cited on page 181.)

[547] Larena, J., Alimi, J.-M., Buchert, T., Kunz, M. and Corasaniti, P.S., "Testing backreaction effects with observations", *Phys. Rev. D*, **79**, 083011 (2009). [DOI], [arXiv:0808.1161 [astro-ph]]. (Cited on page 195.)

[548] Larson, D. et al., "Seven-year Wilkinson Microwave Anisotropy Probe (WMAP) Observations: Power Spectra and WMAP-derived Parameters", *Astrophys. J. Suppl. Ser.*, **192**, 16 (2011). [DOI], [ADS], [arXiv:1001.4635 [astro-ph.CO]]. (Cited on pages 82 and 142.)

[549] Lauer, T.R. and Postman, M., "The motion of the Local Group with respect to the 15,000 kilometer per second Abell cluster inertial frame", *Astrophys. J.*, **425**, 418–438 (1994). [DOI], [ADS]. (Cited on page 84.)

[550] Laureijs, R. et al. (Euclid Science Study Team), *Euclid: Mapping the geometry of the dark Universe. Assessment Study Report*, ESA/SRE(2009)2, (ESA, Paris, 2009). [0912.0914]. URL (accessed 16 May 2013): http://sci.esa.int/jump.cfm?oid=46017. (Cited on pages 86 and 208.)

[551] Laureijs, R. et al. (Euclid Collaboration), *Euclid: Mapping the geometry of the dark Universe. Definition Study Report*, ESA/SRE(2011)12, (ESA, Paris, 2011). [ADS], [arXiv:1110.3193 [astro-ph.CO]]. URL (accessed 16 May 2013): http://sci.esa.int/jump.cfm?oid=48983. (Cited on pages 15, 21, 86, 88, 89, 113, 167, and 208.)

[552] Lavaux, G., Tully, R.B., Mohayaee, R. and Colombi, S., "Cosmic Flow From Two Micron All-Sky Redshift Survey: the Origin of Cosmic Microwave Background Dipole and Implications for ΛCDM Cosmology", *Astrophys. J.*, **709**, 483–498 (2010). [DOI], [ADS], [arXiv:0810.3658]. (Cited on page 85.)

[553] Lee, S., "Constraints on scalar-tensor theories of gravity from observations", *arXiv*, e-print, (2010). [arXiv:1012.2646 [astro-ph.CO]]. (Cited on page 35.)

[554] Lehners, J.-L. and Steinhardt, P.J., "Non-Gaussian density fluctuations from entropically generated curvature perturbations in ekpyrotic models", *Phys. Rev. D*, **77**, 063533 (2008). [DOI], [ADS], [arXiv:0712.3779 [hep-th]]. (Cited on page 173.)

[555] Lesgourgues, J., Matarrese, S., Pietroni, M. and Riotto, A., "Non-linear power spectrum including massive neutrinos: the time-RG flow approach", *J. Cosmol. Astropart. Phys.*, **2009**(06), 017 (2009). [DOI], [ADS], [arXiv:0901.4550 [astro-ph.CO]]. (Cited on page 142.)

[556] Lesgourgues, J., Pastor, S. and Perotto, L., "Probing neutrino masses with future galaxy redshift surveys", *Phys. Rev. D*, **70**, 045016 (2004). [DOI], [ADS], [arXiv:hep-ph/0403296]. (Cited on page 140.)

[557] Lesgourgues, J., Perotto, L., Pastor, S. and Piat, M., "Probing neutrino masses with CMB lensing extraction", *Phys. Rev. D*, **73**, 045021 (2006). [DOI], [ADS], [arXiv:astro-ph/0511735]. (Cited on page 138.)

[558] Lewis, A. and Bridle, S., "Cosmological parameters from CMB and other data: A Monte Carlo approach", *Phys. Rev. D*, **66**, 103511 (2002). [DOI], [ADS], [arXiv:astro-ph/0205436]. (Cited on page 167.)

[559] Lewis, A., Challinor, A. and Lasenby, A., "Efficient Computation of Cosmic Microwave Background Anisotropies in Closed Friedmann-Robertson-Walker Models", *Astrophys. J.*, **538**, 473–476 (2000). [DOI], [ADS], [arXiv:astro-ph/9911177]. (Cited on pages 62, 82, 107, 142, 144, and 166.)

[560] Lewis, A., Challinor, A. and Turok, N., "Analysis of CMB polarization on an incomplete sky", *Phys. Rev. D*, **65**, 023505 (2002). [DOI], [arXiv:astro-ph/0106536]. (Cited on page 76.)

[561] Li, B. and Barrow, J.D., "N-body simulations for coupled scalar-field cosmology", *Phys. Rev. D*, **83**, 024007 (2011). [DOI], [ADS], [arXiv:1005.4231 [astro-ph.CO]]. (Cited on page 66.)

[562] Li, B. and Barrow, J.D., "On the Effects of Coupled Scalar Fields on Structure Formation", *Mon. Not. R. Astron. Soc.*, **413**, 262–270 (2011). [DOI], [ADS], [arXiv:1010.3748 [astro-ph.CO]]. (Cited on pages 34, 66, 72, and 153.)

[563] Li, B., Barrow, J.D. and Mota, D.F., "The Cosmology of Ricci-Tensor-Squared gravity in the Palatini variational approach", *Phys. Rev. D*, **76**, 104047 (2007). [DOI], [arXiv:0707.2664 [gr-qc]]. (Cited on page 40.)

[564] Li, B., Mota, D.F. and Barrow, J.D., "Detecting a Lorentz-Violating Field in Cosmology", *Phys. Rev. D*, **77**, 024032 (2008). [DOI], [arXiv:0709.4581 [astro-ph]]. (Cited on page 50.)

[565] Li, B., Mota, D.F. and Barrow, J.D., "N-body Simulations for Extended Quintessence Models", *Astrophys. J.*, **728**, 109 (2011). [DOI], [arXiv:1009.1400 [astro-ph.CO]]. (Cited on pages 34, 66, 72, and 153.)

[566] Li, B., Mota, D.F. and Shaw, D.J., "Microscopic and macroscopic behaviors of Palatini modified gravity theories", *Phys. Rev. D*, **78**, 064018 (2008). [DOI], [arXiv:0805.3428 [gr-qc]]. (Cited on page 40.)

[567] Li, B., Mota, D.F. and Shaw, D.J., "Indistinguishable Macroscopic Behaviour of Palatini Gravities and General Relativity", *Class. Quantum Grav.*, **26**, 055018 (2009). [DOI], [arXiv:0801.0603 [gr-qc]]. (Cited on page 40.)

[568] Li, N. and Chen, Da-Ming, "Cusp-core problem and strong gravitational lensing", *Res. Astron. Astrophys.*, **9**, 1173–1184 (2009). [DOI], [arXiv:0905.3041 [astro-ph.CO]]. (Cited on page 133.)

[569] Li, N. and Schwarz, D.J., "On the onset of cosmological backreaction", *Phys. Rev. D*, **76**, 083011 (2007). [DOI], [arXiv:gr-qc/0702043 [gr-qc]]. (Cited on page 195.)

[570] Liddle, A.R. and Lyth, D.H., *Cosmological Inflation and Large-Scale Structure*, (Cambridge University Press, Cambridge; New York, 2000). [ADS], [Google Books]. (Cited on page 164.)

[571] Liddle, A.R., Mukherjee, P., Parkinson, D. and Wang, Y., "Present and future evidence for evolving dark energy", *Phys. Rev. D*, **74**, 123506 (2006). [DOI], [arXiv:astro-ph/0610126]. (Cited on page 217.)

[572] Liddle, A.R., Pahud, C. and Ureña-López, L.A., "Triple unification of inflation, dark matter, and dark energy using a single field", *Phys. Rev. D*, **77**, 121301 (2008). [DOI], [ADS], [arXiv:0804.0869]. (Cited on page 151.)

[573] Liddle, A.R. and Scherrer, R.J., "Classification of scalar field potentials with cosmological scaling solutions", *Phys. Rev. D*, **59**, 023509 (1999). [DOI], [arXiv:astro-ph/9809272]. (Cited on page 19.)

[574] Lim, E.A., Sawicki, I. and Vikman, A., "Dust of dark energy", *J. Cosmol. Astropart. Phys.*, **2010**(05), 012 (2010). [DOI], [ADS], [arXiv:1003.5751 [astro-ph.CO]]. (Cited on page 69.)

[575] Lin, C.-M., "Triple Unification of Inflation, Dark matter and Dark energy in Chaotic Braneworld Inflation", *arXiv*, e-print, (2009). [ADS], [arXiv:0906.5021 [hep-ph]]. (Cited on page 151.)

[576] Linde, A.D., "A new inflationary universe scenario: A possible solution of the horizon, flatness, homogeneity, isotropy and primordial monopole problems", *Phys. Lett. B*, **108**, 389–393 (1982). [DOI], [ADS]. (Cited on page 163.)

[577] Linde, A.D., "Chaotic inflation", *Phys. Lett. B*, **129**, 177–181 (1983). [DOI], [ADS]. (Cited on pages 29 and 165.)

[578] Linde, A.D., "Generation of isothermal density perturbations in the inflationary universe", *Phys. Lett. B*, **158**, 375–380 (1985). [DOI], [ADS]. (Cited on page 181.)

[579] Linde, A., "Axions in inflationary cosmology", *Phys. Lett. B*, **259**, 38–47 (1991). [DOI], [ADS]. (Cited on pages 155 and 181.)

[580] Linde, A., "Hybrid inflation", *Phys. Rev. D*, **49**, 748–754 (1994). [DOI], [ADS], [arXiv:astro-ph/9307002]. (Cited on page 170.)

[581] Linde, A., "Inflationary Cosmology", in Lemoine, M., Martin, J. and Peter, P., eds., *Inflationary Cosmology*, XXII IAP colloquium held at the Institut d'Astrophysique de Paris in June 2006, Lecture Notes in Physics, 738, pp. 1–54, (Springer, Berlin; Heidelberg, 2008). [DOI], [ADS], [arXiv:0705.0164 [hep-th]]. (Cited on page 163.)

[582] Linde, A. and Mukhanov, V.F., "Non-Gaussian isocurvature perturbations from inflation", *Phys. Rev. D*, **56**, 535 (1997). [DOI], [ADS], [arXiv:astro-ph/9610219]. (Cited on pages 170 and 181.)

[583] Linde, A. and Noorbala, M., "Measure Problem for Eternal and Non-Eternal Inflation", *J. Cosmol. Astropart. Phys.*, **2010**(09), 008 (2010). [DOI], [ADS], [arXiv:1006.2170 [hep-th]]. (Cited on page 155.)

[584] Linder, E.V., "Exploring the Expansion History of the Universe", *Phys. Rev. Lett.*, **90**, 091301 (2003). [DOI], [ADS], [arXiv:astro-ph/0208512]. (Cited on pages 20, 89, and 212.)

[585] Linder, E.V., "Cosmic growth history and expansion history", *Phys. Rev. D*, **72**, 043529 (2005). [DOI], [arXiv:astro-ph/0507263]. (Cited on pages 23, 26, and 90.)

[586] Linder, E.V., "Extending the gravitational growth framework", *Phys. Rev. D*, **79**, 063519 (2009). [DOI], [arXiv:0901.0918 [astro-ph.CO]]. (Cited on page 26.)

[587] Linder, E.V. and Cahn, R.N., "Parameterized beyond-Einstein growth", *Astropart. Phys.*, **28**, 481–488 (2007). [DOI], [arXiv:astro-ph/0701317]. (Cited on pages 26, 63, and 91.)

[588] Linder, E.V. and Jenkins, A., "Cosmic structure growth and dark energy", *Mon. Not. R. Astron. Soc.*, **346**, 573–583 (2003). [DOI], [ADS], [arXiv:astro-ph/0305286]. (Cited on page 82.)

[589] Lopez Honorez, L., Reid, B.A., Mena, O., Verde, L. and Jimenez, R., "Coupled dark matter-dark energy in light of near universe observations", *J. Cosmol. Astropart. Phys.*, **2010**(09), 029 (2010). [DOI], [ADS], [arXiv:1006.0877 [astro-ph.CO]]. (Cited on page 182.)

[590] Loredo, T.J., "Bayesian Adaptive Exploration", in Erickson, G.J. and Zhai, Y., eds., *Bayesian Inference and Maximum Entropy Methods in Science and Engineering*, Proceedings of the 23rd International Workshop on Bayesian Methods and Maximum Entropy in Science and Engineering, Jackson Hole, WY, USA, 3 – 8 August 2003, AIP Conference Proceedings, 707, pp. 330–346, (American Institute of Physics, Melville, NY, 2004). [DOI], [ADS], [arXiv:astro-ph/0409386]. (Cited on pages 214 and 215.)

[591] LoVerde, M., Miller, A., Shandera, S. and Verde, L., "Effects of scale-dependent non-Gaussianity on cosmological structures", *J. Cosmol. Astropart. Phys.*, **2008**(04), 014 (2008). [DOI], [ADS], [arXiv:0711.4126]. (Cited on page 177.)

[592] Lue, A., Scoccimarro, R. and Starkman, G.D., "Probing Newton's constant on vast scales: Dvali-Gabadadze-Porrati gravity, cosmic acceleration, and large scale structure", *Phys. Rev. D*, **69**, 124015 (2004). [DOI], [arXiv:astro-ph/0401515 [astro-ph]]. (Cited on page 75.)

[593] Luty, M.A., Porrati, M. and Rattazzi, R., "Strong interactions and stability in the DGP model", *J. High Energy Phys.*, **2003**(09), 029 (2003). [DOI], [arXiv:hep-th/0303116 [hep-th]]. (Cited on page 44.)

[594] Lux, H., Read, J.I. and Lake, G., "Determining orbits for the Milky Way's dwarfs", *Mon. Not. R. Astron. Soc.*, **406**, 2312–2324 (2010). [DOI], [ADS], [arXiv:1001.1731 [astro-ph.GA]]. (Cited on page 125.)

[595] Lyth, D.H., "The primordial curvature perturbation in the ekpyrotic Universe", *Phys. Lett. B*, **524**, 1–4 (2002). [DOI], [ADS], [arXiv:hep-ph/0106153]. (Cited on page 173.)

[596] Lyth, D.H., "Generating the curvature perturbation at the end of inflation", *J. Cosmol. Astropart. Phys.*, **2005**(11), 006 (2005). [DOI], [ADS], [arXiv:astro-ph/0510443]. (Cited on page 170.)

[597] Lyth, D.H., Ungarelli, C. and Wands, D., "Primordial density perturbation in the curvaton scenario", *Phys. Rev. D*, **67**, 023503 (2003). [DOI], [ADS], [arXiv:astro-ph/0208055]. (Cited on pages 170 and 181.)

[598] Lyth, D.H. and Wands, D., "Generating the curvature perturbation without an inflaton", *Phys. Lett. B*, **524**, 5–14 (2002). [DOI], [ADS], [arXiv:hep-ph/0110002]. (Cited on page 170.)

[599] Ma, C.-P. and Bertschinger, E., "Cosmological perturbation theory in the synchronous and conformal Newtonian gauges", *Astrophys. J.*, **455**, 7–25 (1995). [DOI], [arXiv:astro-ph/9506072 [astro-ph]]. (Cited on pages 22, 36, and 155.)

[600] Maartens, R., "Is the Universe homogeneous?", *arXiv*, e-print, (2011). [ADS], [arXiv:1104.1300 [astro-ph.CO]]. (Cited on page 190.)

[601] Maartens, R., Ellis, G.F.R. and Stoeger, W.R., "Anisotropy and inhomogeneity of the universe from $\Delta T/T$", *Astron. Astrophys.*, **309**, L7–L10 (1996). [ADS], [arXiv:astro-ph/9510126]. (Cited on page 188.)

[602] Maartens, R. and Majerotto, E., "Observational constraints on self-accelerating cosmology", *Phys. Rev. D*, **74**, 023004 (2006). [DOI], [arXiv:astro-ph/0603353 [astro-ph]]. (Cited on page 91.)

[603] Macciò, A.V., Kang, X., Fontanot, F., Somerville, R.S., Koposov, S. and Monaco, P., "Luminosity function and radial distribution of Milky Way satellites in a ΛCDM Universe", *Mon. Not. R. Astron. Soc.*, **402**, 1995–2008 (2010). [DOI], [ADS], [arXiv:0903.4681 [astro-ph.CO]]. (Cited on page 125.)

[604] Macciò, A.V., Quercellini, C., Mainini, R., Amendola, L. and Bonometto, S.A., "Coupled dark energy: Parameter constraints from N-body simulations", *Phys. Rev. D*, **69**, 123516 (2004). [DOI], [ADS], [arXiv:astro-ph/0309671]. (Cited on pages 34, 66, and 153.)

[605] Mack, K.J., "Axions, Inflation and the Anthropic Principle", *J. Cosmol. Astropart. Phys.*, **2011**(07), 021 (2011). [DOI], [ADS], [arXiv:0911.0421 [astro-ph.CO]]. (Cited on page 155.)

[606] Mack, K.J. and Steinhardt, P.J., "Cosmological Problems with Multiple Axion-like Fields", *J. Cosmol. Astropart. Phys.*, **2011**(05), 001 (2011). [DOI], [ADS], [arXiv:0911.0418 [astro-ph.CO]]. (Cited on page 155.)

[607] MacKay, D.J.C., *Information Theory, Inference, and Learning Algorithms*, (Cambridge University Press, Cambridge; New York, 2003). [Google Books]. (Cited on page 207.)

[608] Maeda, K.-I., "Towards the Einstein-Hilbert Action via Conformal Transformation", *Phys. Rev. D*, **39**, 3159–3162 (1989). [DOI]. (Cited on pages 35 and 39.)

[609] Maggiore, M. and Riotto, A., "The Halo Mass Function from Excursion Set Theory. III. Non-Gaussian Fluctuations", *Astrophys. J.*, **717**, 526–541 (2010). [DOI], [ADS], [arXiv:0903.1251 [astro-ph.CO]]. (Cited on pages 68 and 177.)

[610] Magliocchetti, M. and Porciani, C., "The halo distribution of 2dF galaxies", *Mon. Not. R. Astron. Soc.*, **346**, 186–198 (2003). [DOI], [ADS], [arXiv:astro-ph/0304003]. (Cited on page 175.)

[611] Mainini, R. and Bonometto, S., "Mass functions in coupled Dark Energy models", *Phys. Rev. D*, **74**, 043504 (2006). [DOI], [arXiv:astro-ph/0605621]. (Cited on pages 34, 66, 72, and 153.)

[612] Mainini, R. and Mota, D.F., "ISW-LSS Cross-correlation in Coupled Dark Energy Models with Massive Neutrinos", *Astrophys. J.*, **744**, 3 (2012). [DOI], [ADS], [arXiv:1011.0083 [astro-ph.CO]]. (Cited on pages 34, 66, 152, and 153.)

[613] Majerotto, E., Väliviita, J. and Maartens, R., "Adiabatic initial conditions for perturbations in interacting dark energy models", *Mon. Not. R. Astron. Soc.*, **402**, 2344–2354 (2010). [DOI], [arXiv:0907.4981 [astro-ph.CO]]. (Cited on pages 34, 67, and 153.)

[614] Majerotto, E. et al., "Probing deviations from general relativity with the Euclid spectroscopic survey", *Mon. Not. R. Astron. Soc.*, **424**, 1392–1408 (2012). [DOI], [arXiv:1205.6215]. (Cited on pages 100 and 212.)

[615] Makler, M., de Oliveira, S.Q. and Waga, I., "Constraints on the generalized Chaplygin gas from supernovae observations", *Phys. Lett. B*, **555**, 1–6 (2003). [DOI], [ADS], [arXiv:astro-ph/0209486]. (Cited on page 150.)

[616] Maldacena, J., "Non-gaussian features of primordial fluctuations in single field inflationary models", *J. High Energy Phys.*, **2003**(05), 013 (2003). [DOI], [ADS], [arXiv:astro-ph/0210603]. (Cited on pages 164, 169, and 170.)

[617] Malik, K.A., Wands, D. and Ungarelli, C., "Large-scale curvature and entropy perturbations for multiple interacting fluids", *Phys. Rev. D*, **67**, 063516 (2003). [DOI], [ADS], [arXiv:astro-ph/0211602]. (Cited on page 180.)

[618] Manera, M. and Mota, D.F., "Cluster number counts dependence on dark energy inhomogeneities and coupling to dark matter", *Mon. Not. R. Astron. Soc.*, **371**, 1373 (2006). [DOI], [arXiv:astro-ph/0504519]. (Cited on pages 34, 66, and 153.)

[619] Mangano, G., Miele, G. and Pettorino, V., "Coupled quintessence and the coincidence problem", *Mod. Phys. Lett. A*, **18**, 831–842 (2003). [DOI], [arXiv:astro-ph/0212518]. (Cited on pages 34, 67, 152, and 153.)

[620] Mangilli, A. and Verde, L., "Non-Gaussianity and the CMB bispectrum: Confusion between primordial and lensing-Rees-Sciama contribution?", *Phys. Rev. D*, **80**, 123007 (2009). [DOI], [ADS], [arXiv:0906.2317 [astro-ph.CO]]. (Cited on page 180.)

[621] Mangilli, A., Verde, L. and Beltrán, M., "Isocurvature modes and Baryon Acoustic Oscillations", *J. Cosmol. Astropart. Phys.*, **2010**(10), 009 (2010). [DOI], [ADS], [arXiv:1006.3806 [astro-ph.CO]]. (Cited on page 182.)

[622] Mantz, A., Allen, S.W., Rapetti, D. and Ebeling, H., "The observed growth of massive galaxy clusters – I. Statistical methods and cosmological constraints", *Mon. Not. R. Astron. Soc.*, **406**, 1759–1772 (2010). [DOI], [ADS], [arXiv:0909.3098 [astro-ph.CO]]. (Cited on page 129.)

[623] Maor, I., Brustein, R. and Steinhardt, P.J., "Limitations in using luminosity distance to determine the equation-of-state of the universe", *Phys. Rev. Lett.*, **86**, 6 (2001). [DOI], [arXiv:astro-ph/0007297]. (Cited on page 20.)

[624] March, M.C., Starkman, G.D., Trotta, R. and Vaudrevange, P.M., "Should we doubt the cosmological constant?", *Mon. Not. R. Astron. Soc.*, **410**, 2488–2496 (2011). [DOI], [ADS], [arXiv:1005.3655 [astro-ph.CO]]. (Cited on page 217.)

[625] March, M.C., Trotta, R., Amendola, L. and Huterer, D., "Robustness to systematics for future dark energy probes", *Mon. Not. R. Astron. Soc.*, **415**, 143–152 (2011). [DOI], [ADS], [arXiv:1101.1521 [astro-ph.CO]]. (Cited on page 212.)

[626] March, M.C., Trotta, R., Berkes, P., Starkman, G.D. and Vaudrevange, P.M., "Improved constraints on cosmological parameters from Type Ia supernova data", *Mon. Not. R. Astron. Soc.*, **418**, 2308–2329 (2011). [DOI], [arXiv:1102.3237 [astro-ph.CO]]. (Cited on page 216.)

[627] Marian, L., Hilbert, S., Smith, R.E., Schneider, P. and Desjacques, V., "Measuring Primordial Non-gaussianity Through Weak-lensing Peak Counts", *Astrophys. J. Lett.*, **728**, L13 (2010). [DOI], [ADS], [arXiv:1010.5242 [astro-ph.CO]]. (Cited on page 178.)

[628] Maris, M., Burigana, C., Gruppuso, A., Finelli, F. and Diego, J.M., "Large-scale traces of Solar system cold dust on cosmic microwave background anisotropies", *Mon. Not. R. Astron. Soc.*, **415**, 2546–2552 (2011). [DOI], [ADS], [arXiv:1010.0830 [astro-ph.CO]]. (Cited on page 203.)

[629] Markevitch, M., Gonzalez, A.H., Clowe, D., Vikhlinin, A., Forman, W., Jones, C., Murray, S. and Tucker, W., "Direct Constraints on the Dark Matter Self-Interaction Cross Section from the Merging Galaxy Cluster 1E 0657-56", *Astrophys. J.*, **606**, 819–824 (2004). [DOI], [ADS], [arXiv:astro-ph/0309303]. (Cited on page 131.)

[630] Markovič, K., Bridle, S., Slosar, A. and Weller, J., "Constraining warm dark matter with cosmic shear power spectra", *J. Cosmol. Astropart. Phys.*, **2011**(01), 022 (2011). [DOI], [ADS], [arXiv:1009.0218 [astro-ph.CO]]. (Cited on pages 135, 136, and 162.)

[631] Marra, V. and Rosati, F., "Cosmological evolution of alpha driven by a general coupling with quintessence", *J. Cosmol. Astropart. Phys.*, **2005**(05), 011 (2005). [DOI], [ADS], [arXiv:astro-ph/0501515]. (Cited on page 33.)

[632] Marsh, D.J.E. and Ferreira, P.G., "Ultralight scalar fields and the growth of structure in the Universe", *Phys. Rev. D*, **82**, 103528 (2010). [DOI], [ADS], [arXiv:1009.3501]. (Cited on page 157.)

[633] Marsh, D.J.E., Macaulay, E., Trebitsch, M. and Ferreira, P.G., "Ultralight axions: Degeneracies with massive neutrinos and forecasts for future cosmological observations", *Phys. Rev. D*, **85**, 103514 (2012). [DOI], [ADS], [arXiv:1110.0502 [astro-ph.CO]]. (Cited on pages 158, 159, and 162.)

[634] Martin, J., Ringeval, C. and Trotta, R., "Hunting down the best model of inflation with Bayesian evidence", *Phys. Rev. D*, **81**, 063524 (2011). [DOI], [arXiv:astro-ph/1009.4157 [astro-ph.CO]]. (Cited on page 216.)

[635] Martin, N.F., Ibata, R.A., Chapman, S.C., Irwin, M. and Lewis, G.F., "A Keck-DEIMOS spectroscopic survey of faint Galactic satellites: searching for the least massive dwarf galaxies", *Mon. Not. R. Astron. Soc.*, **380**, 281–300 (2007). [DOI], [ADS], [arXiv:0705.4622]. (Cited on page 124.)

[636] Martinelli, M., Calabrese, E., de Bernardis, F., Melchiorri, A., Pagano, L. and Scaramella, R., "Constraining modified gravitational theories by weak lensing with Euclid", *Phys. Rev. D*, **83**, 023012 (2010). [DOI], [ADS], [arXiv:1010.5755 [astro-ph.CO]]. (Cited on page 111.)

[637] Martinelli, M., Honorez, L.L., Melchiorri, A. and Mena, O., "Future CMB cosmological constraints in a dark coupled universe", *Phys. Rev. D*, **81**, 103534 (2010). [DOI], [ADS], [arXiv:1004.2410 [astro-ph.CO]]. (Cited on page 113.)

[638] Martinez-González, E. and Sanz, J.L., "$\Delta T/T$ and the isotropy of the universe", *Astron. Astrophys.*, **300**, 346 (1995). [ADS]. (Cited on pages 188 and 189.)

[639] Martins, C.J.A.P., Menegoni, E., Galli, S., Mangano, G. and Melchiorri, A., "Varying couplings in the early universe: correlated variations of α and G", *Phys. Rev. D*, **82**, 023532 (2010). [DOI], [arXiv:1001.3418 [astro-ph.CO]]. (Cited on page 33.)

[640] Marulli, F., Baldi, M. and Moscardini, L., "Clustering and redshift-space distortions in interacting dark energy cosmologies", *Mon. Not. R. Astron. Soc.*, **420**, 2377–2386 (2012). [DOI], [ADS], [arXiv:1110.3045 [astro-ph.CO]]. (Cited on page 34.)

[641] Marulli, F., Carbone, C., Viel, M., Moscardini, L. and Cimatti, A., "Effects of massive neutrinos on the large-scale structure of the Universe", *Mon. Not. R. Astron. Soc.*, **418**, 346–356 (2011). [DOI], [ADS], [arXiv:1103.0278 [astro-ph.CO]]. (Cited on pages 140 and 142.)

[642] Masina, I. and Notari, A., "The cold spot as a large void: Rees-Sciama effect on CMB power spectrum and bispectrum", *J. Cosmol. Astropart. Phys.*, **2009**(02), 019 (2009). [DOI], [ADS], [arXiv:0808.1811]. (Cited on page 193.)

[643] Massey, R., Kitching, T. and Nagai, D., "Cluster bulleticity", *Mon. Not. R. Astron. Soc.*, **413**, 1709–1716 (2011). [DOI], [ADS], [arXiv:1007.1924 [astro-ph.CO]]. (Cited on pages 131 and 133.)

[644] Massey, R., Kitching, T. and Richard, J., "The dark matter of gravitational lensing", *Rep. Prog. Phys.*, **73**, 086901 (2010). [DOI], [ADS], [arXiv:1001.1739]. (Cited on page 122.)

[645] Massey, R. et al., "Dark matter maps reveal cosmic scaffolding", *Nature*, **445**, 286–290 (2007). [DOI], [ADS], [arXiv:astro-ph/0701594]. (Cited on page 130.)

[646] Matarrese, S., Baccigalupi, C. and Perrotta, F., "Approaching Λ without fine-tuning", *Phys. Rev. D*, **70**, 061301 (2004). [DOI], [arXiv:astro-ph/0403480]. (Cited on pages 19 and 34.)

[647] Matarrese, S. and Verde, L., "The Effect of Primordial Non-Gaussianity on Halo Bias", *Astrophys. J. Lett.*, **677**, L77–L80 (2008). [DOI], [ADS], [arXiv:0801.4826]. (Cited on pages 175 and 176.)

[648] Matarrese, S., Verde, L. and Heavens, A.F., "Large-scale bias in the Universe: bispectrum method", *Mon. Not. R. Astron. Soc.*, **290**, 651–662 (1997). [DOI], [ADS], [arXiv:astro-ph/9706059]. (Cited on page 83.)

[649] Matarrese, S., Verde, L. and Jimenez, R., "The Abundance of High-Redshift Objects as a Probe of Non-Gaussian Initial Conditions", *Astrophys. J.*, **541**, 10–24 (2000). [DOI], [ADS], [arXiv:astro-ph/0001366]. (Cited on page 177.)

[650] Mateo, M.L., "Dwarf Galaxies of the Local Group", *Annu. Rev. Astron. Astrophys.*, **36**, 435–506 (1998). [DOI], [ADS], [arXiv:astro-ph/9810070]. (Cited on page 124.)

[651] McDonald, P., Trac, H. and Contaldi, C., "Dependence of the non-linear mass power spectrum on the equation of state of dark energy", *Mon. Not. R. Astron. Soc.*, **366**, 547–556 (2006). [DOI], [arXiv:astro-ph/0505565]. (Cited on page 103.)

[652] McEwen, J.D., Hobson, M.P., Lasenby, A.N. and Mortlock, D.J., "Non-Gaussianity detections in the Bianchi VII$_h$ corrected WMAP one-year data made with directional spherical wavelets", *Mon. Not. R. Astron. Soc.*, **369**, 1858–1868 (2006). [DOI], [ADS], [arXiv:astro-ph/0510349]. (Cited on page 188.)

[653] Meerburg, P.D., van der Schaar, J.P. and Corasaniti, P.S., "Signatures of initial state modifications on bispectrum statistics", *J. Cosmol. Astropart. Phys.*, **2009**(05), 018 (2009). [DOI], [ADS], [arXiv:0901.4044 [hep-th]]. (Cited on page 172.)

[654] Meiksin, A. and Davis, M., "Anisotropy of the galaxies detected by IRAS", *Astron. J.*, **91**, 191–198 (1986). [DOI], [ADS]. (Cited on page 85.)

[655] Melchiorri, A., Mena, O., Palomares-Ruiz, S., Pascoli, S., Slosar, A. and Sorel, M., "Sterile neutrinos in light of recent cosmological and oscillation data: a multi-flavor scheme approach", *J. Cosmol. Astropart. Phys.*, **2009**(01), 036 (2009). [DOI], [ADS], [arXiv:0810.5133 [hep-ph]]. (Cited on page 136.)

[656] Ménard, B., Nestor, D., Turnshek, D., Quider, A., Richards, G., Chelouche, D. and Rao, S., "Lensing, reddening and extinction effects of MgII absorbers from $z = 0.4$ to 2", *Mon. Not. R. Astron. Soc.*, **385**, 1053–1066 (2008). [DOI], [ADS], [arXiv:0706.0898]. (Cited on page 184.)

[657] Menard, B., Scranton, R., Fukugita, M. and Richards, G., "Measuring the galaxy-mass and galaxy-dust correlations through magnification and reddening", *Mon. Not. R. Astron. Soc.*, **405**, 1025–1039 (2010). [DOI], [arXiv:0902.4240 [astro-ph.CO]]. (Cited on pages 76 and 77.)

[658] Meneghetti, M., Yoshida, N., Bartelmann, M., Moscardini, L., Springel, V., Tormen, G. and White, S.D.M., "Giant cluster arcs as a constraint on the scattering cross-section of dark matter", *Mon. Not. R. Astron. Soc.*, **325**, 435–442 (2001). [DOI], [ADS], [arXiv:astro-ph/0011405]. (Cited on page 131.)

[659] Milgrom, M., "A modification of the Newtonian dynamics as a possible alternative to the hidden mass hypothesis", *Astrophys. J.*, **270**, 365–370 (1983). [DOI], [ADS]. (Cited on page 49.)

[660] Miranda, V., Jorás, S.E., Waga, I. and Quartin, M., "Viable Singularity-Free $f(R)$ Gravity without a Cosmological Constant", *Phys. Rev. Lett.*, **102**, 221101 (2009). [DOI], [ADS], [arXiv:0905.1941 [astro-ph.CO]]. (Cited on page 41.)

[661] Mollerach, S., "Isocurvature baryon perturbations and inflation", *Phys. Rev. D*, **42**, 313–325 (1990). [DOI], [ADS]. (Cited on page 170.)

[662] Moore, B., Ghigna, S., Governato, F., Lake, G., Quinn, T., Stadel, J. and Tozzi, P., "Dark Matter Substructure within Galactic Halos", *Astrophys. J. Lett.*, **524**, L19–L22 (1999). [DOI], [ADS], [arXiv:astro-ph/9907411]. (Cited on page 124.)

[663] More, S., Bovy, J. and Hogg, D.W., "Cosmic Transparency: A Test with the Baryon Acoustic Feature and Type Ia Supernovae", *Astrophys. J.*, **696**, 1727–1732 (2009). [DOI], [ADS], [arXiv:0810.5553]. (Cited on page 184.)

[664] Moroi, T. and Takahashi, T., "Effects of cosmological moduli fields on cosmic microwave background", *Phys. Lett. B*, **522**, 215–221 (2001). [DOI], [ADS], [arXiv:hep-ph/0110096]. (Cited on pages 170 and 181.)

[665] Mörtsell, E., Bergström, L. and Goobar, A., "Photon-axion oscillations and type Ia supernovae", *Phys. Rev. D*, **66**, 047702 (2002). [DOI], [ADS], [arXiv:astro-ph/0202153]. (Cited on page 184.)

[666] Mota, D.F., "Probing Dark Energy at Galactic and Cluster Scales", *J. Cosmol. Astropart. Phys.*, **2008**(09), 006 (2008). [DOI], [arXiv:0812.4493 [astro-ph]]. (Cited on page 34.)

[667] Mota, D.F., Kristiansen, J.R., Koivisto, T. and Groeneboom, N.E., "Constraining Dark Energy Anisotropic Stress", *Mon. Not. R. Astron. Soc.*, **382**, 793–800 (2007). [DOI], [arXiv:0708.0830 [astro-ph]]. (Cited on page 25.)

[668] Mota, D.F., Pettorino, V., Robbers, G. and Wetterich, C., "Neutrino clustering in growing neutrino quintessence", *Phys. Lett. B*, **663**, 160–164 (2008). [DOI], [arXiv:0802.1515 [astro-ph]]. (Cited on pages 34, 67, 73, 143, and 150.)

[669] Mota, D.F., Sandstad, M. and Zlosnik, T., "Cosmology of the selfaccelerating third order Galileon", *J. High Energy Phys.*, **2010**(12), 051 (2010). [DOI], [ADS], [arXiv:1009.6151 [astro-ph.CO]]. (Cited on page 45.)

[670] Mota, D.F. and Shaw, D.J., "Evading Equivalence Principle Violations, C. and other Experimental Constraints in Scalar Field Theories with a Strong Coupling to Matter", *Phys. Rev. D*, **75**, 063501 (2007). [DOI], [arXiv:hep-ph/0608078 [hep-ph]]. (Cited on page 35.)

[671] Mota, D.F. and van de Bruck, C., "On the Spherical collapse model in dark energy cosmologies", *Astron. Astrophys.*, **421**, 71–81 (2004). [DOI], [arXiv:astro-ph/0401504 [astro-ph]]. (Cited on page 69.)

[672] Mota, D.F. and Winther, H.A., "Cosmology of Chameleons with Power-Law Couplings", *Astrophys. J.*, **733**, 7 (2011). [DOI], [arXiv:1010.5650 [astro-ph.CO]]. (Cited on page 35.)

[673] Motohashi, H., Starobinsky, A.A. and Yokoyama, J., "Phantom behaviour and growth index anomalous evolution in viable $f(R)$ gravity models", in Saijo, M., Miyamoto, U., Harada, T., Sasaki, M., Shiromizu, T. and Mukohyama, S., eds., *Proceedings of the Nineteenth Workshop on General Relativity and Gravitation in Japan (JGRG19)*, Rikkyo University, Tokyo, Japan, 30 November – 4 December 2009, pp. 339–242, (Rikkyo University, Tokyo, 2010). [ADS], [arXiv:1002.0462 [astro-ph.CO]]. URL (accessed 16 August 2013): `http://www2.rikkyo.ac.jp/web/jgrg19/`. (Cited on page 90.)

[674] Motohashi, H., Starobinsky, A.A. and Yokoyama, J., "Phantom boundary crossing and anomalous growth index of fluctuations in viable $f(R)$ models of cosmic acceleration", *Prog. Theor. Phys.*, **123**, 887–902 (2010). [DOI], [arXiv:1002.1141 [astro-ph.CO]]. (Cited on page 68.)

[675] Mukhanov, V.F. and Chibisov, G.V., "Quantum fluctuations and a nonsingular universe", *JETP Lett.*, **33**, 532 (1981). [ADS]. (Cited on page 163.)

[676] Mukherjee, P., Kunz, M., Parkinson, D. and Wang, Y., "Planck priors for dark energy surveys", *Phys. Rev. D*, **78**, 083529 (2008). [DOI], [arXiv:0803.1616 [astro-ph]]. (Cited on pages 118 and 119.)

[677] Mukherjee, P., Parkinson, D., Corasaniti, P.S., Liddle, A.R. and Kunz, M., "Model selection as a science driver for dark energy surveys", *Mon. Not. R. Astron. Soc.*, **369**, 1725–1734 (2006). [DOI], [arXiv:astro-ph/0512484]. (Cited on pages 213 and 216.)

[678] Müller, V., Schmidt, H.-J. and Starobinsky, A.A., "The stability of the de Sitter space-time in fourth order gravity", *Phys. Lett. B*, **202**, 198–200 (1988). [DOI], [ADS]. (Cited on page 41.)

[679] Munshi, D., van Waerbeke, L., Smidt, J. and Coles, P., "From weak lensing to non-Gaussianity via Minkowski functionals", *Mon. Not. R. Astron. Soc.*, **419**, 536–555 (2011). [DOI], [ADS], [arXiv:1103.1876 [astro-ph.CO]]. (Cited on page 175.)

[680] Murayama, H. and Peña-Garay, C., "Neutrinoless double beta decay in light of SNO salt data", *Phys. Rev. D*, **69**, 031301 (2004). [DOI], [ADS], [arXiv:hep-ph/0309114]. (Cited on pages 136 and 137.)

[681] Mustapha, N., Hellaby, C. and Ellis, G.F.R., "Large-scale inhomogeneity versus source evolution: can we distinguish them observationally?", *Mon. Not. R. Astron. Soc.*, **292**, 817 (1997). [DOI], [ADS], [arXiv:gr-qc/9808079]. (Cited on page 192.)

[682] Nariai, H., "Gravitational instability of regular model-universes in a modified theory of general relativity", *Prog. Theor. Phys.*, **49**, 165–180 (1973). [DOI]. (Cited on page 110.)

[683] Navarro, I. and Van Acoleyen, K., "$f(R)$ actions, cosmic acceleration and local tests of gravity", *J. Cosmol. Astropart. Phys.*, **2007**(02), 022 (2007). [DOI], [ADS], [arXiv:gr-qc/0611127]. (Cited on page 41.)

[684] Navarro, J.F., Frenk, C.S. and White, S.D.M., "The Structure of Cold Dark Matter Halos", *Astrophys. J.*, **462**, 563–575 (1996). [DOI], [ADS], [arXiv:astro-ph/9508025]. (Cited on page 129.)

[685] Neto, A.F. et al., "The statistics of ΛCDM halo concentrations", *Mon. Not. R. Astron. Soc.*, **381**, 1450–1462 (2007). [DOI], [ADS], [arXiv:0706.2919]. (Cited on page 129.)

[686] Nicolis, A., Rattazzi, R. and Trincherini, E., "Galileon as a local modification of gravity", *Phys. Rev. D*, **79**, 064036 (2009). [DOI], [ADS], [arXiv:0811.2197 [hep-th]]. (Cited on pages 44, 45, and 172.)

[687] Nojiri, S. and Odintsov, S.D., "Modified gravity with negative and positive powers of curvature: Unification of inflation and cosmic acceleration", *Phys. Rev. D*, **68**, 123512 (2003). [DOI], [ADS], [arXiv:hep-th/0307288]. (Cited on page 40.)

[688] Nojiri, S. and Odintsov, S.D., "Can $F(R)$-gravity be a viable model: the universal unification scenario for inflation, dark energy and dark matter", *arXiv*, e-print, (2008). [ADS], [arXiv:0801.4843]. (Cited on page 151.)

[689] Nolta, M.R. et al. (WMAP Collaboration), "Five-Year Wilkinson Microwave Anisotropy Probe Observations: Angular Power Spectra", *Astrophys. J. Suppl. Ser.*, **180**, 296–305 (2009). [DOI], [ADS], [arXiv:0803.0593 [astro-ph]]. (Cited on page 52.)

[690] Noreña, J., Verde, L., Barenboim, G. and Bosch, C., "Prospects for constraining the shape of non-Gaussianity with the scale-dependent bias", *J. Cosmol. Astropart. Phys.*, **2012**(08), 019 (2012). [DOI], [ADS], [arXiv:1204.6324 [astro-ph.CO]]. (Cited on page 173.)

[691] Noreña, J., Wagner, C., Verde, L., Peiris, H.V. and Easther, R., "Bayesian Analysis of Inflation III: Slow Roll Reconstruction Using Model Selection", *Phys. Rev. D*, **86**, 023505 (2012). [DOI], [arXiv:1202.0304 [astro-ph.CO]]. (Cited on page 169.)

[692] Nunes, N.J. and Mota, D.F., "Structure formation in inhomogeneous dark energy models", *Mon. Not. R. Astron. Soc.*, **368**, 751–758 (2006). [DOI], [arXiv:astro-ph/0409481 [astro-ph]]. (Cited on pages 26 and 69.)

[693] Nusser, A., Branchini, E. and Davis, M., "Bulk flows from galaxy luminosities: Application to 2MASS redshift survey and forecast for next-generation data sets", *Astrophys. J.*, **735**, 77 (2011). [DOI], [ADS], [arXiv:1102.4189 [astro-ph.CO]]. (Cited on page 84.)

[694] Nusser, A. and Davis, M., "The Cosmological Bulk Flow: Consistency with ΛCDM and $z \approx 0$ Constraints on σ_8 and γ", *Astrophys. J.*, **736**, 93 (2011). [DOI], [ADS], [arXiv:1101.1650 [astro-ph.CO]]. (Cited on page 84.)

[695] Olivares, G., Atrio-Barandela, F. and Pavón, D., "Matter density perturbations in interacting quintessence models", *Phys. Rev. D*, **74**, 043521 (2006). [DOI], [arXiv:astro-ph/0607604]. (Cited on page 34.)

[696] Olive, K.A. and Pospelov, M., "Environmental dependence of masses and coupling constants", *Phys. Rev. D*, **77**, 043524 (2008). [DOI], [arXiv:0709.3825 [hep-ph]]. (Cited on page 48.)

[697] Olmo, G.J., "Post-Newtonian constraints on $f(R)$ cosmologies in metric and Palatini formalism", *Phys. Rev. D*, **72**, 083505 (2005). [DOI], [ADS], [arXiv:gr-qc/0505135]. (Cited on pages 40 and 41.)

[698] Orsi, A., Baugh, C.M., Lacey, C.G., Cimatti, A., Wang, Y. and Zamorani, G., "Probing dark energy with future redshift surveys: A comparison of emission line and broad band selection in the near infrared", *Mon. Not. R. Astron. Soc.*, **405**, 1006–1024 (2010). [DOI], [ADS], [arXiv:0911.0669 [astro-ph.CO]]. (Cited on pages 91, 167, and 178.)

[699] Osborne, S.J., Mak, D.S.Y., Church, S.E. and Pierpaoli, E., "Measuring the Galaxy Cluster Bulk Flow from WMAP data", *Astrophys. J.*, **737**, 98 (2011). [DOI], [ADS], [arXiv:1011.2781 [astro-ph.CO]]. (Cited on page 84.)

[700] Oyaizu, H., "Nonlinear evolution of $f(R)$ cosmologies. I. Methodology", *Phys. Rev. D*, **78**, 123523 (2008). [DOI], [arXiv:0807.2449 [astro-ph]]. (Cited on page 68.)

[701] Oyaizu, H., Lima, M. and Hu, W., "Nonlinear evolution of $f(R)$ cosmologies. II. power spectrum", *Phys. Rev. D*, **78**, 123524 (2008). [DOI], [arXiv:0807.2462 [astro-ph]]. (Cited on page 68.)

[702] Paci, F., Gruppuso, A., Finelli, F., Cabella, P., de Rosa, A., Mandolesi, N. and Natoli, P., "Power Asymmetries in the Cosmic Microwave Background Temperature and Polarization patterns", *Mon. Not. R. Astron. Soc.*, **407**, 399–404 (2010). [DOI], [ADS], [arXiv:1002.4745 [astro-ph.CO]]. (Cited on page 206.)

[703] Pahud, C., Liddle, A.R., Mukherjee, P. and Parkinson, D., "Model selection forecasts for the spectral index from the Planck satellite", *Phys. Rev. D*, **73**, 123524 (2006). [DOI], [ADS], [arXiv:astro-ph/0605004]. (Cited on pages 118 and 213.)

[704] Pahud, C., Liddle, A.R., Mukherjee, P. and Parkinson, D., "When can the Planck satellite measure spectral index running?", *Mon. Not. R. Astron. Soc.*, **381**, 489–493 (2007). [DOI], [ADS], [arXiv:astro-ph/0701481]. (Cited on page 213.)

[705] Panda, S., Sumitomo, Y. and Trivedi, S.P., "Axions as Quintessence in String Theory", *Phys. Rev. D*, **83**, 083506 (2011). [DOI], [ADS], [arXiv:1011.5877]. (Cited on pages 154 and 155.)

[706] Park, C., Hwang, J., Park, J. and Noh, H., "Observational constraints on a unified dark matter and dark energy model based on generalized Chaplygin gas", *Phys. Rev. D*, **81**, 063532 (2010). [DOI], [ADS], [arXiv:0910.4202 [astro-ph.CO]]. (Cited on page 152.)

[707] Parkinson, D., Blake, C., Kunz, M., Bassett, B.A., Nichol, R.C. and Glazebrook, K., "Optimizing baryon acoustic oscillation surveys – I: Testing the concordance ΛCDM cosmology", *Mon. Not. R. Astron. Soc.*, **377**, 185–197 (2007). [DOI], [ADS], [arXiv:astro-ph/0702040]. (Cited on page 215.)

[708] Parkinson, D., Kunz, M., Liddle, A.R., Bassett, B.A., Nichol, R.C. and Vardanyan, M., "Optimizing baryon acoustic oscillation surveys – II: Curvature, redshifts and external data sets", *Mon. Not. R. Astron. Soc.*, **401**, 2169–2180 (2010). [DOI], [ADS], [arXiv:0905.3410 [astro-ph.CO]]. (Cited on page 215.)

[709] Parkinson, D. and Liddle, A.R., "Application of Bayesian model averaging to measurements of the primordial power spectrum", *Phys. Rev. D*, **82**, 103533 (2010). [DOI], [arXiv:1009.1394 [astro-ph.CO]]. (Cited on page 217.)

[710] Parkinson, D., Mukherjee, P. and Liddle, A.R., "Bayesian model selection analysis of WMAP3", *Phys. Rev. D*, **73**, 123523 (2006). [DOI], [arXiv:astro-ph/0605003 [astro-ph]]. (Cited on page 216.)

[711] Peacock, J.A., "Statistics of Cosmological Density Fields", in Martinez, V.J., Portilla, M. and Saez, D., eds., *New Insights into the Universe*, Proceedings of a Summer School Held in Valencia, Spain, 23 – 27 September 1991, Lecture Notes in Physics, 408, pp. 1–64, (Springer, Berlin; Heidelberg, 1992). [DOI], [ADS]. (Cited on page 166.)

[712] Peacock, J.A., *Cosmological Physics*, (Cambridge University Press, Cambridge; New York, 1999). [ADS], [Google Books]. (Cited on page 122.)

[713] Peacock, J.A. and Dodds, S.J., "Reconstructing the Linear Power Spectrum of Cosmological Mass Fluctuations", *Mon. Not. R. Astron. Soc.*, **267**, 1020–1034 (1994). [ADS], [arXiv:astro-ph/9311057]. (Cited on page 166.)

[714] Peccei, R.D., "Neutrino models of dark energy", *Phys. Rev. D*, **71**, 023527 (2005). [DOI], [arXiv:hep-ph/0411137]. (Cited on pages 34 and 143.)

[715] Peccei, R.D. and Quinn, H.R., "*CP* Conservation in the Presence of Pseudoparticles", *Phys. Rev. Lett.*, **38**, 1440–1443 (1977). [DOI], [ADS]. (Cited on pages 122, 154, and 181.)

[716] Peebles, P.J.E., "The Peculiar Velocity Field in the Local Supercluster", *Astrophys. J.*, **205**, 318–328 (1976). [DOI]. (Cited on page 90.)

[717] Peebles, P.J.E., *The Large-Scale Structure of the Universe*, Princeton Series in Physics, (Princeton University Press, Princeton, NJ, 1980). [ADS], [Google Books]. (Cited on page 83.)

[718] Peebles, P.J.E., "Tests of cosmological models constrained by inflation", *Astrophys. J.*, **284**, 439–444 (1984). [DOI], [ADS]. (Cited on page 68.)

[719] Peebles, P.J.E., Schramm, D.N., Kron, R.G. and Turner, E.L., "The case for the relativistic hot big bang cosmology", *Nature*, **352**, 769–776 (1991). [DOI], [ADS]. (Cited on page 122.)

[720] Percival, W.J. et al., "Measuring the Matter Density Using Baryon Oscillations in the SDSS", *Astrophys. J.*, **657**, 51–55 (2007). [DOI], [ADS], [arXiv:astro-ph/0608635]. (Cited on page 80.)

[721] Perrotta, F. and Baccigalupi, C., "On the dark energy clustering properties", *Phys. Rev. D*, **65**, 123505 (2002). [DOI], [arXiv:astro-ph/0201335]. (Cited on page 34.)

[722] Perrotta, F., Baccigalupi, C. and Matarrese, S., "Extended quintessence", *Phys. Rev. D*, **61**, 023507 (2000). [DOI], [arXiv:astro-ph/9906066]. (Cited on page 34.)

[723] Pettorino, V., Amendola, L. and Wetterich, C., "How early is early dark energy?", *Phys. Rev. D*, **87**, 083009 (2013). [DOI], [ADS], [arXiv:1301.5279 [astro-ph.CO]]. (Cited on page 59.)

[724] Pettorino, V. and Baccigalupi, C., "Coupled and Extended Quintessence: theoretical differences and structure formation", *Phys. Rev. D*, **77**, 103003 (2008). [DOI], [arXiv:0802.1086 [astro-ph]]. (Cited on pages 32, 34, 35, 39, 91, 113, and 152.)

[725] Pettorino, V., Baccigalupi, C. and Mangano, G., "Extended quintessence with an exponential coupling", *J. Cosmol. Astropart. Phys.*, **2005**(01), 014 (2005). [DOI], [arXiv:astro-ph/0412334]. (Cited on pages 34 and 35.)

[726] Pettorino, V., Baccigalupi, C. and Perrotta, F., "Scaling solutions in scalar tensor cosmologies", *J. Cosmol. Astropart. Phys.*, **2005**(12), 003 (2005). [DOI], [arXiv:astro-ph/0508586]. (Cited on page 34.)

[727] Pettorino, V., Wintergerst, N., Amendola, L. and Wetterich, C., "Neutrino lumps and the cosmic microwave background", *Phys. Rev. D*, **82**, 123001 (2010). [DOI], [ADS], [arXiv:1009.2461 [astro-ph.CO]]. (Cited on pages 34, 66, 67, 73, 143, 150, and 153.)

[728] Pfenniger, D., Combes, F. and Martinet, L., "Is dark matter in spiral galaxies cold gas? I. Observational constraints and dynamical clues about galaxy evolution", *Astron. Astrophys.*, **285**, 79–93 (1994). [ADS], [arXiv:astro-ph/9311043]. (Cited on page 122.)

[729] Piattella, O.F., Bertacca, D., Bruni, M. and Pietrobon, D., "Unified Dark Matter models with fast transition", *J. Cosmol. Astropart. Phys.*, **2010**(01), 014 (2010). [DOI], [ADS], [arXiv:0911.2664 [astro-ph.CO]]. (Cited on page 151.)

[730] Pillepich, A., Porciani, C. and Hahn, O., "Halo mass function and scale-dependent bias from N-body simulations with non-Gaussian initial conditions", *Mon. Not. R. Astron. Soc.*, **402**, 191–206 (2010). [DOI], [ADS], [arXiv:0811.4176]. (Cited on pages 177 and 178.)

[731] Pillepich, A., Porciani, C. and Matarrese, S., "The Bispectrum of Redshifted 21 Centimeter Fluctuations from the Dark Ages", *Astrophys. J.*, **662**, 1–14 (2007). [DOI], [ADS], [arXiv:astro-ph/0611126]. (Cited on pages 174 and 177.)

[732] Pillepich, A., Porciani, C. and Reiprich, T.H., "The X-ray cluster survey with eROSITA: forecasts for cosmology, cluster physics, and primordial non-Gaussianity", *Mon. Not. R. Astron. Soc.*, **422**, 44–69 (2012). [DOI], [ADS], [arXiv:1111.6587 [astro-ph.CO]]. (Cited on page 177.)

[733] Pires, S. and Amara, A., "Weak Lensing Mass Reconstruction: Flexion Versus Shear", *Astrophys. J.*, **723**, 1507–1511 (2010). [DOI], [ADS], [arXiv:1009.0712 [astro-ph.CO]]. (Cited on page 130.)

[734] Pitrou, C., Pereira, T.S. and Uzan, J.-P., "Predictions from an anisotropic inflationary era", *J. Cosmol. Astropart. Phys.*, **2008**(04), 004 (2008). [DOI], [arXiv:0801.3596 [astro-ph]]. (Cited on page 203.)

[735] Planck Science Team, *Planck: The Scientific Programme (Blue Book), Version 2*, ESA-SCI(2005)1, (ESA, Paris, 2009). [arXiv:astro-ph/0604069]. URL (accessed 6 June 2013): http://sci.esa.int/jump.cfm?oid=47334. (Cited on page 165.)

[736] Pogosian, L. and Silvestri, A., "Pattern of growth in viable $f(R)$ cosmologies", *Phys. Rev. D*, **77**, 023503 (2008). [DOI], [arXiv:0709.0296 [astro-ph]]. (Cited on page 74.)

[737] Pogosian, L., Silvestri, A., Koyama, K. and Zhao, G.-B., "How to optimally parametrize deviations from General Relativity in the evolution of cosmological perturbations?", *Phys. Rev. D*, **81**, 104023 (2010). [DOI], [arXiv:1002.2382 [astro-ph.CO]]. (Cited on pages 24, 25, 26, and 63.)

[738] Polarski, D. and Gannouji, R., "On the growth of linear perturbations", *Phys. Lett. B*, **660**, 439–443 (2008). [DOI], [arXiv:0710.1510 [astro-ph]]. (Cited on page 90.)

[739] Polarski, D. and Starobinsky, A.A., "Spectra of perturbations produced by double inflation with an intermediate matter-dominated stage", *Nucl. Phys. B*, **385**, 623–650 (1992). [DOI], [ADS]. (Cited on page 170.)

[740] Pontzen, A. and Peiris, H.V., "The cut-sky cosmic microwave background is not anomalous", *Phys. Rev. D*, **81**, 103008 (2010). [DOI], [arXiv:1004.2706 [astro-ph.CO]]. (Cited on page 188.)

[741] Popov, V.A., "Dark energy and dark matter unification via superfluid Chaplygin gas", *Phys. Lett. B*, **686**, 211–215 (2010). [DOI], [ADS], [arXiv:0912.1609 [gr-qc]]. (Cited on page 151.)

[742] Preskill, J., Wise, MB.. and Wilczek, F., "Cosmology of the invisible axion", *Phys. Lett. B*, **120**, 127–132 (1983). [DOI], [ADS]. (Cited on pages 154 and 181.)

[743] Press, W.H. and Schechter, P., "Formation of Galaxies and Clusters of Galaxies by Self-Similar Gravitational Condensation", *Astrophys. J.*, **187**, 425 (1974). [DOI]. (Cited on page 68.)

[744] Primack, J.R., "Cosmology: small-scale issues", *New J. Phys.*, **11**, 105029 (2009). [DOI], [ADS], [arXiv:0909.2247 [astro-ph.CO]]. (Cited on page 133.)

[745] Pullen, A.R. and Hirata, C.M., "Non-detection of a statistically anisotropic power spectrum in large-scale structure", *J. Cosmol. Astropart. Phys.*, **2010**(05), 027 (2010). [DOI], [ADS], [arXiv:1003.0673 [astro-ph.CO]]. (Cited on pages 205 and 206.)

[746] Pullen, A.R. and Kamionkowski, M., "Cosmic microwave background statistics for a direction-dependent primordial power spectrum", *Phys. Rev. D*, **76**, 103529 (2007). [DOI], [ADS], [arXiv:0709.1144]. (Cited on pages 204, 205, and 206.)

[747] Quartin, M., Calvão, M.O., Jorás, S.E., Reis, R.R.R. and Waga, I., "Dark Interactions and Cosmological Fine-Tuning", *J. Cosmol. Astropart. Phys.*, **2008**(05), 007 (2008). [DOI], [ADS], [arXiv:0802.0546 [astro-ph]]. (Cited on pages 34 and 152.)

[748] Quercellini, C., Bruni, M., Balbi, A. and Pietrobon, D., "Late universe dynamics with scale-independent linear couplings in the dark sector", *Phys. Rev. D*, **78**, 063527 (2008). [DOI], [ADS], [arXiv:0803.1976]. (Cited on pages 34 and 152.)

[749] Quercellini, C., Quartin, M. and Amendola, L., "Possibility of Detecting Anisotropic Expansion of the Universe by Very Accurate Astrometry Measurements", *Phys. Rev. Lett.*, **102**, 151302 (2009). [DOI], [ADS], [arXiv:0809.3675]. (Cited on page 189.)

[750] Randall, S.W., Markevitch, M., Clowe, D., Gonzalez, A.H. and Bradač, M., "Constraints on the Self-Interaction Cross Section of Dark Matter from Numerical Simulations of the Merging Galaxy Cluster 1E 0657-56", *Astrophys. J.*, **679**, 1173–1180 (2008). [DOI], [ADS], [arXiv:0704.0261]. (Cited on pages 131 and 132.)

[751] Räsänen, S., "Dark energy from backreaction", *J. Cosmol. Astropart. Phys.*, **2004**(02), 003 (2004). [DOI], [ADS], [arXiv:astro-ph/0311257 [astro-ph]]. (Cited on page 195.)

[752] Räsänen, S., "Accelerated expansion from structure formation", *J. Cosmol. Astropart. Phys.*, **2006**(11), 003 (2006). [DOI], [ADS], [arXiv:astro-ph/0607626 [astro-ph]]. (Cited on page 195.)

[753] Rassat, A. et al., "Deconstructing Baryon Acoustic Oscillations: A Comparison of Methods", *arXiv*, e-print, (2008). [ADS], [arXiv:0810.0003 [astro-ph]]. (Cited on pages 91, 100, and 178.)

[754] Ratra, B. and Peebles, P.J.E., "Cosmological consequences of a rolling homogeneous", *Phys. Rev. D*, **37**, 3406–3427 (1988). [DOI]. (Cited on pages 18 and 64.)

[755] Rawlings, S., Abdalla, F.B., Bridle, S.L., Blake, C.A., Baugh, C.M., Greenhill, L.J. and van der Hulst, J.M., "Galaxy evolution, cosmology and dark energy with the Square Kilometer Array", *New Astron. Rev.*, **48**, 1013–1027 (2004). [DOI], [ADS], [arXiv:astro-ph/0409479 [astro-ph]]. (Cited on page 117.)

[756] Read, J.I., Pontzen, A.P. and Viel, M., "On the formation of dwarf galaxies and stellar haloes", *Mon. Not. R. Astron. Soc.*, **371**, 885–897 (2006). [DOI], [ADS], [arXiv:astro-ph/0606391]. (Cited on page 125.)

[757] Read, J.I., Saha, P. and Macciò, A.V., "Radial Density Profiles of Time-Delay Lensing Galaxies", *Astrophys. J.*, **667**, 645–654 (2007). [DOI], [ADS], [arXiv:0704.3267]. (Cited on page 126.)

[758] Read, J.I. and Trentham, N., "The baryonic mass function of galaxies", *Philos. Trans. R. Soc. London, Ser. A*, **363**, 2693 (2005). [DOI], [ADS], [arXiv:astro-ph/0502517]. (Cited on page 124.)

[759] Rebolo, R., "Baryonic dark matter", *Nucl. Phys. B (Proc. Suppl.)*, **110**, 16–25 (2002). [DOI], [ADS]. (Cited on page 122.)

[760] Refregier, A., "The Dark UNiverse Explorer (DUNE): proposal to ESA's cosmic vision", *Exp. Astron.*, **23**, 17–37 (2009). [DOI], [ADS], [arXiv:0802.2522]. (Cited on page 15.)

[761] Refsdal, S., "The gravitational lens effect", *Mon. Not. R. Astron. Soc.*, **128**, 295 (1964). [ADS]. (Cited on page 124.)

[762] Reid, B.A., Verde, L., Jimenez, R. and Mena, O., "Robust neutrino constraints by combining low redshift observations with the CMB", *J. Cosmol. Astropart. Phys.*, **2010**(01), 003 (2010). [DOI], [ADS], [arXiv:0910.0008 [astro-ph.CO]]. (Cited on pages 136 and 137.)

[763] Renaux-Petel, S., "Combined local and equilateral non-Gaussianities from multifield DBI inflation", *J. Cosmol. Astropart. Phys.*, **2009**(10), 012 (2009). [DOI], [ADS], [arXiv:0907.2476 [hep-th]]. (Cited on page 172.)

[764] Riazuelo, A. and Uzan, J.-P., "Cosmological observations in scalar-tensor quintessence", *Phys. Rev. D*, **66**, 023525 (2002). [DOI], [arXiv:astro-ph/0107386]. (Cited on page 34.)

[765] Richter, P., Savage, B.D., Sembach, K.R. and Tripp, T.M., "Tracing baryons in the warm-hot intergalactic medium with broad Ly α absorption", *Astron. Astrophys.*, **445**, 827–842 (2006). [DOI], [ADS], [arXiv:astro-ph/0509539]. (Cited on page 122.)

[766] Riess, A.G., Press, W.H. and Kirshner, R.P., "Determining the motion of the local group using type IA supernovae light curve shapes", *Astrophys. J. Lett.*, **445**, L91–L94 (1995). [DOI], [ADS], [arXiv:astro-ph/9412017]. (Cited on page 84.)

[767] Riess, A.G. et al., "A 3% Solution: Determination of the Hubble Constant with the Hubble Space Telescope and Wide Field Camera 3", *Astrophys. J.*, **730**, 119 (2011). [DOI], [ADS], [arXiv:1103.2976 [astro-ph.CO]]. (Cited on page 194.)

[768] Rigopoulos, G.I., Shellard, E.P.S. and van Tent, B.J.W., "Large non-Gaussianity in multiple-field inflation", *Phys. Rev. D*, **73**, 083522 (2006). [DOI], [ADS], [arXiv:astro-ph/0506704]. (Cited on page 170.)

[769] Rinaldi, M., "A new approach to non-commutative inflation", *Class. Quantum Grav.*, **28**, 105022 (2011). [DOI], [ADS], [arXiv:0908.1949 [gr-qc]]. (Cited on page 201.)

[770] Rinaldi, M., "Observational signatures of pre-inflationary and lower dimensional effective gravity", *Class. Quantum Grav.*, **29**, 085010 (2012). [DOI], [ADS]. (Cited on page 200.)

[771] Romano, A.E., "Lemaitre-Tolman-Bondi universes as alternatives to dark energy: Does positive averaged acceleration imply positive cosmic acceleration?", *Phys. Rev. D*, **75**, 043509 (2007). [DOI], [ADS], [arXiv:astro-ph/0612002]. (Cited on page 192.)

[772] Rosa, J.G., "The extremal black hole bomb", *J. High Energy Phys.*, **2010**(06), 015 (2010). [DOI], [ADS], [arXiv:0912.1780 [hep-th]]. (Cited on page 155.)

[773] Rosati, P., Borgani, S., Gilli, R., Paolillo, M. and Tozzi, P., "The Wide Field X-ray Telescope", *Mem. Soc. Astron. Ital. Suppl.*, **17**, 3 (2011). [ADS]. (Cited on page 129.)

[774] Rudd, D.H., Zentner, A.R. and Kravtsov, A.V., "Effects of Baryons and Dissipation on the Matter Power Spectrum", *Astrophys. J.*, **672**, 19–32 (2008). [DOI], [arXiv:astro-ph/0703741]. (Cited on page 104.)

[775] Sachs, R.K., "Gravitational waves in general relativity. VI. The outgoing radiation condition", *Proc. R. Soc. London, Ser. A*, **264**, 309–338 (1961). (Cited on page 76.)

[776] Saha, P. and Read, J.I., "The Cluster Lens ACO 1703: Redshift Contrast and the Inner Profile", *Astrophys. J.*, **690**, 154–162 (2009). [DOI], [ADS], [arXiv:0807.4737]. (Cited on pages 125 and 126.)

[777] Saha, P., Read, J.I. and Williams, L.L.R., "Two Strong-Lensing Clusters Confront Universal Dark Matter Profiles", *Astrophys. J. Lett.*, **652**, L5–L8 (2006). [DOI], [ADS], [arXiv:astro-ph/0610011]. (Cited on page 126.)

[778] Saito, S., Takada, M. and Taruya, A., "Impact of Massive Neutrinos on the Nonlinear Matter Power Spectrum", *Phys. Rev. Lett.*, **100**, 191301 (2008). [DOI], [ADS], [arXiv:0801.0607]. (Cited on page 142.)

[779] Saito, S., Takada, M. and Taruya, A., "Nonlinear power spectrum in the presence of massive neutrinos: Perturbation theory approach, galaxy bias, and parameter forecasts", *Phys. Rev. D*, **80**, 083528 (2009). [DOI], [ADS], [arXiv:0907.2922 [astro-ph.CO]]. (Cited on pages 138 and 142.)

[780] Saito, S., Takada, M. and Taruya, A., "Neutrino mass constraint with the Sloan Digital Sky Survey power spectrum of luminous red galaxies and perturbation theory", *Phys. Rev. D*, **83**, 043529 (2011). [DOI], [ADS], [arXiv:1006.4845 [astro-ph.CO]]. (Cited on page 142.)

[781] Salopek, D.S. and Bond, J.R., "Nonlinear evolution of long-wavelength metric fluctuations in inflationary models", *Phys. Rev. D*, **42**, 3936–3962 (1990). [DOI], [ADS]. (Cited on pages 164 and 169.)

[782] Saltas, I.D. and Kunz, M., "Anisotropic stress and stability in modified gravity models", *Phys. Rev. D*, **83**, 064042 (2011). [DOI], [ADS], [arXiv:1012.3171 [gr-qc]]. (Cited on pages 59 and 60.)

[783] Sanders, R.H. and McGaugh, S.S., "Modified Newtonian Dynamics as an Alternative to Dark Matter", *Annu. Rev. Astron. Astrophys.*, **40**, 263–317 (2002). [DOI], [ADS], [arXiv:astro-ph/0204521]. (Cited on pages 49 and 50.)

[784] Sandvik, H.B., Tegmark, M., Zaldarriaga, M. and Waga, I., "The end of unified dark matter?", *Phys. Rev. D*, **69**, 123524 (2004). [DOI], [ADS], [arXiv:astro-ph/0212114]. (Cited on page 151.)

[785] Sapone, D. and Kunz, M., "Fingerprinting dark energy", *Phys. Rev. D*, **80**, 083519 (2009). [DOI], [arXiv:0909.0007 [astro-ph.CO]]. (Cited on pages 28, 106, and 107.)

[786] Sapone, D., Kunz, M. and Amendola, L., "Fingerprinting dark energy II: weak lensing and galaxy clustering tests", *Phys. Rev. D*, **82**, 103535 (2010). [DOI], [arXiv:1007.2188 [astro-ph.CO]]. (Cited on pages 28, 107, and 110.)

[787] Saracco, F., Pietroni, M., Tetradis, N., Pettorino, V. and Robbers, G., "Non-linear matter spectra in coupled quintessence", *Phys. Rev. D*, **82**, 023528 (2010). [DOI], [arXiv:0911.5396 [astro-ph.CO]]. (Cited on pages 66, 73, and 153.)

[788] Sarkar, D., Feldman, H.A. and Watkins, R., "Bulk flows from velocity field surveys: a consistency check", *Mon. Not. R. Astron. Soc.*, **375**, 691–697 (2007). [DOI], [ADS], [arXiv:astro-ph/0607426]. (Cited on page 84.)

[789] Sartoris, B., Borgani, S., Fedeli, C., Matarrese, S., Moscardini, L., Rosati, P. and Weller, J., "The potential of X-ray cluster surveys to constrain primordial non-Gaussianity", *Mon. Not. R. Astron. Soc.*, **407**, 2339–2354 (2010). [DOI], [ADS], [arXiv:1003.0841 [astro-ph.CO]]. (Cited on page 129.)

[790] Sartoris, B., Borgani, S., Rosati, P. and Weller, J., "Probing dark energy with the next generation X-ray surveys of galaxy clusters", *Mon. Not. R. Astron. Soc.*, **423**, 2503–2517 (2012). [DOI], [ADS], [arXiv:1112.0327 [astro-ph.CO]]. (Cited on page 129.)

[791] Sato, K., "First-order phase transition of a vacuum and the expansion of the Universe", *Mon. Not. R. Astron. Soc.*, **195**, 467–479 (1981). [ADS]. (Cited on page 163.)

[792] Sawicki, I. and Carroll, S.M., "Cosmological structure evolution and CMB anisotropies in DGB braneworlds", *arXiv*, e-print, (2005). [arXiv:astro-ph/0510364]. (Cited on page 75.)

[793] Scaramella, R., Vettolani, G. and Zamorani, G., "The distribution of clusters of galaxies within 300 Mpc/h and the crossover to an isotropic and homogeneous universe", *Astrophys. J. Lett.*, **376**, L1–L4 (1991). [DOI], [ADS]. (Cited on page 85.)

[794] Schaefer, B.M., Caldera-Cabral, G. and Maartens, R., "Constraints on the decay of dark matter to dark energy from weak lensing bispectrum tomography", *arXiv*, e-print, (2008). [arXiv:0803.2154 [astro-ph]]. (Cited on pages 34, 67, and 153.)

[795] Scherrer, R.J., "Purely Kinetic k Essence as Unified Dark Matter", *Phys. Rev. Lett.*, **93**, 011301 (2004). [DOI], [ADS], [arXiv:astro-ph/0402316]. (Cited on page 151.)

[796] Scherrer, R.J. and Sen, A.A., "Thawing quintessence with a nearly flat potential", *Phys. Rev. D*, **77**, 083515 (2008). [DOI], [arXiv:0712.3450 [astro-ph]]. (Cited on page 19.)

[797] Schimd, C., Uzan, J.-P. and Riazuelo, A., "Weak lensing in scalar-tensor theories of gravity", *Phys. Rev. D*, **71**, 083512 (2005). [DOI], [arXiv:astro-ph/0412120]. (Cited on page 34.)

[798] Schirmer, M., Erben, T., Hetterscheidt, M. and Schneider, P., "GaBoDS: the Garching-Bonn Deep Survey. IX. A sample of 158 shear-selected mass concentration candidates", *Astron. Astrophys.*, **462**, 875–887 (2007). [DOI], [ADS], [arXiv:astro-ph/0607022]. (Cited on page 130.)

[799] Schmidt, F. and Kamionkowski, M., "Halo clustering with nonlocal non-Gaussianity", *Phys. Rev. D*, **82**, 103002 (2010). [DOI], [ADS], [arXiv:1008.0638 [astro-ph.CO]]. (Cited on pages 176 and 179.)

[800] Schmidt, F., Lima, M.V., Oyaizu, H. and Hu, W., "Nonlinear evolution of $f(R)$ cosmologies. III. Halo statistics", *Phys. Rev. D*, **79**, 083518 (2009). [DOI], [arXiv:0812.0545 [astro-ph]]. (Cited on page 68.)

[801] Schmoldt, I. et al., "Likelihood analysis of the Local Group acceleration", *Mon. Not. R. Astron. Soc.*, **304**, 893–905 (1999). [DOI], [ADS], [arXiv:astro-ph/9901087]. (Cited on page 85.)

[802] Scoccimarro, R., Hui, L., Manera, M. and Chan, K.C., "Large-scale bias and efficient generation of initial conditions for non-local primordial non-Gaussianity", *Phys. Rev. D*, **85**, 083002 (2012). [DOI], [ADS], [arXiv:1108.5512 [astro-ph.CO]]. (Cited on page 179.)

[803] Scodeller, S., Kunz, M. and Durrer, R., "CMB anisotropies from acausal scaling seeds", *Phys. Rev. D*, **79**, 083515 (2009). [DOI], [arXiv:0901.1845 [astro-ph]]. (Cited on page 54.)

[804] Scranton, R. et al. (SDSS), "Detection of Cosmic Magnification with the Sloan Digital Sky Survey", *Astrophys. J.*, **633**, 589–602 (2005). [DOI], [ADS], [arXiv:astro-ph/0504510]. (Cited on pages 76 and 77.)

[805] Seckel, D. and Turner, M.S., "'Isothermal' density perturbations in an axion-dominated inflationary universe", *Phys. Rev. D*, **32**, 3178–3183 (1985). [DOI], [ADS]. (Cited on page 181.)

[806] Seery, D. and Lidsey, J.E., "Primordial non-Gaussianities in single-field inflation", *J. Cosmol. Astropart. Phys.*, **2005**(06), 003 (2005). [DOI], [ADS], [arXiv:astro-ph/0503692]. (Cited on page 170.)

[807] Sefusatti, E., Fergusson, J.R., Chen, X. and Shellard, E.P.S., "Effects and detectability of quasi-single field inflation in the large-scale structure and cosmic microwave background", *J. Cosmol. Astropart. Phys.*, **2012**(08), 033 (2012). [DOI], [arXiv:1204.6318 [astro-ph.CO]]. (Cited on page 173.)

[808] Sefusatti, E. and Komatsu, E., "Bispectrum of galaxies from high-redshift galaxy surveys: Primordial non-Gaussianity and nonlinear galaxy bias", *Phys. Rev. D*, **76**, 083004 (2007). [DOI], [ADS], [arXiv:0705.0343]. (Cited on page 175.)

[809] Sefusatti, E., Liguori, M., Yadav, A.P.S., Jackson, M.G. and Pajer, E., "Constraining running non-gaussianity", *J. Cosmol. Astropart. Phys.*, **2009**(12), 022 (2009). [DOI], [ADS], [arXiv:0906.0232 [astro-ph.CO]]. (Cited on pages 173 and 178.)

[810] Seiberg, N. and Witten, E., "String theory and noncommutative geometry", *J. High Energy Phys.*, **1999**(09), 032 (1999). [DOI], [arXiv:hep-th/9908142 [hep-th]]. (Cited on page 201.)

[811] Seljak, U., Hamaus, N. and Desjacques, V., "How to Suppress the Shot Noise in Galaxy Surveys", *Phys. Rev. Lett.*, **103**, 091303 (2009). [DOI], [ADS], [arXiv:0904.2963 [astro-ph.CO]]. (Cited on pages 116 and 118.)

[812] Seljak, U., Makarov, A., McDonald, P. and Trac, H., "Can Sterile Neutrinos Be the Dark Matter?", *Phys. Rev. Lett.*, **97**, 191303 (2006). [DOI], [ADS], [arXiv:astro-ph/0602430]. (Cited on pages 126 and 135.)

[813] Semboloni, E., Hoekstra, H., Schaye, J., van Daalen, M.P. and McCarthy, I.G., "Quantifying the effect of baryon physics on weak lensing tomography", *Mon. Not. R. Astron. Soc.*, **417**, 2020–2035 (2011). [DOI], [ADS], [arXiv:1105.1075 [astro-ph.CO]]. (Cited on page 105.)

[814] Senatore, L., Smith, K.M. and Zaldarriaga, M., "Non-Gaussianities in single field inflation and their optimal limits from the WMAP 5-year data", *J. Cosmol. Astropart. Phys.*, **2010**(01), 028 (2010). [DOI], [ADS], [arXiv:0905.3746 [astro-ph.CO]]. (Cited on page 172.)

[815] Seo, H.-J. and Eisenstein, D.J., "Probing dark energy with baryonic acoustic oscillations from future large galaxy redshift surveys", *Astrophys. J.*, **598**, 720–740 (2003). [DOI], [ADS], [arXiv:astro-ph/0307460 [astro-ph]]. (Cited on pages 81, 82, 91, 100, 199, and 211.)

[816] Seo, H.-J. and Eisenstein, D.J., "Improved forecasts for the baryon acoustic oscillations and cosmological distance scale", *Astrophys. J.*, **665**, 14–24 (2007). [DOI], [arXiv:astro-ph/0701079 [astro-ph]]. (Cited on page 83.)

[817] Setare, M.R. and Saridakis, E.N., "Quintom dark energy models with nearly flat potentials", *Phys. Rev. D*, **79**, 043005 (2009). [DOI], [arXiv:0810.4775 [astro-ph]]. (Cited on page 19.)

[818] Shan, H., Qin, B., Fort, B., Tao, C., Wu, X.-P. and Zhao, H., "Offset between dark matter and ordinary matter: evidence from a sample of 38 lensing clusters of galaxies", *Mon. Not. R. Astron. Soc.*, **406**, 1134–1139 (2010). [DOI], [ADS], [arXiv:1004.1475 [astro-ph.CO]]. (Cited on page 132.)

[819] Shan, H.Y., Qin, B. and Zhao, H.S., "Mass discrepancy in galaxy clusters as a result of the offset between dark matter and baryon distributions", *Mon. Not. R. Astron. Soc.*, **408**, 1277–1282 (2010). [DOI], [ADS], [arXiv:1006.3484 [astro-ph.CO]]. (Cited on page 132.)

[820] Shaposhnikov, M. and Zenhäusern, D., "Scale invariance, unimodular gravity and dark energy", *Phys. Lett. B*, **671**, 187–192 (2009). [DOI], [ADS], [arXiv:0809.3395 [hep-th]]. (Cited on page 56.)

[821] Shaw, D.J. and Mota, D.F., "An Improved Semi-Analytical Spherical Collapse Model for Non-linear Density Evolution", *Astrophys. J. Suppl. Ser.*, **174**, 277 (2008). [DOI], [arXiv:0708.0868 [astro-ph]]. (Cited on page 68.)

[822] Shaw, J.R., Bridges, M. and Hobson, M.P., "Efficient Bayesian inference for multimodal problems in cosmology", *Mon. Not. R. Astron. Soc.*, **378**, 1365–1370 (2007). [DOI], [ADS], [arXiv:astro-ph/0701867]. (Cited on page 216.)

[823] Sheth, R.K. and Tormen, G., "Large-scale bias and the peak background split", *Mon. Not. R. Astron. Soc.*, **308**, 119–126 (1999). [DOI], [ADS], [arXiv:astro-ph/9901122]. (Cited on page 68.)

[824] Sheth, R.K. and Tormen, G., "An excursion set model of hierarchical clustering: ellipsoidal collapse and the moving barrier", *Mon. Not. R. Astron. Soc.*, **329**, 61–75 (2002). [DOI], [ADS], [arXiv:astro-ph/0105113]. (Cited on pages 142, 144, and 147.)

[825] Sigad, Y., Branchini, E. and Dekel, A., "Measuring the nonlinear biasing function from a galaxy redshift survey", *Astrophys. J.*, **540**, 62–73 (2000). [DOI], [arXiv:astro-ph/0002170 [astro-ph]]. (Cited on page 92.)

[826] Sikivie, P., "Axion Cosmology", in Kuster, M., Raffelt, G. and Beltrán, B., eds., *Axions: Theory, Cosmology, and Experimental Searches*, Lecture Notes in Physics, 741, pp. 19–50, (Springer, Berlin; Heidelberg, 2008). [DOI], [ADS]. (Cited on pages 123 and 155.)

[827] Sikivie, P., "The dark matter is mostly an axion BEC", *arXiv*, e-print, (2010). [ADS], [arXiv:1012.1553 [astro-ph.CO]]. (Cited on page 155.)

[828] Sikivie, P. and Yang, Q., "Bose-Einstein Condensation of Dark Matter Axions", *Phys. Rev. Lett.*, **103**, 111301 (2009). [DOI], [ADS], [arXiv:0901.1106 [hep-ph]]. (Cited on page 155.)

[829] Silverman, M.P. and Mallett, R.L., "Dark Matter as a Cosmic Bose-Einstein Condensate and Possible Superfluid", *Gen. Relativ. Gravit.*, **34**, 633–649 (2002). [DOI]. (Cited on page 155.)

[830] Silverstein, E. and Tong, D., "Scalar speed limits and cosmology: Acceleration from D-cceleration", *Phys. Rev. D*, **70**, 103505 (2004). [DOI], [ADS], [arXiv:hep-th/0310221]. (Cited on page 171.)

[831] Silverstein, E. and Westphal, A., "Monodromy in the CMB: Gravity waves and string inflation", *Phys. Rev. D*, **78**, 106003 (2008). [DOI], [ADS], [arXiv:0803.3085 [hep-th]]. (Cited on page 172.)

[832] Silvestri, A., Pogosian, L. and Buniy, R.V., "Practical approach to cosmological perturbations in modified gravity", *Phys. Rev. D*, **87**, 104015 (2013). [DOI], [ADS], [arXiv:1302.1193 [astro-ph.CO]]. (Cited on page 62.)

[833] Simon, J.D., Bolatto, A.D., Leroy, A., Blitz, L. and Gates, E.L., "High-Resolution Measurements of the Halos of Four Dark Matter-Dominated Galaxies: Deviations from a Universal Density Profile", *Astrophys. J.*, **621**, 757–776 (2005). [DOI], [ADS], [arXiv:astro-ph/0412035]. (Cited on pages 124 and 133.)

[834] Simon, J.D. and Geha, M., "The Kinematics of the Ultra-faint Milky Way Satellites: Solving the Missing Satellite Problem", *Astrophys. J.*, **670**, 313–331 (2007). [DOI], [ADS], [arXiv:0706.0516]. (Cited on page 124.)

[835] Simon, P., Taylor, A.N. and Hartlap, J., "Unfolding the matter distribution using three-dimensional weak gravitational lensing", *Mon. Not. R. Astron. Soc.*, **399**, 48–68 (2009). [DOI], [ADS], [arXiv:0907.0016 [astro-ph.CO]]. (Cited on page 130.)

[836] Simon, P. et al., "Spatial matter density mapping of the STAGES Abell A901/2 supercluster field with 3D lensing", *Mon. Not. R. Astron. Soc.*, **419**, 998–1016 (2012). [DOI], [ADS], [arXiv:1109.0932 [astro-ph.CO]]. (Cited on page 130.)

[837] Simpson, F., "Scattering of dark matter and dark energy", *Phys. Rev. D*, **82**, 083505 (2010). [DOI], [ADS], [arXiv:1007.1034 [astro-ph.CO]]. (Cited on page 132.)

[838] Simpson, F. and Bridle, S., "The redshift sensitivities of dark energy surveys", *Phys. Rev. D*, **73**, 083001 (2006). [DOI], [arXiv:astro-ph/0602213 [astro-ph]]. (Cited on pages 56 and 215.)

[839] Sivia, D.S., *Data Analysis: A Bayesian Tutorial*, (Oxford University Press, Oxford; New York, 1996). [Google Books]. (Cited on page 207.)

[840] Skordis, C., "The tensor-vector-scalar theory and its cosmology", *Class. Quantum Grav.*, **26**, 143001 (2009). [DOI], [ADS], [arXiv:0903.3602 [astro-ph.CO]]. (Cited on page 51.)

[841] Skordis, C., Mota, D.F., Ferreira, P.G. and Boehm, C., "Large scale structure in Bekenstein's theory of relativistic MOND", *Phys. Rev. Lett.*, **96**, 011301 (2006). [DOI], [arXiv:astro-ph/0505519]. (Cited on pages 51, 52, and 161.)

[842] Slosar, A., Hirata, C., Seljak, U., Ho, S. and Padmanabhan, N., "Constraints on local primordial non-Gaussianity from large scale structure", *J. Cosmol. Astropart. Phys.*, **2008**(08), 031 (2008). [DOI], [ADS], [arXiv:0805.3580]. (Cited on page 176.)

[843] Slosar, A., Melchiorri, A. and Silk, J., "Did Boomerang hit MOND?", *Phys. Rev. D*, **72**, 101301 (2005). [DOI], [arXiv:astro-ph/0508048]. (Cited on page 52.)

[844] Smith, R.E. et al., "Stable clustering, the halo model and non-linear cosmological power spectra", *Mon. Not. R. Astron. Soc.*, **341**, 1311–1332 (2003). [DOI]. (Cited on pages 68, 85, 101, and 103.)

[845] Smoot, G.F. et al., "Structure in the COBE differential microwave radiometer first-year maps", *Astrophys. J. Lett.*, **396**, L1–L5 (1992). [DOI], [ADS]. (Cited on page 124.)

[846] Snyder, H.S., "Quantized Space-Time", *Phys. Rev.*, **71**, 38–41 (1947). [DOI], [ADS]. (Cited on page 201.)

[847] Sollom, I., Challinor, A. and Hobson, M.P., "Cold dark matter isocurvature perturbations: Constraints and model selection", *Phys. Rev. D*, **79**, 123521 (2009). [DOI], [ADS], [arXiv:0903.5257 [astro-ph.CO]]. (Cited on page 182.)

[848] Song, Y.-S., Hollenstein, L., Caldera-Cabral, G. and Koyama, K., "Theoretical Priors On Modified Growth Parametrisations", *J. Cosmol. Astropart. Phys.*, **2010**(04), 018 (2010). [DOI], [ADS], [arXiv:1001.0969 [astro-ph.CO]]. (Cited on pages 24, 25, and 86.)

[849] Song, Y.-S., Hu, W. and Sawicki, I., "Large scale structure of $f(R)$ gravity", *Phys. Rev. D*, **75**, 044004 (2007). [DOI], [ADS], [arXiv:astro-ph/0610532]. (Cited on page 41.)

[850] Song, Y.-S., Peiris, H. and Hu, W., "Cosmological constraints on $f(R)$ acceleration models", *Phys. Rev. D*, **76**, 063517 (2007). [DOI], [arXiv:0706.2399 [astro-ph]]. (Cited on page 110.)

[851] Soucail, G., Fort, B., Mellier, Y. and Picat, J.P., "A blue ring-like structure, in the center of the A 370 cluster of galaxies", *Astron. Astrophys.*, **172**, L14–L16 (1987). [ADS]. (Cited on page 124.)

[852] Soussa, M.E. and Woodard, R.P., "Letter: The Force of Gravity from a Lagrangian Containing Inverse Powers of the Ricci Scalar", *Gen. Relativ. Gravit.*, **36**, 855–862 (2004). [DOI], [ADS], [arXiv:astro-ph/0308114]. (Cited on page 40.)

[853] Spergel, D.N. and Steinhardt, P.J., "Observational Evidence for Self-Interacting Cold Dark Matter", *Phys. Rev. Lett.*, **84**, 3760–3763 (2000). [DOI], [ADS], [arXiv:astro-ph/9909386]. (Cited on page 131.)

[854] Spergel, D.N. and Zaldarriaga, M., "CMB polarization as a direct test of inflation", *Phys. Rev. Lett.*, **79**, 2180–2183 (1997). [DOI], [arXiv:astro-ph/9705182 [astro-ph]]. (Cited on page 54.)

[855] Spergel, D.N. et al., "Three-Year Wilkinson Microwave Anisotropy Probe (WMAP) Observations: Implications for Cosmology", *Astrophys. J. Suppl. Ser.*, **170**, 377–408 (2007). [DOI], [ADS], [arXiv:astro-ph/0603449]. (Cited on pages 52 and 124.)

[856] Spitzer, C., "Stability in MaVaN Models", *arXiv*, e-print, (2006). [ADS], [arXiv:astro-ph/0606034]. (Cited on pages 34 and 143.)

[857] Springel, V., "The cosmological simulation code GADGET-2", *Mon. Not. R. Astron. Soc.*, **364**, 1105–1134 (2005). [DOI], [arXiv:astro-ph/0505010]. (Cited on pages 64 and 66.)

[858] Springel, V., White, S.D.M., Tormen, G. and Kauffmann, G., "Populating a cluster of galaxies – I. Results at $z = 0$", *Mon. Not. R. Astron. Soc.*, **328**, 726–750 (2001). [DOI], [ADS], [arXiv:astro-ph/0012055]. (Cited on page 142.)

[859] Stadel, J.G., *Cosmological N-body Simulations and their Analysis*, Ph.D. thesis, (University of Washington, Seattle, WA, 2001). [ADS]. (Cited on page 104.)

[860] Starck, J.-L., Pires, S. and Réfrégier, A., "Weak lensing mass reconstruction using wavelets", *Astron. Astrophys.*, **451**, 1139–1150 (2006). [DOI], [ADS], [arXiv:astro-ph/0503373]. (Cited on page 130.)

[861] Starobinsky, A.A., "Spectrum of relict gravitational radiation and the early state of the universe", *JETP Lett.*, **30**, 682 (1979). [ADS]. (Cited on page 163.)

[862] Starobinsky, A.A., "A new type of isotropic cosmological models without singularity", *Phys. Lett. B*, **91**, 99–102 (1980). [DOI], [ADS]. (Cited on page 40.)

[863] Starobinsky, A.A., "Dynamics of phase transition in the new inflationary universe scenario and generation of perturbations", *Phys. Lett. B*, **117**, 175–178 (1982). [DOI], [ADS]. (Cited on page 163.)

[864] Starobinsky, A.A., "Disappearing cosmological constant in $f(R)$ gravity", *JETP Lett.*, **86**, 157–163 (2007). [DOI], [ADS], [arXiv:0706.2041]. (Cited on pages 41, 91, and 95.)

[865] Steffen, F.D., "Dark-matter candidates. Axions, neutralinos, gravitinos, and axinos", *Eur. Phys. J. C*, **59**, 557–588 (2009). [DOI], [ADS], [arXiv:0811.3347 [hep-ph]]. (Cited on page 124.)

[866] Steinhardt, P.J. and Turner, M.S., "Saving the invisible axion", *Phys. Lett. B*, **129**, 51–56 (1983). [DOI]. (Cited on page 154.)

[867] Steinhardt, P.J., Wang, L. and Zlatev, I., "Cosmological tracking solutions", *Phys. Rev. D*, **59**, 123504 (1999). [DOI], [arXiv:astro-ph/9812313]. (Cited on page 19.)

[868] Strauss, M.A., Yahil, A., Davis, M., Huchra, J.P. and Fisher, K., "A redshift survey of IRAS galaxies. V. The acceleration on the Local Group", *Astrophys. J.*, **397**, 395–419 (1992). [DOI], [ADS]. (Cited on page 85.)

[869] Strigari, L.E., Bullock, J.S., Kaplinghat, M., Diemand, J., Kuhlen, M. and Madau, P., "Redefining the Missing Satellites Problem", *Astrophys. J.*, **669**, 676–683 (2007). [DOI], [ADS], [arXiv:0704.1817 [astro-ph]]. (Cited on page 133.)

[870] Sutter, P.M. and Ricker, P.M., "Structure and evolution of Zel'dovich pancakes as probes of dark energy models", *Astrophys. J.*, **674**, 1–10 (2008). [DOI], [ADS], [arXiv:0707.2968 [astro-ph]]. (Cited on pages 34, 66, and 153.)

[871] Svrcek, P. and Witten, E., "Axions in string theory", *J. High Energy Phys.*, **2006**(06), 051 (2006). [DOI], [ADS], [arXiv:hep-th/0605206]. (Cited on pages 123, 154, and 185.)

[872] 't Hooft, G., "Computation of the quantum effects due to a four-dimensional pseudoparticle", *Phys. Rev. D*, **14**, 3432–3450 (1976). [DOI]. (Cited on page 154.)

[873] 't Hooft, G., "Symmetry Breaking through Bell-Jackiw Anomalies", *Phys. Rev. Lett.*, **37**, 8 (1976). [DOI]. (Cited on page 154.)

[874] Takahashi, R. and Tanimoto, M., "Speed of sound in the mass varying neutrinos scenario", *J. High Energy Phys.*, **2006**(05), 021 (2006). [DOI], [arXiv:astro-ph/0601119]. (Cited on pages 34 and 143.)

[875] Tammann, G.A., Yahil, A. and Sandage, A., "The velocity field of bright nearby galaxies. II. Luminosity functions for various Hubble types and luminosity classes: The peculiar motion of the local group relative to the Virgo cluster", *Astrophys. J.*, **234**, 775–784 (1979). [DOI], [ADS]. (Cited on page 84.)

[876] Tanaka, T., Suyama, T. and Yokoyama, S., "Use of δN formalism – difficulties in generating large local-type non-Gaussianity during inflation", *Class. Quantum Grav.*, **27**, 124003 (2010). [DOI], [ADS], [arXiv:1003.5057 [astro-ph.CO]]. (Cited on page 170.)

[877] Taruya, A., Koyama, K. and Matsubara, T., "Signature of primordial non-Gaussianity on the matter power spectrum", *Phys. Rev. D*, **78**, 123534 (2008). [DOI], [ADS], [arXiv:0808.4085]. (Cited on page 178.)

[878] Taylor, A.N. and Kitching, T.D., "Analytic methods for cosmological likelihoods", *Mon. Not. R. Astron. Soc.*, **408**, 865–875 (2010). [DOI], [ADS], [arXiv:1003.1136 [astro-ph.CO]]. (Cited on pages 208 and 212.)

[879] Taylor, A.N. et al., "Mapping the 3D dark matter with weak lensing in COMBO-17", *Mon. Not. R. Astron. Soc.*, **353**, 1176–1196 (2004). [DOI], [ADS], [arXiv:astro-ph/0402095]. (Cited on page 130.)

[880] Tegmark, M., "Measuring Cosmological Parameters with Galaxy Surveys", *Phys. Rev. Lett.*, **79**, 3806–3809 (1997). [DOI], [ADS], [arXiv:astro-ph/9706198]. (Cited on pages 82 and 211.)

[881] Tegmark, M., "Measuring the metric: A parametrized post-Friedmannian approach to the cosmic dark energy problem", *Phys. Rev. D*, **66**, 103507 (2002). [DOI], [ADS], [arXiv:astro-ph/0101354]. (Cited on page 20.)

[882] Tegmark, M., Aguirre, A.N., Rees, M.J. and Wilczek, F., "Dimensionless constants, cosmology, and other dark matters", *Phys. Rev. D*, **73**, 023505 (2006). [DOI], [ADS], [arXiv:astro-ph/0511774]. (Cited on page 155.)

[883] Tegmark, M., Hamilton, A.J.S., Strauss, M.A., Vogeley, M.S. and Szalay, A.S., "Measuring the Galaxy Power Spectrum with Future Redshift Surveys", *Astrophys. J.*, **499**, 555 (1998). [DOI], [ADS], [arXiv:astro-ph/9708020]. (Cited on page 167.)

[884] Tegmark, M., Taylor, A. and Heavens, A., "Karhunen-Loeve eigenvalue problems in cosmology: how should we tackle large data sets?", *Astrophys. J.*, **480**, 22 (1997). [DOI], [arXiv:astro-ph/9603021]. (Cited on page 211.)

[885] Thakur, P., Ghose, S. and Paul, B.C., "Modified Chaplygin gas and constraints on its B parameter from cold dark matter and unified dark matter energy cosmological models", *Mon. Not. R. Astron. Soc.*, **397**, 1935–1939 (2009). [DOI], [ADS], [arXiv:0905.2281 [astro-ph.CO]]. (Cited on page 151.)

[886] Thomas, S.A., Abdalla, F.B. and Weller, J., "Constraining modified gravity and growth with weak lensing", *Mon. Not. R. Astron. Soc.*, **395**, 197–209 (2009). [DOI], [ADS], [arXiv:0810.4863]. (Cited on page 85.)

[887] Thomas, S.A., Appleby, S.A. and Weller, J., "Modified gravity: the CMB, weak lensing and general parameterisations", *J. Cosmol. Astropart. Phys.*, **2011**(03), 036 (2011). [DOI], [ADS], [arXiv:1101.0295 [astro-ph.CO]]. (Cited on pages 111 and 113.)

[888] Tikhonov, A.V., Gottlöber, S., Yepes, G. and Hoffman, Y., "The sizes of minivoids in the local Universe: an argument in favor of a warm dark matter model?", *Mon. Not. R. Astron. Soc.*, **399**, 1611–1621 (2009). [DOI], [ADS], [arXiv:0904.0175 [astro-ph.CO]]. (Cited on page 133.)

[889] Tisserand, P. et al. (EROS-2 Collaboration), "Limits on the Macho content of the Galactic Halo from the EROS-2 Survey of the Magellanic Clouds", *Astron. Astrophys.*, **469**, 387–404 (2007). [DOI], [ADS], [arXiv:astro-ph/0607207]. (Cited on page 122.)

[890] Tojeiro, R., Heavens, A.F., Jimenez, R. and Panter, B., "Recovering galaxy star formation and metallicity histories from spectra using VESPA", *Mon. Not. R. Astron. Soc.*, **381**, 1252–1266 (2007). [DOI], [ADS], [arXiv:0704.0941]. (Cited on page 190.)

[891] Tomita, K., "Distances and Lensing in Cosmological Void Models", *Astrophys. J.*, **529**, 38–46 (2000). [DOI], [ADS], [arXiv:astro-ph/9906027]. (Cited on page 191.)

[892] Tomita, K., "A local void and the accelerating Universe", *Mon. Not. R. Astron. Soc.*, **326**, 287–292 (2001). [DOI], [ADS], [arXiv:astro-ph/0011484]. (Cited on page 191.)

[893] Treu, T. and Koopmans, L.V.E., "The internal structure of the lens PG1115+080: breaking degeneracies in the value of the Hubble constant", *Mon. Not. R. Astron. Soc.*, **337**, L6–L10 (2002). [DOI], [ADS], [arXiv:astro-ph/0210002]. (Cited on page 125.)

[894] Trotta, R., "Applications of Bayesian model selection to cosmological parameters", *Mon. Not. R. Astron. Soc.*, **378**, 72–82 (2007). [DOI], [arXiv:astro-ph/0504022]. (Cited on pages 57, 209, and 216.)

[895] Trotta, R., "Forecasting the Bayes factor of a future observation", *Mon. Not. R. Astron. Soc.*, **378**, 819–824 (2007). [DOI], [arXiv:astro-ph/0703063]. (Cited on page 213.)

[896] Trotta, R., "The isocurvature fraction after WMAP 3-year data", *Mon. Not. R. Astron. Soc.*, **375**, L26–L30 (2007). [DOI], [arXiv:astro-ph/0608116]. (Cited on page 182.)

[897] Trotta, R., "Bayes in the sky: Bayesian inference and model selection in cosmology", *Contemp. Phys.*, **49**, 71–104 (2008). [DOI], [arXiv:0803.4089 [astro-ph]]. (Cited on pages 207 and 216.)

[898] Trotta, R., Feroz, F., Hobson, M.P., Roszkowski, L. and Ruiz de Austri, R., "The impact of priors and observables on parameter inferences in the constrained MSSM", *J. High Energy Phys.*, **2008**(12), 024 (2008). [DOI], [arXiv:0809.3792 [hep-ph]]. (Cited on page 216.)

[899] Trotta, R., Kunz, M. and Liddle, A.R., "Designing decisive detections", *Mon. Not. R. Astron. Soc.*, **414**, 2337–2344 (2011). [DOI], [ADS], [arXiv:1012.3195 [astro-ph.CO]]. (Cited on pages 213 and 215.)

[900] Trotta, R., Kunz, M., Mukherjee, P. and Parkinson, D., "Bayesian experimental design and model selection forecasting", in Hobson, M.P., Jaffe, A.H., Liddle, A.R., Mukherjee, P. and Parkinson, D., eds., *Bayesian Methods in Cosmology*, pp. 99–124, (Cambridge University Press, Cambridge; New York, 2010). [Google Books]. (Cited on pages 57 and 212.)

[901] Trotta, R. and Melchiorri, A., "Indication for primordial anisotropies in the neutrino background from WMAP and SDSS", *Phys. Rev. Lett.*, **95**, 011305 (2005). [DOI], [arXiv:astro-ph/0412066]. (Cited on page 139.)

[902] Trotta, R., Riazuelo, A. and Durrer, R., "Cosmic Microwave Background Anisotropies with Mixed Isocurvature Perturbations", *Phys. Rev. Lett.*, **87**, 231301 (2001). [DOI], [ADS], [arXiv:astro-ph/0104017]. (Cited on page 182.)

[903] Trotta, R., Riazuelo, A. and Durrer, R., "Cosmological constant and general isocurvature initial conditions", *Phys. Rev. D*, **67**, 063520 (2003). [DOI], [arXiv:astro-ph/0211600]. (Cited on page 182.)

[904] Tsujikawa, S., "Observational signatures of $f(R)$ dark energy models that satisfy cosmological and local gravity constraints", *Phys. Rev. D*, **77**, 023507 (2008). [DOI], [ADS], [arXiv:0709.1391]. (Cited on pages 41, 91, and 95.)

[905] Tsujikawa, S., Maartens, R. and Brandenberger, R.H., "Non-commutative inflation and the CMB", *Phys. Lett. B*, **574**, 141–148 (2003). [DOI], [ADS], [arXiv:astro-ph/0308169]. (Cited on page 188.)

[906] Tsujikawa, S., Uddin, K., Mizuno, S., Tavakol, R. and Yokoyama, J., "Constraints on scalar-tensor models of dark energy from observational and local gravity tests", *Phys. Rev. D*, **77**, 103009 (2008). [DOI], [arXiv:0803.1106 [astro-ph]]. (Cited on page 110.)

[907] Tsujikawa, S., Uddin, K. and Tavakol, R., "Density perturbations in $f(R)$ gravity theories in metric and Palatini formalisms", *Phys. Rev. D*, **77**, 043007 (2008). [DOI], [arXiv:0712.0082 [astro-ph]]. (Cited on page 42.)

[908] Turner, M.S., "Cosmic and local mass density of 'invisible' axions", *Phys. Rev. D*, **33**, 889–896 (1986). [DOI]. (Cited on page 154.)

[909] Turner, M.S., "The Case for $\Omega_M = 0.33 \pm 0.035$", *Astrophys. J. Lett.*, **576**, L101–L104 (2002). [DOI], [ADS], [arXiv:astro-ph/0106035]. (Cited on page 122.)

[910] Turner, M.S. and Wilczek, F., "Inflationary axion cosmology", *Phys. Rev. Lett.*, **66**, 5–8 (1991). [DOI], [ADS]. (Cited on page 181.)

[911] Turner, M., Wilczek, F. and Zee, A., "Formation of structure in an axion-dominated universe", *Phys. Lett. B*, **125**, 35–40 (1983). [DOI]. (Cited on page 154.)

[912] Uzan, J.-P., "Cosmological scaling solutions of non-minimally coupled scalar fields", *Phys. Rev. D*, **59**, 123510 (1999). [DOI], [arXiv:gr-qc/9903004]. (Cited on page 34.)

[913] Vainshtein, A.I., "To the problem of nonvanishing gravitation mass", *Phys. Lett. B*, **39**, 393–394 (1972). [DOI]. (Cited on pages 44, 47, and 48.)

[914] Väliviita, J. and Giannantonio, T., "Constraints on primordial isocurvature perturbations and spatial curvature by Bayesian model selection", *Phys. Rev. D*, **80**, 123516 (2009). [DOI], [ADS], [arXiv:0909.5190 [astro-ph.CO]]. (Cited on page 182.)

[915] Väliviita, J., Maartens, R. and Majerotto, E., "Observational constraints on an interacting dark energy model", *Mon. Not. R. Astron. Soc.*, **402**, 2355–2368 (2010). [DOI], [arXiv:0907.4987 [astro-ph.CO]]. (Cited on pages 34, 67, and 153.)

[916] Väliviita, J., Majerotto, E. and Maartens, R., "Instability in interacting dark energy and dark matter fluids", *J. Cosmol. Astropart. Phys.*, **2008**(07), 020 (2008). [DOI], [ADS], [arXiv:0804.0232 [astro-ph]]. (Cited on pages 34, 38, 67, and 153.)

[917] Vardanyan, M., Trotta, R. and Silk, J., "Applications of Bayesian model averaging to the curvature and size of the Universe", *Mon. Not. R. Astron. Soc.*, **413**, L91–L95 (2011). [DOI], [ADS], [arXiv:1101.5476 [astro-ph.CO]]. (Cited on page 217.)

[918] Verde, L., "Non-Gaussianity from Large-Scale Structure Surveys", *Adv. Astron.*, **2010**, 768675 (2010). [DOI], [ADS], [arXiv:1001.5217 [astro-ph.CO]]. (Cited on page 177.)

[919] Verde, L., "Statistical Methods in Cosmology", in Wolschin, G., ed., *Lectures on Cosmology: Accelerated Expansion of the Universe*, Lecture Notes in Physics, 800, pp. 147–177, (Springer, Berlin; Heidelberg, 2010). [DOI], [arXiv:0911.3105 [astro-ph.CO]]. (Cited on page 212.)

[920] Verde, L. and Heavens, A.F., "On the Trispectrum as a Gaussian Test for Cosmology", *Astrophys. J.*, **553**, 14–24 (2001). [DOI], [ADS], [arXiv:astro-ph/0101143]. (Cited on page 175.)

[921] Verde, L., Heavens, A.F. and Matarrese, S., "Projected bispectrum in spherical harmonics and its application to angular galaxy catalogues", *Mon. Not. R. Astron. Soc.*, **318**, 584–598 (2000). [DOI], [ADS], [arXiv:astro-ph/0002240]. (Cited on page 175.)

[922] Verde, L. and Matarrese, S., "Detectability of the Effect of Inflationary Non-Gaussianity on Halo Bias", *Astrophys. J. Lett.*, **706**, L91–L95 (2009). [DOI], [ADS], [arXiv:0909.3224 [astro-ph.CO]]. (Cited on page 177.)

[923] Verde, L., Peiris, H.V. and Jimenez, R., "Considerations in optimizing CMB polarization experiments to constrain inflationary physics", *J. Cosmol. Astropart. Phys.*, **2006**(01), 019 (2006). [DOI], [ADS], [arXiv:astro-ph/0506036]. (Cited on page 166.)

[924] Verde, L., Wang, L., Heavens, A.F. and Kamionkowski, M., "Large-scale structure, the cosmic microwave background and primordial non-Gaussianity", *Mon. Not. R. Astron. Soc.*, **313**, 141–147 (2000). [DOI], [ADS], [arXiv:astro-ph/9906301]. (Cited on pages 169, 174, and 175.)

[925] Verde, L. et al., "The 2dF Galaxy Redshift Survey: the bias of galaxies and the density of the Universe", *Mon. Not. R. Astron. Soc.*, **335**, 432–440 (2002). [DOI], [ADS], [arXiv:astro-ph/0112161]. (Cited on pages 83, 92, and 175.)

[926] Vernizzi, F. and Wands, D., "Non-Gaussianities in two-field inflation", *J. Cosmol. Astropart. Phys.*, **2006**(05), 019 (2006). [DOI], [ADS], [arXiv:astro-ph/0603799]. (Cited on page 170.)

[927] Viel, M., Becker, G.D., Bolton, J.S., Haehnelt, M.G., Rauch, M. and Sargent, W.L.W., "How Cold Is Cold Dark Matter? Small-Scales Constraints from the Flux Power Spectrum of the High-Redshift Lyman-α Forest", *Phys. Rev. Lett.*, **100**, 041304 (2008). [DOI], [ADS], [arXiv:0709.0131 [astro-ph]]. (Cited on pages 126 and 135.)

[928] Viel, M., Haehnelt, M.G. and Springel, V., "The effect of neutrinos on the matter distribution as probed by the intergalactic medium", *J. Cosmol. Astropart. Phys.*, **2010**(06), 015 (2010). [DOI], [ADS], [arXiv:1003.2422 [astro-ph.CO]]. (Cited on page 142.)

[929] Viel, M., Lesgourgues, J., Haehnelt, M.G., Matarrese, S. and Riotto, A., "Constraining warm dark matter candidates including sterile neutrinos and light gravitinos with WMAP and the Lyman-α forest", *Phys. Rev. D*, **71**, 063534 (2005). [DOI], [arXiv:astro-ph/0501562]. (Cited on page 135.)

[930] Vielva, P., Martínez-González, E., Barreiro, R.B., Sanz, J.L. and Cayón, L., "Detection of Non-Gaussianity in the Wilkinson Microwave Anisotropy Probe First-Year Data Using Spherical Wavelets", *Astrophys. J.*, **609**, 22–34 (2004). [DOI], [ADS], [arXiv:astro-ph/0310273]. (Cited on page 187.)

[931] Vikhlinin, A. et al., "X-ray Cluster Cosmology", in *Astro2010: The Astronomy and Astrophysics Decadal Survey – Science White Papers*, 91, (National Academy of Sciences, Washington, DC, 2009). [ADS], [arXiv:0903.5320 [astro-ph.CO]]. URL (accessed 6 June 2013): http://sites.nationalacademies.org/bpa/BPA_050603. (Cited on page 129.)

[932] Visinelli, L. and Gondolo, P., "Dark Matter Axions Revisited", *Phys. Rev. D*, **80**, 035024 (2009). [DOI], [ADS], [arXiv:0903.4377 [astro-ph.CO]]. (Cited on page 154.)

[933] Wagner, C., Verde, L. and Boubekeur, L., "N-body simulations with generic non-Gaussian initial conditions I: power spectrum and halo mass function", *J. Cosmol. Astropart. Phys.*, **2010**(10), 022 (2010). [DOI], [ADS], [arXiv:1006.5793 [astro-ph.CO]]. (Cited on pages 176 and 179.)

[934] Walker, M.G., Mateo, M., Olszewski, E.W., Gnedin, O.Y., Wang, X., Sen, B. and Woodroofe, M., "Velocity Dispersion Profiles of Seven Dwarf Spheroidal Galaxies", *Astrophys. J. Lett.*, **667**, L53–L56 (2007). [DOI], [ADS], [arXiv:0708.0010]. (Cited on page 124.)

[935] Walsh, D., Carswell, R.F. and Weymann, R.J., "0957 + 561 A, B: Twin quasistellar objects or gravitational lens?", *Nature*, **279**, 381–384 (1979). [DOI], [ADS]. (Cited on page 124.)

[936] Wands, D., "Extended gravity theories and the Einstein–Hilbert action", *Class. Quantum Grav.*, **11**, 269–280 (1994). [DOI], [arXiv:gr-qc/9307034]. (Cited on pages 35 and 39.)

[937] Wang, L.-M. and Steinhardt, P.J., "Cluster abundance constraints on quintessence models", *Astrophys. J.*, **508**, 483–490 (1998). [DOI], [arXiv:astro-ph/9804015 [astro-ph]]. (Cited on pages 23, 68, 90, and 103.)

[938] Wang, Y., "Differentiating dark energy and modified gravity with galaxy redshift surveys", *J. Cosmol. Astropart. Phys.*, **2008**(05), 021 (2008). [DOI], [ADS], [arXiv:0710.3885 [astro-ph]]. (Cited on page 81.)

[939] Wang, Y., "Figure of Merit for Dark Energy Constraints from Current Observational Data", *Phys. Rev. D*, **77**, 123525 (2008). [DOI], [arXiv:0803.4295 [astro-ph]]. (Cited on pages 20 and 212.)

[940] Wang, Y., "Forecasts of Dark Energy Constraints from Baryon Acoustic Oscillations", *Mod. Phys. Lett. A*, **25**, 3093–3113 (2010). [DOI], [ADS], [arXiv:0904.2218 [astro-ph.CO]]. (Cited on page 82.)

[941] Wang, Y. and Freese, K., "Probing dark energy using its density instead of its equation of state", *Phys. Lett. B*, **632**, 449–452 (2006). [DOI], [ADS], [arXiv:astro-ph/0402208]. (Cited on page 20.)

[942] Wang, Y. and Garnavich, P.M., "Measuring Time Dependence of Dark Energy Density from Type IA Supernova Data", *Astrophys. J.*, **552**, 445–451 (2001). [DOI], [ADS], [arXiv:astro-ph/0101040]. (Cited on page 20.)

[943] Wang, Y., Kratochvil, J.M., Linde, A. and Shmakova, M., "Current observational constraints on cosmic doomsday", *J. Cosmol. Astropart. Phys.*, **2004**(12), 006 (2004). [DOI], [ADS], [arXiv:astro-ph/0409264]. (Cited on page 20.)

[944] Wang, Y. and Tegmark, M., "New Dark Energy Constraints from Supernovae, Microwave Background, and Galaxy Clustering", *Phys. Rev. Lett.*, **92**, 241302 (2004). [DOI], [ADS], [arXiv:astro-ph/0403292]. (Cited on page 20.)

[945] Wang, Y. et al., "Designing a space-based galaxy redshift survey to probe dark energy", *Mon. Not. R. Astron. Soc.*, **409**, 737–749 (2010). [DOI], [arXiv:1006.3517 [astro-ph.CO]]. (Cited on pages 81, 96, 100, and 212.)

[946] Watanabe, M., Kanno, S. and Soda, J., "The Nature of Primordial Fluctuations from Anisotropic Inflation", *Prog. Theor. Phys.*, **123**, 1041–1068 (2010). [DOI], [arXiv:1003.0056 [astro-ph.CO]]. (Cited on page 203.)

[947] Watkins, R., Feldman, H.A. and Hudson, M.J., "Consistently large cosmic flows on scales of $100h^{-1}$Mpc: a challenge for the standard ΛCDM cosmology", *Mon. Not. R. Astron. Soc.*, **392**, 743–756 (2009). [DOI], [ADS], [arXiv:0809.4041]. (Cited on pages 84 and 150.)

[948] Weinberg, S., "Anthropic bound on the cosmological constant", *Phys. Rev. Lett.*, **59**, 2607–2610 (1987). [DOI], [ADS]. (Cited on page 68.)

[949] Weinberg, S., "Adiabatic modes in cosmology", *Phys. Rev. D*, **67**, 123504 (2003). [DOI], [ADS], [arXiv:astro-ph/0302326]. (Cited on page 180.)

[950] Weinberg, S., "Must cosmological perturbations remain nonadiabatic after multifield inflation?", *Phys. Rev. D*, **70**, 083522 (2004). [DOI], [ADS], [arXiv:astro-ph/0405397]. (Cited on page 180.)

[951] Weinberg, S., "Effective field theory for inflation", *Phys. Rev. D*, **77**, 123541 (2008). [DOI], [ADS], [arXiv:0804.4291 [hep-th]]. (Cited on page 172.)

[952] Weiner, N. and Zurek, K.M., "New matter effects and BBN constraints for mass varying neutrinos", *Phys. Rev. D*, **74**, 023517 (2006). [DOI], [arXiv:hep-ph/0509201]. (Cited on pages 34 and 143.)

[953] Weller, J. and Albrecht, A., "Opportunities for future supernova studies of cosmic acceleration", *Phys. Rev. Lett.*, **86**, 1939–1942 (2001). [DOI], [arXiv:astro-ph/0008314]. (Cited on page 20.)

[954] Wetterich, C., "Cosmology and the Fate of Dilatation Symmetry", *Nucl. Phys. B*, **302**, 668–696 (1988). [DOI]. (Cited on pages 18, 32, 34, 35, 39, and 64.)

[955] Wetterich, C., "An asymptotically vanishing time-dependent cosmological 'constant"', *Astron. Astrophys.*, **301**, 321–328 (1995). [ADS], [arXiv:hep-th/9408025]. (Cited on pages 34, 91, and 113.)

[956] Wetterich, C., "Phenomenological parameterization of quintessence", *Phys. Lett. B*, **594**, 17–22 (2004). [DOI], [arXiv:astro-ph/0403289]. (Cited on pages 19, 64, and 73.)

[957] Wetterich, C., "Growing neutrinos and cosmological selection", *Phys. Lett. B*, **655**, 201–208 (2007). [DOI], [arXiv:0706.4427 [hep-ph]]. (Cited on pages 34, 138, and 143.)

[958] Wetterich, C., "Naturalness of exponential cosmon potentials and the cosmological constant problem", *Phys. Rev. D*, **77**, 103505 (2008). [DOI], [ADS], [arXiv:0801.3208 [hep-th]]. (Cited on page 33.)

[959] Wetterich, C. and Pettorino, V., "Growing neutrino cosmology", *arXiv*, e-print, (2009). [ADS], [arXiv:0905.0715 [astro-ph.CO]]. (Cited on page 138.)

[960] Will, C.M., "Theoretical Frameworks for Testing Relativistic Gravity. II. Parametrized Post-Newtonian Hydrodynamics, and the Nordtvedt Effect", *Astrophys. J.*, **163**, 611–628 (1971). [DOI], [ADS]. (Cited on page 61.)

[961] Will, C.M. and Nordtvedt Jr, K.L., "Conservation Laws and Preferred Frames in Relativistic Gravity. I. Preferred-Frame Theories and an Extended PPN Formalism", *Astrophys. J.*, **177**, 757–774 (1972). [DOI], [ADS]. (Cited on page 61.)

[962] Wintergerst, N. and Pettorino, V., "Clarifying spherical collapse in coupled dark energy cosmologies", *Phys. Rev. D*, **82**, 103516 (2010). [DOI], [arXiv:1005.1278 [astro-ph.CO]]. (Cited on pages 34, 66, 71, 72, 73, 74, 143, 150, and 153.)

[963] Wintergerst, N., Pettorino, V., Mota, D.F. and Wetterich, C., "Very large scale structures in growing neutrino quintessence", *Phys. Rev. D*, **81**, 063525 (2010). [DOI], [arXiv:0910.4985 [astro-ph.CO]]. (Cited on pages 34, 67, 73, 143, and 150.)

[964] Winther, H.A., Mota, D.F. and Li, B., "Environment Dependence of Dark Matter Halos in Symmetron Modified Gravity", *Astrophys. J.*, **756**, 166 (2012). [DOI], [ADS], [arXiv:1110.6438 [astro-ph.CO]]. (Cited on page 68.)

[965] Witten, E., "Some properties of O(32) superstrings", *Phys. Lett. B*, **149**, 351–356 (1984). [DOI], [ADS]. (Cited on page 123.)

[966] Wong, Y.Y.Y., "Higher order corrections to the large scale matter power spectrum in the presence of massive neutrinos", *J. Cosmol. Astropart. Phys.*, **2008**(10), 035 (2008). [DOI], [ADS], [arXiv:0809.0693]. (Cited on page 142.)

[967] Woodard, R., "Avoiding Dark Energy with $1/R$ Modifications of Gravity", in Papantonopoulos, L., ed., *The Invisible Universe: Dark Matter and Dark Energy*, Proceedings of the 3rd Aegean Summer School, Chios, 26 September – 1 October, 2005, Lecture Notes in Physics, 720, pp. 403–433, (Springer, Berlin; Heidelberg, 2007). [DOI], [ADS], [arXiv:astro-ph/0601672], [Google Books]. (Cited on pages 59 and 62.)

[968] Wright, E.L. et al., "Interpretation of the cosmic microwave background radiation anisotropy detected by the COBE Differential Microwave Radiometer", *Astrophys. J. Lett.*, **396**, L13–L18 (1992). [DOI], [ADS]. (Cited on page 124.)

[969] Wu, P., Yu, H. and Fu, X., "A parametrization for the growth index of linear matter perturbations", *J. Cosmol. Astropart. Phys.*, **2009**(06), 019 (2009). [DOI], [ADS], [arXiv:0905.3444 [gr-qc]]. (Cited on page 90.)

[970] Xia, J.-Q., "Constraint on coupled dark energy models from observations", *Phys. Rev. D*, **80**, 103514 (2009). [DOI], [arXiv:0911.4820 [astro-ph.CO]]. (Cited on page 34.)

[971] Xia, J.-Q., Bonaldi, A., Baccigalupi, C., De Zotti, G., Matarrese, S., Verde, L. and Viel, M., "Constraining primordial non-Gaussianity with high-redshift probes", *J. Cosmol. Astropart. Phys.*, **2010**(08), 013 (2010). [DOI], [ADS], [arXiv:1007.1969 [astro-ph.CO]]. (Cited on page 176.)

[972] Yahil, A., Sandage, A. and Tammann, G.A., "The velocity field of bright nearby galaxies. III. The distribution in space of galaxies within 80 megaparsecs: The north galactic density anomaly", *Astrophys. J.*, **242**, 448–468 (1980). [DOI], [ADS]. (Cited on page 85.)

[973] Yokoyama, S. and Soda, J., "Primordial statistical anisotropy generated at the end of inflation", *J. Cosmol. Astropart. Phys.*, **2008**(08), 005 (2008). [DOI], [ADS], [arXiv:0805.4265]. (Cited on page 204.)

[974] Zavala, J., Jing, Y.P., Faltenbacher, A., Yepes, G., Hoffman, Y., Gottlöber, S. and Catinella, B., "The Velocity Function in the Local Environment from ΛCDM and ΛWDM Constrained Simulations", *Astrophys. J.*, **700**, 1779–1793 (2009). [DOI], [ADS], [arXiv:0906.0585 [astro-ph.CO]]. (Cited on pages 133 and 135.)

[975] Zehavi, I. et al., "The Luminosity and Color Dependence of the Galaxy Correlation Function", *Astrophys. J.*, **630**, 1–27 (2005). [DOI], [ADS], [arXiv:astro-ph/0408569]. (Cited on page 175.)

[976] Zentner, A.R., Rudd, D.H. and Hu, W., "Self-calibration of tomographic weak lensing for the physics of baryons to constrain dark energy", *Phys. Rev. D*, **77**, 043507 (2008). [DOI], [arXiv:0709.4029 [astro-ph]]. (Cited on pages 68 and 104.)

[977] Zhang, P. and Pen, U.-L., "Mapping dark matter with cosmic magnification", *Phys. Rev. Lett.*, **95**, 241302 (2005). [DOI], [arXiv:astro-ph/0506740]. (Cited on pages 76 and 77.)

[978] Zhang, P. and Pen, U.-L., "Precision measurement of cosmic magnification from 21 cm emitting galaxies", *Mon. Not. R. Astron. Soc.*, **367**, 169–178 (2006). [DOI], [arXiv:astro-ph/0504551]. (Cited on pages 76, 77, and 78.)

[979] Zhang, X., Wu, F.-Q. and Zhang, J., "New generalized Chaplygin gas as a scheme for unification of dark energy and dark matter", *J. Cosmol. Astropart. Phys.*, **2006**(01), 003 (2006). [DOI], [ADS], [arXiv:astro-ph/0411221]. (Cited on page 151.)

[980] Zhao, G.-B., Giannantonio, T., Pogosian, L., Silvestri, A., Bacon, D.J., Koyama, K., Nichol, R.C. and Song, Y.-S., "Probing modifications of general relativity using current cosmological observations", *Phys. Rev. D*, **81**, 103510 (2010). [DOI], [ADS], [arXiv:1003.0001 [astro-ph.CO]]. (Cited on pages 25, 26, 34, 35, 63, 66, and 153.)

[981] Zhao, G.-B., Li, B. and Koyama, K., "N-body simulations for $f(R)$ gravity using a self-adaptive particle-mesh code", *Phys. Rev. D*, **83**, 044007 (2011). [DOI], [ADS], [arXiv:1011.1257 [astro-ph.CO]]. (Cited on page 68.)

[982] Zhao, G.-B., Pogosian, L., Silvestri, A. and Zylberberg, J., "Cosmological tests of GR – a look at the principals", *Phys. Rev. Lett.*, **103**, 241301 (2009). [DOI], [arXiv:0905.1326 [astro-ph.CO]]. (Cited on page 26.)

[983] Zhao, G.-B., Pogosian, L., Silvestri, A. and Zylberberg, J., "Searching for modified growth patterns with tomographic surveys", *Phys. Rev. D*, **79**, 083513 (2009). [DOI], [arXiv:0809.3791 [astro-ph]]. (Cited on page 111.)

[984] Zhao, H.S., "Constraining TeVeS gravity as effective dark matter and dark energy", *Int. J. Mod. Phys. D*, **16**, 2055–2063 (2008). [DOI], [ADS], [arXiv:astro-ph/0610056]. (Cited on page 51.)

[985] Zhu, Z.-H., "Generalized Chaplygin gas as a unified scenario of dark matter/energy: Observational constraints", *Astron. Astrophys.*, **423**, 421–426 (2004). [DOI], [ADS], [arXiv:astro-ph/0411039]. (Cited on page 151.)

[986] Zibin, J.P. and Moss, A., "Linear kinetic Sunyaev-Zel'dovich effect and void models for acceleration", *Class. Quantum Grav.*, **28**, 164005 (2011). [DOI], [arXiv:1105.0909 [astro-ph.CO]]. (Cited on page 194.)

[987] Zlosnik, T.G., Ferreira, P.G. and Starkman, G.D., "Vector-tensor nature of Bekenstein's relativistic theory of modified gravity", *Phys. Rev. D*, **74**, 044037 (2006). [DOI], [ADS], [arXiv:gr-qc/0606039]. (Cited on page 51.)

[988] Zlosnik, T.G., Ferreira, P.G. and Starkman, G.D., "Modifying gravity with the aether: An alternative to dark matter", *Phys. Rev. D*, **75**, 044017 (2007). [DOI], [ADS], [arXiv:astro-ph/0607411]. (Cited on page 49.)

[989] Zlosnik, T.G., Ferreira, P.G. and Starkman, G.D., "Growth of structure in theories with a dynamical preferred frame", *Phys. Rev. D*, **77**, 084010 (2008). [DOI], [ADS], [arXiv:0711.0520 [astro-ph]]. (Cited on pages 50 and 159.)

[990] Zumalacárregui, M., García-Bellido, J. and Ruiz-Lapuente, P., "Tension in the void: cosmic rulers strain inhomogeneous cosmologies", *J. Cosmol. Astropart. Phys.*, **2012**(10), 009 (2012). [DOI], [ADS], [arXiv:1201.2790 [astro-ph.CO]]. (Cited on page 194.)

[991] Zuntz, J., Zlosnik, T.G., Bourliot, F., Ferreira, P.G. and Starkman, G.D., "Vector field models of modified gravity and the dark sector", *Phys. Rev. D*, **81**, 104015 (2010). [DOI], [ADS], [arXiv:1002.0849 [astro-ph.CO]]. (Cited on page 50.)

[992] Zwicky, F., "Die Rotverschiebung von extragalaktischen Nebeln", *Helv. Phys. Acta*, **6**, 110–127 (1933). [ADS]. (Cited on page 122.)

[993] Zwicky, F., "On the Masses of Nebulae and of Clusters of Nebulae", *Astrophys. J.*, **86**, 217–246 (1937). [DOI], [ADS]. (Cited on pages 122 and 124.)